frontiers | Research Topics

Enhanced weathering and synergistic combinations with other CDR methods

Edited by
Jens Hartmann, David Beerling, Mathilde Hagens and Sara Vicca

Published in
Frontiers in Climate

ISSN 1664-8714
ISBN 978-2-8325-3026-9
DOI 10.3389/978-2-8325-3026-9

About Frontiers

Frontiers is more than just an open access publisher of scholarly articles: it is a pioneering approach to the world of academia, radically improving the way scholarly research is managed. The grand vision of Frontiers is a world where all people have an equal opportunity to seek, share and generate knowledge. Frontiers provides immediate and permanent online open access to all its publications, but this alone is not enough to realize our grand goals.

Frontiers journal series

The Frontiers journal series is a multi-tier and interdisciplinary set of open-access, online journals, promising a paradigm shift from the current review, selection and dissemination processes in academic publishing. All Frontiers journals are driven by researchers for researchers; therefore, they constitute a service to the scholarly community. At the same time, the *Frontiers journal series* operates on a revolutionary invention, the tiered publishing system, initially addressing specific communities of scholars, and gradually climbing up to broader public understanding, thus serving the interests of the lay society, too.

Dedication to quality

Each Frontiers article is a landmark of the highest quality, thanks to genuinely collaborative interactions between authors and review editors, who include some of the world's best academicians. Research must be certified by peers before entering a stream of knowledge that may eventually reach the public - and shape society; therefore, Frontiers only applies the most rigorous and unbiased reviews. Frontiers revolutionizes research publishing by freely delivering the most outstanding research, evaluated with no bias from both the academic and social point of view. By applying the most advanced information technologies, Frontiers is catapulting scholarly publishing into a new generation.

What are Frontiers Research Topics?

Frontiers Research Topics are very popular trademarks of the *Frontiers journals series*: they are collections of at least ten articles, all centered on a particular subject. With their unique mix of varied contributions from Original Research to Review Articles, Frontiers Research Topics unify the most influential researchers, the latest key findings and historical advances in a hot research area.

Find out more on how to host your own Frontiers Research Topic or contribute to one as an author by contacting the Frontiers editorial office: frontiersin.org/about/contact

Enhanced weathering and synergistic combinations with other CDR methods

Topic editors

Jens Hartmann — University of Hamburg, Germany
David Beerling — The University of Sheffield, United Kingdom
Mathilde Hagens — Wageningen University and Research, Netherlands
Sara Vicca — University of Antwerp, Belgium

Citation

Hartmann, J., Beerling, D., Hagens, M., Vicca, S., eds. (2023). *Enhanced weathering and synergistic combinations with other CDR methods*. Lausanne: Frontiers Media SA. doi: 10.3389/978-2-8325-3026-9

Table of contents

frontiers | Frontiers in Climate

TYPE Editorial
PUBLISHED 04 July 2023
DOI 10.3389/fclim.2023.1244396

OPEN ACCESS

EDITED AND REVIEWED BY
Phil Renforth,
Heriot-Watt University, United Kingdom

*CORRESPONDENCE
Mathilde Hagens
✉ mathilde.hagens@wur.nl

RECEIVED 22 June 2023
ACCEPTED 23 June 2023
PUBLISHED 04 July 2023

CITATION
Hagens M, Hartmann J, Vicca S and Beerling DJ (2023) Editorial: Enhanced weathering and synergistic combinations with other CDR methods. *Front. Clim.* 5:1244396. doi: 10.3389/fclim.2023.1244396

Editorial: Enhanced weathering and synergistic combinations with other CDR methods

Mathilde Hagens[1]*, Jens Hartmann[2], Sara Vicca[3] and David J. Beerling[4]

[1]Soil Chemistry and Chemical Soil Quality, Wageningen University & Research, Wageningen, Netherlands, [2]Institute for Biogeochemistry and Marine Chemistry, KlimaCampus, Universität Hamburg, Hamburg, Germany, [3]PLECO (Plants and Ecosystems), Department of Biology, University of Antwerp, Antwerp, Belgium, [4]Leverhulme Centre for Climate Change Mitigation, School of Biosciences, University of Sheffield, Sheffield, United Kingdom

KEYWORDS

enhanced weathering, carbon dioxide removal (CDR), mineral dissolution kinetics, soil quality, monitoring reporting and verification (MRV), long-term field trials

Editorial on the Research Topic
Enhanced weathering and synergistic combinations with other CDR methods

1. Introduction

Weathering of silicate minerals stabilizes climate on geologic time scales by consuming carbon dioxide (CO_2) (Walker et al., 1981; Berner et al., 1983). Artificially enhancing weathering rates on land by crushing and spreading silicate mineral-bearing rocks is a promising carbon dioxide removal (CDR) technology (Hartmann et al., 2013) that exploits acceleration of these natural weathering reactions with potential to scale to gigatons of CDR annually when deployed on croplands (Strefler et al., 2018; Beerling et al., 2020). Over the past 1.5 decades, research interest on Enhanced Weathering (EW) has increased with research foci including process modeling of the CDR potential of nations (Beerling et al., 2020; Kantzas et al., 2022), capacity of rivers and oceans to transport sequestered CO_2 (Kohler et al., 2010; Zhang et al., 2022; Kanzaki et al., 2023), field trials aiming to understand the performance of this technology in agricultural systems under real world conditions (Haque et al., 2020; Larkin et al.), and the requirement for robust monitoring, reporting and verification (MRV) of CDR. The collection of papers in this Research Topic focuses on the application of EW on land and in the oceans and the resulting feedback mechanisms and potential co-benefits.

2. Overview of publications in this Research Topic

Out of the 11 publications in this Research Topic, some deal with fundamental factors controlling mineral dissolution kinetics. Fuhr et al. used a batch reactor to investigate dissolution of sand-sized olivine-rich rocks in artificial seawater. They showed an unexpected decline in total alkalinity (TA), which they attributed to authigenic clay mineral formation exceeding olivine dissolution. Amann et al. investigated the role of partial pressure

of CO_2 (pCO_2) and mineral grain size on CO_2 uptake in a series of column experiments. In most columns, they observed a fourfold increase in CO_2 uptake when comparing saturated vs. ambient pCO_2. Interestingly, while the absolute CO_2 uptake was highest with smallest grain size, the CO_2 uptake normalized per reactive surface area was highest with coarser grains. Pogge von Strandmann et al. compared olivine weathering in soil cores at 4–19°C and showed that the olivine dissolution rate was two orders of magnitude lower at the lower temperature. Since many laboratory or greenhouse studies investigate mineral weathering at relatively high ambient temperatures, this finding has important implications when translating small-scale experiments to larger-scale settings.

Other studies investigated the co-benefits of EW in relation to various aspects of soil quality at a range of spatial scales. te Pas et al. compared the potential of five different silicates for both CO_2 sequestration and soil quality improvements. They showed that while wollastonite and olivine had the highest CDR potential, columns amended with the latter mineral also exceeded nickel (Ni) groundwater threshold values in their leachates. Furthermore, most treatments produced a net carbon loss due to enhanced losses of organic carbon (OC). This highlights the need to investigate both inorganic carbon (IC) and OC dynamics in EW experiments to fully understand CO_2 sequestration at multiple timescales, a common finding in this Research Topic (e.g., Almaraz et al.; Janssens et al.). Vienne et al. investigated co-benefits of EW in a mesocosm experiment growing potato in so far understudied alkaline soil. Besides finding no negative impact of basalt amendment on potato yield despite higher soil aluminum and Ni availability, the study also showed reduced nitrogen leaching for the basalt-amended treatments. The authors additionally used a 1-dimensional reactive transport model (RTM) to estimate CO_2 sequestration during the experiment. Combining mesocosm experiments with RTMs allows assessment of the underlying processes of EW and CO_2 sequestration on timescales exceeding the duration of experiments (Kelland et al., 2020).

A couple of perspectives in this Research Topic had a broader look at factors that should be considered in the upscaling of EW. To address the abovementioned heavy metal release resulting from EW, Suhrhoff investigated whether phytoremediation strategies can prevent the accumulation of Ni and chromium in soils. He proposes the use of either hyperaccumulating plants in crop rotation strategies, or accumulating plants with a high biomass production, as a way of preventing long-term heavy metal contamination. Janssens et al. looked at the use of EW in combination with biochar amendment and OC sequestration in soils suffering from low fertility and water retention capacity. They argue that these CDR technologies do not only result in negative CO_2 emissions, but also in negative erosion, through improving soil structure and increasing both cation and anion exchange capacities. Their work highlights that combined applications of CDR technologies may synergistically contribute to multiple Sustainable Development Goals (SDGs) (Beerling et al., 2018).

EW requires long-term field trials investigating its performance on working lands under a wide range of environmental and agronomical settings. Larkin et al. present for the first time the results of such a field trial in a tropical environment using TA export, thereby accounting for possible lower CDR due to either carbonate mineral dissolution or silicate mineral dissolution with acids other than CO_2. They show higher CDR in one of the three catchments in their study design, likely due to EW of silicate minerals in this catchment. Almaraz et al. conducted a literature review on the use of mineral amendments as a CDR technology, as well as methodologies used to studying mineral weathering by both geologists and agronomists. Their work highlights the need for both groups to collaborate in interdisciplinary projects and involve stakeholders. Besides large-scale field trials of EW, a low-cost method for MRV of CO_2 removal in such settings is required. Acknowledging that TA can be used to track CO_2 removal due to mineral weathering, Amann and Hartmann propose such a method. Their work shows linear correlations between electrical conductivity (EC) and TA both in column experiments and at the catchment scale. These promising results for using EC as a proxy for CO_2 sequestration will need further calibration with a range of both abiotic and biotic factors.

While the studies in this Research Topic mostly focused on EW of silicate rocks, also enhancing carbonate mineral weathering may contribute to CDR because of its relatively high mineral dissolution rates. However, reprecipitation of carbonate minerals before the produced TA reaches the ocean fully reverts CO_2 capture. To investigate this potential reprecipitation (Knapp and Tipper) conducted a modeling study in almost 150 river basins. They show that the key factor controlling the efficacy of carbonate weathering for CDR is riverine transport of the weathering products, and not the capacity of soils to dissolve carbonate minerals.

3. Conclusion

The publications in this Research Topic offer guidance on possible future directions of EW research, ranging from fundamental mineral dissolution kinetics to practical applications in naturally heterogenous fields. A unified, synchronized global research agenda to develop a robust MRV framework, and to understand if and how EW and its interaction with other CDR-methods might contribute to the significant CDR-necessities to stabilize climate within this century, is urgently necessary.

Author contributions

MH wrote the draft, with input from JH, SV, and DB. All authors listed have made a substantial, direct, and intellectual contribution to the work and approved it for publication.

Funding

MH, SV, and JH acknowledge funding from the European Union Horizon 2020 framework program for research and innovation (No. 964545).

Acknowledgments

We thank all authors and reviewers who contributed to this Research Topic for their stimulating inputs. We also acknowledge the Editorial Team of Frontiers in Climate—Negative Emission

Technologies for their professional support during the publication process of this Research Topic.

Conflict of interest

The authors declare that the research was conducted in the absence of any commercial or financial relationships that could be construed as a potential conflict of interest.

Publisher's note

References

Beerling, D. J., Kantzas, E. P., Lomas, M. R., Wade, P., Eufrasio, R. M., Renforth, P., et al. (2020). Potential for large-scale CO_2 removal via enhanced rock weathering with croplands. *Nature* 583, 242–248. doi: 10.1038/s41586-020-2448-9

Beerling, D. J., Leake, J. R., Long, S. P., Scholes, J. D., Ton, J., Nelson, P. N., et al. (2018). Farming with crops and rocks to address global climate, food and soil security. *Nat. Plants* 4, 138–147. doi: 10.1038/s41477-018-0108-y

Berner, R. A., Lasaga, A. C., and Garrels, R. M. (1983). The carbonate-silicate geochemical cycle and its effect on atmospheric carbon dioxide over the past 100 million years. *Am. J. Sci.* 283, 641–683. doi: 10.2475/ajs.283.7.641

Haque, F., Santos, R. M., and Chiang, Y. W. (2020). CO2 sequestration by wollastonite-amended agricultural soils – an Ontario field study. *Int. J. Greenh. Gas Control* 97, 103017. doi: 10.1016/j.ijggc.2020.103017

Hartmann, J., West, A. J., Renforth, P., Köhler, P., De La Rocha, C. L., Wolf-Gladrow, D., et al. D., et al. (2013). Enhanced chemical weathering as a geoengineering strategy to reduce atmospheric carbon dioxide, supply nutrients, and mitigate ocean acidification. *Rev. Geophys.* 51, 113–149. doi: 10.1002/rog.20004

Kantzas, E. P., Val Martin, M., Lomas, M. R., Eufrasio, R. M., Renforth, R., Lewis, A. L., et al. (2022). Substantial carbon drawdown potential from enhanced rock weathering in the United Kingdom. *Nat. Geosci.* 15, 382–389. doi: 10.1038/s41561-022-00925-2

Kanzaki, Y., Planavsky, N. J., and Reinhard, C. T. (2023). New estimates of the storage permanence and ocean co-benefits of enhanced rock weathering. *PNAS Nexus* 2, pgad059. doi: 10.1093/pnasnexus/pgad059

Kelland, M. E., Wade, P. W., Lewis, A. L., Taylor, L. L., Sarkar, B., Andrews, M. G., et al. (2020). Increased yield and CO2 sequestration potential with the C4 cereal Sorghum bicolor cultivated in basaltic rock dust-amended agricultural soil. *Glob. Chang. Biol.* 26, 3658–3676. doi: 10.1111/gcb.15089

Kohler, P., Hartmann, J., and Wolf-Gladrow, D. A. (2010). Geoengineering potential of artificially enhanced silicate weathering of olivine. *Proc. Nat. Acad. Sci.* 107, 20228–20233. doi: 10.1073/pnas.1000545107

Strefler, J., Amann, T., Bauer, N., Kriegler, E., and Hartmann, J. (2018). Potential and costs of carbon dioxide removal by enhanced weathering of[[Inline Image]] rocks. *Environ. Res. Lett.* 13. doi: 10.1088/1748-9326/aaa9c4

Walker, J. C. G., Hays, P. B., and Kasting, J. F. (1981). A negative feedback mechanism for the long-term stabilization of Earth's surface temperature. *J. Geophys. Res.* 86, 9776. doi: 10.1029/JC086iC10p09776

Zhang, S., Planavsky, N. J., Katchinoff, J., Raymond, P. A., Kanzaki, Y., Reershemius, T., et al. (2022). River chemistry constraints on the carbon capture potential of surficial enhanced rock weathering. *Limnol. Oceanogr.* 67(S2), S148–S157. doi: 10.1002/lno.12244

frontiers in Climate

PERSPECTIVE
published: 17 January 2022
doi: 10.3389/fclim.2021.820204

Phytoprevention of Heavy Metal Contamination From Terrestrial Enhanced Weathering: Can Plants Save the Day?

*Tim Jesper Suhrhoff**

Department of Earth Sciences, Institute of Geochemistry and Petrology, ETH Zurich, Zurich, Switzerland

Enhanced weathering is a promising approach to remove carbon dioxide from the atmosphere. However, it may also pose environmental risks through the release of heavy metals, in particular nickel and chromium. In this perspective article I explore the potential role of plants in modulating these heavy metal fluxes. Agricultural basaltic soils may be valuable study sites in this context. However, the effect of biomass harvesting on the accumulation of heavy metals is currently not well studied. Mostly caused by different parent rock concentrations, there is a large variability of heavy metal concentrations in basaltic and ultramafic soils. Hence, to minimize environmental risks of enhanced weathering, basalts with low heavy metal concentrations should be favored. Existing phytoremediation strategies may be used to "phytoprevent" the accumulation of nickel and chromium released from enhanced weathering in soils. As a result, elevated nickel and chromium concentrations in rocks must not preclude enhanced weathering in all settings. In particular, hyperaccumulating plants could be used as part of a crop rotation to periodically remove heavy metals from soils. Enhanced weathering could also be employed on fields or forests of (non-hyper) accumulating plants that have a high primary production of biomass. Both approaches may have additional synergies with phytomining or bioenergy carbon capture and storage, increasing the total amount of carbon dioxide drawdown and at the same time preventing heavy metal accumulation in soils.

Keywords: enhanced weathering, heavy metals, chromium, nickel, phytoprevention, phytoremediation, hyperaccumulating plants, basalt

OPEN ACCESS

Edited by:
Sara Vicca,
University of Antwerp, Belgium

Reviewed by:
Fatima Haque,
University of Guelph, Canada
Rafael Mattos Dos Santos,
University of Guelph, Canada
Sofie Thijs,
University of Hasselt, Belgium

***Correspondence:**
Tim Jesper Suhrhoff
jesper.suhrhoff@erdw.ethz.ch

Specialty section:
This article was submitted to Negative Emission Technologies, a section of the journal Frontiers in Climate

Received: *22 November 2021*
Accepted: *20 December 2021*
Published: *17 January 2022*

Citation:
Suhrhoff TJ (2022) Phytoprevention of Heavy Metal Contamination From Terrestrial Enhanced Weathering: Can Plants Save the Day? Front. Clim. 3:820204. doi: 10.3389/fclim.2021.820204

INTRODUCTION

Limiting global warming to below 1.5 °C will require the development and implementation of carbon dioxide removal (CDR) technologies to offset residual and potential overshoot emissions (Fuss et al., 2018; IPCC, 2018). Among other CDR approaches (Fuss et al., 2018), terrestrial enhanced weathering (TEW) of silicate rocks has the potential to limit the accumulation of CO_2 in the atmosphere through the acceleration of natural weathering processes. Although TEW removes only ~0.3–1.1 tCO_2 per ton of rock (Köhler et al., 2010; Moosdorf et al., 2014; Strefler et al., 2018), when scaled up to large application rates (e.g. 40 t ha^{-1}; Beerling et al., 2020) it can remove between 0.5 and 4 $GtCO_2$ yr^{-1} (Fuss et al., 2018; Beerling et al., 2020; Goll et al., 2021) or even up to 95 $GtCO_2$ yr^{-1} (Strefler et al., 2018). Co-benefits of EW include (i) increasing the alkalinity of natural

waters which ameliorates ocean acidification and decreasing aragonite saturation (Taylor et al., 2016), (ii) stabilizing the soil pH which benefits plants and reduces emissions of other greenhouse gases (Kantola et al., 2017), (iii) improving soil hydrology (de Oliveira Garcia et al., 2020), and (iv) the release of nutrients which stimulates further biological carbon sequestration (Goll et al., 2021). Carbon dioxide removal through TEW does not require underground storage in geological reservoirs but still stores CO_2 in stable non-biological reservoirs such as the marine alkalinity pool or marine/pedogenic carbonates. Furthermore, selling carbon credits from TEW may also support livelihoods in the Global South and help progress toward multiple sustainable development goals (Smith et al., 2019).

Although models suggest that TEW could be a suitable CDR strategy (Strefler et al., 2018; Beerling et al., 2020; Goll et al., 2021), and pot and sediment core experiments detect increasing cation fluxes or bioavailable concentrations (Anda et al., 2009, 2013, 2015; ten Berge et al., 2012; Renforth et al., 2015; Amann et al., 2020), first field trials of TEW in agricultural settings do not detect an enhanced weathering signal in drainage waters (Andrews and Taylor, 2019). This is problematic because drainage waters integrate weathering signals over their catchment and would therefore be ideal to quantify TEW processes. Possible reasons include the retardation of weathering signals by the soil exchangeable cation pool (Pogge von Strandmann et al., 2021), precipitation of solutes in pedogenic carbonate (Haque et al., 2019, 2020b,c) and other secondary minerals, as well as the incorporation of released cations into biomass (Andrews and Taylor, 2019). Support for the latter mechanism can be drawn from (i) the fertilization potential of TEW implying cation uptake by plants (Hartmann et al., 2013; Amann and Hartmann, 2018; Goll et al., 2021), (ii) detectable cation flux responses in TEW experiments in forests (Peters et al., 2004; Shao et al., 2016; Taylor et al., 2021), and (iii) the observation that biomass constitutes a missing sink in weathering flux mass balances (von Blanckenburg et al., 2021).

Suitable rocks for enhanced weathering include basalt and dunite, an ultramafic rock mostly comprised of olivine. Both rocks, particularly dunite, often have elevated concentrations of Ni and Cr (Alloway, 2012). Alternatives with lower HM concentrations exist, for example wollastonite (Peters et al., 2004; Shao et al., 2016; Haque et al., 2019, 2020b,c; Taylor et al., 2021). However, they can be limited by availability (∼0.1Gt global wollastonite reserves; USGS, 2021) or price. Upon release through weathering, Ni and Cr have the tendency to be incorporated into secondary phases or adsorb onto surfaces (Alloway, 2012). Hence, TEW may result in accumulation of these heavy metals in soils and biomass which can be toxic to living organisms at high concentrations (Miranda et al., 2009; Alloway, 2012; Hartmann et al., 2013; Beerling et al., 2018; Amann et al., 2020). For example, in an experiment using an agricultural soil core, ∼99% of Ni and Cr released from olivine weathering are retained in the soil, limiting addition of olivine to soils to 95 t ha^{-1} before permissible Ni concentrations are exceeded (Renforth et al., 2015). However, plants also take up trace elements like Ni and Cr (Pulford and Watson, 2003; Etim, 2012), which might result in accumulation of these elements in periodically harvested and removed biomass. As a result, grass grown on basaltic soils may have Ni and Cr concentrations of 2.2 and 0.3 ppm (Néel et al., 2007), and 11–39 and 0.4–7.1 ppm when grown on ultramafic soils (Miranda et al., 2009). While this may have implications for food safety, it could also mean that concentrations could remain at safe levels in both soil and biomass.

Clearly, both the quantification of TEW fluxes as well as TEW related heavy metal (HM) cycling require a deeper understanding of how plants interact with the solutes released through TEW. Focusing on the latter aspect, in this perspective article I explore the lessons from existing literature on HM in basaltic soils as well as using phytoremediation strategies to "phytoprevent" accumulation of HM in soils. Phytoprevention might prove useful since understanding and mitigating detrimental environmental consequences of TEW is an important prerequisite for its large-scale implementation. It is also important from a global climate justice perspective, as TEW might be employed in countries of the Global South (Strefler et al., 2018; Beerling et al., 2020; Goll et al., 2021) that have not substantially contributed to the climate crisis.

HEAVY METALS IN BASALTIC SOILS

Soils formed from ultramafic and basaltic parent materials exist in various locations where these rocks occur naturally. Many of these soils are well studied, giving the opportunity to derive implications for TEW. Although basalt weathers (and removes CO_2 from the atmosphere) much slower than ultramafic lithologies (Strefler et al., 2018), I focus on basalt due to the high abundance of basalt outcrops (Hartmann and Moosdorf, 2012), its phosphorous fertilization potential (Gillman et al., 2002; Hartmann et al., 2013), and lower HM concentrations of ∼130 ppm Ni and ∼250 ppm Cr compared to ∼2000 ppm Ni and ∼2300 ppm Cr in ultramafic rocks like dunite (Alloway, 2012). As an upper limit for acceptable concentrations of Ni and Cr in soils I use 100 ppm and 200 ppm respectively, which are broadly representative of average limits throughout the EU (Tóth et al., 2016).

Globally, Ni and Cr concentrations in basaltic soils vary over two (Ni) to three (Cr) orders of magnitude (**Figure 1**). Some soils fall below, and some above, these thresholds. The main factor controlling soil concentrations is the composition of the parent material (Tra and Egashira, 2001; Dœlsch et al., 2006a,b; de Oliveira et al., 2011; Mendoza-Grimón et al., 2014; Cabral Pinto et al., 2015; Cox et al., 2017; Mazhari et al., 2017; Vlček et al., 2017; Fabrício Neta et al., 2018; Memoli et al., 2018; Iskandar et al., 2019; Bocardi et al., 2020; Wang et al., 2020). This is expected given the tendency of Ni and Cr to be retained in soils (Alloway, 2012). Similarly, reflecting elevated parent materials concentrations, soils formed from ultramafic rocks have much higher concentrations of Ni and Cr – on average ∼2000 ppm Ni and ∼2750 ppm Cr (Kierczak et al., 2021). Only few studies assess the impact of biology on HM concentrations in basaltic soils. On La Réunion, Ni and Cr concentrations are similar in

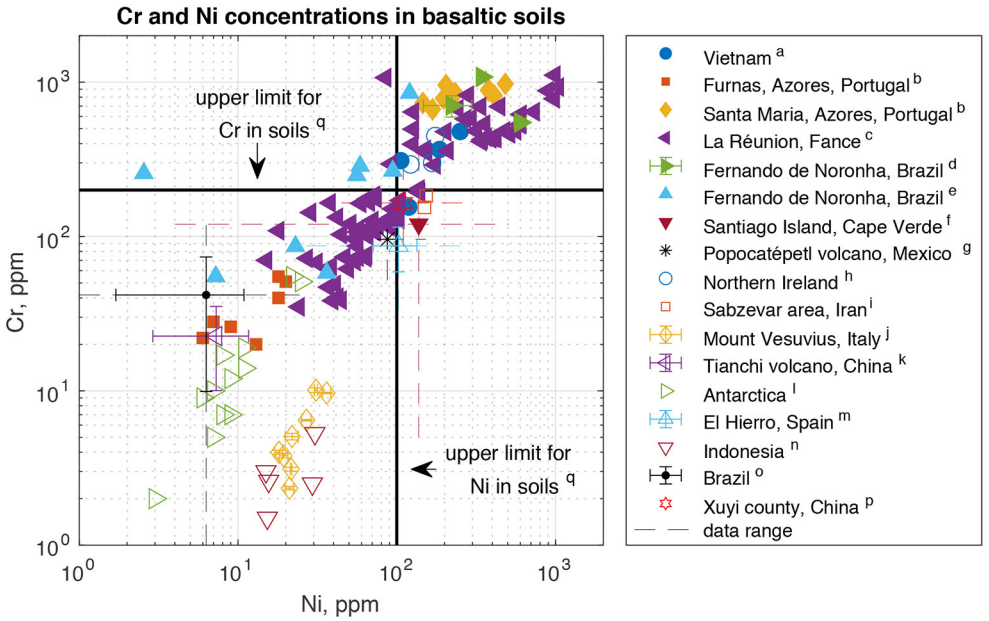

FIGURE 1 | Chromium and Ni concentrations in soils derived from basaltic rocks. The chosen acceptable limits for agricultural soils are representative of average limits throughout the EU (Tóth et al., 2016), although both higher or lower values are adopted into legislature in various countries (Tóth et al., 2016; Iskandar et al., 2019). For studies where individual sample data were not reported, the mean as well as the range of results (stippled lines) are shown. Where reported, the standard deviation around the mean (error bars) is plotted as well. (a) Tra and Egashira, 2001, (b) Amaral et al., 2006, (c) Dœlsch et al., 2006a, (d) de Oliveira et al., 2011, (e) Fabrício Neta et al., 2018, (f) Cabral Pinto et al., 2015, (g) Rodriguez-Espinosa et al., 2015, (h) Cox et al., 2017, (i) Mazhari et al., 2017, (j) Memoli et al., 2018, (k) Ma et al., 2019, (l) Vlček et al., 2017, (m) Mendoza-Grimón et al., 2014, (n) Iskandar et al., 2019, (o) Bocardi et al., 2020, (p) Wang et al., 2020, (q) Tóth et al., 2016.

cultivated and uncultivated soils (Dœlsch et al., 2006b), though it is not clear whether this is due to vegetation having no effect, or a canceling out of HM removal in biomass and inputs from fertilizer which can contain HM like Ni (McMurtry et al., 1995). At Mount Vesuvius, plant cover determines the HM fraction that is reducible or oxidizable mostly through its control on soil organic matter quality and associated impacts on pH, oxidation state and element mobility (Memoli et al., 2018). Although few studies report the composition of the parent material, some find HM concentrations in soils that are lower than in the parent material (McMurtry et al., 1995; Wang et al., 2020), indicating the presence of a HM sink.

This analysis shows that, first, there is large variability of Ni and Cr concentrations in soils formed from basalt (**Figure 1**), which is also valid for soils formed from ultramafic rocks (Kierczak et al., 2021). Second, much of this variability seems to depend on the composition of the parent material. This highlights that if HM exposure is to be minimized based exclusively on parent rock composition, the variability within the respective rock classes should be taken into account, favoring rocks with low concentrations in both rock types (i.e. also differentiating between high and low HM concentrations in basalts). Thus, choosing basalt or ultramafic rocks becomes a decision based on other factors like the required rate of CO_2 uptake or nutrient requirements, rather than environmental risk alone. Third, the extent to which biology effects buildup of HM in basaltic soils is currently poorly understood. Given this limited state of knowledge and the fact that additional sinks of Ni and Cr exist at least in some settings (McMurtry et al., 1995; Wang et al., 2020), further studies assessing the effect of different types of vegetation cover and agricultural practices on HM concentrations in basaltic (and ultramafic) soils would be valuable in the TEW context.

PHYTOREMEDIATION

Although high concentrations of HM in ultramafic soils make them toxic for many plants, they are also a niche habitat for plant species that are adapted to coping with these conditions by either excluding HM from, or (hyper-)accumulating HM in, their plant tissues (Kierczak et al., 2021). While hyperaccumulation has probably evolved as a defense mechanism of plants against herbivores (Rascio and Navari-Izzo, 2011), excluders use one or several separate strategies to either break down contaminants or make them less bioavailable (e.g. phytodegradation, rhizodegradation, and phytostabilization; Etim, 2012; Yadav et al., 2021).

In phytoremediation, appropriate plants are used to decontaminate soils or water bodies polluted from anthropogenic impacts either by extracting HM or making them less bioavailable. To remove metals from soils, phytoextracting plants that accumulate metals of interest, ideally in the above ground biomass, are particularly useful (Pulford and Watson,

2003; Vara Prasad and de Oliveira Freitas, 2003; Etim, 2012; Yadav et al., 2021). These plants are usually separated into hyperaccumulators having a metal concentration of >1000 ppm of some HM (including Ni and Cr) in their dried biomass (Baker and Brooks, 1989) and non-hyperaccumulators that have lower HM concentrations but may still accumulate HM from soils (called accumulators here). Hyperaccumulating plants usually have a lower biomass production (Pulford and Watson, 2003). As a result, accumulating plants of lower HM concentration but high biomass production can be just as effective at removing HM from soils.

"PHYTOPREVENTION" OF HEAVY METAL CONTAMINATION FROM TEW

In phytoremediation, plants are used to treat soils *after* they have been contaminated. The existence of these approaches suggests that they could be used preemptively to prevent accumulation and contamination of soils with HM released from TEW (Haque et al., 2020a) – termed "phytoprevention" here. In combination with TEW, this seems a promising approach given that plant species have been identified that (hyper-)accumulate Ni and Cr from soils and waters. While several hundred Ni hyperaccumulating taxa have been identified (Lone et al., 2008), Cr hyperaccumulation is generally scarce (Han et al., 2004; Singh et al., 2013; Teuchies et al., 2013; van der Ent et al., 2013) due to the low bioavailability of Cr(III) (dominating over Cr(IV) in most soils; Kotaś and Stasicka, 2000; Alloway, 2012). In the context of phytoprevention, I outline two synergistic approaches between phytoprevention and TEW below, as well a third approach to remove HM from effluent waters. A comprehensive review of potentially suitable species is beyond the scope of this perspective article, but a selection of promising species for each approach can be found in **Table 1**.

In approach one, TEW is employed on agricultural fields (including for food production) and hyperaccumulating plants periodically remove Ni and Cr from the soils as part of a crop rotation. Many hyperaccumulators can reach metal concentrations of 1–3% of Ni. Given that their ashes may contain 12% to >20% of Ni, this approach might also enable the commercial retrieval of the metals initially contained in the basalt or ultramafic rocks, i.e. phytomining (Chaney et al., 2007; Alloway, 2012) in addition to limiting HM buildup in soil and biomass. Although some examples like southern cutgrass (*Leersia hexandra*) or Chinese brake (*Pteris vittate*; in hydroponic experiments) of Cr hyperaccumulation exist (Zhang et al., 2007; Kalve et al., 2011), it is not clear whether this strategy could work for Cr due to its limited bioavailability.

In approach two, managed fields or forests of accumulating plants, ideally grown for non-food applications, are used for TEW. While the concentrations of HM in these plants are lower, their larger biomass production may still make them suitable for phytoprevention. This approach has potential synergies with bioenergy carbon capture and storage (BECCS) discussed in the next section. Low translocation from roots to above ground biomass may limit HM extraction efficiency for some of these plants or require laborious root harvesting (Pulford et al., 2001; Pulford and Watson, 2003; Were et al., 2017; Ranieri et al., 2020). An additional benefit of this approach is that many involved plant species, like bamboo and willow, stabilize soils and prevent erosion, decreasing the risk of spreading potential contamination to adjacent areas (Riddell-Black, 1994; Were et al., 2017). Intercropping accumulating plants with hyperaccumulating plants may increase overall crop metal accumulation, protect the accumulating plants, and increase overall biomass production (Kidd et al., 2015; Bian et al., 2020).

In the third approach, hyperaccumulating aquatic freshwater plants are used to remove HM from surface runoff and/or groundwater springs or wells to prevent contamination of rivers and freshwater resources. Many terrestrial hyperaccumulators like Indian mustard (*Brasicca juncea*) or Chinese brake (*Pteris vittate*) presented in approach one can also extract HM from hydroponic solutions (Diwan et al., 2008; Kalve et al., 2011; Ansari et al., 2015) enlarging the pool of suitable species.

POTENTIAL SYNERGIES WITH BECCS

Using accumulating plants of high biomass production for phytoprevention of HM pollution from TEW, i.e. approach two above, has the benefit that this biomass might be used for other CDR approaches like BECCS. For example, bamboo has a high net primary productivity of 12-26 t ha^{-1} yr^{-1} (Nath et al., 2015). Willows can be frequently harvested and yield as much as 10–15 t ha^{-1} dry biomass (Pulford and Watson, 2003). Both plants have been suggested as energy feedstocks in BECCS (Fajardy and Mac Dowell, 2017; Quader and Ahmed, 2017; Albanito et al., 2019). Removal of nutrients from soils through harvested biomass results in soils that are often nutrient deficient in terms of P and K in bamboo forests (Guan et al., 2017) and forests in general (Thiffault et al., 2011), limiting biomass production. As a result, combining TEW and phytoprevention with BECCS may produce a synergistic system where TEW supplies additional nutrients, increases growth rates, and CO_2 fixation of the BECCS feedstock. At the same time, regular harvesting of HM bearing biomass could phytoprevent the accumulation of HM in soils. While increased HM concentrations in biomass may pose challenges to bioenergy power plants from a pollution point of view, it may be possible to extract these metals through phytomining (Edgar et al., 2021).

FURTHER PHYTOPREVENTION OPPORTUNITIES

For all three approaches, plants should be chosen that are adjusted to the local climate conditions, favoring native plant varieties (Arreghini et al., 2017; Wei et al., 2021). Further research and a large database of plants that can potentially ameliorate HM contamination would therefore greatly benefit the management of environmental consequences of TEW.

Phytoremediation draws on a few other strategies, which may also be relevant in the context of phytoprevention. Examples

TABLE 1 | Selected plants that have been used to remove Cr and/or Ni from soils or water and might be useful in one of the three phytoprevention scenarios outlined in the main text.

Plant	Enriched metal	Concentration in dry biomass, ppm	Comment	Reference
Hyperaccumulating plants with potential for crop rotation (approach one)				
Mustard family plants (*Brassicaceae*), e.g. *Alyssum markgrafi, Brasicca juncea,* and *Thlaspi apterum*	Ni, Cr, HM	19100 (Ni, *A. markgrafi*) and 21500 (Ni, *T. apterum*), 890 (Cr, *Brasicca juncea*)	Mustard family plants can thrive in polymetallic contaminated soils. Indian Mustard (*Brasicca juncea*): Ni concentration in roots is 208 times higher than in medium, Cr 179 times; ∼1.2 t ha^{-1} biomass production. Can also extract HM from hydroponic solutions.	Dushenkov et al., 1995; Kidd and Monterroso, 2005; Diwan et al., 2008; Bani et al., 2010; Ansari et al., 2015; Rathore et al., 2019
Fern species Chinese brake (*Pteris vittate*)	Cr	20675 (in the stem) at 150 mg L^{-1}	Grown in hydroponic solution for 20 days (concentration might be lower when grown in soils due to lower bioavailability of Cr). Cr concentration in biomass increased until 150 mg L^{-1} and decreased at higher concentrations.	Kalve et al., 2011
Pycnandra (formerly *Sebertia*) *acuminata* (Sapotaceae)	Ni	257400 (latex), 24500 (trunk bark), 1700 (wood)	One of many hyperaccumulating species discovered in New Caledonia, others include *Psychotria gabriellae*, *Hybanthus austrocaledonicus*, *H. caledonicus* (Violaceae), *Geissois pruinosa* (Cunoniaceae), and *Homalium guillainii* (Salicaceae).	Brooks et al., 1974; Jaffr and Schmid, 1974; Jaffré et al., 1976, 2013
Accumulating plants with high biomass production (approach two)				
Bamboo (e.g. *Bambusa bambos)*	Cr	547 in plant shoots	Bamboo has been successfully used to extract Cr from a contaminated tannery site, Ni requires further studies. Chromium concentration is higher in roots than shoots.	Were et al., 2017; Bian et al., 2020; Ranieri et al., 2020
Black poplar (*Populus nigra*) and princess tree (*Paulownia tomentosa*)	Ni		In a study of soils contaminated with hydrocarbons and heavy metals, these trees removed on average ∼40% of Ni within three years.	Macci et al., 2013
Combination of five different woody species (*Terminalia arjuna, Prosopis juliflora, Populus alba, Eucalyptus tereticornis and Dendrocalamus strictus*)	Cr, Ni	∼250–250 (Cr), ∼12–17 (Ni)	Concentrations in tannery sludge (628 ppm Cr, 76 ppm Ni) were reduced by 70% (Cr) and 59% (Ni) after 1 year.	Shukla et al., 2011
Willow (*Salix* spp.)	HM		Willow has shown potential to remove metals from soils. The translocation from root to plan is possibly low and requires further studies.	Pulford et al., 2001; Pulford and Watson, 2003
Aquatic hyperaccumulators removing HM from TEW runoff (approach three)				
Water hyacinth (*Eichhornia crassipes*)	Cr, Ni	2000 (Cr) and 1000 (Ni) in culturing experiments at 10 mg L^{-1}	Water hyacinths have been widely used to remove both Cr and Ni from natural and industrial waste waters, removing up to 95% of Ni and 99% of Cr.	Zaranyika and Ndapwadza, 1995; Zhu et al., 1999; Ingole and Bhole, 2003; Mishra and Tripathi, 2009; Fazal et al., 2015; Pandharipande and Gadpayle, 2016; Saha et al., 2017; Panneerselvam and Priya, 2021
Floating ferns (*Salvinia natans, Salvina minima*)	Cr, Ni	∼12000 (Cr) of which ∼9000 after 48 h in 50 mg L^{-1} (*Salvinia natans*), 2210 (Cr) in submerged leaves in 10 mg L^{-1} (*Salvinia minima*), 16300 (Ni at 160 mg L^{-1}; *Salvinia minima*)	Uptake increases at higher aqueous concentrations. Uptake is quick in early stages (6-12h for Ni, 24 h for Cr), followed by slower uptake.	Dhir et al., 2009; Prado et al., 2010; Fuentes et al., 2014
Eel grass (*Vallisneria spiralis*)	Cr, Ni	2870 (Cr) and 2100 (Ni) at 30 mg L^{-1} in a polymetallic solution	Uptake increases at higher aqueous concentrations.	Verma et al., 2008
Lesser bulrush (*Typha angustifolia*), marshpennywort (*Hydrocotyle umbellata*)	Cr	130 (*T. angustifolia*) and ∼1850 (*H. umbellata*), both grown at 50 mg L^{-1})	*T. angustifolia* removed 99.78% of Cr from the water within 9 days, *H. umbellata* 99.67%.	Taufikurahman et al., 2019

are the use of rhizobacteria (Yadav et al., 2021) or mycorrhiza (Coninx et al., 2017) that may encourage plant growth, and increase the bioavailability and uptake efficiency of metals. The latter effect could also be achieved by adding chelating agents like EDTA to soils (Lim et al., 2004; Wu et al., 2004), although this should be viewed with caution and tested meticulously as the increased bioavailability and element mobility might promote runoff of HM into surface and groundwaters (Cooper et al., 1999; Pulford and Watson, 2003; Wu et al., 2004). Another interesting potential phytoprevention strategy common in phytoremediation is using phytostabilizing plants, which may have a similar effect as biochar in that they reduce HM bioavailability and runoff (Amann and Hartmann, 2018).

Upper limits of environmentally safe addition of olivine or basalt to soils may easily be calculated based on the cumulative amount of rocks added and their HM concentrations (Renforth et al., 2015). However, this may overestimate the environmental impact in the presence of additional HM sinks. In principle, a limit to TEW application at which HM do not accumulate in soils may be calculated from the heavy metal fluxes in biomass and rock:

$$max.\ TEW\ rock\ flux = \frac{(biomass\ flux)\ (max.\ HM\ concentration\ in\ biomass)\ u}{(HM\ concentration\ in\ TEW\ rock)\ d}$$

Where u is the uptake efficiency of HM in biomass, and d the fraction of source rock dissolved in the given period. For example, in a simplified case where u and d are 1 (biomass HM concentration as high as it is at high soil concentrations, source rock dissolved completely), bamboo could extract the Cr equivalent of up to ∼55 t basalt $ha^{(-1)}$ $yr^{(-1)}$, and mustard family plants the Ni equivalent of ∼180 t basalt $ha^{(-1)}$ $yr^{(-1)}$. In practice, this would require a more realistic parametrization of weathering (d) and plant HM uptake (u) processes at the given soil and source rock conditions, including of concentrations of HM in biomass at lower concentrations in soils. Potentially, elevated HM concentrations in rocks must not preclude TEW in all settings: If HM are continuously removed from soils through phytoprevention, even prolonged TEW might not exceed acceptable HM thresholds in either soil, drainage water, or harvested biomass. Overall, the approach of phytoprevention highlights the need for TEW studies to assess the fate of HM, as well as weathering fluxes in general, in terms of all input and output fluxes including biomass.

DATA AVAILABILITY STATEMENT

Publicly available datasets were analyzed in this study. The data sources are referenced in the article.

AUTHOR CONTRIBUTIONS

The author confirms being the sole contributor of this work and has approved it for publication.

FUNDING

The publication costs were covered by ETH Zurich.

ACKNOWLEDGMENTS

I would like to thank Prof. Dr. Jens Hartmann for discussing this idea with me, encouraging me to write this paper, and his constructive suggestions on how it may be improved. I further thank Prof. Dr. Derek Vance, Dr. Jörg Rickli, and Clara Leonie Bütow for editing, Lydia Ruth Bailey for proofreading an early version of this manuscript, and finally Dr. Fatima Haque, Dr. Rafael Mattos Dos Santos, and Dr. Sofie Thijs for their constructive reviews.

REFERENCES

Albanito, F., Hastings, A., Fitton, N., Richards, M., Martin, M., and Mac Dowell, N. (2019). Mitigation potential and environmental impact of centralized versus distributed BECCS with domestic biomass production in Great Britain. *GCB Bioenergy*. 11, 1234–1252. doi: 10.1111/gcbb.12630

Alloway, B. J. (2012). *Heavy Metals in Soils - Trace Metals and Metalloids in Soils and their Bioavailability*. Springer. doi: 10.1007/978-94-007-4470-7

Amann, T., and Hartmann, J. (2018). Ideas and perspectives: Synergies from co-deployment of negative emission technologies. *Biogeosc. Discus.* 16, 2949–2960. doi: 10.5194/bg-16-2949-2019

Amann, T., Hartmann, J., Struyf, E., Oliveira Garcia, D., e., Fischer, W., Janssens, E. K., et al. (2020). Enhanced Weathering and related element fluxes - A cropland mesocosm approach. *Biogeosciences*. 17, 103–119. doi: 10.5194/bg-17-103-2020

Amaral, A., Cruz, J., Cunha, R., and Rodrigues, A. (2006). Baseline levels of metals in volcanic soils of the Azores (Portugal). *Soil Sediment Contamin.* 15, 123–130. doi: 10.1080/15320380500506255

Anda, M., Shamshuddin, J., and Fauziah, C. I. (2013). Increasing negative charge and nutrient contents of a highly weathered soil using basalt and rice husk to promote cocoa growth under field conditions. *Soil Tillage Res.* 132, 1–11. doi: 10.1016/j.still.2013.04.005

Anda, M., Shamshuddin, J., and Fauziah, C. I. (2015). Improving chemical properties of a highly weathered soil using finely ground basalt rocks. *Catena.* 124, 147–161. doi: 10.1016/j.catena.2014.09.012

Anda, M., Shamshuddin, J., Fauziah, C. I., and Omar, S. R. S. (2009). Dissolution of ground basalt and its effect on oxisol chemical properties and cocoa growth. *Soil Sci.* 174, 264–271. doi: 10.1097/SS.0b013e3181a56928

Andrews, M. G., and Taylor, L. L. (2019). Combating climate change through enhanced weathering of agricultural soils. *Elements,* 15, 253–258. doi: 10.2138/gselements.15.4.253

Ansari, M. K. A., Ahmad, A., Umar, S., Zia, M. H., Iqbal, M., and Owens, G. (2015). Genotypic variation in phytoremediation potential of indian mustard exposed to nickel stress: a hydroponic study. *Int. J. Phytoremed.* 17, 135–144. doi: 10.1080/15226514.2013.862206

Arreghini, S., de Cabo, L., Serafini, R., and de Iorio, A. F. (2017). Effect of the combined addition of Zn and Pb on partitioning in sediments and their accumulation by the emergent macrophyte Schoenoplectus californicus. *Environ. Sci. Pollut. Res.* 24, 8098–8107. doi: 10.1007/s11356-017-8478-7

Baker, A. J. M., and Brooks, R. R. (1989). Terrestrial higher plants which hyperaccumulate metallic elements - a review of their distribution, ecology and phytochemistry. *Biorecovery*. 1, 81–126.

Bani, A., Pavlova, D., Echevarria, G., Mullaj, A., Reeves, R. D., and Morel, J. L., et al. (2010). Nickel hyperaccumulation by the species of Alyssum and Thlaspi (Brassicaceae) from the ultramafic soils of the Balkans. *Botanica Serbica*. 34, 3–14. Available online at: https://botanicaserbica.bio.bg.ac.rs/arhiva/pdf/2010_34_1_502_full.pdf

Beerling, D. J., Kantzas, E. P., Lomas, M. R., Wade, P., Eufrasio, R. M., Renforth, P., et al. (2020). Potential for large-scale CO 2 removal via enhanced rock weathering with croplands. *Nature*. 583, 242–248. doi: 10.1038/s41586-020-2448-9

Beerling, D. J., Leake, J. R., Long, S. P., Scholes, J. D., Ton, J., Nelson, P. N., et al. (2018). Farming with crops and rocks to address global climate, food and soil security. *Nat. Plants*. 4, 138–147. doi: 10.1038/s41477-018-0108-y

Bian, F., Zhong, Z., Zhang, X., Yang, C., and Gai, X. (2020). Bamboo – An untapped plant resource for the phytoremediation of heavy metal contaminated soils. *Chemosphere*. 246, 125750. doi: 10.1016/j.chemosphere.2019.125750

Bocardi, J. M. B., Pletsch, A. L., Melo, F., and Quinaia, S. P. (2020). Quality reference values for heavy metals in soils developed from basic rocks under tropical conditions. *J. Geochem. Explor.* 217, 106591. doi: 10.1016/j.gexplo.2020.106591

Brooks, R. R., Lee, J., and Jaffre, T. (1974). Some New Zealand and new caledonian plant accumulators of nickel. *J. Ecol.* 62, 493–499. doi: 10.2307/2258995

Cabral Pinto, M., da Silva, E. F., Silva, M. M. G., and Melo-Gonçalves, P. (2015). Heavy metals of Santiago Island (Cape Verde) top soils: Estimated Background Value maps and environmental risk assessment. *J. Afri. Earth Sci.* 101, 162–176. doi: 10.1016/j.jafrearsci.2014.09.011

Chaney, R. L., Angle, J. S., Broadhurst, C. L., Peters, C. A., Tappero, R. V., and Sparks, D. L. (2007). Improved understanding of hyperaccumulation yields commercial phytoextraction and phytomining technologies. *J. Environ. Qual.* 36, 1429–1443. doi: 10.2134/jeq2006.0514

Coninx, L., Martinova, V., and Rineau, F. (2017). Mycorrhiza-Assisted Phytoremediation. *Adv. Botan. Res.* 83, 127–188. doi: 10.1016/bs.abr.2016.12.005

Cooper, E. M., Sims, J. T., Cunningham, S. D., Huang, J. W., and Berti, W. R. (1999). Chelate-assisted phytoextraction of lead from contaminated soils. *J. Environ. Qual.* 28, 1709–1719. doi: 10.2134/jeq1999.00472425002800060004x

Cox, S. F., Rollinson, G., and McKinley, J. M. (2017). Mineralogical characterisation to improve understanding of oral bioaccessibility of Cr and Ni in basaltic soils in Northern Ireland. *J. Geochem. Explor.* 183, 166–177. doi: 10.1016/j.gexplo.2017.02.006

de Oliveira Garcia, W., Amann, T., Hartmann, J., Karstens, K., Popp, A., and Boysen, L. R. (2020). Impacts of enhanced weathering on biomass production for negative emission technologies and soil hydrology. *Biogeosciences*. 17, 2107–2133. doi: 10.5194/bg-17-2107-2020

de Oliveira, S., Pessenda, L. C., Gouveia, S. E., and Favaro, D. I. (2011). Heavy metal concentrations in soils from a remote oceanic island Fernando de Noronha, Brazil. *Anais Acade. Brasileira Ciencias.* 83, 1193–1206. doi: 10.1590/S0001-37652011005000042

Dhir, B., Sharmila, P., Pardha Saradhi, P., and Nasim, S. A. (2009). Physiological and antioxidant responses of Salvinia natans exposed to chromium-rich wastewater. *Ecotoxicol. Environ. Safety*. 72, 1790–1797. doi: 10.1016/j.ecoenv.2009.03.015

Diwan, H., Ahmad, A., and Iqbal, M. (2008). Genotypic variation in the phytoremediation potential of indian mustard for chromium. *Environ. Manage.* 41, 734–741. doi: 10.1007/s00267-007-9020-3

Dœlsch, E., Saint Macary, H., and Van de Kerchove, (2006b). Sources of very high heavy metal content in soils of volcanic island (La Réunion). *J. Geochem. Explor.* 88, 194–197. doi: 10.1016/j.gexplo.2005.08.037

Dœlsch, E., Van de Kerchove, V., and Saint Macary, H. (2006a). Heavy metal content in soils of Réunion (Indian Ocean). *Geoderma.* 134, 119–134. doi: 10.1016/j.geoderma.2005.09.003

Dushenkov, V., Nanda Kumar, P. B. A., Motto, H., and Raskin, I. (1995). Rhizofiltration: the use of plants to remove heavy metals from aqueous streams. *Environ. Sci. Technol.* 29, 1239–1245. doi: 10.1021/es0005a015

Edgar, N., Fabián, F. L., Julián Mario, P. C., and Ileana, R. (2021). Coupling plant biomass derived from phytoremediation of potential toxic-metal-polluted soils to bioenergy production and high-value by-products-a review. *Appl. Sci.* 11, 1–35. doi: 10.3390/app11072982

Etim, E. E. (2012). Phytoremediation and its mechanisms: a review. *Int. J. Environ. Bioenergy*. 2, 120–136. Available online at: http://www.modernscientificpress.com/Journals/ViewArticle.aspx?gkN1Z6Pb60HNQPymfPQlZIsaO1oMajYkT5i8/SIthV/i1509l3XqlgX4XSDiXBec

Fabrício Neta, A. D. B., do Nascimento, C. W. A., Biondi, C. M., van Straaten, P., and Bittar, S. M. B. (2018). Natural concentrations and reference values for trace elements in soils of a tropical volcanic archipelago. *Environ. Geochem. Health*. 40, 163–173. doi: 10.1007/s10653-016-9890-5

Fajardy, M., and Mac Dowell, N. (2017). Can BECCS deliver sustainable and resource efficient negative emissions? *Energy Environ. Sci.* 10, 1389–1426. doi: 10.1039/C7EE00465F

Fazal, S., Zhang, B., and Mehmood, Q. (2015). Biological treatment of combined industrial wastewater. *Ecol Eng*. 84, 551–558. doi: 10.1016/j.ecoleng.2015.09.014

Fuentes, I. I., Espadas-Gil, F., Talavera-May, C., Fuentes, G., and Santamaría, J. M. (2014). Capacity of the aquatic fern (Salvinia minima Baker) to accumulate high concentrations of nickel in its tissues, and its effect on plant physiological processes. *Aquatic Toxicol*. 155, 142–150. doi: 10.1016/j.aquatox.2014.06.016

Fuss, S., Lamb, W. F., Callaghan, M. W., Hilaire, J., Creutzig, F., Amann, T., et al. (2018). Negative emissions - Part 2: costs, potentials and side effects. *Environ. Res. Lett.* 13, 063002. doi: 10.1088/1748-9326/aabf9f

Gillman, G. P., Burkett, D. C., and Coventry, R. J. (2002). Amending highly weathered soils with finely ground basalt rock. *Appl. Geochem*. 17, 987–1001. doi: 10.1016/S0883-2927(02)00078-1

Goll, D. S., Ciais, P., Amann, T., Buermann, W., Chang, J., Eker, S., et al. (2021). Potential CO2 removal from enhanced weathering by ecosystem responses to powdered rock. *Nat Geosci*. 14, 545–549. doi: 10.1038/s41561-021-00798-x

Guan, F., Xia, M., Tang, X., and Fan, S. (2017). Spatial variability of soil nitrogen, phosphorus and potassium contents in Moso bamboo forests in Yong'an City, China. *Catena*. 150, p. 161–172. doi: 10.1016/j.catena.2016.11.017

Han, F. X., Sridhar, B. B. M., Monts, D. L., and Su, Y. (2004). Phytoavailability and toxicity of trivalent and hexavalent chromium to Brassica juncea. *New Phytol*. 162, 489–499. doi: 10.1111/j.1469-8137.2004.01027.x

Haque, F., Chiang, Y. W., and Santos, R. M. (2020a). Risk assessment of Ni, Cr, and Si release from alkaline minerals during enhanced weathering. *Open Agric*. 5, 166–175. doi: 10.1515/opag-2020-0016

Haque, F., Santos, R. M., and Chiang, Y. W. (2020b). CO2 sequestration by wollastonite-amended agricultural soils – An Ontario field study. *Int. J. Greenhouse Gas Control*. 97, 103017. doi: 10.1016/j.ijggc.2020.103017

Haque, F., Santos, R. M., and Chiang, Y. W. (2020c). Optimizing inorganic carbon sequestration and crop yield with wollastonite soil amendment in a microplot study. *Front. Plant Sci*. 11, 1–12. doi: 10.3389/fpls.2020.01012

Haque, F., Santos, R. M., Dutta, A., Thimmanagari, M., and Chiang, Y. W. (2019). Co-benefits of wollastonite weathering in agriculture: CO2 sequestration and promoted plant growth. *ACS Omega*. 4, 1425–1433. doi: 10.1021/acsomega.8b02477

Hartmann, J., and Moosdorf, N. (2012). The new global lithological map database GLiM: a representation of rock properties at the Earth surface. *Geochem. Geophys. Geosyst.* 13, 1–37. doi: 10.1029/2012GC004370

Hartmann, J., West, A. J., Renforth, P., Köhler, P., De La Rocha, C. L., Wolf-Gladrow, D. A., et al. (2013). Enhanced chemical weathering as a geoengineering strategy to reduce atmospheric carbon dioxide, supply nutrients, and mitigate ocean acidification. *Rev. Geophys.* 51, 113–149. doi: 10.1002/rog.20004

Ingole, N. W., and Bhole, A. G. (2003). Removal of heavy metals from aqueous solution by water hyacinth (Eichhornia crassipes). *J. Water Supply. Res. Technol. AQUA*. 52, 119–128. doi: 10.2166/aqua.2003.0012

IPCC, (2018). *Summary for Policy makers, in Global Warming of 1, 5.°C. An IPCC Special Report on the impacts of global warming of 1.5°C above pre-industrial levels and related global greenhouse gas emission pathways, in the context of strengthening the global response to the threat of climate change*. World Meteorological Organization, Geneva, Switzerland, p. 32.

Iskandar, Darmawan, Sudadi, U., and Mulyanto, B. (2019). Ambient concentration of soil heavy metals in Indonesian tertiary and quaternary geologic formations: an explorative study. In: *IOP Conference Series: Earth and Environmental Science*. Vol. 399, p. 012017. doi: 10.1088/1755-1315/399/1/012017

Jaffr,é, T., and Schmid, M. (1974). Accumulation du nickel par une Rubiacée de Nouvelle-Calédonie, Psychotria douarrei (G. Beauvisage) Däniker: Comptes Rendus de l'Académie des Sciences. *Série D: Sci. Naturel.* 278, 1727–1730.

Jaffré, T., Brooks, R. R., Lee, J., and Reeves, R. D. (1976). Sebertia acuminata: a hyperaccumulator of nickel from New Caledonia. *Science*. 193, 579–580. doi: 10.1126/science.193.4253.579

Jaffré, T., Pillon, Y., Thomine, S., and Merlot, S. (2013). The metal hyperaccumulators from New Caledonia can broaden our understanding of nickel accumulation in plants. *Front. Plant Sci*. 4, 1–7. doi: 10.3389/fpls.2013.00279

Kalve, S., Sarangi, B. K., Pandey, R. A., and Chakrabarti, T. (2011). Arsenic and chromium hyperaccumulation by an ecotype of Pteris vittata - prospective for phytoextraction from contaminated water and soil. *Current Sci*. 100, 888–894. Available online at: https://www.jstor.org/stable/24076481

Kantola, I. B., Masters, M. D., Beerling, D. J., Long, S. P., and DeLucia, E. H. (2017). Potential of global croplands and bioenergy crops for climate change mitigation through deployment for enhanced weathering. *Biol. Lett*. 13, 20160714. doi: 10.1098/rsbl.2016.0714

Kidd, P., Mench, M., Alvarez-Lopez, V., Bert, V., Dimitriou, I., Friesl-Hanl, W., et al. (2015). Agronomic Practices for Improving Gentle Remediation of Trace Element-Contaminated Soils. *Int. J. Phytoremed.* 17, 1005–1037. doi: 10.1080/15226514.2014.1003788

Kidd, P. S., and Monterroso, C. (2005). Metal extraction by Alyssum serpyllifolium ssp. lusitanicum on mine-spoil soils from Spain. *Sci. Total Environ.* 336, 1–11. doi: 10.1016/j.scitotenv.2004.06.003

Kierczak, J., Pietranik, A., and Pedziwiatr, A. (2021). Ultramafic geoecosystems as a natural source of Ni, Cr, and Co to the environment: a review. *Sci Total Environ*. 755, 142620. doi: 10.1016/j.scitotenv.2020.142620

Köhler, P., Hartmann, J., and Wolf-Gladrow, D. A. (2010). Geoengineering potential of artificially enhanced silicate weathering of olivine. In: *Proceedings of the National Academy of Sciences of the United States of America*. vol.107, 20228–pp. 20233. doi: 10.1073/pnas.1000545107

Kotaś, J., and Stasicka, Z. (2000). Chromium occurrence in the environment and methods of its speciation. *Environ. Pollut*. 107, 263–283. doi: 10.1016/S0269-7491(99)00168-2

Lim, J. M., Salido, A. L., and Butcher, D. J. (2004). Phytoremediation of lead using Indian mustard (Brassica juncea) with EDTA and electrodics. *Microchem. J*. 76, 3–9. doi: 10.1016/j.microc.2003.10.002

Lone, M. I., He, Z. L., Stoffella, P. J., and Yang, X. E. (2008). Phytoremediation of heavy metal polluted soils and water: Progresses and perspectives. *J. Zhejiang Univ. Sci. B*. 9, 210–220. doi: 10.1631/jzus.B0710633

Ma, Q., Han, L., Zhang, J., Zhang, Y., Lang, Q., Li, F., et al. (2019). Environmental risk assessment of metals in the volcanic soil of Changbai mountain. *Int. J. Environ. Res. Public Health*. 16, 2047. doi: 10.3390/ijerph16112047

Macci, C., Doni, S., Peruzzi, E., Bardella, S., Filippis, G., Ceccanti, B., et al. (2013). A real-scale soil phytoremediation. *Biodegradation*. 24, 521–538. doi: 10.1007/s10532-012-9608-z

Mazhari, S. A., Sharifiyan Attar, R., and Haghighi, F. (2017). Heavy metals concentration and availability of different soils in Sabzevar area, NE of Iran. *J. Afr. Earth Sci*. 134, 106–112. doi: 10.1016/j.jafrearsci.2017.06.017

McMurtry, G. M., Wiltshire, J. C., and Kauahikaua, J. P. (1995). Heavy metal anomalies in coastal sediments of Oahu, Hawaii. *Pacific Sci.* 49, 452–470.

Memoli, V., Eymar, E., García-Delgado, C., Esposito, F., Santorufo, L., and De Marco, A. (2018). Total and fraction content of elements in volcanic soil: Natural or anthropogenic derivation. *Sci. Total Environ.* 625, 16–26. doi: 10.1016/j.scitotenv.2017.12.223

Mendoza-Grimón, V., Hernández-Moreno, J. M., Rodríguez Martín, J. A., Fernández-Vera, J. R., and Palacios-Díaz, M. P. (2014). Trace and major element associations in basaltic ash soils of El Hierro Island. *J. Geochem. Explor.* 147, 277–282. doi: 10.1016/j.gexplo.2014.06.010

Miranda, M., Benedito, J. L., Blanco-Penedo, I., López-Lamas, C., Merino, A., and López-Alonso, M. (2009). Metal accumulation in cattle raised in a serpentine-soil area: Relationship between metal concentrations in soil, forage and animal tissues. *J. Trace Elements Med. Biol.* 23, 231–238. doi: 10.1016/j.jtemb.2009.03.004

Mishra, K., and Tripathi, B. D. (2009). Accumulation of chromium and zinc from aqueous solutions using water hyacinth (Eichhornia crassipes). *J. Hazard. Mater*. 164, 1059–1063. doi: 10.1016/j.jhazmat.2008.09.020

Moosdorf, N., Renforth, P., and Hartmann, J. (2014). Carbon dioxide efficiency of terrestrial enhanced weathering. *Environ. Sci. Technol*. 48, 4809–4816. doi: 10.1021/es4052022

Nath, A. J., Lal, R., and Das, A. K. (2015). Managing woody bamboos for carbon farming and carbon trading. *Global Ecol. Conserv*. 3, 654–663. doi: 10.1016/j.gecco.2015.03.002

Néel, C., Soubrand-Colin, M., Piquet-Pissaloux, A., and Bril, H. (2007). Mobility and bioavailability of Cr, Cu, Ni, Pb and Zn in a basaltic grassland: comparison of selective extractions with quantitative approaches at different scales. *Appl. Geochem.* 22, 724–735. doi: 10.1016/j.apgeochem.2006.11.008

Pandharipande, S., and Gadpayle, P. (2016). Phytoremediation studies for removal of copper and chromium using azolla pinnata and water hyacinth. *Int. J. Innov. Res. Sci. Eng. Technol*. 5, 7078–7083. doi: 10.15680/IJIRSET.2016.0505064

Panneerselvam, B., and Priya, K. S. (2021). Phytoremediation potential of water hyacinth in heavy metal removal in chromium and lead contaminated water. *Int. J. Environ. Analyt. Chem.* 1–16. doi: 10.1080/03067319.2021.1901896

Peters, S. C., Blum, J. D., Driscoll, C. T., and Likens, G. E. (2004). Dissolution of wollastonite during the experimental manipulation of Hubbard Brook Watershed. *Biogeochemistry*. 67, 309–329. doi: 10.1023/B:BIOG.0000015787.44175.3f

Pogge von Strandmann, P. A. E., Renforth, P., West, A. J., Murphy, M. J., Luu, T. H., and Henderson, G. M. (2021). The lithium and magnesium isotope signature of olivine dissolution in soil experiments. *Chem. Geol*. 560, 120008. doi: 10.1016/j.chemgeo.2020.120008

Prado, C., Rodríguez-Montelongo, L., González, J. A., Pagano, E. A., Hilal, M., and Prado, F. E. (2010). Uptake of chromium by Salvinia minima: effect on plant growth, leaf respiration and carbohydrate metabolism. *J. Hazard. Mater*. 177, 546–553. doi: 10.1016/j.jhazmat.2009.12.067

Pulford, I. D., and Watson, C. (2003). Phytoremediation of heavy metal-contaminated land by trees - a review. *Environ. Int.* 29, 529–540. doi: 10.1016/S0160-4120(02)00152-6

Pulford, I. D., Watson, C., and McGregor, S. D. (2001). Uptake of chromium by trees: prospects for phytoremediation. *Environ. Geochem. Health.* 23, 307–311. doi: 10.1023/A:1012243129773

Quader, M. A., and Ahmed, S. (2017). *Bioenergy with carbon capture and storage (BECCS): Future prospects of carbon-negative technologies*. Elsevier Inc., p. 91–140. doi: 10.1016/B978-0-12-805423-9.00004-1

Ranieri, E., Tursi, A., Giuliano, S., Spagnolo, V., Ranieri, A. C., and Petrella, A. (2020). Phytoextraction from chromium-contaminated soil using moso bamboo in mediterranean conditions. *Water, Air, Soil Pollut.* 231, 1–12. doi: 10.1007/s11270-020-04759-9

Rascio, N., and Navari-Izzo, F. (2011). Heavy metal hyperaccumulating plants: How and why do they do it? And what makes them so interesting? *Plant Sci.* 180, 169–181. doi: 10.1016/j.plantsci.2010.08.016

Rathore, S. S., Shekhawat, K., Dass, A., Kandpal, B. K., and Singh, K. (2019). Phytoremediation mechanism in indian mustard (Brassica juncea) and its enhancement through agronomic interventions. *Proc. Nation. Acad. Sci. India Section B – Biol. Sci*. 89, 419–427. doi: 10.1007/s40011-017-0885-5

Renforth, P., von Strandmann, P. P., and Henderson, G. M. (2015). The dissolution of olivine added to soil: Implications for enhanced weathering. *Appl. Geochem.* 61, 109–118. doi: 10.1016/j.apgeochem.2015.05.016

Riddell-Black, D. (1994). *Heavy metal uptake by fast growing willow species, in Willow vegetation filters for municipal wastewaters and sludges. A biological purification system*. Uppsala: Swedish University of Agricultural Sciences, *p*. 145–151.

Rodriguez-Espinosa, P. F., Jonathan, M. P., Morales-García, S. S., Villegas, L. E. C., Martínez-Tavera, E., Muñoz-Sevilla, N. P., et al. (2015). Metal enrichment of soils following the April 2012–2013 eruptive activity of the Popocatépetl volcano, Puebla, Mexico. *Environ. Monitor. Assess.* 187, 1–7. doi: 10.1007/s10661-015-4938-z

Saha, P., Shinde, O., and Sarkar, S. (2017). Phytoremediation of industrial mines wastewater using water hyacinth. *Int. J. Phytoremed*. 19, 87–96. doi: 10.1080/15226514.2016.1216078

Shao, S., Driscoll, C. T., Johnson, C. E., Fahey, T. J., Battles, J. J., and Blum, J. D. (2016). Long-term responses in soil solution and stream-water chemistry at Hubbard Brook after experimental addition of wollastonite. *Environ. Chem*. 13, 528–540. doi: 10.1071/EN15113

Shukla, O. P., Juwarkar, A. A., Singh, S. K., Khan, S., and Rai, U. N. (2011). Growth responses and metal accumulation capabilities of woody plants during the phytoremediation of tannery sludge. *Waste Manage.* 31, 115–123. doi: 10.1016/j.wasman.2010.08.022

Singh, H. P., Mahajan, P., Kaur, S., Batish, D. R., and Kohli, R. K. (2013). Chromium toxicity and tolerance in plants. *Environ. Chem. Lett.* 11, 229–254. doi: 10.1007/s10311-013-0407-5

Smith, P., Adams, J., Beerling, D. J., Beringer, T., Calvin, K. V., Fuss, S., et al. (2019). Land-management options for greenhouse gas removal and their impacts on ecosystem services and the sustainable development goals. *Ann. Rev. Environ. Resour.* 44, 255–286. doi: 10.1146/annurev-environ-101718-033129

Strefler, J., Amann, T., Bauer, N., Kriegler, E., and Hartmann, J. (2018). Potential and costs of carbon dioxide removal by enhanced weathering of rocks. *Environ. Res. Lett.* 13, 034010. doi: 10.1088/1748-9326/aaa9c4

Taufikurahman, T., Pradisa, M. A. S., Amalia, S. G., and Hutahaean, G. E. M. (2019). Phytoremediation of chromium (Cr) using Typha angustifolia L., Canna indica L. and Hydrocotyle umbellata L. in surface flow system of constructed wetland: IOP Conference Series. *Earth Environ. Sci.* 308, 012020. doi: 10.1088/1755-1315/308/1/012020

Taylor, L. L., Driscoll, C. T., Groffman, P. M., Rau, G. H., Blum, J. D., and Beerling, D. J. (2021). Increased carbon capture by a silicate-treated forested watershed affected by acid deposition. *Biogeosciences.* 18, 169–188. doi: 10.5194/bg-18-169-2021

Taylor, L. L., Quirk, J., Thorley, R. M. S., Kharecha, P. A., Hansen, J., Ridgwell, A., et al. (2016). Enhanced weathering strategies for stabilizing climate and averting ocean acidification. *Nat. Clim. Change.* 6, 402–406. doi: 10.1038/nclimate2882

ten Berge, H. F. M., van der Meer, H. G., Steenhuizen, J. W., Goedhart, P. W., Knops, P., and Verhagen, J. (2012). Olivine weathering in soil, and its effects on growth and nutrient uptake in ryegrass (Lolium perenne L.): a pot experiment. *PLoS ONE.* 7, 1–8. doi: 10.1371/journal.pone.0042098

Teuchies, J., Jacobs, S., Oosterlee, L., Bervoets, L., and Meire, P. (2013). Role of plants in metal cycling in a tidal wetland: Implications for phytoremidiation. *Sci. Total Environ.* 445, 146–154. doi: 10.1016/j.scitotenv.2012.11.088

Thiffault, E., Hannam, K. D., Paré, D., Titus, B. D., Hazlett, P. W., Maynard, D. G., et al. (2011). Effects of forest biomass harvesting on soil productivity in boreal and temperate forests-A review. *Environ. Rev.* 19, 278–309. doi: 10.1139/a11-009

Tóth, G., Hermann, T., Da Silva, M. R., and Montanarella, L. (2016). Heavy metals in agricultural soils of the European Union with implications for food safety. *Environ. Int.* 88, 299–309. doi: 10.1016/j.envint.2015.12.017

Tra, H. T. L., and Egashira, K. (2001). Status of heavy metals in agricultural soils of Vietnam. *Soil Sci. Plant Nutr.* 47, 419–422. doi: 10.1080/00380768.2001.10408405

USGS, (2021). *Mineral commodity summaries 2021: U.S.* Geological Survey. p. 1–200.

van der Ent, A., Baker, A. J. M., Reeves, R. D., Pollard, A. J., and Schat, H. (2013). Hyperaccumulators of metal and metalloid trace elements: facts and fiction. *Plant and Soil.* 362, 319–334. doi: 10.1007/s11104-012-1287-3

Vara Prasad, M. N., and de Oliveira Freitas, H. M. (2003). Metal hyperaccumulation in plants - Biodiversity prospecting for phytoremediation technology. *Electr. J. Biotechnol.* 6, 285–321. doi: 10.2225/vol6-issue3-fulltext-6

Verma, K., Tewari, S., and Rai, J. P. N. (2008). Ion exchange during heavy metal bio-sorption from aqueous solution by dried biomass of macrophytes. *Bioresource Technol.* 99, 1932–1938. doi: 10.1016/j.biortech.2007.03.042

Vlček, V., Jurička, D., and Míkov,á, J. (2017). Heavy metal concentration in selected soils and sediments of Livingston Island, Deception Island, King George Island, James Ross Island (Antarctica). *Czech Polar Rep.* 7, 18–33. doi: 10.5817/CPR2017-1-3

von Blanckenburg, F., Schuessler, J. A., Bouchez, J., and Frings, P. J. (2021). Rock weathering and nutrient cycling along an erodosequence. *Am. J. Sci.* 321, 1111–1163. doi: 10.2475/08.2021.01

Wang, H., Li, X., Chen, Y., Li, Z., Hedding, D. W., Nel, W., et al. (2020). Geochemical behavior and potential health risk of heavy metals in basalt-derived agricultural soil and crops: a case study from Xuyi County, eastern China. *Sci Total Environ.* 729, 139058. doi: 10.1016/j.scitotenv.2020.139058

Wei, Z., Van Le, Q., Peng, W., Yang, Y., Yang, H., Gu, H., et al. (2021). A review on phytoremediation of contaminants in air, water and soil. *J. Hazard. Mater.* 403, 123658. doi: 10.1016/j.jhazmat.2020.123658

Were, F. H., Wafula, G. A., and Wairungu, S. (2017). Phytoremediation using bamboo to reduce the risk of chromium exposure from a contaminated tannery site in Kenya. *J. Health Pollut.* 7, 12–25. doi: 10.5696/2156-9614-7.16.12

Wu, L. H., Luo, Y. M., Xing, X. R., and Christie, P. (2004). EDTA-enhanced phytoremediation of heavy metal contaminated soil with Indian mustard and associated potential leaching risk. *Agric. Ecosyst. Environ.* 102, 307–318. doi: 10.1016/j.agee.2003.09.002

Yadav, M., Singh, G., and Jadeja, R. N. (2021). Phytoremediation for heavy metal removal. *Pollut. Water Manage.* 128–150. doi: 10.1002/9781119693635.ch6

Zaranyika, M. F., and Ndapwadza, T. (1995). Uptake of Ni, Zn, Fe, Co, Cr, Pb, Cu and Cd by water hyacinth (eichhornia crassipes) in mukuvisi and manyame rivers, Zimbabwe: Journal of Environmental Science and Health. *Part A: Environ. Sci. Eng. Toxicol.* 30, 157–169. doi: 10.1080/10934529509376193

Zhang, X. H., Liu, J., Huang, H. T., Chen, J., Zhu, Y. N., and Wang, D. Q. (2007). Chromium accumulation by the hyperaccumulator plant Leersia hexandra Swartz. *Chemosphere.* 67, 1138–1143. doi: 10.1016/j.chemosphere.2006.11.014

Zhu, Y. L., Zayed, A. M., Qian, J., Souza, M., and Terry, N. (1999). Phytoaccumulation of Trace Elements by Wetland Plants: II. *Water Hyacinth. J. Environ. Quality.* 28, 339–344. doi: 10.2134/jeq1999.00472425002800010042x

Conflict of Interest: The author declares that the research was conducted in the absence of any commercial or financial relationships that could be construed as a potential conflict of interest.

Publisher's Note: All claims expressed in this article are solely those of the authors and do not necessarily represent those of their affiliated organizations, or those of the publisher, the editors and the reviewers. Any product that may be evaluated in this article, or claim that may be made by its manufacturer, is not guaranteed or endorsed by the publisher.

frontiers in Climate

ORIGINAL RESEARCH
published: 10 February 2022
doi: 10.3389/fclim.2022.827698

The Dissolution of Olivine Added to Soil at 4°C: Implications for Enhanced Weathering in Cold Regions

Philip A. E. Pogge von Strandmann[1,2]*, *Chloe Tooley*[2], *Josephina J. P. A. Mulders*[2,3] and *Phil Renforth*[4]

[1] Mainz Isotope and Geochemistry Centre, Institute of Geosciences, Johannes Gutenberg University, Mainz, Germany, [2] London Geochemistry and Isotope Centre (LOGIC), Institute of Earth and Planetary Sciences, University College London and Birkbeck, University of London, London, United Kingdom, [3] Witteveen+Bos, Deventer, Netherlands, [4] School of Engineering & Physical Sciences, Heriot-Watt University, Edinburgh, United Kingdom

Crushed olivine was added to a soil core to mimic enhanced weathering, and water was continually dripped through for ~6 months. Our experiments were conducted at 4°C, and are compared to previously run identical experiments at 19°C. Olivine dissolution rates in both experiments start out similar, likely due to fines and sharp crystal corners. However, after >100 days of reaction, the dissolution rate at 4°C was two orders of magnitude lower than at 19°C. The accumulation of heavy metals, such as Ni and Cd, was low in both experiments, but soil retention of these elements was proportionally higher at higher temperatures, likely due to enhanced sorption and formation of clays. Overall, this study suggests that olivine dissolution rates in experiments that mimic natural settings are orders of magnitude slower than in normal laboratory experiments, and that enhanced weathering may be a considerably less efficient method of carbon dioxide removal at low climatic temperatures. Both of these conclusions have implications for the application of enhanced weathering as a CO_2 removal method.

Keywords: weathering, carbon sequestration, weathering experiment, enhanced weathering of minerals, temperature effect on weathering

OPEN ACCESS

Edited by:
Mathilde Hagens, Wageningen University and Research, Netherlands

Reviewed by:
Fatima Haque, National Taiwan University, Taiwan
Andrew Lenton, Commonwealth Scientific and Industrial Research Organization, Australia

***Correspondence:**
Philip A. E. Pogge von Strandmann
ppoggevo@uni-mainz.de

Specialty section:
This article was submitted to Negative Emission Technologies, a section of the journal Frontiers in Climate

Received: *02 December 2021*
Accepted: *18 January 2022*
Published: *10 February 2022*

Citation:
Pogge von Strandmann PAE, Tooley C, Mulders JJPA and Renforth P (2022) The Dissolution of Olivine Added to Soil at 4°C: Implications for Enhanced Weathering in Cold Regions. Front. Clim. 4:827698. doi: 10.3389/fclim.2022.827698

INTRODUCTION

Projections of future climate scenarios clearly show that to avoid climate warming above dangerous levels of 1.5°C, large quantities of CO_2 will have to be removed from the atmosphere (IPCC, 2014, 2018), in addition to rapid and deep emissions reduction. Negative emissions technologies have been proposed for removing and storing atmospheric CO_2 (The Royal Society, 2018), which have a range of carbon drawdown efficiencies, environmental requirements, energy inputs and costs (e.g., Shepherd et al., 2009; Matter et al., 2016; Taylor et al., 2016; Pogge von Strandmann et al., 2019a). Perhaps the processes that most lend themselves to be efficient and cost-effective are those that draw on the natural carbon cycles. Hence, techniques like ocean fertilization (e.g., Bowie et al., 2001; Williamson et al., 2012) and afforestation (e.g., Nilsson and Schopfhauser, 1995; Yosef et al., 2018) enhance the organic pathway of the long-term carbon cycle, while others like mineral carbonation (Gislason and Oelkers, 2014; Matter et al., 2016; Pogge von Strandmann et al., 2019a) and enhanced weathering increase the rates of the inorganic pathway of the long-term carbon cycle. This study

examines the latter of these processes, enhanced weathering (Schuiling and Krijgsman, 2006; Hangx and Spiers, 2009; Koehler et al., 2010, 2013; Schuiling and de Boer, 2010; Renforth, 2012; Hartmann et al., 2013; Renforth et al., 2013, 2015; Renforth and Campbell, 2021).

Chemical weathering is the Earth's primary process of long-term atmospheric CO_2 drawdown (Walker et al., 1981; Saenger and Wang, 2014). Dissolution of silicate rocks, in particular in rivers and soil pore waters, leads to carbon dissolution in water as alkalinity, and also carries critical cations such as Ca and Mg. When transported to the oceans, these initially contribute to elevated ocean alkalinity (Renforth and Henderson, 2017), then over ∼10–100 ka precipitate as marine carbonate, sequestering CO_2. At the same time, rock-derived cations such as P, Fe and Si are also dissolved and transported to the coastal oceans, where they fertilize organic carbon growth (Lalonde et al., 2012; Hawley et al., 2017). The burial of this organic carbon is also assisted by the supply of continent-derived particulate material (Kennedy and Wagner, 2011). Hence, silicate weathering influences both the inorganic and organic pathways of the long-term carbon cycle, on timescales from yearly (for organic carbon) to tens of kyr (for carbonate precipitation) (e.g., Colbourn et al., 2015; Pogge von Strandmann et al., 2017, 2021a).

The limiting steps on weathering reactions therefore significantly affects climate. In natural settings, these are both climate-based (temperature, runoff, etc.) and supply-based (availability of primary silicates for weathering) (Berner et al., 1983; Raymo and Ruddiman, 1992; West et al., 2005). Slow clay mineral precipitation rates have also been considered as limiting reactions (Maher, 2010; Zhang et al., 2010), although more recently both laboratory and field experiments suggest that the formation of clays (or at least their amorphous versions) can be fairly rapid, and on the order of days to months (e.g., Oelkers et al., 2019; Pogge von Strandmann et al., 2019b, 2021b). Enhanced weathering intends to circumvent especially the limitation of supply, by providing fine-grained silicates for weathering, for example by plowing mafic material into agricultural lands (Hartmann et al., 2013; Taylor et al., 2016; Beerling et al., 2020). The smaller the grain size and greater the surface area, the faster dissolution rates and CO_2 drawdown will be, but the more CO_2 will be emitted by grinding (Renforth, 2012). However, as yet little is known about precise dissolution rates of various silicate grain sizes in natural settings, in part due to surface passivation, where unreactive secondary minerals (e.g., carbonates and clays) precipitate on primary mineral surfaces, inhibiting dissolution (Taylor et al., 2016; Beerling et al., 2020). Laboratory-derived dissolution rates are generally several orders of magnitude higher than field-derived rates (White and Brantley, 2003), and dissolution rates of artificially-added silicates are even less well-known (Peters et al., 2004; ten Berge et al., 2012; Manning et al., 2013; Renforth et al., 2015). Effectively, at the fast end of this potential dissolution rate scale, enhanced weathering is a highly efficient carbon sequestration method, while at the slow end, less carbon would be sequestered than emitted during grinding, transport and installation.

In an attempt to reconcile laboratory- and field-derived weathering rates, Renforth et al. (2015) used natural soil columns and brought them into the laboratory to control and measure material inputs and outputs. Two identical soil cores were used, one as a control and the other with crushed olivine to mimic enhanced weathering. By monitoring dissolved output fluxes, a dissolution rate per grain size of olivine was determined for an air temperature of 19°C. Here, we determine the effect of temperature on olivine dissolution, by reproducing the Renforth et al. (2015) experiments at a temperature of 4°C. The goal is to assess to what degree temperature limits the geographical application of olivine as an enhanced weathering technique. While it is clear that temperature is a key control on the dissolution rate of silicate material, it is less clear whether temperature dominates in a system where there is no supply limitation (West et al., 2005). Also, it is not clear how the exchangeable fraction responds to differences in temperature.

Further, we have revisited the original experiments, and pre-concentrated solutions to better assess the behavior of toxic heavy metals (e.g., Ni, Cr) during the dissolution of olivine. This is in order to determine whether the use of olivine can lead to dangerous accumulations of such metals in either soils or surface waters (Haque et al., 2020).

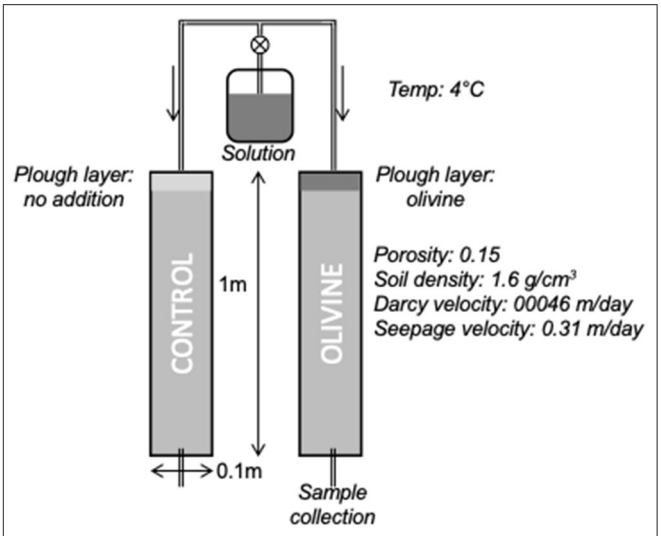

FIGURE 1 | Diagram of the soil column experiments. Adapted from Pogge von Strandmann et al. (2021b) and Renforth et al. (2015).

EXPERIMENTAL DESIGN

The original experiments of Renforth et al. (2015) took 1 m long soil cores from agricultural land in North Oxfordshire. This bedrock in this area is Jurassic limestone and mudstone, and the soils are calcareous. The cores span the transition from the plowed layer, though the B and C horizons, to the parent rock material. One core was used to examine the compositions of the bulk soil and leachable phases. The other two were used as column reactors, and a modified Hoagland nutrient solution (to mimic the addition of fertilizer) was dripped onto them at a rate of 15 ml/h (∼200 μg/ml K, N, 30 μg/ml P, 37 ng/ml Ca, 30 ng/ml S; 69 ng/ml Mg). Crushed olivine (100 g), from Western Norway

TABLE 1 | Elemental concentrations from the 4°C experiments, and the heavy metal concentrations also from the 19°C experiment.

Day	pH		Ca		Mg		Si		Cr		Ni		Cu	
			μg/ml						ng/ml					
	Olivine	Control	Olivine	Control	Olivine	Control	Olivine	Control	Olivine	Control	Olivine	Control	Olivine	Control
Initial Water	6.9		0.042		0.070		bdl		0.178		0.324		7.13	
4°C														
5	7.13	7.20	271	182	3.95	2.31	1.64	0.942	0.874	0.599	1.91	1.12	7.22	3.13
10	7.22	7.39	182	185	2.60	2.38	1.28	1.18	1.25	0.590	1.38	1.00	5.96	3.82
14			117	95.8	1.66	1.21	0.898	0.579	1.15	0.645	1.33	1.02	5.06	3.54
25	7.04	7.21	65.0	93.1	0.90	1.18	0.526	0.896	0.946	0.580	1.34	1.17	5.08	4.92
39	7.15	7.30	40.4	19.2	0.55	0.23	0.577	0.184	0.777	0.651	1.34	1.00	5.90	4.71
46	7.09	7.27	147	141	2.19	1.78	2.07	1.43	0.870	0.806	1.57	1.38	8.63	6.85
61	7.11	7.29	157	138	2.36	1.76	2.27	1.65	0.316	0.281	0.96	0.646	2.56	1.84
77			42.7	152	0.616	1.93	0.699	1.86	0.340	0.368	1.07	0.790	3.30	2.61
85	7.13	7.27	21.9	108	0.291	1.39	0.444	2.11	0.301	0.255	1.04	0.715	2.74	2.84
109	7.15	7.28	77.7	70.2	1.12	0.883	1.87	1.14	0.315	0.317	0.922	0.694	3.61	2.34
134	7.12	7.27	27.9	18.2	0.370	0.213	0.787	0.322	0.370	0.355	1.10	0.725	4.25	3.26
19°C														
8	7.25	7.59							0.128	0.173	1.91	0.90	2.48	2.33
18	7.17	7.56							0.073	0.125	0.98	0.98	2.59	1.98
43	7.01	7.51							0.132	0.191	0.70	0.50	2.56	2.72
55	7.28	7.71							0.090	0.237	0.61	0.55	3.40	2.82
60									0.127	0.190	0.34	0.38	2.79	3.10
67	7.29	7.52							0.131	0.161	0.34	0.33	3.14	3.19
76									0.152	0.114	0.37	0.33	2.60	3.01
120	7.31	7.57							0.145	0.13	0.38	0.32	2.55	2.87

bdl stands for below detection limit.

(Minelco Ltd.), was stirred into the top 10 cm of one core, while the other was stirred, but without olivine addition, and used as a control core. This addition amount of olivine equals ∼12.7 kg/m^2, which is around 2.5× higher than the highest rate of 5 kg/m^2/yr proposed by the modeling study of Taylor et al. (2016). Effluent drip waters were collected periodically from the base of each core (**Figure 1**).

In this study's experiments, additional cores drilled from the same site at the same time were used. The same olivine and identical Hoagland solution were used. The two primary differences compared to the original experiments were (1) our experiments were conducted in a cold room at 4° at the department of Earth Sciences, University College London rather than at 19°C; (2) the original experiments showed a general decrease in control core effluent Ca and Mg concentrations, due to the added Hoagland solution being out of equilibrium with the soil exchangeable fraction at the start of the experiment (Pogge von Strandmann et al., 2021b). To counteract this, we dripped Hoagland solution through our columns for 45 days before addition of the olivine. After this, solution was dripped through both columns for a further 6 months.

METHODS

Major element concentrations in bulk soils and olivine powder were determined by XRF (Renforth et al., 2015). Elemental concentrations of the effluent solutions were determined by a Varian 820-MS inductively-coupled plasma mass spectrometer (ICP-MS) at the LOGIC laboratories at UCL. The analyses were calibrated using multi-element solutions mixed from single-element standards, and accuracy was assessed by analyzing the international reference standards SLRS-5 and TMDA. The analytical reproducibility was better than ±4%.

Calcium concentrations were analyzed by a Varian ICP-OES (Optical emission spectrometry), also at UCL's LOGIC laboratories. This was because Ca concentrations were very high due to the presence of Ca in the influent Hoagland solutions, and because of the carbonate rock in the columns dissolving.

In order to determine the concentrations of Cr, Ni, and Cu, 15 ml of solution from both these experiments, and those of Renforth et al. (2015), were dried down and also analyzed by ICP-MS.

RESULTS

Data from the bulk soils and olivine composition, initially published by Renforth et al. (2015) are repeated in **Supplementary Material**.

Effluent Concentrations From the 4°C Experiment

As for the 19°C experiments (Renforth et al., 2015), the pH of the input solution was circumneutral, and the passage through the columns had little effect on the pH. Effluent pH was 7.1 ± 0.4 (1sd) for the olivine column and 7.3 ± 0.5 for the control column. All results are presented in **Table 1**. Overall, the effluent major element concentrations exhibit more scatter than observed in the 19°C experiment by Renforth et al. (2015). Magnesium and calcium concentrations in both of the columns' effluent show a general decrease with time (**Figure 2**). In most samples the concentrations of the olivine core's effluent are higher than in the control core's, and the difference between the cores decreases slightly with time. For example, initially, the Mg effluent concentrations from the olivine column were ∼1.6 μg/ml higher than that of the control column. By day 134 this difference had decreased to ∼0.1 μg/ml. Silicon concentrations, in contrast, are highly scattered in the effluent from both cores, with no straightforward trends.

Heavy Metal Effluent Concentrations

In general, the concentrations of Cu, Ni, and Cr in the 4°C experiment start out with greater concentrations in the olivine core over the control core (**Figure 3**). After approximately 50 days the concentrations tend to decrease by ∼50% (for Cr and Cu) to ∼80% (for Ni). For Ni and Cu, the olivine core's effluent always is more concentrated, while for Cr, the difference between the cores is effectively zero after 60 days. The behavior of Ni between the 4° and 19°C experiment is fairly similar, in that both show a decline with time. In contrast, in the 19°C experiment there is little difference between the effluent from the olivine and control cores for Cr or Cu with time, meaning that the behavior of these elements is different at different temperatures.

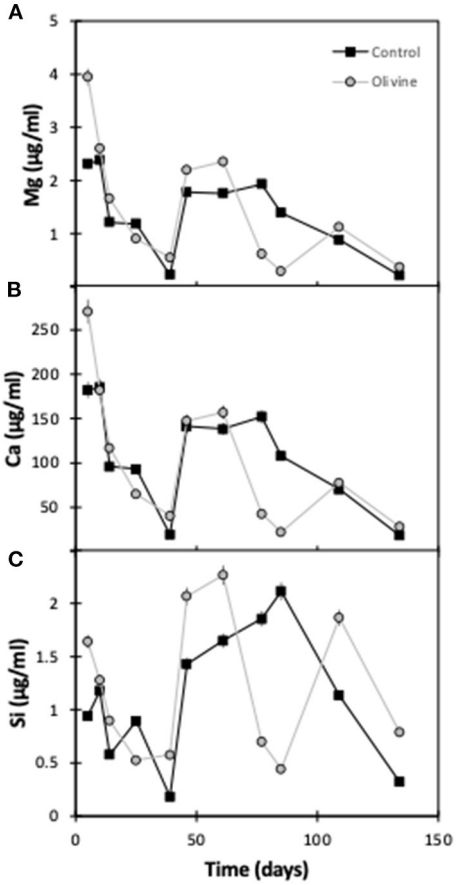

FIGURE 2 | Effluent major element concentrations as a function of experimental time for both columns: **(A)** magnesium, **(B)** calcium, **(C)** silicon. The error bars represent the 2sd analytical uncertainties.

DISCUSSION

Source of Dissolved Cations

In order to determine the source of effluent cations such as Mg, a mass balance can be constructed. This is based on the assumptions that all (input-corrected) control core effluent Ca stems from the dissolution of carbonate rock, and all control core effluent Si is from the dissolution of silicates (clays, given the absence of primary silicates). We then use the Mg/Ca of carbonate leaches, and the Mg/Si of residual material (Renforth et al., 2015) to determine the amount of Mg coming from carbonates and secondary silicates. It is then assumed that all remaining Mg in the input-correct control core effluent stems from the exchangeable pool. Then we assume that the control and olivine cores are identical except for the added dissolution of olivine. According to these calculations, ∼73% of Mg in the control core effluent stems from dissolution of carbonate by the end of the experiment, and ∼26% from the exchangeable fraction, and only 1% from the dissolution of silicates. By comparison, in the 19°C experiment, these numbers are 65, 32, and 1%, respectively (Pogge von Strandmann et al., 2021b). In other words, increased temperature appears to decrease the proportion of carbonate contribution, and increase that of the exchangeable fraction. Error propagation of the analytical uncertainties yields ± ∼ 6% relative error on the mass balance.

In the olivine core, by the end of the 4°C experiment, olivine dissolution only makes up ∼3% of the total Mg, while in the 19°C experiment this number is ∼45% (Pogge von Strandmann et al., 2021b). Overall, then, it is clear that lower temperatures do not favor the dissolution of olivine, but in relative terms the dissolution of carbonate is more favored. In general, a relative decrease in carbonate weathering and increase in silicate weathering as temperature increases has been observed before (West et al., 2005; Kasemann et al., 2014; Gaillardet et al., 2019; Romero-Mujalli et al., 2019). Further, the exchangeable pool is relatively less dominant in the colder experiments, likely due to kinetic effects on the exchange rate.

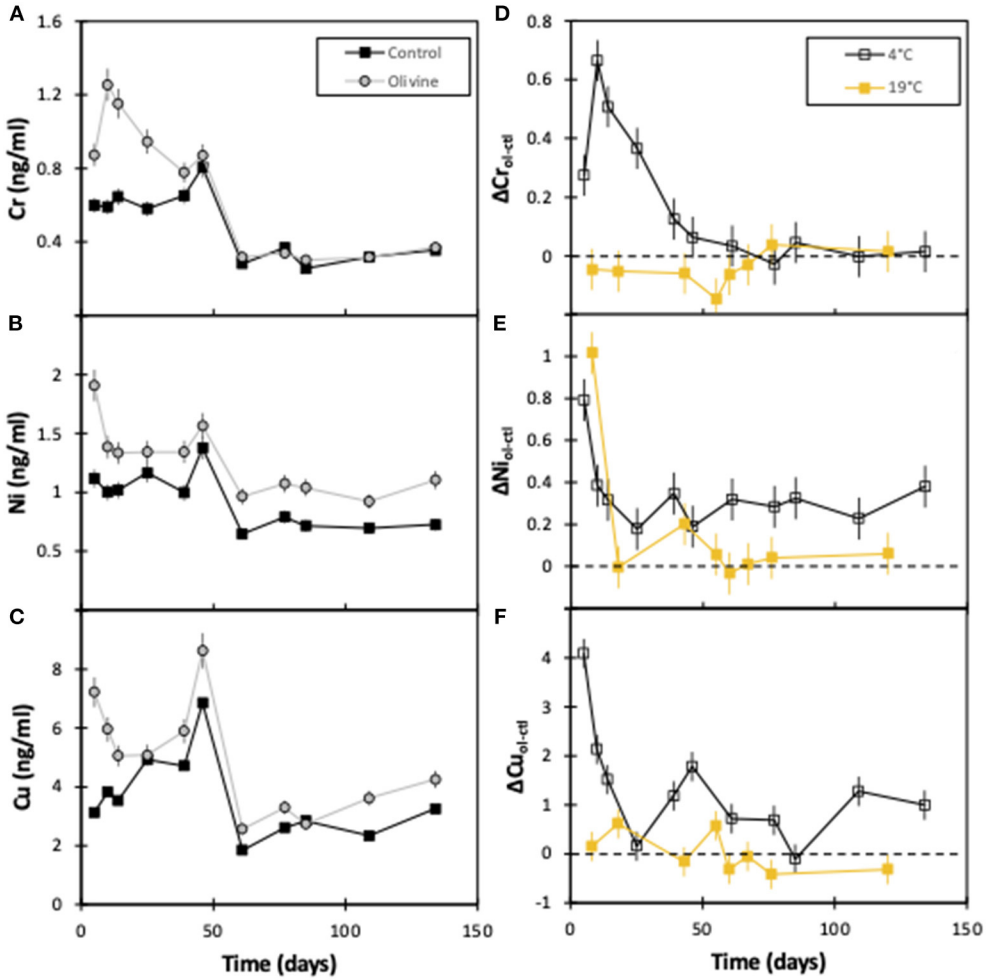

FIGURE 3 | Effluent trace element concentrations as a function of experimental time for both columns: **(A)** chromium, **(B)** nickel, **(C)** copper. **(D–F)** show the difference in heavy metal concentration between the olivine and control core for this (4°C) and the 19°C experiments (Renforth et al., 2015). The error bars represent the 2sd analytical uncertainties. For the Δ panels **(D–F)**, the analytical uncertainty has been compounded through the calculations.

Further evidence for very little dissolution of olivine at 4°C is shown when plotting [Mg] against [Ca] for all experiments. The 4°C control and olivine core effluents, as well as the 19°C control core effluent exhibit an identical gradient that is largely due to the dissolution of carbonate. The Mg/Ca ratio of the leached carbonate is 0.01 ± 0.005, while the Mg:Ca gradients of those three cores are 0.013–0.015 (**Figure 4**), demonstrating a likely carbonate source. In contrast, the 19°C olivine core's effluent has a similar gradient, but is considerably more Mg-enriched.

Magnesium vs. silicon trends follow a similar relationship, albeit more scattered (**Figure 4**). Combined, these trends clearly suggest that while a Mg- and Si-rich phase (olivine) is being dissolved in the 19°C experiment, this is occurring far less, if at all, in the 4°C experiment.

Olivine Dissolution Rates

Based on the assumption that the only difference between the effluent from the olivine and from the control core is due to olivine dissolution (Renforth et al., 2015; Pogge von Strandmann et al., 2021b), the rate of that dissolution can be calculated. Using the difference in effluent Mg concentrations, dissolution rates were calculated using a surface area normalized approach:

$$W_r = \frac{Q_{soln}(Mg_{ol} - Mg_{ctl})}{SSA} \quad (1)$$

where W_r is the surface area normalized weathering rate, Q is the solution flux (in ml/s) and Mg is the concentration of Mg from the olivine and control cores, respectively. SSA is the surface area of the olivine, which is 3.04×10^4 cm^2/g (Renforth et al., 2015).

Thus, the weathering rate of the 19°C experiment starts at $10^{-16.1}$ mol(Mg)/cm^2/s and then increases slightly, before stabilizing at $10^{-15.8}$ mol(Mg)/cm^2/s after ∼50 days. However, while the 4°C experiment's weathering rate is initially almost identical to the 19°C experiment ($10^{-16.0}$ compared to $10^{-16.1}$ mol(Mg)/cm^2/s, respectively), it subsequently rapidly decreases with time. After 134 days the rate is $10^{-17.1}$ mol(Mg)/cm^2/s, and

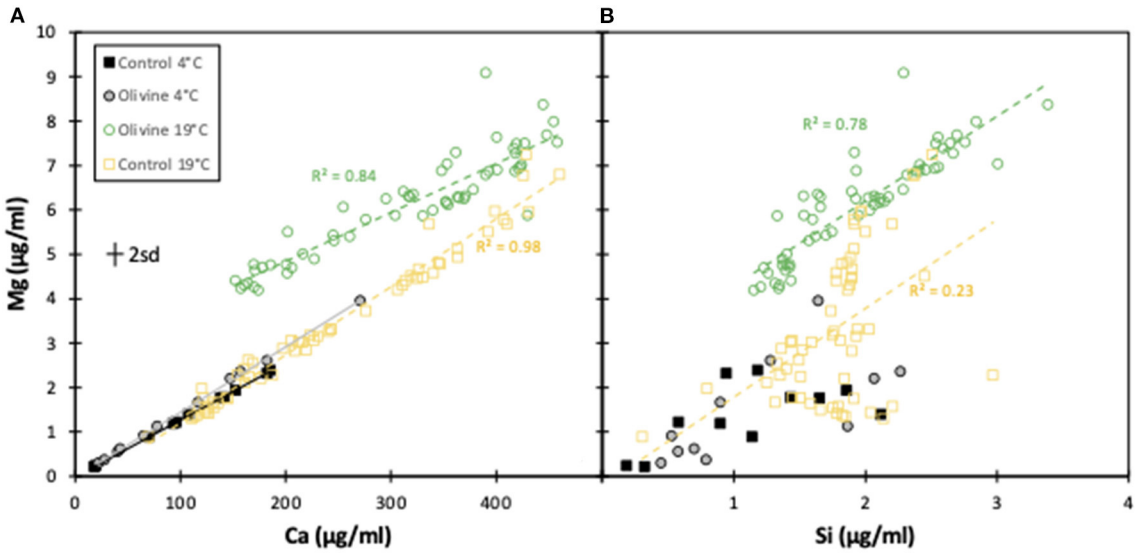

FIGURE 4 | Mg concentrations plotted against Ca and Si concentrations for the effluents from this experiment and the 19°C experiment (Renforth et al., 2015). In all cases, only the effluent from the 19°C olivine column shows dissolution of olivine, and not the 4°C olivine column. The error bar represents the 2sd analytical uncertainty.

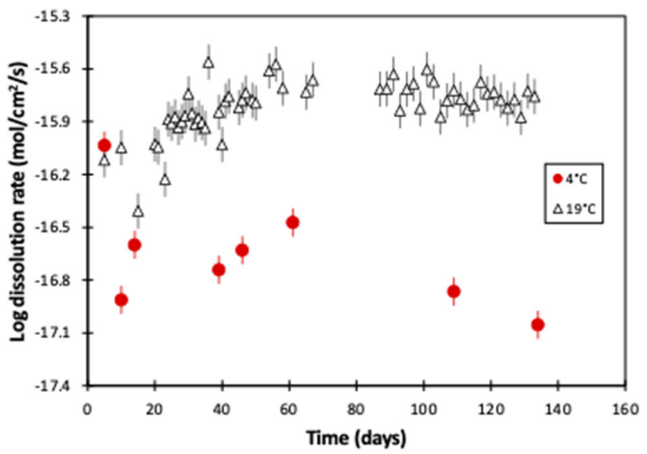

FIGURE 5 | Magnesium-derived olivine dissolution rates of this 4°C experiment, and the 19°C experiment (Renforth et al., 2015), as a function of experimental time. The error bars represent the compounded 2sd uncertainty.

there is over two orders of magnitude difference between the two experiments (**Figure 5**).

The similarity of the weathering rates between the two experiments at the start is likely due to initial dissolution of the fresh outer surface of the crushed olivine, including many relatively high surface area sharp corners (Anbeek, 1992). The subsequent reduction in weathering rate may be attributed to the reduced availability of reactive surface sites on the olivine surface (Orkoula and Koutsoukos, 2002; Appelo and Postma, 2004), suggesting dissolution rate is partially controlled by the mechanism of surface reaction (Renforth, 2012).

Using the dissolution rate law:

$$r = Aa_{H^+}^{n} e^{\frac{-E_a}{RT}} \quad (2)$$

where R is the gas constant (8.3145 kJ mol^{-1} K^{-1}), E_a is the activation energy (52.9 ± 6.9 kJ mol^{-1} K^{-1}), A represents a pre-exponential factor (0.0854), n is the reaction order with respect to H^+ = 0.46, T is temperature (K) and a is the activity (Pokrovsky and Schott, 2000; Hänchen et al., 2006), we can calculate the idealized temperature-dependent dissolution of forsterite (**Figure 6**). Interestingly, while these idealized dissolution rates show the same temperature-dependent slope as our two experiments, they are an order of magnitude faster. In conventional laboratory dissolution rate studies, the fluid to mineral ratio is much higher to ensure effective transport of the solutes from the mineral surface, and laboratory studies tend to be run at far-from-equilibrium conditions. In contrast, in our soil core experiments, there was likely only imperfect contact between minerals and fluid, as well as closer to equilibrium conditions, and the possibility that the surface of the olivine became less reactive with time as it was weathered. As such, this highlights the difference between pure dissolution experiments and soil core (and natural) experiments, and clearly shows that idealized laboratory experiments should not be used to estimate dissolution rates in enhanced weathering. Further, olivine dissolution rates (in laboratory experiments) are pH dependent, and decrease with increasing pH (Oelkers et al., 2018). In the experimentally analyzed pH range of 1–12, neutral pH causes an approximately median dissolution rate (Oelkers et al., 2018), but also highlights that olivine dissolution rates during enhanced weathering will also vary depending on the pH of the source water.

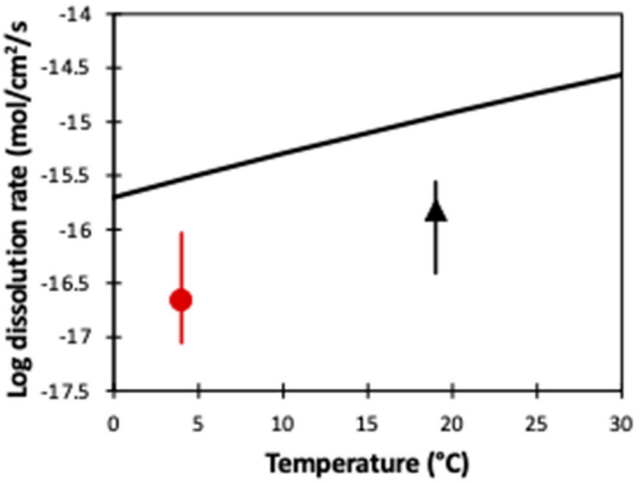

FIGURE 6 | A comparison of olivine dissolution rates from pure laboratory experiments (black line) and our soil column experiments (this study and Renforth et al., 2015), as a function of temperature. The symbols represent the average value, while the error bars represent the entire observed range of dissolution rates (**Figure 5**).

Heavy Metals

One of the key areas of research surrounding the potential of enhanced weathering is the investigation into the build-up of toxic elements in soils and the water column (Renforth, 2012; Hartmann et al., 2013; Renforth et al., 2015; Haque et al., 2020). This potential environmental risk could limit the application of enhanced silicate weathering as a method of carbon sequestration. Both Cr and Ni have been used to assess this risk here. In the 4°C solutions, Cr concentrations in the olivine core effluent are up to 2× that of the control core for the first ∼50 days. Following this, overall concentrations decrease, and are also similar in waters from both cores (**Figure 3**).

Using an Mg/Cr ratio of 3,000 for this olivine (Renforth et al., 2015), it is estimated that ∼0.5 ± 0.07 μg Cr is released by the dissolution of ∼5 mg of olivine at 4°C. This compares to a total difference between the Cr flux of the control and olivine cores for the whole experiment of 0.33 ± 0.02 μg, meaning that ∼0.17 ± 0.01 μg was retained in the soil, which is a retention efficiency of 34 ± 4%. In the 19°C experiment, 37 ± 3 μg Cr was released from the olivine, and 9.6 ± 0.7 μg was retained in the soil column, giving a retention efficiency of 26 ± 4%.

Similarly, ∼1 ± 0.07 μg Ni was in the effluent from the 4°C experiment, while the olivine dissolution led to release of ∼14 ± 1 μg Ni. Hence Ni retention by the soil is ∼90 ± 6%. Similarly, in the 19°C experiment, ∼5 ± 0.4 μg Ni was in the effluent, compared to 1060 ± 70 μg released from olivine dissolution, leading to a retention efficiency of 99%. A high percentage build-up of Ni in soil has been observed in other experiments (Raveh-Rubin et al., 2015), where 90% of the initial Ni mass was extracted from the soil after experiment completion.

High retention of heavy metals in soils is observed throughout the world in relation to mature soils (Haque et al., 2020), both in secondary minerals (largely clays) and adsorbed. Some laterites have high Ni content (Lewis et al., 2006), with some serpentinite zones showing >2% Ni. Raveh-Rubin et al. (2015) show evidence of fast Ni retention at higher temperatures, with the expectation that Ni is not released into a mobile stage for a considerable time. In relation to temperature, the accumulation of Cr and Ni in soils will be slower in colder temperatures compared to warmer climates, due to slower dissolution rates. On the other hand, the build-up of Ni in the soil is considerably slower at 4°C compared to 19°C, which could be partially related to the increased availability of secondary clay minerals in the 19°C column providing easily sorbed surfaces for Ni (Raveh-Rubin et al., 2015).

The European Union's human drinking water standard (98/83/EC) is 50 ng/ml Cr. For the first 60 days in our experiments (before Cr concentrations in the control and olivine core became effectively identical), the 4°C experiment released 0.015 ng/ml Cr, which the 19°C experiment released 0.9 ng/ml. Hence, addition of this amount of olivine (for this Cr concentration in the olivine) is over an order of magnitude from breaching drinking water guidelines. Further, the Finland Ministry of the Environment has a soil Cr limit of 200 mg/kg. Given our experiments' retention of Cr, it would take over 2 million years at 4°C and ∼44,000 years at 19°C of this level of enhanced weathering to breach these limits.

Equally, the Ni guidelines for drinking water is 20 ng/ml. The 4°C experiment released 0.05 ng/ml, while the 19°C experiment released 0.2 ng/ml. The higher Ni retention by soils, compared to Cr, means that this example of enhanced weathering would be even further from breaching drinking water guidelines. The soil limit for Ni is 100 mg/kg, and it would take ∼15,800 years to reach this at 4°C, and ∼200 years at 19°C.

It must be stressed, however, that using less pure olivine, or other silicates, for enhanced weathering (Taylor et al., 2016) could lead to a faster build-up of heavy metals. Equally, using materials whose weathering produces secondary minerals (clays, oxides, etc.), such as basalt, may also enhance the retention of heavy metals in soils. Further, the type of initial soil being seeded will have an effect, as of course the thicker application or faster dissolution of olivine. For example, Taylor et al. (2016) suggest the application of 1–5 kg/m^2/yr of rock powder in their models of the global application of enhanced weathering. This amount is 2.5–13 times less than that applied during this experiment. This would suggest that olivine application on a global scale is unlikely to rapidly increase the heavy metal component of soils. However, it must be noted that fresh application on an annual basis would potentially cause a disproportionately greater heavy metal addition, because there would be a fairly constant supply of rapidly dissolving fresh mineral edges and fines. This is also further discussed below.

Possibility of Using Enhanced Weathering

The possible maximum carbon dioxide capture potential (enhanced weathering potential EWp, kgCO_2 per ton) of the olivine used in this experiment has been calculated using the modified Steinour equation (see Renforth, 2019).

$$EW_P = \frac{M_{CO_2}}{100} \cdot \left(\alpha \frac{CaO}{M_{CaO}} + \beta \frac{MgO}{M_{MgO}} + \epsilon \frac{Na_2O}{M_{Na_2O}} + \gamma \frac{K_2O}{M_{K_2O}} + \theta \frac{SO_3}{M_{SO_3}} + \delta \frac{P_2O_5}{M_{P_2O_5}} \right) \cdot 10^3 \cdot \eta \quad (3)$$

where CaO, MgO, SO3, P2O5, Na_2O, and K_2O, are the elemental concentrations of Ca, Mg, S, P, Na, and K, expressed as oxides, M is the molecular mass of those oxides; coefficients α, β,ϵ, θ (equal to +1), γ (equal to −1), and δ (equal to −2) consider the relative contribution of each oxide; and η is molar ratio of CO_2 to divalent cation sequestered during enhanced weathering; we have used η = 1.5 in this study, which is a conservative global average.

EW_P for the olivine used in this experiment is 0.79 tCO_2/t. The land area normalized dissolution rate for the olivine has been calculated at 30 t/km^2/yr for 4°C, and at 200 t/km^2/yr at 19°C (Renforth et al., 2015).

However, these estimates are based on a constant olivine surface area, and do not consider the effects of comminution on dissolution rates. The feasibility of enhanced olivine weathering can be analyzed using a shrinking core model to estimate the reaction times for dissolution (Hangx and Spiers, 2009). Using the calculated weathering rates from this experiment and Renforth et al. (2015), a model for dissolution as a function of time for various grain sizes can be calculated (**Figure 7**). The model also assumes a distribution in the grain size, because a uniform grain size does not occur during grinding. Here we assume a relative standard deviation on the grain size distribution of 2.5, which occurs during ball milling of olivine.

With an average grain size of 125 μm [80% of the grains in the olivine used in this experiment were >125 μm (Renforth et al., 2015)] dissolution of olivine at 4°C reaches ∼20% in 10 years, sequestering ∼0.2 kg CO_2 /m^2/yr for this experiment's application rate. For this grain size it takes >>10,000 years to reach 80% dissolution (**Figure 7**). In contrast, dissolution (of an average grain size of 125 μm) at 19°C reaches 20% after 1.5 years (sequestering ∼1.3 kg CO_2 /m^2/yr), and 80% after ∼4,000 years. The model of Taylor et al. (2016), which suggests global enhanced weathering in the tropics, assumes a uniform grain size of 10 μm. Our model suggests that 80% of olivine with an average grain size of 10 μm would take >200 years to dissolve at 4°C, and 20–30 years at 19°C, highlighting the importance of temperature and grain size on the dissolution rate and CO_2 sequestration. This suggests that even at 19°C grain size must be reduced to ∼1 μm to dissolve ∼80% within <10 years. However, the extra processing (grinding) of olivine would then release additional CO_2 (Renforth, 2012). A similar result was seen in Hangx and Spiers (2009), where olivine dissolution in a coastal setting was modeled for two temperatures using a shrinking core model, with the 15°C model showing rates three times longer than that of the 25°C simulation.

Clearly, if enhanced weathering is applied to natural settings, soil temperature will vary both diurnally and seasonally. Diurnal soil temperature changes at 1 m depth (the depth of our soil columns) are on the order of 1–2°C in Europe (German National Meteorological Service). Average monthly soil temperatures at 1 m depth vary between 1 and 22°C in, for example, central and western Europe (i.e., Germany, northern France, UK, Benelux; German National Meteorological Service), with mean annual soil temperatures of 8.8–12.7°C in the UK (Busby, 2015), which match fairly well to the range used in these experiments. At such temperatures (assuming a linear extrapolation between the dissolution rates at 4° and 19°C; **Figure 6**), it would take ∼5,800 years for 80% of a mean grain size of 125 μm to dissolve (2.5 years for 20%). If the mean grain size were 10 μm, 20% would dissolve in ∼1.2 years, and 80% in ∼50 years. For a 1 μm mean grain size, these values are ∼1 and ∼14 years, respectively.

Overall, this study highlights that olivine dissolution rates are considerably lower in field-like experiments than in "normal" laboratory experiments. More experiments are needed to assess dissolution rates at higher, tropical, temperatures, but if our dissolution rates can be extrapolated to tropical temperatures, then a yearly application of material (Taylor et al., 2016) may not be feasible without accumulation of unweathered silicate material over time.

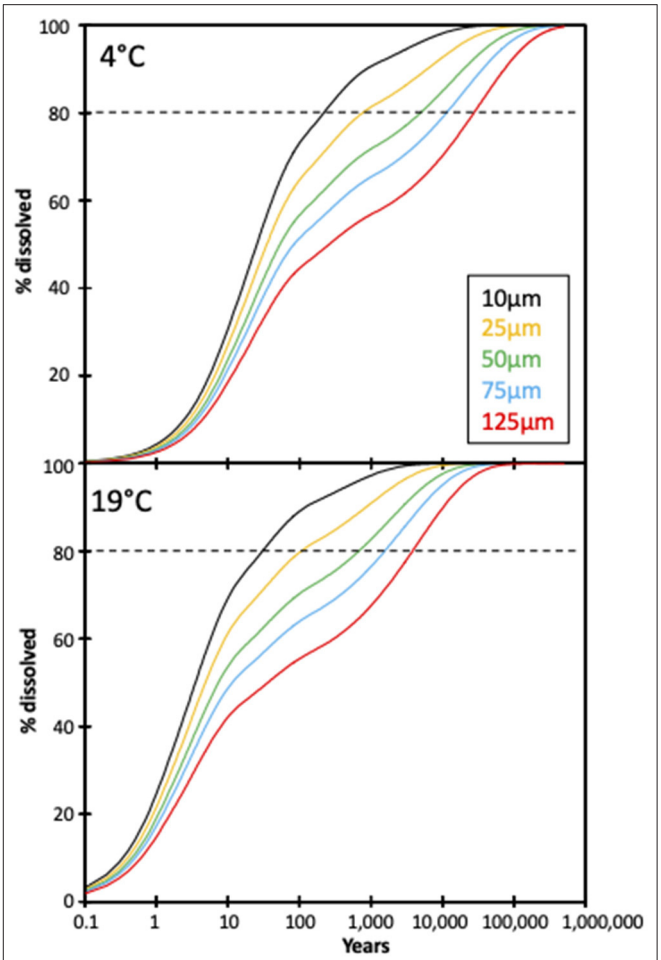

FIGURE 7 | Modeled extents of dissolution for different olivine grain sizes based on a shrinking core model (see text for details). The horizontal dashed lines represent a target dissolution proportion of 80% (given that the final 20% take a significant amount of time to finally dissolve).

CONCLUSIONS

Soil core experiments with olivine addition, used to evaluate enhanced weathering at 4°C, show that olivine dissolution is almost two orders of magnitude lower than in identical experiments at 19°C. In general, the two experiments at different temperatures exhibit the same temperature-dependent gradient as idealized laboratory experiments, but offset to lower values. This is likely because soil columns do not represent ideal fluid-rock contact conditions, and suggests that, as observed previously, natural experiments show significantly lower dissolution rates.

Heavy metals, such as Cd and Ni, were examined to assess whether olivine addition can contaminate water or soils. While in this experiment concentrations in both phases were significantly lower than guidelines, retention of heavy metals in soils was higher at elevated temperatures. This represents an increased retention beyond that caused by higher dissolution of minerals and higher temperatures, and is likely due to enhanced secondary mineral (e.g., clay) formation at higher temperatures. In themselves, clays present a potential problem for enhanced weathering, as clay accumulation can inhibit plant growth.

Overall, as anticipated, enhanced weathering may be considerably less feasible in cold conditions. Kinetic-limitation of weathering reactions results in substantially longer dissolution times for olivine. For example, for an average grain size of 50μm, 50% of olivine would dissolve in <10 years at 19°C, but in ∼50 years at 4°C. Thus, for example, enhanced weathering rates will be very low during northern and central European and American winters, and this must be factored into calculations.

DATA AVAILABILITY STATEMENT

The original contributions presented in the study are included in the article/**Supplementary Material**, further inquiries can be directed to the corresponding author/s.

AUTHOR CONTRIBUTIONS

PP designed the project and wrote the manuscript. CT conducted the experiment and performed the analyses. PR also designed the project and interpreted the data. JM performed the dissolution calculations. All authors contributed to the article and approved the submitted version.

FUNDING

PP were funded by ERC Consolidator grant 682760 CONTROLPASTCO2. PR acknowledges UKRI funding under the UK Greenhouse Gas Removal Programme (NE/P019943/1, NE/P019730/1).

ACKNOWLEDGMENTS

Birkbeck, University of London is thanked for the MSc of CT. Gary Tarbuck is thanked for assistance during concentration analyses. We thank two reviewers for their useful comments.

SUPPLEMENTARY MATERIAL

The Supplementary Material for this article can be found online at: https://www.frontiersin.org/articles/10.3389/fclim.2022.827698/full#supplementary-material

REFERENCES

Anbeek, C. (1992). The dependence of dissolution rates on grain size for some fresh and weathered feldspars. *Geochim. Cosmochim. Acta* 56, 3957–3970. doi: 10.1016/0016-7037(92)90009-8

Appelo, C. A. J., and Postma, A. (2004). *Geochemistry, Groundwater and Pollution*. Rotterdam: A.A Balkema Publishers. doi: 10.1201/9781439833544

Beerling, D. J., Kantzas, E. P., Lomas, M. R., Wade, P., Eufrasio, R. M., Renforth, P., et al. (2020). Potential for large-scale CO2 removal via enhanced rock weathering with croplands. *Nature* 583, 242–248. doi: 10.1038/s41586-020-2448-9

Berner, R. A., Lasaga, A. C., and Garrels, R. M. (1983). The carbonate-silicate geochemical cycle and its effect on atmospheric carbon-dioxide over the past 100 million years. *Am. J. Sci.* 283, 641–683. doi: 10.2475/ajs.283.7.641

Bowie, A. R., Maldonado, M. T., Frew, R. D., Croot, P. L., Achterberg, E. P., Mantoura, R. F. C., et al. (2001). The fate of added iron during a mesoscale fertilisation experiment in the Southern Ocean. *Deep Sea Res. II Top. Stud. Oceanogr.* 48, 2703–2743. doi: 10.1016/S0967-0645(01)00015-7

Busby, J. (2015). UK shallow ground temperatures for ground coupled heat exchangers. *Q. J. Eng. Geol. Hydrol.* 48, 248–260. doi: 10.1144/qjegh2015-077

Colbourn, G., Ridgwell, A., and Lenton, T. M. (2015). The time scale of the silicate weathering negative feedback on atmospheric CO2. *Glob. Biogeochem. Cycles* 29, 583–596. doi: 10.1002/2014GB005054

Gaillardet, J., Calmels, D., Romero-Mujalli, G., Zakharova, E. A., and Hartmann, J. (2019). Global climate control on carbonate weathering intensity. *Chem. Geol.* 2019, 118762. doi: 10.1016/j.chemgeo.2018.05.009

Gislason, S. R., and Oelkers, E. H. (2014). Carbon storage in basalt. *Science* 344, 373–374. doi: 10.1126/science.1250828

Hänchen, M., Prigiobbe, V., and Storti, G. (2006). Dissolution kinetics of fosteritic olivine at 90-150°C including effects of the presence of CO2. *Geochim. Cosmochim. Acta* 70, 4403–4416. doi: 10.1016/j.gca.2006.06.1560

Hangx, S. J. T., and Spiers, C. J. (2009). Coastal spreading of olivine to control atmospheric CO2 concentrations: a critical analysis of viability. *Int. J. Greenhouse Gas Control* 3, 757–767. doi: 10.1016/j.ijggc.2009.07.001

Haque, F., Chiang, Y. W., and Santos, R. M. (2020). Risk assessment of Ni, Cr, and Si release from alkaline minerals during enhanced weathering. *Open Agric.* 5, 166–175. doi: 10.1515/opag-2020-0016

Hartmann, J., West, A. J., Renforth, P., Kohler, P., De la Rocha, C. L., Wolf-Gladrow, D. A., et al. (2013). Enhanced chemical weathering as a geoengineering strategy to reduce atmopsheric carbon dioxide, supply nutrients, and mitigate ocean acidification. *Rev. Geophys.* 51, 113–150. doi: 10.1002/rog.20004

Hawley, S. M., Pogge von Strandmann, P. A. E., Burton, K. W., Williams, H. M., and Gislason, S. R. (2017). Continental weathering and terrestrial (oxyhydr)oxide export: comparing glacial and non-glacial catchments in Iceland. *Chem. Geol.* 462, 55–66. doi: 10.1016/j.chemgeo.2017.04.026

IPCC (2014). *Intergovernmental Panel on Climate Change, 5th Assessment Report.*

IPCC (2018). *"Global Warming of 1.5°C", in: Special Report on Global warming (SR15).*

Kasemann, S. A., Pogge von Strandmann, P. A. E., Prave, A. R., Fallick, A. E., Elliott, T., and Hoffmann, K. H. (2014). Continental weathering following a

Cryogenian glaciation: evidence from calcium and magnesium isotopes. *Earth Planet. Sci. Lett.* 396, 66–77. doi: 10.1016/j.epsl.2014.03.048

Kennedy, M. J., and Wagner, T. (2011). Clay mineral continental amplifier for marine carbon sequestration in a greenhouse ocean. *Proc. Natl. Acad. Sci. U.S.A.* 108, 9776–9781. doi: 10.1073/pnas.1018670108

Koehler, P., Abrams, J. F., Voelker, C., Hauck, J., and Wolf-Gladrow, D. A. (2013). Geoengineering impact of open ocean dissolution of olivine on atmospheric CO2, surface ocean pH and marine biology. *Environ. Res. Lett.* 8:014009. doi: 10.1088/1748-9326/8/1/014009

Koehler, P., Hartmann, J., and Wolf-Gladrow, D. A. (2010). Geoengineering potential of artificially enhanced silicate weathering of olivine. *Proc. Natl. Acad. Sci. U.S.A.* 107, 20228–20233. doi: 10.1073/pnas.1000545107

Lalonde, K., Mucci, A., Ouellet, A., and Gelinas, Y. (2012). Preservation of organic matter in sediments promoted by iron. *Nature* 483, 198–200. doi: 10.1038/nature10855

Lewis, J. F., Draper, G., Proenza, J. A., Espaillat, J., and Jimenez, J. (2006). Ophiolite-related ultramafic rocks (serpentinites) in the Caribbean Region: a review of their occurrence, composition, origin emplacement and Ni-laterite soil formation. *Geologica Acta*. 4, 237–263.

Maher, K. (2010). The dependence of chemical weathering rates on fluid residence time. *Earth Planet. Sci. Lett.* 294, 101–110. doi: 10.1016/j.epsl.2010.03.010

Manning, D. A. C., Renforth, P., Lopez-Capel, E., Robertson, S., and Ghazireh, N. (2013). Carbonate precipitation in artificial soils produced from basaltic quarry fines and composts: an opportunity for passive carbon sequestration. *Int. J. Greenhouse Gas Control* 17, 309–317. doi: 10.1016/j.ijggc.2013.05.012

Matter, J. M., Stute, M., Snaebjornsdottir, S. O., Oelkers, E. H., Gislason, S. R., Aradottir, E. S., et al. (2016). Rapid carbon mineralization for permanent disposal of anthropogenic carbon dioxide emissions. *Science* 352, 1312–1314. doi: 10.1126/science.aad8132

Nilsson, S., and Schopfhauser, W. (1995). The carbon-sequestration potential of a global afforestation program. *Clim. Change* 30, 267–293. doi: 10.1007/BF01091928

Oelkers, E. H., Butcher, R., Pogge von Strandmann, P. A. E., Schuessler, J. A., von Blanckenburg, F., Snaebjornsdottir, S. O., et al. (2019). Using stable Mg isotope signatures to assess the fate of magnesium during the *in situ* mineralisation of CO2 and H2S at the CarbFix site in SW-Iceland. *Geochim. Cosmochim. Acta* 245, 542–555. doi: 10.1016/j.gca.2018.11.011

Oelkers, E. H., Declerqc, J., Saldi, G. D., Gislason, S. R., and Schott, J. (2018). Olivine dissolution rates: a critical review. *Chem. Geol.* 500, 1–19. doi: 10.1016/j.chemgeo.2018.10.008

Orkoula, M. G., and Koutsoukos, P. G. (2002). Variability of dissolution rates at constant undersaturation. *J. Colloid Interface Science* 253, 185–189. doi: 10.1006/jcis.2002.8536

Peters, S. C., Blum, J. D., Driscoll, C. T., and Likens, G. E. (2004). Dissolution of wollastonite during the experimental manipulation of Hubbard Brook Watershed 1. *Biogeochemistry* 67, 309–329. doi: 10.1023/B:BIOG.0000015787.44175.3f

Pogge von Strandmann, P. A. E., Burton, K. W., Snaebjornsdottir, S. O., Sigfusson, B., Aradottir, E. S. P., Gunnarsson, I., et al. (2019a). Rapid CO2 mineralisation into calcite at the CarbFix storage site quantified using calcium isotopes. *Nat. Commun.* 10:1983. doi: 10.1038/s41467-019-10003-8

Pogge von Strandmann, P. A. E., Fraser, W. T., Hammond, S. J., Tarbuck, G., Wood, I. G., Oelkers, E. H., et al. (2019b). Experimental determination of Li isotope behaviour during basalt weathering. *Chem. Geol.* 517, 34–43. doi: 10.1016/j.chemgeo.2019.04.020

Pogge von Strandmann, P. A. E., Jones, M. T., West, A. J., Murphy, M. J., Stokke, E. W., Tarbuck, G., et al. (2021a). Lithium isotope evidence for enhanced weathering and erosion during the Paleocene-Eocene Thermal Maximum. *Sci. Adv.* 7, eabh4224. doi: 10.1126/sciadv.abh4224

Pogge von Strandmann, P. A. E., Renforth, P., West, A. J., Murphy, M. J., Luu, T.-H., and Henderson, G. M. (2021b). The lithium and magnesium isotope signature of olivine dissolution in soil experiments. *Chem. Geol.* 560, 120008. doi: 10.1016/j.chemgeo.2020.120008

Pogge von Strandmann, P. A. E., Vaks, A., Bar-Matthews, M., Ayalon, A., Jacob, E., and Henderson, G. M. (2017). Lithium isotopes in speleothems: temperature-controlled variation in silicate weathering during glacial cycles. *Earth Planet. Sci. Lett.* 469, 64–74. doi: 10.1016/j.epsl.2017.04.014

Pokrovsky, O. S., and Schott, J. (2000). Kinetics and mechanism of forsterite dissolution at 25 degrees C and pH from 1 to 12. *Geochim. Cosmochim. Acta* 64, 3313–3325. doi: 10.1016/S0016-7037(00)00434-8

Raveh-Rubin, S., Edery, Y., Dror, I., and Berkowitz, B. (2015). Nickel migration and retention dynamics in natural soil columns. *Water Resour. Res.* 51, 7702–7722. doi: 10.1002/2015WR016913

Raymo, M. E., and Ruddiman, W. F. (1992). Tectonic forcing of late cenozoic climate. *Nature* 359, 117–122. doi: 10.1038/359117a0

Renforth, P. (2012). The potential of enhanced weathering in the UK. *Int. J. Greenhouse Gas Control* 10, 229–243. doi: 10.1016/j.ijggc.2012.06.011

Renforth, P. (2019). The negative emission potential of alkaline materials. *Nat. Commun.* 10, 1401. doi: 10.1038/s41467-019-09475-5

Renforth, P., and Campbell, J. S. (2021). The role of soils in the regulation of ocean acidification. *Philos. Trans. R. Soc. B Biol. Sci.* 376, 1834. doi: 10.1098/rstb.2020.0174

Renforth, P., and Henderson, G. (2017). Assessing ocean alkalinity for carbon sequestration. *Rev. Geophys.* 55, 636–674. doi: 10.1002/2016RG000533

Renforth, P., Jenkins, B. G., and Kruger, T. (2013). Engineering challenges of ocean liming. *Energy* 60, 442–452. doi: 10.1016/j.energy.2013.08.006

Renforth, P., Pogge von Strandmann, P. A. E., and Henderson, G. M. (2015). The dissolution of olivine added to soil: implications for enhanced weathering. *Appl. Geochem.* 61, 109–118. doi: 10.1016/j.apgeochem.2015.05.016

Romero-Mujalli, G., Hartmann, J., and Börker, J. (2019). Temperature and CO2 dependency of global carbonate weathering fluxes - implications for future carbonate weathering research. *Chem. Geol.* 527, 118874. doi: 10.1016/j.chemgeo.2018.08.010

Saenger, C., and Wang, Z. (2014). Magnesium isotope fractionation in biogenic and abiogenic carbonates: implications for paleoenvironmental proxies. *Q. Sci. Rev.* 90, 1–21. doi: 10.1016/j.quascirev.2014.01.014

Schuiling, R. D., and de Boer, P. L. (2010). Coastal spreading of olivine to control atmospheric CO2 concentrations: a critical analysis of viability. Comment: Nature and laboratory models are different. *Int. J. Greenhouse Gas Control* 4, 855–856. doi: 10.1016/j.ijggc.2010.04.012

Schuiling, R. D., and Krijgsman, P. (2006). Enhanced weathering: an effective and cheap tool to sequester CO2. *Clim. Change* 74, 349–354. doi: 10.1007/s10584-005-3485-y

Shepherd, J., Caldeira, K., Cox, P., Haigh, J. E., Keith, D., Launder, B., et al. (2009). *Geoengineering the Climate: Science, Governance and Uncertainty*. The Royal Society.

Taylor, L. L., Quirk, J., Thorley, R. M. S., Kharecha, P. A., Hansen, J., Ridgwell, A., et al. (2016). Enhanced weathering strategies for stabilizing climate and averting ocean acidification. *Nat. Clim. Change* 6, 402–406. doi: 10.1038/nclimate2882

ten Berge, H. F. M., van der Meer, H. G., Steenhuizen, J. W., Goedhart, P. W., Knops, P., and Verhagen, J. (2012). Olivine weathering in soil, and its effects on growth and nutrient uptake in ryegrass (*Lolium perenne* L.): a pot experiment. *PLoS ONE* 7, e42098. doi: 10.1371/journal.pone.0042098

The Royal Society (2018). *Greenhouse Gas Removal*. The Royal Society.

Walker, J. C. G., Hays, P. B., and Kasting, J. F. (1981). A negative feedback mechanism for the long-term stabilization of earths surface-temperature. *J. Geophys. Res. Oceans Atmos.* 86, 9776–9782. doi: 10.1029/JC086iC10p09776

West, A. J., Galy, A., and Bickle, M. (2005). Tectonic and climatic controls on silicate weathering. *Earth Planet. Sci. Lett.* 235, 211–228. doi: 10.1016/j.epsl.2005.03.020

White, A. F., and Brantley, S. L. (2003). The effect of time on the weathering of silicate minerals: why do weathering rates differ in the laboratory and field? *Chem. Geol.* 202, 479–506. doi: 10.1016/j.chemgeo.2003.03.001

Williamson, P., Wallace, D. W. R., Law, C. S., Boyd, P. W., Collos, Y., Croot, P., et al. (2012). Ocean fertilization for geoengineering: a review of effectiveness, environmental impacts and emerging governance. *Process Saf. Environ. Protect.* 90, 475–488. doi: 10.1016/j.psep.2012.10.007

Yosef, G., Walko, R., Avisar, R., Tatarinov, F., Rotenberg, E., and Yakir, D. (2018). Large-scale semi-arid afforestation can enhance precipitation and carbon sequestration potential. *Sci. Rep.* 8,996. doi: 10.1038/s41598-018-19265-6

Zhang, D., Zhou, C. H., Lin, C. X., Tong, D. S., and Yu, W. H. (2010). Synthesis of clay minerals. *Appl. Clay Sci.* 50, 1–11. doi: 10.1016/j.clay.2010.06.019

Conflict of Interest: JM was employed by Witteveen+Bos.

The remaining authors declare that the research was conducted in the absence of any commercial or financial relationships that could be construed as a potential conflict of interest.

Publisher's Note: All claims expressed in this article are solely those of the authors and do not necessarily represent those of their affiliated organizations, or those of the publisher, the editors and the reviewers. Any product that may be evaluated in this article, or claim that may be made by its manufacturer, is not guaranteed or endorsed by the publisher.

frontiers in Climate

ORIGINAL RESEARCH
published: 22 March 2022
doi: 10.3389/fclim.2022.831587

Kinetics of Olivine Weathering in Seawater: An Experimental Study

Michael Fuhr[1], Sonja Geilert[1], Mark Schmidt[1], Volker Liebetrau[1], Christoph Vogt[2], Brendan Ledwig[3] and Klaus Wallmann[1]*

[1] GEOMAR Helmholtz Centre for Ocean Research Kiel, Kiel, Germany, [2] FB05 Geosciences and MARUM - Center for Marine Environmental Sciences, University of Bremen, Bremen, Germany, [3] Christian-Albrechts-Universität zu Kiel, Kiel, Germany

Enhanced weathering of mafic and ultra-mafic minerals has been suggested as a strategy for carbon dioxide removal (CDR) and a contribution to achieve a balance between global CO_2 sources and sinks (net zero emission). This study was designed to assess CDR by dissolution of ultramafic sand (UMS) in artificial seawater (ASW). Fine grained UMS with an olivine content of ∼75% was reacted in ASW for up to 134 days at 1 bar and 21.5–23.9°C. A decline in total alkalinity (TA) was observed over the course of the experiments. This unexpected result indicates that TA removal *via* precipitation of cation-rich authigenic phases exceeded the production of TA induced by olivine dissolution. The TA decline was accompanied by a decrease in dissolved inorganic carbon and Ca concentrations presumably induced by $CaCO_3$ precipitation. Temporal changes in dissolved Si, Ca, Mg, and TA concentrations observed during the experiments were evaluated by a numerical model to identify secondary mineral phases and quantify rates of authigenic phase formation. The modeling indicates that $CaCO_3$, FeOOH and a range of Mg-Si-phases were precipitated during the experiments. Chemical analysis of precipitates and reacted UMS surfaces confirmed that these authigenic phases accumulated in the batch reactors. Nickel released during olivine dissolution, a potential toxic element for certain organisms, was incorporated in the secondary phases and is thus not a suitable proxy for dissolution rates as proposed by earlier studies. The overall reaction stoichiometry derived from lab experiments was applied in a box model simulating atmospheric CO_2 uptake in a continental shelf setting induced by olivine addition. The model results indicate that CO_2 uptake is reduced by a factor of 5 due to secondary mineral formation and the buffering capacity of seawater. In comparable natural settings, olivine addition may thus be a less efficient CDR method than previously believed.

Keywords: silicate weathering, carbon sequestration, olivine dissolution, seawater, sequestration efficiency

OPEN ACCESS

Edited by:
David Beerling,
The University of Sheffield,
United Kingdom

Reviewed by:
Peter Köhler,
Alfred Wegener Institute Helmholtz Centre for Polar and Marine Research (AWI), Germany
James Campbell,
Heriot-Watt University,
United Kingdom

****Correspondence:***
Michael Fuhr
mfuhr@geomar.de

Specialty section:
This article was submitted to Negative Emission Technologies, a section of the journal Frontiers in Climate

Received: *08 December 2021*
Accepted: *22 February 2022*
Published: *22 March 2022*

Citation:
Fuhr M, Geilert S, Schmidt M, Liebetrau V, Vogt C, Ledwig B and Wallmann K (2022) Kinetics of Olivine Weathering in Seawater: An Experimental Study. Front. Clim. 4:831587. doi: 10.3389/fclim.2022.831587

INTRODUCTION

The CO_2 content in the atmosphere has continuously increased over the last 120 years to a current maximum of 412 ppm (Keeling et al., 2001; MacFarling Meure et al., 2006; Howe, 2015). Since CO_2 acts as a greenhouse gas (Feldman et al., 2015), it is mainly responsible for the anthropogenic greenhouse effect (Lindzen, 2007; Solomon et al., 2009). The 2015 Paris Climate Change Conference COP21 agreed on limiting global warming to <2°C compared to the preindustrial level. Furthermore, it was stated that reaching this goal can only be reached if

zero net emissions of CO_2 are attained between 2030 and 2050 (Rhodes, 2016). The 2018 IPCC (Intergovernmental Panel on Climate Change) special report "Global Warming of 1.5°C" has made clear that this goal is only achievable if in addition to the reduction of CO_2 emissions, CO_2 is actively sequestered from the atmosphere in form of negative emissions (Friedlingstein et al., 2011; IPCC, 2021).

A vast variety of carbon dioxide removal (CDR) techniques has been proposed and critically reviewed over the last 20 years (Lackner, 2003; Iizuka et al., 2004; Lal, 2004; Fuss et al., 2018; Saran et al., 2018). Amongst other methods, CO_2 sequestration by alkalinity enhancement through silicate weathering has been highlighted as an affordable and effective CDR technique (Oelkers, 2001; Hartmann and Kempe, 2008; Renforth and Henderson, 2014; Montserrat et al., 2017). The general concept behind this technique is the chemical reaction of an idealized magnesium silicate, i.e., forsterite (Mg_2SiO_4), with water, following:

$$Mg_2SiO_4 + 4H_2O + 4CO_2 \rightarrow 2Mg^{2+} + H_4SiO_4 + 4HCO_3^- \quad (1)$$

This reaction has been thoroughly studied in soils on land (Oelkers, 1999; Olsen and Rimstidt, 2008; Oelkers et al., 2015; Amann et al., 2020) but to a smaller extent in seawater, despite the fact that enhanced olivine weathering would have a triple positive effect if applied in the ocean: (1) CO_2 would be sequestered from the atmosphere into the ocean, (2) the acidification of the oceans would be reduced, and (3) the supply of silica and iron, which are limiting nutrients in many parts of the ocean, would increase primary production and could lead to further CO_2 uptake (Hartmann et al., 2013; Montserrat et al., 2017).

The idea behind this concept is to distribute fine grained olivine (Strefler et al., 2018) in coastal areas, along beaches and/or on shelf regions (Meysman and Montserrat, 2017; Montserrat et al., 2017). Subsequently, olivine dissolves following Equation (1) and thus takes up CO_2 by contributing total alkalinity (TA) to the water column.

A vast number of studies have investigated or reviewed the dissolution kinetics of olivine in aqueous solutions (Pokrovsky and Schott, 2000; Oelkers, 2001; Davis et al., 2009; Rimstidt et al., 2012; Méheut and Schauble, 2014; Maher et al., 2016; Oelkers et al., 2018) including filtered seawater (FSW) (Montserrat et al., 2017) and artificial seawater (ASW) (Montserrat et al., 2017; Rigopoulos et al., 2018). Montserrat et al. (2017) showed that during the dissolution of olivine in SW and ASW the amount of TA increase is up to ∼80% lower than theoretically expected. This TA deficit was left unexplained but loosely related to the possible but not observed formation of secondary minerals.

Other studies suggested that the low TA increase was caused by lower dissolution rates due to the formation of passivating surface layers that either consist of a deprotonated surface complex (Pokrovsky and Schott, 2000; Palandri and Kharaka, 2004) or repolymerized silicic acid (Maher et al., 2016) or the formation of secondary mineral phases on the olivine grains, which reduce the reactive surface (Béarat et al., 2006; King et al., 2010; Sissmann et al., 2013; Oelkers et al., 2018).

These secondary minerals, including the formation of $CaCO_3$, have also been linked to direct TA loss and thus low TA increase observed in several studies (Béarat et al., 2006; Hangx and Spiers, 2009; Köhler et al., 2013; Sissmann et al., 2013; Meysman and Montserrat, 2017; Montserrat et al., 2017). However, the rates and mechanisms of their formation are poorly constrained especially in SW and ASW.

Furthermore, the release of toxic elements such as nickel has been subject to speculations about a possible negative effect on the environment if olivine is applied in coastal ecosystems (Montserrat et al., 2017; Flipkens et al., 2021).

In this study, batch experiments were carried out in which ultramafic olivine sand was weathered in ASW. A special focus is laid on the formation of secondary phases and their impact on the CO_2 sequestration efficiency. The implications for the application of enhanced olivine weathering as a CDR measure for climate change mitigation are assessed. Furthermore, the release of potentially toxic elements such as nickel is investigated, which allows a better assessment of environmental risks associated with enhanced olivine weathering.

MATERIALS AND METHODS

Materials

Commercially available ultra-mafic sand (UMS) was received from AdL Sandstrahltechnik, which, according to oral information from the company, ultimately derives from several quarries in northern Italy, presumably located in the mafic-ultramafic complex near Vidracco (Kremer et al., 2019). The olivine content of UMS was determined as 74.6 wt-%. For a detailed chemical composition see **Table 1** and **Supplementary Table 4**.

The UMS was milled and subsequently sieved to separate grains with a diameter of 100–125 μm, based on the recommendation by Strefler et al. (2018). The 100–125 μm fraction was then thoroughly washed with ASW until the supernatant was clear. Subsequently, the diluted salts were removed by at least three wash cycles with deionized water (18.2 MΩ-Milli-Q system, hereafter: MQe) until the supernatant was clear. The composition of ASW was calculated for a salinity of 35.0 (Millero et al., 2008). Additionally, 2.3 mmol/l $NaHCO_3$ were added to reach an alkalinity of ∼2.3 mmol/l. All chemical components listed in **Supplementary Table 3** were dissolved in MQe. The initial Ca content was lower than listed (∼320 mg/l instead of 422 mg/l). After day 50, the ASW used for replacement after sample taking contained the correct amount of Ca (422 mg/l). The lower initial Ca content was applied to keep the saturation state with respect to aragonite and calcite within natural ranges of the surface ocean (Feely et al., 2012) and to avoid strong oversaturation that can appear during the early stage of the experiment due to rapid dissolution of high-energy surface sites created during the milling process.

Experimental Setup

The UMS was permitted to react with artificial seawater in 250 ml polyethylene (PE) batch reactors. Three different batches with variable amounts of UMS were prepared, each containing

TABLE 1 | Mineralogical model for UMS (bulk) combining XRD, WDX, and ICP-OES data.

Species	Al	Ca	Cr	Fe	K	Mg	Mn	Na	Ni	Ti	Si	Oxy	% (wt.)
Phase													
Forsterite	0.002		0.002	1.182		11.02	0.018	0.003	0.036		5.868	24	74.62
Opx	0.663	0.093	0.034	0.767		7.032	0.019	0.055	0.007	0.010	7.504	24	15.92
Cpx	1.104	3.352	0.091	0.288		3.350		0.360	0.005	0.042	7.471	24	3.55
Amph.	1.454	1.905	0.071	0.393	0.174	4.518		0.369	0.008	0.096	7.242	24	5.40
Spinel	10.24		1.603	1.597		4.605	0.015		0.032	0.004		24	0.07
Sulfide				1.900					0.350				0.45
	0.039	0.039	0.002	0.174	0.002	1.543	0.003	0.007	0.006	0.001	1.0	3.822	100
	0.035	0.034	0.002	0.174	0.000	1.543	0.003	–	0.006	0.001	1.0	3.822	

*Element concentrations in minerals are given as atomic proportion relative to 24 oxygen. Oxygen is not measured but set to 24. The mineral phases were determined based on XRD measurements, the elementary compositions of mineral phases are based on WDX measurements (**Supplementary Table 5**). Opx, Orthopyroxene; Cpx, Clinopyroxene; Amph, Amphibole.* $C_{i,bulk}$ $\left(\frac{mol_{element}}{mol_{Si_{bulk}}}\right)$ *represents the calculated bulk concentration of each element normalized to bulk Si,* $C_{i,UMS}$ $\left(\frac{mol_{element}}{mol_{Si_{UMS}}}\right)$ *are measured element concentrations obtained by full digestion of UMS normalized to the measured Si content of the UMS.*

three replicates ($n = 3$) to verify the reproducibility of the experiments. The amount of ASW was 200 ml for all replicates and batches. Fifty milliliter of ambient air were included to allow for equilibration with the atmosphere. The amount of UMS was varied from 20 g for Batch20 to 10 g for Batch10 and 5 g for Batch5 in order to investigate the effect of the solid/liquid ratio. The air was partly exchanged with the laboratory atmosphere every time samples were taken. All batch reactors with artificial seawater, UMS and gas phase were subjected to constant movement in Heidolph™ Reax2© over-head shakers at ∼40 rpm. The experiment was conducted under controlled laboratory conditions ($p = 1$ bar, $21.5°C < T < 23.9°C$).

Sampling Procedure From Batch Reactors and Water Analysis

For each sample (23 in total), two aliquots (2 ml and 5 ml) were taken for further measurements and the same volume of artificial seawater was added to ensure a constant solid/liquid ratio. For the same reason it was made sure that no UMS grains were removed *via* sample taking. Sampling intervals increased from minutes to hours during day one to every 2 weeks between day 50 and day 134. The 5 ml aliquot was filtered through a 0.2 µm cellulose membrane filter and refrigerated in 5.2 ml Zinsser™ scintillation bottles. The 2 ml aliquot was used for direct pH measurements (see below) and not filtered to ensure a pristine chemical milieu. At the end of the experiments, the ASW in the batch reactors was carefully decanted over a 0.2 µm regenerated cellulose filter to recover the grayish suspended matter that had formed in the batch reactors during the experiment. Fine particles possibly stuck to the UMS grains were eluted by refilling the batch reactor with fresh ASW, shaking and decanting it. This procedure was repeated until the supernatant was clear. Withal, it was made sure that all precipitates, which left the bottles, were recovered on the filters. Subsequently, the wet cake was rinsed with pH neutral MQe to elute dissolved species (e.g., salinity). Furthermore, the UMS used in Batch20 was recovered, very carefully rinsed with pH neutral MQe (to only elute salinity), and dried for scanning electron microscope energy-dispersive X-ray spectroscopy (SEM–EDX).

The water samples were analyzed for pH following Dickson (1993). TA was analyzed by titration with diluted HCl to an end point of pH = 4.5 (Gieskes et al., 1991; Stumm and Morgan, 1996) and element concentrations were determined using inductively coupled plasma optical emission spectrometry (ICP-OES).

Solid Phase Analysis

Pristine (unused and washed) and weathered UMS as well as the precipitates recovered from the batch reactors were digested after a modified alkali-fusion method of van den Boorn et al. (2006), in order to preserve Si, which is lost using conventional HF digestion methods. In contrast to van den Boorn et al. (2006), we used Teflon beakers on a hot plate instead of an oven. Between 20 and 40 mg of NaOH (Merck™ Suprapure®) and a drop of MQe were added and the sample set to reflux for 72 h at 120°C. Afterwards the sample was diluted with 1 ml MQe and transferred to a 1.5 ml save-lock tube and centrifuged at 11,000 rpm. The supernatant was separately stored and the undissolved residues retransferred to the Teflon vial, together with 200 µl of concentrated HNO_3 and set to reflux for 72 h at 120°C. After the second reflux 1 ml of MQe was added to the sample and the sample centrifuged and the supernatant removed, as described above. The entire procedure was then repeated. Subsequently, the dissolved samples (e.g., all aliquots of each sample) were retransferred to the Teflon beakers and measured with ICP-OES.

Additionally, major and trace elements were determined using the Panalytical Axios Plus X-ray spectrometer at the Institut für Chemie und Biologie des Meeres (ICBM) in Oldenburg. In brief, 700 mg of freeze-dried and homogenized ultra-mafic sand was mixed with 4,200 mg lithiumtetraborate ($Li_2 B_4 O_7$ Spektromelt) and fused to glass beads. The accuracy and precision were determined by simultaneous runs of certified sediment standards BE-N and BIR-1 (IGGE; e.g., Govindaraju, 1994) and in-house standard (PSS) with better than 2.6% RSD for major elements and 3.3% RSD for trace elements.

In order to determine the precise composition of the single mineral phases, the UMS before and after the experiment was

investigated using a JXA-8200 SuperProbe high resolution SEM and a WDX/EDX Combined Electron Probe Microanalyzer (EPMA) at GEOMAR. For this purpose, a small portion of reacted UMS (see section Sampling Procedure From Batch Reactors and Water Analysis) and small portion of fresh UMS were poured on a self-sticking carbon plate. Thereby it was made sure that both samples did not mix and that the grains were placed solitarily. Furthermore, fresh UMS and reacted UMS were embedded in resin and the hardened samples were whetted to create a suitable surface for element analysis along a profile. Afterwards the samples were evaporated with carbon and placed in the EPMA. A large number of measuring points were evenly distributed along a profile with a distance between the measuring points of ∼1.5 µm. The spatial resolution of each measuring point is ∼5 µm. Hence, neighboring data points overlapped along the profile. The measured values were reported as atomic proportion normalized to 24 oxygen atoms with an RSD better than 0.7% for simultaneously measured standards and better than 1.5% for major elements. Finally, the element abundance was normalized to 100 wt.-% and the atomic proportion normalized to 24 oxygen. For the analysis of carbonate grains, the carbon content was pre-set to 12.01 wt.-%. Apart from quantitative measurements, scanning electron microscope (SEM) images were taken with the same device.

In order to verify the mineral composition, the pristine UMS as well as the precipitates recovered from the batch reactors were measured on a Phillips X-ray diffractometer (XRD) equipped with an automatic divergency slit, monochromator and a Co-cube at 40 kV and 35 mA. The samples were finely ground, pressed on an Si monocrystalline plate and measured with $2\theta = [4; 75]$ at 0.01° steps for 1 s at each step. The analysis of the XRD diffractograms was performed *via* the xPowder™ software and the standard PDF2 database. The results and interpretations are shown in **Supplementary Figures 1–4**.

Model Setup

A dissolution-precipitation model was set up with Wolfram Mathematica to simulate the chemical reactions for each batch experiment. The kinetic box model considers dissolution of olivine after Rimstidt et al. (2012), precipitation of the secondary phases aragonite/calcite, sepiolite, crysotile, talc and $Fe(OH)_3$ based on saturation state calculations (**Supplementary Section 1**). The model also calculates the concentration of dissolved Mg, Si, Ca, Fe as well as TA and is used to infer the overall reaction stoichiometry.

For each species in solution, ordinary differential equations (ODEs) were formulated as:

$$\frac{dC}{dt} = \varphi_{ol} * r_{ol} - \sum\nolimits_j \varphi_{m,j} * r_{m,j} - r_s * (C - C_{in}) \quad (2)$$

where C is concentration of the considered species in the dissolved phase, t is time, φ_{ol} represents the abundance of the species in olivine (ol) and r_{ol} is the olivine dissolution rate. Precipitation of secondary mineral phases (j) is calculated by multiplying the respective precipitation rate ($r_{m,j}$) with a corresponding stoichiometric coefficient ($\varphi_{m,j}$) defining the content of the considered element in the respective mineral. Sampling and replacement by fresh ASW are considered by applying the sampling rate r_S and the concentration difference between sample (C) and unreacted ASW (C_{in}).

The model is solved using the solver for ordinary differential equations of MATHEMATICA (version 11.3).

The precipitation rate of secondary minerals depends on the corresponding saturation state ($\Omega_i(t)$):

$$r_{pre_i} = \varepsilon_{pre1_i} * UnitStep\,(\Omega_i\,(t) - 1)\ * |\Omega_i(t) - 1|^{\varepsilon_{pre2_i}} \quad (3)$$

UnitStep expresses a function that returns 0 for arguments smaller than or equal to 0 and 1 for all arguments larger than 0. Hence, precipitation was assumed to take place only when the solutions were oversaturated with respect to the considered mineral ($\Omega_i(t) > 1$). ε_{pre2_i} defines the order of the reaction and ε_{pre1_i} is defined as

$$\varepsilon_{pre1_i} = k_{pre_i} * \left(1 - \frac{1}{1 + e^{\frac{t-\alpha_i}{\beta_i}}}\right) \quad (4)$$

k_{pre_i} is a kinetic constant, α represents the time delay until the precipitation starts and β steers the speed with which the precipitation starts. ε_{pre1_i} was introduced because the solids used in our experiments did not contain seed material for the precipitation of secondary minerals. Hence, the precipitation did not start immediately after oversaturation was reached but with a delay expressed by ε_{pre1_i}. The kinetic constants k_{prei} (Equation 4) were employed to consider the fact that precipitation rates are not only determined by the degree of oversaturation but also by kinetic factors that may either slowdown or accelerate the precipitation reaction.

The oxidation of ferrous iron released during olivine dissolution was simulated applying the kinetic rate for abiotic iron oxidation (Millero et al., 1987).

The mineralogical composition of the UMS and the precipitates was determined with a simple mixing calculation. In a first step, element concentrations measured *via* ICP-OES were normalized to the measured Si content following:

$$C_{i,\,S} = conc_i / Si_S \quad (5)$$

where $C_{i,\,S}$ $\left(\frac{mol_{element}}{mol_{Si_S}}\right)$ is the concentration of an element normalized to the Si concentration in the respective solid S (UMS or precipitates), $conc_i$ $\left(\frac{mol_{element}}{mg_S}\right)$ is the concentration of an element per milligram solid and Si_S $\left(\frac{mol_{Si_S}}{mg_S}\right)$ is the Si concentration in the solid.

In a second step, the composition was calculated following:

$$C_{i,bulk} = \sum\nolimits_i \left(C_{i,\min} * f_{bulk}\right) / Si_{bulk} \quad (6)$$

$C_{i,bulk}$ $\left(\frac{mol_{element}}{mol_{Si_{bulk}}}\right)$ represents the molar fraction of an element i in the calculated composition normalized to mol of Si;

$C_{i,\min}\left(\frac{mol_{element}}{mol_{mineral}}\right)$ is the molar content of the element in a certain mineral. $f_{bulk}\left(\frac{mol_{mineral}}{mol_{bulk}}\right)$ denotes the fraction of a certain mineral in the calculated composition and $Si_{bulk}\left(\frac{mol_{Si_{bulk}}}{mol_{bulk}}\right)$ represents the corresponding Si content (**Table 1**). The mineral phases used for this calculation were estimated from XRD and WDX measurements. The amount of each mineral (f_{bulk}) was then iterated until $C_{i,bulk}$ values for each element were acceptably close to the measured $C_{i,S}$ values. Normalization to Si was used to allow comparing concentrations (mol/mg) measured *via* ICP-OES to atomic proportions (normalized to 24 O) obtained *via* WDX and XRD.

RESULTS

Composition of the Ultra-Mafic Sand (UMS)

The major and trace element measurements (ICP-OES and XRF) of the UMS are mainly in good agreement with the oxide composition provided by the manufacturer (**Supplementary Table 6**). Furthermore, 5% of the UMS consisted of accessory oxides such as MnO, K_2O, CaO, and Al_2O_3 which were not accounted for in the manufacturer information. According to WDX measurements the olivine used consists of 90.3% forsterite and 9.7% fayalite leading to the formula $(Mg_{0.90}Fe_{0.10})_2SiO_4$ (Fo90) and based on the simple mineral model accounts for 74.62% of the UMS (**Table 1**). The second largest fraction is Orthopyroxene (Opx) with the simplified structural formula $(Mg_{0.9}Fe_{0.1})_2(Al_{0.15}Si_{0.85})_2O_6$ accounting for 15.92% followed by an amphibole (Amph., likely tremolite) with the structural formula $(Na_{0.36}K_{0.14})(Ca_{0.95}Mg_{0.05})_2(Cr_{0.014}Fe_{0.079}Mg_{0.79}Al_{0.087}Ti_{0.03})_5(Si_{7.4}Al_{0.6})O_{22}(OH)_2$ (5.41%) and a Clinopyroxene (Cpx) with 3.5% and the structural formula $(CaMg)_2(Si_{0.9}Al_{0.1})_2O_6$. Additionally, WDX measurements revealed the presence of accessory spinel and Ni and Fe sulfides. The abundance of these phases was estimated employing ICP-OES data and EDX observations.

Concentrations of Dissolved Species Measured During the Experiments

All experiments show a common trend of increasing TA in the early stage of the experiment and a decrease below initial values (2.36 ± 0.011 meq/l) after a certain period of time (**Figure 1A**). The highest and lowest values (2.65 ± 0.011 meq/l; 1.266 ± 0.019 meq/l), were measured in Batch20 (solid/liquid = 1/10) after 1 day (highest) and at the very end of the experiment (lowest). Batch5 (solid/liquid = 1/40) shows the lowest overall temporal gradient. The peak values occur the latest for Batch5, which also shows the highest final TA values, even though associated with the largest errors. Dissolved silicon concentrations [Si] increase persistently over the entire experiment (**Figure 1B**). The fastest increase is observed during the initial stage of the experiment (e.g., **Supplementary Tables 8–10**). The rate of [Si] increase then stabilizes during the experiment to nearly constant values toward the end. An exception to that trend is visible in Batch5. Here, the rate increases abruptly around day 78 (**Supplementary Table 10**) before a steady increase is attained. This rate change does not occur in all three replicates, which is reflected in high double standard deviation (2SD) values for [Si] toward the end of the experiment (**Figure 1B**). The highest concentrations are observed at the end of the experiment with a final [Si] of 421.8 ± 1.3 µmol/l (Batch20), 286.6 ± 6.4 µmol/l [Batch10 (solid/liquid = 1/20)] and 190.3 ± 42.1 µmol/l (Batch5). Calcium concentrations [Ca] (**Figure 1C**) show a common trend for all three batches: During the early stage of the experiment, [Ca] stays relatively constant, before the concentrations start to drop. Toward the end of the experiment, [Ca] increases again. Similar to TA values, the initial decrease appears latest in Batch5 and earliest and strongest in Batch20. Interestingly, until day three [Ca] follows a pattern that is similar to Mg concentrations ([Mg]) values (**Supplementary Figure 5**) with a well-pronounced peak in Batch20 after 115 min which, at the same time, represents the highest measured [Ca] value of all three batches ([Ca] = 8.26 ± 0.02 mmol/l). However, the temporal changes in [Mg] do not exceed the standard deviation of the three replicates due to the high [Mg] values in the ASW. In Batch20, [Ca] decreases constantly after 1 day from 8.10 ± 0.01 mmol/l to a minimum value of 6.58 ± 0.01 mmol/l at day 78. The decrease is weaker after day 50. For Batch10 and Batch5 the [Ca] decrease is less pronounced and occurs with a delay of 2 days in Batch10 and after 4 days in Batch5. After 50 days, the replenishment of ASW with high Ca concentrations (see section Materials) caused an increase in [Ca] in all three batches.

Final experimental [Ca] is 6.83 ± 0.01 mmol/l for Batch20, 7.32 ± 0.01 mmol/l for Batch10 and 7.78 ± 0.01 mmol/l for Batch5. Overall, the behavior of [Si], [Ca], and TA reflects the amount of USM used in the experiments. Elevated solid/water ratios induce high [Si] and low [Ca] and TA values at the end of the experiments.

For all batches, the model used for the simulation was able to reproduce measured values very accurately (**Figures 1A–C**). The sum of squared errors ranged between 0.03 and 0.52 with highest errors in Batch5. Additional data used in the modeling are provided and described in detail in the **Supplementary Section 1**.

Secondary Mineral Formation and Precipitation Rates

The change in water chemistry by dissolution of olivine and the subsequent accumulation of cations change the saturation state with respect to a variety of mineral phases containing these ions (**Figure 2**). Saturation states (Ω_i) were calculated using PHREEQ (Parkhurst and Appelo, 1999) where values above 1 indicate oversaturation (**Supplementary Materials**). During all experiments, DIC calculated from measured TA and pH values follows the same trend as TA (**Figure 1A**) and [Ca] (**Figure 1C**). In contrast, pH values (**Figure 2B**) follow a different trend. In all batches an initial increase in pH can be observed. This increase is strongest and appears earliest (until day 1) in Batch20. In Batch10 and Batch5 pH values rise less rapidly and highest values were measured latest in Batch5. Subsequently, the pH values decrease again in all batches. Again, this decrease ends first in Batch20

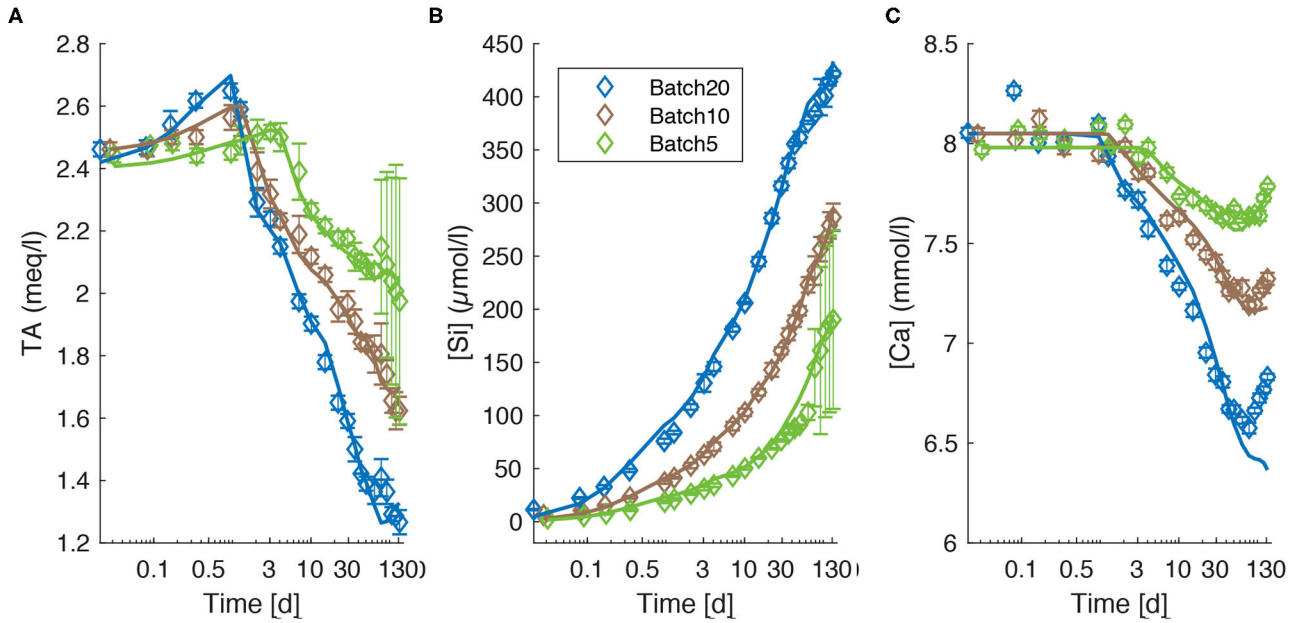

FIGURE 1 | TA **(A)**, [Si] **(B)**, and [Ca] **(C)** values measured during the experiments. Symbols indicate mean values of three replicates for each batch. Error bars are reported as ± 2SD of the mean values. Lines represent modeled concentrations (blue; Batch20, brown: Batch10, green; Batch5). A logarithmic scale is used for the time axis.

followed by Batch10 and is observed latest in Batch5. Contrary to the first increase, the subsequent drop has a similar magnitude in all batches which leads to lowest values in Batch5. After a well-pronounced peak, pH values decrease in Batch10 and Batch20 toward the end of the experiment. In Batch5 pH values plateau until day 78 before they slowly decrease toward the end. Note that the standard deviation of the three replicates in Batch5 becomes very large during the last days which leads to the assumption that an external input might have occurred in one of the Batch5 batch reactors.

In all three batches, the system is oversaturated with respect to aragonite (saturation state >1) over the entire course of the experiment (**Figure 2C**). Following DIC (**Figure 2A**) and TA, the saturation states increase toward an initial peak that occurs first in Batch20, then Batch10 and less pronounced in Batch5. During the subsequent decrease that persists until the end of the experiment, the saturation states in all three batches converge toward a common value of ∼1.5.

For the phyllosilicate phases considered in this study (serpentinite, talc, sepiolite), the saturation states, which depend on [Si], [Mg], and pH, develop differently from saturation with respect to aragonite. Since Si and Mg concentrations increase persistently, saturations follow this trend which is, though, overlain by changes in pH values (**Figures 2D–F**). The most striking features are the time after which the solution exceeds oversaturation with respect to the individual minerals (saturation values >1) and the extent of oversaturation attained at the end of experiments. Whilst serpentine saturation (**Figure 2D**) increases to a state of oversaturation very early in all batches (first Batch20 after ∼0.1 day, latest Batch5 after ∼1 day), saturations with respect to talc increase later and reveal higher differences between the batches (**Figure 2E**). A similar trend but with overall lower oversaturation is visible for sepiolite (**Figure 2F**). Thus, saturation with respect to both minerals (talc and sepiolite) rise above 1 in Batch5 only after day ∼50 and day ∼80 respectively.

Trace Metal Concentrations

Manganese concentrations [Mn] increase over the first 3 days during all experiments (**Figure 3A**). A well-pronounced peak is clearly visible in all batches at day 3, followed by a minimum at day 4. Subsequently, [Mn] values increase again but do not follow a common trend anymore. Important features are the strong increase in Batch5 between day 46 and day 78 which coincides with a strong increase in [Si] (**Figure 1B**) and the fact that lowest final values are observed in Batch20 (∼0.3 µmol/l), whereas the concentrations in Btach10 and Batch5 are equal within the error (∼0.5 µmol/l).

Despite the larger 2SD compared to [Mn], Ni concentrations show a clearly increasing trend throughout the experiment (**Figure 3B**) with a tendency toward highest values for Batch20 until day 22. A strong final increase for Batch5, that coincides with the increase in [Si], leads to values that are equal within the error for all batches (Batch201.23 ± 0.26 µmol/l, Batch10: 1.31 ± 0.23, Batch5: 1.42 ± 0.26 µmol/l).

Model Results: Composition of Precipitates and Overall Stoichiometry

The kinetic rate law employed in the model allows for secondary mineral precipitation only after the solutions reach oversaturation with respect to the considered mineral

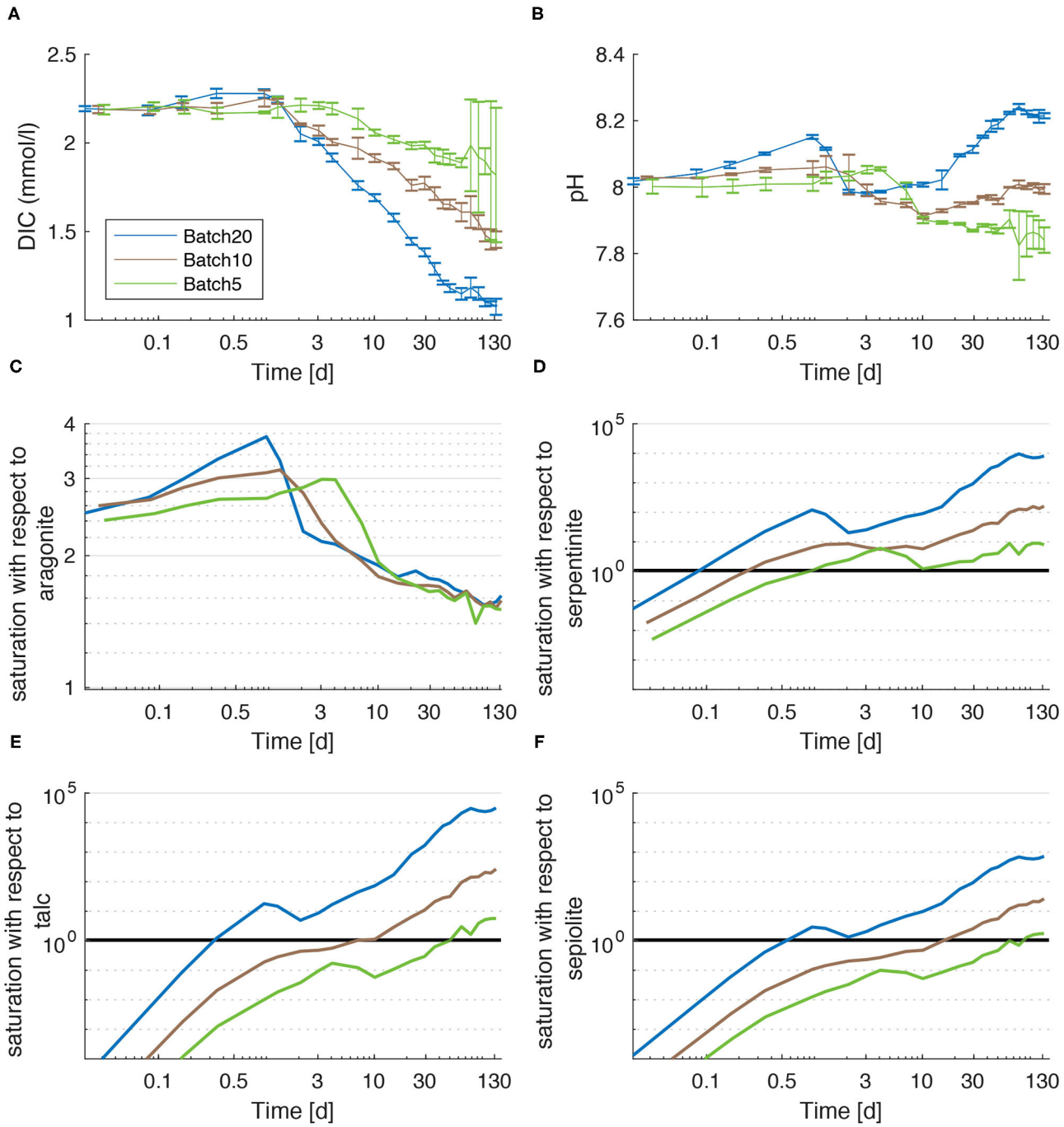

FIGURE 2 | DIC **(A)**, pH **(B)** and saturation states with respect to aragonite **(C)**, serpentine **(D)**, talc **(E)**, and sepiolite **(F)** as calculated for Batch20 (blue), Batch10 (brown), and Batch5 (green). Error bars in **(A)** reflect ± 2SD that are calculated form the standard deviations of measured pH and TA values.

(Equations 3, 4). Precipitation does not start immediately after oversaturation is reached, since nucleation has to occur before precipitation can remove substantial amounts of solutes from solution. The time delay accounting for nucleation and the kinetic constants are derived by fitting the model to the measured dissolved species concentrations. The least deviation of modeled values from measured ones is reached with relatively low rates for talc and sepiolite precipitation compared to serpentine formation (**Figures 4B–D**). It also becomes clear that apparently phyllosilicate formation is less dependent on the saturation state compared to aragonite precipitation (**Figure 4E**; Equations 3, 4; **Supplementary Table 1**). The fastest precipitation is applied for

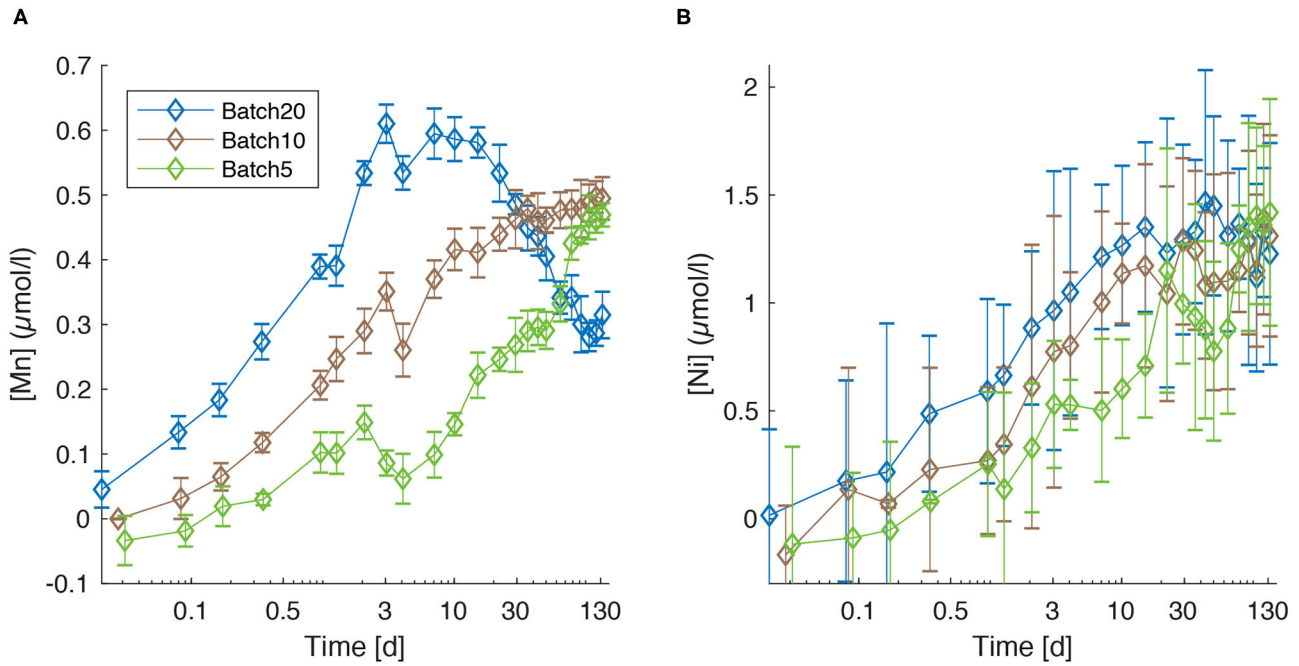

FIGURE 3 | Concentration of dissolved Mn **(A)** and Ni **(B)** for Batch20 (blue), Batch10 (brown), and Batch5 (green). Error bars are reported as ± 2SD.

$Fe(OH)_3$ because dissolved ferrous Fe released from olivine is rapidly oxidized to ferric iron and precipitated as iron hydroxide (**Figures 4A,F**).

The time-integrated rates of olivine dissolution and secondary phase precipitation calculated in the model are employed to derive the overall reaction stoichiometry for each of the three batches:

Batch20:

$$0.77H_2O + \left(Mg_{0.90}Fe_{0.10}\right)_2 SiO_4 + 0.055O_2 + 0.89Ca^{2+} + 0.53CO_2 + 0.36HCO_3^- \rightarrow 0.18Fe(OH)_3 + 0.25Si(OH)_4 + 0.89CaCO_3 + 0.025Mg_2Si_3O_{7.5}\,(OH)\,(H_2O)_3 + 0.32Mg_3Si_2O_5(OH)_4 + 0.0090Mg_3Si_4O_{10}(OH)_2 + 0.016Fe^{3+} + 0.77Mg^{2+} \quad (7)$$

Batch10:

$$0.79H_2O + \left(Mg_{0.90}Fe_{0.10}\right)_2 SiO_4 + 0.055O_2 + 0.98Ca^{2+} + 0.45CO_2 + 0.53HCO_3^- \rightarrow 0.18Fe(OH)_3 + 0.27Si(OH)_4 + 0.98CaCO_3 + 0.021Mg_2Si_3O_{7.5}\,(OH)\,(H_2O)_3 + 0.32Mg_3Si_2O_5(OH)_4 + 0.0061Mg_3Si_4O_{10}(OH)_2 + 0.012Fe^{3+} + 0.77Mg^{2+} \quad (8)$$

Batch5:

$$0.79H_2O + \left(Mg_{0.90}Fe_{0.10}\right)_2 SiO_4 + 0.055O_2 + 0.98Ca^{2+} + 0.51CO_2 + 0.47HCO_3^- \rightarrow 0.19Fe(OH)_3 + 0.32Si(OH)_4 + 0.98CaCO_3 + 0.007Mg_2Si_3O_{7.5}\,(OH)\,(H_2O)_3 + 0.32Mg_3Si_2O_5(OH)_4 + 0.0025Mg_3Si_4O_{10}(OH)_2 + 0.013Fe^{3+} + 0.80Mg^{2+} \quad (9)$$

To verify these model results, the composition of the grayish suspended matter that had formed in the batch reactors was determined applying a simple mixing calculation (Equations 3, 4). Especially the amount of fine-grained UMS in the suspended matter was scrutinized to subsequently estimate the composition of the actual precipitate. In contrast to the UMS procedure, no WDX measurements were performed on the precipitate. Hence, the mixing calculations are only based on XRD scans (**Supplementary Figures 1–4**) and full digestion, followed by ICP-OES measurements (**Supplementary Table 6**). The results of the calculations are presented in **Table 2** and suggest a molar portion of UMS from 25% for Batch5 to 37.5% for Batch10. After the subtraction of these portions the result reveals very similar compositions for all batches with ∼16–23% sepiolite and >70% aragonite as the major components. Minor phases are chrysotile (∼3–4%), $Fe(OH)_3$ (∼3–4%), and Al_2O_3. Even though Al_2O_3 is unlikely to have formed, it was included for the precipitates to match the measured compositions. It is most likely incorporated into the different partly amorphous Mg-Si-phases. Overall, the solid phase data and model results are broadly consistent as both

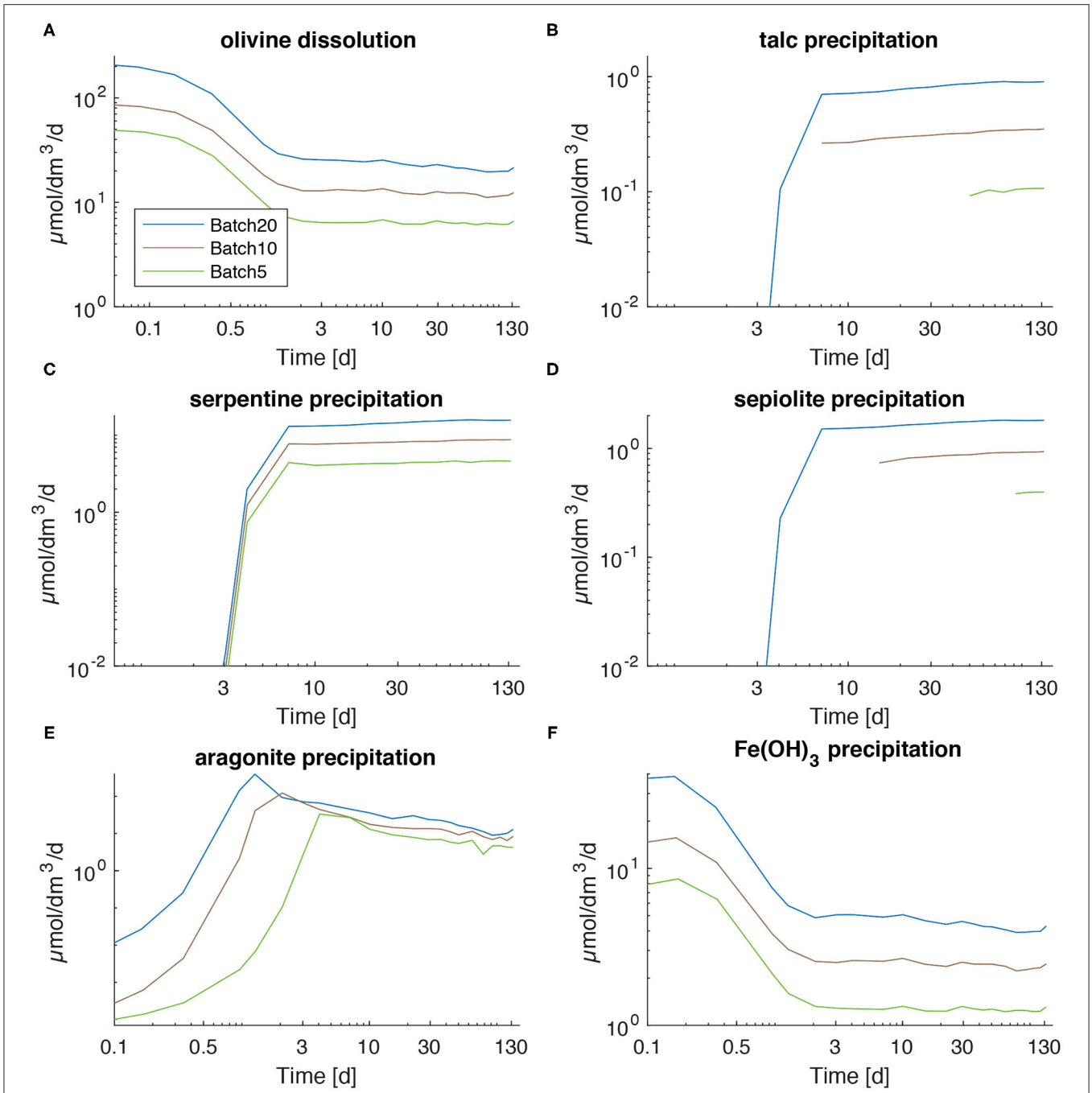

FIGURE 4 | Dissolution rate for olivine **(A)** and precipitation rates for secondary phases **(B–F)** as calculated *via* the model for all batches.

indicate that $CaCO_3$ and a range of Mg-Si phases are the major secondary phases formed during the experiments.

EDX/WDX Observations of Weathered UMS

After 134 days of agitation in batch reactors, grains of UMS were distinctively rounded with secondary mineral phases grown in indentations and fissures (**Figure 5**). The WDX measurement on the blank grain (**Figure 5**a2) revealed that the Mg/Si ratio was elevated for the olivine grain (Mg/Si = 2.33) compared to the pristine value (Mg/Si = 1.78) (**Supplementary Table 5**). The secondary mineral phase measured in inundations clearly indicates calcium carbonate and a very small contribution of iron (**Figure 5**a1).

In **Figure 5b**, the elementary distribution suggests orthopyroxene as host mineral for secondary mineral formation (**Figure 5**b2). Here again, the data clearly indicate that the

TABLE 2 | Calculated composition of suspended matter filtered from batch reactors.

	Component	mol%	% (M)	mol on filter	mg on filter	mol % precipitate
Batch5	UMS	25.00	31.721	0.0258	3.735	
	Sepiolite	12.35	12.229	0.0127	1.440	16.73
	Serpentinite	2.60	3.167	0.0027	0.373	3.52
	Talc	1.10	0.917	0.0011	0.108	1.49
	$CaCO_3$	55.40	48.745	0.0572	5.739	75.07
	$Fe(OH)_3$	2.35	2.146	0.0024	0.253	3.18
	Al_2O_3	1.20	1.076	0.0012	0.127	1.63
Batch10	UMS	37.05	45.762	0.0417	6.014	
	Sepiolite	14.40	13.304	0.0162	1.748	23.34
	Serpentinite	1.10	1.304	0.0012	0.171	1.78
	Talc	0.40	0.325	0.0005	0.043	0.65
	$CaCO_3$	43.40	37.172	0.0488	4.885	70.34
	$Fe(OH)_3$	2.40	2.133	0.0027	0.280	3.89
	Al_2O_3	1.25	1.091	0.0014	0.143	2.03
Batch20	UMS	29.90	37.819	0.0675	9.733	
	Sepiolite	11.10	10.502	0.0190	2.703	16.04
	Serpentinite	2.00	2.428	0.0029	0.625	2.89
	Talc	0.40	0.332	0.0005	0.086	0.58
	$CaCO_3$	53.80	47.189	0.0610	12.145	77.75
	$Fe(OH)_3$	1.90	1.729	0.0020	0.445	2.75
	Al_2O_3	0.90	0.804	0.0009	0.207	1.30

*Values represent mean values of three replicates per batch. For the precise composition of the UMS, see **Table 1**.*

secondary phase is largely composed of calcium carbonate (**Figure 5**b1). The cross-section measured on an altered olivine grain (**Figures 5c–e**) illustrates that the material found on the grains not only consists of calcium carbonates. Instead, it is a heterogenous mixture of different phases with different densities (indicated by different shades of gray, **Figure 5c**). The atomic proportion (relative to 24 oxygen atoms) along the profile (**Figures 5d,e**) indicates a smooth transition from the host material olivine to different Mg-Si phases and back. The smoothness is an artifact of the measuring precision of the micro-probe indicated by the blurred area around the profile line. Hence the material is too fine grained to be examined in detail. Still, the asymmetric increase of Al and Ca indicates the presence of different phases along the profile which is underpinned by the jagged distribution of trace elements along the profile (**Figure 5f**). Overall, the measurements revealed that the agglomerations are most likely a mix of fine-grained UMS remnants cemented with a mix of calcium carbonate and hardly determinable secondary Mg-Si-phases. The examples in **Figure 5** represent typical patterns obtained during a series of measurements.

DISCUSSION

Robustness of Modeled and Measured Results

The consistency of measurements and model results suggests a step forward toward the precise understanding of the processes operating during olivine dissolution in seawater. For the interpretation of the results, however, it is necessary to shine a light on uncertainties. A crucial aspect is the surface area of the olivine grains. Rough edges that originate from the grinding process represent high energy sites which enhance the reactive surface of the grains but are worked off quickly during the early stage of the experiment. Even though, the initially enhanced reactive surface was considered in the kinetic model (**Figure 4A**, **Supplementary Equation 11**), all calculations are based on the geometrical surface area for spherical grains with a diameter of $\sim$100 μm. Hence, the actual reactive surface is most certainly larger than assumed in the kinetic model of olivine dissolution. It is thus possible that the dissolution rates were actually higher than those calculated in the model. Moreover, idealized mineral phases were used in the modeling of authigenic mineral precipitation whereas the solid phase analyses indicate the formation of amorphous phases with a poorly defined composition (**Figure 5**).

Moreover, the model may not consider all processes occurring in the experiment. In general, olivine was assumed to be the only mineral phase that dissolves. Despite the considerably lower dissolution rates of other mineral phases (Lerman et al., 1975; Wolff-Boenisch et al., 2011; Gruber et al., 2019), their dissolution can play an important role at the beginning of the experiment due to the enhanced surface area. The admixture of very fine UMS particles that made up to 30% of the recovered precipitates (**Table 2**) and enhanced surface roughness can lead to a large number of possibly fast initial dissolution-precipitation reactions that might explain fluctuations in elementary concentrations in the early stage of the experiment.

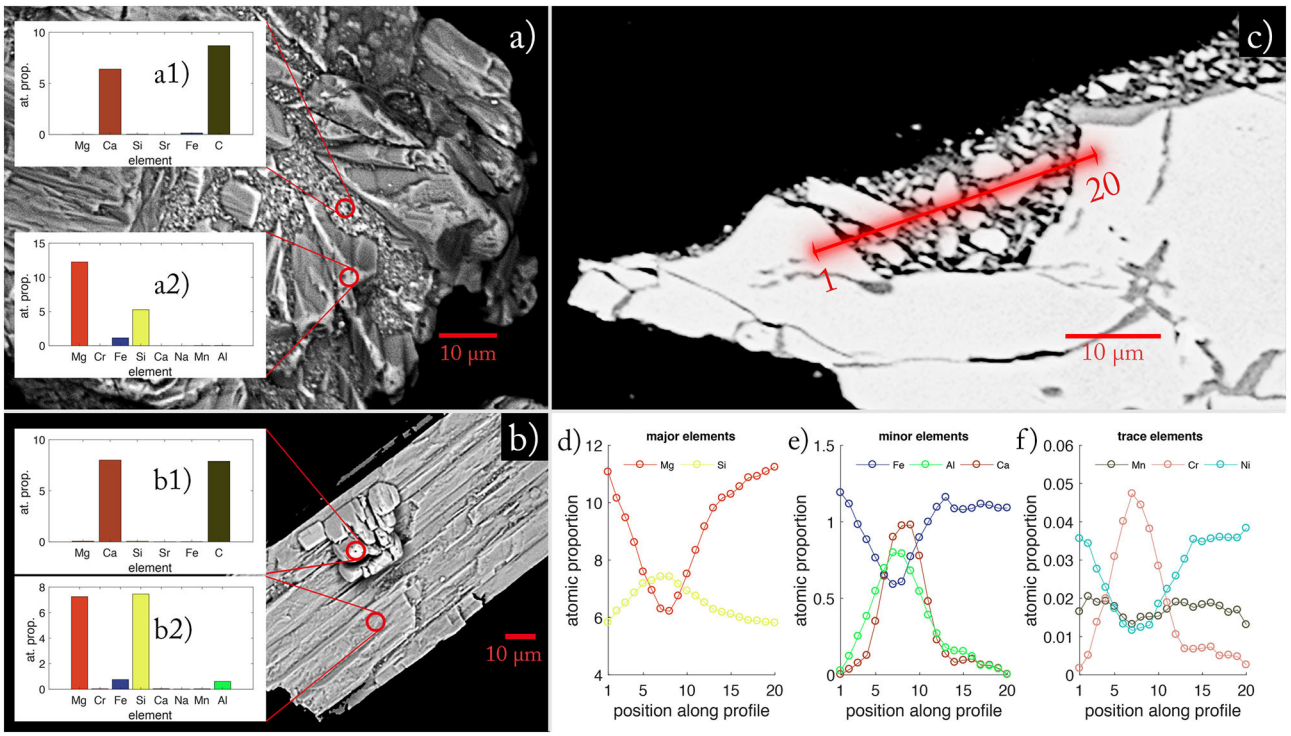

FIGURE 5 | EDX images of reacted UMS grains taken at the end of the experiments. **(a)** Olivine grain with secondary mineral phases. (a1) Atomic proportions in secondary minerals grown on olivine. (a2) Atomic proportion of host mineral. **(b)** Orthopyroxene grain with on-grown aragonite crystal. (b1) Atomic proportion of secondary mineral grown on Orthopyroxene. (b2) Atomic proportion of host mineral for secondary phase (b1). Red circles indicate areas of WDX composition measurements. **(c)** Illustrates the transect through secondary minerals on an olivine grain. The red line denotes the measured transect. **(d)** Shows the atomic proportion of major elements measured along the profile shown in **(c)**. **(e)** Shows the atomic proportion of minor elements measured along the profile shown in **(c)**. **(f)** Shows the atomic proportion of trace elements measured along the profile shown in **(c)**.

Despite these uncertainties, the model is able to reproduce the concentrations of dissolved species measured over the course of the experiments (**Figure 1**). This and the fact that the same kinetic rate laws, functions and parameter values were used for all batches, suggests that the overall stoichiometries derived from the model are adequate.

Secondary Mineral Phases

The major goal of this study was to close the gaps in knowledge regarding the impact of secondary phases on the sequestration efficiency of ESW. Thus, the experiments were designed to allow investigating the precipitation of secondary phases under the following premises:

In order to reduce the number of unknown quantities, ASW was used instead of filtered seawater.

- Commercially available ultramafic sand was used since future large-scale applications of enhanced silicate weathering as CDR measure will rely on widely available rocks rather than purified olivine.
- Different solid-phase/water ratios were applied to investigate the dependency of secondary mineral formation on saturation states.
- A kinetic model was specifically designed to provide a deeper understanding of the kinetics and overall stoichiometry of authigenic mineral formation.

The most striking feature in the data presented in this study are the counterintuitively decreasing TA values (**Figure 1A**) as the weathering of olivine is supposed to lead to the exact opposite (Rimstidt et al., 2012; Köhler et al., 2013; Renforth and Henderson, 2014; Meysman and Montserrat, 2017; Montserrat et al., 2017; Fuss et al., 2018; Oelkers et al., 2018; Rigopoulos et al., 2018). The formation of secondary minerals has been invoked as a possible mechanism to reduce the net gain in TA during olivine weathering (Griffioen, 2017; Meysman and Montserrat, 2017; Montserrat et al., 2017; Oelkers et al., 2018; Torres et al., 2019) but to our knowledge have never been investigated in ASW in great detail. They appear in the form of phyllosilicates and carbonates. In seawater with a low rock/water ratio, the latter ones mainly exist in form of aragonite, calcite and Mg-calcite as these are the major authigenic carbonate phases that are formed in this chemical environment (Lein, 2004; Wallmann et al., 2008; Schrag et al., 2013; Torres et al., 2020). Mg-carbonates can be neglected as they only form under very special conditions mainly in highly alkaline facies with very high rock/water ratios, which do not match our experimental set-up (Moore et al., 2004; Ferrini

et al., 2009; Power et al., 2013; Dehouck et al., 2014; Entezari Zarandi et al., 2017).

Precipitation of $CaCO_3$

The direct comparison of [Ca] and DIC (**Figures 1C**, **2A**) reveals that the decrease in [Ca] is accompanied by a corresponding decrease in DIC. Meanwhile, [Mg] concentrations increased (**Supplementary Figure 5**). Combined with the low Mg/Si ratios in the recovered precipitates (**Supplementary Tables 6, 7**), the most likely explanation for these values is the formation of $CaCO_3$ either in the form of aragonite or calcite, as this process is the only one that has the potential to reduce both C and Ca to an equal amount. This is underlined by the composition of the precipitates (**Table 2**, **Supplementary Table 7**) that were calculated *via* Equations (5) and (6). Stockmann et al. (2014) suggest that forsterite has the potential to foster the nucleation of calcite on its surface. The major difference in the experimental design of Stockmann et al. (2014) and this study is the reagent in which forsterite was dissolved. Whilst in this study ASW with a pH of ∼8 was used, Stockmann et al. (2014) dissolved forsterite in Na-carbonate and Ca-chlorite solutions at a pH of ∼9. XRD measurements of precipitates recovered from the batch reactors in this study revealed no significant calcite content but indicated the presence of aragonite (**Supplementary Figures 1–3**). Despite the fact that these measurements have a very high noise/signal ratio and are therefore fraught with a very large error this is consistent with the findings of Rigopoulos et al. (2018), who found aragonite as the only $CaCO_3$ species in weathering experiments with dunite, and with the fact that aragonite is preferably precipitated in Mg rich solutions (De Choudens-Sánchez and González, 2009; Sun et al., 2015). Mixing calculations revealed that the precipitates recovered from the batch reactors consisted of ∼72% (molar) $CaCO_3$ averaged over all batches, which is very close to the modeled values of ∼65% (molar) as average for all batches. For natural seawater, Burton and Walter (1987) ascertained growth rates of aragonite 3 times higher compared to calcite at 25°C with highest aragonite dominance for calcite saturations of ∼5, which corresponds to the values during the early stage of the experiment of this study. These findings are supported by Zhong and Mucci (1989) who used a different rate equation but found very similar total rates. In order to match measured and modeled [Ca] and TA values, aragonite precipitation needed to be considered in the model used in this study (**Figures 4E**, **6B**). When comparing the rate parameters for aragonite precipitation which lead to the best model fit in this study, with the constants of Burton and Walter (1987), the values were higher compared to the values of Burton and Walter (1987) for Batch20 and Batch10 but matched for Batch5. The slightly higher values in this study indicate possible catalyzation of $CaCO_3$ precipitation on the surface of the UMS grains, as for the same saturation stronger precipitation takes place. Our data clearly show that, contrary to findings of Montserrat et al. (2017), calcium carbonate is formed during the experiments and is responsible for most of the observed TA loss.

Secondary Phyllosilicate and $Fe(OH)_3$ Phases

Next to calcium carbonate, phyllosilicates have the potential to form during olivine weathering (Delvigne et al., 1979; Buurman et al., 1988; Suárez et al., 2011; Hellmann et al., 2012; Sissmann et al., 2013; Griffioen, 2017; Montserrat et al., 2017; Rigopoulos et al., 2018). Hence, precipitation of serpentine, sepiolite and talc is investigated in this study (**Figures 4B–D**). Calculated saturation states vary largely for the different minerals (**Figure 2**). In the model, the precipitation of each mineral depends on the magnitude of oversaturation and a kinetic constant (Lasaga, 1998). The best fit to the Si, Mg, and TA data was reached applying a very small rate constant for talc precipitation compared to rate constants for serpentine and sepiolite. Hence, talc is least represented in the model results (0.25% (molar), averaged over all models). This is fairly congruent to the calculated composition of the recovered precipitates where the average content of talc was 0.89% (molar) (**Table 2**). Large discrepancies between the model and the calculated mineral composition based on measurements occur with regard to the ratio of sepiolite to serpentine $\left(\frac{sep}{serp}\right)$. The numerical model suggests a $\left(\frac{sep}{serp}\right)$ of ∼0.066 (average of all batches) whereas the mineralogic model reveals a $\left(\frac{sep}{serp}\right)$ of 7.8. The saturation states (**Figure 2**) clearly show that ASW was least oversaturated with respect to sepiolite in all batches and undersaturated in Batch10 and Batch5 for at least half the experimental period. Thus, sepiolite appears highly unlikely to be the major precipitated phase (**Figure 4D**).

Hence, the remaining explanation is that a major portion of secondary phases with low Mg/Si ratios had stuck on the grains and was therefore not recovered. This is supported by EDS images (**Figure 5**). Several grains were found that were covered with secondary phases. Next to $CaCO_3$ the WDX analysis of these secondary phases indicates a large variety of Mg-Si-phases. Via their composition, though, these phases could hardly be identified as any of the Si-phases considered in the model.

Also, XRD measurements do not indicate high amounts of the phyllosilicate phases that were considered in the model. It is thus likely that the Mg-Si bearing phases in this study show the same amorphous character as the phases found by Davis et al. (2009) who described a "deweylite assemblage" which stands for a mix of different Mg-silicates whose precise chemical composition can vary strongly (Hövelmann et al., 2011). Thus, the mixed composition of all Si-bearing precipitates could be understood as the composition of a Si-Mg-rich partly amorphous bulk phase, which is well represented by the noisy XRD diffractograms (**Supplementary Figures 1–3**).

Similarly to secondary phyllosilicates, $Fe(OH)_3$ seems to have attached to UMS grains, as the measured (and subsequently calculated) content of $Fe(OH)_3$ in the suspended matter recovered from the batch reactors was ∼3% on average and the model calculated ∼13% (averaged over all batches). This is evidenced by little dense flakes that were found on the weathered grains during EDX/WDX measurements that consisted mainly of Fe and is supported by the fact that less precipitate was recovered, than the suggested by the model. Like the precipitation of

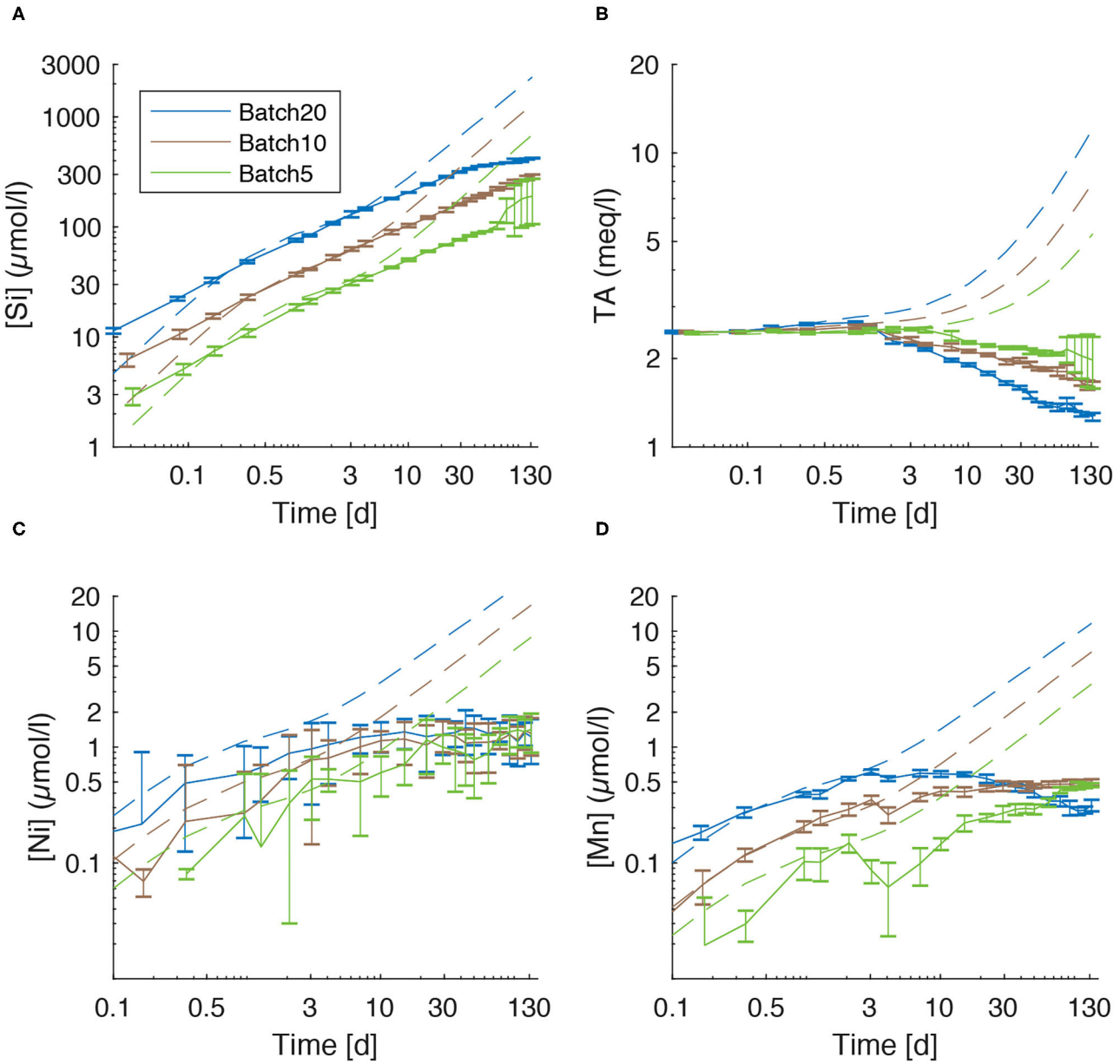

FIGURE 6 | Comparison of measured values (solid lines) for dissolved species and modeled concentrations that would result from congruent dissolution of UMS without formation of secondary minerals (dashed lines). **(A)** silicon, **(B)** TA, **(C)** nickel, and **(D)** manganese.

phyllosilicates and carbonates, the formation of $Fe(OH)_3$ releases protons. It is therefore important to consider this process with regards to the overall efficiency of enhanced silicate weathering.

Dissolution Kinetics of Olivine

Over the first 2–4 days of the experiments dissolved [Si] and TA values are close to those predicted by the kinetic rate law for olivine dissolution used in our model (Rimstidt et al., 2012). However, the measured concentrations are significantly lower than the predicted value over the following period (**Figures 6A,B**) This observation could in principle either be explained by a decline in the olivine dissolution rate due to surface passivation/occupation by secondary minerals, or by the removal of Si and TA from solution *via* precipitation of secondary minerals.

Montserrat et al. (2017), whose experiment A3 was very similar to the experiments of this study, proposed a dissolution rate for olivine in dependence of the changing saturation state with respect to olivine that was calculated after Palandri and Kharaka (2004). For the validation of this hypothesis, they

fitted their model to the accumulation of Si in solution $\left(\frac{d[Si]}{dT}\right)$, regardless of Si removal by secondary phases. The outcome is a good approximation of the apparent dissolution rate.

A passivation of the surface as a result of incongruent weathering has previously been invoked as one explanation for the decrease in dissolution rate over time (Wolff-Boenisch et al., 2011; Hellmann et al., 2012; Maher et al., 2016; Montserrat et al., 2017). Apart from Mg isotopes (Hellmann et al., 2012), which were not measured in this study, one indication for such processes is the cation depletion of the reactive surface of the olivine grains after the weathering process. Hellmann et al. (2012) as well as Maher et al. (2016) used HCl and NaCl solutions respectively which did not contain Mg. Likewise, Montserrat et al. (2017) reported highest Mg depletion on reactive surfaces for experiments with Mg-reduced ASW. Extensive WDX measurements applied in this study have not revealed such depletion. Instead, highest Mg/Fe ratios in olivine were measured on blank surfaces of weathered olivine that were not covered with secondary mineral phases (**Figure 5**a2). Thus, the depletion and subsequent passivation of forsterite surfaces observed in other studies during dissolution seems to be a result of diffusive equilibration between a depleted reagent and the crystal surface. This effect did not occur in in our study, as the background activity of Mg is very high in ASW (Millero et al., 2008). Hence, following the idea of an equilibrated steady state for surface layers (Maher et al., 2016), olivine grains might as well be considered a temporary sink for Mg, assuming the diffusive replacement of Fe^{2+} with Mg^{2+} supplied from the ambient seawater, similar to the process of Mg-replacement by H^{+} described by Oelkers et al. (2018). Additionally, elevated (Mg+Fe)/Si ratios point toward the results of Pokrovsky and Schott (2000), who described the preferential release of Si during the early stage of dissolution (100 days in their experiment) for non-acidic solutions.

Further passivation of the grain surface due to occupation with secondary minerals (Béarat et al., 2006; King et al., 2010; Sissmann et al., 2013; Oelkers et al., 2018) appears unlikely as the portion of reactive surface covered by authigenic phases was relatively small in this study (data not shown). Considering these observations and the solid phase data that were obtained in our experimental set-up, it is likely that most of the Si and TA deficit (**Figures 6A,B**) in the dissolved phase is induced by the precipitation of secondary phases rather than a decline in dissolution rate.

Fate of Nickel and Its Usability as a Dissolution Proxy

Ni concentrations were suggested as a possible proxy for olivine dissolution by Montserrat et al. (2017). The comparison of [Ni] values (**Figures 3B**, **6C**), though, clearly shows that the accumulation of Ni is not proportional to the amount of dissolved olivine calculated by the model (**Supplementary Tables 11–13**) and not even proportional to the accumulation of [Si] in solution (**Figures 1B**, **6A**). Incongruent weathering of olivine (Montserrat et al., 2017) can be excluded as, during the early stage of the experiment and thus before the precipitation of secondary minerals started, the accumulation of dissolved Si and Mn (which have a satisfyingly small 2SD) are proportional to the amount of olivine used in the experiments. Now under the assumption of congruent weathering, the expected [Ni] values would be 5.70 μmol/l for Batch20, 4.28 μmol/l for Batch10, and 2.26 μmol/l for Batch5. The measured values were significantly lower (**Figure 3B**). Therefore, some removal process must be operating, that is apparently strongest in Batch20 and weakest in Batch5, leading to values that are identical within the error in all batches at the end of the experiment. Ni and Mn can be adsorbed on the surface of phyllosilicate phases, FeOOH and $CaCO_3$ and incorporated in the crystal lattice of calcite and aragonite during carbonate precipitation (Hoffmann and Stipp, 2001; Lakshtanov and Stipp, 2007; Lazarević et al., 2010; Castillo Alvarez et al., 2020; Alvarez et al., 2021). Carré et al. (2017) even proposed aragonite precipitation as a way to remove dissolved Ni from seawater. Therefore, it is likely that the Ni and Mn deficits (**Figures 6C,D**) observed at the end of the experiments are due to uptake of these trace elements in authigenic $CaCO_3$, Mg-Si and FeOOH phases.

As a conclusion, it becomes clear that the variety of processes affecting Ni and Mn concentrations in batch experiments excludes both as a reliable proxy for olivine dissolution rate determination. However, the proposed strong Ni uptake in authigenic phases reduces toxic metal release that would limit the applicability of olivine weathering for CO_2 sequestration (Blewett and Leonard, 2017).

Sequestration Efficiency

In a first approach the CO_2 conversion observed in the experiments (R_{ex}) can be expressed as a function of total inorganic carbon (TIC) following:

$$R_{ex} = \Delta TIC = (DIC_{final} + PIC_{final}) - (DIC_{ini} + \sum_j (DIC_{ini} * 0.007 - DIC\,(t)\, * 0.007)) \quad (10)$$

where DIC_{final} is the DIC at the end of the experiment, PIC_{final} is the amount of particulate inorganic carbon in form of $CaCO_3$ at the end of the experiment and DIC_{ini} is the initial DIC at the beginning of the experiment. $\sum_j (DIC_{ini} * 0.007 - DIC\,(t)\, * 0.007)$ represents the amount of DIC added during sample taking (0.007 l per sample).

PIC_{final} was calculated *via* the entire [Ca] loss during the experiment following,

$$PIC_{final} = [Ca]_{ini} - [Ca]_{final} + \sum_j ([Ca]_{in}\,(t) * 0.007 - [Ca]\,(t)\, * 0.007) \quad (11)$$

where $[Ca]_{ini}$ is the initial Ca concentration, $[Ca]_{final}$ is the final concentration and $[Ca]_{in}\,(t)$ is the function of the Ca input derived on sample taking that changes over time. The calculated net uptake was 0.21 mmol (Batch20), 0.166 mmol (Batch10), and 0.143 mmol (Batch5). Still, these values derive from a quasi-closed system with very limited CO_2 supply.

Hence, the efficiency of CO_2 uptake was investigated using a 1-box model where olivine with a grain diameter of 100 μm is dissolved in a 50 m deep water layer representative for the coastal ocean. The model box defines the seafloor at 50 m water depth. Hence, settling olivine grains that are rapidly deposited at the seafloor (Köhler et al., 2013) are kept within the system and continuously take part in the dissolution process. Hence, all olivine grains contribute equally to the overall dissolution rate whether they are kept in suspension or deposited at the seabed (Feng et al., 2017). Concentration and grain size of olivine were kept constant over the simulation period, for simplicity reasons. It is, thus, assumed that new olivine is added to the system to compensate for any olivine loss induced by dissolution. The concentration of olivine in the model box was set to a constant value of 10 mg dm^{-3} and the box was equilibrated with the atmosphere by applying a constant atmospheric pCO_2 of 400 μatm.

Mass balance equations (ordinary differential equations) for TA and DIC were set up and solved numerically to simulate temporal changes in DIC and TA. The TA mass balance considers TA production *via* olivine dissolution (4 × olivine dissolution rate) with the olivine dissolution rate depending on olivine concentration, grain size, temperature and pH (Rimstidt et al., 2012). TA consumption *via* authigenic mineral formation is considered applying the stoichiometry derived from dissolution experiments (Batch10, Equation 8). Rates of mineral precipitation were calculated from olivine dissolution rates applying the corresponding stoichiometric coefficient. The DIC mass balance considers DIC removal *via* $CaCO_3$ precipitation and DIC gain induced by CO_2 uptake from the atmosphere.

Initial values applied in the model (salinity: 34.77, temperature: 17.88°C, pressure: 1 bar, total alkalinity: 2,308 μmol kg^{-1}, total boron: 415 μmol kg^{-1}) correspond to the mean composition of surface water in the global ocean (Spivack and Edmond, 1987; Sarmiento and Gruber, 2006). The initial DIC concentration was set to 2,053 μmol kg^{-1} to obtain an initial pCO_2 of 400 μatm in surface water. Equilibrium calculations were conducted using stability constants valid for seawater (Zeebe and Wolf-Gladrow, 2001). Total alkalinity (TA) was defined as:

$$TA = HCO_3^- + 2CO_3^- + B(OH)_4^- + OH^- - H^+ \quad (12)$$

while CO_2 uptake from the atmosphere was calculated as:

$$FCO_2 = v_p(CO_2\,(eq) - CO_2) \quad (13)$$

where v_P is the piston velocity [20 cm h^{-1} (Sarmiento and Gruber, 2006)], CO_2(eq) is the concentration of dissolved CO_2 at equilibrium with the atmosphere and CO_2 is the time-dependent concentration calculated from TA and DIC (Sarmiento and Gruber, 2006).

In a first model run, olivine dissolution was simulated without secondary mineral formation to constrain the loss in CO_2 uptake efficiency induced by the buffer capacity of seawater (Middelburg et al., 2020). The efficiency (eff) is calculated as the ratio of the CO_2 uptake flux (FCO_2) and the depth-integrated rate of CO_2 consumption (RCO_2) induced by olivine dissolution ($RCO_2 = 4$ x olivine dissolution rate, $eff = FCO_2/RCO_2$). The model was run over a period of 10 years to equilibrate the water column with the overlying atmosphere (**Figure 7**). The shift in acid-base equilibria induced by olivine-driven CO_2 consumption (e.g., $2HCO_3^- \rightarrow CO_2 + CO_3^{2-} + H_2O$) reduces the efficiency by about 42% at the end of the simulation period. TA and DIC increase continuously due to alkalinity release by olivine dissolution and CO_2 uptake from the atmosphere, respectively, while the CO_2 uptake flux approaches a plateau after the water column is equilibrated with the atmosphere. The depth-integrated rate of olivine dissolution was almost constant over the model run. The small increase in pH from 8.035 at the start to 8.075 at the end of simulation (data not shown) induced a small decrease in RCO_2 from an initial value of 147 mmol m^{-2} yr^{-1} to a final value of 145 mmol m^{-2} yr^{-1}.

In a second model run, precipitation of ferric iron oxides and Si-Mg-phases was implemented employing the stoichiometry derived from batch experiments (batch10, Equation 8). Precipitation of ferric iron oxides and Si-Mg-phases strongly affects the model results. The increase in TA and DIC is reduced, whereas CO_2 uptake and CO_2 efficiency are strongly diminished since protons are released during the precipitation reactions. The efficiency at the end of the model period decreased from 0.58 in the model run without secondary mineral formation to only 0.25. Most of the efficiency loss is caused by the precipitation of Mg-Si-phases that consumes large amounts of alkalinity due to the strong proton release induced by these reactions (6 mol H^+ per mol of serpentinite/talc, 4 mol H^+ per mol of sepiolite).

In a final model run, all secondary phases including $CaCO_3$ are allowed to precipitate. $CaCO_3$ formation has a strong effect on solution composition and induces a decline in both TA and DIC. The CO_2 uptake is further reduced such that the efficiency drops to 0.21 after 10 years. $CaCO_3$ formation has a smaller effect on CO_2 fluxes than Mg-Si-phase precipitation even though $CaCO_3$ is the major secondary phase formed during the experiments. This somewhat surprising model result is related to the acid-base stoichiometry of carbonate precipitation where only two moles of alkalinity are removed per mol of $CaCO_3$, while the coeval DIC loss promotes CO_2 uptake from the atmosphere.

Additional model runs were conducted to explore the effects of olivine concentration (1–1,000 mg dm^{-3}) and grain size (10–100 μM) on CO_2 uptake efficiency (data not shown). The experiments showed that olivine dissolution rates and CO_2 uptake fluxes strongly increase when higher concentrations and smaller grain sizes are applied. However, the CO_2 uptake efficiency was constant (0.21) over the explored parameter space when the stoichiometry derived from our lab experiments was applied. Hence, the low efficiency obtained in the box model simulations seems to be a robust result, if the overall stoichiometry that we observed in our lab experiments is also valid in the field. There are, however, a number of factors that may induce a change in the rates of olivine dissolution and secondary mineral precipitation. Hence, the solid/liquid ratio and the rates of water replacement, CO_2 uptake from the atmosphere and biological activity may affect the ratios between

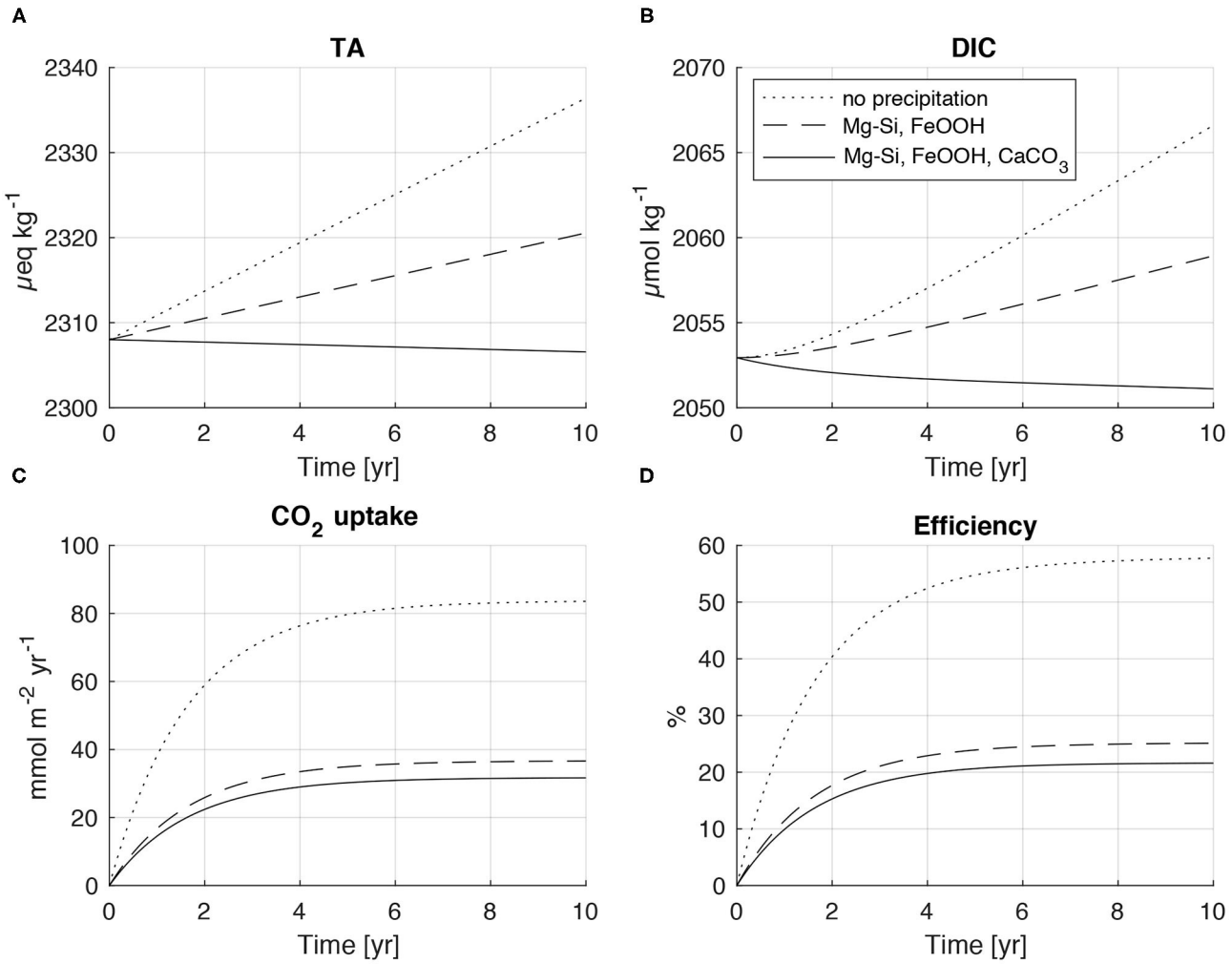

FIGURE 7 | Model experiments simulating the effect of olivine dissolution on seawater composition and CO_2 uptake from the atmosphere. Dotted lines show results for a model run without secondary mineral formation. Broken lines represent model results for the precipitation of ferric iron oxides (FeOOH) and Mg-Si-phases (serpentinite, talc, sepiolite). Solid lines indicate the results for a model run where all authigenic phases (FeOOH, Mg-Si-phases, $CaCO_3$) precipitate according to the stoichiometry observed in our lab experiments. **(A)** Total alkalinity. **(B)** Dissolved inorganic carbon. **(C)** CO_2 uptake from the atmosphere (FCO_2). **(D)** Efficiency of CO_2 uptake is defined as FCO_2/RCO_2 where RCO_2 is the depth-integrated rate of CO_2 consumption induced by olivine dissolution (= 4 x olivine dissolution rate).

dissolution and precipitation reactions. These factors should be investigated in future lab and field experiments.

Implications for Field Application

The experimental results of this study show that precipitation of secondary minerals ($CaCO_3$, Mg-Si-phases, FeOOH) compromises the efficiency of CO_2 uptake by olivine dissolution. It should, however be noted that the stoichiometry that we observed in our lab experiments may not be valid for all field conditions. Moreover, we found higher rates of alkalinity removal than previous studies with pure olivine that were conducted under comparable experimental conditions (Montserrat et al., 2017). This observation may be due to the high solid/solution ratios applied in our experiments and could be related to the fact that we used commercially available olivine (UMS) that was not pure but contained a number of accessory minerals. Our use of ultramafic sand rather than pure olivine may be justified since large-scale CDR will probably not be conducted with pure olivine but with rocks containing other minerals and impurities. The range of dissolved Si concentrations attained in our experiments (**Figure 1**) is similar to the concentrations observed in bioturbated surface sediments (Dale et al., 2021). Since grains added to seawater will rapidly sink to the seafloor where they are mixed into surface sediments by benthic biota, the experimental conditions may be close to those in benthic habitats where most of the dissolution is expected to occur.

Precipitation rates of authigenic Mg-Si-phases may be lower than observed in our experiments, though, when olivine is

applied to highly dynamic environments such as the coastal zone (beaches, surf zones), where dissolution products are rapidly removed (Hangx and Spiers, 2009; Meysman and Montserrat, 2017; Montserrat et al., 2017). It is, however, possible that $CaCO_3$ precipitation may also occur in these coastal environments since our data imply that carbonate precipitation is catalyzed by olivine surfaces even at low degrees of aragonite oversaturation. Further work is needed to scrutinize whether the abrasive effects of wave action may suppress $CaCO_3$ precipitation (Meysman and Montserrat, 2017).

Anyhow, fine-grained olivine added to the shelf environment will ultimately be transported by bottom currents to local depo-centers where low bottom current velocities allow for the permanent burial of sediments. These environments are marked by high accumulation rates of both sediments and organic matter (De Haas et al., 2002). The low pH values induced by the release of metabolic CO_2 during organic matter degradation largely inhibit $CaCO_3$ precipitation in these sedimentary environments while FeOOH formation is limited to surface sediments due to the reducing conditions prevailing in these deposits (Van Cappellen and Wang, 1996; Silburn et al., 2017). However, authigenic Mg-Si- phases and clays are formed in these benthic environments (Michalopoulos and Aller, 1995). Since the formation of cation-rich phases induces CO_2 release, the overall efficiency of CO_2 uptake might be strongly diminished as observed in our experiments. It is, hence, possible that, when applied in the field, olivine weathering is less efficient than previously believed. On the other hand, adverse environmental effects may be smaller than previously anticipated since data obtained during the experiments in this study indicate that Ni and other toxic metals will largely be fixed in authigenic phases. However, more work needs to be done to explore how variable conditions in pelagic and benthic environments may affect the ratio between olivine dissolution and authigenic mineral precipitation and, hence, the efficiency of CO_2 uptake from the atmosphere and the rate of toxic metal release.

SUMMARY, CONCLUSION AND OUTLOOK

This study presents a first dedicated attempt to investigate the formation of secondary mineral phases in artificial seawater (ASW) during olivine weathering. For this purpose, ultramafic sand (UMS) was brought to reaction with ASW applying different solid/liquid ratios. The results strongly suggest the formation of $CaCO_3$, as evidenced by the congruent loss of Ca and DIC observed over the course of the experiments. XRD measurements suggest, that aragonite is the major $CaCO_3$ species precipitated which is underlined by the fact that this variation is more likely to be precipitated in Mg-rich solutions. This is further supported by WDX measurements that showed pure $CaCO_3$ crystals on the surface of weathered olivine grains. These observations are confirmed by the results of a numerical model that simulated the dissolution of olivine and the precipitation of several secondary mineral phases including aragonite. Moreover, the model results allowed estimating the overall stoichiometry of the combined dissolution-precipitation reaction. The thorough analysis of ASW and precipitates recovered from the batch reactors underline that Si-bearing phases must also have formed during the experiment. The precise character (amorphous or crystalline) and chemical composition of these phases, though, afford further dedicated studies. Via the different accumulation rates of Ni in the different batches, this study revealed that these secondary mineral phases most likely are a major sink for this toxic element, excluding it as a proxy for olivine dissolution rates. This makes the precise knowledge of secondary phase formation and characteristics crucial for the feasibility of enhanced olivine weathering on the one hand and for the understanding of the dissolution kinetics of olivine on the other. Experimental combined with modeling results suggest that the formation of secondary phases lowers the overall sequestration efficiency to ∼20% during the application of enhanced olivine weathering in a shallow shelf sea. This bears implications for possible application sites, as not only physical parameters, but, more importantly, chemical parameters in the field steer secondary mineral formation and thus the overall efficiency.

Sandy shelf sediments and specifically the surf zone may be appropriate sites for enhanced olivine dissolution since the flushing of surface sediments by ambient bottom waters may mitigate the accumulation of dissolution products and the formation of secondary silicate and carbonate minerals in these permeable and physically dynamic deposits. Alternatively, application sites where pore and or bottom waters are undersaturated with respect to the major secondary phases would be a promising target for enhanced coastal weathering of olivine.

Our experimental and modeling results hence indicate that it may be promising to also investigate $CaCO_3$ as alkaline mineral for CO_2 removal since secondary mineral formation is usually not observed during $CaCO_3$ dissolution. $CaCO_3$ could be added to sediment depo-centers on the shelf where large amounts of metabolic CO_2 are formed (about 3 Pg yr^{-1} at global scale) that can be converted into bicarbonate by $CaCO_3$ dissolution (Dunne et al., 2007). This process would accelerate the CO_2 shelf pump (Bozec et al., 2005) and promote further CO_2 uptake from the atmosphere. This approach may be most successful in marine environments where bottom waters are enriched in CO_2 and undersaturated with respect to calcite and aragonite. These conditions occur, e.g., in oxygen minimum zones and partly anoxic marginal basins such as the Baltic Sea (Tyrrell et al., 2008). The CO_2 release from Baltic Sea sediments amounts to 80 Tg yr^{-1} (Nilsson et al., 2019). The addition of a corresponding amount of $CaCO_3$ may thus dramatically enhance CO_2 uptake from the atmosphere. Moreover, $CaCO_3$ addition may support the formation of authigenic carbonate fluorapatite and could thereby reduce benthic phosphate fluxes (Ruttenberg and Berner, 1993). Hence, $CaCO_3$ addition may mitigate eutrophication, which is a major problem in many shelf regions, while olivine addition would promote Si and Fe release and potentially amplify eutrophication. Further lab studies, field experiments and numerical modeling also focusing on the biological impact are needed to better constrain the efficiency and environmental effects of these CDR approaches and their large-scale applicability.

DATA AVAILABILITY STATEMENT

The original contributions presented in the study are included in the article/**Supplementary Materials**, further inquiries can be directed to the corresponding author.

AUTHOR CONTRIBUTIONS

MF carried out the experiments, processed most of the samples in the laboratory, and wrote the manuscript. SG helped with sample preparation in the clean-lab and contributed with discussions. MS supervised XRD interpretation and contributed with discussions. VL initiated and supervised EDX/WDX measurements and contributed with discussions. CV supported XRD interpretation. BL carried out additional XRD measurements and helped with XRD interpretation. KW designed the numerical models used in this study and contributed with discussions. All authors contributed to the article and approved the submitted version.

FUNDING

This study was funded by the Bundesministerium für Bildung und Forschung (BMBF) (Project RETAKE, granted to SG) in the framework of the Deutsche Allianz für Meeresforschung (DAM) mission CDRmare.

ACKNOWLEDGMENTS

We would like to thank Philipp Böning (ICBM, Oldenburg) for carrying out XRF measurements and interpretation. We also acknowledge Anke Bleyer (GEOMAR), Bettina Domeyer (GEOMAR), and Regina Surberg (GEOMAR) for their help with technical and analytical procedures in the clean laboratory, respectively. Additionally we thank Mario Thöner (GEOMAR) for his great support during EDX/WDX measurements. In deep mourning we commemorate our dear friend and highly respected and regarded colleague VL who deceased short before the publication of this study. Our thoughts are with his family and beloved ones.

SUPPLEMENTARY MATERIAL

The Supplementary Material for this article can be found online at: https://www.frontiersin.org/articles/10.3389/fclim.2022.831587/full#supplementary-material

REFERENCES

Alvarez, C. C., Quitté, G., Schott, J., and Oelkers, E. H. (2021). Nickel isotope fractionation as a function of carbonate growth rate during Ni coprecipitation with calcite. *Geochim. Cosmochim. Acta* 299, 184–198. doi: 10.1016/j.gca.2021.02.019

Amann, T., Hartmann, J., Struyf, E., De Oliveira Garcia, W., Fischer, E. K., Janssens, I., et al. (2020). Enhanced weathering and related element fluxes - a cropland mesocosm approach. *Biogeosciences* 17, 103–119. doi: 10.5194/bg-17-103-2020

Béarat, H., J., McKelvy, M., V. G., Chizmeshya, A., Gormley, D., et al. (2006). Carbon sequestration via aqueous olivine mineral carbonation: role of passivating layer formation. *Environ. Sci. Technol.* 40, 4802–4808. doi: 10.1021/es0523340

Blewett, T. A., and Leonard, E. M. (2017). Mechanisms of nickel toxicity to fish and invertebrates in marine and estuarine waters. *Environ. Pollut.* 223, 311–322. doi: 10.1016/j.envpol.2017.01.028

Bozec, Y., Thomas, H., Elkalay, K., and De Baar, H. J. W. (2005). The continental shelf pump for CO2 in the North Sea-evidence from summer observation. *Mar. Chem.* 93, 131–147. doi: 10.1016/j.marchem.2004.07.006

Burton, E. A., and Walter, L. M. (1987). Relative precipitation rates of aragonite and Mg calcite from seawater: Temperature or carbonate ion control? *Geology* 15, 111–114. doi: 10.1130/0091-7613(1987)15<111:RPROAA>2.0.CO;2

Buurman, P., Meijer, E. L., and Wijck, J. H. V. (1988). Weathering of chlorite and vermiculite in ultramafic rocks of Cabo Ortegal, northwestern Spain. *Clays Clay Miner.* 36, 263–269. doi: 10.1346/CCMN.1988.0360308

Carré, C., Gunkel-Grillon, P., Serres, A., Jeannin, M., Sabot, R., and Quiniou, T. (2017). Calcareous electrochemical precipitation, a new method to trap nickel in seawater. *Environ. Chem. Lett.* 15, 151–156. doi: 10.1007/s10311-016-0602-2

Castillo Alvarez, C., Quitté, G., Schott, J., and Oelkers, E. H. (2020). Experimental determination of Ni isotope fractionation during Ni adsorption from an aqueous fluid onto calcite surfaces. *Geochim. Cosmochim. Acta* 273, 26–36. doi: 10.1016/j.gca.2020.01.010

Dale, A. W., Paul, K. M., Clemens, D., Scholz, F., Schroller-Lomnitz, U., Wallmann, K., et al. (2021). Recycling and burial of biogenic silica in an open margin oxygen minimum zone. *Global Biogeochem. Cycles* 35, e2020GB006583. doi: 10.1029/2020GB006583

Davis, M. C., Brouwer, W. J., Wesolowski, D. J., Anovitz, L. M., Lipton, A. S., and Mueller, K. T. (2009). Magnesium silicate dissolution investigated by 29Si MAS, 1H-29Si CPMAS, 25Mg QCPMG, and 1H-25Mg CP QCPMG NMR. *Phys. Chem. Chem. Phys.* 11, 7013–7021. doi: 10.1039/b907494e

De Choudens-Sánchez, V., and González, L. A. (2009). Calcite and aragonite precipitation under controlled instantaneous supersaturation: elucidating the role of CaCO3 saturation state and Mg/Ca ratio on calcium carbonate polymorphism. *J. Sediment. Res.* 79, 363–376. doi: 10.2110/jsr.2009.043

De Haas, H., Van Weering, T. C. E., and De Stigter, H. (2002). Organic carbon in shelf seas: sinks or sources, processes and products. *Cont. Shelf Res.* 22, 691–717. doi: 10.1016/S0278-4343(01)00093-0

Dehouck, E., Gaudin, A., Mangold, N., Lajaunie, L., Dauzères, A., Grauby, O., et al. (2014). Weathering of olivine under CO2 atmosphere: a martian perspective. *Geochim. Cosmochim. Acta* 135, 170–189. doi: 10.1016/j.gca.2014.03.032

Delvigne, J., Bisdom, E. B. A., Sleeman, J., and Stoops, G. (1979). Olivines, their pseudomorphs and secondary products. *Pedologie* 29, 247–309.

Dickson, A. G. (1993). pH buffers for sea water media based on the total hydrogen ion concentration scale. *Deep Sea Res. Part I Oceanogr. Res. Pap.* 40, 107–118. doi: 10.1016/0967-0637(93)90055-8

Dunne, J. P., Sarmiento, J. L., and Gnanadesikan, A. (2007). A synthesis of global particle export from the surface ocean and cycling through the ocean interior and on the seafloor. *Global Biogeochem. Cycles* 21:GB4006. doi: 10.1029/2006GB002907

Entezari Zarandi, A., Larachi, F., Beaudoin, G., Plante, B., and Sciortino, M. (2017). Nesquehonite as a carbon sink in ambient mineral carbonation of ultramafic mining wastes. *Chem. Eng. J.* 314, 160–168. doi: 10.1016/j.cej.2017.01.003

Feely, R. A., Sabine, C. L., Byrne, R. H., Millero, F. J., Dickson, A. G., Wanninkhof, R., et al. (2012). Decadal changes in the aragonite and calcite saturation state of the Pacific Ocean. *Global Biogeochem. Cycles* 26:GB3001. doi: 10.1029/2011GB004157

Feldman, D. R., Collins, W. D., Gero, P. J., Torn, M. S., Mlawer, E. J., and Shippert, T. R. (2015). Observational determination of surface radiative forcing by CO2 from 2000 to 2010. *Nature* 519, 339–343. doi: 10.1038/nature14240

Feng, E. Y., Koeve, W., Keller, D. P., and Oschlies, A. (2017). Model-based assessment of the CO2 sequestration potential of coastal ocean Alkalinization. *Earth. Futur.* 5, 1252–1266. doi: 10.1002/2017EF000659

Ferrini, V., De Vito, C., and Mignardi, S. (2009). Synthesis of nesquehonite by reaction of gaseous CO2 with Mg chloride solution: Its potential role in the sequestration of carbon dioxide. *J. Hazard. Mater.* 168, 832–837. doi: 10.1016/j.jhazmat.2009.02.103

Flipkens, G., Blust, R., and Town, R. M. (2021). Deriving nickel (Ni(II)) and chromium (Cr(III)) based environmentally safe olivine guidelines for coastal enhanced silicate weathering. *Environ. Sci. Technol.* 55, 12362–12371. doi: 10.1021/acs.est.1c02974

Friedlingstein, P., Solomon, S., Plattner, G.-K., Knutti, R., Ciais, P., and Raupach, M. R. (2011). Long-term climate implications of twenty-first century options for carbon dioxide emission mitigation. *Nat. Clim. Chang.* 1, 457–461. doi: 10.1038/nclimate1302

Fuss, S., Lamb, W. F., Callaghan, M. W., Hilaire, J., Creutzig, F., Amann, T., et al. (2018). Negative emissions - part 2: Costs, potentials and side effects. *Environ. Res. Lett.* 13:063002. doi: 10.1088/1748-9326/aabf9f

Gieskes, J., Gamo, T., and Brumsack, H. (1991). *Chemical Methods for Interstitial Water Analysis Aboard JOIDES Resolution.* ODP Tech Note 15. doi: 10.2973/odp.tn.15.1991

Govindaraju, K. (1994). (1994). Compilation of working values and sample description for 383 geostandards. *Geostand. Newsl.* 18, 1–158. doi: 10.1046/j.1365-2494.1998.53202081.x-i1

Griffioen, J. (2017). Enhanced weathering of olivine in seawater: the efficiency as revealed by thermodynamic scenario analysis. *Sci. Total Environ.* 575, 536–544. doi: 10.1016/j.scitotenv.2016.09.008

Gruber, C., Harlavan, Y., Pousty, D., Winkler, D., and Ganor, J. (2019). Enhanced chemical weathering of albite under seawater conditions and its potential effect on the Sr ocean budget. *Geochim. Cosmochim. Acta* 261, 20–34. doi: 10.1016/j.gca.2019.06.049

Hangx, S. J. T., and Spiers, C. J. (2009). Coastal spreading of olivine to control atmospheric CO2 concentrations: a critical analysis of viability. *Int. J. Greenh. Gas Control* 3, 757–767. doi: 10.1016/j.ijggc.2009.07.001

Hartmann, J., and Kempe, S. (2008). What is the maximum potential for CO 2 sequestration by "stimulated" weathering on the global scale? *Naturwissenschaften* 95, 1159–1164. doi: 10.1007/s00114-008-0434-4

Hartmann, J., West, A. J., Renforth, P., Köhler, P., De La Rocha, C. L., Wolf-Gladrow, D. A., et al. (2013). Enhanced chemical weathering as a geoengineering strategy to reduce atmospheric carbon dioxide, supply nutrients, and mitigate ocean acidification. *Rev. Geophys.* 51, 113–149. doi: 10.1002/rog.20004

Hellmann, R., Wirth, R., Daval, D., Barnes, J. P., Penisson, J. M., Tisserand, D., et al. (2012). Unifying natural and laboratory chemical weathering with interfacial dissolution-reprecipitation: a study based on the nanometer-scale chemistry of fluid-silicate interfaces. *Chem. Geol.* 294–295, 203–216. doi: 10.1016/j.chemgeo.2011.12.002

Hoffmann, U., and Stipp, S. L. S. (2001). The behavior of Ni2+ on calcite surfaces. *Geochim. Cosmochim. Acta* 65, 4131–4139. doi: 10.1016/S0016-7037(01)00691-3

Hövelmann, J., Austrheim, H., Beinlich, A., and Anne Munz, I. (2011). Experimental study of the carbonation of partially serpentinized and weathered peridotites. *Geochim. Cosmochim. Acta* 75, 6760–6779. doi: 10.1016/j.gca.2011.08.032

Howe, J. P. (2015). This is nature; This is un-nature: reading the keeling curve. *Environ. Hist. Durh. N. C.* 20, 286–293. doi: 10.1093/envhis/emv005

Iizuka, A., Fujii, M., Yamasaki, A., and Yanagisawa, Y. (2004). Development of a new CO2 sequestration process utilizing the carbonation of waste cement. *Ind. Eng. Chem. Res.* 43, 7880–7887. doi: 10.1021/ie0496176

IPCC (2021). "Climate change 2021: the physical science basis," in *Contribution of Working Group I to the Sixth Assessment Report of the Intergovernmental Panel on Climate Change*, eds V. Masson-Delmotte, P. Zhai, A. Pirani, S.L. Connors, C. Péan, S. Berger, et al. (Cambridge: Cambridge University Press).

Keeling, C. D., Stephen, C., Piper, S. C., Bacastow, R. B., Wahlen, M., Whorf, T. P., et al. (2001). Exchanges of atmospheric CO2 and 13CO2 with the terrestrial biosphere and oceans from 1978 to 2000. *Glob. Asp. SIO Ref. Ser. Scripps Inst. Ocean* (San Diego, CA), 01–06.

King, E. H., and Plümper, O., Putnis, A. (2010). Effect of secondary phase formation on the carbonation of olivine. *Environ. Sci. Technol.* 44, 6503–6509. doi: 10.1021/es9038193

Köhler, P., Abrams, J. F., Völker, C., Hauck, J., and Wolf-Gladrow, D. A. (2013). Geoengineering impact of open ocean dissolution of olivine on atmospheric CO2, surface ocean pH and marine biology. *Environ. Res. Lett.* 8:014009. doi: 10.1088/1748-9326/8/1/014009

Kremer, D., Etzold, S., Boldt, J., Blaum, P., Hahn, K. M., Wotruba, H., et al. (2019). Geological mapping and characterization of possible primary input materials for the mineral sequestration of carbon dioxide in Europe. *Minerals* 9:485. doi: 10.3390/min9080485

Lackner, K. S. (2003). A guide to CO2 sequestration. *Science* 300, 1677–1678. doi: 10.1126/science.1079033

Lakshtanov, L. Z., and Stipp, S. L. S. (2007). Experimental study of nickel(II) interaction with calcite: adsorption and coprecipitation. *Geochim. Cosmochim. Acta* 71, 3686–3697. doi: 10.1016/j.gca.2007.04.006

Lal, R. (2004). Soil carbon sequestration to mitigate climate change. *Geoderma.* 123, 1–22. doi: 10.1016/j.geoderma.2004.01.032

Lasaga, A. C. (1998). *Kinetic Theory in the Earth Sciences*. Princeton, NJ: Princeton University Press. doi: 10.1515/9781400864874

Lazarević, S., Janković-Castvan, I., Djokić, V., Radovanović, Z., Janaćković, D., and Petrović, R. (2010). Iron-modified sepiolite for Ni2+ sorption from aqueous solution: an equilibrium, kinetic, and thermodynamic study. *J. Chem. Eng. Data* 55, 5681–5689. doi: 10.1021/je100639k

Lein, A. Y. (2004). Authigenic carbonate formation in the ocean. *Lithol. Miner. Resour.* 39, 1–30. doi: 10.1023/B:LIMI.0000010767.52720.8f

Lerman, A., Mackenzie, F. T., and Bricker, O. P. (1975). Rates of dissolution of aluminosilicates in seawater. *Earth Planet. Sci. Lett.* 25, 82–88. doi: 10.1016/0012-821X(75)90213-7

Lindzen, R. S. (2007). Taking greenhouse warming seriously. *Energy Environ.* 18, 937–950. doi: 10.1260/095830507782616823

MacFarling Meure, C., Etheridge, D., Trudinger, C., Steele, P., Langenfelds, R., van Ommen, T., et al. (2006). Law Dome CO2, CH4 and N2O ice core records extended to 2000 years BP. *Geophys. Res. Lett.* 33:L14810. doi: 10.1029/2006GL026152

Maher, K., Johnson, N. C., Jackson, A., Lammers, L. N., Torchinsky, A. B., Weaver, K. L., et al. (2016). A spatially resolved surface kinetic model for forsterite dissolution. *Geochim. Cosmochim. Acta* 174, 313–334. doi: 10.1016/j.gca.2015.11.019

Méheut, M., and Schauble, E. A. (2014). Silicon isotope fractionation in silicate minerals: Insights from first-principles models of phyllosilicates, albite and pyrope. *Geochim. Cosmochim. Acta* 134, 137–154. doi: 10.1016/j.gca.2014.02.014

Meysman, F. J. R., and Montserrat, F. (2017). Negative CO2 emissions via enhanced silicate weathering in coastal environments. *Biol. Lett.* 13:20160905. doi: 10.1098/rsbl.2016.0905

Michalopoulos, P., and Aller, R. C. (1995). Rapid clay mineral formation in amazon delta sediments: reverse weathering and oceanic elemental cycles. *Science* 270, 614–617. doi: 10.1126/science.270.5236.614

Middelburg, J. J., Soetaert, K., and Hagens, M. (2020). Ocean alkalinity, buffering and biogeochemical processes. *Rev. Geophys.* 58, e2019RG000681. doi: 10.1029/2019RG000681

Millero, F. J., Feistel, R., Wright, D. G., and McDougall, T. J. (2008). The composition of Standard Seawater and the definition of the Reference-Composition Salinity Scale. *Deep. Res. Part I Oceanogr. Res. Pap.* 55, 50–72. doi: 10.1016/j.dsr.2007.10.001

Millero, F. J., Sotolongo, S., and Izaguirre, M. (1987). The oxidation kinetics of Fe(II) in seawater. *Geochim. Cosmochim. Acta* 51, 793–801. doi: 10.1016/0016-7037(87)90093-7

Montserrat, F., Renforth, P., Hartmann, J., Leermakers, M., Knops, P., and Meysman, F. J. R. (2017). Olivine dissolution in seawater: implications for CO2 sequestration through enhanced weathering in coastal environments. *Environ. Sci. Technol.* 51, 3960–3972. doi: 10.1021/acs.est.6b05942

Moore, T. S., Murray, R. W., Kurtz, A. C., and Schrag, D. P. (2004). Anaerobic methane oxidation and the formation of dolomite. *Earth Planet. Sci. Lett.* 229, 141–154. doi: 10.1016/j.epsl.2004.10.015

Nilsson, M. M., Kononets, M., Ekeroth, N., Viktorsson, L., Hylén, A., Sommer, S., et al. (2019). Organic carbon recycling in Baltic Sea sediments - an integrated estimate on the system scale based on in situ measurements. *Mar. Chem.* 209, 81–93. doi: 10.1016/j.marchem.2018.11.004

Oelkers, E. H. (1999). "A comparison of forsterite and enstatite dissolution rates and mechanisms," in: *Growth, Dissolution and Pattern Formation in Geosystems*, eds B. Jamtveit, and P. Meakin (Dordrecht: Springer), 253–267. doi: 10.1007/978-94-015-9179-9_12

Oelkers, E. H. (2001). An experimental study of forsterite dissolution rates as a function of temperature and aqueous Mg and Si concentrations. *Chem. Geol.* 175, 485–494. doi: 10.1016/S0009-2541(00)00352-1

Oelkers, E. H., Benning, L. G., Lutz, S., Mavromatis, V., Pearce, C. R., and Plümper, O. (2015). The efficient long-term inhibition of forsterite dissolution by common soil bacteria and fungi at Earth surface conditions. *Geochim. Cosmochim. Acta* 168, 222–235. doi: 10.1016/j.gca.2015.06.004

Oelkers, E. H., Declercq, J., Saldi, G. D., Gislason, S. R., and Schott, J. (2018). Olivine dissolution rates: a critical review. *Chem. Geol.* 500, 1–19. doi: 10.1016/j.chemgeo.2018.10.008

Olsen, A. A., and Rimstidt, J. D. (2008). Oxalate-promoted forsterite dissolution at low pH. *Geochim. Cosmochim. Acta* 72, 1758–1766. doi: 10.1016/j.gca.2007.12.026

Palandri, J. L., and Kharaka, Y. K. (2004). *A Compilation of Rate Parameters of Water-Mineral Interaction Kinetics for Application to Geochemical Modeling*. USGS Open File Report.

Parkhurst, D. L., and Appelo, C. A. J. (1999). *User's Guide to PHREEQC (Version 2): A Computer Program for Speciation, Batch-Reaction, One-Dimensional Transport, and Inverse Geochemical Calculations*. Water-Resources Investigations Report, 99–4259.

Pokrovsky, O. S., and Schott, J. (2000). Kinetics and mechanism of forsterite dissolution at 25°C and pH from 1 to 12. *Geochim. Cosmochim. Acta* 64, 3313–3325. doi: 10.1016/S0016-7037(00)00434-8

Power, I. M., Wilson, S. A., and Dipple, G. M. (2013). Serpentinite carbonation for CO2 sequestration. *Elements* 9, 115–121. doi: 10.2113/gselements.9.2.115

Renforth, P., and Henderson, G. (2014). Assessing ocean alkalinity for carbon sequestration. *Rev. Geophys.* 55, 636–674. doi: 10.1002/2016RG000533

Rhodes, C. J. (2016). The 2015 Paris climate change conference: COP21. *Sci. Prog.* 99, 97–104. doi: 10.3184/003685016X14528569315192

Rigopoulos, I., Harrison, A. L., Delimitis, A., Ioannou, I., Efstathiou, A. M., Kyratsi, T., et al. (2018). Carbon sequestration via enhanced weathering of peridotites and basalts in seawater. *Appl. Geochem.* 91, 197–207. doi: 10.1016/j.apgeochem.2017.11.001

Rimstidt, J. D., Brantley, S. L., and Olsen, A. A. (2012). Systematic review of forsterite dissolution rate data. *Geochim. Cosmochim. Acta* 99, 159–178. doi: 10.1016/j.gca.2012.09.019

Ruttenberg, K. C., and Berner, R. A. (1993). Authigenic apatite formation and burial in sediments from non-upwelling, continental margin environments. *Geochim. Cosmochim. Acta* 57, 991–1007. doi: 10.1016/0016-7037(93)90035-U

Saran, R. K., Arora, V., and Yadav, S. (2018). CO2 sequestration by mineral carbonation: a review. *Glob. Nest J.* 20, 497–503. doi: 10.30955/gnj.002597

Sarmiento, J. L., and Gruber, N. (2006). J. L. Sarmiento and N. Gruber 2006. Ocean Biogeochemical Dynamics. xiii + 503 pp. Princeton, Woodstock: Princeton University Press. 0 691 01707 7. *Geol. Mag.* 144, 1034. doi: 10.1017/S0016756807003755

Schrag, D. P., Higgins, J. A., Macdonald, F. A., and Johnston, D. T. (2013). Authigenic carbonate and the history of the global carbon cycle. *Science* 339, 540–543. doi: 10.1126/science.1229578

Silburn, B., Kröger, S., Parker, E. R., Sivyer, D. B., Hicks, N., Powell, C. F., et al. (2017). Benthic pH gradients across a range of shelf sea sediment types linked to sediment characteristics and seasonal variability. *Biogeochemistry* 135, 69–88. doi: 10.1007/s10533-017-0323-z

Sissmann, O., Daval, D., Brunet, F., Guyot, F., Verlaguet, A., Pinquier, Y., et al. (2013). The deleterious effect of secondary phases on olivine carbonation yield: Insight from time-resolved aqueous-fluid sampling and FIB-TEM characterization. *Chem. Geol.* 357, 186–202. doi: 10.1016/j.chemgeo.2013.08.031

Solomon, S., Plattner, G.-K., Knutti, R., and Friedlingstein, P. (2009). Irreversible climate change due to carbon dioxide emissions. *Proc. Natl. Acad. Sci.* 106, 1704 LP—1709. doi: 10.1073/pnas.0812721106

Spivack, A. J., and Edmond, J. M. (1987). Boron isotope exchange between seawater and the oceanic crust. *Geochim. Cosmochim. Acta* 51, 1033–1043. doi: 10.1016/0016-7037(87)90198-0

Stockmann, G. J., Wolff-Boenisch, D., Bovet, N., Gislason, S. R., and Oelkers, E. H. (2014). The role of silicate surfaces on calcite precipitation kinetics. *Geochim. Cosmochim. Acta* 135, 231–250. doi: 10.1016/j.gca.2014.03.015

Strefler, J., Amann, T., Bauer, N., Kriegler, E., and Hartmann, J. (2018). Potential and costs of carbon dioxide removal by enhanced weathering of rocks. *Environ. Res. Lett.* 13:034101. doi: 10.1088/1748-9326/aaa9c4

Stumm, W., and Morgan, J. J. (1996). Aquatic chemistry: chemical equilibria and rates in natural waters. *Choice Rev. Online* 33, 171–229. doi: 10.5860/CHOICE.33-6312

Suárez, S., Nieto, F., Velasco, F., and Martín, F. J. (2011). Serpentine and chlorite as effective Ni-Cu sinks during weathering of the Aguablanca sulphide deposit (SW Spain). TEM evidence for metal-retention mechanisms in sheet silicates. *Eur. J. Mineral.* 23, 179–196. doi: 10.1127/0935-1221/2011/0023-2084

Sun, W., Jayaraman, S., Chen, W., Persson, K. A., and Ceder, G. (2015). Nucleation of metastable aragonite $CaCO_3$ in seawater. *Proc. Natl. Acad. Sci. U.S.A.* 112, 3199 LP—3204. doi: 10.1073/pnas.1423898112

Torres, M. A., Dong, S., Nealson, K. H., and West, A. J. (2019). The kinetics of siderophore-mediated olivine dissolution. *Geobiology* 17, 401–416. doi: 10.1111/gbi.12332

Torres, M. E., Hong, W.-L., Solomon, E. A., Milliken, K., Kim, J.-H., Sample, J. C., et al. (2020). Silicate weathering in anoxic marine sediment as a requirement for authigenic carbonate burial. *Earth Sci. Rev.* 200, 102960. doi: 10.1016/j.earscirev.2019.102960

Tyrrell, T., Schneider, B., Charalampopoulou, A., and Riebesell, U. (2008). Coccolithophores and calcite saturation state in the Baltic and Black Seas. *Biogeosciences* 5, 485–494. doi: 10.5194/bg-5-485-2008

Van Cappellen, P., and Wang, Y. (1996). Cycling of iron and manganese in surface sediments; a general theory for the coupled transport and reaction of carbon, oxygen, nitrogen, sulfur, iron, and manganese. *Am. J. Sci.* 296, 197 LP—243. doi: 10.2475/ajs.296.3.197

van den Boorn, S. H. J. M., Vroon, P. Z., van Belle, C. C., van der Wagt, B., Schwieters, J., and van Bergen, M. J. (2006). Determination of silicon isotope ratios in silicate materials by high-resolution MC-ICP-MS using a sodium hydroxide sample digestion method. *J. Anal. At. Spectrom.* 21, 734–742. doi: 10.1039/b600933f

Wallmann, K., Aloisi, G., Haeckel, M., Tishchenko, P., Pavlova, G., Greinert, J., et al. (2008). Silicate weathering in anoxic marine sediments. *Geochim. Cosmochim. Acta* 72, 2895–2918. doi: 10.1016/j.gca.2008.03.026

Wolff-Boenisch, D., Wenau, S., Gislason, S. R., and Oelkers, E. H. (2011). Dissolution of basalts and peridotite in seawater, in the presence of ligands, and CO_2: implications for mineral sequestration of carbon dioxide. *Geochim. Cosmochim. Acta* 75, 5510–5525. doi: 10.1016/j.gca.2011.07.004

Zeebe, R. E., and Wolf-Gladrow, D. (2001). *CO2 in Seawater: Equilibrium, Kinetics, Isotopes*. Gulf Professional Publishing.

Zhong, S., and Mucci, A. (1989). Calcite and aragonite precipitation from seawater solutions of various salinities: precipitation rates and overgrowth compositions. *Chem. Geol.* 78, 283–299. doi: 10.1016/0009-2541(89)90064-8

Conflict of Interest: The authors declare that the research was conducted in the absence of any commercial or financial relationships that could be construed as a potential conflict of interest.

frontiers | Frontiers in Climate

ORIGINAL RESEARCH
published: 05 May 2022
doi: 10.3389/fclim.2022.849948

Carbon Accounting for Enhanced Weathering

Thorben Amann[*†] *and Jens Hartmann*[†]

Institute for Geology, Center for Earth System Sciences and Sustainability, Universität Hamburg, Hamburg, Germany

The inevitable deployment of negative emission technologies requires carbon accounting to incentivise the investment and to foster an active CO_2 certificate trading schema. Enhanced Weathering as one of the negative emission technologies is being tested in the field now, but lacks a verifiable and cost-effective carbon accounting approach. Based on results from a lab scale column experiment and field observations, it is hypothesized that the observed stable positive correlation between total alkalinity and electrical conductivity may present a way to easily predict the initial CO_2 sequestration at the application site by chemical mineral weathering at low costs. Alkalinity is a measure to track weathering products. It is not difficult to measure, yet continuous and mid- to high-frequency sampling and analyses are expensive and time consuming. The observed strong correlation of alkalinity with electrical conductivity could be harnessed and enable a CO_2 uptake monitoring by simple electrical conductivity measurements in soils or any point in the discharge system. For a successful implementation and calibration, data are needed, covering the most likely employment scenarios of soil, climate, hydrology, rock product, application scenario and plant abundance. Incorporated in a growing public database, this could be used as an assessment and benchmark system for future EW deployment.

Keywords: CO_2, carbon dioxide removal, carbon accounting, negative emissions, enhanced weathering, climate change

OPEN ACCESS

Edited by:
Keith Paustian,
Colorado State University,
United States

Reviewed by:
Grace Andrews,
University of Southampton,
United Kingdom
Curtis Monger,
New Mexico State University,
United States

***Correspondence:**
Thorben Amann
science@thorbenamann.de

***ORCID:**
Thorben Amann
orcid.org/0000-0001-9347-0615
Jens Hartmann
orcid.org/0000-0003-1878-9321

Specialty section:
This article was submitted to Negative Emission Technologies, a section of the journal Frontiers in Climate

Received: *06 January 2022*
Accepted: *21 March 2022*
Published: *05 May 2022*

Citation:
Amann T and Hartmann J (2022) Carbon Accounting for Enhanced Weathering. Front. Clim. 4:849948. doi: 10.3389/fclim.2022.849948

INTRODUCTION

To limit effects of global warming, the 1.5° target was stipulated in the Paris Agreement (United Nations, 2015). By now it is almost impossible to reach the target by mitigation, without the help of negative emission technologies (NET) (Gasser et al., 2015; Sanderson et al., 2016; IPCC, 2018). When these negative emission technologies are integrated in a global carbon emission trading scheme that compensates entities for their costs in carbon capture undertakings, it will be an important issue to monitor, report and verify the removal of CO_2 and its permanence (Mclaren, 2012; Brander et al., 2021; Carton et al., 2021). While some methods capture CO_2 and create a point source, like Direct Air Capture and Storage (DACS), which makes it easy to quantify the mass of CO_2 captured, other methods rely on the diffuse uptake and sequestration of CO_2, like afforestation or Enhanced Weathering (EW). Exemplary, afforestation may have an advantage in proving the CO_2 uptake by the simple quantification of grown biomass, yet accounting of actual carbon stocks in growing forests includes more, e.g., soil carbon changes and further greenhouse gas emissions (Lefebvre et al., 2021).

The inorganic sequestration of CO_2 by EW on the other hand, relies on the natural process of chemical weathering (Ebelmen, 1845), which is, in principle, a well-understood process. To counteract climate change by removal of CO_2 from the atmosphere through chemical weathering, the use of rock products was briefly proposed by Seifritz (1990) but made prominent in the climate science community by Schuiling and Krijgsman (2006).

Since, the assessment of a realistic potential of EW as a tool for carbon dioxide removal (CDR) was in the focus of literature reviews (Hartmann and Kempe, 2008; Hartmann et al., 2013), a few laboratory (e.g., Renforth et al., 2015), micro- to mesocosm studies (Ten Berge et al., 2012; Dietzen et al., 2018; Amann et al., 2020), and field trials (e.g., Haque et al., 2020). Globally representative field data coverage for the various combinations of soil, climate, plant abundance, and applied rock source (including rate and quality) is still missing.

Besides the assessment of realistic CDR boundaries of EW under lab or field conditions, it remains an open question of how to track and prove inorganic and organic CO_2 removal by EW with cheap and robust methods. Organic carbon captured due to EW application may be assessed by measuring the carbon content in plants and soils. The inorganic CO_2 sink in the form of alkalinity (predominantly as HCO_3^-) is determined by the hydrochemistry of percolating waters leaving the soil system. But frequent sampling and analyses in the laboratory is expensive. Reports on co-variation of total alkalinity (TA) and electrical conductivity (EC) (Sechriest, 1960; Bouillon et al., 2014; Proulx et al., 2018) suggest that the EC may be a good predictor for TA under given soil and land use settings, thus rendering it an interesting tool to identify and track the initial CO_2 uptake by EW at the application site. Results from EW laboratory column experiments with dunite (rich in olivine), a basaltic rock (rich in nepheline), and a mixture of laterite with the basaltic rock are reviewed in this respect and compared to field data from basaltic catchments as basalt is the proposed rock type for EW. In addition, data from a loess column experiment and loess catchments are discussed as an analogy for natural EW due to the deposition of glacially-derived fine (silty) rock dust. Considered data also contains samples from agricultural catchments with partly elevated nitrate fluxes, which are compared to the silicate material columns and basalt catchments to assess the impact of fertilization on the EC-TA relationship.

METHODS

In a small-scale laboratory experiment, multiple columns were filled with varying materials and watered periodically to simulate intensive tropical rainfall (8,000 mm a^{-1}). The columns contained dunite, basaltic rock [basanite, after Streckeisen (1980) and TAS (Total Alkaline Silica) classification (Le Bas et al., 1986)], lateritic soil (oxisol), and a blend of this soil and the basanite. One set of columns was treated under ambient CO_2 concentrations (∼0.046%) while a second set was put under 100% CO_2 atmosphere. Details on the setup and the used materials can be found **Supplementary Material S1**.

To test the EC-TA relationship, water chemistry data from rivers draining basaltic catchments on Madeira Island, Portugal, and loess dominated catchments in Germany were collected (**Supplementary Material S3**).

Temperature, pH, and EC of field samples were measured *in situ* with a handheld multimeter probe (WTW Multimeter 350i). Samples from the lab experiment were measured similarly in the bottles collecting the outflow water.

In the lab, TA was measured by automated titration (Metrohm Titrando) with 0.005 N HCl. Major anions and cations were determined by ion chromatography (Metrohm 881 Compact IC Pro system).

Individual sample tables and more specific method descriptions are given **Supplementary Materials S1, S3**.

The contributions of ion specific electrical conductivities were calculated using the empirical equations from Mccleskey et al. (2012) after modeling the speciation in each solution with PhreeqC and the phreeqc.dat database (Parkhurst and Appelo, 2013) using the Python package PhreeqPython (Vitens, 2021). Calculated EC (based on available major ion data) is in good agreement with measured EC (**Supplementary Figure S4-4**).

Linear least squares regressions were calculated using Python and the *scipy.stats.linregress* function of SciPy (Virtanen et al., 2020). Regression equation and parameters are given in **Supplementary Material S5**.

RESULTS

With the start of the column experiment, an initial flush of cations and TA can be observed due to the experimental setup, with stabilizing concentrations after 3 weeks (**Supplementary Material S2**). Looking at the entire experiment phase, including the initial flushing phase, EC correlates very well with TA in most cases (**Figure 1**). The experiments with laterite and loess showed, at the first glance, no or limited correlation (**Figures 1A,D**). However, disregarding the initial 21 day flushing phase, the correlations between TA and EC improved markedly, except for dunite under the atmospheric treatment and loess under the extreme scenario with a saturated CO_2 treatment, showing relatively constant high TA levels in the leached water from this carbonate rich soil (**Figures 1B,D**).

DISCUSSION

The relationship between concentrations of TA and EC clearly reflects the underlying physical principle, that all elements dissolved in the water carry an electrical current which can be put into relation with the TA, sensu stricto the carbonate alkalinity, i.e., equivalent concentrations of HCO_3^- and CO_3^-, produced during the chemical weathering and dissolution of rock material. This linkage is known and utilized in the characterization of natural waters (Sechriest, 1960; Krawczyk and Ford, 2006; Thompson et al., 2012; Proulx et al., 2018). Other processes like respiration and nitrification may influence the TA but not the carbonate alkalinity. As such TA is a sum parameter that

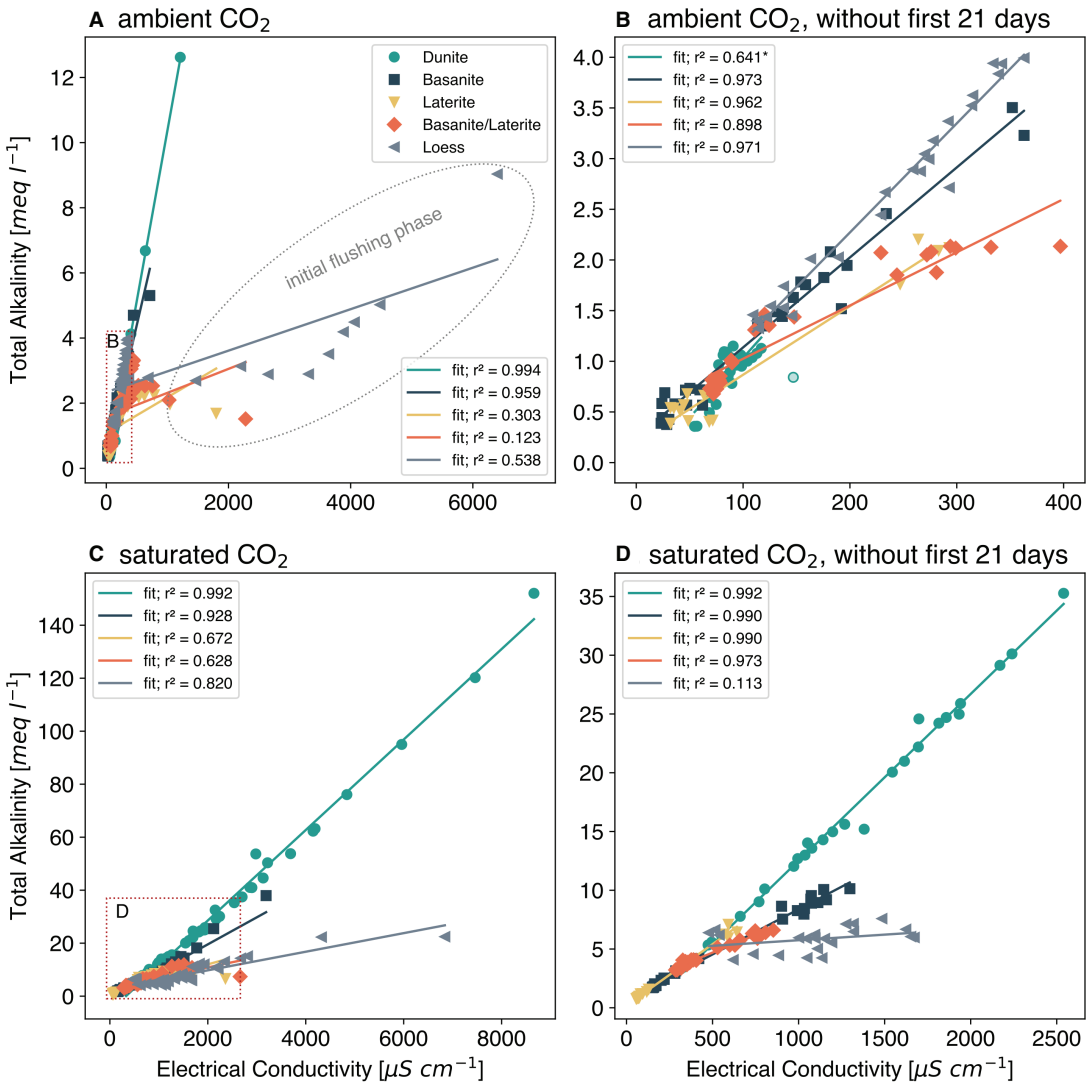

FIGURE 1 | Relationship between alkalinity and electrical conductivity in the outflow of columns which were filled with different rock and soil materials and watered for about 300 days. Data fit: linear least squares fit with the coefficient of determination r^2 given in the legend. *One outlier data point (transparent green circle) was removed to calculate this regression. Red rectangles indicate the areas of figures **(B,D)**. **(A)** Experiment under ambient (~0.046%) CO_2. **(B)** Ambient CO_2, without first 21 days. **(C)** Experiment under saturated (100%) CO_2. **(D)** Saturated CO_2, without first 21 days.

is most likely dominated by bicarbonate, but may, especially in agricultural settings, be manipulated by fertilizer addition.

Co-variation between TA and dominating cations are causing the clear relationship between TA levels and EC. This effect points toward a potential method to track and report site-specific CO_2 consumption rates. Carbon accounting is important when it comes to the field application of NETs (Brander et al., 2021), as it provides a base for comparison between methods. As for EW, the use of established methods should allow for the settlement and validation of pay-outs within a CO_2 certification scheme (Hartmann and Kempe, 2008; Peters and Geden, 2017), which is required to incentivise negative emission approaches (Peters and Geden, 2017).

Each of the released ions contributes specifically to the overall EC of a solution (Gustafson and Behrman, 1939) based on its specific ionic molar conductivity. The ionic composition of water draining the columns creates an individual EC signal (e.g., Pawlowicz, 2008). This explains the slope differences in the regression lines of TA and EC because the column material compositions and resulting chemical composition of the draining waters are different. The higher r^2 of the saturated CO_2 setups (except for loess) are the effect of overall higher TA generated and accompanying released cations, resulting in higher EC values assuming that measurement errors and individual fluctuations remain constant. Because the water addition to columns was constant with time the slope of TA-EC relationship represents

predominantly the evolution of the system with time, as can be seen by the TA-concentration change during the experiments (**Supplementary Figure S2-1**).

The column experiments had idealized properties with intensive watering, to simulate extreme conditions. To test if the TA-EC-relationship is also observable in field data more comparable to EW application sites, exemplary waters of basaltic and loess catchments were evaluated. The contribution of bicarbonate (as the major component of TA) to EC can be high - in the selected samples around 30% (**Figure 2D**). Therefore, the deduction of TA from EC should be possible if released cations (by EW) covary with TA, adding proportionally to the added EC. This is further corroborated by observations from a field trial in which wollastonite ($CaSiO_3$) rock flour was spread on a controlled forested watershed (Peters et al., 2004), basically simulating EW application. Here, EC and TA signals clearly increase after the onset of the experiment (**Figures 2A,B**) and the modeled contribution of bicarbonate to overall EC increases notably (**Figure 2C**). As the draining waters from this watershed are naturally very low in TA (around zero in the control watershed, **Figure 2B**), the observed signal is pinpointed to the wollastonite application.

From these data, the link between TA and EC can be well-demonstrated (**Figure 3A**), with a clear, yet low r^2 of 0.531, probably due to the unique composition of the waters, with very low conductivities and near zero TA at the start. Here, the abundance of organic acids, sulfate and nitrate in the watershed, partly lead to dissolution of rock material without TA generation (Taylor et al., 2021). Furthermore, under such low TA conditions slight absolute variations have a high relative impact on the coefficient of determination. As the higher TA values indicate, the correlation might become stronger, if the baseline level of TA and

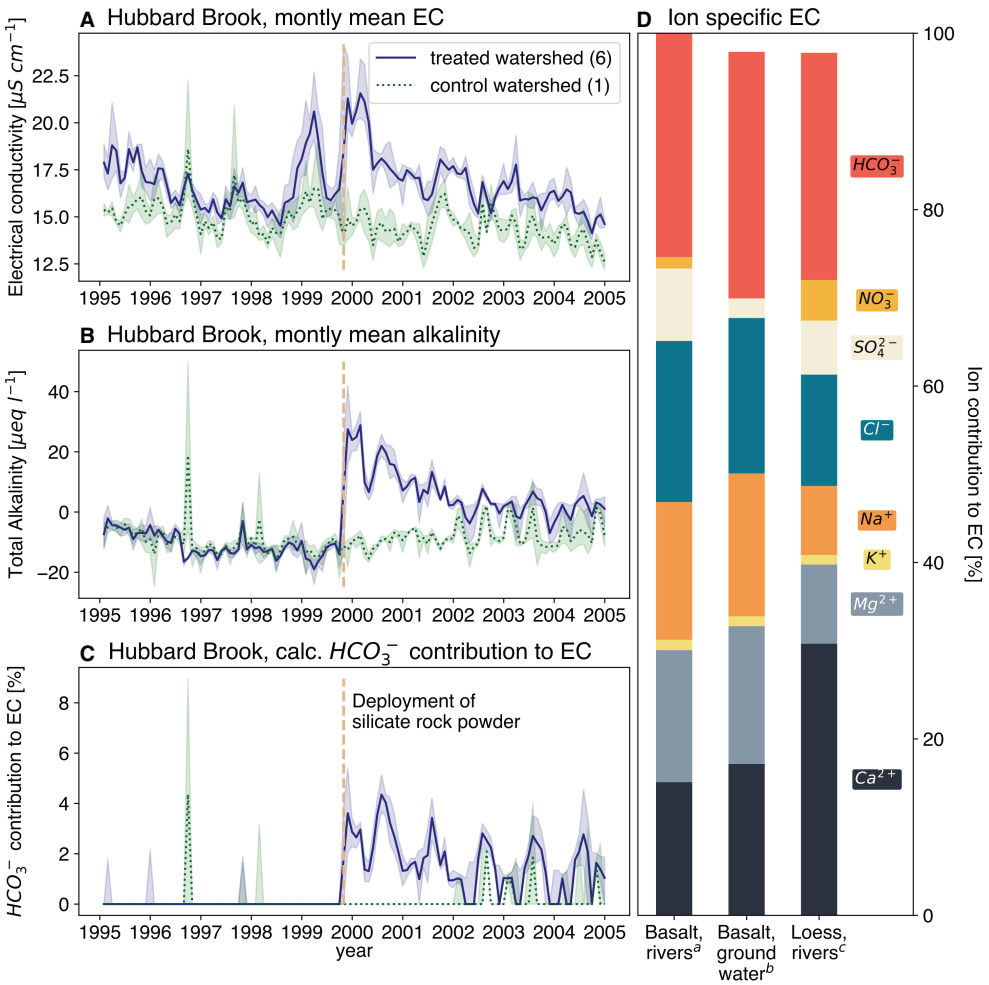

FIGURE 2 | Selective time series of two Hubbard Brook experimental forest watershed (Likens, 2017), watershed 1 data as control baseline (dotted, green) and watershed 6 data representing effects of silicate rock powder spreading (solid, blue): monthly mean and 10 and 90 percentiles for electrical conductivity **(A)**, total alkalinity **(B)** and the calculated HCO_3^- contribution to the electrical conductivity **(C)**; Individual ionic conductivity contributions to overall electrical conductivity, mean values **(D)**, individual sample results, can be found in **Supplementary Material S4**. [a]data from rivers of Madeira island, collected by the authors; [b]data from Van Der Weijden and Pacheco (2003); [c]data from rivers of a loess dominated catchment in Germany, collected by the authors.

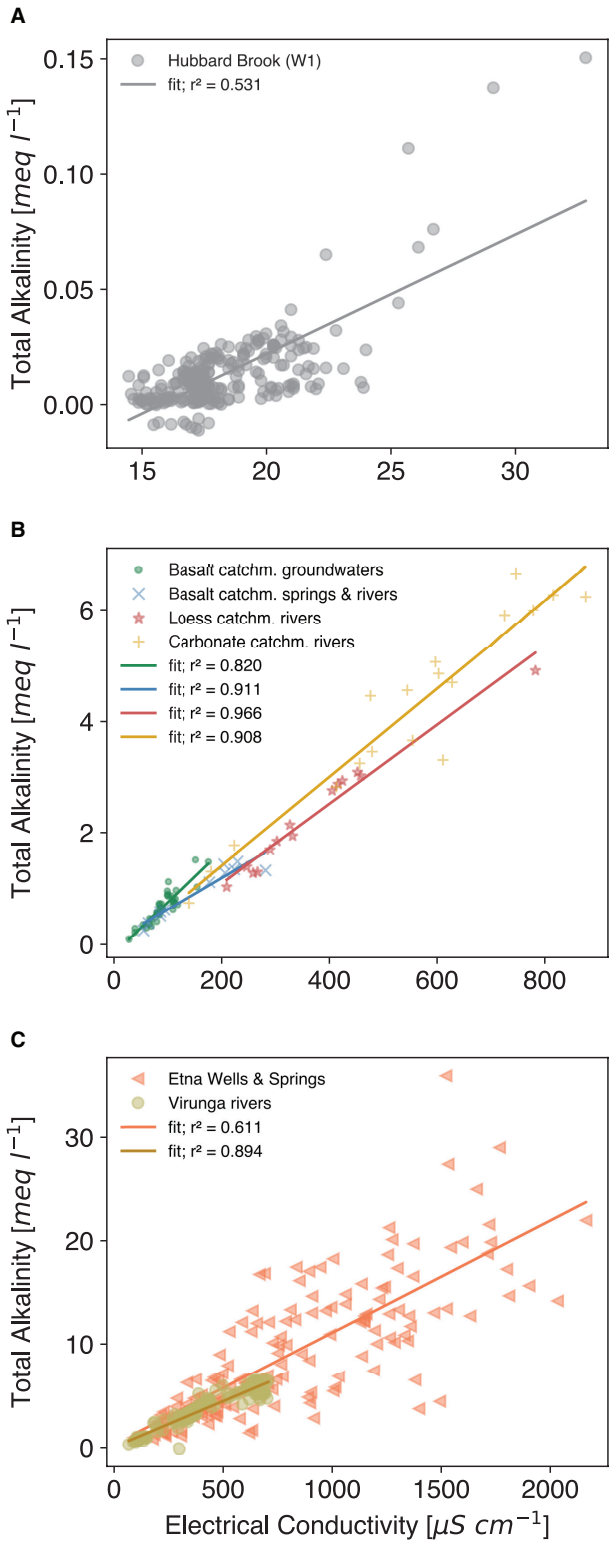

FIGURE 3 | Data fit: linear least squares fit with the coefficient of determination r^2 given in the legend. Regression parameters are provided in **Supplementary Material S5**. **(A)** Data from Likens (2017) for watershed 1 of the Hubbard

(Continued)

FIGURE 3 | Brook experimental forest, which was amended with wollastonite rock flour, considered period from 1999-10-24 to 2004-10-24, cf. **Figures 2A–C**; **(B)** Groundwater data from Van Der Weijden and Pacheco (2003) (green dot); Observations from river water and springs from basaltic catchments on Madeira island (blue x); river water data from a loess dominated catchment in central Germany (see Methods section) (red *); averaged river water data from Perrin et al. (2008) from the calcareous molassic Gascogne area located in the Garonne river basin (south-western France) (yellow +); **(C)** Data from active volcanoes: water from wells and springs of the Etna, Italy (Brusca et al., 2001) (red triangles); Virunga National Park, Kongo: river water from basaltic catchments (Balagizi et al., 2015) (brown circles).

therefore EC would be elevated for longer times (in the case of the Hubbard Brook experiment, treated and control values converge because of the one-time deployment of rock dust).

Basalt is a material more recently discussed for EW application (e.g., Beerling et al., 2018; Amann and Hartmann, 2019). Therefore, ground- and river water samples from catchments in Madeira, a basaltic volcanic island (Gardner, 1882), were tested for the TA-EC relationship, with a distinctly positive result (**Figure 3B**). Loess as a very reactive material, here considered as a natural EW analog, supports the TA-EC correlation hypothesis, too (**Figure 3B**). Even in watersheds with elevated nitrate levels due to agriculture, the relationship is maintained (Loess and carbonate catchment rivers in **Figure 3B**) and NO_3 is not conclusively impacting EC (**Figure 4A**). Measurements from highly active volcanic systems with fresh mafic to ultramafic material (Virunga and Etna volcanic systems) also confirm the relationship (**Figure 3C**). However, groundwater data of the Etna area are more scattered, likely due to the influence of acidic volcanic gases, which would not be present in regular EW application scenarios on agricultural or forested land. In summary, the field data results corroborate the findings from the column experiment (**Figure 1**).

From these observations, it is suggested that EC is a promising proxy for tracking EW related inorganic CO_2 consumption via TA production. The slope differences of the regression lines from the TA-EC relationship of the different treatments in the lab experiment as well in the field observations suggest that no generalized equation could be derived to be used in a carbon accounting scheme. However, after an initial calibration period, easily to perform EC measurements may enable local farmers to track and report CO_2 consumption based on EC measurements in water from their individual land, with an uncertainty, which might be averaged for specific conditions over a larger area of land. Because catchment runoff is possibly underestimating the TA produced by EW, as some TA remains in the soil and groundwater for a longer time, soil bulk EC might be used to more precisely track EC increases, as it is right within the application area.

Water EC from streams is different to interpret than soil bulk EC, as latter is naturally impacted by a plethora of factors (Corwin and Lesch, 2005), which are not necessarily connected with TA in the first instance. As such, changes in those independent

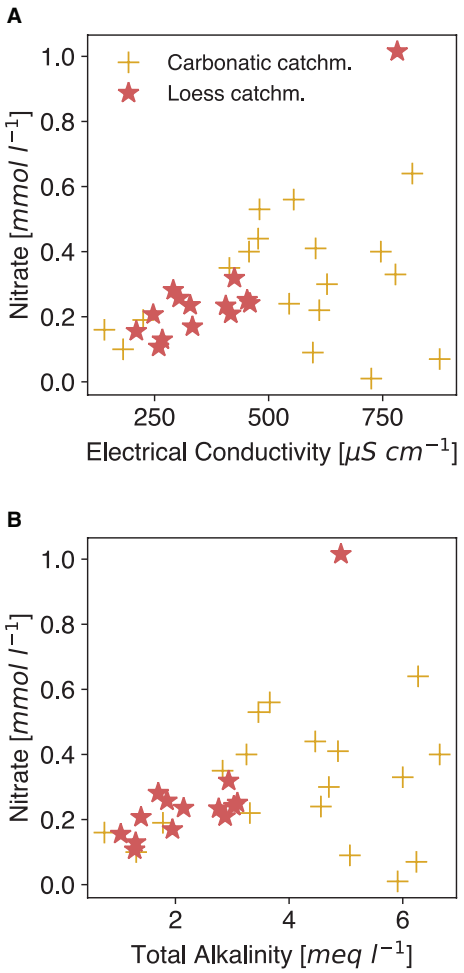

FIGURE 4 | Relation between nitrate and electrical conductivity **(A)** and total alkalinity **(B)**. Data from rivers draining carbonatic catchments from Perrin et al. (2008) and loess catchment data as in **Figure 3B**. Both datasets contain water from catchments which are influenced by agricultural activities.

factors must be closely monitored and evaluated to single out the weathering signal. EC might be most prominently influenced by periodical fertilization, which adds ions that don't contribute to TA (Phong et al., 2020). These fertilizers may alter the slope of the TA-EC relationship temporarily, as they can consist of compounds that release ions, which do not change TA (like K^+ and Cl^- from muriate of potash (MOP), a commonly applied K fertilizer). Looking at N fertilizer, in the data at hand, the elevated nitrate levels are not clearly related to EC, nor is there a negative tendency with TA (**Figure 4**), even though the data contains waters from agriculturally impacted areas. The specific molar conductivity of fertilizer-released compounds (NO_3^-, NH_4^+, Cl^-) is not distinctly high (Adamson, 1979) but spikes from the periodic application of fast dissolving fertilizer could alter the signal temporarily. Transformation processes like (de-)nitrification can alter the TA in soil solution (Gandois et al., 2011), without changing the EC in the same proportion. As an additional effect, fertilizer dissolution can lead to the formation of strong acids, which dissolve added rock material (Perrin et al., 2008; Pierson-Wickmann et al., 2009) without increasing TA. Intense rain events may also lead to a wash-out effect marked by nitrate peaks, which level out within a few days (Ferrant et al., 2013).

Once the likely additional sources and sinks for TA and impacts on EC are identified, a correction function could be applied, as the influencing factors should be rather controllable on a well-defined agricultural soil under standardized agricultural practices. Exemplary, a study on weathering of the Aso caldera, Japan, with intensive rice agriculture revealed low nitrate loads (average: 0.03 mmol l^{-1}), probably due to optimized application procedures (Hosono et al., 2018). In EW application areas not impacted by agricultural activities and with human interferences at a minimum, like tropical hinterland as discussed in Goll et al. (2021), the aforementioned influences should be low and as such, EC less impacted by anthropogenic activities. Here the measurement of EC changes may be an even more reliable approach to monitor CO_2 uptake.

At the catchment scale, EC measurements using low-cost equipment is possible (e.g., Hund et al., 2016). This method requires a sampling point which represents the catchment outflow, and thus the water draining the rock flour amended land. This approach may prove to be difficult as individual fields may not have confined catchments with controlled outflow, yet the signal should also be visible in the greater discharge system and could be measured there. Alternatively, in a more detailed approach, EC sensors could be buried in the field (Scudiero et al., 2012), tracking the percolating soil solution. In this case further model development is needed, as soil bulk EC depends also on soil humidity and other physical properties and is therefore different from EC measured in sample water. The relationship between both parameters needs to be used to calibrate functions for TA production by EW in the soil system. This requires further research, before soil bulk EC might be used as a proxy for and therefore its use as a carbon accounting tool.

As the technology for soil bulk EC and humidity monitoring to track agricultural productivity is already available (Noborio, 2001; Kitchen et al., 2003; Fortes et al., 2014; Akanji et al., 2018), it could be used for CDR accounting without additional investment costs. Newer developments suggest the use of simple easy-to-deploy EC probes to monitor soil conditions in smart and precision farming applications (Othaman et al., 2020). With this, the transfer of data from field to user via wireless networks is possible (Citoni et al., 2019; Terence and Purushothaman, 2020). This provides perspectives for the remote monitoring of EW and achieved carbon sequestration.

As carbon sequestration must be tracked and verified for carbon accounting, simple and cost-efficient physical measurement of waters draining the treated areas is necessary ensure sustained monitoring. The application of one technique for two purposes would therefore create a win-win-situation.

The TA prediction approach described here, would not account for carbon bound in precipitated carbonate minerals as particulate inorganic carbon (PIC) in the soil system. To account for this carbon fraction, additional soil PIC analyses

would be necessary, which could be done during mandatory or cross compliance routine sampling for soil quality monitoring (i.e., based on the framework of common agricultural policy of the EU).

In addition to the CDR purpose, the application of rock products was much earlier suggested to improve soil conditions for agricultural production (Missoux, 1853; Leonardos et al., 1987; Van Straaten, 2002). Improved biomass growth leads to additional CO_2 uptake and storage as organic carbon, propelling the overall CDR potential of EW (Amann and Hartmann, 2019; Goll et al., 2021). This effect would necessitate an additional tracking of yield/biomass increases to account for the complete CO_2 sequestration potential of EW. Current techniques of remote plant monitoring for carbon accounting in above ground biomass would add to a scenario, in which the additional organic carbon sequestration path of EW could be tracked and monitored remotely.

CONCLUSION

Proper accounting for deliberate carbon sequestration is inevitable. All CDR methods have to solve this issue before entering the emission trading market. Experimental studies show that the weathering signal can be tracked well in confined column setups by measuring outflow cation concentrations (Renforth et al., 2015; Amann et al., 2020; Kelland et al., 2020). Yet it remains an open question how the signal can be tracked reliably in the field and how the CO_2 uptake can be quantified with low-cost and robust methods.

To provide a means of monitoring the initial CO_2 drawdown at the application site, we propose a deeper investigation into the use of EC measurements to derive TA levels which indicate CO_2 sequestration. Data from a lab experiment and selected natural waters support the approach by showing very clear relationships between EC and TA.

It remains to be investigated how this new approach of carbon accounting can be implemented in the field. Practical issues to be solved are sensor placement in the ground and calibration, considering seasonal variability of soil humidity, and the application of fertilizer or other soil amendments which might affect the EC.

The general caveat of the described approach is that the tracking of EC in waters from agricultural land represents only the initial uptake of CO_2 from the atmosphere. Downstream processes in groundwater, rivers, and the ocean are not covered by the proposed approach and require separate recognition.

Globally representative field data covering various combinations of soil, climate, plant abundance and applied rock source (including rate and quality) would be needed to create a framework for easy implementation of a functional carbon accounting scheme after testing and verification. Ideally, a global database for case scenarios is established, fostering business models for farmers. A high-quality monitoring database covering typical application scenarios may enable a reliable pre-application assessment of the efficiency, based on standardized conditions delivering a reliable, statistically grounded base reference of the amount of CO_2 transferred to alkalinity.

Ideally, a set of coordinated global field campaigns will provide these data, so that low-cost conductivity and humidity measurements can replace more expensive hydrochemical sampling and analysis of CO_2 consumption by EW.

The approach to remove CO_2, monitor, and verify (RMV) must be simple, robust, cost-efficient, and reproducible. As such, applicability of EW for CDR could benefit from the expanding remote sensor utilization.

DATA AVAILABILITY STATEMENT

The original contributions presented in the study are included in the article/**Supplementary Material**, further inquiries can be directed to the corresponding author/s.

AUTHOR CONTRIBUTIONS

TA and JH conceived the study design and wrote the text. Both authors contributed to the article and approved the submitted version.

FUNDING

This work was funded by Germany's Excellence Strategy – EXC 2037 'Climate, Climatic Change, and Society' – project number 390683824, contribution to the Center for Earth System Research and Sustainability (CEN) of Universität Hamburg.

ACKNOWLEDGMENTS

We acknowledge the help of Tom Jäppinen, Peggy Bartsch, Aman Malik, Rhiannon Breider, Mark Brosell, Marvin Keitzel, Eric Marques, and Walid Karimi for valuable contributions from the wet lab. We thank the Carbon Drawdown Initiative (Project Carbdown) for fruitful discussions and support around the need for carbon accounting methods.

SUPPLEMENTARY MATERIAL

The Supplementary Material for this article can be found online at: https://www.frontiersin.org/articles/10.3389/fclim.2022.849948/full#supplementary-material

REFERENCES

Adamson, A. W. (1979). *A Textbook of Physical Chemistry*. New York, NY; San Francisco, CA: Academic Press.

Akanji, M. A., Oshunsanya, S. O., and Alomran, A. (2018). Electrical conductivity method for predicting yields of two yam (*Dioscorea alata*) cultivars in a coarse textured soil. *Int. Soil Water Conserv. Res.* 6, 230–236. doi: 10.1016/j.iswcr.2018.03.006

Amann, T., and Hartmann, J. (2019). Ideas and perspectives: synergies from co-deployment of negative emission technologies. *Biogeosciences* 16, 2949–2960. doi: 10.5194/bg-16-2949-2019

Amann, T., Hartmann, J., Struyf, E., De Oliveira Garcia, W., Fischer, E. K., Janssens, I., et al. (2020). Enhanced Weathering and related element fluxes – a cropland mesocosm approach. *Biogeosciences* 17, 103–119. doi: 10.5194/bg-17-103-2020

Balagizi, C. M., Darchambeau, F., Bouillon, S., Yalire, M. M., Lambert, T., and Borges, A. V. (2015). River geochemistry, chemical weathering, and atmospheric CO2consumption rates in the Virunga Volcanic Province (East Africa). *Geochem. Geophys. Geosyst.* 16, 2637–2660. doi: 10.1002/2015GC005999

Beerling, D. J., Leake, J. R., Long, S. P., Scholes, J. D., Ton, J., Nelson, P. N., et al. (2018). Farming with crops and rocks to address global climate, food and soil security. *Nat Plants*. 4, 138–147. doi: 10.1038/s41477-018-0108-y

Bouillon, S., Yambele, A., Gillikin, D. P., Teodoru, C., Darchambeau, F., Lambert, T., et al. (2014). Contrasting biogeochemical characteristics of the Oubangui River and tributaries (Congo River basin). *Sci. Rep.* 4, 5402. doi: 10.1038/srep05402

Brander, M., Ascui, F., Scott, V., and Tett, S. (2021). Carbon accounting for negative emissions technologies. *Clim. Policy.* 21, 1–19. doi: 10.1080/14693062.2021.1878009

Brusca, L., Aiuppa, A., D'alessandro, W., Parello, F., Allard, P., and Michel, A. (2001). Geochemical mapping of magmatic gas-water-rock interactions in the aquifer of Mount Etna volcano. *J. Volcanol. Geothermal Res.* 108, 199–218. doi: 10.1016/S0377-0273(00)00286-9

Carton, W., Lund, J. F., and Dooley, K. (2021). Undoing equivalence: rethinking carbon accounting for just carbon removal. *Front. Clim.* 3, 664130. doi: 10.3389/fclim.2021.664130

Citoni, B., Fioranelli, F., Imran, M. A., and Abbasi, Q. H. (2019). Internet of things and LoRaWAN-enabled future smart farming. *IEEE Int. Things Mag.* 2, 14–19. doi: 10.1109/IOTM.0001.1900043

Corwin, D. L., and Lesch, S. M. (2005). Apparent soil electrical conductivity measurements in agriculture. *Comp. Electron. Agric.* 46, 11–43. doi: 10.1016/j.compag.2004.10.005

Dietzen, C., Harrison, R., and Michelsen-Correa, S. (2018). Effectiveness of enhanced mineral weathering as a carbon sequestration tool and alternative to agricultural lime: an incubation experiment. *Int. J. Greenhouse Gas Control* 74, 251–258. doi: 10.1016/j.ijggc.2018.05.007

Ebelmen, J. J. (1845). *Sur les produits de la décomposition des espèces minérales de la famille des silicates*. Paris: Carilian-G.ury et Vor Dalmont, Libraires des Corps Royaux des Ponts et Chausees et dus Mines.

Ferrant, S., Laplanche, C., Durbe, G., Probst, A., Dugast, P., Durand, P., et al. (2013). Continuous measurement of nitrate concentration in a highly event-responsive agricultural catchment in south-west of France: is the gain of information useful? *Hydrol. Process.* 27, 1751–1763. doi: 10.1002/hyp.9324

Fortes, R., Prieto, M. H., Terron, J. M., Blanco, J., Millan, S., and Campillo, C. (2014). Using apparent electric conductivity and Ndvi measurements for yield estimation of processing tomato crop. *Transact. Asabe* 57, 827–835. doi: 10.13031/trans.57.10456

Gandois, L., Perrin, A.-S., and Probst, A. (2011). Impact of nitrogenous fertiliser-induced proton release on cultivated soils with contrasting carbonate contents: a column experiment. *Geochim. Cosmochim. Acta* 75, 1185–1198. doi: 10.1016/j.gca.2010.11.025

Gardner, J. S. (1882). The geology of madeira. *Q. J. Geol. Soc.* 38, 277–281. doi: 10.1144/GSL. JGS.1882.038.01-04.30

Gasser, T., Guivarch, C., Tachiiri, K., Jones, C. D., and Ciais, P. (2015). Negative emissions physically needed to keep global warming below 2°C. *Nat. Commun.* 6, 7958. doi: 10.1038/ncomms8958

Goll, D. S., Ciais, P., Amann, T., Buermann, W., Chang, J., Eker, S., et al. (2021). Potential CO2 removal from enhanced weathering by ecosystem responses to powdered rock. *Nat. Geosci.* 14, 545–549. doi: 10.1038/s41561-021-00798-x

Gustafson, H., and Behrman, A. S. (1939). Determination of total dissolved solids in water by electrical conductivity. *Ind. Eng. Chem. Anal. Ed.* 11, 355–357. doi: 10.1021/ac50135a001

Haque, F., Santos, R. M., and Chiang, Y. W. (2020). CO2 sequestration by wollastonite-amended agricultural soils – An Ontario field study. *Int. J. Greenhouse Gas Control* 97:103017. doi: 10.1016/j.ijggc.2020.103017

Hartmann, J., and Kempe, S. (2008). What is the maximum potential for CO(2) sequestration by "stimulated" weathering on the global scale? *Naturwissenschaften* 95, 1159–1164. doi: 10.1007/s00114-008-0434-4

Hartmann, J., West, A. J., Renforth, P., Köhler, P., De La Rocha, C. L., Wolf-Gladrow, D. A., et al. (2013). Enhanced chemical weathering as a geoengineering strategy to reduce atmospheric carbon dioxide, supply nutrients, and mitigate ocean acidification. *Rev. Geophys.* 51, 113–149. doi: 10.1002/rog.20004

Hosono, T., Hartmann, J., Louvat, P., Amann, T., Washington, K. E., West, A. J., et al. (2018). Earthquake-induced structural deformations enhance long-term solute fluxes from active volcanic systems. *Sci. Rep.* 8, 14809. doi: 10.1038/s41598-018-32735-1

Hund, S. V., Johnson, M. S., and Keddie, T. (2016). Developing a hydrologic monitoring network in data-scarce regions using open-source arduino dataloggers. *Agric. Environ. Lett.* 1:160011. doi: 10.2134/ael2016.02.0011

IPCC. (2018). "Global warming of 1.5○C," in *An IPCC Special Report on the Impacts of Global Warming of 1.5○C Above Pre-Industrial Levels and Related Global Greenhouse Gas Emission Pathways, in the Context of Strengthening the Global Response to the Threat of Climate Change, Sustainable Development, and Efforts to Eradicate Poverty*, eds V. Masson-Delmotte, P. Zhai, H. -O. Pörtner, D. Roberts, J. Skea, P. R. Shukla, A. Pirani, W. Moufouma-Okia, C. Péan, R. Pidcock, S. Connors, J. B. R. Matthews, Y. Chen, X. Zhou, M. I. Gomis, E. Lonnoy, T. Maycock, M. Tignor, and T. Waterfield. [In Press].

Kelland, M. E., Wade, P. W., Lewis, A. L., Taylor, L. L., Sarkar, B., Andrews, M. G., et al. (2020). Increased yield and CO2 sequestration potential with the C4 cereal Sorghum bicolor cultivated in basaltic rock dust-amended agricultural soil. *Glob. Chang. Biol.* 26, 3658–3676. doi: 10.1111/gcb.15089

Kitchen, N. R., Drummond, S. T., Lund, E. D., Sudduth, K. A., and Buchleiter, G. W. (2003). Soil electrical conductivity and topography related to yield for three contrasting soil-crop systems. *Agron. J.* 95, 483–495. doi: 10.2134/agronj2003.4830

Krawczyk, W. E., and Ford, D. C. (2006). Correlating specific conductivity with total hardness in limestone and dolomite karst waters. *Earth Surf. Process. Landforms* 31, 221–234. doi: 10.1002/esp.1232

Le Bas, M. J., Maitre, R. W. L., Streckeisen, A., and Zanettin, B. (1986). A chemical classification of volcanic rocks based on the total alkali-silica diagram. *J. Petrol.* 27, 745–750. doi: 10.1093/petrology/27.3.745

Lefebvre, D., Williams, A. G., Kirk, G. J. D., Paul, Burgess, J., Meersmans, J., Silman, M. R., et al. (2021). Assessing the carbon capture potential of a reforestation project. *Sci. Rep.* 11, 19907. doi: 10.1038/s41598-021-99395-6

Leonardos, O. H., Fyfe, W. S., and Kronberg, B. I. (1987). The use of ground rocks in laterite systems: an improvement to the use of conventional soluble fertilizers? *Chem. Geol.* 60, 361–370. doi: 10.1016/0009-2541(87)90143-4

Likens, G. E. (2017). Fifty years of continuous precipitation and stream chemistry data from the Hubbard Brook ecosystem study (1963-2013). *Ecology* 98, 2224. doi: 10.1002/ecy.1894

Mccleskey, R. B., Nordstrom, D. K., Ryan, J. N., and Ball, J. W. (2012). A new method of calculating electrical conductivity with applications to natural waters. *Geochim. Cosmochim. Acta* 77, 369–382. doi: 10.1016/j.gca.2011.10.031

Mclaren, D. (2012). A comparative global assessment of potential negative emissions technologies. *Process Saf. Environ. Protect.* 90, 489–500. doi: 10.1016/j.psep.2012.10.005

Missoux, M. (1853). Sur l'emploi de la poudre des roches granitiques comme excitant de la vegetation. *Compt. Rend. Acad. Sci.* 36, 1136.

Noborio, K. (2001). Measurement of soil water content and electrical conductivity by time domain reflectometry: a review. *Comp. Electron. Agric.* 31, 213–237. doi: 10.1016/S0168-1699(00)00184-8

Othaman, N. N. C., Isa, M. N. M., Ismail, R. C., Ahmad, M. I., and Hui, C. K. (2020). "Factors that affect soil electrical conductivity (EC) based system for smart farming application," in *The 2nd International Conference on Applied Photonics and Electronics 2019 (InCAPE 2019)*.

Parkhurst, D. L., and Appelo, C. A. J. (2013). "Description of input and examples for PHREEQC version 3—A computer program for speciation, batch-reaction, one-dimensional transport, and inverse geochemical calculations," in *U. S. Geological Survey Techniques and Methods*. U.S. Geological Survey.

Pawlowicz, R. (2008). Calculating the conductivity of natural waters. *Limnol. Oceanogr. Methods* 6, 489–501. doi: 10.4319/lom.2008.6.489

Perrin, A.-S., Probst, A., and Probst, J.-L. (2008). Impact of nitrogenous fertilizers on carbonate dissolution in small agricultural catchments: implications for weathering CO2 uptake at regional and global scales. *Geochim. Cosmochim. Acta* 72, 3105–3123. doi: 10.1016/j.gca.2008.04.011

Peters, G. P., and Geden, O. (2017). Catalysing a political shift from low to negative carbon. *Nat. Clim. Chang.* 7, 619–621. doi: 10.1038/nclimate3369

Peters, S. C., Blum, J. D., Driscoll, C. T., and Likens, G. E. (2004). Dissolution of wollastonite during the experimental manipulation of hubbard brook watershed 1. *Biogeochemistry* 67, 309–329. doi: 10.1023/B:BIOG.0000015787.44175.3f

Phong, P. H., Anh, P. B. V., Ha, V. T. T., Hung, L. Q., and Thanh, L. M. (2020). Simulating and monitoring the temporal and spatial transfer of NPK Fertilizer In Agricultural Soils Using A Mathematical Model And Multi-Channel Electrical Conductivity Measurement. *J. Soil Sci. Plant Nutr.* 21, 374–388. doi: 10.1007/s42729-020-00367-y

Pierson-Wickmann, A. C., Aquilina, L., Martin, C., Ruiz, L., Molénat, J., Jaffrézic, A., et al. (2009). High chemical weathering rates in first-order granitic catchments induced by agricultural stress. *Chem. Geol.* 265, 369–380. doi: 10.1016/j.chemgeo.2009.04.014

Proulx, C. L., Kilgour, B. W., Francis, A. P., Bouwhuis, R. F., and Hill, J. R. (2018). Using a conductivity–alkalinity relationship as a tool to identify surface waters in reference condition across Canada. *Water Qual. Res. J.* 53, 231–240. doi: 10.2166/wqrj.2018.030

Renforth, P., Pogge Von Strandmann, P. A. E., and Henderson, G. M. (2015). The dissolution of olivine added to soil: implications for enhanced weathering. *Appl. Geochem.* 61, 109–118. doi: 10.1016/j.apgeochem.2015.05.016

Sanderson, B. M., O'neill, B. C., and Tebaldi, C. (2016). What would it take to achieve the Paris temperature targets? *Geophys. Res. Lett.* 43, 7133–7142. doi: 10.1002/2016GL069563

Schuiling, R. D., and Krijgsman, P. (2006). Enhanced weathering: an effective and cheap tool to sequester CO2. *Clim. Change* 74, 349–354. doi: 10.1007/s10584-005-3485-y

Scudiero, E., Berti, A., Teatini, P., and Morari, F. (2012). Simultaneous monitoring of soil water content and salinity with a low-cost capacitance-resistance probe. *Sensors* 12, 17588–17607. doi: 10.3390/s121217588

Sechriest, R. E. (1960). Relationship between total alkalinity, conductivity, original pH, and buffer action of natural water. *Ohio J. Sci.* 60, 303–308.

Seifritz, W. (1990). CO2 disposal by means of silicates. *Nature* 345, 486–486. doi: 10.1038/345486b0

Streckeisen, A. (1980). Classification and nomenclature of volcanic rocks, lamprophyres, carbonatites and melilitic rocks IUGS subcommission on the systematics of igneous rocks. *Geol. Rundschau* 69, 194–207. doi: 10.1007/BF01869032

Taylor, L. L., Driscoll, C. T., Groffman, P. M., Rau, G. H., Blum, J. D., and Beerling, D. J. (2021). Increased carbon capture by a silicate-treated forested watershed affected by acid deposition. *Biogeosciences* 18, 169–188. doi: 10.5194/bg-18-169-2021

Ten Berge, H. F. M., Van Der Meer, H. G., Steenhuizen, J. W., Goedhart, P. W., Knops, P., and Verhagen, J. (2012). Olivine weathering in soil, and its effects on growth and nutrient uptake in ryegrass *Lolium perenne* L.: a pot experiment. *PLoS ONE* 7, e42098. doi: 10.1371/journal.pone.0042098

Terence, S., and Purushothaman, G. (2020). Systematic review of Internet of Things in smart farming. *Transact. Emerg. Telecommun. Technol.* 31:e3958. doi: 10.1002/ett.3958

Thompson, M. Y., Brandes, D., and Kney, A. D. (2012). Using electronic conductivity and hardness data for rapid assessment of stream water quality. *J. Environ. Manage.* 104, 152–157. doi: 10.1016/j.jenvman.2012.03.025

United Nations (2015). *Chapter XXVII Environment, 7.d Paris Agreement*. New York, NY.

Van Der Weijden, C. H., and Pacheco, F. A. L. (2003). Hydrochemistry, weathering and weathering rates on Madeira island. *J. Hydrol.* 283, 122–145. doi: 10.1016/S0022-1694(03)00245-2

Van Straaten, P. (2002). *Rocks for Crops: Agrominerals of sub-Saharan Africa*. Nairobi, Kenya: ICRAF.

Virtanen, P., Gommers, R., Oliphant, T. E., Haberland, M., Reddy, T., Cournapeau, D., et al. (2020). SciPy 1.0: fundamental algorithms for scientific computing in Python. *Nat. Methods* 17, 261–272. doi: 10.1038/s41592-019-0686-2

Vitens (2021). *PhreeqPython*. Available online at: https://github.com/Vitens/phreeqpython (accessed December 15, 2021).

Conflict of Interest: The authors declare that the research was conducted in the absence of any commercial or financial relationships that could be construed as a potential conflict of interest.

Publisher's Note: All claims expressed in this article are solely those of the authors and do not necessarily represent those of their affiliated organizations, or those of the publisher, the editors and the reviewers. Any product that may be evaluated in this article, or claim that may be made by its manufacturer, is not guaranteed or endorsed by the publisher.

frontiers | Frontiers in Climate

ORIGINAL RESEARCH
published: 17 May 2022
doi: 10.3389/fclim.2022.869456

Enhanced Weathering Using Basalt Rock Powder: Carbon Sequestration, Co-benefits and Risks in a Mesocosm Study With *Solanum tuberosum*

Arthur Vienne[1]*, *Silvia Poblador*[1], *Miguel Portillo-Estrada*[1], *Jens Hartmann*[2], *Samuel Ijiehon*[1], *Peter Wade*[3] *and Sara Vicca*[1]

[1] PLECO (Plants and Ecosystems), Department of Biology, University of Antwerp, Antwerp, Belgium, [2] Institute for Biogeochemistry and Marine Chemistry, KlimaCampus, Universität Hamburg, Hamburg, Germany, [3] (GLOBAL) Future Forest Company LTD, Darlington, United Kingdom

OPEN ACCESS

Edited by:
Ben W. Kolosz,
University of Pennsylvania,
United States

Reviewed by:
Rafael Mattos Dos Santos,
University of Guelph, Canada
Davide Ciceri,
Agroplantae, United States

***Correspondence:**
Arthur Vienne
arthur.vienne@uantwerpen.be

Specialty section:
This article was submitted to Negative Emission Technologies, a section of the journal Frontiers in Climate

Received: 04 February 2022
Accepted: 04 April 2022
Published: 17 May 2022

Citation:
Vienne A, Poblador S, Portillo-Estrada M, Hartmann J, Ijiehon S, Wade P and Vicca S (2022) Enhanced Weathering Using Basalt Rock Powder: Carbon Sequestration, Co-benefits and Risks in a Mesocosm Study With Solanum tuberosum. Front. Clim. 4:869456. doi: 10.3389/fclim.2022.869456

Enhanced weathering (EW) of silicate rocks can remove CO_2 from the atmosphere, while potentially delivering co-benefits for agriculture (e.g., reduced nitrogen losses, increased yields). However, quantification of inorganic carbon sequestration through EW and potential risks in terms of heavy metal contamination have rarely been assessed. Here, we investigate EW in a mesocosm experiment with *Solanum tuberosum* growing on alkaline soil. Amendment with 50 t basalt/ha significantly increased alkalinity in soil pore water and in the leachate losses, indicating significant basalt weathering. We did not find a significant change in TIC, which was likely because the duration of the experiment (99 days) was too short for carbonate precipitation to become detectable. A 1D reactive transport model (PHREEQC) predicted 0.77 t CO_2/ha sequestered over the 99 days of the experiment and 1.83 and 4.48 t CO_2/ha after 1 and 5 years, respectively. Comparison of experimental and modeled cation pore water Mg concentrations at the onset of this experiment showed a factor three underestimation of Mg concentrations by the model and hence indicates an underestimation of modeled CO_2 sequestration. Moreover, pore water Ca concentrations were underestimated, indicating that the calcite precipitation rate was overestimated by this model. Importantly, basalt amendment did not negatively affect potato growth and yield (which even tended to increase), despite increased Al availability in this alkaline soil. Soil and pore water Ni increased upon basalt addition, but Ni levels remained below regulatory environmental quality standards and Ni concentrations in leachates and plant tissues did not increase. Last, basalt amendment significantly decreased nitrogen leaching, indicating the potential for EW to provide benefits for agriculture and for the environment.

Keywords: enhanced weathering, basalt, carbon sequestration, DIC, TIC, nitrate, nickel, PHREEQC

INTRODUCTION

In order to limit global warming to well below 2°C, model projections indicate that both rapid decarbonisation and negative emission technologies (NETs) will be required (Gasser et al., 2015). Hence, in addition to conventional mitigation there is an urgent need for development of scalable NETs that safely remove CO_2 from the atmosphere. A promising, yet poorly studied NET, is enhanced weathering (EW) of silicate minerals, which is particularly of interest due to its application potential in agriculture (van Straaten, 2002; Hartmann et al., 2013; Haque et al., 2019; Beerling et al., 2020). This technique aims to accelerate natural weathering, a process that has been responsible for stabilizing climate over geological timescales, which naturally captures 1.1 Gt of CO_2 per year (or ca. 3% of current global CO_2-emissions; Strefler et al., 2018; Roser and Ritchie, 2020). The idea behind EW is to speed up this natural process by grinding silicate rocks to powder, hence increasing the surface area (Schuiling and Krijgsman, 2006; Hartmann et al., 2013) and bringing these in a moisture-retaining environment favorable to weathering, e.g., agricultural soils.

Agricultural enhanced weathering is considered a promising NET because co-utilization of surface area with agricultural land is possible and competition with food production is avoided (in contrast to some other NETs such as afforestation). Furthermore, the cost of terrestrial EW was recently estimated to be competitive to those of other NETs, such as Direct Air Carbon Capture and Storage (DACCS) (Strefler et al., 2018; Beerling et al., 2020). As the original focus of agricultural silicate rock amendment was delivering agricultural benefits rather than CO_2 sequestration (van Straaten, 2002), only few studies have quantified the associated CO_2 sequestration.

Silicate weathering involves the reaction of silicate minerals with CO_2 and water to form bicarbonate (HCO_3^-) and carbonate (CO_3^{2-}) ions and cations (mainly Ca^{2+}, Mg^{2+}, Na^+, and K^+). Ca^{2+} and Mg^{2+} may either precipitate in the soil (degassing one mole of CO_2 per mole of divalent cation) to form solid carbonates or are transported to streams and ultimately the ocean. Hence, in order to quantify total inorganic CO_2 sequestration through EW, both changes in total inorganic carbon (TIC) in the soil (solid phase) and the exported dissolved inorganic carbon (DIC) through runoff should be considered. The few studies that estimated CO_2 sequestration thus far, usually calculated CO_2 sequestration based on cation changes in leachates or soil exchangeable pools (ten Berge et al., 2012; Dietzen et al., 2018; Amann et al., 2020). However, changes in soil cations are confounded by plant uptake, soil adsorption, and cation exchange. Others considered soil TIC changes but did not account for DIC leaching (Manning et al., 2013). Quantification of DIC leaching losses is difficult in the field, but may be estimated using a reactive transport model such as PHREEQC. This model can account for the carbonate and cation flows through the soil and estimate CO_2 sequestration through EW, but these estimates have not yet been verified with experimental data.

A key abiotic factor influencing weathering rates (and therefore carbon sequestration) is pH. Weathering rates are typically assumed to increase with decreasing pH, but this relationship differs between silicate minerals. According to Brantley et al. (2008), mineral dissolution of the silicate minerals contained in basalt (mainly olivine, augite, plagioclase) proceeds *via* an acidic and *via* an alkaline pathway and is lowest around pH five. While olivine and augite dissolution increase with decreasing pH, weathering of Al-containing Ca-plagioclases increases at alkaline pH (Qian and Schoenau, 2002) (**Supplementary Figure SF1**). Not only dissolution of ions into the liquid phase is a pH dependent process. Reprecipitation of these ions is also influenced by pH. In alkaline soils, precipitation of HCO_3^- in carbonates is promoted, which can stimulate weathering rates in the longer term by removing weathering products from soil solutions (Bose and Satyanarayana, 2017). For example, Fe can be removed from solution at alkaline pH through precipitation of $Fe(OH)_3$ and Fe-bearing carbonates such as siderite, ankerite and ferroan calcite. Likewise, Al can precipitate as $Al(OH)_3$ at alkaline pH. Alkaline pH can thus increase both dissolution of Al-bearing plagioclases and Al hydroxide precipitation, indicating that, in contrast to what has been suggested in some studies (Beerling et al., 2018), EW application should not necessarily be focused on acidic soils.

Although research on the drivers of EW has mostly focused on abiotic factors, several biotic processes can also strongly influence mineral weathering, and some of these effects may be stronger in alkaline soils (Vicca et al., 2022). For example, enzymes of the group carbonic anhydrases (CAs) (which catalyse HCO_3^- formation and are found in all domains of life) were found to be most efficient at pH above seven and may support the silicate dissolution process in alkaline soils (Demir et al., 2001). Xiao et al. (2015) observed promoted wollastonite ($CaSiO_3$) weathering (Ca-release) upon addition of CA from *Bacillus mucilaginosus*.

Apart from potential enhancement of mineral dissolution through (a)biotic mechanisms, a considerable share of land area is alkaline. According to the Harmonized World Soil Database (FAO), about 23% of all soils have an alkaline pH (>7) (Fischer et al., 2008). Although EW is currently considered to be most effective for CO_2 removal in tropical areas (Hartmann et al., 2013), alkaline soils clearly hold considerable potential for CO_2 removal through EW, but their CO_2 sequestration potential, as well as potential side-effects require experimental verification.

Silicate rock dust have been previously applied to agricultural soil because of its potential benefits for agriculture. These include increased cation exchange capacity (CEC) and crop yields, increased plant nutrient concentrations and countered soil acidification. Moreover, silicate addition can also increase plant pest- and drought resistance (Hartmann et al., 2013; Blanc-Betes et al., 2021) and reduce N-losses (N_2O and NO_3^- emissions). Similarly to agricultural liming, EW induces a pH increase in acid soils, which is hypothesized to reduce nitrogen losses because the activity of denitrifying enzymes was found to increase at neutral pH (Bakken et al., 2012; Qu et al., 2014; Kantola et al., 2017).

On the other hand, large-scale EW adoption may hold the risk of heavy metal (especially Ni) contamination, particularly when fast-weathering ultramafic minerals are used (Haque et al., 2020a). In this context, basalt rock is proposed as an alternative for the ultramafic mineral olivine, as basalt contains less Ni (Amann and Hartmann, 2019). Interestingly, alkaline soils may

reduce the risk of Ni leaching to surface waters, as more Ni can be adsorbed in soils at alkaline pH. Ni can form insoluble hydroxides and the presence of carbonates may also lead to an increase in the retention of Ni as carbonate salt in soil (Sathya and Mahimairaja, 2015). Although terrestrial EW focus shifted to basalt and less problems in Ni contamination are expected with this rock in alkaline soils, a comparison with regulatory environmental quality standards (EQSs) remains necessary to ensure environmental safety. As aforementioned, Al release by weathering of Al-bearing plagioclases is stimulated in alkaline soils, as well as $Al(OH)_3$ precipitation. The resulting effect may increase Al concentration (Al toxicity) in alkaline soil pore water, in contrast with EW in acid soils, where pH increase decreases Al availability.

We set up a mesocosm experiment to investigate carbon sequestration, risks and co-benefits of EW using basalt rock powder with potatoes (*Solanum tuberosum*) as this is the world's third most important crop in terms of human consumption, after wheat and rice (FAOSTAT, 2013). In addition, from a sustainable development goals (SDGs) perspective, it is also a highly relevant crop as potatoes are grown in regions that are experiencing high poverty and malnutrition (Campos and Ortiz, 2019). We quantified CO_2 sequestration through EW based on experimental data and using the PHREEQC 1D reactive transport model. Further, we hypothesized that potato tuber yield would benefit from the increase in base cations (released from the basalt), while we expected Ni leaching to remain within the safe range according to environmental quality standards. In addition, we expected that basalt addition would reduce N leaching.

MATERIALS AND METHODS

Experimental Set-Up

A mesocosm experiment with 10 mesocosms (five Control and five basalt-amended) was constructed at the experimental site at the Drie Eiken Campus of the University of Antwerp (Belgium, 51°09′ N, 04°24′ E). The mesocosms (1 m height, radius = 0.25 m) were placed under a transparent shelter, hence excluding natural rainfall. In April 2019, the mesocosms were filled with loamy soil (**Table 1**). In the basalt amended mesocosms, a mass equivalent to 50 t basalt ha-1 was homogeneously mixed into the upper 20 cm. On 21 May 2019, three potatoes (*Solanum tuberosum* "Nicola," purchased at AVESTA, Belgium) were planted in each mesocosm and all pots received 60 g of NPK fertilizers (5 – 4 – 15 + Bacillus). All mesocosms were watered regularly with tap water (composition: see **Supplementary Table ST7**). Soil pore water was sampled from two rhizon samplers (Rhizon Flex, Rhizosphere Research Products B.V., Wageningen, NL) installed at five cm depth in each mesocosm. To allow leachate collection, mesocosms had a two cm diameter hole at the bottom. On the inside, the bottom of the pot was covered with a root exclusion math to prevent soil export through leaching. A glass collector (one liter volume) was placed under the mesocosm to collect the leachates. Leachate volumes were determined throughout the experiment and samples for chemical analyses were collected on six occasions (23/5; 28/5; 6/6; 16/6; 7/8; 13/8; 20/8 in 2019). Nitrogen in leachates was analyzed on the last three dates.

TABLE 1 | Characterization of soil (pH, texture, and organic C) and basalt (composition, specific surface area, particle size distribution, and XRF data).

Control soil characteristics*	
pH	7.72 ± 0.03
Texture class (Sand, clay, silt %)	Silt (18.39, 0.83, 92.21%)
Inorganic C (%)	0.16 ± 0.02 (standard error)
Organic C (%)	0.83 ± 0.03 (standard error)
Basalt characteristics (type: DURUBAS, RPBL)	
Mineralogical composition	(g/g)
Augite	0.50
Plagioclase (modeled as labradorite)	0.35
Olivine (modeled as Mg1.04Fe0.96SiO4)	0.05
Illite	0.05
Chlorite	0.05
Specific surface area	(9.226 ± 0.076) m²/g
Particle size	
>2,000 μm	0.25%
500–2,000 μm	0.52%
250–500 μm	22.30%
63–250 μm	59.82%
32–63 μm	14.73%
<32 μm	2.38%
XRF basalt	(m%)
SiO_2	44.6
MgO	12.9
CaO	10.8
K_2O	0.7
Na_2O	2.6
P_2O_5	0.9
Al_2O_3	11.5
Fe_2O_3	11.7
TiO_2	2.30

Model assumptions for the minerals are also included.
**Control soil characteristics were measured after the experimental period of 99 days.*

Soil and Basalt Characteristics

Basalt characteristics are given in **Table 1**. Surface area was measured in triplicate with Kr using a Quantachrome surface area analyser. Basalt (type: DURUBAS) composition was determined by the supplier [Rheinischen Provinzial-Basalt- und Lavawerke (RPBL)]. Basalt particle size distribution was determined by sieve separation.

Plant Responses

On the 27th of August 2019, all plants were harvested and separated into aboveground and belowground parts. After drying (48 h at 70°C, potatoes were cut to speed up the drying process), above- and belowground (potato tuber) biomass was determined. Potato tubers were analyzed for Mg, Ca, K, Si, Al, and Ni

by ICP-OES (iCAP 6300 duo, Thermo Scientific). Ni and Al were determined after a destruction of 0.2 g sample with 20 mL HNO_3. For Ca, Mg and K, 0.3 g of sample was destructed with a $H2SO_4$/Se/salicylic acid mixture according to the protocol of Walinga et al. (1989). For Si, 30 mg sample was destructed with 20 mL of 0.5 N NaOH, this was done in triplicate.

Soil Analyses

Soil cores (5 cm length) were taken across the depth of the mesocosm (0–10 cm, 10–20 cm, 20–30 cm, 30–50 cm, 50–75 cm, and 75–100 cm). Immediately after collection, the cores were dried at 105°C for 3 days to determine water content (g H_2O/g soil) and bulk density. Water-filled porosity was calculated by multiplying water content with bulk density. The soil samples were ground to pass a 0.2 mm sieve with an ultra-centrifugal mill (Model ZM 200, Retsch GmbH, Haan, Germany).

Soil Total Carbon (TC) was determined with an elemental analyzer (Flash 2000 CN Soil Analyser, Interscience, Louvain-la-Neuve, Belgium). Total Organic Carbon (TOC) of each 20 cm across mesocosms was determined in the elemental analyser after acid hydrolysis of the original sample: 1 g of soil was digested with excess of 6N HCl at 80°C to and the residue dried. The remaining sample was analyzed giving TOC as a result, and TIC was calculated as the difference between TC and TOC.

Other soil elements (Mg, Ca, K, Al, and Ni) for samples taken at 10, 25, and 40 cm depth were determined using ICP-OES. In this way, concentrations in the topsoil, the basalt-soil mixing layer and deeper layers were measured. Brown's procedures (1943) were used for CEC and total exchangeable bases (TEB), for which 1M NH_4Acetate at pH seven served as the extractant (Brown, 1943). CEC and TEB were also measured in soils sampled at 10, 25, and 40 cm depth.

Leachate and Pore Water Analysis

Leachate and pore water samples for Ca, Mg, K, Fe, Al analyses were filtered over a 0.45 µm PET filter and were conserved adding 1.5 mL 15.8 N HNO_3 (69%) to 30 mL of sample until analysis with ICP-OES (iCAP 6300 duo, Thermo Scientific). Nitrogen (NH_4^+-N, NO_3^--N) and alkalinity were determined using a Skalar (SAN++) continuous flow analyzer. Nitrogen samples were conserved in tubes with 20 µL 10 N HCl before analysis. pH was determined using a HI3220 pH/ORP meter. For monitoring soil nutrient availability, we used commercially available PRS™ probes (Western Ag Global, Saskatoon, SK, Canada), which provide proxies for plant available ions in soil solution while in contact with the soil (Gudbrandsson et al., 2011). Eight PRS probes (four for cation and four for anion, **Figure 1**) were installed in each mesocosm twice during the growing season, on 7th of June and 6th of August, and were retrieved 7 days after burial. Total N leaching was calculated as the sum of NH_4-N and NO_3-N leaching.

Soil CO_2 Efflux

Soil CO_2 efflux was measured on three occasions on a shallow stainless steel collar (8 cm high, 10 cm diameter) which was installed at four cm depth in each mesocosm (**Figure 1**). Measurements were made using a custom-built soil chamber (0.98 L), which was connected to a portable EGM-5 infrared gas analyzer (PP Systems, Hitchin, UK). We measured the increase in soil CO_2 concentration until a CO_2 concentration difference of 50 ppm was reached, or during 120 s in case of lower increases.

FIGURE 1 | A mesocosm containing three potato plants, a stainless steel collar, PRS probes and rhizon samplers.

PHREEQC Reactive Transport Model for CO_2 Sequestration

Carbon sequestration was modeled using the PHREEQC geochemical platform (Parkhurst and Appelo, 2013). We followed the approach of Kelland et al. (2020), an overview of the model's required inputs is given in **Figure 2**. The model details and calculation of the model's inputs can be found in **Supplementary Material 2**. The model includes different PHREEQC functionalities (phases, dissolution rates, solutions, transport, equilibrium phases, cation exchange, and surface adsorption) which are indicated in bold. The 1 m long mesocosms were divided into 20 cells of 5 cm height. Basalt was added to the four top layers (20 cm topsoil). Hence, in the phases block, basalt mineralogy and thermodynamic data of mineral dissolution (log k and enthalpy) are entered for the first four cells. The possibility of inclusion of minerals within other mineral phases may occur but was not included in our model. Basalt mineral dissolution according to the rate law of Palandri and Kharaka (2004) is inserted in the Rates functionality. The selection of parameters for this rate law is discussed in Section 1.1 of **Supplementary Material 1**. For the mineral augite (50 m% of the utilized DURUBAS basalt), two different rate laws were considered in different simulations (the first rate law utilizes parameters as in Palandri and Kharaka (2004), while the second follows the approach of Knauss et al. (1993) at 25°C with an Arrhenius temperature correction to the experimental temperature (**Supplementary Table ST1**). Plagioclase was simulated as labradorite because labradorite is intermediate in the Na-Ca plagioclase series and the Ca content of the plagioclase in the durubas basalt is unknown.

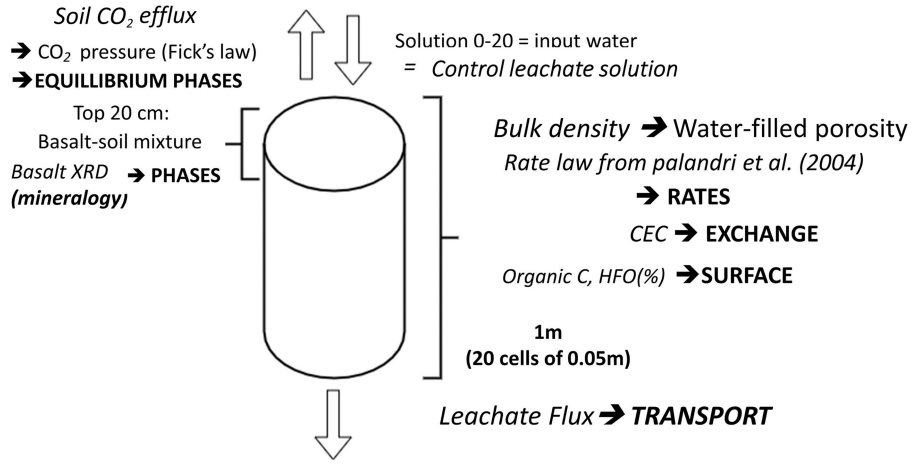

FIGURE 2 | Overview of the PHREEQC reactive transport model. PHREEQC functions are indicated in bold, model inputs are written in italics.

For labradorite, alkaline dissolution kinetic parameters were considered (**Supplementary Figure SF1**). In order to simulate mineral weathering in the control soil, the input solution (that is added on the top layer of all simulated columns) equals the composition of the efflux soil solution in the control treatment. Cations (e.g., Ca or Mg) are added to this control solution according to the abovementioned rate law. This solution is in equilibrium with equilibrium phases (gases and minerals, e.g., CO_2, calcite and $Al(OH)_3$).

CO_2 partial pressure was entered in the equilibrium phases functionality and was calculated using Fick's law (as in Roland et al., 2015), using the average experimental soil CO_2 efflux (F in Equation 1). The difference between the CO_2 concentration in the atmosphere and soil (**C**) increases with depth (**z**). Assuming a constant atmospheric CO_2 concentration of 414 ppm, soil CO_2 concentration at each soil depth was calculated and converted to pressure by multiplying with the universal gas constant and the average experimental soil temperature (285 K). Water-filled porosity was calculated from the soil bulk density (1.40 kg soil.l-1 soil) and equaled 0.141 H2O/l soil (Equation 3). The diffusion coefficient, Ds (Equation 4), was calculated from the total and water-filled porosity (Equations 2, 3) as in Roland et al. (2015).

$$F = -Ds \cdot \frac{\Delta C}{z} \quad (1)$$

$$Total\ porosity\ (\%) = 100 \cdot \left(1 - \frac{Bulk\ density\left[\frac{g}{cm^3}\right]}{2.65\frac{g}{cm^3}}\right) \quad (2)$$

$$water\ filled\ porosity\ (\%) = 100 \cdot Bulk\ density\ [\frac{g\ soil}{cm^3 soil}] \cdot soil\ moisture[\frac{cm^3 H2O}{g\ soil}] \quad (3)$$

$$Ds = 1.47 \cdot 10^{-5} \cdot \left(\frac{285.2}{273.2}\right)^{1.75} \cdot \frac{\left(total\ porosity - water\ filled\ porosity\ (\%)\right)^2}{total\ porosity\ (\%)^{\frac{2}{3}}} \quad (4)$$

Cations can complex on surfaces such as organic matter or ferrihydrite (HFO). Surface complexation of species on organic matter is included by implementing the WHAM model using the organic carbon content of the soil (control group) (Lawlor, 1998). Exchange of cations with soils is also included as the measured cation exchange capacity (CEC) is inserted in the "Exchange" functionality. Finally, in the transport functionality, the average observed leachate flux (7.61L/99 days/mesocosm) was inserted.

The 1D reactive transport model was run for a scenario with and without basalt amendment. Simulated results of weathering products (Ca, Mg) in the first cells were compared with experimental concentrations of Mg and Ca in the topsoil pore water (**Figure 6**).

Data Analysis and Calculation of CO_2 Sequestration

One-way Anova was used for detecting statistical differences in biomass and soil composition among treatments. For analyses that were repeated in time (leachate and pore water chemistry measurements), a repeated measures one-way Anova was used using the lmer package in R studio Version 1.4.1106. Normality and homoscedasticity assumptions underlying statistical tests were evaluated with the Shapiro-Wilk test. If residuals were not normally distributed a log10 transformation on the variable was performed. Total mesocosm TIC was calculated using Equation

5 (with n = number of depths).

$$\frac{kg\ TIC}{mesocosm} = \sum_{i=1}^{n} \frac{\Delta TIC,i\ (\%)}{100} \cdot \Delta depth,i\ [m] \cdot \frac{0.196m^2}{mesocosm} \cdot BulkDensity,i \left[\frac{kg}{m^3}\right] \quad (5)$$

In order to calculate total inorganic CO_2 (IC) sequestration, the total sequestered mass of carbon as DIC in leachates and as TIC changes are summed. The CO_2 sequestration through DIC leaching losses was calculated by multiplying the observed leachate flow (7.61 L/mesocosm/99 days) with the difference in average DIC concentration among treatments. DIC was calculated from the experimentally measured alkalinity with a slope of 6.70 gDIC/Equivalent (**Supplementary Figure SF5**).

RESULTS

Inorganic Carbon Sequestration

Weathering Products

Basalt addition significantly altered soil and soil pore water chemistry. The strongest changes of basalt amendment were observed for Mg, for which the basalt effect increased the topsoil Mg concentration with about 200% (**Table 2**). A clear negative basalt x depth interaction effect was found: the basalt effect on soil Mg decreased with depth. Likewise, basalt amendment increased soil CEC (and TEB), especially in the topsoil (a significantly negative basalt x depth interaction effect was found for CEC and TEB). Soil pore water Mg concentration also increased significantly, and the Ca concentration tended to increase (**Table 3**). On the other hand, the PRS probes indicated no significant basalt effect on Mg and Ca availability, although we observed a tendency for an increase at the start of the experiment. These PRS probe data also revealed a strong decline in availability of Ca, Mg and other cations over the course of the experiment.

Topsoil K decreased with basalt addition, and increased at lower depths in the basalt treatment (i.e., a significantly positive depth × basalt interaction was found). This decrease in topsoil K is not due to a soil dilution effect because this basalt contains more K than background soil (**Table 4**). PRS probes in the topsoil showed an increase in topsoil K in June, but not in August. Al increased significantly in the soil ($p = 0.03^*$). The PRS probes revealed a borderline significant increase in Al (**Table 3**; $p = 0.08$), indicating weathering of Al-bearing silicate minerals Ca-plagioclase and/or augite. Basalt did not increase Fe in PRS probes ($p = 0.99$). We observe a decrease of P in PRS probes of the basalt treatment, leading to a borderline significant negative basalt effect ($p = 0.07$). pH in the pore water and leachates did not significantly change upon basalt amendment, and the system was buffered at pH 7.7 (**Table 3**).

Experimental Inorganic Carbon Sequestration

On average, basalt weathering increased leachate and topsoil pore water (0–5 cm) alkalinity with 8 and 29%, respectively (**Figure 3**). After 99 days of experiment, a higher amount of DIC (calculated from TA), equivalent to only 4.77 $kgCO_2$/ha, had leached from the basalt amended system compared to the control system (**Table 4**). We found no significant basalt effect on soil TIC content (**Figure 4**). Note that the large uncertainty on TIC resulted in a large uncertainty on the estimate of ΔIC.

During the timespan of the experiment, the PHREEQC model predicts a difference of 4.39 gTIC/mesocosm formation between basalt and control treatment in the top 20 cm mesocosm. Given the mass of soil in the column (54.9 kg in the top 20 cm column), this results in an increase of about only 0.01% inorganic carbon (**Supplementary Table ST3**; **Supplementary Figure SF9**). Hence, given the variation in measured TIC percentages (**Figure 4A**), this indicates that the uncertainty on the measurements is larger than the modeled differences in TIC. Indeed, although TIC tended to be higher in the basalt amended soils, this increase was not statistically significant (**Figure 4B**).

TABLE 2 | Multiple regression parameters of different soil elements analysed (Ca, Mg, Al, K, Ni), cation exchange capacity (CEC) and total exchangable bases (TEB).

Soil characteristic	Intercept	Basalt effect	Depth effect	Interaction
Ca	1,707.9	+307.17 **($p = 0.04^*$)**	N.S.	N.S.
Mg	670.04	+1,345.6 **($p < 0.001^{***}$)**	−5.8500 ($p = 0.32$)	−28.490 **($p < 0.01^{**}$)**
Al	2,845.3	+450.46 **($p = 0.03^*$)**	+28.370 **($p = 0.001^{**}$)**	N.S.
K	1,197.4	−373.01 **($p = 0.05$)**	+1.2100 ($p = 0.78$)	+15.310 **($p = 0.02^*$)**
Ni	56.510	+23.070 **($p = 0.05$)**	N.S.	N.S.
CEC	5.22	+1.81 **($p < 0.01^*$)**	0.0100 ($p = 0.45$)	−0.0600 **($p < 0.01^{**}$)**
TEB	5.19	+1.82 **($p < 0.01^{**}$)**	0.0120 ($p = 0.46$)	−0.0600 **($p < 0.01^{**}$)**

*N.S., Not Significant; Elements units are expressed in mg element/kg soil, CEC and TEB are expressed in mEQ/100 g soil. (Borderline) Significant increases ($p < 0.10$) are indicated in bold. Significance codes *, ** and *** refer to p-values in the ranges 0.01–0.05, 0.001–0.01 and 0–0.001 respectively.*

PHREEQC Modeled Inorganic Carbon Sequestration

Modeled IC sequestration during the duration of the experiment was 0.77 t CO_2/ha (**Figure 5**). A model run beyond the experimental period indicated a CO_2 sequestration of 1.83 and 4.48 t CO_2/ha after 1 and 5 years, respectively (**Supplementary Table ST3**). The evolution of olivine, labradorite and augite dissolution is shown in **Supplementary Figure SF8**.

We calculated the difference in Mg and Ca pore water concentration between the basalt and control treatment and compared this delta for experimental data and simulated values (**Figure 6**). This indicated that the model underestimated initial increases of Mg in the pore water by a factor 3. For Ca, simulated concentrations were lower in the basalt treatment than

TABLE 3 | Overview of weathering products (Ca, Mg, K, and P) concentrations ± standard error observed in leachates and pore water samples over the entire season and in PRS probes at two occasions (June and August).

Weathering products in:	Control	Basalt	*p*-value
Leachates	**Concentration (mg element/L)**		
Ca	226.61 ± 34.05	273.21 ± 30.67	0.92
Mg	18.83 ± 2.74	23.26 ± 2.54	0.05
K	16.37 ± 2.88	22.56 ± 2.52	0.45
P	0.138 ± 0.027	0.135 ± 0.012	0.66
pH	7.67 ± 0.05	7.67 ± 0.04	0.92
Top 5 cm pore water	**Concentration (mg element/L)**		
Ca	76.31 ± 13.16	110.88 ± 25.78	0.13
Mg	6.99 ± 1.11	11.88 ± 2.87	**0.02***
K	118.10 ± 33.71	104.08 ± 8.53	0.45
P	0.483 ± 0.169	0.379 ± 0.068	0.66
pH	7.71 ± 0.06	7.76 ± 0.04	0.33

PRS-probes	**μg Element/10 cm²/7 days**				
Element	**Ca**	**Mg**	**K**	**P**	**Al**
June, Control treatment	327.25 ± 36.41	23.15 ± 2.66	188.33 ± 28.76	2.83 ± 0.34	4.05 ± 0.26
June, Basalt treatment	361.17 ± 54.84	30.29 ± 4.26	240.79 ± 18.73	2.52 ± 0.41	7.49 ± 2.58
August, Control treatment	1,149.63 ± 95.35	80.46 ± 8.82	81.76 ± 8.39	8.23 ± 1.17	8.00 ± 0.83
August, Basalt treatment	1,084.43 ± 61.97	80.84 ± 4.11	79.62 ± 8.49	5.76 ± 0.73	11.20 ± 1.64
Basalt effect	$p = 0.81$	$p = 0.49$	$p = 0.23$	**$p = 0.07$**	**$p = 0.08$**
Time effect	**$P < 0.001$*****	**$P < 0.001$*****	**$P < 0.001$*****	**$P < 0.001$*****	**$P < 0.001$*****
Time × Basalt effect	N.S.	N.S.	N.S.	N.S.	N.S.

In the most right column, p-values of one way Anova are displayed. (Borderline) Significant increases ($p < 0.10$) are indicated in bold.
N.S, Not significant.
*Significance codes *, ** and *** refer to p-values in the ranges 0.01–0.05, 0.001–0.01 and 0–0.001 respectively.*

TABLE 4 | Inorganic carbon balance in tonCO_2/ha/99 days (experimental timeframe).

ΔTIC (Basalt-control)	**se ΔTIC**	**ΔDIC (Basalt-control)**	**se ΔDIC**	**ΔIC (Basalt-control)**	**se ΔIC**
12.4	24.7	0.0048	0.0024	12.4	24.7

With IC = DIC (derived from TA) + TIC formation, se, standard error.

in the control treatment, while experimental results showed the opposite pattern.

Co-benefits for Biomass, Nutrient Stocks, and Nitrogen Leaching

Basalt addition tended to increase aboveground biomass and potato tuber yield (albeit not statistically significantly; $p = 0.16$, $p = 0.45$). No significant changes in potato tuber Mg, Ca, P, Si, and Ni concentrations were detected upon basalt amendment (**Table 5**). However, basalt induced a positive trend in potato stocks of K ($p = 0.16$), Mg ($p = 0.21$), Ca ($p = 0.24$), and P ($p = 0.31$).

Nitrogen leaching was significantly lower in the basalt treatment than in the control (**Figure 7**). This reduction in nitrogen leaching was mainly due to the decrease in NO_3^--N leaching. Average N leaching decreased with about 45% upon basalt amendment.

Risks of Basalt Amendment in Alkaline Soil

In the soil (0–50 cm), a 41% increase of Ni was observed ($p = 0.05$). Ni also increased significantly in the topsoil (0–5 cm) pore water (**Figure 8**). In contrast, leached Ni tended to decrease upon basalt addition ($p = 0.40$). Hence, the added Ni was retained in the soil system. Potato tuber Ni content did not significantly differ among treatments ($p = 0.80$). Despite the borderline significant Al increase observed in PRS probes, potato tuber Al was not significantly increased in the basalt treatment ($p = 0.70$; **Table 5**).

DISCUSSION

Inorganic CO_2 Sequestration

Based on the XRF data of our, we estimate a maximum CO_2 sequestration of 223 and 416 kg CO_2/t basalt, after complete dissolution and reaction *via* mineral carbonation (MC; all

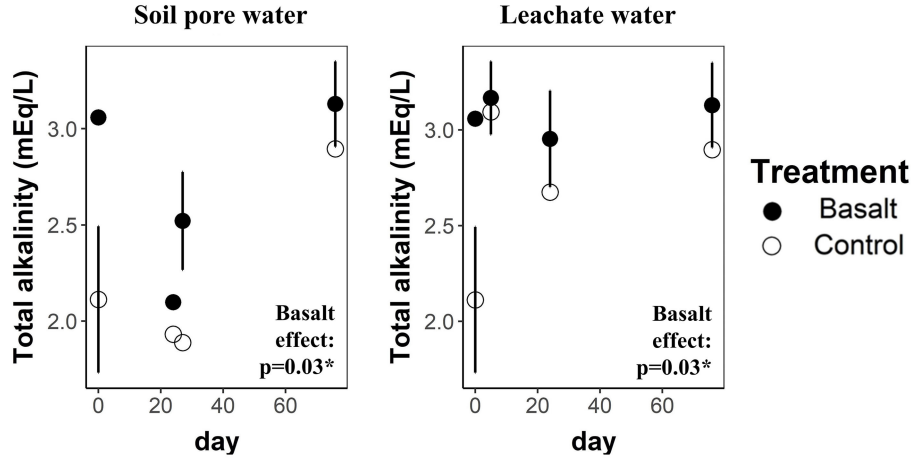

FIGURE 3 | Total alkalinity (mEq L-1) in pore water and leachates in function of time (days) for basalt and control treatments. Error bars represent averages ± standard errors. Significance codes *, ** and *** refer to p-values in the ranges 0.01–0.05, 0.001–0.01 and 0–0.001 respectively.

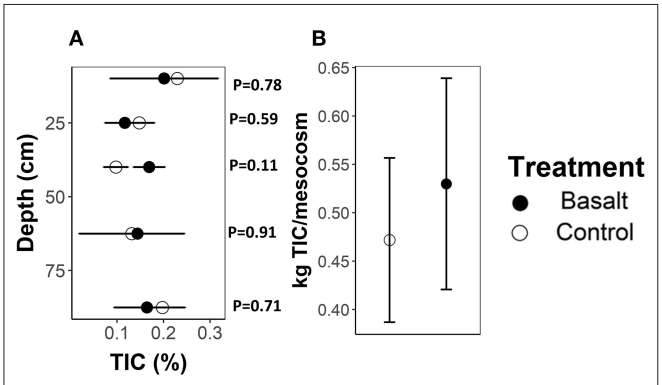

FIGURE 4 | (A) TIC (%) for different soil depths (cm) and **(B)** total kg TIC mesocosm-1 for basalt and control treatments. Error bars represent averages ± standard errors.

inorganic carbon precipitates) or enhanced weathering (EW; all inorganic carbon is rinsed out of the system as dissolved C), respectively (Renforth, 2019) (see also Section 1.11 in **Supplementary Material 1**). Hence, applying 50 t of our basalt per ha corresponds with a theoretical maximum of 20.8 and 11.2 t CO_2/ha through EW and MC, respectively. It may take several decades for this to be reached. We recognize that applying several tens of tonnes basalt ha^{-1} in practice would result in substantial transportation costs and that this application rate is higher than for conventional fertilizers. However, costs of C sequestration through enhanced weathering of basalt are estimated at about US$80–180 t^{-1} CO_2 (Beerling et al., 2020), which corresponds roughly to the world bank estimate of the carbon price in 2050 (100–150$ $t^{-1}CO_2$) and current EU-ETS carbon price, which already exceeded 100 US$ t^{-1} CO_2 in 2022.

We investigated inorganic CO_2 sequestration by experimentally quantifying changes in both DIC and TIC. Over the short duration of our experiment, only a small amount of DIC (4.77 kgCO_2-eq/ha) had leached out. The experiment was conducted during summer season, when evapotranspiration was high and leaching losses were small. More DIC might leach out during winter, when evapotranspiration is low. Our PHREEQC simulations predicted carbonates to precipitate only in the basalt amended topsoil and not in deeper layers, indicating that in our experiment sequestered inorganic carbon should be retained in the top soil. Large uncertainty on TIC measurements, resulting from heterogeneity in background soil TIC complicated exact determination of IC sequestration. This result is in line with Kelland et al. (2020), who found no significant TIC changes in a similar short-term mesocosm experiment with basalt rock powder. In contrast, Haque et al. (2019) did detect a significant CO_2 sequestration of 39.3 t CO_2/ha through TIC changes in a mesocosm experiment of 55 days. Also in some field studies with smaller application rates, TIC changes were detectable after 5 months (Haque et al., 2020b). The latter experiments used the faster weathering silicate mineral wollastonite. Besides addition of large amounts of fast-weathering silicates, long-term monitoring also increases the potential to detect TIC changes upon basalt amendment. In a field experiment in which soil was amended with basaltic quarry fines, Manning et al. (2013) detected a significant increase of TIC after 4 years and estimated CO_2 sequestration at 17.6 t CO_2/ha/y.

For detection of significant TIC changes with rocks and minerals that have weathering rates similar to basalt, our results indicate that multi-year experiments are required. PHREEQC simulations show that the standard error on TIC measurements (ranging from 0.03 to 0.12% across the different depths) was larger than the modeled differences in TIC (of about 0.01%) obtained for the experimental duration. Based on our simulations, we estimate that, in our experiment, a TIC increase of ∼0.05% would have occurred after about 5 years, which we assume would be detectable (given the standard error on TIC ranged between 0.03 and 0.12). In reality, weathering was likely underestimated by the model (see below), and hence, TIC might become detectable earlier.

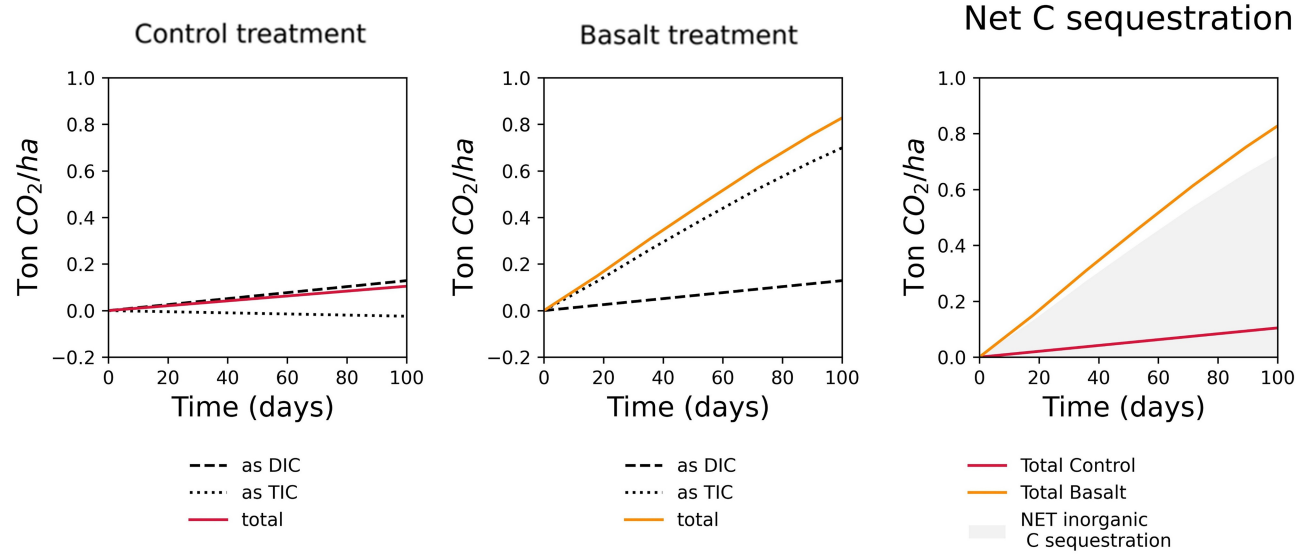

FIGURE 5 | Simulated inorganic carbon sequestration (ton CO_2 ha-1) in function of time (days), for 100 days of experiment in the control and basalt treatment. Net inorganic C sequestration (in grey) results from the difference between the basalt and control treatment.

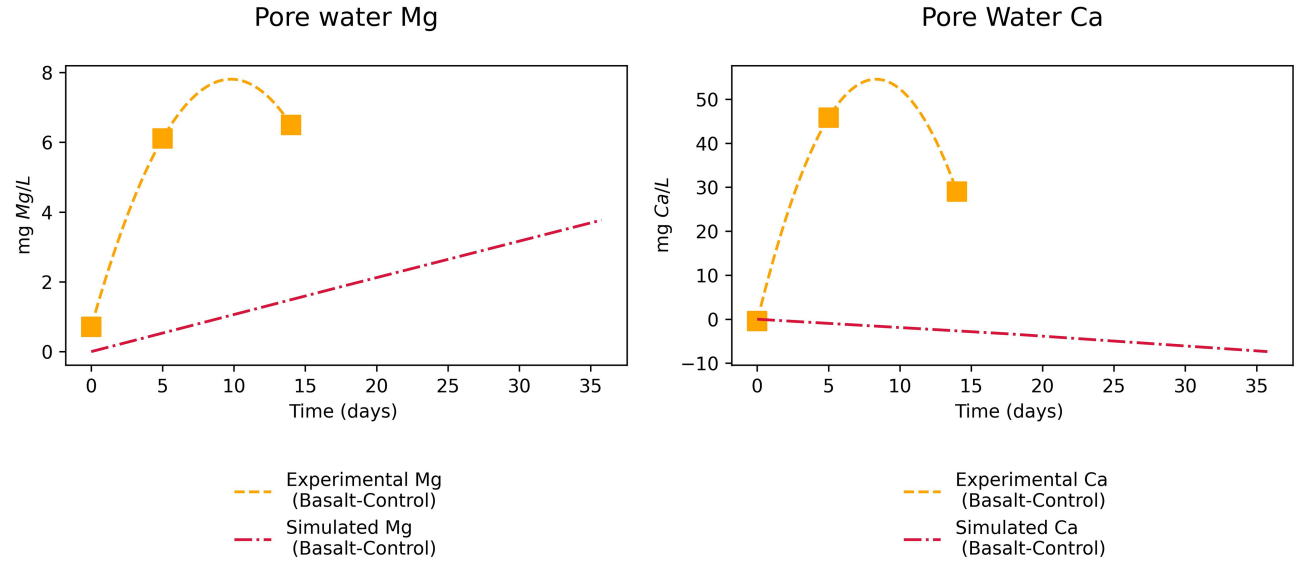

FIGURE 6 | Experimental and simulated Mg and Ca increase in pore water (mg L-1) after basalt amendment in function of time (days).

We used the 1D reactive transport model to estimate CO_2 sequestration after 1 and 5 years. Predicted CO_2 sequestration was 1.83 and 4.48 t CO_2/ha sequestration after 1 and 5 years, respectively, which corresponds to about 13 and 35% of the maximum MC potential. Kelland et al. (2020) modeled a similar system that captured a similar 3 t CO_2/ha despite applying twice as much (100 t/ha) basalt and columns were watered more intensely. This can be explained as in their simulation, net inorganic CO_2 sequestration did not further increase after year one, when olivine and diopside were fully dissolved. In the model, the dissolution of Al-containing minerals diopside, plagioclases and basaltic glass were inhibited through precipitation of amorphous $Al(OH)_3$, which was included as an equilibrium phase in the work of Kelland et al. (2020). As in Kelland et al. (2020), the latter mechanism inhibited dissolution of the Al-bearing labradorite (a Ca-plagioclase) also in our model simulations (**Supplementary Figure SF8**). Model assumptions are further discussed in Section 1.2 of **Supplementary Material 1**.

TABLE 5 | Overview of (aboveground, potato tuber or total) biomass and element stocks in potato tuber (96 m% of the total biomass).

	Control		Basalt		*p*-value
	Biomass (g DM) (±standard error)	**% of total biomass**	**Biomass (g DM) (±standard error)**	**% of total biomass**	
Potato tuber biomass	2,092 ± 74	96.54	2,208 ± 14	96.60	0.16
Aboveground Biomass	75 ± 3	3.46	78 ± 1	3.40	0.45
total biomass	2,167 ± 76	100.00	2,285 ± 14	100.00	0.17
Potato tuber composition	**mg/kg DM (±standard error)**				
P	2,765 ± 81		2,846 ± 137		0.62
K	22,755 ± 486		23,494 ± 393		0.27
Ca	485 ± 34		536 ± 51		0.43
Mg	979 ± 43		1,036 ± 43		0.38
Al	63 ± 14		69 ± 11		0.76
Si	0.060 ± 0.018		0.050 ± 0.022		0.72
Ni	0.31 ± 0.04		0.33 ± 0.07		0.80
Total stock of element in Potato tubers	**mg/mesocosm (±standard error)**				
P	5,792 ± 314		6,287 ± 329		0.31
K	47,688 ± 2,435		51,881 ± 1,152		0.16
Ca	1,012 ± 71		1,184 ± 117		0.24
Mg	2,053 ± 136		2,288 ± 108		0.21
Al	134 ± 33		151 ± 25		0.70
Si	0.129 ± 0.039		0.110 ± 0.048		0.77
Ni	0.65 ± 0.08		0.74 ± 0.16		0.63

All masses reported in this table represent dry matter (DM).

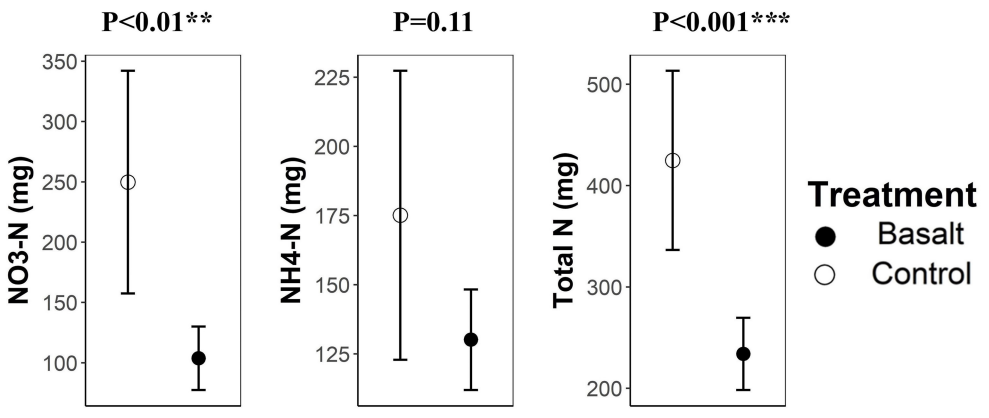

FIGURE 7 | Nitrogen leaching (mg N mesocosm-1) among treatments. Error bars represent averages ± standard errors. Significance codes *, ** and *** refer to p-values in the ranges 0.01–0.05, 0.001–0.01, and 0–0.001 respectively.

Comparison of pore water Mg revealed that the rate law parameters for weathering of the pyroxene mineral augite by Knauss et al. (1993) provide a better estimate than the parameters used by Palandri and Kharaka (2004) (**Supplementary Figure SF2**). Given the abundance of pyroxene minerals in basalt and mine tailings (Bullock et al., 2022), the latter is relevant for improving modeling CO_2 sequestration of these rocks near neutral pH conditions. Still, a factor three difference in Mg in pore water remains with this rate law. This discrepancy between measured and modeled Mg concentration cannot result from overestimation of carbonate precipitation as the model did not predict precipitation of Mg-carbonates.

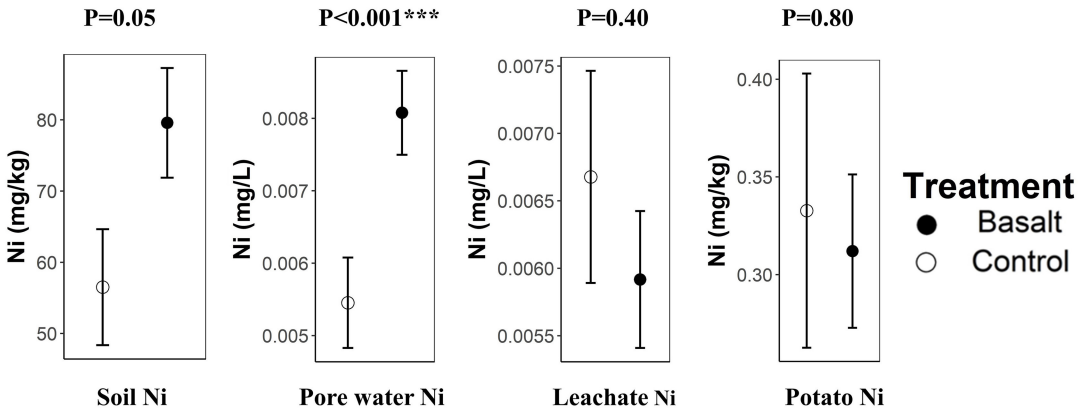

FIGURE 8 | Nickel differences among treatments in the soil (mg Ni kg-1 soil), pore water (mg Ni L-1), leachates (mg Ni L-1), and potato tubers (mg Ni kg-1 tuber). Error bars represent averages ± standard errors. Significance codes *, ** and *** refer to p-values in the ranges 0.01–0.05, 0.001–0.01, and 0–0.001 respectively.

Furthermore, only small changes of surface adsorbed Mg are simulated (**Supplementary Table ST6**). This suggests that the difference between measured and modeled Mg concentration in pore water is likely due to an underestimation of Mg mineral dissolution and/or an overestimation of Mg cation exchange. As PHREEQC is a geochemical model, the influence of biologically synthesized substances (e.g., siderophores, CAs, protons) is not taken into account. Biological substances can enhance weathering rates and may (partly) explain why the model underestimated the release of cations and hence weathering rates (Vicca et al., 2022). Moreover, also pore water Ca concentrations were underestimated by the model, indicating that the calcite precipitation rate (and hence degassing rate) was overestimated, leading to an underestimation of modeled CO_2 sequestration.

To the best of our knowledge, we are the first to assess model predictions of CO_2 sequestration through EW based on experimental pore water cation composition in real soils (**Figure 6**). Our study builds on the work of Kelland et al. (2020), who implemented this model, but did not compare experimental pore water data with simulated values. Additional research is needed to determine long-term weathering dynamics as well as to improve model simulations. Long-term studies are needed in which soil pore water chemistry is monitored. Our results demonstrate that in short-term EW-experiments with basalt, measurements of soil pore water chemistry are critical for monitoring weathering rates and for estimating CO_2 sequestration. Future studies could consider specific elements (e.g., Ti, Al, and Na; depending on the mineral composition) that can provide insights in the weathering behavior of mineral phases containing these atoms. This would also allow verification of the modeled Al-silicate weathering inhibition by amorphous $Al(OH)_3$.

Risks of Basalt Amendment in Alkaline Soils

A trade-off of utilizing fast-weathering ultramafic minerals for EW is Ni contamination; Ni leaching is expected to be smaller using mafic basalt rocks (which contain relatively little olivine) in alkaline soils where Ni precipitation is higher. Nonetheless, a comparison with EQSs is necessary for EW adoption in practice. Ni increased significantly in the soil and topsoil pore water. The addition of 50 t basalt/ha resulted in a topsoil (0–50 cm) Ni increase of 23 ppm, which is well below the Flemish threshold of 48 ppm for soil quality (VLAREBO, 2008). The pore water Ni concentration was increased with 2.5 μg/L. The EQSs for Ni in freshwater in the EU, Australia, the US and Canada, respectively, range from 4, over 8, 52, and 200 μg/L, respectively. Hence pore water Ni concentration remained below legislative freshwater thresholds of all of the above countries/regions. As Ni is associated with the fast weathering mineral olivine within basalt, we expect Ni in pore water to decrease over time. Information about initial soil Ni content and legal limits could provide a theoretical maximum on the amount of basalt that can be applied. In our experiment, the Flemish threshold would be reached after amendment with 104 t basalt/ha (if initial soil Ni equals zero). However, Ni would gradually leach out to surface waters, and might be taken up by plants, increasing the possible amount of application. Despite the increased Ni in soil and soil pore water, Ni concentrations in edible plant parts did not significantly increase with basalt amendment. This is in correspondance with results from Stasinos and Zabetakis (2013), who grew potatoes on soils irrigated with Ni-contaminated (0–250 μgNi/L) wastewater and found no increase in tuber Ni content. In fact, they even found tuber Ni concentration to decrease with increasing irrigation Ni levels.

In our experiment, basalt weathering increased Al availability, which induces Al toxicity and may reduce plant growth. Hence, during this experiment the alkaline catalyzed dissolution of Al by Ca plagioclase and Al-release by augite weathering was higher than the sum of Al precipitation and Al uptake. Dorneles et al. (2016) investigated Al toxicity in *Solanum tuberosum* and found that Si can ameliorate Al toxicity through formation of alumino silicate compounds in the walls of root cortex cells that inhibit uptake of Al into the protoplast. Hence, EW can influence Al toxicity in contrasting ways through release of Si and Al. In our alkaline soil, the weathering-induced increase in Al availability did not result in significantly higher potato tuber Al and Si stocks. Most importantly, the increased Al availability in the

aqueous phase did not result in a decrease in tuber biomass, lifting concerns of reduced yield for EW with *Solanum tuberosum* in alkaline soils.

A risk that was not evaluated here concerns the potential health issues due to spreading fine silicate particles (Webb, 2020). To overcome this, basalt can be applied in a pelletized form to disintegrate again when applied in soils. Avoiding additional grinding of basalt quarry fines, which may not be warranted in terms of additional carbon sequestration gains (Lewis et al., 2021) can also reduce dust formation.

Co-benefits of Basalt Amendment in Alkaline Soils

In our experiment with potatoes growing on alkaline soil, basalt amendment significantly increased soil CEC and Ca and Mg and tended to increase average potato tuber yield by 6%. This potato yield increase is lower than that in some studies on acid soil. Lafond and Simard (1999) amended an acid Canadian soil (low in Ca and K) with cement kiln dust (a silicate by-product from the cement industry) for growing *Solanum tuberosum,* which resulted in a tuber yield increases of over 50% at several locations. These yield gains were correlated with soil extractable K and Mg (Lafond and Simard, 1999). It is likely that potato tuber yield is increased more in agricultural systems where cations are more depleted than in our experimental soil. Still, positive trends in Ca, Mg, and K potato stocks were observed. The K decrease in the top soil of the basalt treatment presumably resulted from the high mobility of K and higher uptake by potato plants.

Interestingly, silicate amendment reduced potato harvest losses due to stem lodging and increased potato tuber yield in drought stress experiments (Crusciol et al., 2009). Silicate amendment may thus be even more attractive for potato cultivation in dry regions such as Africa or India (the third largest potato producing country globally) (FAO, 2008) and in future, when droughts increase in frequency and intensity with negative consequences for potato yield (Hijmans, 2003; IPCC, 2021).

Another co-benefit that we observed was the effect of basalt amendment on nitrogen leaching. Nitrogen leaching significantly decreased upon basalt amendment. In acid soils, the latter is hypothesized to result from pH increases. However, pH was buffered at 7.7 in both control and basalt amended soil. Hence, other mechanisms were likely at play in our experiment. Mechanistically, basalt amendment may have increased the trace element molybdenum (Mo) (which is present in rhyolite basalt in concentrations up to 4 ppm) (Arnórsson and Óskarsson, 2007). Soil and freshwater environments often contain Mo at concentrations that naturally limit denitrification. Mo is a cofactor of the enzyme nitrate reductase, which catalyzes the conversion of nitrate into nitrite (Vaccaro et al., 2016). Possibly, Mo released by basalt stimulated denitrifying microbial communities, but further research is needed to verify this.

CONCLUSION

Simulated CO_2 sequestration was 0.77 t CO_2/ha in the experimental timeframe (99 days) and 1.83 and 4.48 t CO_2/ha after 1 and 5 years, respectively. This first study comparing experimental and modeled pore water chemistry in an EW mesocosm experiment indicated an underestimation of modeled CO_2 sequestration, as simulated Ca and Mg pore water concentration were substantially lower than measured concentrations. Nonetheless, we did not detect a significant increase in TIC, probably because TIC increases were too small compared to soil heterogeneity. More detailed, long term assessments in future mesocosm and field experiments can help to further improve experimental and modeled estimates of CO_2 sequestration through EW. As a co-benefit, nitrogen leaching significantly decreased with basalt addition, despite the fact that pH was not affected, suggesting that other processes were at play. In order to draw conclusions about the basalt effect on total soil nitrogen losses, future analyses should also consider gaseous N losses such as NH_3 and N_2O.

Plant Ni did not significantly increase, and increases in soil and pore water Ni were below allowed environmental quality standards. Importantly, in our alkaline soil, the weathering-induced risk of increased Al availability did not result in lower potato biomass. Despite the positive trends in Ca, Mg and K potato stocks, potato biomass was not significantly increased.

DATA AVAILABILITY STATEMENT

The original contributions presented in the study are included in the article/**Supplementary Material**, further inquiries can be directed to the corresponding author. Raw data can be consulted at https://zenodo.org/record/6477990#.YmLAPNpBw2x.

AUTHOR CONTRIBUTIONS

SV designed the research. SI, SP, and SV conducted the experimental work. MP-E did the CN analysis. AV did the data analyses and PHREEQC modeling with help from PW and JH and AV drafted the paper. All authors contributed to the interpretation of the results and the writing of the paper, and contributed to the article and approved the submitted version.

FUNDING

This research was supported by the Research Foundation—Flanders (FWO), and by the Research Council of the University of Antwerp.

ACKNOWLEDGMENTS

We thank Sebastian Wieneke and Cristina Ariza Carricondo for help during the experimental setup.

SUPPLEMENTARY MATERIAL

The Supplementary Material for this article can be found online at: https://www.frontiersin.org/articles/10.3389/fclim.2022.869456/full#supplementary-material

REFERENCES

Amann, T., and Hartmann, J. (2019). Ideas and perspectives: synergies from co-deployment of negative emission technologies. *Biogeosciences* 16, 2949–2960. doi: 10.5194/bg-16-2949-2019

Amann, T., Hartmann, J., Struyf, E., De Oliveira Garcia, W., Fischer, E. K., Janssens, I., et al. (2020). Enhanced Weathering and related element fluxes - A cropland mesocosm approach. *Biogeosciences* 17, 103–119. doi: 10.5194/bg-17-103-2020

Arnórsson, S., and Óskarsson, N. (2007). Molybdenum and tungsten in volcanic rocks and in surface and <100 °C ground waters in Iceland. *Geochim. Cosmochim. Acta* 71, 284–304. doi: 10.1016/j.gca.2006.09.030

Bakken, L. R., Bergaust, L., Liu, B., and Frostegård, Ä. (2012). Regulation of denitrification at the cellular level: a clue to the understanding of N2O emissions from soils. *Philosop. Trans. R. Soc. B Biol. Sci.* 367, 1226–1234. doi: 10.1098/rstb.2011.0321

Beerling, D. J., Kantzas, E. P., Lomas, M. R., Wade, P., Eufrasio, R. M., Renforth, P., et al. (2020). Potential for large-scale CO_2 removal *via* enhanced rock weathering with croplands. *Nature* 583, 242–248. doi: 10.1038/s41586-020-2448-9

Beerling, D. J., Leake, J. R., Long, S. P., Scholes, J. D., Ton, J., Nelson, P. N., et al. (2018). Farming with crops and rocks to address global climate, food and soil security /631/449 /706/1143 /704/47 /704/106 perspective. *Nature Plants* 4, 138–147. doi: 10.1038/s41477-018-0108-y

Blanc-Betes, E., Kantola, I. B., Gomez-Casanovas, N., Hartman, M. D., Parton, W. J., Lewis, A. L., et al. (2021). *In silico* assessment of the potential of basalt amendments to reduce N_2O emissions from bioenergy crops. *GCB Bioenergy* 13, 224–241. doi: 10.1111/gcbb.12757

Bose, H., and Satyanarayana, T. (2017). Microbial carbonic anhydrases in biomimetic carbon sequestration for mitigating global warming: prospects and perspectives. *Front. Microbiol.* 8, 1–20. doi: 10.3389/fmicb.2017.01615

Brantley, S. L., White, A. F., and Kubicki, J. D. (2008). *Kinetics of Water-Rock Interaction*. New York: Springer. doi: 10.1007/978-0-387-73563-4

Brown, I. C. (1943). A rapid method of determining exchangeable hydrogen and total exchangeable bases of soils. *Soil Sci.* 56, 353–357. doi: 10.1097/00010694-194311000-00004

Bullock, L. A., Yang, A., and Darton, R. C. (2022). Kinetics-informed global assessment of mine tailings for CO_2 removal. *Sci. Total Environ.* 808, 152111. doi: 10.1016/j.scitotenv.2021.152111

Campos, H., and Ortiz, O. (2019). The potato crop: its agricultural, nutritional and social contribution to humankind. In: *The Potato Crop: Its Agricultural, Nutritional and Social Contribution to Humankind*. (Cham: Springer Nature), 518. doi: 10.1007/978-3-030-28683-5

Crusciol, C. A. C., Pulz, A. L., Lemos, L. B., Soratto, R. P., and Lima, G. P. P. (2009). Effects of silicon and drought stress on tuber yield and leaf biochemical characteristics in potato. *Crop Sci.* 49, 949–954. doi: 10.2135/cropsci2008.04.0233

Demir, N., Demir, Y., and Coşkun, F. (2001). Purification and characterization of carbonic anhydrase from human erythrocyte plasma membrane. *Turk. J. Med. Sci.* 31, 477–482. doi: 10.1080/10826060008544944

Dietzen, C., Harrison, R., and Michelsen-Correa, S. (2018). Effectiveness of enhanced mineral weathering as a carbon sequestration tool and alternative to agricultural lime: an incubation experiment. *Int. J. Greenhouse Gas Control* 74, 251–258. doi: 10.1016/j.ijggc.2018.05.007

Dorneles, A. O. S., Pereira, A. S., Rossato, L. V., Possebom, G., Sasso, V. M., Bernardy, K., et al. (2016). Silício reduz o conteúdo de alumínio em tecidos e ameniza seus efeitos tóxicos sobre o crescimento de plantas de batata. *Ciencia Rural* 46, 506–512. doi: 10.1590/0103-8478cr20150585

FAO (2008). *Potato World*. Available online at: https://www.fao.org/potato-2008/en/world/index.html (accessed December 20, 2021).

FAOSTAT (2013). *Food Balances 2010*. Available online at: https://www.fao.org/faostat/en/#data/FBS (accessed March 16, 2022).

Fischer, G., Nachtergaele, F., Prieler, S., van Velthuizen, H. T., Verelst, L., and Wiberg, D. (2008). *Global Agro-ecological Zones Assessment for Agriculture (GAEZ 2008)*. Rome: IIASA, Laxenburg, Austria and FAO.

Gasser, T., Guivarch, C., Tachiiri, K., Jones, C. D., and Ciais, P. (2015). Negative emissions physically needed to keep global warming below 2°C. *Nat Commun.* 6, 958. doi: 10.1038/ncomms8958

Gudbrandsson, S., Wolff-Boenisch, D., Gislason, S. R., and Oelkers, E. H. (2011). An experimental study of crystalline basalt dissolution from 2pH11 and temperatures from 5 to 75°C. *Geochimica et Cosmochimica Acta.* 75, 5496–5509. doi: 10.1016/j.gca.2011.06.035

Haque, F., Chiang, Y. W., and Santos, R. M. (2020a). Risk assessment of Ni, Cr, and Si release from alkaline minerals during enhanced weathering. *Open Agric.* 5, 166–175. doi: 10.1515/opag-2020-0016

Haque, F., Santos, R. M., and Chiang, Y. W. (2020b). CO2 sequestration by wollastonite-amended agricultural soils – An Ontario field study. *Int. J. Greenhouse Gas Control* (2019) 97:103017. doi: 10.1016/j.ijggc.2020.103017

Haque, F., Santos, R. M., Dutta, A., Thimmanagari, M., and Chiang, Y. W. (2019). Co-benefits of wollastonite weathering in agriculture: CO_2 sequestration and promoted plant growth [research-article]. *ACS Omega* 4, 1425–1433. doi: 10.1021/acsomega.8b02477

Hartmann, J., West, A. J., Renforth, P., Köhler, P., De La Rocha, C. L., Wolf-Gladrow, D. A., et al. (2013). Enhanced chemical weathering as a geoengineering strategy to reduce atmospheric carbon dioxide, supply nutrients, and mitigate ocean acidification. *Rev. Geophys.* 51, 113–149. doi: 10.1002/rog.20004

Hijmans, R. J. (2003). The effect of climate change on global potato production. *Am. J. Potato Res.* 80, 8–280. doi: 10.1007/BF02855363

IPCC. (2021). *Climate Change 2021: The Physical Science Basis. Contribution of Working Group I to the Sixth Assessment Report of the Intergovernmental Panel on Climate Change*, eds V. Masson-Delmotte, P. Zhai, A. Pirani, S. L. Connors, C. Péan, S. Berger, N. Caud, Y. Chen, L. Goldfarb, M.I. Gomis, M. Huang, K. Leitzell, E. Lonnoy, J. B. R. Matthews, T. K. Maycock, T. Waterfield, O. Yelekçi, R. Yu, and B. Zhou (Cambridge University Press).

Kantola, I. B., Masters, M. D., Beerling, D. J., Long, S. P., and DeLucia, E. H. (2017). Potential of global croplands and bioenergy crops for climate change mitigation through deployment for enhanced weathering. *Biol. Lett.* 13, 20160714. doi: 10.1098/rsbl.2016.0714

Kelland, M. E., Wade, P. W., Lewis, A. L., Taylor, L. L., Sarkar, B., Andrews, M. G., et al. (2020). Increased yield and CO_2 sequestration potential with the C4 cereal Sorghum bicolor cultivated in basaltic rock dust-amended agricultural soil. *Global Change Biol.* 26, 3658–3676. doi: 10.1111/gcb.15089

Knauss, K. G., Nguyen, S. N., and Weed, H. C. (1993). Diopside dissolution kinetics as a function of pH, CO_2, temperature, and time. *Geochim. Cosmochim. Acta* 57, 285–294. doi: 10.1016/0016-7037(93)90431-U

Lafond, J., and Simard, R. R. (1999). Effects of cement kiln dust on soil and potato crop quality. *Am. J. Potato Res.* 76, 83–90. doi: 10.1007/BF02855204

Lawlor, E. T. S. L. A. (1998). *Modelling the Chemical Speciation of Trace Metals in the Surface Waters of the Humber System*.

Lewis, A. L., Sarkar, B., Wade, P., Kemp, S. J., Hodson, M. E., Taylor, L. L., et al. (2021). Effects of mineralogy, chemistry and physical properties of basalts on carbon capture potential and plant-nutrient element release *via* enhanced weathering. *Appl. Geochem.* 132, 105023. doi: 10.1016/j.apgeochem.2021.105023

Manning, D. A. C., Renforth, P., Lopez-Capel, E., Robertson, S., and Ghazireh, N. (2013). Carbonate precipitation in artificial soils produced from basaltic quarry fines and composts: an opportunity for passive carbon sequestration. *Int. J. Greenhouse Gas Control* 17, 309–317. doi: 10.1016/j.ijggc.2013.05.012

Palandri, J. L., and Kharaka, Y. K. (2004). A compilation of rate parameters of water-mineral interaction kinetics for application to geochemical modeling. *USGS Open File Report* 2004–1068, 71. doi: 10.3133/ofr20041068

Parkhurst, D. L., and Appelo, C. A. J. (2013). "Description of input and examples for PHREEQC version 3—A Computer Program for Speciation, Batch-Reaction, One-Dimensional Transport, and Inverse Geochemical Calculations," in *U.S. Geological Survey Techniques and Methods*. (Denver, Colorado), Book 6, Chapter A43, 497 p. 6–43A. Available online at: http://pubs.usgs.gov/tm/06/a43/

Qian, P., and Schoenau, J. J. (2002). Practical applications of ion exchange resins in agricultural and environmental soil research. *Canadian Journal of Soil Science.* 82(1), 9–21.

Qu, Z., Wang, J., Almøy, T., and Bakken, L. R. (2014). Excessive use of nitrogen in Chinese agriculture results in high $N_2O/(N_2O+N_2)$ product ratio of denitrification, primarily due to acidification of the soils. *Global Change Biol.* 20, 1685–1698. doi: 10.1111/gcb.12461

Renforth, P. (2019). The negative emission potential of alkaline materials_Supplementary information. *Nat. Commun.* 10, 1–29. doi: 10.1038/s41467-019-09475-5

Roland, M., Vicca, S., Bahn, M., Ladreiter-Knauss, T., Schmitt, M., and Janssens, I. A. (2015). Importance of nondiffusive transport for soil CO_2 efflux in a temperate mountain grassland. *J. Geophys. Res. Biogeosci.* 120, 502–512. doi: 10.1002/2014JG002788

Roser, M., and Ritchie, H. (2020). *CO_2 Emissions*. Available online at: https://ourworldindata.org/co2-emissions (accessed April 23, 2021).

Sathya, V., and Mahimairaja, S. (2015). Adsorption of nickel on vertisol: effect of pH of soil organic matter and co-contaminants. *Res. J. Chem. Environ.* 19, 1–8. Available online at: https://www.researchgate.net/publication/340933868_Adsorption_of_Nickel_on_Vertisol_Effect_of_pH_of_soil_Organic_Matter_and_Co-contaminants

Schuiling, R. D., and Krijgsman, P. (2006). Enhanced weathering: an effective and cheap tool to sequester CO_2. *Clim. Change* 74, 349–54. doi: 10.1007/s10584-005-3485-y

Stasinos, S., and Zabetakis, I. (2013). The uptake of nickel and chromium from irrigation water by potatoes, carrots and onions. *Ecotoxicol. Environ. Safety* 91, 122–128. doi: 10.1016/j.ecoenv.2013.01.023

Strefler, J., Amann, T., Bauer, N., Kriegler, E., and Hartmann, J. (2018). Potential and costs of carbon dioxide removal by enhanced weathering of rocks. *Environ. Res. Letters* 13:034010. doi: 10.1088/1748-9326/aaa9c4

ten Berge, H. F. M., van der Meer, H. G., Steenhuizen, J. W., Goedhart, P. W., Knops, P., and Verhagen, J. (2012). Olivine weathering in soil, and its effects on growth and nutrient uptake in ryegrass (*Lolium perenne* L.): a pot experiment. *PLoS ONE* 7, e004298. doi: 10.1371/journal.pone.0042098

Vaccaro, B. J., Thorgersen, M. P., Lancaster, W. A., Price, M. N., Wetmore, K. M., Poole, F. L., et al. (2016). Determining roles of accessory genes in denitrification by mutant fitness analyses. *Appl. Environ. Microbiol.* 82, 51–61. doi: 10.1128/AEM.02602-15

van Straaten, P. (2002). *Rocks for Crops: Agrominerals of sub-Saharan Africa*. Nairobi: ICRAF, 338.

Vicca, S., Goll, D., Hagens, M., Hartmann, J., Janssens, I. A., Neubeck, A., et al. (2022). Is the climate change mitigation effect of enhanced silicate weathering governed by biological processes? *Global Change Biol.* 28, 711–26. doi: 10.1111/gcb.15993

VLAREBO (2008). *VLAREBO 2008 14 DECEMBER 2007 - Besluit van de Vlaamse Regering houdende vaststelling van het Vlaams reglement betreffende de bodemsanering en de bodembescherming*. 1–115. Available online at: https://navigator.emis.vito.be/mijn-navigator?woId=23569andwoLang=nl (accessed November 13, 2021).

Walinga, I., van Vark, W., Houba, V. J. G., and van der Lee, J. J. (1989). *Plant Analysis Procedures. Soil and Plant Analysis, Part 7*. Wageningen: Agricultural University, p. 13–16.

Webb, R. M. (2020). *The Law of Enhanced Weathering for Carbon Dioxide Removal*. New York: Sabin Center for Climate Change Law, Columbia Law School. Available online at SSRN: https://ssrn.com/abstract=3698944 (accessed September 22, 2020).

Xiao, L., Lian, B., Hao, J., Liu, C., and Wang, S. (2015). Effect of carbonic anhydrase on silicate weathering and carbonate formation at present day CO_2 concentrations compared to primordial values. *Sci. Rep.* 5, 1–10. doi: 10.1038/srep07733

Conflict of Interest: PW was employed by (GLOBAL) Future Forest Company Ltd.

The remaining authors declare that the research was conducted in the absence of any commercial or financial relationships that could be construed as a potential conflict of interest.

Publisher's Note: All claims expressed in this article are solely those of the authors and do not necessarily represent those of their affiliated organizations, or those of the publisher, the editors and the reviewers. Any product that may be evaluated in this article, or claim that may be made by its manufacturer, is not guaranteed or endorsed by the publisher.

frontiers | Frontiers in Climate

TYPE Original Research
PUBLISHED 22 July 2022
DOI 10.3389/fclim.2022.929268

OPEN ACCESS

EDITED BY
Fatima Haque,
National Taiwan University, Taiwan

REVIEWED BY
Davide Ciceri,
Agroplantae, United States
Debanjan Chandra,
Indian Institute of Technology Bombay, India

*CORRESPONDENCE
Thorben Amann
science@thorbenamann.de

SPECIALTY SECTION
This article was submitted to Negative Emission Technologies, a section of the journal Frontiers in Climate

RECEIVED 26 April 2022
ACCEPTED 27 June 2022
PUBLISHED 22 July 2022

CITATION
Amann T, Hartmann J, Hellmann R, Pedrosa ET and Malik A (2022) Enhanced weathering potentials—the role of *in situ* CO_2 and grain size distribution. *Front. Clim.* 4:929268. doi: 10.3389/fclim.2022.929268

Enhanced weathering potentials—the role of *in situ* CO_2 and grain size distribution

Thorben Amann [1]*, Jens Hartmann [1], Roland Hellmann [2], Elisabete Trindade Pedrosa [3] and Aman Malik [4]

[1]Center for Earth System Sciences and Sustainability, Institute for Geology, Universität Hamburg, Hamburg, Germany, [2]Université Grenoble Alpes, CNRS, ISTerre, Grenoble, France, [3]Alfred-Wegener-Institut Helmholtz-Zentrum für Polar- und Meeresforschung Bremerhaven, Bremerhaven, Germany, [4]Potsdam Institute for Climate Impact Research, Member of the Leibniz Association, Potsdam, Germany

The application of rock powder on agricultural land to ameliorate soils and remove carbon dioxide (CO_2) from the air by chemical weathering is still subject to many uncertainties. To elucidate the effects of grain size distribution and soil partial pressure of carbon dioxide (pCO_2) levels on CO_2 uptake rates, two simple column experiments were designed and filled nearly daily with an amount of water that simulates humid tropical conditions, which prevail in areas known for being hotspots of weathering. Multiple materials (dunite, basanite, agricultural oxisol, a combination of the latter two, and loess) were compared under ambient and 100% CO_2 atmosphere. In a second series, single material columns (dunite) were filled with three different grain size distributions. Total alkalinity, pH, major ions, and dissolved silica were determined in the outflow water of the columns for about 300 days. Under ambient atmospheric conditions, the CO_2 consumption was the lowest in the oxisol column, with 100 t CO_2 km^{-2} $year^{-1}$, while dunite and basanite showed similar consumption rates (around 220 t CO_2 km^{-2} $year^{-1}$). The values are comparable to high literature values for ultramafic lithologies. Interestingly, the mixture of basanite and oxisol has a much higher consumption rate (around 430 t CO_2 km^{-2} $year^{-1}$) than the basanite alone. The weathering fluxes under saturated CO_2 conditions are about four times higher in all columns, except the dunite column, where fluxes are increased by a factor of more than eleven. Grain size distribution differences also play a role, with the highest grain surface area normalized weathering rates observed in the columns with coarser grains, which at first seems counterintuitive. Our findings point to some important issues to be considered in future experiments and a potential rollout of EW as a carbon dioxide removal method. Only in theory do small grain sizes of the spread-material yield higher CO_2 drawdown potentials than coarser material. The hydrologic conditions, which determine the residence times in the pore space, i.e., the time available for weathering reactions, can be more important than small grain size. Saturated-CO_2 column results provide an upper limit for weathering rates under elevated CO_2.

KEYWORDS

climate change, negative emissions, carbon dioxide removal, enhanced weathering, column experiment

Introduction

Chemical weathering of silicate rocks exposed to meteoric water is a process that removes carbon dioxide (CO_2) from the atmosphere (Ebelmen, 1845). To counteract rising CO_2 levels by removal of CO_2 from the atmosphere, the use of rock products was briefly proposed by Seifritz (1990) and made popular in the climate science community as Enhanced Weathering (EW) by Schuiling and Krijgsman (2006). Since then, assessing the realistic potential of EW as a tool for carbon dioxide removal (CDR) has become the focus of literature reviews (Hartmann et al., 2013) and modeling studies (e.g., Hartmann and Kempe, 2008; Hartmann et al., 2013; Taylor et al., 2015; Beerling et al., 2018; Strefler et al., 2018a). However, these studies have relied on several assumptions for the parameterization of the weathering process. Moreover, robust experimental data are still missing, aside from a few laboratories (Renforth et al., 2015), mesocosm (ten Berge et al., 2012; Dietzen et al., 2018; Amann et al., 2020; Kelland et al., 2020; Vienne et al., 2022), and field trials (Haque et al., 2020).

In addition to CDR, the application of rock products has also been thought to improve soil conditions (*via* fertilization and physical amelioration effects), thereby increasing agricultural production (Julius, 1894; Leonardos et al., 1987; van Straaten, 2002). The resulting increase in biomass growth leads to additional CO_2 uptake and storage as organic carbon, thereby augmenting the overall CDR potential of EW.

The sensitivity of weathering reactions to CO_2 concentrations in a system, i.e., the magnitude of chemical weathering effects from CO_2 concentration changes, has implications for estimates of weathering rates of EW applications, and therefore CO_2 removal. The parameterization of Earth system models targeting long time scales relies on, for example, realistic assumptions of the CO_2 and related climate sensitivity (e.g., Royer et al., 2007). In general, the sensitivity of weathering rates to CO_2 levels also has consequences for the evolution of the atmospheres on other planets and is important for, e.g., habitability assessments for early Mars (Teitler et al., 2014; Cockell et al., 2016; Foley and Smye, 2018).

Small grain sizes (i.e., with high surface areas) are favorable for fast reaction rates in the system, but the comminution of rock to fine grain sizes implies energy costs that may render EW less attractive. Thus, an ideal grain size range that balances these two constraint needs must be defined for different types of source material and soil targets. This energy constraint may not be relevant if side products from the mining process, often deposited as fines, are used.

To address these issues, column experiments were set up to better understand the effects of the grain size distribution (also referred to as particle size distribution) and partial pressure of CO_2 in soils with respect to CO_2 uptake rates, these being important controls on weathering rates in the field, and thus the overall CDR potential. One of the objectives of this study was therefore to test realistic upper limits of weathering rates and CDR potential considering CO_2 levels as the primary driver of weathering rates.

To explore the CO_2 effect, different materials were treated under humid tropical conditions, typical for weathering hotspots, with two soil CO_2 conditions, ambient (0.046%) and saturated (100%) CO_2, where the latter is an upper limit for this parameter, which is of course not realized in soils. Four rock types were used: dunite, basanite, laterite, and loess. Olivine-rich dunite was selected as a chemically simple model rock type that is primarily composed of olivine, while basaltoids (like the basanite used here) were proposed as a more suitable rock type for EW (Hartmann et al., 2013; Amann and Hartmann, 2019) that is widely available (Börker, 2019). Laterite or oxisol was included as a representative of typically abundant soil types associated with weathering hotspots in humid tropical regions. As a commonly proposed EW substrate, this laterite was used in pure form and as a laterite-basanite mixture. The last material type is loess sediment from aeolian deposits—these can be considered a natural analog for EW. The effect of grain sizes and their distribution was tested using the dunite with three different grain size distributions under fixed ambient CO_2 conditions.

Methods

Material origin and characterization

Materials used in the experiments were dunite, basanite, laterite, a basanite-laterite mix, and loess. The bulk chemical composition of all materials (Table 1) was determined by Panalytical Magix Pro wavelength dispersive X-ray fluorescence (XRF) analysis. Specific surface areas (Table 2) were measured by BET analyses using Kr adsorption (Brunauer et al., 1938) with a Quantachrome autosorb iQ. Particle size characteristics (Table 2, Figure 1) were determined using Sympatec Helos KFMagic laser granulometry coupled to a Quixel wet dispersing unit, covering a range of 0.5/18–3,200 μm.

Dunite

The dunite rock used here, also deployed in Amann et al. (2020), contains ~93% forsterite (Mg-endmember olivine, Mg_2SiO_4). The other 7% are comprised of lizardite (Mg-rich serpentine), Cr-bearing chlorite (including chromite or chrome-spinel inclusions), and traces of chabazite (zeolite group) and Mg-hornblende (amphibole). The mineralogical composition was determined by energy-dispersive X-ray spectroscopy (Zeiss LEO 1455 VP coupled with an Oxford Instruments EDX detector). The sample originates from the Almklovdalen peridotite complex (Åheim mineral deposit mined by the North Cape Minerals Company, Norway). More information on the

TABLE 1 Geochemical analysis of the source material.

Oxide	Dunite	Basanite	Laterite a	Laterite b	Loess
	[Mass–%]				
SiO_2	40.14	43.49	63.78	54.2	63.59
Al_2O_3	0.7	14.32	16.64	22.65	9.28
Fe_2O_3	6.75	11.1	5.5	6.67	3.91
MgO	44.99	9.05	0.1	0.05	1.68
MnO	0.09	0.18	0.02	0.01	0.1
CaO	0.4	11.52	0.21	0.13	6.77
Na_2O	0.03	2.98	0.09	0.11	0.79
K_2O	0.06	3.37	0.29	0.17	1.7
TiO_2	0.01	2.69	0.75	1.01	0.65
P_2O_5	0.01	0.51	0.08	0.06	0.13
SO_3	n.d.	0.02	0.05	0.05	0.09
LOI*	6.48	0.44	11.4	13.9	10.25
SUM	99.66	99.67	98.91	99.01	98.94

*Loss on ignition, determined gravimetrically at 1,050°C for 1 h (Lechler and Desilets, 1987).

geochemistry of the material can be found in Beyer (2006), Hövelmann et al. (2012) describes the geological setting. The material was provided in two-grain sizes, a fine and a coarse fraction (Figure 1).

Basanite (basaltoid)

The material used is a commercially available rock powder called Eifelgold, produced by Lava Union GmbH (https://www.rpbl.de) and sourced from the Eifel, a low mountain range in western Germany with notable volcanic rock occurrences. It was used in an "as delivered" condition with a grain size similar to the fine dunite, with 44 µm as the dominant grain size fraction (Figure 1). Based on the geochemical composition the calculated normative mineralogy (based on the CIPW norm by Cross et al. (1902) is diopside (32%), plagioclase (16%), leucite (15%), olivine (14%), nepheline (14%), and others (10%). Based on the modal mineralogical QAPF classification of volcanic rocks (Streckeisen, 1980) or the TAS classification (Le Bas et al., 1986), this nepheline-rich material is of basaltic composition, and more specifically, it is classified as *basanite*.

Laterite (oxisol/ultisol)

This material, received from coffee farmers through private contact, originates from the area of Conceição de Ipanema, Minas Gerais, Brazil. According to the USDA soil taxonomy (Soil Survey Staff, 1999), it can be considered to be oxisol or ultisol, yet a more detailed soil description is not available. We use the more generic term laterite here and chose this material based on its cation-depleted character and high iron and aluminum content. As this soil material comes from an actively used agricultural plot, it is known that some fertilizer had been applied to the soil, but more precise information on the fertilizer type and quantities used is not known. There are two types of laterite (Table 1), which were sampled at different locations of the same plot. One type was used for the pure laterite column experiments, and due to insufficient material, the second type was used for the basanite-laterite mix.

Loess

The loess material was freshly collected from a well-described Upper Pleistocene loess occurrence in Remagen, western Germany (50.5611°N, 7.2435°E; Klasen et al., 2015) during a field trip in 2017. It was dried at 40°C to remove moisture. The average $CaCO_3$ content is reported as 17–19%, depending on the formation (Schirmer, 2011).

Experimental setup

Acrylic cylindrical tubes (outer-ø/inner-ø/length: 60/56/250 mm) were filled with the untreated materials (Table 3) to a height of 20 cm while tapping the cylinder to gently settle the powder. All cylinders were fixed vertically using clamps and clamp stands (Figure 2). The top/inlet was covered to decrease water loss by evaporation. A 20-µm nylon mesh was fixed at the bottom of each column to allow water to pass through while retaining the fill material. The experiments were carried out in a temperature-regulated room at about 23°C (Table 3 for details) during the duration of each run. In total, 75 ml of deionized water was added (all at once) to each cylinder every morning, 5 days a week. This amounts to about 8,000 mm a^{-1} (= 8 m^3 m^{-2} a^{-1}), to simulate intensive tropical rainfall (e.g., up to 10,000 mm a^{-1} on La Réunion (Strasberg et al., 2005) or Hawai'i (Giambelluca et al., 2013). In contrast to these natural settings where a variable, but significant amount of water is surface runoff, water is forced through the column material in the experiments.

The effluent solution was collected in polyethylene (PE) bottles, and initially, collected and measured daily. The sampling frequency was then decreased in the later stages of the experiment when the fluid composition showed decreasing variability. The experiments ran for about 10 months (Table 3). Samples were not pooled over multiple watering events. It should be noted that each daily-collected fluid only represents the water that flowed through the column starting from the day before. The samples were stored in a cool and dark environment until analyses.

TABLE 2 Specific surface areas of the source material, derived by BET analyses, as well as grain size distribution characteristics.

Grain size category	Specific surface area [m^2 g^{-1}]	p80* [μm]	Dominant size fraction diameter [μm]	Dominant size fraction [%]	Smallest diameter [μm]	Share of a smallest fraction [%]
Dunite, fine	14.75 ± 0.24	43.5	30.5	6.7	<0.9[§]	2.7
Dunite, coarse	1.61 ± 0.03	1020	860	10.8	<18	1.5
Basanite	1.98 ± 0.01	74.0	44.0	10.5	<18	25.0
Laterite a	N.D.	21.5	18.0	6.5	<0.45	1.0
Laterite b	N.D.	25.5	18.0	6.4	<0.45	1.6
Loess	19.77 ± 0.17	43.5	43.5	6.8	<0.45	0.7

*80% of grains are smaller than the given diameter. [§]this class is divided into five smaller classes but was summed to show the share below 0.9 μm.

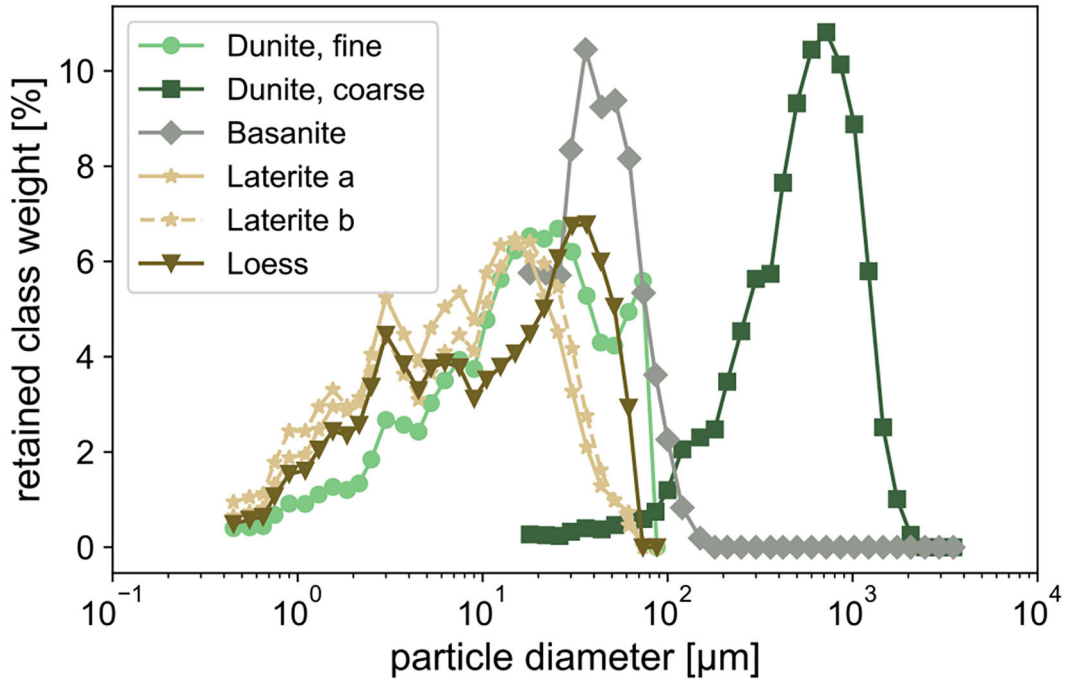

FIGURE 1
Grain size distribution of the applied material.

CO_2 experiment

One series of columns was treated with deionized water in equilibrium with ambient air. The saturated-CO_2 series used deionized water that was sparged with a pure CO_2 stream for 15 min before application. These columns were capped with a gas-tight cover.

Stock solutions had an average pH of 5.34 (5.58; note that all values in parentheses were calculated with PhreeqC) and an average electrical conductivity (EC) of 0.9 ± 0.6 μS cm^{-1} (1.0) when in equilibrium with the ambient lab atmosphere. Under CO_2-saturated conditions, the average pH was 3.93 (3.91) and the average EC was 43.9 ± 5.6 μS cm^{-1} (48.0).

Grain size experiment

This experiment was run with dunite (Table 3). Three replicates of three-grain size distributions were prepared: a coarse fraction, a fine fraction, and a 1:1 mix by mass of the two-grain size fractions. The mass of the dunite powder in each cylinder was subsequently measured.

Fluid composition analysis

The fluid effluent samples were measured for pH, alkalinity, dissolved silica, and major ion composition. Alkalinity was measured by automated titration to pH 4.3, using a Metrohm

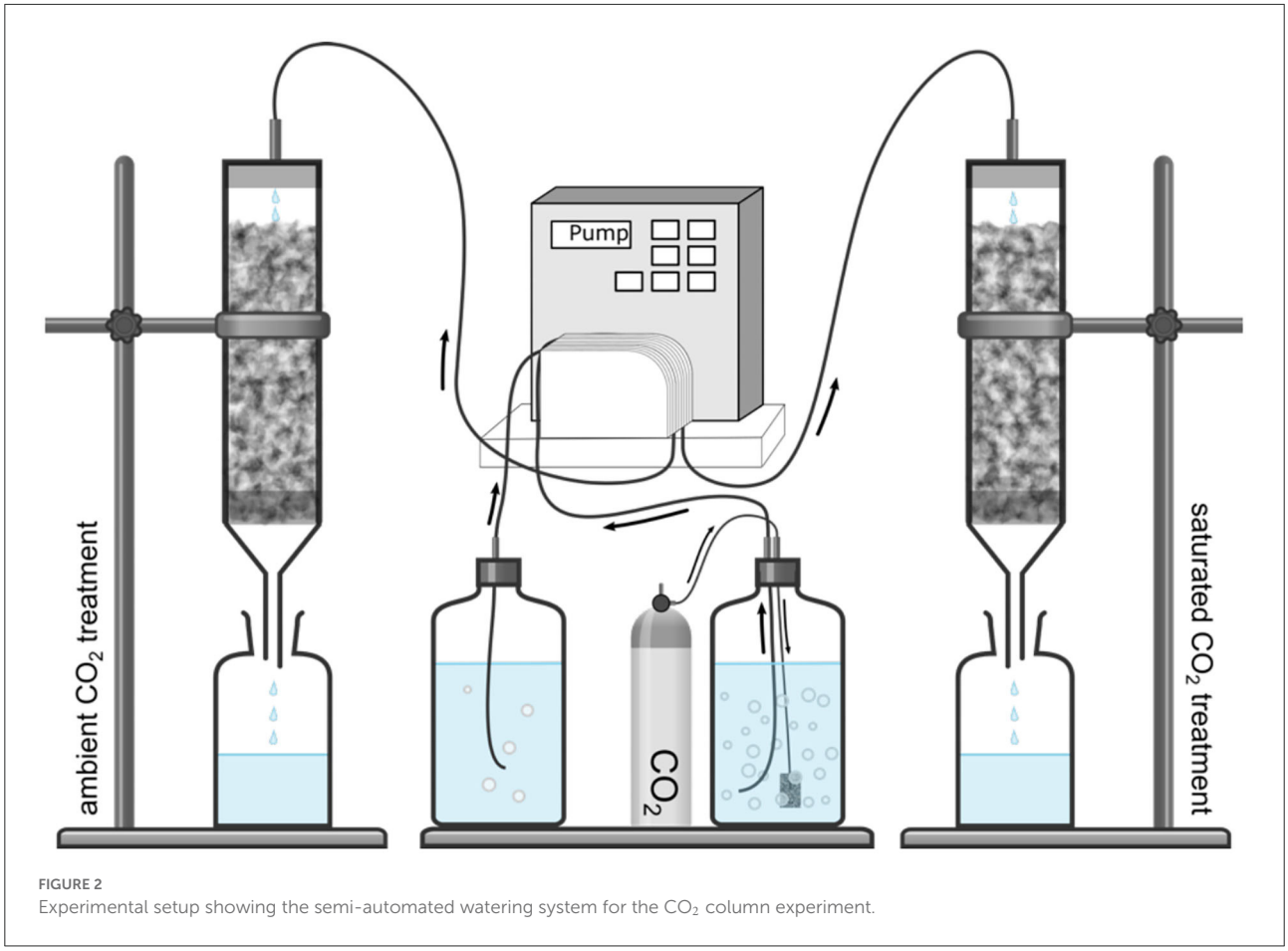

FIGURE 2
Experimental setup showing the semi-automated watering system for the CO_2 column experiment.

Titrando. The titration method determines total alkalinity (TA), defined by Dickson (1981) as:

$$TA = \left[HCO_3^-\right] + 2\left[CO_3^{2-}\right] + \left[B(OH)_4^-\right] + \left[OH^-\right] + \left[HPO_4^{2-}\right] + 2\left[PO_4^{3-}\right] + \left[SiO(OH)_3^-\right] + \left[HS^-\right] + 2\left[S^{2-}\right] + \left[NH_3\right] - \left[H^+\right] - \left[HSO_4^+\right] - \left[HF\right] - \left[H_3PO_4\right] \quad (1)$$

Measurements were calibrated with certified references by A. Dickson (recovery ≥ 99%). Dissolved silica was measured using the molybdate blue colorimetric method (after Hansen and Koroleff, 1999). The average and standard deviation of the coefficients of variation from multiple measurements were 0.6 ± 0.8% for all measured samples. The major cations, Na^+, K^+, Ca^{2+}, and Mg^{2+}, were determined by ion chromatography (Metrohm 881 Compact IC Pro system). Measurements were considered valid when the standard recovery (done every ten samples) was ≥ 95%. The pH was measured using a WTW handheld pH meter calibrated with 3 buffer standards. The effluent solution was routinely sampled before new water was added, implying that the solution was in equilibrium with the atmosphere (time for equilibration was generally ~24 h).

Cation release

To estimate the total cation loss from the column material, data gaps in the obtained time series were approximated by linear interpolations between measured values. In the next step, daily fluxes of each major cation were summed over the entire experimental period. To derive the percentage loss of cations relative to the amount present in the initial fresh material, the following expression was employed:

$$Cation\ loss\ (\%) = \left(1 - \frac{n_{cat} - \sum_{t=1}^{t_{max}} Q(t) \times c_{cat}(t)}{n_{cat}}\right) \times 100 \quad (2)$$

here Q [L] is the solution outflux volume from the column per time step t [day] and c [mol L^{-1}] is the concentration of

TABLE 3 Experimental series and parameters.

Series	Solids	pCO_2 (%)	Column replicates	Column filling mass (g)	Duration (days)	Temp (°C)	Total flow-run through volume (ml)
Ambient-CO_2	1:1 mix of coarse + fine dunite	0.046[a]	1	1,023.65	295	22.6[c]	16,404
	Basanite			810.25	304		16,886
	Laterite			561.00	304		16,886
	1:1 mix of basanite and laterite			620.00	286		15,921
	Loess			794.32	304		16,886
Saturated-CO_2	1:1 mix of coarse + fine dunite	100	1	1,019.96	295	22.6[c]	16,404
	Basanite			789.69	304		16,886
	Laterite			528.00	304		16,886
	1:1 mix of basanite + laterite			620.00	286		15,761
	Loess			849.22	304		16,886
Grain size distribution	Fine dunite	0.046[a]	3	901.13[b]	284	22.6[d]	15,814
	Coarse dunite			982.97[b]			
	1:1 mix of coarse + fine dunite			655.47[b]			

[a]Ambient air average over the experimental period: 459 ± 43 ppm CO_2, measured with a Picarro CRDS G2101-i; [b]Average of three replicates (all values given in Table 1-1 in Supplementary Material). [c]Average over the experimental period ± 2.2°C (q25/q75: 22.3/24.0°C). [d]Data from this period missing—since the lab was continuously temperature-controlled, we assume a value similar to the other experiments.

the considered cation. The moles of a given cation are initially present, n_{cat} [mol], can be calculated using this expression:

$$n_{cat} = \frac{\left(m_{Cat_xO} \times \frac{M_{Cat}}{(M_{Cat}+M_O)}\right)}{M_{Cat}} \quad (3)$$

where M_{Cat} and M_O are the molar mass of the given cation and oxygen, $m_{Cat_\chi O}$ is the column-specific available mass [g] of the considered cation oxide (Cat_x%), as derived by XRF and found in Table 1:

$$m_{Cat_xO} = \frac{Cat_x\%}{100} \times m_c \quad (4)$$

with m_c [g] being the initial mass of the solid material in the column.

Weathering rate calculations

TA release rate

To calculate the "average" instantaneous release rate of TA from a particular material, we used the following equation:

$$R_{TA} = \frac{Q(t) \times c_{TA}(t)}{A_{TSA} \times \tau} \quad (5)$$

As is commonly the case, weathering or elemental release rates are typically reported in terms of moles per unit area of solid reactant per unit time (mol m^{-2} s^{-1}). In the above equation, Q [L] is the solution outflux volume from the column per time step t, c [mol L^{-1}] is the concentration of total alkalinity (TA) at timestep t, A_{TSA} [m^2] is the initial total surface area of the column material (which changes over time but is approximated here as being constant), and τ [s] is the residence time of the solution occupying the pore space of the material.

The total surface area is given by:

$$A_{TSA} = m_c \times A_{SSA} \quad (6)$$

where m_c [g] is the material mass and A_{SSA} [m^2 g^{-1}] is the specific surface area.

The residence time is calculated by:

$$\tau = \frac{V_p}{V_o(t)} \times t \quad (7)$$

with V_p as the calculated porespace within the column and $V_o(t)$ is the volume of outflowing water per timestep t, with t being the length of each time step (sampling interval).

The pore space is derived from the density differences as:

$$V_p = V_c - \frac{m_c}{\rho_s} \quad (8)$$

where ρ_s is the material-specific density [g m^{-3}] and V_c [m^3] is the volume of the empty column. Column mass and material density data are given in Supplementary Material 1.

Equation 5 is equivalent to the standard equation used to calculate mineral dissolution rates using mixed-flow reactors (e.g., Equation 2 in Hellmann, 1994). Nonetheless, the release rates based on Equation 5 provide what can be considered to be a 'column-averaged' elemental release rate, which in all cases would be less than the corresponding rate based on the dissolution of the same amount of material in an MFR. The reason for this is that as the solution flows from top to bottom in a column, non-linear chemical gradients will develop along the column axis, such that the rate of dissolution of material at the top of the reactor will be higher than that at the bottom. For the purposes of this study, the use of an "average rate" should be an acceptable proxy.

Land surface-based CO_2 consumption rate (R_{land})

Based on the weathering reactions for two common silicate minerals, forsterite:

$$\overbrace{Mg_2SiO_4}^{Forsterite} + 4CO_2 + 4H_2O \rightarrow 2Mg^{2+} + 4HCO_3^- + H_4SiO_4 \rightarrow 2MgCO_3 \downarrow + SiO_2 \downarrow + 2CO_2 \uparrow + 4H_2O \quad (9)$$

or albite:

$$\overbrace{2NaAlSi_3O_8}^{Albite} + 2CO_2 + 11H_2O \rightarrow 2Na^+ + 2HCO_3^- + 4H_4SiO_4 + \overbrace{Al_2Si_2O_5(OH)_4}^{Kaolinite} \downarrow \rightarrow 2Na^+ + 2HCO_3^- + 4SiO_2 \downarrow + 8H_2O \quad (10)$$

we assume a 1:1 conversion of CO_2 into alkalinity in the second step of the reaction, which represents the initial weathering product, while the second steps in Equations 9 and 10 represent the long-term final stages of the reaction.

Based on this conversion, we use the TA concentrations together with outflow volumes to calculate a first-order estimate of land surface-based weathering rates, which are equal to the CO_2 consumption rates.

The annual CO_2 consumption is estimated based on average TA fluxes during the final stages of the experiments, based on the assumption that dynamic near-equilibrium conditions are representative of long-term fluxes. The values used were $t > 225$ days for dunite, $t > 268$ days for basanite-laterite, and $t > 289$ days for basanite, laterite, and loess experiments.

Individual, daily TA fluxes were calculated according to

$$F_d = Q(t) \times c_{TA}(t) \quad (11)$$

based on the measured data for outfluxes $Q(t)$ [L d^{-1}] and TA concentrations $c_{TA}(t)$ [mol L^{-1}] from the aforementioned experiments and corresponding periods.

With these individual fluxes, an average annual CO_2 consumption (in t km^{-2} a^{-1}) was calculated by

$$R_{land} = \frac{\frac{1}{n}\sum_{d=1}^{n} F_d}{A_c} \times M_{CO_2} \times 365 \quad (12)$$

where n is the number of available flux values, A_c is the cross-sectional surface area of the column, M_{CO_2} is the molar mass of CO_2, and the factor of 365 serves to convert daily to annual CO_2 uptake.

To evaluate the additional CO_2 uptake over the first year, which is characterized by non-equilibrium fluxes, a simplified approach was chosen. Since TA concentrations were not determined every day due to economic and time constraints, the available data were fitted to a non-linear function in order to derive an estimate of the TA fluxes over the course of the experiments (curve fits shown in Supplementary Material 2). Based on the fitting parameters, modeled daily TA concentrations were summed over 1 year:

$$R_{land\,year1} = \frac{\sum_{d=1}^{365} F_d}{A_c} \times M_{CO_2} \quad (13)$$

The additional CO_2 consumption in the first year is then simply calculated by

$$R_{land_{add}} = R_{land\,year1} - R_{land} \quad (14)$$

Saturation indices

All saturation indices were calculated using the Python package *PhreeqPython* (Vitens, 2021), which is based on *PhreeqC* (Parkhurst and Appelo, 2013). Thermodynamic input was taken from the *WATEQ4F* database (Ball and Nordstrom, 1991). Calculations consider the major cation concentrations, dissolved silica, phosphate, alkalinity, pH, and temperature as input variables.

Results

CO_2 experiment

Total alkalinity and pH

All experiments show an immediate effect of watering after the start of each experiment, for both ambient CO_2 and saturated CO_2 conditions (Figure 3). There is an initial phase in which all materials show an immediate spike in TA concentration, followed by a slow exponential decrease, and then the attainment of a roughly linear relation characterized by slowly decreasing concentrations (Figures 3A,B). The weak linear (downward) trends remain, even during the final stages

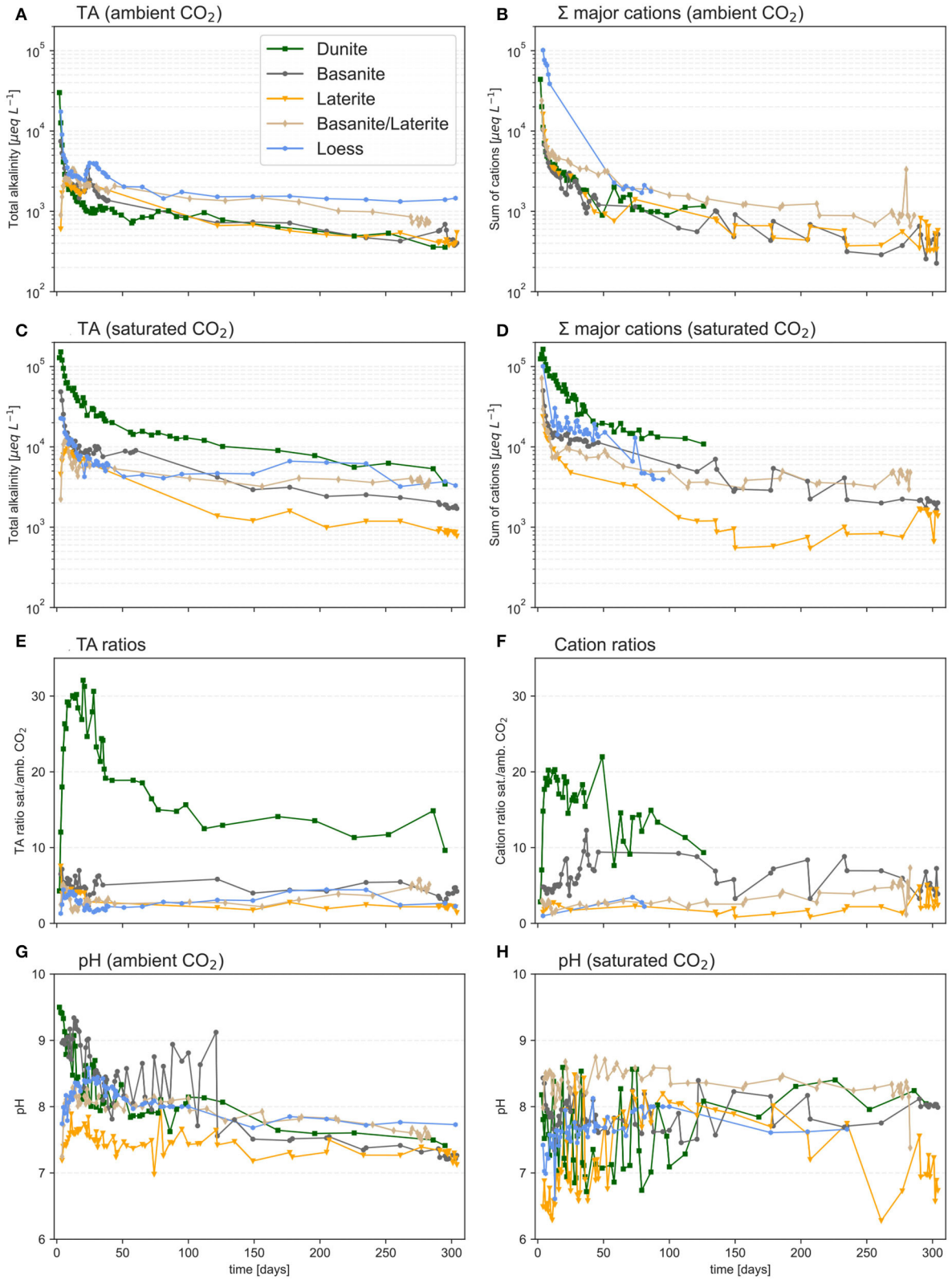

FIGURE 3
Development of TA, the sum of cation equivalent concentrations, and pH in the columns treated under ambient **(A,B,G)** and saturated **(C,D,H)** CO_2 conditions. The ratios of TA and total cations ($CO_{2\ saturated}/CO_{2\ ambient}$) are shown in **(E,F)**. pH is given in **(G,H)**, note the starting pH for water under ambient CO_2 was on average 5.34, while the starting pH under 100% CO_2 was on average 3.93.

of each experiment, indicating that true steady-state conditions were not yet fully reached.

Except for the first week, the highest TA concentrations under ambient CO_2 were observed for basanite, with values around 2,000 μmol L^{-1} (Figure 3A), whereas under CO_2-saturated conditions, dunite showed the highest concentrations, with values starting >100,000 μmol L^{-1}, and then leveling out further on to around 10,000 μmol L^{-1} (Figure 3C).

The strongest effect of CO_2 saturation on TA was observed for dunite, as evidenced by a TA ratio (CO_2-saturated/CO_2-ambient) equalling 15–30. The effect was less pronounced for the other materials, but all columns showed higher TA concentrations under saturated conditions (Figure 3E).

The pH measurements in the effluent solutions are quite scattered, but nonetheless, there is an overall trend of decreasing pH with time for CO_2-ambient conditions, which does not seem to be the case in saturated-CO_2 conditions. In general, it appears that higher pH values occurred during the first half of all experiments for CO_2-ambient conditions, but during the second half, the output pH values were slightly higher at saturated-CO_2 conditions (Figures 3G,H). The effluent pH values reflect in large part the significant differences in the starting pH values of the input solutions.

Cation release

The sum of cation equivalents released follows trends similar to those for TA (Figures 3B,D,F), in particular the sharp initial spike followed by an exponential decrease and then the attainment of a weak but negative linear relation (Figures 3B,D).

The relative loss of cations after the experimental period was generally higher under CO_2-saturated conditions in all materials (Table 4). The ratio between the losses at ambient and saturated CO_2 varies, depending on the cation and source material. On average, the loss ratio is 3.7 ± 3.8. The loss ratio of Mg is highest in the dunite column, where the presence of high CO_2 concentrations leads to a nearly 16× higher flux than under ambient-CO_2 conditions (Table 4). While the ratio is highest for Mg, it stands out that major cation losses from the dunite are dominated by monovalent K and Na. Also, basanite and basanite/laterite released relatively higher Na and K contents than Mg under saturated-CO_2 conditions (Table 4). Losses from the laterite are markedly high for Mg, Ca, and K. The loess column lost predominantly divalent cations.

The relative release of elements is not proportional to their content in the untreated substrates (Figure 4). The major cation release of dunite is dominated by Na and K, even though their abundance is only 1% in the dunite. The basanite columns predominantly show Mg release under saturated CO_2 conditions, but Ca, Na, and K contribute 35% under atmospheric conditions (Figure 4). Compared to the original material, laterite shows a pronounced release of K at ambient CO_2 and of Ca at saturated CO_2. The cation release from loess is proportionally larger for Mg at both CO_2 concentrations, while Na and K releases are very low compared to the original composition.

Grain size

This series of experiments was designed to shed light on the effects of grain sizes (their distribution and specific surface area) on weathering rates and ion fluxes using dunite. Columns with smaller grain sizes resulted in higher Mg, TA, and effluent pH (Figure 5). The mixed granulometry results approximated those of the fine grain size rather than the coarse grains. Results for Mg (Figure 5B) and TA concentrations (Figure 5C) show similar trends, as was the case for dunite under ambient CO_2 in the CO_2 experimental series (Figures 3A,C). The effluent pH trends are very similar to TA and show a sharp initial spike, and then an exponential decrease to values of ∼8 (Figure 5D). Si concentrations do not follow the generally observed trends of TA, Mg, and pH (Figure 5A). Dissolved silica concentrations are very low (<90 μmol L^{-1}, Figure 5A) in comparison to the released magnesium (>1,500 μmol L^{-1}). Moreover, Si release showed very similar trends for the three-grain sizes, with the mixed case showing three anomalous concentration excursions of unknown origin (Figure 5B). Si values generally fluctuate between 5 and 20 μmol L^{-1}, with four outliers.

The Mg/Si molar ratios are always well above the theoretical value of 2 (Figure 5E), with values >100 at the beginning and an average long-term average of 47.8. The mechanism responsible for this non-stoichiometry can (in theory) result from either preferential Mg release, or preferential Si retention, and can only be elucidated with nanometer-scale solid-state surface analyses (e.g., Hellmann et al., 2012, 2021; Zandanel et al., 2022).

Annual CO_2 sequestration based on TA fluxes

The initial period spanning the first few weeks showed substantially elevated TA concentrations (Figures 3, 5), which in turn corresponded to initially higher land surface-based release rates. Over significantly longer time periods (up to 1 year) the TA concentrations, and consequently the CO_2 removal rates, decreased until a baseline characterized by a more constant behavior was reached, which can be considered to be representative of the first year (Figure 6). These lower, but constant weathering rates show that, under ambient-CO_2 conditions, CO_2 consumption is highest in the loess column and lowest in the laterite column, with 730 and 100 t CO_2 km^{-2} a^{-1}, respectively (Figure 6A). Dunite (all-grain sizes under ambient CO_2) and basanite have similar consumption rates (around 220 t CO_2 km^{-2} a^{-1}). These values are comparable to the plotted literature values for ultramafic lithologies (Figure 6A).

TABLE 4 Fraction of major cations (mole %) relative to the cation content of the fresh/unreacted column material released during the experiment phase. The resulting ratios between saturated and ambient CO_2 treatment can be interpreted as the maximum achievable ratios in the field since watering volumes were chosen to simulate tropical humid high precipitation rates with enhanced complete drainage.

	Dunite			Basanite			Basanite/Laterite			Laterite			Loess		
	Amb. CO_2	Sat. CO_2	Ratio	Amb. CO_2	Sat. CO_2	Ratio	Amb. CO_2	Sat. CO_2	Ratio	Amb. CO_2	Sat. CO_2	Ratio	Amb. CO_2	Sat. CO_2	Ratio
Mg	0.09	1.44	15.87	0.09	0.49	5.51	0.32	0.87	2.70	12.91	31.48	2.44	3.98	9.18	2.30
Ca	1.78	2.98	1.67	0.16	0.95	5.83	0.59	2.01	3.39	14.69	51.44	3.50	2.28	3.09	1.36
Na	23.75	24.82	1.04	0.48	5.98	12.54	4.14	10.42	2.52	0.68	1.10	1.61	0.95	1.02	1.08
K	14.27	12.77	0.90	0.65	3.52	5.44	2.75	5.11	1.86	24.19*	27.72*	1.15	0.11	0.23	2.14

*High K-fraction in the laterite is assumed to be from highly soluble fertilizer contained in the original soil.

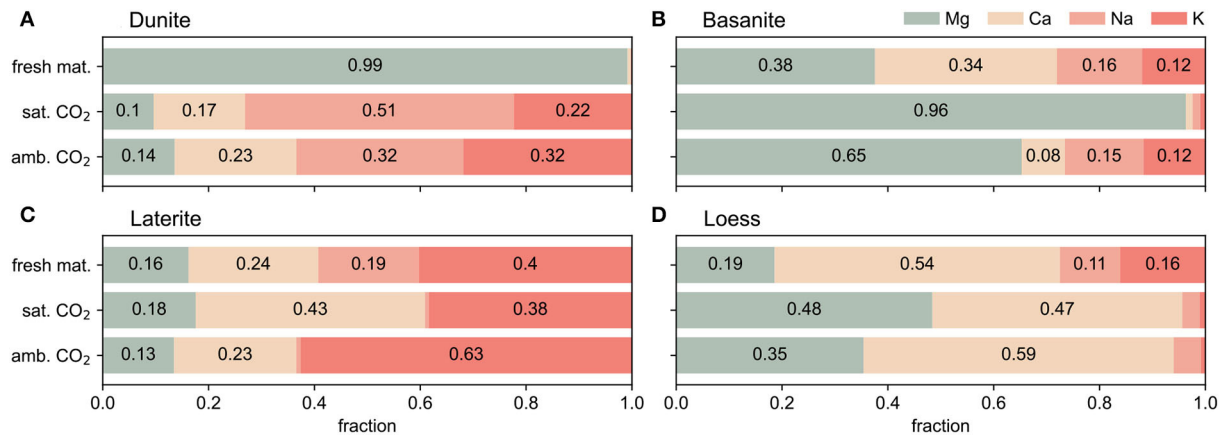

FIGURE 4
Relative fractions of major cations [from left to right: Mg (green), Ca (light orange), Na (light red), K (red)] in the original, unreacted material (see XRF analyses, Table 1) and the relative cumulative fractions of each cation released over the 300-day reaction time under ambient and saturated-CO_2 conditions. **(A)** Dunite, **(B)** Basanite, **(C)** Laterite, **(D)** Loess.

The mix of basanite and laterite has a much higher consumption rate (around 430 t CO_2 km^{-2} a^{-1}) compared to the basanite alone. If the initial intensive weathering period is considered representative of the first year, CO_2 consumption rates are significantly higher in all ambient-CO_2 experiments (by 20–250%). The CO_2-saturated experiments show higher CO_2 consumption rates (Figure 6B), compared to the ambient CO_2 treatment by roughly a factor of four for the basanite, laterite, and basanite/laterite, but around 11 for the dunite column, excluding the initial flushing phase (Figure 6C).

Mineral saturation states

As a simplified indicator for potential secondary mineral precipitation, saturation indices (SI) were calculated. It should be kept in mind that these are thermodynamic calculations, and therefore may not correctly predict precipitation, given that kinetics may in fact be rate-controlling. The SI of calcite and amorphous silica throughout the experiments was calculated using the composition of the outflow solution from all columns (Figure 7). Under ambient conditions, the saturation indices of the effluent solutions suggest that the precipitation of carbonate minerals (e.g., calcite, Figures 7A–D) was thermodynamically favorable only for a short period at the beginning of the experiment. Beyond this initial period, the solutions were undersaturated with respect to all considered carbonate species (Supplementary Material 3). Under CO_2-saturated conditions, water draining the columns was, after equilibration with the atmosphere, most of the time oversaturated or near saturation with respect to calcite for the basanite and basanite-laterite columns (Figures 7A,B). These SI indices change if it is assumed that the effluent water remained 100% CO_2-saturated; in this scenario, the solutions were then consistently undersaturated with respect to calcite. When the dunite columns were considered with the same scenario (100% CO_2-saturated effluent solution), calcite was also undersaturated, except over the first few weeks. Similar results were calculated for aragonite and dolomite

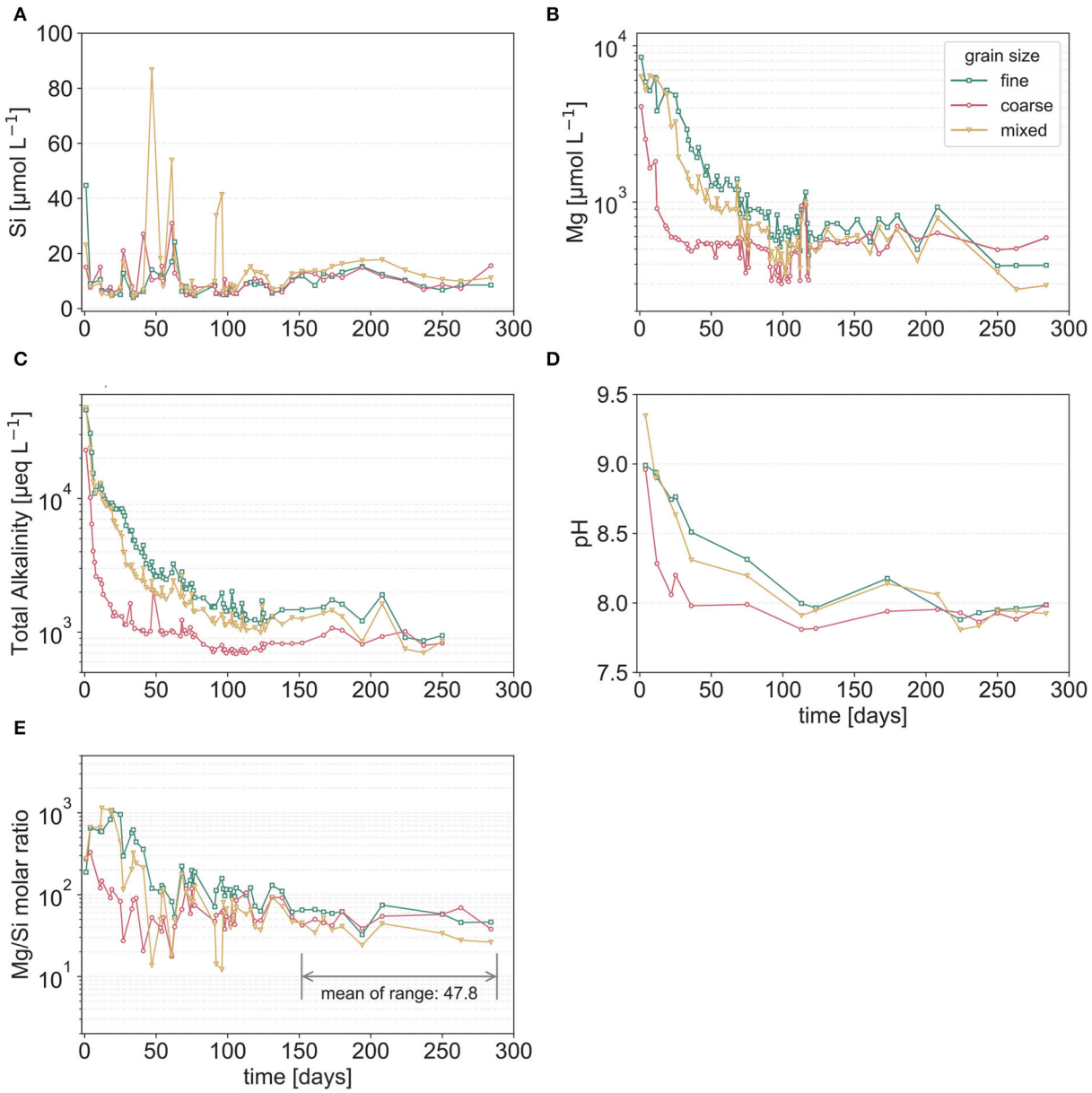

FIGURE 5
Temporal evolution of averaged dissolved silica [Si, **(A)**], magnesium [Mg, **(B)**], total alkalinity [TA, **(C)**] concentrations, and pH **(D)** in the outflow of the columns filled with dunite of different grain size distributions under ambient CO_2 conditions. **(E)** Evolution of the Mg/Si molar ratio; here the y-axis minimum was chosen to represent the nominal ratio of Mg/Si in olivine, i.e., congruent dissolution ($Mg_2SiO_4 \rightarrow$ 2:1), Note that during the final period, values are far higher than 2, indicating a non-stoichiometric alteration process. All the data are differentiated by fine (green squares), coarse (red circles), and mixed (yellow triangles) grain sizes.

(Supplementary Material 3-1). The hydrous magnesium mineral nesquehonite was always undersaturated, even in the dunite experiment (Supplementary Material 3-2). Magnesite may have precipitated throughout the experiment if equilibration with the atmosphere occurred.

All solutions were generally below saturation with respect to amorphous SiO_2 under ambient-CO_2 conditions, while at saturated-CO_2 conditions values fluctuated around zero, indicating that precipitation could have occurred (Figures 7E,F).

Discussion

Land surface-based CO_2 consumption

The CO_2 consumption rates shown in Figure 6 were calculated with a straightforward approach based on TA fluxes from the columns. Two perspectives on achievable CO_2 sequestration rates can be drawn from our results. When scaled to 1 year, total CO_2 uptake of nearly 1,000 t CO_2

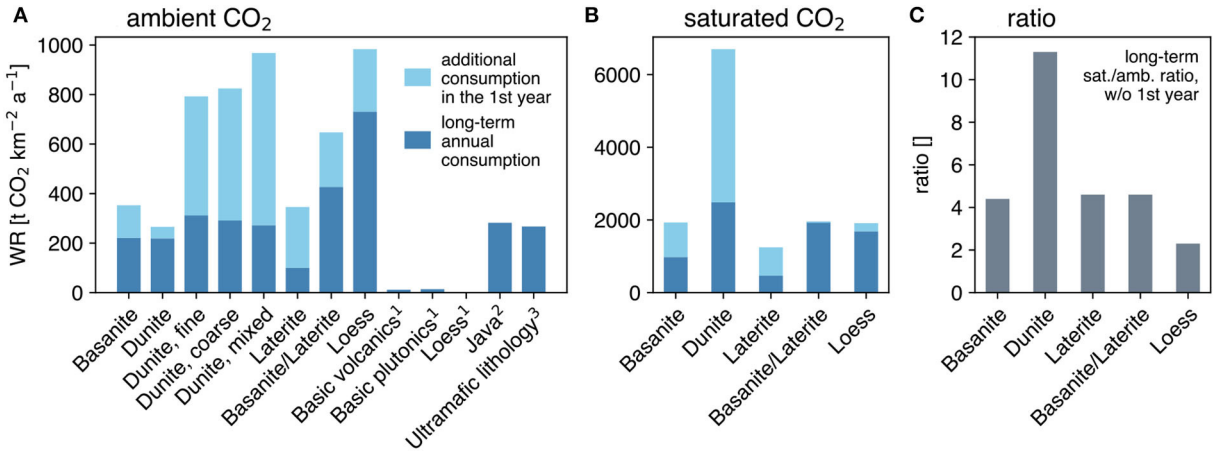

FIGURE 6
The long-term annual CO_2 consumption normalized to land surface area in t CO_2 km^{-2} a^{-1} under ambient-CO_2 **(A)** and saturated-CO_2 conditions **(B)**. The light blue bars indicate the additional CO_2 consumption during the first year, as rates steeply increase during the first weeks of deployment. **(C)** The ratio between rates of saturated over ambient CO_2 conditions is based on the expected annual consumption without the initial flushing phase. [1]from Table 1 in Hartmann et al. (2009): 11.77, 13.97, and 2.05 t CO_2 km^{-2} a^{-1}, respectively; [2]from Table 1 in Dessert et al. (2003); [3]from Table 6 in Schopka et al. (2011).

km^2 a^{-1} was calculated for loess and dunite. However, this estimate is only valid for the first year of application, which includes a very elevated weathering signal contribution from the first 3 weeks. Further on in time, the systems approach an approximate dynamic steady-state state that leads to markedly lower overall CO_2 uptake rates. The possible explanations for the decline in rates are discussed in Section 4.2. The dynamic steady-state in the later stages of the experiments yields significantly lower CO_2 uptake rates, which for dunite and basanite are comparable to the highest reported literature values of catchments found for tropical areas with volcanic rocks. This order of magnitude equivalence in CO_2 removal validates the applied environmental parameters in this study (temperature and precipitation simulating tropical conditions). Applying the observed rates to the globally available tropical agricultural areas [5.1×10^6 km^2, Strefler et al. (2018a), yields a total annual CO_2 uptake of 1.1 Gt CO_2 a^{-1}]. This is about 14% of the annual minimum required CDR to attain the 1.5° target estimate, stipulated in the Paris Agreement (United Nations, 2015; Strefler et al., 2018b), and indicates that inorganic carbon uptake by EW based on atmospheric CO_2 levels in soils might contribute significantly to a portfolio of CDR methods. Moreover, *in situ* soil pCO_2 is normally considerably higher than ambient atmospheric values, where estimates of up to 70,000 ppm in tropical soils are not unusual (Brook et al., 1983; Davidson and Trumbore, 2017; Hashimoto et al., 2017; Romero-Mujalli et al., 2018). Higher CO_2 levels increase CO_2 drawdown rates, by a factor of more than four under a scenario of 100% CO_2-saturated conditions compared to ambient levels, as demonstrated in this study. Counterintuitively, the land surface-normalized CO_2 sequestration rate of dunite is roughly equal to that of basanite under ambient-CO_2 conditions (Figure 6A), and yet the ratio of CO_2-saturated to ambient-CO_2 uptake in the dunite columns is more than two times higher than for all other materials (11.3 vs. ~4.5). We hypothesize that the weathering reaction in the dunite column under ambient-CO_2 conditions was limited by the available CO_2.

To put into perspective the weathering rates that we present, it needs to be re-iterated that the experiments in this study were designed to simulate plausible maximum weathering rates, under specific conditions of (very) humid tropics, and an (unlikely) 100% drainage of water within the columns (water flowing through a bed of rock powder). Although the investigated effects of saturated-CO_2 conditions are not realistic for natural soils, the results likely represent the upper limit for inorganic weathering, without considering the potential contributions of plants, microbes, and bioturbation. The CO_2-enhancement factor for elevated realistic CO_2 levels in soils compared to ambient conditions remains to be determined and might not be linear (c.f. discussion Section The CO_2 effect and feedback constraints in Earth system model parameterizations).

Decrease of weathering rates with time

The surface area normalized weathering rates, here represented by TA (Figure 8), are in general lower than far-from-equilibrium rates using mixed-flow or batch reactors (cf., Palandri and Kharaka, 2004). Dissolution experiments using the latter types of reactors are generally characterized by very low solid to solution ratios, pre-treatment of grains to remove fines, uniform grain sizes, and run times commonly on the order

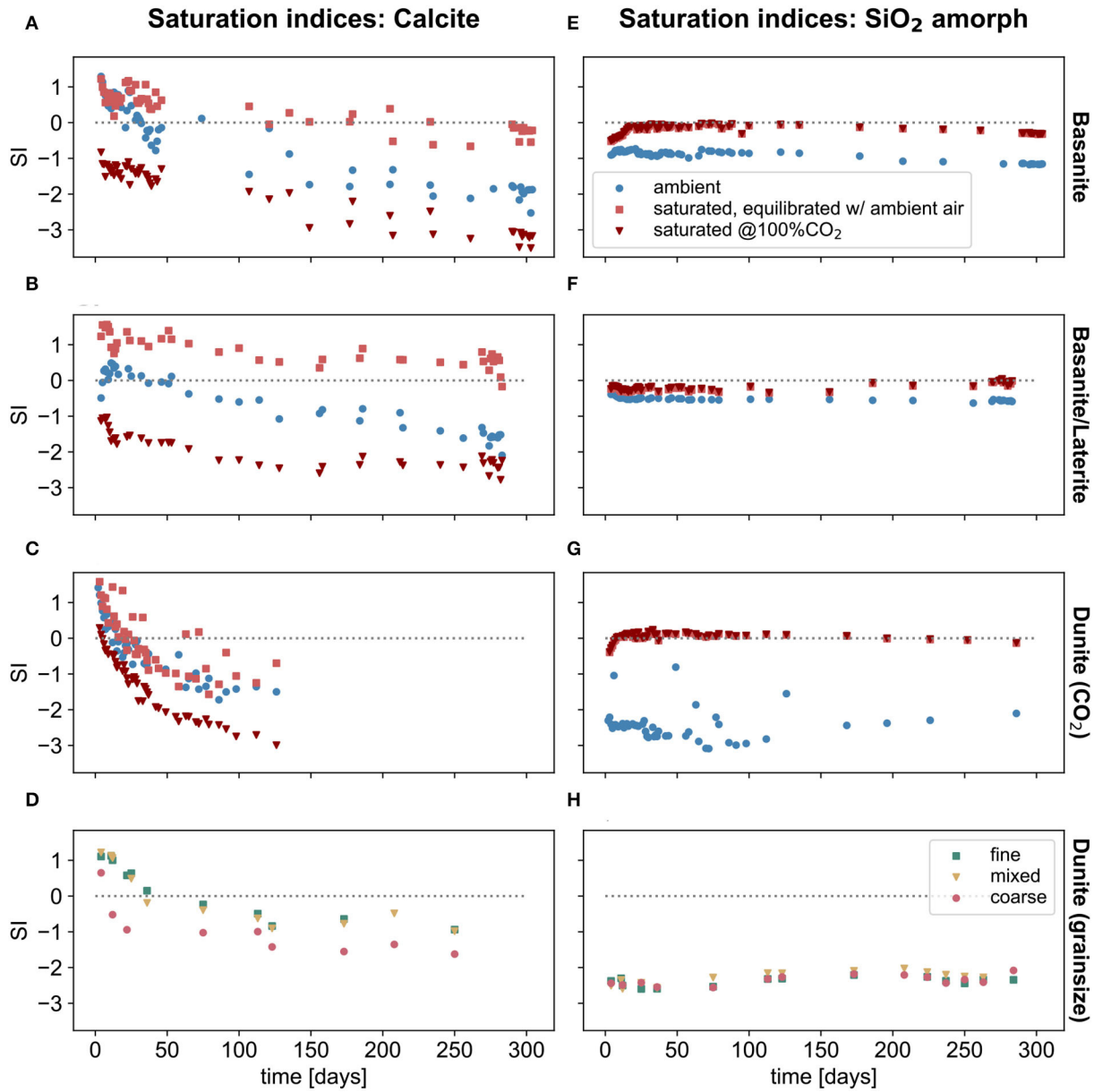

FIGURE 7
Calculated saturation indices for calcite **(A–D)** and amorphous silica **(E–H)** based on the composition of the outflow solution of the column experiments. Values were calculated using PhreeqC. Ambient and saturated values in **(A–C,E,F)** are calculated based on the outflow solution, which was equilibrated for 24 h or longer with the laboratory atmosphere. In addition, saturation indices were calculated assuming the effluent solutions remained CO_2-saturated.

of hundreds of hours to several tens of days. In contrast, our column experiments, which have a high rock-to-water volume ratio, provide rates that have maximum values below (ambient) or in the lower range of one standard deviation of fitted reported literature values [basanite columns, Figures 8C,D, comparison with fitted data from Bandstra and Brantley (2008)]. Moreover, in column experiments rates can decrease by up to two orders of magnitude within the first year (Figures 8E,F).

The decrease in reaction rates with time can be attributed to several processes. Initially, sample preparation conditions can lead to hardly quantifiable decreases in observed dissolution rates (Eggleston et al., 1989). Furthermore, a natural continuous decrease of available material may also influence the observed rate to a minor extent.

More importantly, dissolution rate declines may be attributed to the very rapid dissolution of fine particles, and/or

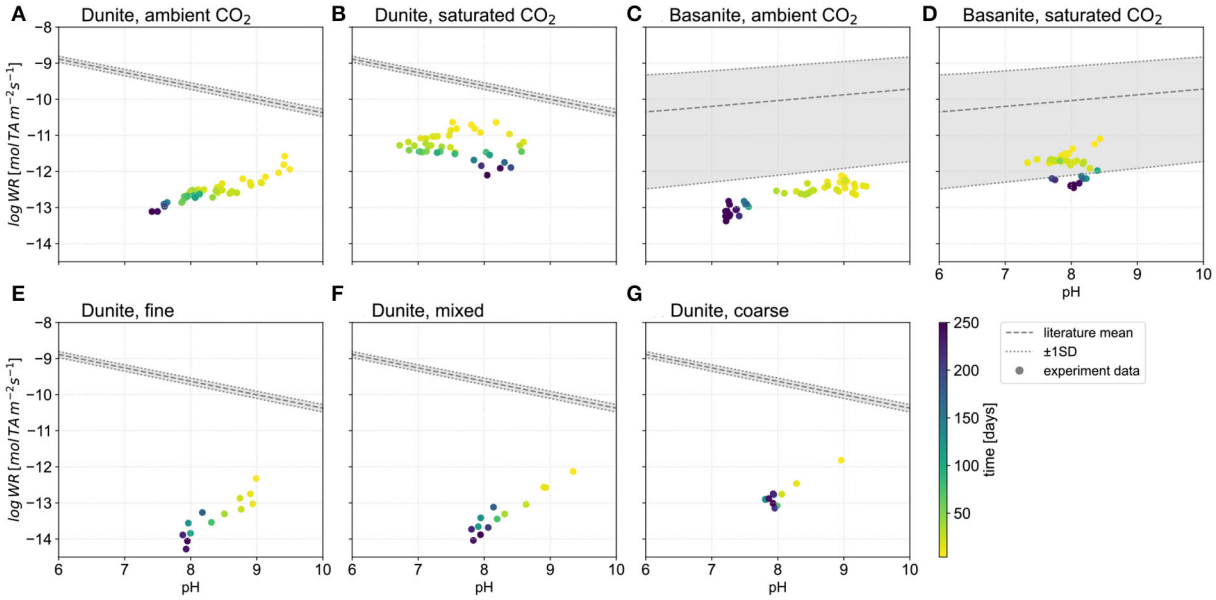

FIGURE 8
TA based weathering rates plotted against pH. Fitted data for literature weathering rates (gray area and dashed lines) from Bandstra and Brantley (2008); rate values were recalculated with a stoichiometric factor to get TA to release rates. Four moles TA are produced from one mole forsterite (Equation 9). Rates for basalt are reported as mol Si m-2 s-1; here, the conversion to TA release rates is based on a generalized basalt composition (from Navarre-Sitchler and Brantley, 2007), where the equivalent of one mole Si yields 2.5 moles TA. Gradient colors indicate elapsed time of the experiment. Note that in configurations e.g., there are more rate values available, yet no corresponding pH values were recorded. **(A)** Dunite, ambient CO_2, **(B)** Dunite, saturated CO_2, **(C)** Basanite, ambient CO_2, **(D)** Basanite, saturated CO_2, **(E)** Dunite, fine, **(F)** Dunite, mixed, **(G)** Dunite, coarse.

surface sites having high surface energies (Holdren and Berner, 1979; Brantley, 2008). The crushed materials used in this study contain fines (no effort was made to remove them, e.g., see SEM images of dunite in Supplementary Material 4 and Table 2, column "share of smallest class"), and most likely also grain surfaces with sites of high energy density that were created during comminution.

Reaction rates reported in the literature based on mixed-flow and batch reactors, typically with agitators stirring a few grams of the minerals in a fluid medium, mitigate against transport-limited conditions of mineral dissolution and rather favor surface-controlled reactions (Awad et al., 2000; Martinez et al., 2014).

In a column reactor, the somewhat fast and preferential flow of water through channels, canals, or pore interconnections will be similar and also surface reaction controlled. Water with dissolved CO_2 is moving through the pore system, and not all pores will exchange water at the same rate. We observed slight compaction of the material during the experimental runs, decreasing the pore space and the surface area available for solid-fluid contact, which also could have contributed to the reduction of dissolution rates.

In addition, the material will be in contact with stagnant fluids trapped within very tiny fluid pore spaces where it is unlikely that the reactions are transport controlled.

Past experiments on forsterite dissolution have observed non-stochiometric release of Mg/Si in the initial phase of dissolution, becoming stoichiometric after a few 100 h of reaction (Pokrovsky and Schott, 2000b). This was attributed to the formation of an amorphous silica-rich layer (ASL) on the mineral surface and has been reported for many other silicate minerals including albite, labradorite, diopside, wollastonite, and garnet (Wogelius and Walther, 1992; Pokrovsky and Schott, 2000b; Hellmann et al., 2012). At steady-state, the layer thickness varies and depends on the mineral, as well as the fluid dynamics, solution chemistry and pH, and temperature. Reported thicknesses range from <1 nm for laboratory altered forsterite [Zandanel et al., 2022; see also evidence for slightly thicker layers in Pokrovsky and Schott (2000a)] to 50 nm on naturally weathered K-feldspars and 200 nm on serpentine (Hellmann et al., 2012). The high Mg/Si ratio at the end of the dunite experiment (Figure 5E) suggests that Si is actively precipitating, even after 250 days. These results indicate that the system was still far from the steady-state, unlike in experiments with low mineral to water ratios, where steady-state and stoichiometric dissolution were often observed within a few 100 h (Wogelius and Walther, 1992; Pokrovsky and Schott, 2000b; Hellmann et al., 2012).

If it is assumed that the formation of the ASL is governed by a coupled interfacial dissolution-reprecipitation (CIDR)

mechanism (Hellmann et al., 2003, 2012, 2021), and the ASL is porous, it should not impede dissolution of the silicates (Putnis and Putnis, 2007). However, if the ASL is non-porous and impermeable to fluid exchange between the dissolving silicate surface and the surrounding bulk fluid, the dissolution reaction may become kinetically hindered, or in a worst-case scenario, the reaction rate would evolve to such low values so as to be unmeasurable (Putnis and Putnis, 2007). Even if the ASL is porous and permeable, the distance between the exterior bulk fluid and the reacting silicate surface might result in a decline in rates over the course of the reaction (Pedrosa et al., 2016), at least for low pressure and temperature conditions (Pedrosa et al., 2017). Moreover, recent studies suggest that ASLs are heterogeneous and can structurally evolve with time, e.g., an increase in density. As a consequence, dissolution rates may decline further over time (Daval et al., 2011, 2017; Maher et al., 2016). Considering all of our experiments, after 1 year of reaction there was no evidence that the dissolution of the minerals stopped, even if some of the release curves are noisy and do not display clear trends (Figure 3).

Si can also precipitate with different morphologies. In an experiment by Lazaro et al. (2012), it was found that amorphous silica precipitated during intense olivine dissolution as nano-silica colloids, with a high SSA of 100–300 m^2g^{-1}. The observed nano-silica has primary particles of 10–25 nm that were agglomerated in clusters with an average pore size of ∼20 nm. An increase in mesopores could (further) increase the water holding capacity of the soil (Schaller et al., 2020). This probably important aspect in the context of drought conditions needs further research to assess application consequences from the evolution of amorphous silica in quality and quantity, depending on the applied amount of silicate minerals, their grain sizes, and shapes.

Comparing pH-controlled dissolution experiments from the literature and the column-derived data from this study is difficult as the experiment conditions are different, yet they can provide a reference for the discussion. In the ambient-CO_2 column experiments, dunite rates increase with pH (Figure 8) with values >7, as opposed to the trends shown by literature data fits (from Bandstra and Brantley, 2008). While in the literature, rates are measured at fixed pH in a system far from equilibrium, the column experiment is a system that reacts dynamically with water and CO_2 input by proton production or consumption. Under ambient conditions, the capacity to consume protons declines toward the end of the experiment, indicated by lower pH and decreased weathering rates. Under CO_2-saturated conditions, rates also decline with time, but the pH range is greater and not directly correlated with alkalinity production (Figures 8B,D). Weathering rates are still higher at the end of the experiment compared to rates under ambient conditions.

Effect of grain size (distribution)

It is often assumed that finer rock material grain sizes purposed for enhanced weathering would yield higher CO_2 capture rates (e.g., Strefler et al., 2018a), simply due to the higher surface area available for reaction. This hypothesis is not supported by our experiment results for EW.

The experimental series designed to evaluate the effect of different grain sizes using the same dunite material shows higher TA fluxes from the fine grain size column, especially over the first 100 days. However, when normalized to the total grain surface areas, this result changes: while the total grain surface area of the fine column material is on average 8.4 ± 0.2 times higher than the surface area of the material in the coarse columns, the CO_2 consumption of the fine material is only ∼7% higher. Although the porosity is much higher in the fine grain size column (Table 1-3 in Supplementary Material), which would indicate a larger potential contact area for rock-water interaction, it is assumed that the characteristics of this larger pore space do not allow for rate-stimulating effects. The pore sizes may be much smaller, reflected in decreased hydraulic conductivity, qualitatively observed by longer residence times of the supernatant water (which percolated more slowly through the column). Moreover, significantly smaller pores likely did not contribute much to the transport of water through the column, which was more likely characterized by preferential fluid channels. In contrast, fluid flow through the coarse material with larger and inter-connected pores likely enabled a greater material-water contact area, leading to enhanced dissolution.

A comparable effect may explain the higher weathering fluxes of the laterite/basanite mix, compared to basanite alone, although the mix is only comprised of 50% basanite. The plain tropical soil, laterite, naturally dominated by very small grains (p80 < 30 μm) showed little hydraulic conductivity and long retention times of the supernatant water. Mixing with the coarse basanite yielded a grain size distribution more suitable for enhanced weathering, so the effect of hydrology, an increase of hydraulic conductivity, and enhanced grain-water contact time may lead to the enhanced observed weathering fluxes.

Both observed effects underline the importance of the hydrologic conditions within the material, which are controlled by the grain size distribution (as also hypothesized in Amann et al., 2020; c.f., modeled hydrological effects from EW in de Oliveira Garcia et al., 2020) and the nature of grain packing, which in the experiment was also influenced by manually filling the columns. Preferential flow along the column walls, or clogging and missing pore interconnections (as could be visually observed in the columns) may decrease apparent weathering rates, while a grain size distribution optimized for water residence times, with a balance between sufficient reaction time and oversaturation, can maximize the weathering effect and thus the CO_2 uptake efficiency (de Oliveira Garcia et al., 2020).

For a real-world application, simply testing the rock flour material alone, without considering the soils it is applied to, will not be an effective strategy. Besides testing material mixed with the target soil, it seems imperative that hydrological effects should also be considered. Moreover, the effects of bioturbation, plant roots, or uptake of elements by plants (Akter and Akagi, 2010; Taylor et al., 2015; Krahl, 2020; Verbruggen et al., 2021) affect the transferability of the column experiment results to real-world soil-plant systems. Such effects on EW must be studied in more detail to enable enhanced predictions by models in the future, backed up of course, by experimental data.

Cation release

Studies of major cation leaching are relevant for the assessment of different rock types to act as potential CO_2 sinks *via* weathering. Our results (Table 4) suggest that the total dissolution of any of the evaluated materials under the conditions in this study would take about a century or longer under atmospheric pCO_2 while being accelerated in the CO_2-saturated environment. It is relevant for a CDR application scenario to understand the cation release rate and alkalinity production as a function of CO_2 levels in the amended soils.

The relative release of major cations from the substrate diverges from its relative content in the parent mineral (Figure 4). Cation release is largely determined by the dissolution kinetics of dominant minerals. Mg dominates the cation flux from the dunite column, which is expected, as forsterite (Mg_2SiO_4) dominates the source rock. In the dunite experiment, notable amounts of K were released, which might be unexpected, given the general composition of the material. This behavior may be traced back to the occurrence of chabazite (Supplementary Material 5), a mineral from the zeolite group, which can contain K and has rather rapid weathering rates (Schofield et al., 2015; Moravec et al., 2021). K is relevant for achieving additional carbon sequestration *via* EW through biological processes (Goll et al., 2021), as K is an important nutrient to most plants. The release of Na and K from the basanite columns could be explained by the abundance of nepheline [$(Na,K)AlSiO_4$], a feldspathoid mineral that commonly occurs in the silica-depleted magmas of the Eifel (Mertes and Schmincke, 1985). The dissolution rate of nepheline is significantly higher than other Na-dominated rock-forming minerals, i.e., albite (Lasaga et al., 1994; Franke, 2009). The high dissolution rate indicates that rocks rich in this mineral may be a preferable source for EW, even if a monovalent ion is associated with ~50% less CO_2 drawdown compared to a divalent cation.

Target materials for EW application should be tested for available water (rainfall) and CO_2 concentration gradients in the soil, as these two external parameters predominantly govern CO_2 uptake. However, since K, but also Mg and Ca, are taken up by plants, their removal from the soil-water system is likely to decrease the instantaneous CO_2 sequestration rate because plant uptake of cations is counterbalanced by the release of protons (Britto and Kronzucker, 2008), and cation concentrations in the water phase leaving the system should be lower due to their temporal storage in plants. The quantity of these elements that remain in agricultural fields after crop/tree harvest will affect the final long-term field-based CO_2 removal rate. At the same time, given sufficient time, the leftover organic matter could re-release cations. These processes call for further investigations to provide a better picture of full inorganic CO_2 sequestration through EW. To assess the full EW potential, inorganic and organic CO_2 sequestration should be studied in parallel, focusing additionally on the effects of P release, an important micro-nutrient for plants that are commonly used in fertilizers, and which is abundant in the basanite (Table 1) but was not the focus of this study.

Riverine cation elemental ratios in watersheds (e.g., Ca/Na) can be used to distinguish between carbonate and silicate weathering (Gaillardet et al., 1999). Results here suggest that EW application with high amounts of nepheline might change Ca/Na ratios due to the non-stoichiometry of the alteration process, which potentially affects the interpretation of weathering sources, and also can alter the geochemical baselines of rivers (Hartmann et al., 2007). Under a large-scale EW deployment scenario, the influence of altered geochemical fluxes in natural systems on scientific interpretations has to be considered as a side effect not addressed so far.

The CO_2 effect and feedback constraints in earth system model parameterizations

The CO_2 feedback on weathering rates and CO_2 consumption in Earth system or planetary models is often represented by the factor $\alpha = (p_{CO_2}/preind.p_{CO_2})^n$ (Walker et al., 1981). In an abiotic world, as in our column experiments, this feedback would represent the direct effect of CO_2 dissolution and consumption in water, in addition to hydrological feedback, as the weathering flux is largely controlled by water throughflow, given a fixed lithological composition. In general, it is not possible to distinguish the proportions each of these effects contribute to the feedback. The exponent n is often modulated to fit an assumed feedback-strength range (Uchikawa and Zeebe, 2008; Lehmer et al., 2020). We can compare our results with the resulting feedback strength for $n = 0.1$ to $n = 0.5$ using a p_{CO_2} of 400 ppm as a baseline, instead of the pre-industrial value. This comparison would only consider the CO_2 effect and no further hydrological feedback due to elevated CO_2 in the atmosphere. Solving the above equation for n with $\alpha = 4.5$, representative of the results in this experiment (Figure 6C) leads to $n = 0.2$, a value that matches the assumed default conditions in the simulations of Uchikawa and

Zeebe (2008). This value might be representative of conditions on Mars or other planets with a high pCO_2 atmosphere. With $n = 0.3$ the feedback is comparable to results from the dunite column, where it must be assumed that observed weathering fluxes are diffusion-limited (see above). The case of $n = 0.5$ would result in an even higher CO_2-enhancement factor of 50. This would imply that in a basalt-dominated world, the additional hydrological effect would be stronger by a factor of 10. As the early, primitive surfaces of Earth or Mars were more likely to be comparable to a basaltic than to an olivine-dominated surface, this comparison invites a discussion about the combined effects of CO_2 and hydrology in a planetary system, and how they can be best represented. If the CO_2 feedback effect due to EW is modeled at the planetary scale, one should distinguish CO_2 effects on mineral weathering and on hydrology separately.

Results suggest that n values in the lower range of values considered are more realistic. As only two CO_2 conditions were tested, a simple scaling law would suggest that for humid tropical areas a doubling to tripling in weathering rates can be assumed for elevated (>70,000 ppm) CO_2 conditions compared to ambient CO_2 conditions (Table 5).

Enhancement of weathering by rhizosphere processes

As the column experiment was primarily abiotic, the influence of biological processes on weathering rates was not explicitly considered, although microbial components may have exerted a minor influence on the columns filled with soils, as these were not sterilized. Processes in the rhizosphere can speed up dissolution processes and therefore increase EW potentials (Krahl, 2020; Verbruggen et al., 2021). Beerling et al. (2020) deduced a biotic weathering enhancement factor normalized to net primary productivity in the range of 1–7 (from work of Akter and Akagi, 2005, 2010; Quirk et al., 2012, 2014). This factor incorporates the effects of rhizosphere biologically accelerated weathering. Given the overall scarcity of data, but the relevant influence of plants and the rhizosphere, these processes need to be considered to determine realistic constraints on the boundaries of EW for diverse environmental settings in the future.

TABLE 5 Weathering rate factor $\alpha = (p_{CO_2}/p_{CO_{2-baseline}})^n$, normalized to the baseline condition of 400 ppm CO_2 as applied in common Earth system models to simulate weathering rate changes with increased p_{CO_2}, depending on the choice of exponent n.

CO_2 (ppm)	$n = 0.1$	$n = 0.2$	$n = 0.3$	$n = 0.5$
400[a]	1.00	1.00	1.00	1.00
1,000	1.10	1.20	1.32	1.58
70,000[b]	1.68	2.81	4.71	13.23
1,000,000[c]	2.19	4.78	10.46	50.00

[a]Reference value, ambient-CO_2 concentration; [b]Elevated soil pCO_2, from Davidson and Trumbore (2017); [c]Saturated-CO_2 conditions (100%).

Precipitation of carbonates

The secondary precipitation of carbonates as the final long-term step in the weathering process can release half of the captured CO_2 counterbalanced by Ca and to some proportion of Mg. Thus, carbonate precipitation should be monitored to evaluate the overall carbon sequestration potential of an agricultural system. However, carbonate mineral saturation indices indicate that carbonate formation only occurred during the initial phases of our experiments, since long-term oversaturation was not observed. Consequently, the precipitation of carbonates may not be expected in agricultural soils under long-term treatment with rock material, given the humid, tropical conditions. Precipitation downstream of the application area might occur after water is re-equilibrating with the atmosphere (Figure 7). See further discussion on efficacy of enhancing carbonate weathering for carbon dioxide sequestration in Knapp and Tipper (2022).

Conclusion

Our counter-intuitive finding that the smallest grain sizes may not lead to the fastest CO_2 uptake (Figure 6) calls for a more detailed investigation of the influence of grain size distributions and packing density of soils in individual application cases. Larger target grain sizes will decrease the energy requirements for comminution. This will lower costs and the potential CO_2 penalty from fossil energy use.

The pronounced alkalinity production during the initial phases of the experiments suggests that a modified application scheme might be considered: rock flour replenishment at shorter intervals (e.g., annually) may be preferable over a one-time application of a larger amount of material to achieve higher CO_2 drawdown rates. This, however, needs to be tested with further experiments, as biological processes were not simulated in this study.

We have also shown that the individual mineral compositions making up applied rock material is important for the evaluation of CO_2 uptake speeds and side effects. A site-specific material selection process, going further than a simple search for local "basalt," can optimize dissolution rates (and thus CO_2 uptake potential), as well as plant nutrient potential. Looking beyond basaltic material, loess can sustain rather high dissolution rates over millennia (Börker et al., 2020), which also showed high dissolution rates in the experiments. As such, it may even be a well-suited material to produce alkalinity—and

remove CO_2–in the context of CDR as it is often regionally available, easily extractable, and fertile. Material-specific aging processes and the formation of secondary precipitates will be issues that also need to be understood in more detail.

Overall, future models and projections for EW-related CDR should consider the dissolution rates obtained from column experiments under 100% CO_2, as they will represent an upper boundary in an inorganic system. Further studies should assess the soil pCO_2 gradients, simulating conditions in soils of different climates and environments with up to more than 100,000 ppm. Biologic processes should further accelerate the observed rates, which demands tailored experiments, distinguishing biological and inorganic geochemical processes, to improve EW-CDR-potential assessments.

A further observation from the experiments, the promising utilization of electrical conductivity as a predictor for TA production, a proxy for the CO_2 sequestration effect, is discussed in a complementary publication (Amann and Hartmann, 2022).

Data availability statement

The original contributions presented in the study are included in the article/supplementary material, further inquiries can be directed to the corresponding author.

Author contributions

JH, TA, and AM designed the study. AM ran the first experiment comparing grain sizes and contributed to the discussion. TA wrote the manuscript with input from JH, RH, EP, and AM. EP contributed to the discussion. RH provided input throughout the manuscript and especially to section decrease of weathering rates with time. All authors approved the submitted version.

Funding

This work was funded by Germany's Excellence Strategy—EXC 2037 Climate, Climatic Change, and Society—project number 390683824, contribution to the Center for Earth System Research and Sustainability (CEN) of the Universität Hamburg.

Acknowledgments

We acknowledge the help of Tom Jäppinen, Peggy Bartsch, Rhiannon Breider, Mark Brosell, Marvin Keitzel, Eric Marques, and Walid Karimi for valuable contributions from the wet lab, and Sebastian Lindhorst for providing granulometric analyses (all from the Institute for Geology, Universität Hamburg). We thank Stephan Jung and Joachim Ludwig (from the Institute for Mineralogy and Petrography, Universität Hamburg) for contributing to the XRF and XRD analyses. Discussions were further stimulated by work with the Carbon Drawdown Initiative (Project Carbdown).

Conflict of interest

The authors declare that the research was conducted in the absence of any commercial or financial relationships that could be construed as a potential conflict of interest.

Publisher's note

Supplementary material

The Supplementary Material for this article can be found online at: https://www.frontiersin.org/articles/10.3389/fclim.2022.929268/full#supplementary-material

References

Akter, M., and Akagi, T. (2005). Effect of fine root contact on plant-induced weathering of basalt. *Soil Sci. Plant Nutr.* 51, 861–871. doi: 10.1111/j.1747-0765.2005.tb00121.x

Akter, M., and Akagi, T. (2010). Dependence of plant-induced weathering of basalt and andesite on nutrient conditions. *Geochem. J.* 44, 137–150. doi: 10.2343/geochemj.1.0052

Amann, T., and Hartmann, J. (2019). Ideas and perspectives: synergies from co-deployment of negative emission technologies. *Biogeosciences* 16, 2949–2960. doi: 10.5194/bg-16-2949-2019

Amann, T., and Hartmann, J. (2022). Carbon accounting for enhanced weathering. *Front. Clim.* 4, 849948. doi: 10.3389/fclim.2022.849948

Amann, T., Hartmann, J., Struyf, E., de Oliveira Garcia, W., Fischer, E. K., Janssens, I., et al. (2020). Enhanced weathering and related element fluxes – a cropland mesocosm approach. *Biogeosciences* 17, 103–119. doi: 10.5194/bg-17-103-2020

Awad, A., Koster van Groos, A. F., and Guggenheim, S. (2000). Forsteritic olivine: effect of crystallographic direction on dissolution kinetics. *Geochim. Cosmochim. Acta* 64, 1765–1772. doi: 10.1016/S0016-7037(99)00442-1

Ball, J. W., and Nordstrom, D. K. (1991). "User's manual for WATEQ4F, with revised thermodynamic data base and text cases for calculating speciation of major, trace, and redox elements in natural waters," in *Open-File Report. Version 2.0* (Menlo Park, CA). doi: 10.3133/ofr91183

Bandstra, J. Z., and Brantley, S. L. (2008). "Data fitting techniques with applications to mineral dissolution kinetics," in *Kinetics of Water-Rock Interaction,* eds S. L. Brantley, J. D. Kubicki, and A. F. White (New York, NY: Springer), 211–257. doi: 10.1007/978-0-387-73563-4_6

Beerling, D. J., Kantzas, E. P., Lomas, M. R., Wade, P., Eufrasio, R. M., Renforth, P., et al. (2020). Potential for large-scale CO2 removal via enhanced rock weathering with croplands. *Nature* 583, 242–248. doi: 10.1038/s41586-020-2448-9

Beerling, D. J., Leake, J. R., Long, S. P., Scholes, J. D., Ton, J., Nelson, P. N., et al. (2018). Farming with crops and rocks to address global climate, food and soil security. *Nat. Plants* 4, 138–147. doi: 10.1038/s41477-018-0108-y

Beyer, E. E. (2006). Transformation of archaean lithospheric mantle by refertilization: evidence from exposed peridotites in the western Gneiss Region, Norway. *J. Petrol.* 47, 1611–1636. doi: 10.1093/petrology/egl022

Börker, J. (2019). *Quantifications of Global Chemical Weathering Fluxes Applying New Lithological Maps and New Parameterizations*. Hamburg: Staats- und Universitätsbibliothek Hamburg.

Börker, J., Hartmann, J., Amann, T., Romero-Mujalli, G., Moosdorf, N., and Jenkins, C. (2020). Chemical weathering of loess and its contribution to global alkalinity fluxes to the coastal zone during the last glacial maximum, mid-holocene, and present. *Geochem. Geophys. Geosyst.* 21, e2020GC008922. doi: 10.1029/2020GC008922

Brantley, S. L. (2008). "Kinetics of mineral dissolution," in *Kinetics of Water-Rock Interaction,* eds S. L. Brantley, J. D. Kubicki, and A. F. White (New York, NY: Springer), 151–210. doi: 10.1007/978-0-387-73563-4_5

Britto, D. T., and Kronzucker, H. J. (2008). Cellular mechanisms of potassium transport in plants. *Physiol. Plant.* 133, 637–650. doi: 10.1111/j.1399-3054.2008.01067.x

Brook, G. A., Folkoff, M. E., and Box, E. O. (1983). A world model of soil carbon dioxide. *Earth Surf. Proc. Landf.* 8, 79–88. doi: 10.1002/esp.3290080108

Brunauer, S., Emmett, P. H., and Teller, E. (1938). Adsorption of gases in multimolecular layers. *J. Am. Chem. Soc.* 60, 309–319. doi: 10.1021/ja01269a023

Cockell, C. S., Bush, T., Bryce, C., Direito, S., Fox-Powell, M., Harrison, J. P., et al. (2016). Habitability: a review. *Astrobiology* 16, 89–117. doi: 10.1089/ast.2015.1295

Cross, W. I., Joseph, P.;, Pirsson, L. V., and Washington, H. S. (1902). A quantitative chemico-mineralogical classification and nomenclature of igneous rocks. *J. Geol.* 10, 555–690. doi: 10.1086/621030

Daval, D., Bernard, S., Rémusat, L., Wild, B., Guyot, F., Micha, J. S., et al. (2017). Dynamics of altered surface layer formation on dissolving silicates. *Geochim. Cosmochim. Acta* 209, 51–69. doi: 10.1016/j.gca.2017.04.010

Daval, D., Sissmann, O., Menguy, N., Saldi, G. D., Guyot, F., Martinez, I., et al. (2011). Influence of amorphous silica layer formation on the dissolution rate of olivine at 90 °C and elevated pCO2. *Chem. Geol.* 284, 193–209. doi: 10.1016/j.chemgeo.2011.02.021

Davidson, E. A., and Trumbore, S. E. (2017). Gas diffusivity and production of CO2in deep soils of the eastern Amazon. *Tellus B Chem. Phys. Meteorol.* 47, 550–565. doi: 10.3402/tellusb.v47i5.16071

de Oliveira Garcia, W., Amann, T., Hartmann, J., Karstens, K., Popp, A., Boysen, L. R., et al. (2020). Impacts of enhanced weathering on biomass production for negative emission technologies and soil hydrology. *Biogeosciences* 17, 2107–2133. doi: 10.5194/bg-17-2107-2020

Dessert, C., Dupré, B., Gaillardet, J., François, L. M., and Allègre, C. J. (2003). Basalt weathering laws and the impact of basalt weathering on the global carbon cycle. *Chem. Geol.* 202, 257–273. doi: 10.1016/j.chemgeo.2002.10.001

Dickson, A. G. (1981). An exact definition of total alkalinity and a procedure for the estimation of alkalinity and total inorganic carbon from titration data. *Deep Sea Res. Part A Oceanogr. Res. Pap.* 28, 609–623. doi: 10.1016/0198-0149(81)90121-7

Dietzen, C., Harrison, R., and Michelsen-Correa, S. (2018). Effectiveness of enhanced mineral weathering as a carbon sequestration tool and alternative to agricultural lime: an incubation experiment. *Int. J. Greenh. Gas Con.* 74, 251–258. doi: 10.1016/j.ijggc.2018.05.007

Ebelmen, J. J. (1845). *Sur les Produits de la Décomposition des Espèces Minérales de la Famille des Silicates*. Paris: Carilian-G.ury et Vor Dalmont, Libraires des Corps Royaux des Ponts et Chausees et dus Mines.

Eggleston, C. M., Hochella, M. F., and George, P. A. (1989). Sample preparation and aging effects on the dissolution rate and surface composition of diopside. *Geochim. Cosmochim. Acta* 53, 797–804. doi: 10.1016/0016-7037(89)90026-4

Foley, B. J., and Smye, A. J. (2018). Carbon cycling and habitability of earth-sized stagnant lid planets. *Astrobiology* 18, 873–896. doi: 10.1089/ast.2017.1695

Franke, W. A. (2009). The durability of rocks–Developing a test of rock resistance to chemical weathering. *Am. J. Sci.* 309, 711–730. doi: 10.2475/08.2009.04

Gaillardet, J., Dupré, B., Louvat, P., and Allègre, C. J. (1999). Global silicate weathering and CO2 consumption rates deduced from the chemistry of large rivers. *Chem. Geol.* 159, 3–30. doi: 10.1016/S0009-2541(99)00031-5

Giambelluca, T. W., Chen, Q., Frazier, A. G., Price, J. P., Chen, Y.-L., Chu, P.-S., et al. (2013). Online rainfall atlas of Hawai'i. *Bull. Am. Meteorol. Soc.* 94, 313–316. doi: 10.1175/BAMS-D-11-00228.1

Goll, D. S., Ciais, P., Amann, T., Buermann, W., Chang, J., Eker, S., et al. (2021). Potential CO2 removal from enhanced weathering by ecosystem responses to powdered rock. *Nat. Geosci.* 14, 545–549. doi: 10.1038/s41561-021-00798-x

Hansen, H. P., and Koroleff, F. (1999). "Determination of nutrents," in *Methods of Seawater Analysis*. doi: 10.1002/9783527613984.ch10

Haque, F., Santos, R. M., and Chiang, Y. W. (2020). CO2 sequestration by wollastonite-amended agricultural soils – an Ontario field study. *Int. J. Greenh. Gas Con.* 97, 103017. doi: 10.1016/j.ijggc.2020.103017

Hartmann, J., Jansen, N., Dürr, H. H., Kempe, S., and Köhler, P. (2009). Global CO_2-consumption by chemical weathering: what is the contribution of highly active weathering regions? *Glob. Planet. Change* 69, 185–194. doi: 10.1016/j.gloplacha.2009.07.007

Hartmann, J., Jansen, N., Kempe, S., and Dürr, H. (2007). Geochemistry of the river rhine and the upper danube: recent trends and lithological influence on baselines. *J. Environ. Sci. Sustain. Soc.* 1, 39–46. doi: 10.3107/jesss.1.39

Hartmann, J., and Kempe, S. (2008). What is the maximum potential for CO(2) sequestration by "stimulated" weathering on the global scale? *Naturwissenschaften* 95, 1159–1164. doi: 10.1007/s00114-008-0434-4

Hartmann, J., West, A. J., Renforth, P., Köhler, P., De La Rocha, C. L., Wolf-Gladrow, D. A., et al. (2013). Enhanced chemical weathering as a geoengineering strategy to reduce atmospheric carbon dioxide, supply nutrients, and mitigate ocean acidification. *Rev. Geophys.* 51, 113–149. doi: 10.1002/rog.20004

Hashimoto, S., Tanaka, N., Suzuki, M., Inoue, A., Takizawa, H., Kosaka, I., et al. (2017). Soil respiration and soil CO2 concentration in a tropical forest, Thailand. *J. For. Res.* 9, 75–79. doi: 10.1007/s10310-003-0046-y

Hellmann, R. (1994). The albite-water system: part I. The kinetics of dissolution as a function of pH at 100, 200 and 300°C. *Geochim. Cosmochim. Acta* 58, 595–611. doi: 10.1016/0016-7037(94)90491-X

Hellmann, R., Penisson, J. M., Hervig, R. L., Thomassin, J. H., and Abrioux, M. F. (2003). An EFTEM/HRTEM high-resolution study of the near surface of labradorite feldspar altered at acid pH: evidence for interfacial dissolution-reprecipitation. *Phys. Chem. Min.* 30, 192–197. doi: 10.1007/s00269-003-0308-4

Hellmann, R., Wirth, R., Daval, D., Barnes, J.-P., Penisson, J.-M., Tisserand, D., et al. (2012). Unifying natural and laboratory chemical weathering with interfacial dissolution–reprecipitation: a study based on the nanometer-scale chemistry of fluid–silicate interfaces. *Chem. Geol.* 294–295, 203–216. doi: 10.1016/j.chemgeo.2011.12.002

Hellmann, R., Zhai, Y., Robin, E., Findling, N., Mayanna, S., Wirth, R., et al. (2021). The hydrothermal alkaline alteration of potassium feldspar: a nanometer-scale investigation of the orthoclase interface. *Chem. Geol.* 569. doi: 10.1016/j.chemgeo.2021.120133

Holdren, G. R., and Berner, R. A. (1979). Mechanism of feldspar weathering—I. Experimental studies. *Geochim. Cosmochim. Acta* 43, 1161–1171. doi: 10.1016/0016-7037(79)90109-1

Hövelmann, J., Austrheim, H., and Jamtveit, B. (2012). Microstructure and porosity evolution during experimental carbonation of a natural peridotite. *Chem. Geol.* 334, 254–265. doi: 10.1016/j.chemgeo.2012.10.025

Julius, H. (1894). *Bread from Stones - A New and Rational System of Land Fertilization and Physical Regeneration (Translated From the German)*, ed A. J. Tafel. Philadelphia, PA.

Kelland, M. E., Wade, P. W., Lewis, A. L., Taylor, L. L., Sarkar, B., Andrews, M. G., et al. (2020). Increased yield and CO2 sequestration potential with the C4 cereal Sorghum bicolor cultivated in basaltic rock dust-amended agricultural soil. *Glob. Chang. Biol.* 26, 3658–3676. doi: 10.1111/gcb.15089

Klasen, N., Fischer, P., Lehmkuhl, F., and Hilgers, A. (2015). Luminescence dating of loess deposits from the Remagen-Schwalbenberg site, Western Germany. *Geochronometria* 42. doi: 10.1515/geochr-2015-0008

Knapp, W., and Tipper, E. (2022). The efficacy of enhancing carbonate weathering for carbon dioxide sequestration. *Front. Clim.* doi: 10.17863/CAM.85785

Krahl, L. L. (2020). *Mineral Formation and Element Release From Aluminosilicate Rocks Promoted by Maize Rhizosphere (Ph.D)*. Available online at: https://repositorio.unb.br/bitstream/10482/38678/1/2020_LuiseLotticiKrahl.pdf

Lasaga, A. C., Soler, J. M., Ganor, J., Burch, T. E., and Nagy, K. L. (1994). Chemical weathering rate laws and global geochemical cycles. *Geochim. Cosmochim. Acta* 58, 2361–2386. doi: 10.1016/0016-7037(94)90016-7

Lazaro, A., Brouwers, H. J. H., Quercia, G., and Geus, J. W. (2012). The properties of amorphous nano-silica synthesized by the dissolution of olivine. *Chem. Eng. J.* 211–212, 112–121. doi: 10.1016/j.cej.2012.09.042

Le Bas, M. J., Maitre, R. W. L., Streckeisen, A., and Zanettin, B. (1986). A chemical classification of volcanic rocks based on the total alkali-silica diagram. *J. Petrol.* 27, 745–750. doi: 10.1093/petrology/27.3.745

Lechler, P. J., and Desilets, M. O. (1987). A review of the use of loss on ignition as a measurement of total volatiles in whole-rock analysis. *Chem. Geol.* 63, 341–344. doi: 10.1016/0009-2541(87)90171-9

Lehmer, O. R., Catling, D. C., and Krissansen-Totton, J. (2020). Carbonate-silicate cycle predictions of earth-like planetary climates and testing the habitable zone concept. *Nat. Commun.* 11, 6153. doi: 10.1038/s41467-020-19896-2

Leonardos, O. H., Fyfe, W. S., and Kronberg, B. I. (1987). The use of ground rocks in laterite systems: an improvement to the use of conventional soluble fertilizers? *Chem. Geol.* 60, 361–370. doi: 10.1016/0009-2541(87)90143-4

Maher, K., Johnson, N. C., Jackson, A., Lammers, L. N., Torchinsky, A. B., Weaver, K. L., et al. (2016). A spatially resolved surface kinetic model for forsterite dissolution. *Geochim. Cosmochim. Acta* 174, 313–334. doi: 10.1016/j.gca.2015.11.019

Martinez, R. E., Weber, S., and Bucher, K. (2014). Quantifying the kinetics of olivine dissolution in partially closed and closed batch reactor systems. *Chem. Geol.* 367, 1–12. doi: 10.1016/j.chemgeo.2013.12.017

Mertes, H., and Schmincke, H. U. (1985). Mafic potassic lavas of the quaternary west eifel volcanic field.1. Major and trace-elements. *Contribut. Mineral. Petrol.* 89, 330–345. doi: 10.1007/BF00381555

Moravec, B. G., Keifer, V., Root, R. A., White, A. M., Wang, Y., Olshansky, Y., et al. (2021). Experimental weathering of a volcaniclastic critical zone profile: Key role of colloidal constituents in aqueous geochemical response. *Chem. Geol.* 559, 119886. doi: 10.1016/j.chemgeo.2020.119886

Navarre-Sitchler, A., and Brantley, S. (2007). Basalt weathering across scales. *Earth Planet. Sci. Lett.* 261, 321–334. doi: 10.1016/j.epsl.2007.07.010

Palandri, J. L., and Kharaka, Y. K. (2004). *A Compilation of Rate Parameters of Water-Mineral Interaction Kinetics for Application to Geochemical Modeling*. Menlo Park, CA: U.S. Geological Survey. doi: 10.3133/ofr20041068

Parkhurst, D. L., and Appelo, C. A. J. (2013). "Description of input and examples for PHREEQC version 3—a computer program for speciation, batch-reaction, one-dimensional transport, and inverse geochemical calculations," in *U.S. Geological Survey Techniques and Methods* (Denver, CO). doi: 10.3133/tm6A43

Pedrosa, E. T., Boeck, L., Putnis, C. V., and Putnis, A. (2017). The replacement of a carbonate rock by fluorite: kinetics and microstructure. *Am. Min.* 102, 126–134. doi: 10.2138/am-2017-5725

Pedrosa, E. T., Putnis, C. V., Renard, F., Burgos-Cara, A., Laurich, B., and Putnis, A. (2016). Porosity generated during the fluid-mediated replacement of calcite by fluorite. *Cryst. Eng. Comm.* 18, 6867–6874. doi: 10.1039/C6CE01150K

Pokrovsky, O. S., and Schott, J. (2000a). Forsterite surface composition in aqueous solutions: a combined potentiometric, electrokinetic, and spectroscopic approach. *Geochim. Cosmochim. Acta* 64, 3299–3312. doi: 10.1016/S0016-7037(00)00435-X

Pokrovsky, O. S., and Schott, J. (2000b). Kinetics and mechanism of forsterite dissolution at 25°C and pH from 1 to 12. *Geochim. Cosmochim. Acta* 64, 3313–3325. doi: 10.1016/S0016-7037(00)00434-8

Putnis, A., and Putnis, C. V. (2007). The mechanism of reequilibration of solids in the presence of a fluid phase. *J. Solid State Chem.* 180, 1783–1786. doi: 10.1016/j.jssc.2007.03.023

Quirk, J., Andrews, M. Y., Leake, J. R., Banwart, S. A., and Beerling, D. J. (2014). Ectomycorrhizal fungi and past high CO2 atmospheres enhance mineral weathering through increased below-ground carbon-energy fluxes. *Biol. Lett.* 10, 20140375. doi: 10.1098/rsbl.2014.0375

Quirk, J., Beerling, D. J., Banwart, S. A., Kakonyi, G., Romero-Gonzalez, M. E., and Leake, J. R. (2012). Evolution of trees and mycorrhizal fungi intensifies silicate mineral weathering. *Biol. Lett.* 8, 1006–1011. doi: 10.1098/rsbl.2012.0503

Renforth, P., Pogge von Strandmann, P. A. E., and Henderson, G. M. (2015). The dissolution of olivine added to soil: implications for enhanced weathering. *Appl. Geochem.* 61, 109–118. doi: 10.1016/j.apgeochem.2015.05.016

Romero-Mujalli, G., Hartmann, J., Börker, J., Gaillardet, J., and Calmels, D. (2018). Ecosystem controlled soil-rock pCO2 and carbonate weathering – constraints by temperature and soil water content. *Chem. Geol.* 527, 118634. doi: 10.1016/j.chemgeo.2018.01.030

Royer, D. L., Berner, R. A., and Park, J. (2007). Climate sensitivity constrained by CO2 concentrations over the past 420 million years. *Nature* 446, 530–532. doi: 10.1038/nature05699

Schaller, J., Cramer, A., Carminati, A., and Zarebanadkouki, M. (2020). Biogenic amorphous silica as main driver for plant available water in soils. *Sci. Rep.* 10, 2424. doi: 10.1038/s41598-020-59437-x

Schirmer, W. (2011). Rhine loess at Schwalbenberg II — MIS 4 and 3. *E&G Q. Sci. J.* 61, 32–47. doi: 10.3285/eg.61.1.03

Schofield, R. E., Hausrath, E. M., and Gainey, S. R. (2015). "Zeolite weathering in laboratory and natural settings, and implications for mars," in *46th Lunar and Planetary Science Conference* (The Woodlands, TX).

Schopka, H. H., Derry, L. A., and Arcilla, C. A. (2011). Chemical weathering, river geochemistry and atmospheric carbon fluxes from volcanic and ultramafic regions on Luzon Island, the Philippines. *Geochim. Cosmochim. Acta* 75, 978–1002. doi: 10.1016/j.gca.2010.11.014

Schuiling, R. D., and Krijgsman, P. (2006). Enhanced weathering: an effective and cheap tool to sequester CO2. *Clim. Change* 74, 349–354. doi: 10.1007/s10584-005-3485-y

Seifritz, W. (1990). CO2 disposal by means of silicates. *Nature* 345, 486–486. doi: 10.1038/345486b0

Soil Survey Staff (1999). "Soil taxonomy: a basic system of soil classification for making and interpreting soil surveys," in *Natural Resources Conservation Service. U.S. Department of Agriculture Handbook 436, 2nd edn* (Soil Survey Staff). Available online at: https://www.nrcs.usda.gov/wps/portal/nrcs/main/soils/survey/class/taxonomy/

Strasberg, D., Rouget, M., Richardson, D. M., Baret, S., Dupont, J., and Cowling, R. M. (2005). An Assessment of habitat diversity and transformation on la réunion island (Mascarene Islands, Indian Ocean) as a basis for identifying broad-scale conservation priorities. *Biodivers. Conserv.* 14, 3015–3032. doi: 10.1007/s10531-004-0258-2

Streckeisen, A. (1980). Classification and nomenclature of volcanic rocks, lamprophyres, carbonatites and melilitic rocks IUGS Subcommission on the systematics of igneous rocks. *Geol. Rundschau* 69, 194–207. doi: 10.1007/BF01869032

Strefler, J., Amann, T., Bauer, N., Kriegler, E., and Hartmann, J. (2018a). Potential and costs of carbon dioxide removal by enhanced weathering of rocks. *Environ. Res. Lett.* 13, 034010. doi: 10.1088/1748-9326/aaa9c4

Strefler, J., Bauer, N., Kriegler, E., Popp, A., Giannousakis, A., and Edenhofer, O. (2018b). Between scylla and charybdis: delayed mitigation narrows the passage between large-scale CDR and high costs. *Environ. Res. Lett.* 13, 044015. doi: 10.1088/1748-9326/aab2ba

Taylor, L. L., Quirk, J., Thorley, R. M. S., Kharecha, P. A., Hansen, J., Ridgwell, A., et al. (2015). Enhanced weathering strategies for stabilizing climate and averting ocean acidification. *Nat. Clim. Chang.* 6, 402–406. doi: 10.1038/nclimate2882

Teitler, Y., Le Hir, G., Fluteau, F., Philippot, P., and Donnadieu, Y. (2014). Investigating the Paleoproterozoic glaciations with 3-D climate modeling. *Earth Planet. Sci. Lett.* 395, 71–80. doi: 10.1016/j.epsl.2014.03.044

ten Berge, H. F. M., van der Meer, H. G., Steenhuizen, J. W., Goedhart, P. W., Knops, P., and Verhagen, J. (2012). Olivine weathering in soil, and its effects on growth and nutrient uptake in ryegrass *Lolium perenne* L.: a pot experiment. *PLoS ONE* 7, e42098. doi: 10.1371/journal.pone.0042098

Uchikawa, J., and Zeebe, R. E. (2008). Influence of terrestrial weathering on ocean acidification and the next glacial inception. *Geophys. Res. Lett.* 35, L23608. doi: 10.1029/2008GL035963

United Nations (2015). *Chapter XXVII Environment, 7.d Paris Agreement*. New York, NY: United Nations.

van Straaten, P. (2002). *Rocks for Crops: Agrominerals of Sub-Saharan Africa*. Nairobi: ICRAF. doi: 10.1046/j.1465-5101.2001.132.x

Verbruggen, E., Struyf, E., and Vicca, S. (2021). Can arbuscular mycorrhizal fungi speed up carbon sequestration by enhanced weathering? *Plants People Planet* 3, 445–453. doi: 10.1002/ppp3.10179

Vienne, A., Ibanez, S. P., Portillo-Estrada, M., Hartmann, J., Ijiehon, S., Wade, P., et al. (2022). Enhanced weathering using basalt rock powder: carbon sequestration, co-benefits and risks in a mesocosm study with Solanum tuberosum. *Front. Clim.* 4, 869456. doi: 10.3389/fclim.2022.869456

Vitens (2021). *PhreeqPython*. Vitens. Available online at: https://github.com/Vitens/phreeqpython).

Walker, J. C. G., Hays, P. B., and Kasting, J. F. (1981). A negative feedback mechanism for the long-term stabilization of earth's surface temperature. *J. Geophys. Res.* 86, 9776–9782. doi: 10.1029/JC086iC10p09776

Wogelius, R. A., and Walther, J. V. (1992). Olivine dissolution kinetics at near-surface conditions. *Chem. Geol.* 97, 101–112. doi: 10.1016/0009-2541(92)90138-U

Zandanel, A., Hellmann, R., Truche, L., Roddatis, V., Mermoux, M., Choblet, G., et al. (2022). Geologically rapid aqueous mineral alteration at subfreezing temperatures in icy worlds. *Nat. Astron.* 6, 554–559. doi: 10.1038/s41550-022-01613-2

frontiers | Frontiers in Climate

TYPE Original Research
PUBLISHED 11 August 2022
DOI 10.3389/fclim.2022.928215

OPEN ACCESS

EDITED BY
Jens Hartmann,
University of Hamburg, Germany

REVIEWED BY
Rafael Mattos Dos Santos,
University of Guelph, Canada
Klaus Wallmann,
Helmholtz Association of German Research Centres (HZ), Germany

*CORRESPONDENCE
William J. Knapp
wjk27@cam.ac.uk

SPECIALTY SECTION
This article was submitted to Negative Emission Technologies, a section of the journal Frontiers in Climate

RECEIVED 25 September 2022
ACCEPTED 23 June 2022
PUBLISHED 11 August 2022

CITATION
Knapp WJ and Tipper ET (2022) The efficacy of enhancing carbonate weathering for carbon dioxide sequestration. *Front. Clim.* 4:928215. doi: 10.3389/fclim.2022.928215

The efficacy of enhancing carbonate weathering for carbon dioxide sequestration

William J. Knapp* and Edward T. Tipper

Department of Earth Sciences, University of Cambridge, Cambridge, United Kingdom

Enhanced weathering is a geoengineering strategy aiming to increase continental weathering rates, thereby increasing the delivery of atmospheric carbon (as HCO_3^-) to the oceans. Most enhanced weathering studies focus on the capacity of silicate rocks (e.g., basalt) and minerals (e.g., olivine, Mg_2SiO_4, or wollastonite $CaSiO_3$) to remove atmospheric CO_2. However, carbonate minerals (e.g., calcite, $CaCO_3$) could provide an additional, rapid way to increase HCO_3^- export to the oceans. Recent studies suggest that 0.84 Gt C yr^{-1} could be removed from the atmosphere through the enhanced dissolution of calcite in soils, provided carbonic acid is the main dissolution agent. What is not clear is whether atmospheric CO_2 dissolved in soils can be transported by rivers, which typically have lower [pCO_2], to the oceans. This difference in calcite solubility between soils (where weathering occurs) and rivers (where HCO_3^- is transported) may lead to large amounts of secondary carbonate formation during transport, releasing the CO_2 consumed through dissolution. Here, we present a modeling study comparing the estimated soil dissolution capacity (SDC) in 149 of Earth's largest river basins, to the potential transport capacity of carbon (PTCC) in corresponding rivers. We find the SDC can only be exported to the oceans, without secondary carbonate precipitation, if rivers are in disequilibrium with respect to calcite (i.e., SIc = 1). In this instance, 0.92 Gt C yr^{-1} may be sequestered above background weathering rates, which is ~20% of annual increases in atmospheric carbon. If rivers are at equilibrium with calcite (i.e., SIc = 0), approximately two-thirds of the carbon dissolved in soil waters are lost due to calcite precipitation in rivers, and just 0.26 Gt of additional atmospheric C yr^{-1} can be transported to the oceans. Overall, the efficacy of enhanced carbonate weathering is a function of the capacity rivers have for transporting the products from carbonate weathering to the oceans, rather than the dissolution capacity of soils. These findings have implications for the efficiency of enhancing silicate weathering for ocean alkalinity enhancement, as secondary carbonate precipitation during transport is not always considered.

KEYWORDS

carbonate weathering, soil pCO_2, carbon sequestration, rivers, enhanced weathering in soils, calcite dissolution capacity

1. Introduction

The riverine flux of dissolved inorganic carbon (DIC, mostly present as the bicarbonate HCO_3^- ion in natural waters), derived from continental weathering, forms a vital link between Earth's atmosphere and oceans, acting to regulate atmospheric [CO_2] on million year timescales (Berner and Berner, 2012). A novel approach to combatting the current anthropogenically forced increase in atmospheric CO_2, and concomitant global warming, is to artificially increase the flux of solutes from chemical weathering processes, in particular, HCO_3^- (Seifritz, 1990; Lackner et al., 1995; Schuiling and Krijgsman, 2006; Köhler et al., 2010; Kelemen et al., 2011; Hartmann et al., 2013). This process of increasing HCO_3^- export is known as enhanced weathering (Schuiling and Krijgsman, 2006). The majority of studies concerning enhanced weathering have evaluated the potential of mafic silicate rocks (e.g., basalt) and minerals (e.g., forsterite, Mg_2SiO_4 and wollastonite, $CaSiO_3$) as reactants (Schuiling and Tickell, 2010; Moosdorf et al., 2014; Renforth et al., 2015; Taylor et al., 2016; Griffioen, 2017; Montserrat et al., 2017; Rigopoulos et al., 2018; Andrews and Taylor, 2019; Haque et al., 2019). The potential of calcium carbonate ($CaCO_3$) and calcium hydroxide (CaOH) dissolution to consume CO_2 is poorly constrained (Oh and Raymond, 2006; Zeng et al., 2022b). Carbonate rocks and minerals have faster dissolution kinetics over a range of temperature and pH values in comparison to silicates. For example, experimental studies show calcite dissolution can be >4 orders of magnitude faster than forsterite dissolution at pH 6, c.f. Brantley et al. (2008), Chou et al. (1989), and Plummer et al. (1979). Field observations of silicate mineral dissolution suggest this difference may be even larger (Renforth et al., 2015; White, 2018). Therefore, enhancing carbonate dissolution may be an efficient way to increase the rate of the terrestrial weathering response to increased atmospheric CO_2 increase (Rau et al., 2007). Carbonate rocks are also ubiquitous and are often extracted to create aggregates and for other industrial purposes (Hudson et al., 1997; Rau et al., 2007).

Carbonate dissolution with carbonic acid (H_2CO_3) is often overlooked as a potential method for enhanced weathering since the weathering of carbonates is considered to be a carbon neutral process on geological timescales (Berner and Berner, 2012). However, on the shorter timescales of mineral dissolution reactions and transport to the oceans, carbonate weathering reactions (Equations 1 and 2) dissolve one mole of atmospheric CO_2 into solution (HCO_3^-) per mole of Ca^{2+} released from a carbonate mineral to aqueous cation. Carbonate rocks are estimated to account for over half of the atmospheric CO_2 consumed by rock weathering each year, making carbonate weathering integral to the current understanding of global carbon cycling (Gaillardet et al., 1999).

$$CO_{2\,atmospheric} + H_2O_{(l)} \rightarrow H_2CO_{3(aq)} \quad (1)$$

$$CaCO_{3(s)} + H_2CO_{3(aq)} \rightarrow Ca^{2+}{}_{(aq)} + 2\,HCO_3^-{}_{(aq)} \quad (2)$$

The influx of anthropogenic CO_2 into the global oceans is initially buffered by the dissolution of pre-existing carbonate sediment on the ocean floor (i.e., calcium carbonate neutralization Archer, 1996; Archer et al., 1997), resulting in a shoaling of the carbonate compensation depth (CCD). This initial shoaling is subsequently balanced by a terrestrial input of HCO_3^- as weathering rates increase as a consequence of increased atmospheric CO_2 (Archer, 1996). The timescales on which these neutralization processes occur are on the order of 1,000–10,000 years (Ridgwell and Hargreaves, 2007). Enhanced weathering increases the rate at which HCO_3^- is delivered to the oceans, restoring the equilibrium between seafloor carbonate dissolution and carbonate sedimentation more rapidly than natural weathering rates could achieve. Ultimately, this slows the rate of CCD shoaling, as carbonate weathering products are transferred to the deep ocean to neutralize the influx of atmospheric CO_2.

Proposed methods of enhancing carbonate weathering range from point source industrial scale reaction of flue gasses with a limestone seawater mixture (e.g., Rau and Caldeira, 1999; Caldeira and Rau, 2000; Rau et al., 2007), to a large-scale reaction of lime powder on agricultural land with atmospheric CO_2 (e.g., Zeng et al., 2022b). In the present study, we focus on liming, a commonplace agricultural method, which involves the spreading of carbonate powder on farm land. Canonically, the carbon in the H_2CO_3 is derived from the dissolution of atmospheric CO_2 into water (Equation 1), but this CO_2 can also be derived from the respiration of modern organic matter (e.g., soil carbon <1,000 years old) in the critical zone (Trumbore et al., 1996; Shi et al., 2020). Therefore, the release of cations (chiefly Ca^{2+}) and HCO_3^- involved in Equation 2 can help ameliorate the effects of soil acidification, replenish nutrients in the soil profile and increase the ionic strength of soil solutions. Liming has been practiced since antiquity (Connor et al., 2011), and is thought to have played a critical role in the agricultural revolution in Europe, allowing successful intensive crop rotations (Narbarte-Hernandez et al., 2021). Liming is commonplace and considered safe. This is advantageous in comparison to other methods of enhanced weathering, e.g., olivine weathering, which has been shown (in some cases) to release potentially toxic metals in dissolution experiments (Renforth et al., 2015).

Previous studies have demonstrated that liming has the potential to remove appreciable amounts of CO_2 from the atmosphere *via* dissolution. For example, Zeng et al. (2022b) estimate that liming at a global scale could remove ~ 0.84 Gt C yr^{-1} (Gt = gigaton = 1×10^9 tons), or ~15% of annual increases in atmospheric CO_2 (Friedlingstein et al., 2020). For enhanced carbonate weathering *via* liming to be an effective

CO_2 consumption mechanism over timescales relevant to the anthropogenic increase in CO_2, it is imperative that i) the additional HCO_3^-, derived from enhancing carbonate weathering, is not precipitated as secondary carbonate on the continents, and ii) the source of acidity is carbonic acid, with carbon recently derived from the atmosphere. However, many rivers and streams are saturated with respect to calcite, and as these waters outgas and equilibrate with atmospheric CO_2 the precipitation of travertines in rivers and calcretes in soils is likely (Dandurand et al., 1982; Drever, 1988; Dreybrodt et al., 1992; Yan et al., 2020; Erlanger et al., 2021). Indeed, the precipitation of carbonates from supersaturated solutions is a well documented phenomenon in a range of climatic settings (Ford and Pedley, 1996; Hudson et al., 1997; Galy et al., 1999; Tipper et al., 2006; Lacelle, 2007; Thomazo et al., 2017; Erlanger et al., 2021). As carbonate precipitation is the reverse of Equation 2, rapid carbonate precipitation in rivers and soils means there is no net consumption of CO_2. To date, there has been no systematic study pertaining to whether the carbon (as bicarbonate, HCO_3^-) derived from enhancing carbonate weathering can be successfully transported from the continents to the oceans, without precipitating as secondary carbonate during transit. Therefore, a key issue to quantify is the extent to which the supersaturation of natural waters, induced by liming, limits the transport potential for carbon transfer between the continents and oceans, limiting carbon consumption *via* enhanced carbonate weathering.

In the present contribution, we define the concept of a potential transport capacity of carbon (PTCC). The PTCC is the difference between the measured HCO_3^- concentration in a river basin ($HCO_{3\,measured}^-$), and the theoretical equilibrium HCO_3^- concentration before calcite will precipitate ($HCO_{3\,equib}^-$). The equilibrium calcite solubility (and also $HCO_{3\,equib}^-$) can be determined on the regional or catchment scale as a function of temperature and river $pCO_{2(aq)}$. This solubility represents a chemical equilibrium between a dissolving carbonate mineral (in this case calcite) and river with measured chemistry, constraining the maximum possible HCO_3^- concentration river water can have prior to calcite precipitation. As all natural waters already have a HCO_3^- concentration resulting from rock and mineral dissolution, the viability of CO_2 consumption by enhanced carbonate weathering depends on the difference between the maximum [HCO_3^-] (calculated from maximum calcite solubility), and the measured [HCO_3^-] within a given river basin. This comparison serves as a PTCC with respect to HCO_3^- (or DIC). Our simple calculations highlight that river basins already at or above calcite saturation have very little (or no) capacity to transport additional HCO_3^-, which is charge balanced by Ca^{2+}, to the oceans and would be a poor choice for liming. River basins with a low measured [HCO_3^-], and are undersaturated with respect to $CaCO_3$, have higher PTCC values and may be appropriate for carbonate weathering by liming. Since many rivers are supersaturated with respect to $CaCO_3$ we evaluate two global simulations of riverine $CaCO_3$ transport capacities, the first at saturation index for calcite (SIc, see methods for definition) = 0 and the second at SIc = 1. These two modeling scenarios provide a baseline PTCC and a maximum PTCC. As a point of reference, the PTCC estimates are compared to a soil dissolution capacity (SDC). This is defined as the total amount of calcite a soil may dissolve, while maintaining a SIc = 0 and a calculated pCO_2. Soil pCO_2 is often greater than riverine pCO_2 (Romero-Mujalli et al., 2019b), and this discrepancy has been observed to result in secondary carbonate precipitation in rivers and other terrestrial environments (Erlanger et al., 2021). Therefore, the SDC serves as an upper bound for estimating CO_2 consumption, since degassing and mixing processes will likely lead to soil waters becoming oversaturated and precipitating secondary carbonates.

This approach contributes to the growing body of evidence in favor of enhancing carbonate weathering through liming (Oh and Raymond, 2006; Hamilton et al., 2007; Zeng et al., 2022b), and suggests tenable carbon sequestration potentials.

2. Materials and methods

The modeling approach assumes that it is possible to elevate the concentrations of Ca^{2+} and HCO_3^- in solution through enhanced calcite dissolution until saturation (SIc = 0), or supersaturation (SIc = 1), is reached.

SIc is defined as:

$$SIc = \log_{10}\left(\frac{\alpha Ca^{2+}\alpha CO_3^{2-}}{K_{sp(calcite)}}\right) \quad (3)$$

Where αCa^{2+} and αCO_3^{2-} are the activities of Ca^{2+} and CO_3^{2-} in solution respectively, and $K_{sp(calcite)}$ is the equilibrium constant of calcite for a given temperature. Where:

$$K_{sp(calcite)} = \alpha Ca^{2+}\alpha CO_3^{2-} \quad (4)$$

αCa^{2+} and αCO_3^{2-} are the activities at saturation.

2.1. Calculation of $HCO_{3\,equib}^-$ in rivers and soils

To calculate $HCO_{3\,equib}^-$ (i.e., the [HCO_3^-] at a given SIc), dissolution, and transport of calcite were assumed to take place under open system conditions, as such it was assumed rivers and soil waters are able to exchange gases with the atmosphere, a constant supply of CO_2 from organic matter is available, and rapid dissolution kinetics of calcite. Assuming open system

conditions, equilibrium [HCO_3^-] in a non-ideal solution can be modeled after after (Drever, 1988; Calmels et al., 2014):

$$[HCO_{3\ equib}^-] = \left(\frac{2K_{Ca}K_1K_HpCO_2}{K_2\gamma_{Ca^{2+}}\gamma_{HCO_3^-}^2}\right)^{\frac{1}{3}} \quad (5)$$

Where K_1 and K_2 are the first and second dissociation constants of carbonic acid, K_{Ca} is the equilibrium constant for calcite dissolution, K_H is Henry's law constant for CO_2 in water, $\gamma_{Ca^{2+}}$ and $\gamma_{HCO_3^-}$ are the activity coefficients for calcium and bicarbonate in solution, respectively, and pCO_2 is the partial pressure of CO_2 in either river or soil waters. A full derivation of Equation (5) is provided in the Supplementary material. The amount of calcite required to reach saturation can then be calculated based on the stoichiometry of Equation 2.

Enhanced rates of organic carbon respiration in soil waters mean pCO_2 is generally elevated in soils in comparison to rivers (Romero-Mujalli et al., 2019a; Erlanger et al., 2021). Consequently, according to Equation 5, the $HCO_{3\ equib}^-$ at a given temperature and ionic strength in soil waters is typically greater than that of rivers (Erlanger et al., 2021). This is an important distinction. While dissolution rates and [HCO_3^-] can be elevated in the soil environment, it is not possible to transport these weathering products under equilibrium conditions in rivers to the oceans, where carbonate dissolution products can contribute to long-term carbon storage. This phenomenon has been observed in the poly-lithic Northern-Apenines, where the discrepancy in [HCO_3^-] between the soil and river environment is caused by a quantitative removal of Ca^{2+} and HCO_3^- from river waters, *via* authigenic carbonate mineral formation (Erlanger et al., 2021). Therefore, it is critical that the discrepancy between the SDC (where most weathering occurs), and the capacity of rivers to transport this carbon (PTCC) is addressed on a global scale.

To compare the open system transport capacity of rivers with the dissolution capacity of high pCO_2 soils, soil pCO_2 was estimated at a global scale at a grid resolution of 0.5° (Romero-Mujalli et al., 2019b):

$$\log_{10}(pCO_2) = \frac{e^{(b_1+\theta)} + \left(\frac{b_2}{\theta}\right)}{\left(b_3 + e_{4T}^b\right)} + \log_{10}(pCO_{2atm}) \quad (6)$$

Where θ is the mean annual volumetric water content of the soil (v/v), T is surface temperature in degrees Celsius, $\log_{10}(pCO_{2atm})$ is logarithm of CO_2 partial pressure in the atmosphere (a value of −3.4 is used), b_1, b_2, b_3, and b_4 are fitted constants (Romero-Mujalli et al., 2019b). Soil moisture data is from the European Space Agency Climate Change Initiative data portal (ESA, http://www.esa-soilmoisture-cci.org/).

Calculated soil pCO_2 values were used in Equation 5 when calculating the carbonate derived SDC. Global gridded riverine pCO_2 data were taken from Lauerwald et al. (2015). Riverine pCO_2 data were used in Equation 5 when calculating the PTCC for rivers. The solubility of calcite in the river and soil environments was calculated in PHREEQC V3 (Parkhurst and Appelo, 2013) using the Frezchem.dat database (Marion et al., 2010). The Frezchem database was preferred for this analysis as many basins have sub zero annual average temperatures.

2.2. Calculating the PTCC of river waters and the SDC

This study uses [$HCO_3^-{}_{measured}$] for 148 river basins from the GEMS-GLORI database (Figure 1; Meybeck and Ragu, 2012), and Congo data was taken from HYBAM (available at: http://www.ore-hybam.org). This represents ∼55% of global runoff (Fekete et al., 2002, 21,000 km^3 yr^-1). The PTCC, (tons yr^{-1}) is calculated as follows:

$$PTCC = \frac{(HCO_{3\ equib}^- - HCO_{3\ measured}^-) * Q * 12 * 0.5}{10^3} \quad (7)$$

Where HCO_{3equib}^- is the modeled equilibrium [HCO_3^-] of each river (Mol/L) calculated using Equation 5, $HCO_{3measured}^-$ is the observed [HCO_3^-] of each river (Mol/L), Q is the annual discharge of each basin (m^3 yr^{-1}), 12 is the atomic mass of carbon, the factor of 0.5 is because half of the C in the HCO_3^- is atmospherically derived from the recent atmosphere (Equation 2), and 10^3 is a conversion factor from kg to tons.

The SDC in each basin was calculated to provide a comparison between the amount of HCO_3^- that could be dissolved in soils *via* the weathering of carbonates, compared to the amount of HCO_3^- that can be transported by rivers globally (i.e., PTCC). The SDC (tons yr^{-1}) is calculated as:

$$SDC = \frac{[HCO_{3\ equib}^-] * Q * 12 * 0.5}{10^3} \quad (8)$$

Where HCO_{3equib}^- is calculated by substituting Equation 6 into Equation 5. The HCO_{3equib}^- here is assumed to be entirely derived from the neutralization of CO_2 in solution, replicating previous studies (e.g., Zeng et al., 2022b).

2.3. Estimation of average river basin pCO_2, temperature, and soil moisture

K_1, K_2, K_{Ca}, and K_{CO_2} in Equation 5 are all temperature dependent constants, meaning calcite solubility in a given river basin is a function of both temperature and pCO_2, and in soils; temperature, soil moisture, and pCO_2. Global gridded land temperature data was taken from Fick and Hijmans (2017).

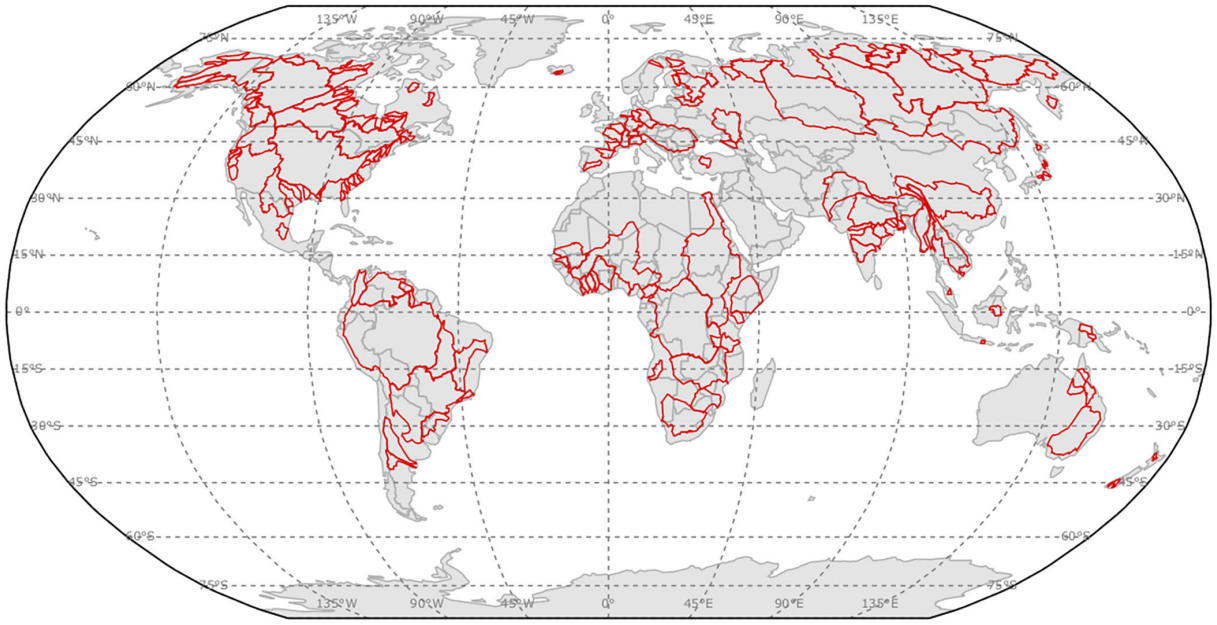

FIGURE 1
The world map with catchments used in this study is outlined in red.

Temperature, soil moisture, and pCO_2 data were extracted as raster files at 0.5° resolution. Data were then clipped to basin polygon shapefiles (GRDC, 2020), and mean and SD values for temperature, pCO_2, and soil moisture were extracted. A Monte Carlo error propagation routine was then used to estimate the mean and error for each basin (Supplementary material), based on 1,000 randomly resampled synthetic values derived from the SD of the raw raster data for each catchment (Monte Carlo routine described in Supplementary material). Some larger basins extend over a wide latitude or have significant topography - hence, show more temperature, pCO_2, and soil moisture variability. Input data was not available at a high enough resolution to account for seasonal variations. A 40-year average annual temperature was chosen for all model runs.

Three different model scenarios were evaluated:

Model 1: The baseline SDC scenario (assumes SIc = 0). In this scenario, thermodynamic equilibrium with respect to calcite is maintained, meaning calcite dissolution will occur until SIc = 0 for that soil water. This baseline scenario provides a minimum estimate for the dissolution capacity of soil waters and broadly replicates the model conditions estimated by Zeng et al. (2022b).

Model 2: Minimum PTCC scenario, assuming SIc = 0 in the river (transport) environment. In this scenario, river waters can transport carbonate derived HCO_3^- until SIc = 0 is reached.

Model 3: Maximum PTCC scenario, assuming SIc = 1 (refer to Section 4.2 for justification) since many rivers draining carbonate lithologies are supersaturated with respect to calcite (Romero-Mujalli et al., 2019b). In this scenario, river waters can transport carbonate derived HCO_3^- until SIc = 1 is reached.

The three scenarios outlined are intended to understand i) the difference between the dissolution capacity of soils (SDC) and the transport capacity of rivers (PTCC) with respect to HCO_3^-, and ii) the effect of supersaturation vs. saturation on PTCC.

3. Results

Model results for all catchments are shown in Figure 2, and the 5 catchments with the greatest SDC for Model 1, and PTCC for Models 2 and 3 are shown in Table 1. Full results are shown in the Supplementary material.

3.1. Model 1: SDC, SIc = 0

In the soil environment (when SIc = 0), Model 1 estimates equilibrium dissolution conditions with respect to calcite (Figure 2 and Table 1). Model 1 assumes that the soil HCO_3^- is entirely derived from calcite dissolution by carbonic acid and the HCO_{3equib}^- is a function of soil pCO_2 (calculated using Equation 6) and temperature. Assuming half of the carbon in the solution is derived from the atmosphere in the reaction between carbonate powder and soil water (Equation 5), Model 1 estimates that the SDC of soils in the river basins in this study is ~0.47 Gt C yr^{-1}. Extrapolated to global discharge this is 0.86 Gt C yr^{-1}, in agreement with Zeng et al. (2022b) (0.84 Gt C

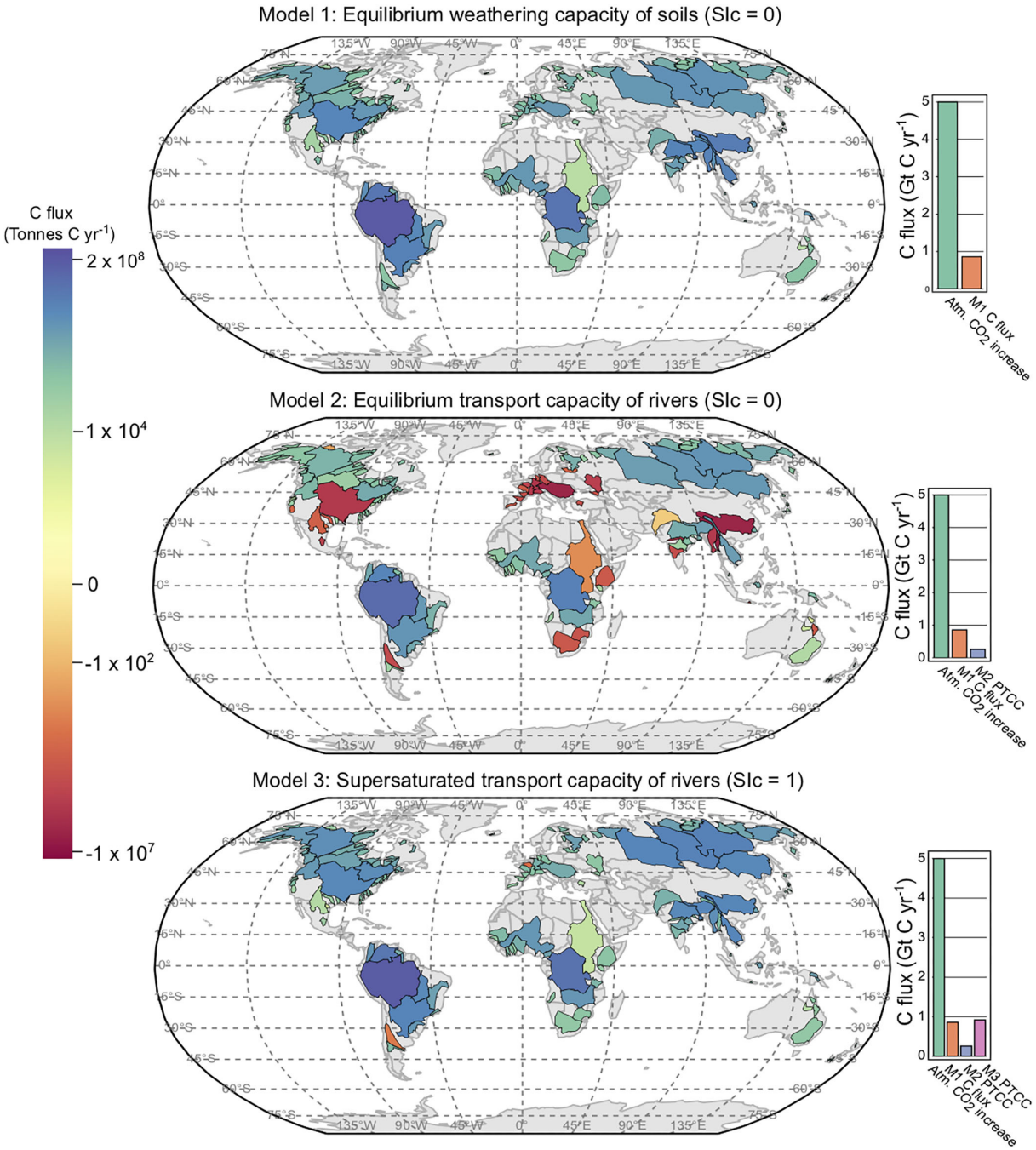

FIGURE 2
Model 1, 2, and 3 results plotted per river basin. Model 1 shows the SDC per basin. Models 2 and 3 display PTCC (potential transport capacity of carbon) values. Marginal bar plots provide a comparison between the SDC of Model 1, and the PTCC of Models 2 and 3 in comparison to annual increases of C in the atmosphere from Friedlingstein et al. (2020).

yr^{-1}). Current increases in atmospheric C are ~5 Gt C yr^{-1} (Friedlingstein et al., 2020), therefore, Model 1 represents a 17% removal of C from the atmosphere when extrapolated to global runoff (Figure 2). The amount of $CaCO_3$ required to saturate all soil waters in this study is 4 Gt $CaCO_3$ yr^{-1}, and for all soil waters globally 7.1 Gt $CaCO_3$ yr^{-1}. It is worth noting that these values do not account for the natural weathering of carbonate and silicate already occurring in soils, which can be a substantial

source of alkalinity. The SDC serves as a calcite dissolution capacity, rather than an atmospheric carbon sequestration flux. In order for this calcite dissolution to be meaningful as a carbon sequestration strategy, the HCO_3^- in the soil environment needs to be transported to the oceans without precipitating as a secondary carbonate phase. This transport is principally done *via* rivers, and the following two models assess the transport capacity of large rivers with respect to calcite.

3.2. Model 2: River water PTCC, SIc = 0

This model scenario reproduces equilibrium conditions with respect to the aqueous transport of HCO_3^- in rivers, i.e., SIc = 0 (Figure 2). The PTCC of Model 2 is 0.15 Gt C yr^{-1}, which extrapolated to global runoff is 0.26 Gt C yr^{-1} - only 5% of annual increases in atmospheric C (Figure 2). The current rate of C consumption *via* carbonate weathering is 0.15 Gt C yr^{-1} (Gaillardet et al., 1997; Zeng et al., 2022b), Model 2 results suggest that the large rivers in this study have the capacity to transport double the amount of HCO_3^- derived from carbonate weathering each year, and twice that when extrapolated to global discharge. Saturating all rivers in this study *via* liming would require 2.1 Gt $CaCO_3$ yr^{-1}, and 3.9 Gt $CaCO_3$ yr^{-1} at a global scale. Model 2 shows that only one-third of the HCO_3^- that can be dissolved in the soil environment can be transported to the ocean *via* rivers (without precipitating as secondary carbonates) at SIc = 0 (bar charts, (Figure 2).

3.3. Model 3: River water PTCC, SIc = 1

This model scenario reproduces supersaturated transport conditions with respect to HCO_3^- in rivers, i.e., SIc = 1 (Figure 2). The PTCC of Model 3 is 0.5 Gt C yr^{-1}, which when extrapolated to global runoff is 0.92 Gt C yr^{-1} - ~20% of annual increases in atmospheric C. These model results suggest that the amount of calcite derived HCO_3^- that can be transported by rivers globally could be increased by a factor of 6 if supersaturation can be achieved. Saturating all rivers in this study *via* liming would require 5.1 Gt CaCO3 yr^{-1}, and 9.3 Gt $CaCO_3$ yr^{-1} on a global scale. Model 3 shows that the transport capacity of rivers at SIc = 1 is similar to the amount of HCO_3^- that can be dissolved in the soil environment under equilibrium conditions (Figure 2). Therefore, rivers are required to maintain a supersaturated state to transport for all of the HCO_3^-, derived from critical zone weathering, to be delivered to the oceans without secondary carbonate precipitation—where it may act to increase the rate of carbonate compensation.

4. Discussion

4.1. Discrepancies between maximum $[HCO_3^-]$ in dissolution and transport environments

Respiration and decay of organic matter in soil profiles results in soil waters developing a pCO_2 content that can be orders of magnitude greater than that of the atmosphere (Figure 3A; Drever, 1988; Friedlingstein et al., 2020). The dominant control on soil respiration, hence soil pCO_2, is net primary production, which in itself is largely controlled by temperature (Lloyd and Taylor, 1994), and volumetric soil pore water content (Ilstedt et al., 2000; Blagodatsky and Smith, 2012). Models of respiration rates show that maximum respiration rates occur at soil pore water volumes of ~ 0.3 m^3 m^{-3} (Ilstedt et al., 2000; Romero-Mujalli et al., 2019b), and temperatures >15°C. In most soils, pCO_2 values are ~ 10^{-2} atm (Drever, 1988), ~ 15 times greater than atmospheric pCO_2 $10^{-3.4}$ atm, (Figure 3A). River waters have intermediate pCO_2 values between soils and the atmosphere (Figure 3A) because they are unconfined systems and can degas, equilibrating with the atmosphere. Rivers also have much lower organic carbon concentrations compared to soils, hence high pCO_2 concentrations cannot be sustained *via* organic carbon respiration (Lauerwald et al., 2015).

Since calcite solubility is a function of pCO_2 (Equation 5), soil waters in warm climates have a much greater calcite solubility (hence equilibrium $[HCO_3^-]$) in comparison to their corresponding river waters (Figure 3). For example, the Amazon River (a globally important transport environment) has a calculated $HCO_{3\ equib}^-$ concentration of 2.2 mMol/L at SIc = 0 (Model 2) and 5.2 mMol/L at SIc = 1 (Model 3), whereas soil pore waters in the Amazon basin (i.e., where most weathering takes place) have an equilibrium weathering capacity of 4.7 mMol/L (Table 1). Therefore, the supply of Ca^{2+} and HCO_3^- *via* calcite dissolution in the soil environment can be double that which can be transported to the oceans in the fluvial environment without carbonate precipitation, at SIc = 0 (Figure 3A and Table 1). Comparison of modeled soil $[HCO_3^-]$ and spring water $[HCO_3^-]$ in karst environments show soils often have greater $[HCO_3^-]$ (Zeng et al., 2022a). This demonstrates the HCO_{3equib}^- of soils multiplied by discharge is not a true measure of carbon capture potential, as the river (assuming calcite saturation), does not have the capacity to transfer this carbon to the oceans at equilibrium conditions (Figure 3B).

However, if rivers are supersaturated with respect to calcite (equivalent to there being a kinetic barrier of nucleation and growth of calcite in the river environment) then HCO_{3equib}^- in rivers is within the uncertainty of the SDC calculated in this study (Figure 3B and Table 1). Therefore, it is clear that the main control on the carbon capture and sequestration potential of enhanced carbonate weathering is not only the dissolution

TABLE 1 Top 5 river basins from each model simulation by SDC (Model 1) and PTCC (Model 2 and 3).

River	Discharge ($L\ yr^{-1}$) $\times 10^{15}$	(mMol/L)	pCO_2 (μatm)	Temperature (°C)	$HCO3^-_{equib}$ (mMol/L)	pH_{pot}	SDC ($T\ C\ yr^{-1}$) $\times 10^8$	PTCC ($T\ C\ yr^{-1}$) $\times 10^8$
Model 1 - Soil (SIc = 0)								
Amazon	6.19	0.36	29124	24.7	4.7	7.0	1.7	-
Congo	1.25	0.18	24815	23.7	4.4	7.1	0.33	-
Orinoco	1.05	0.16	29779	25.9	4.7	7.0	0.29	-
Chang Jiang	0.932	2.00	12713	10.1	3.4	7.4	0.19	-
Parana	0.504	0.53	25173	21.7	4.6	7.1	0.14	-
Model 2 - Rivers (SIc = 0)								
Amazon	6.19	0.36	3757	24.7	2.2	7.6	-	0.68
Congo	1.25	0.18	3865	23.7	2.3	7.6	-	0.16
Orinoco	1.05	0.16	3247	25.9	2.1	7.6	-	0.12
Lena	0.524	0.78	809	-11.5	2.3	8.1	-	0.047
Parana	0.504	0.53	2442	21.7	2.0	7.7	-	0.044
Model 3 - Rivers (SIc = 1)								
Amazon	6.19	0.36	3757	24.7	5.2	7.9	-	1.8
Congo	1.25	0.18	3865	23.7	5.3	7.9	-	0.38
Orinoco	1.05	0.16	3247	25.9	4.8	8.0	-	0.30
Lena	0.524	0.78	809	-11.5	5.5	8.5	-	0.15
Yenisey	0.597	1.03	861	-7.0	5.1	8.4	-	0.15

10.3389/fclim.2022.928215

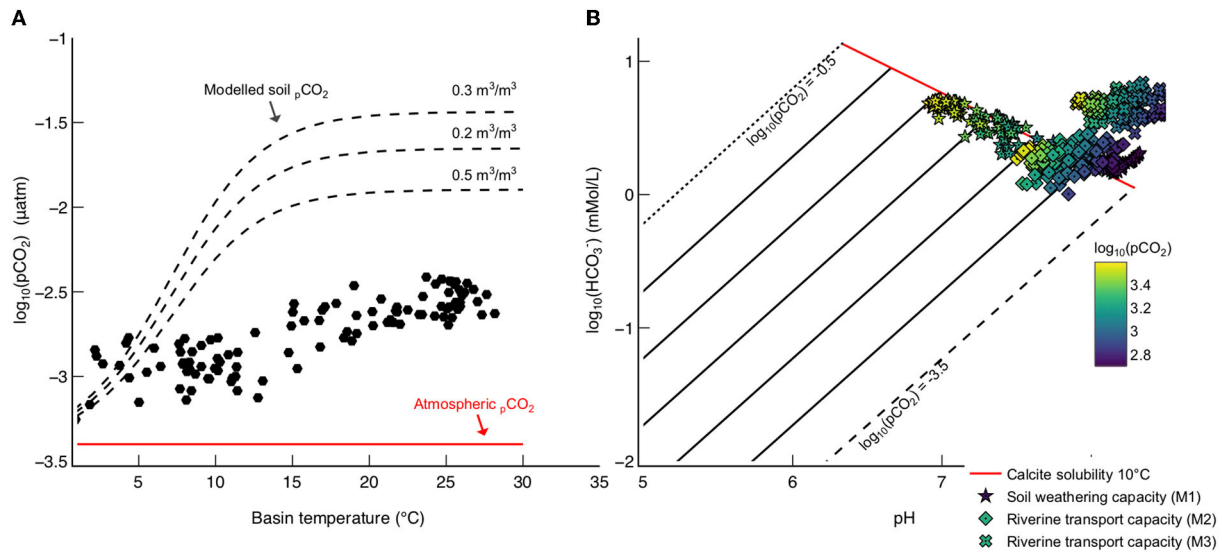

FIGURE 3
(A) Difference in pCO_2 values between river waters (hexagonal-black points) transporting HCO_3^-, and soil waters weathering lime powder (dashed lines). Soil pCO_2 values are calculated using Equation 6 (Romero-Mujalli et al., 2019b), labels refer to soil water volume, river pCO_2 values are derived from Lauerwald et al. (2015). The difference between soil and river pCO_2 values are greatest at higher temperatures, i.e., tropical basins. The mean soil pore water volume for basins in this study is 0.25 m^3 m^{-3}, which is derived from ESA soil moisture data. Atmospheric pCO_2 (red line) = -3.4. **(B)** Open system model for different pCO_2 solution paths at 10°C and initial pH = 5 (approximate value for rainwater). Modelled equilibrium soil weathering capacity (Model 1), equilibrium riverine transport (Model 2), and supersaturated riverine transport (Model 3) are shown.

capacity of soils but the controls on HCO_{3equib}^- in rivers, where carbon is transferred to the oceans.

4.2. Controls on HCO_{3equib}^- in the riverine environment

Both pCO_2 and HCO_{3equib}^- are greater in the soil environment than in the riverine environment at calcite saturation (e.g., Model 1 vs. Model 2, Figure 3). However, rivers draining carbonate rocks are frequently supersaturated with respect to calcite (Romero-Mujalli et al., 2019a), hence could transport atmospherically derived carbon above their prescribed equilibrium at calcite saturation without it being lost to secondary carbonate precipitation. The global river databases GLORICH (Hartmann et al., 2014) and GEMS-GLORI (Meybeck and Ragu, 2012) were filtered to remove anthropogenic inputs (after Gaillardet et al., 2019). The calcite saturation index was calculated for each river using PHREEQC V3. (frezchem.dat, n = 2,412 Parkhurst and Appelo, 2013). Saturation states >0 are common, 47% of the rivers surveyed were calculated to be oversaturated with respect to calcite (Figure 4). This supports the idea that Model 2 (SIc = 0) serves as a baseline potential transport capacity, and the lack of rivers with SIc >1 suggests Model 3 (SIc = 1) serves as a reasonable upper potential transport limit. A critical question for enhancing carbonate weathering is why rivers become supersaturated with respect to calcite, and how this supersaturation is maintained in a steady-state.

As the pCO_2 of a soil environment is much greater than that of the atmosphere, soil waters will outgas CO_2 as they supply the fluvial environment, lowering $pCO_{2(aq)}$ as equilibration with the lower pCO_2 atmosphere proceeds (Figure 5; Lauerwald et al., 2015). This outgassing drives calcite supersaturation in river waters (horizontal arrow on Figure 5). Secondly, mixing between atmospherically derived runoff and soil waters can cause a mixture of two fluids which may become supersaturated with respect to calcite (diagonal arrow on Figure 5). Calcite saturation may drive calcite precipitation *via* the reverse of Equation 2, lowering $[HCO_3^-]$ by removal of DIC species to form $CaCO_3$ (vertical arrow on Figure 5). In this instance, the HCO_3^- in excess of the calculated HCO_{3equib}^- (at calcite saturation) will be removed through calcite deposition (Erlanger et al., 2021). CO_2 degassing (Lauerwald et al., 2015) and subsequent travertine formation are a well documented phenomena in carbonate terrains (Herman and Lorah, 1987; Dreybrodt et al., 1992; Yan et al., 2020), playing an important role in terrestrial carbon cycling (Raymond et al., 2013). Often, the spontaneous precipitation of carbonate in the fluvial environment is concentrated around specific turbulent environments, e.g., waterfalls and steps (Rogerson et al., 2014). In some cases, calcite precipitation can be microbially mediated

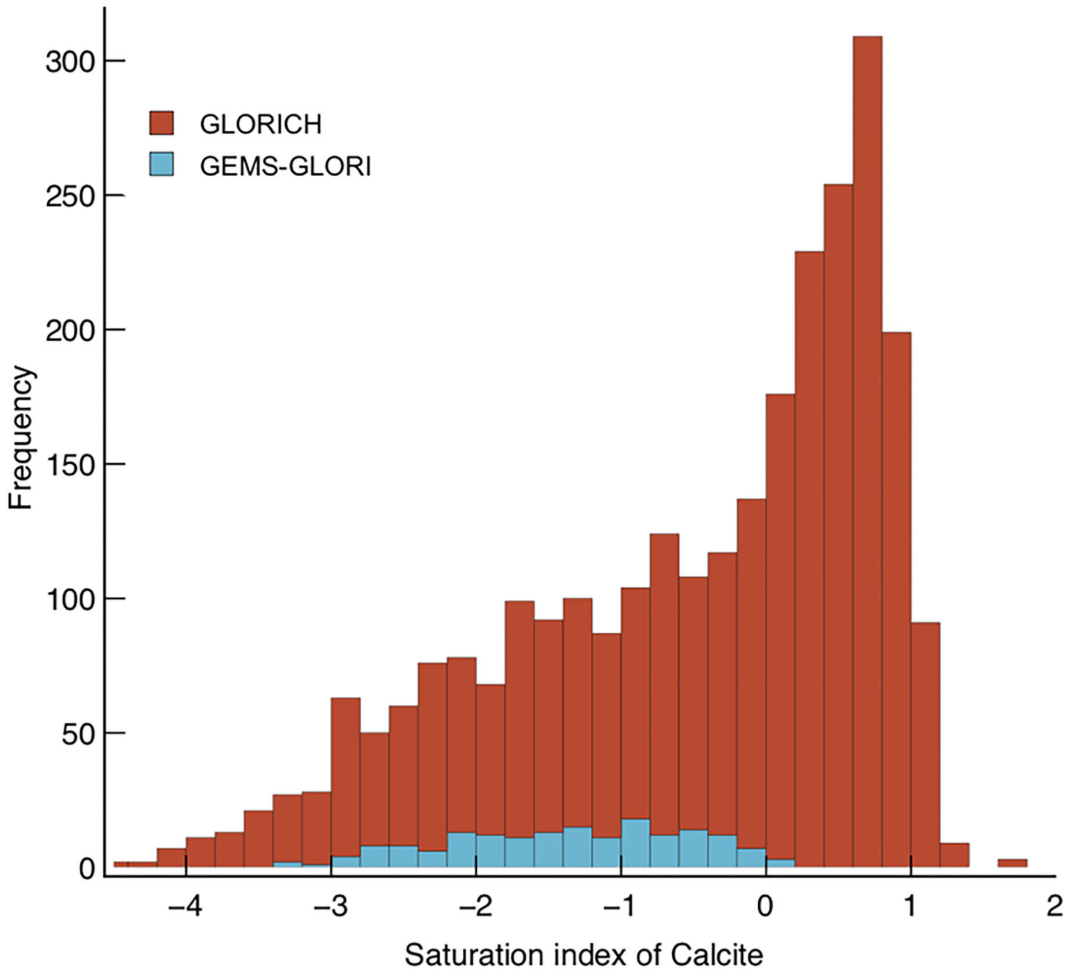

FIGURE 4
Stacked histogram displaying calculated SIc values for rivers in the GEMS-GLORI (Meybeck and Ragu, 2012) and GLORICH (Hartmann et al., 2014) databases. Mean discharge for GLORICH data is 5 $km^3\ yr^{-1}$, the mean for GEMS-GLORI is 170 $km^3\ yr^{-1}$.

(Rogerson et al., 2014). When quantitative precipitation to re-equilibrate waters with respect to calcite does not happen, supersaturation is achieved. Reasons for calcite not precipitating from natural waters with SIc >0 are varied and are explored in the next section. Critically, results from Models 1 and 3 show that for atmospheric carbon dissolved in the soil environment to remain in solution before reaching the oceans, precipitation of calcite (and other Ca or Mg carbonates) must be inhibited in river waters and supersaturation achieved.

4.3. Current understanding of calcite supersaturation and precipitation inhibitors in rivers

For calcite supersaturation to be maintained in rivers the precipitation of carbonate minerals must be inhibited, such that concentrations of $HCO^-_{3(aq)}$ can remain above equilibrium. It is important to understand how calcite supersaturation can be maintained in rivers (where HCO^-_3 is transported) because this will ultimately control the efficiency of CO_2 consumption *via* carbonate weathering. Calcite precipitation can be inhibited in several ways. For example, precipitation can be inhibited by the presence of nucleation inhibitors such as Mg^{2+}, SO^{2-}_4, and organic complexes, which adsorb onto crystal lattices resulting in sluggish calcite precipitation kinetics (Mann, 1988; Astilleros et al., 2010; Dobberschütz et al., 2018). The effect of nucleation inhibitors may then be exacerbated in catchments with short water residence times. If the reaction kinetics of calcite precipitation are slower than the residence time of water in the catchment then disequilibrium in the carbonate system can occur (Herman and Lorah, 1987). The controls on precipitation inhibitors raise interesting points with regards to methods of enhancing carbonate weathering. This study

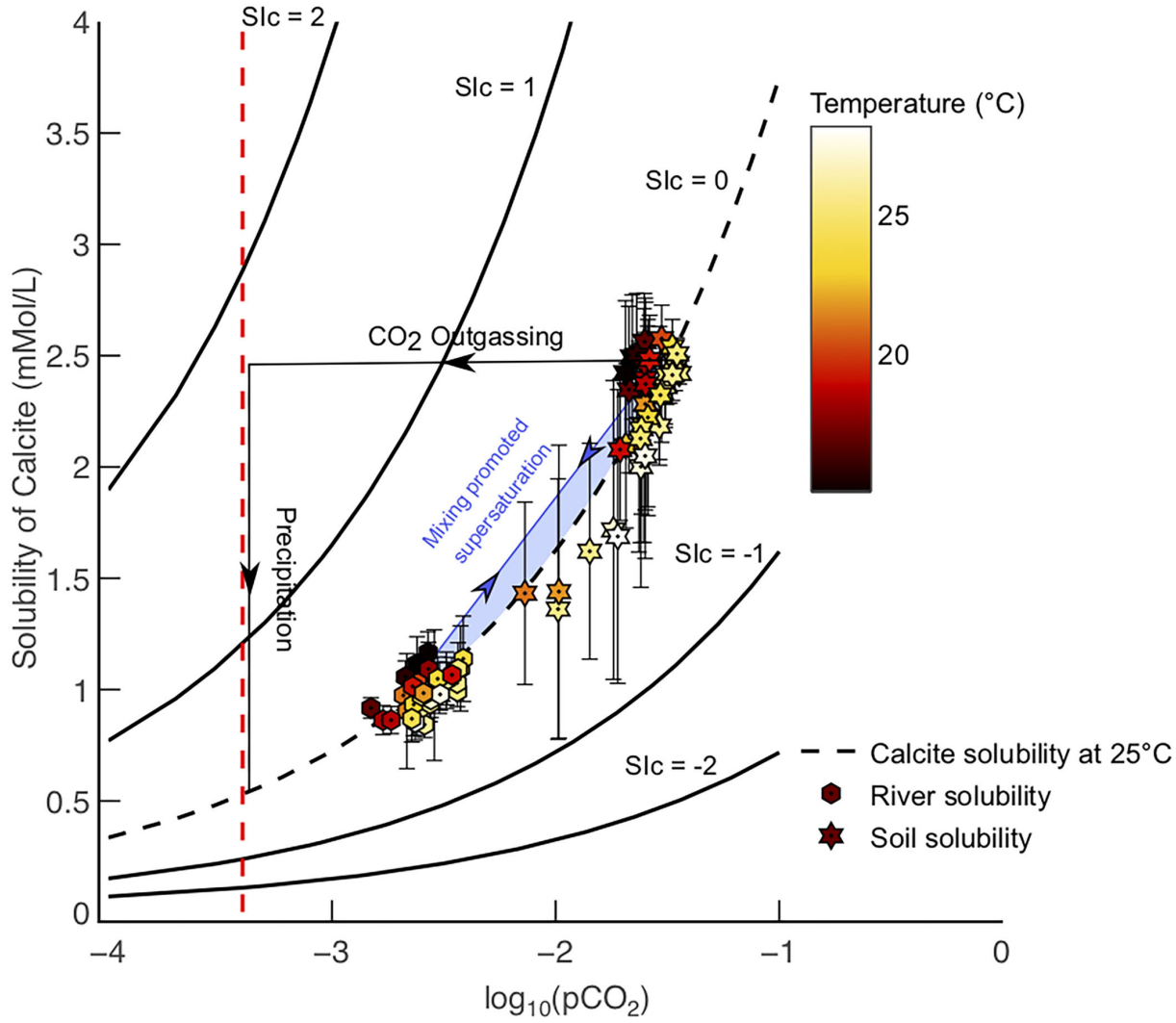

FIGURE 5
Schematic figure presenting two plausible mechanisms for calcite precipitation, or supersaturation, to be achieved. River basins with a mean temperature >15°C and are undersaturated prior to liming (i.e., positive PTCC) are shown with corresponding modelled soil pore water calcite solubilities from Model 1 and 2 (i.e., SIc = 0). Atmospheric pCO_2 is shown as the red line. Precipitation may be triggered either by soil waters degassing when in contact with the atmosphere, or mixing with river waters, creating fluids with even higher SIc values (blue shaded area). Supersaturation *via* mixing is exacerbated further when river waters are saturated with calcite. All SIc contours are calculated for 25°C.

focuses on 149 of the world's largest rivers by discharge, which have long water residence times. Approximately 55% of global discharge is captured in this study, meaning that much smaller streams and rivers draining into the oceans must make up the remaining 45%. Therefore, small rivers could potentially play a crucial role in carbon transfer between the continents and oceans, which is currently unaccounted for. Furthermore, the role of Mg^{2+} as a calcite precipitation inhibitor suggests that other Mg-bearing carbonates (e.g., dolomite) could make good candidates for enhancing carbonate weathering.

4.4. Principal controls on PTCC

Model 1 calculates an equilibrium dissolution capacity of soils (SDC). In the context of this study, this represents the potential [HCO_3^-] in soils that can be achieved by reacting all soil derived pCO_2 with calcite. This is the premise of other literature models e.g., Zeng et al. (2022b) and produces similar results. The assumption being that the soil dissolved load shifts from being bedrock dominated to carbonate dominated as a consequence of liming (Zeng et al., 2022b). This has been suggested to represent a weathering flux (Zeng et al., 2022a,b),

but this must be an upper limit given 1) the difference in pCO_2 between soil waters and rivers (e.g., Figure 2, 3), and 2) natural weathering fluxes will also produce HCO_3^-. Natural critical zone fluxes have not been quantified at a global scale and, therefore, cannot be subtracted from the SDC calculated in this study. As such, in this study, it is used as a representative soil dissolution capacity of calcite, to which riverine transport potentials (PTCC) are compared, rather than a potential soil weathering flux for CO_2 sequestration as suggested by Zeng et al. (2022b).

Model 2 calculates the transport capacity (PTCC) of HCO_3^- in rivers, if the SIc is 0, a conservative estimate. As many river basins are already oversaturated or close to oversaturation with respect to $CaCO_3$ (Figure 2, 4) many basins in Model 2 have negative PTCC values, meaning they already transport HCO_3^- in excess of a SIc = 0, i.e., they are oversaturated with respect to calcite. Therefore, they have no capacity to increase carbon consumption through enhanced carbonate weathering. The reasons for this are varied. For example, liming has been prevalent in the Mississippi basin, and much of North America, since the 1950s (Oh and Raymond, 2006)—contributing to the negative transport potentials observed in this basin and much of the U.S. (Figure 2). Negative transport potentials in much of Europe are likely explained by extensive carbonate rock outcrop and karst systems (Goldscheider, 2005), in addition to pollution (Roy et al., 1999, e.g., Seine). Similarly, rivers draining the Himalayan region are known to have dissolved loads dominated by carbonate weathering and precipitate secondary carbonate minerals (Tipper et al., 2006; Bickle et al., 2015). Rivers with their source in the Himalayas with positive transport potentials (e.g., the Mekong) are likely to be supply limited with respect to carbonates—hence may benefit from liming.

Model 3 simulates the transport capacity (PTCC) of HCO_3^- if SIc of global rivers is capped at 1 (an upper estimate). Few river basins globally have SIc values >1 (Figure 4), and so PTCC values in Model 3 are largely positive and qualitatively align with SDC results from Model 1 (e.g., comparison of model output in Figure 2). This reiterates the notion that supersaturated transport environments (i.e., Model 3 parameters) are required to transport the products from equilibrium calcite dissolution in the soil environment (i.e., Model 1 parameters, Figure 3).

Basins with the greatest PTCC in Model 2 are those which have both high discharge values and are currently undersaturated with respect to calcite (Figure 6). The largest PTCC values are observed in the tropical and Siberian cratons (e.g., Amazon, Congo, Orinoco, Lena, and Yenisey), which are known to be supply limited (West et al., 2005). Supply limited basins are defined by low erosion rates in comparison to chemical leaching capacities, meaning the capacity for weathering in that particular system outstrips the supply of rock to the critical zone.

At both low (<0°C) and high (>20°C) temperatures, HCO_{3equib}^- at SIc = 0 exceeds $HCO_{3measured}^-$ for the GEMS river data set (Figure 7). This is indicative of rivers in these temperature ranges being able to enhance their HCO_3^- concentrations *via* enhanced carbonate weathering, and this is reflected in their calculated PTCC predictions (Model 2, Figure 2 and Table 1). Whereas in temperate climates (i.e., 7–20°C) $HCO_{3measured}^-$ exceeds or is equivalent to HCO_{3equib}^-, and HCO_3^- fluxes cannot be increased in these rivers.

Northern high latitude basins have low pCO_2 concentrations (Table 1), and as such do not have leaching capacities as great as those in tropical basins. However, these high latitude basins have large PTCC values because of their very low temperatures, which increases calcite solubility—hence, HCO_{3equib}^-. Therefore, cold river basins with appreciable discharges (e.g., Lena, Yenisey) will have a large potential to transport more HCO_3^- in solution *via* enhanced carbonate weathering, simply because calcite is far more soluble in colder water in comparison to warm (Figure 7).

If calcite solubility is negatively correlated with temperature then it seems counter-intuitive that warm basins (>20°C) also have an HCO_{3equib}^- >$HCO_{3measured}^-$ (Figure 7). Calcite solubility, hence HCO_{3equib}^- can be high in these warm climates because microbially derived pCO_2 production increases with temperature (Equation 6, Lloyd and Taylor, 1994; Romero-Mujalli et al., 2019b), hence the solubility of calcite of is a trade-off between increasing temperature and decreasing calcite solubility, and pCO2 generation increasing calcite solubility as a function of temperature (Figure 7).

Interestingly, the global minimum of the modeled fit representing HCO_{3equib}^- occurs at ∼10°C (Figure 7), where it is hypothesized carbonate weathering is most intense (Gaillardet et al., 2019; Romero-Mujalli et al., 2019a). This is intriguing as our thermodynamic solubility model suggests this is the least favorable place to transport carbonate derived HCO_3^- in rivers to the oceans, whilst maintaining equilibrium (SIc = 0). If temperate climates are relatively poor at transporting the products of carbonate dissolution, as suggested by this model (Figure 7), then we speculate that authigenic carbonate precipitation would be more abundant in temperate climates. Differences in river and bedrock Mg/Ca and stable isotope ratios (e.g., Ca isotope ratios) in temperate climates have been suggested to be a consequence of large amounts of secondary carbonate precipitation (Tipper et al., 2010; Bickle et al., 2015), which provides some credence to this idea. Overall, the intensity of carbonate weathering, and the possibility of secondary carbonate precipitation, make enhancing carbonate weathering in temperate climates unfavorable (Figure 7).

In summary, tropical basins like the Amazon and Congo are ideal for liming as sustained rapid denudation kinetics over periods of millions of years has resulted in shield exposure and thick regolith development (Gaillardet et al., 1997; Braun et al., 2005). High solubility phases, such as $CaCO_3$, have long since been weathered and tropical rivers are often dilute due to high discharges—making them very undersaturated with respect to calcite. A combination of these factors and

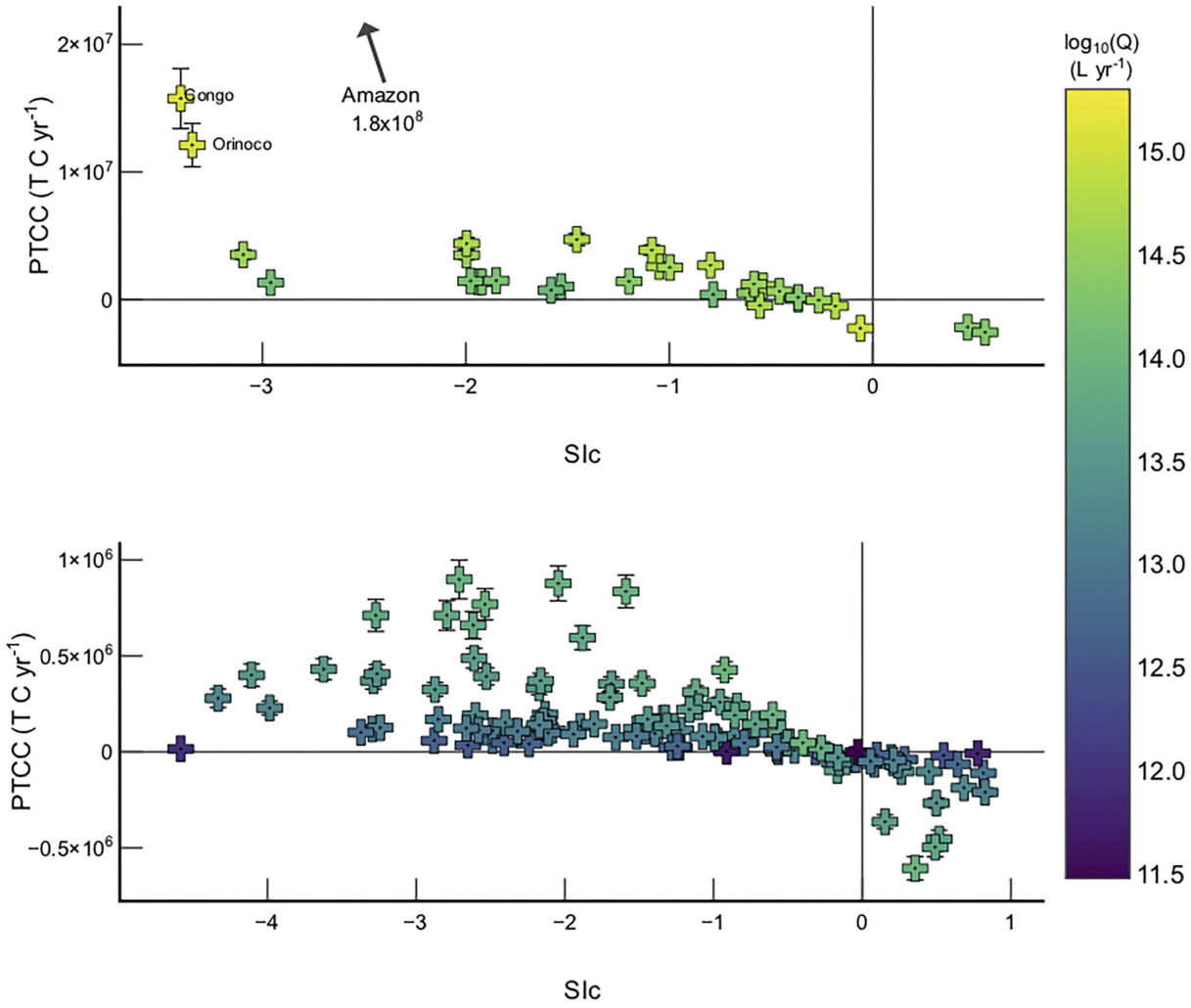

FIGURE 6
Sic vs PTCC >1 × 10^{14} L yr^{-1} (top) and rivers with discharge <1 × 10^{14} L yr^{-1} (bottom). Error bars are not visible for data where the error is smaller than the data symbol.

high organic carbon respiration rates, i.e., very high pCO_2 concentrations (Lauerwald et al., 2015), results in tropical basins being ideal for transporting large quantities of carbonate dissolution products (i.e., HCO_3^-) in solution to the oceans (Figure 2, Table 1). Similarly, Siberian rivers could export more HCO_3^- than they currently do to the oceans without authigenic carbonate precipitation, on account of their low temperatures, but the effects of tributaries freezing during boreal winter may mean transport capacities are hindered during colder seasons. Freezing rivers at high latitudes may also produce cryogenic carbonate (Lacelle, 2007; Thomazo et al., 2017), but it is difficult to predict the effects of this phenomenon on transport potentials. A potential benefit of liming high latitudes is that carbonate weathering is known to be rapid in sub-arctic climates, in contrast to silicate weathering. For example, carbonate weathering dominates the dissolved loads of poly-lithic basins such as the Mackenzie (Millot et al., 2003). In these cold environments enhancing the weathering of silicate rocks is less feasible as dissolution kinetics are slower (Pogge von Strandmann et al., 2022).

4.5. Benefits of liming

The main purpose of liming in the past has been to amend soil pH, which is often low on account of organic matter respiration in the soil environment generating rich pore waters. It is common for soils to have a pH of

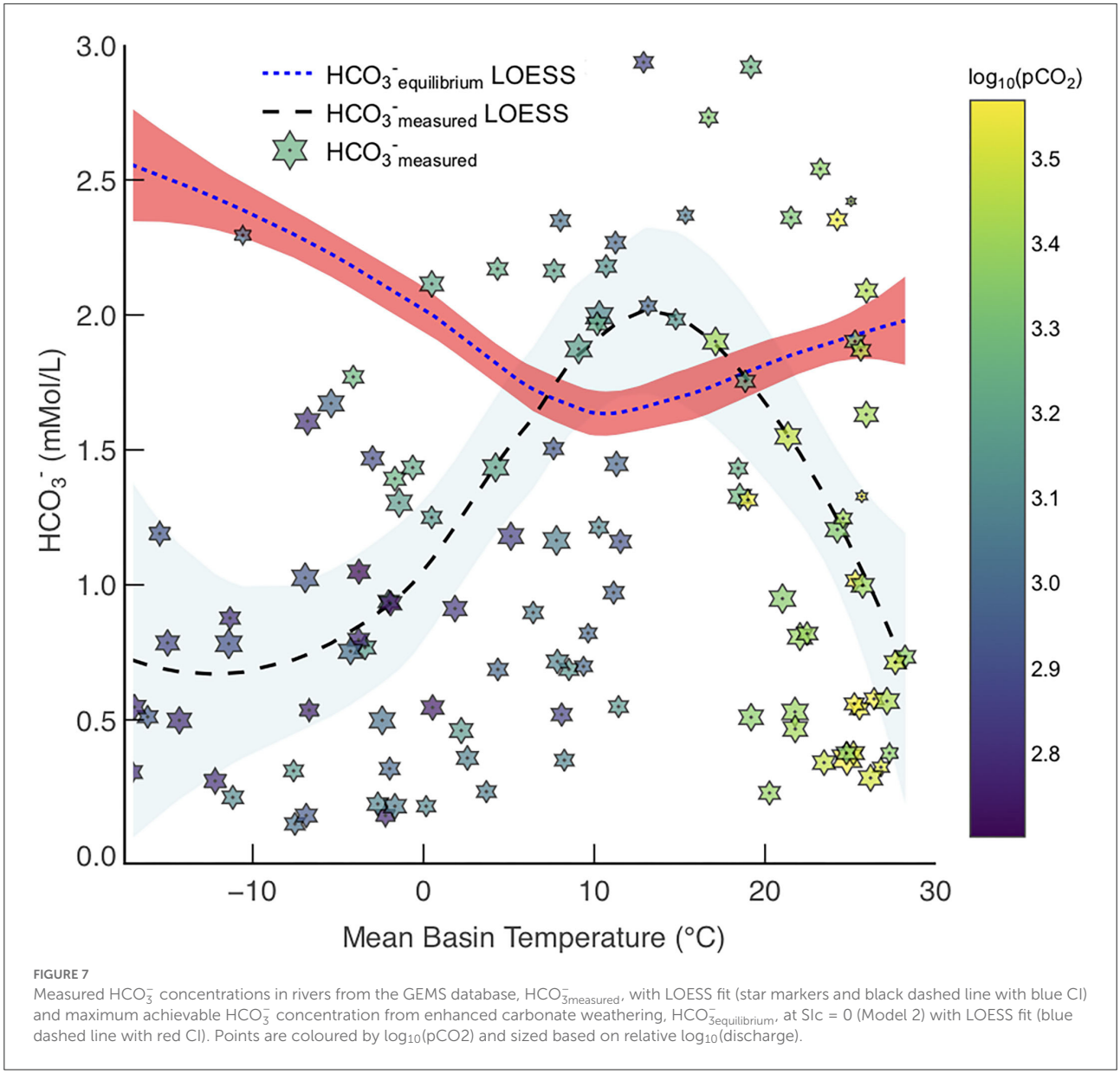

FIGURE 7
Measured HCO_3^- concentrations in rivers from the GEMS database, $HCO_{3measured}^-$, with LOESS fit (star markers and black dashed line with blue CI) and maximum achievable HCO_3^- concentration from enhanced carbonate weathering, $HCO_{3equilibrium}^-$, at SIc = 0 (Model 2) with LOESS fit (blue dashed line with red CI). Points are coloured by log_{10}(pCO2) and sized based on relative log_{10}(discharge).

~5.5 in temperate northern hemisphere climates (Tunney et al., 2010), whereas pH values in in tropical soils can be as low as 3.9 (Motavalli et al., 1995) due to higher rates of organic carbon respiration. Ideal soil pH values for agriculture vary with soil type, but generally neutral pH values (7) are required to grow most crops (Oshunsanya, 2019). Reacting the prescribed amount of calcite for each basin with the modeled soil waters in those basins results in modest increases in soil pH, to values sustainable for farming in most conditions (Figure 8). At lower temperatures it is plausible that liming could elevate soil pH to values too alkaline for growing traditional crops in those areas (Figure 8), and this must be recognized as a plausible side effect of using farmland to enhance carbonate weathering. However, it is worth noting that the elevation of soil water pH associated with enhanced carbonate weathering is much lower than that for enhanced silicate weathering, particularly in tropical basins (Köhler et al., 2010).

Additional benefits of liming include increasing the availability of nutrients, such as nitrate and phosphate, by changing soil water pH (Haynes, 1982). Increasing nutrient availability reduces fertilizer requirements and increases soil health. Liming can also decrease the mobility of heavy metals in soil profiles, reducing the risk of plants incorporating heavy metals into soft tissues (Bolan and Duraisamy, 2003).

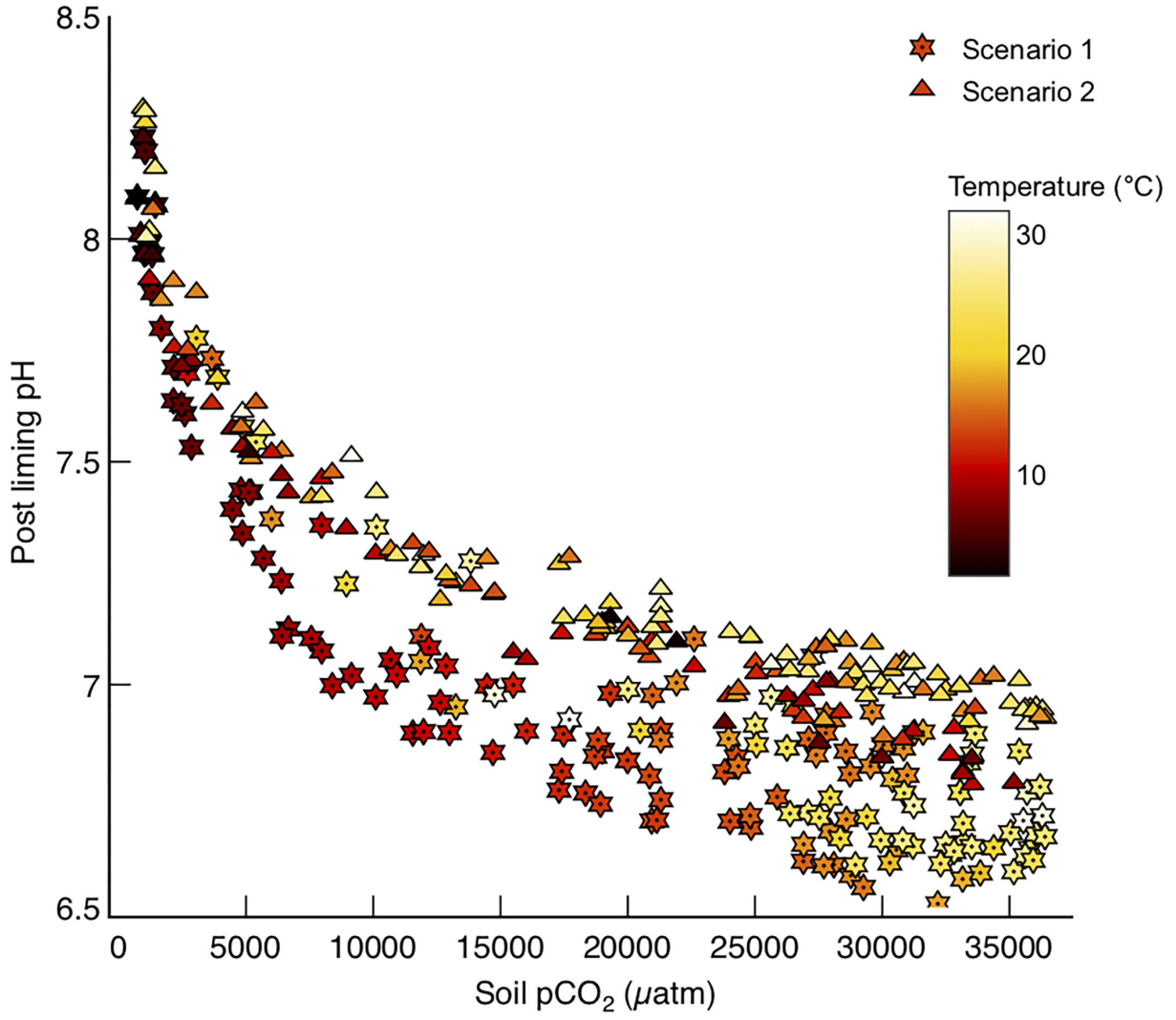

FIGURE 8
pH values for soil waters in each basin, after reaction with the prescribed amount of calcite to reach the saturation states required for Model 2 (SIc = 0) and Model 3 (SIc = 1).

4.6. Potential risks of liming agricultural land

Farmland is one potential location to practice liming, though other land types may also be used - e.g., reforestation projects. This study focuses on farmland because i) many parts of North America already practice liming, and this has resulted in an increased export of bicarbonate in waters draining farmland (Oh and Raymond, 2006; Hamilton et al., 2007), and ii) global coverage of farmland is well quantified (e.g., GlobCover database Arino et al., 2008).

CO_2 is consumed by enhancing carbonate weathering, provided that the agricultural lime is dissolved by carbonic acid. However, one caveat for enhancing carbonate weathering is a growing body of evidence suggesting that strong acids (e.g., H_2SO_4) play an important role in rock weathering in large river basins such as the Mekong and Mackenzie (e.g., Calmels et al., 2007; Torres et al., 2016; Relph et al., 2021). Agricultural fertilization can also result in the production of strong acids. Nitrification of nitrate-based fertilizers, used in agriculture, can produce nitric acid (HNO_3) (Zbieranowski and Aherne, 2013). The reaction between strong acids (e.g., H_2SO_4 and HNO_3) and $CaCO_3$ results in CO_2 release into the atmosphere.

Some modeling studies have assumed that agricultural liming acts as a direct source of CO_2 (e.g., Houghton et al., 1997; West and McBride, 2005), and often account for the relatively long timescale process of carbonate precipitation in the ocean. Field trials have demonstrated that liming acts as a sink of CO_2

(e.g., Oh and Raymond, 2006; Hamilton et al., 2007), with the reaction of lime and strong acids generally accounting for less than 15% of the charge balance in the soil and river waters (Oh and Raymond, 2006; Hamilton et al., 2007; Biasi et al., 2008). It appears, based on the evidence of field trials, that enhancing carbonate weathering on agricultural land would be a net sink of CO_2, but the efficiency can be compromised by the strong acid reaction. The reduction in efficiency of enhancing carbonate weathering can be quantified by understanding how much excess nitrogen, derived from fertilizers, is in each catchment in this study (Supplementary material for calculation, Figure 9). Literature studies (Oh and Raymond, 2006; Hamilton et al., 2007; Biasi et al., 2008) stipulate that ∼15% of this excess nitrate (Figure 9) would react with lime products. Assuming the reaction between strong acids and agricultural lime is:

$$2HNO_{3(aq)} + CaCO_{3(s)} \rightarrow Ca^{2+}{}_{(aq)} + 2NO_3^-{}_{(aq)} + CO_{2(g)} + H_2O_{(l)} \quad (9)$$

Then Equation 9 stoichiometry dictates 1 mol of CO_2 is released for every 2 mol of HNO_3 reacted with $CaCO_3$. Based on these assumptions the PTCC of Model 2 may decrease from 0.26 to 0.20 Gt C yr^{-1} (Figure 9) as a consequence of a strong acid reaction. This is assuming that the amount of lime required to reach equilibrium for Model 2 without accounting for a strong acid weathering is applied to the soil, such that strong acid reaction would result in equilibrium saturation with respect to calcite not being achieved. Areas worst affected are unsurprisingly those which have the greatest excess of nitrate (e.g., SE Asia, Figure 9), and qualitatively it is shown that the catchments affected in Figure 9 already have low or negative PTCC values in Figure 2. The PTCC calculated from Model 3 would change from 0.92 Gt C yr^{-1} to 0.86 Gt C yr^{-1}, adjusting for the reaction of limestone with excess nitrate in soils. Overall, Strong acid weathering of agricultural lime may reduce the efficacy of enhanced carbonate weathering by 5–25% (Figure 9; Oh and Raymond, 2006; Hamilton et al., 2007; Biasi et al., 2008).

The obvious downside to enhanced carbonate weathering is that the dissolution of lime products by strong acids results in CO_2 emission, in comparison to silicate weathering, where strong acid weathering only results in a reduction in CO_2 draw down efficiency—if ocean alkalinity enhancement is the study aim (Köhler et al., 2010; Taylor et al., 2016). Pedogenic carbonate formation is the aim of other enhanced silicate weathering studies (e.g., Andrews and Taylor, 2019; Haque et al., 2019) because the residence time of pedogenic carbonates is estimated to be long (i.e., 10^4 years). Strong acid generation from fertilizers may significantly reduce the residence time of pedogenic carbonates, or stop formation altogether (Zamanian et al., 2016). Dissolution of pedogenic carbonates by strong acids would result in a rapid re-release of CO_2 to the atmosphere. Indeed, strong acid weathering is an unknown variable in the agricultural enhanced weathering hypothesis and requires dedicated research with meticulous field trials for appropriate quantification of the impacts on carbon cycling.

4.7. Logistics of liming at a global scale

To assess the practicality of agricultural liming at a global scale, the quantity of farmland in the 5 catchments with the largest SDC (Model 1) and PTCC values (Models 2 and 3) for each scenario were determined using the GlobCover database (Arino et al., 2008). The thickness of limestone powder needing to be spread on farmland annually was then calculated using the molar volume of $CaCO_3$ (36.95 Mol cm^3), the mass of limestone required to reach saturation, and the surface area of farmland in each basin. The results for all model scenarios are shown in Table 2.

To satisfy Model 1, which represents an equilibrium dissolution capacity of soils, with respect to calcite (SIc = 0), ∼1–10 mm yr^{-1} of limestone powder is required to be spread on all farmland in each basin. This would saturate soil waters with respect to calcite. Typically, <20 mm yr^{-1} thickness of lime powder is required for rivers to reach SIc = 0 (Model 2) and SIc = 1 (Model 3), though the small amount of farmland in Siberia (i.e., Lena and Yenisey) could require >20 mm yr^{-1} of lime powder to achieve saturation (Table 2). The amount of lime powder required to achieve saturation or supersaturation with respect to calcite in the 149 rivers modeled is 4.0, 2.1, and 5.1 Gt $CaCO_3$ yr^{-1} for Model scenarios 1, 2, and 3, respectively. As shown in Figure 9, it is likely the true amount of lime required to reach saturation (Model 2) or supersaturation (Model 3) may be more than this.

Though no database exists for lime powder availability globally, limestone is frequently quarried to create aggregate and cement. Limestone extraction during the 1990s was ∼ 1 Gt yr^{-1} in the U.S. alone, and lime powder is produced as a by-product of this extraction and processing (Hudson et al., 1997; Rau et al., 2007). To satisfy the amount of limestone required for model scenarios in this study, U.S. limestone extraction would require either doubling (Model 2), or increasing five-fold (Models 1 and 3). Investigating sources of alkaline feedstocks for enhancing weathering is not the aim of this study, but it is useful to note that limestone powder is not the only available alkaline material to enhance carbonate weathering. Industrially produced cement, blast furnace slag, kiln dust, and slaked lime could all be used for enhancing weathering (Renforth, 2019). This is with a caveat that of these materials only slaked lime has long term field trials, meaning lime powder and slaked lime are the most attractive materials from an environmental perspective.

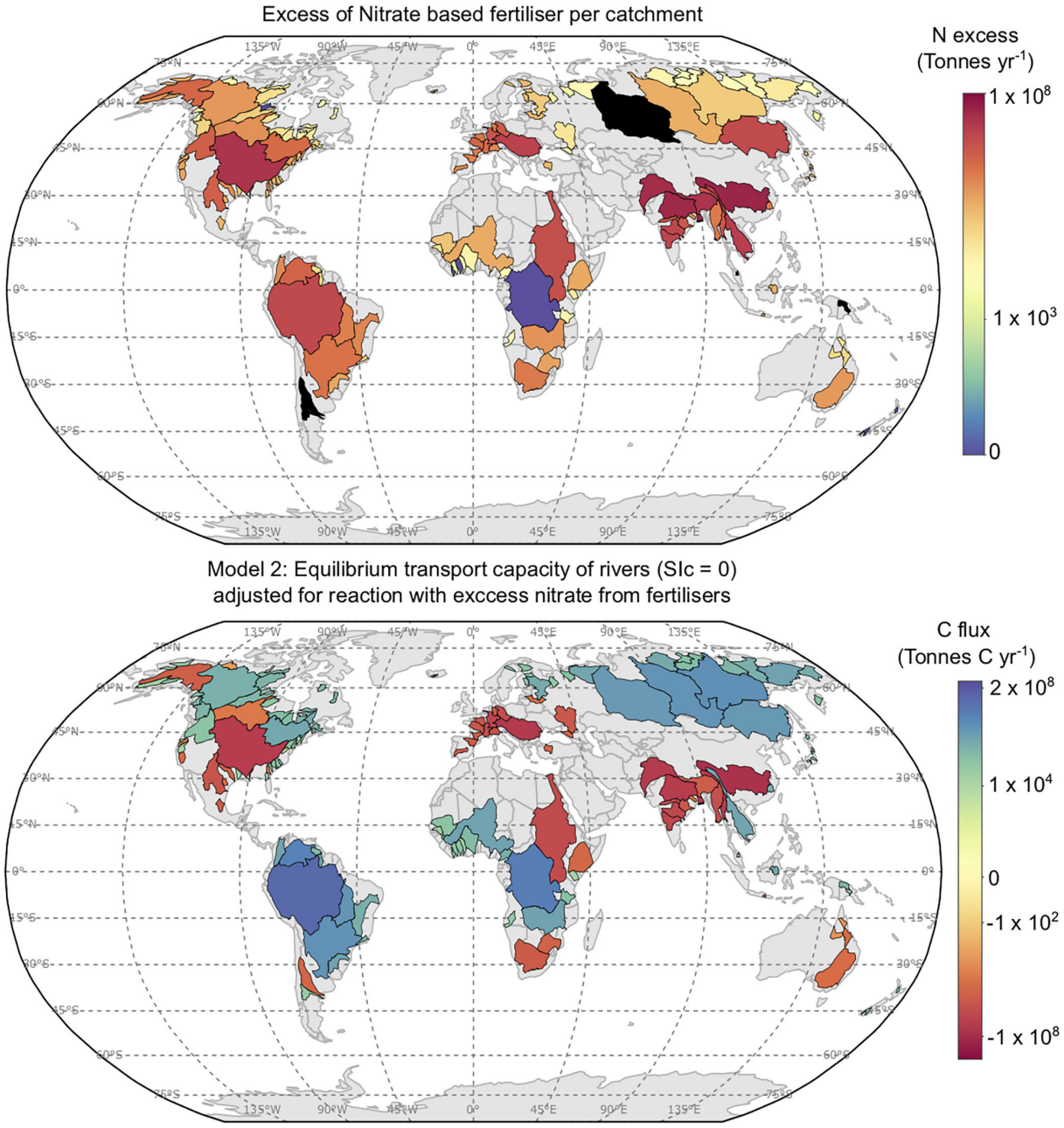

FIGURE 9
Top: Excess nitrogen based fertiliser per catchment studied (Tonnes yr^{-1}). Nitrogen excess data from Lassaletta et al. (2014), and the mass of nitrogen used is available from: https://www.fao.org/faostat/en/?dat. Black catchments occur for areas where nitrogen mining occurs, which skews estimates of nitrogen use efficiency. Bottom: PTCC values (Tonnes C yr^{-1}) for Model 2, recalculated assuming 15% of excess nitrate in each catchment reacts with agricultural lime applied to aribal land.

5. Conclusion

Rapid increases in atmospheric CO_2 concentrations require that novel methods for carbon sequestration are developed before 2050. Enhancing the dissolution of carbonate rocks on land has been suggested as a potential strategy to remove appreciable amounts of atmospheric CO_2 on the timescale of human life. Indeed, carbonates have been shown to react rapidly with atmospheric CO_2, but require this dissolved carbon to be delivered to the ocean for sequestration on meaningful timescales (1,000s of years), and that strong acids are of minor importance for dissolution reactions. This study provides

TABLE 2 The calculated thickness of lime required to be spread on farmland each year to achieve the estimated SDC (soil dissolution capacity) for Model 1, and estimated PTCC (potential transport capacities of carbon) for Models 2 and 3.

River	Area (m^2) $\times 10^{12}$	Farmland (%)	Lime required (T $CaCO_3$ yr^{-1}) $\times 10^9$	Lime thickness (mm yr^{-1})
Model 1				
Amazon	6.13	6	1.5	11
Congo	3.64	12	0.27	2
Orinoco	1.01	15	0.25	5
Chang Jiang	1.27	56	0.16	<1
Parana	2.81	46	0.12	<1
Model 2				
Amazon	6.13	6	0.68	5
Congo	3.64	12	0.14	1
Orinoco	1.01	15	0.11	2
Lena	2.46	<1	0.060	13
Parana	2.81	46	0.050	<1
Model 3				
Amazon	6.13	6	1.6	12
Congo	3.64	12	0.33	2
Orinoco	1.01	15	0.25	5
Lena	2.46	<1	0.14	32
Yenisey	2.54	1	0.15	16

estimates for the amount of additional dissolved HCO_3^- Earth's rivers can deliver to the oceans under two saturation scenarios—providing both an optimistic and pessimistic scenario for carbon sequestration *via* enhancing carbonate weathering.

In both transport simulations (Models 2 and 3) continental cratons (tropical South America and Africa and Siberia) were the ideal locations to enhance riverine HCO_3^- export *via* liming, without precipitating authigenic carbonate minerals. This would be expected as these rivers are supply-limited, hence are dilute and often have high discharges (e.g., in tropical areas). A lack of farmland in Siberia may mean that alternative land types for enhancing carbonate weathering need to be used, e.g., shrub land or forests. The efficacy of enhanced weathering in these locations is not known, though the reactivity of carbonate phases could make them plausible land types for liming. High northern latitudes may be ideal places for enhancing carbonate weathering, as olivine dissolution rates in these climates are unfeasible to enhance silicate weathering on meaningful timescales. The amounts of limestone required for rivers to reach saturation in either scenario may be feasible at the large basin scale in comparison to dunite extraction, and alternatives to limestone powder (e.g., blast furnace slag, slaked lime) are available. Liming is also a well understood and relatively widely practiced agricultural technique already, meaning costs and benefits are known. The degree of liming to reach the saturation states proposed in this study results in practical increases in soil water pH in most cases.

Overall, increasing the saturation index of calcite in global rivers to either 0 or 1 *via* enhancing carbonate weathering will result in a 5–20% sequestration of increases in atmospheric C per year. These values come with the caveat that a weak carbonic acid must be the dissolving agent, as strong acids will release CO_2 into the atmosphere. The impact of strong acid dissolution for any agricultural enhanced weathering study requires careful and dedicated field trials. Our model estimates align with literature results for the dissolution capacity of calcite in soils, but these data require that rivers globally maintain an oversaturated state with respect to calcite for successful CO_2 sequestration in the global oceans. The plausibility of oversaturation is poorly understood on a global scale, and to develop a deeper understanding of the feasibility of enhanced carbonate weathering more study is needed to understand this phenomenon.

Data availability statement

The original contributions presented in the study are included in the article/Supplementary material, further inquiries can be directed to the corresponding author.

Author contributions

WK contributed to the conception, modeling, and writing of this manuscript. ET contributed to the conception and writing of this manuscript. Both authors contributed to the article and approved the final submission.

Funding

This study was funded by a UKRI grant [NE/S007164/1]. WK acknowledges funding from NERC studentship NE/S007164/1. ET acknowledges funding from NERC grants NE/T007214/1, NE/P011659/1, and NE/M001865/1.

Acknowledgments

We thank Emily Stevenson, Luke Bridgestock, Mike Bickle, and Alasdair Knight for helpful discussions and two anonymous reviewers.

Conflict of interest

The authors declare that the research was conducted in the absence of any commercial or financial relationships that could be construed as a potential conflict of interest.

Publisher's note

All claims expressed in this article are solely those of the authors and do not necessarily represent those of their affiliated organizations, or those of the publisher, the editors and the reviewers. Any product that may be evaluated in this article, or claim that may be made by its manufacturer, is not guaranteed or endorsed by the publisher.

Supplementary material

The Supplementary Material for this article can be found online at: https://www.frontiersin.org/articles/10.3389/fclim.2022.928215/full#supplementary-material

References

Andrews, M. G., and Taylor, L. L. (2019). Combating climate change through enhanced weathering of agricultural soils. *Elements* 15, 253–258. doi: 10.2138/gselements.15.4.253

Archer, D. (1996). A data-driven model of the global calcite lysocline. *Glob. Biogeochem. Cycles* 10, 511–526. doi: 10.1029/96GB01521

Archer, D., Kheshgi, H., and Maier-Reimer, E. (1997). Multiple timescales for neutralization of fossil fuel CO_2. *Geophys. Res. Lett.* 24, 405–408. doi: 10.1029/97GL00168

Arino, O., Bicheron, P., Achard, F., Latham, J., Witt, R., and Weber, J.-L. (2008). The most detailed portrait of earth. Eur. *Space Agency* 136, 25–31. doi: 10.1109/IGARSS.2007.4423328

Astilleros, J., Fernández-Díaz, L., and Putnis, A. (2010). The role of magnesium in the growth of calcite: an afm study. *Chem. Geol.* 271, 52–58. doi: 10.1016/j.chemgeo.2009.12.011

Berner, E. K., and Berner, R. A. (2012). *Global Environment: Water, Air, and Geochemical Cycles*. Princeton, NJ: Princeton University Press.

Biasi, C., Lind, S. E., Pekkarinen, N. M., Huttunen, J. T., Shurpali, N. J., Hyvönen, N. P., et al. (2008). Direct experimental evidence for the contribution of lime to CO_2 release from managed peat soil. *Soil Biol. Biochem.* 40, 2660–2669. doi: 10.1016/j.soilbio.2008.07.011

Bickle, M. J., Tipper, E., Galy, A., Chapman, H., and Harris, N. (2015). On discrimination between carbonate and silicate inputs to himalayan rivers. *Am. J. Sci.* 315, 120–166. doi: 10.2475/02.2015.02

Blagodatsky, S., and Smith, P. (2012). Soil physics meets soil biology: towards better mechanistic prediction of greenhouse gas emissions from soil. *Soil Biol. Biochem.* 47, 78–92. doi: 10.1016/j.soilbio.2011.12.015

Bolan, N. S., and Duraisamy, V. (2003). Role of inorganic and organic soil amendments on immobilisation and phytoavailability of heavy metals: a review involving specific case studies. *Soil Res.* 41, 533–555. doi: 10.1071/SR02122

Brantley, S. L., Kubicki, J. D., and White, A. F. (2008). *Kinetics of Water-Rock Interaction*. New York, NY: Springer.

Braun, J.-J., Ngoupayou, J. R. N., Viers, J., Dupre, B., Bedimo, J.-P. B., Boeglin, J.-L., et al. (2005). Present weathering rates in a humid tropical watershed: Nsimi, south cameroon. *Geochim. Cosmochim. Acta* 69, 357–387. doi: 10.1016/j.gca.2004.06.022

Caldeira, K., and Rau, G. H. (2000). Accelerating carbonate dissolution to sequester carbon dioxide in the ocean: geochemical implications. *Geophys. Res. Lett.* 27, 225–228. doi: 10.1029/1999GL002364

Calmels, D., Gaillardet, J., Brenot, A., and France-Lanord, C. (2007). Sustained sulfide oxidation by physical erosion processes in the mackenzie river basin: climatic perspectives. *Geology*. 35, 1003–1006. doi: 10.1130/G24132A.1

Calmels, D., Gaillardet, J., and François, L. (2014). Sensitivity of carbonate weathering to soil CO_2 production by biological activity along a temperate climate transect. *Chem. Geol.* 390, 74–86. doi: 10.1016/j.chemgeo.2014.10.010

Chou, L., Garrels, R. M., and Wollast, R. (1989). Comparative study of the kinetics and mechanisms of dissolution of carbonate minerals. *Chem. Geol.* 78, 269–282. doi: 10.1016/0009-2541(89)90063-6

Connor, D. J., Loomis, R. S., and Cassman, K. G. (2011). *Crop Ecology: Productivity and Management in Agricultural Systems*. Cambridge: Cambridge University Press.

Dandurand, J., Gout, R., Hoefs, J., Menschel, G., Schott, J., and Usdowski, E. (1982). Kinetically controlled variations of major components and carbon and oxygen isotopes in a calcite-precipitating spring. *Chem. Geol.* 36, 299–315. doi: 10.1016/0009-2541(82)90053-5

Dobberschütz, S., Nielsen, M., Sand, K., Civioc, R., Bovet, N., Stipp, S., et al. (2018). The mechanisms of crystal growth inhibition by organic and inorganic inhibitors. *Nat. Commun.* 9, 1–6. doi: 10.1038/s41467-018-04022-0

Drever, J. I. (1988). *The Geochemistry of Natural Waters, Vol. 437*. Englewood Cliffs, NJ: Prentice Hall.

Dreybrodt, W., Buhmann, D., Michaelis, J., and Usdowski, E. (1992). Geochemically controlled calcite precipitation by CO_2 outgassing: field measurements of precipitation rates in comparison to theoretical predictions. *Chem. Geol.* 97, 285–294. doi: 10.1016/0009-2541(92)90082-G

Erlanger, E., Rugenstein, J., Bufe, A., Picotti, V., and Willett, S. (2021). Controls on physical and chemical denudation in a mixed carbonate-siliciclastic orogen. *J. Geophys. Res.* 126, e2021JF006064. doi: 10.1002/essoar.10505807.1

Fekete, B. M., Vörösmarty, C. J., and Grabs, W. (2002). High-resolution fields of global runoff combining observed river discharge and simulated water balances. *Glob. Biogeochem. Cycles* 16, 15–11. doi: 10.1029/1999GB001254

Fick, S. E., and Hijmans, R. J. (2017). Worldclim 2: new 1-km spatial resolution climate surfaces for global land areas. *Int. J. Climatol.* 37, 4302–4315. doi: 10.1002/joc.5086

Ford, T., and Pedley, H. (1996). A review of tufa and travertine deposits of the world. *Earth Sci. Rev.* 41, 117–175. doi: 10.1016/S0012-8252(96)00030-X

Friedlingstein, P., O'sullivan, M., Jones, M. W., Andrew, R. M., Hauck, J., Olsen, A., et al. (2020). Global carbon budget 2020. *Earth Syst. Sci. Data* 12, 3269–3340. doi: 10.5194/essd-12-3269-2020

Gaillardet, J., Calmels, D., Romero-Mujalli, G., Zakharova, E., and Hartmann, J. (2019). Global climate control on carbonate weathering intensity. *Chem. Geol.* 527, 118762. doi: 10.1016/j.chemgeo.2018.05.009

Gaillardet, J., Dupre, B., Allegre, C. J., and Négrel, P. (1997). Chemical and physical denudation in the amazon river basin. *Chem. Geol.* 142, 141–173. doi: 10.1016/S0009-2541(97)00074-0

Gaillardet, J., Dupré, B., Louvat, P., and Allegre, C. (1999). Global silicate weathering and CO_2 consumption rates deduced from the chemistry of large rivers. *Chem. Geol.* 159, 3–30. doi: 10.1016/S0009-2541(99)00031-5

Galy, A., France-Lanord, C., and Derry, L. A. (1999). The strontium isotopic budget of himalayan rivers in nepal and bangladesh. *Geochim. Cosmochim. Acta* 63, 1905–1925. doi: 10.1016/S0016-7037(99)00081-2

Goldscheider, N. (2005). Karst groundwater vulnerability mapping: application of a new method in the swabian alb, germany. *Hydrogeol. J.* 13, 555–564. doi: 10.1007/s10040-003-0291-3

GRDC. (2020). *Major River Basins of the World / Global Runoff Data Centre, GRDC, 2nd Revised Edn*. Koblenz: Federal Institute of Hydrology (BfG).

Griffioen, J. (2017). Enhanced weathering of olivine in seawater: the efficiency as revealed by thermodynamic scenario analysis. *Sci. Total Environ.* 575, 536–544. doi: 10.1016/j.scitotenv.2016.09.008

Hamilton, S. K., Kurzman, A. L., Arango, C., Jin, L., and Robertson, G. P. (2007). Evidence for carbon sequestration by agricultural liming. *Glob. Biogeochem. Cycles* 21, 2738. doi: 10.1029/2006GB002738

Haque, F., Santos, R. M., Dutta, A., Thimmanagari, M., and Chiang, Y. W. (2019). Co-benefits of wollastonite weathering in agriculture: CO_2 sequestration and promoted plant growth. *ACS Omega* 4, 1425–1433. doi: 10.1021/acsomega.8b02477

Hartmann, J., Lauerwald, R., and Moosdorf, N., (2014). A brief overview of the global river chemistry database, GLORICH. *Procedia Earth Planet. Sci.* 10, 23–27. doi: 10.1016/j.proeps.2014.08.005

Hartmann, J., West, A. J., Renforth, P., Köhler, P., De La Rocha, C. L., Wolf-Gladrow, D. A., et al. (2013). Enhanced chemical weathering as a geoengineering strategy to reduce atmospheric carbon dioxide, supply nutrients, and mitigate ocean acidification. *Rev. Geophys.* 51, 113–149. doi: 10.1002/rog.20004

Haynes, R. (1982). Effects of liming on phosphate availability in acid soils. *Plant Soil.* 68, 289–308. doi: 10.1007/BF02197935

Herman, J. S., and Lorah, M. M. (1987). CO_2 outgassing and calcite precipitation in falling spring creek, virginia, usa. *Chem. Geol.* 62, 251–262. doi: 10.1016/0009-2541(87)90090-8

Houghton, J. T., Filho, L. G. M., Lim, B., Treanton, K., and Mamaty, I. (1997). *Revised 1996 IPCC Guidelines for National Greenhouse Gas Inventories*. v. 1: Greenhouse gas Inventory Reporting Instructions.-v. 2: Greenhouse Gas Inventory Workbook.-v. 3: Greenhouse Gas Inventory Reference Manual. Bracknell.

Hudson, W. R., Little, D. N., Razmi, A. M., Anderson, V., and Weissmann, A. J. (1997). *An investigation of the status of by-product fines in the united states*. Technical report, University of Texas at Austin. International Center for Aggregates Research.

Ilstedt, U., Nordgren, A., and Malmer, A. (2000). Optimum soil water for soil respiration before and after amendment with glucose in humid tropical acrisols and a boreal mor layer. *Soil Biol. Biochem.* 32, 1591–1599. doi: 10.1016/S0038-0717(00)00073-0

Kelemen, P. B., Matter, J., Streit, E. E., Rudge, J. F., Curry, W. B., and Blusztajn, J. (2011). Rates and mechanisms of mineral carbonation in peridotite: natural processes and recipes for enhanced, in situ CO_2 capture and storage. *Annu. Rev. Earth Planet. Sci.* 39, 545–576. doi: 10.1146/annurev-earth-092010-152509

Köhler, P., Hartmann, J., and Wolf-Gladrow, D. A. (2010). Geoengineering potential of artificially enhanced silicate weathering of olivine. *Proc. Natl. Acad. Sci. U.S.A.* 107, 20228–20233. doi: 10.1073/pnas.1000545107

Lacelle, D. (2007). Environmental setting, (micro) morphologies and stable c-o isotope composition of cold climate carbonate precipitatesa review and evaluation of their potential as paleoclimatic proxies. *Quat. Sci. Rev.* 26, 1670–1689. doi: 10.1016/j.quascirev.2007.03.011

Lackner, K. S., Wendt, C. H., Butt, D. P., Joyce Jr, E. L., and Sharp, D. H. (1995). Carbon dioxide disposal in carbonate minerals. *Energy* 20, 1153–1170. doi: 10.1016/0360-5442(95)00071-N

Lassaletta, L., Billen, G., Grizzetti, B., Anglade, J., and Garnier, J. (2014). 50 year trends in nitrogen use efficiency of world cropping systems: the relationship between yield and nitrogen input to cropland. *Environ. Res. Lett.* 9, 105011. doi: 10.1088/1748-9326/9/10/105011

Lauerwald, R., Laruelle, G. G., Hartmann, J., Ciais, P., and Regnier, P. A. (2015). Spatial patterns in CO_2 evasion from the global river network. *Glob. Biogeochem. Cycles* 29, 534–554. doi: 10.1002/2014GB004941

Lloyd, J., and Taylor, J. (1994). On the temperature dependence of soil respiration. *Funct. Ecol.* 8, 315–323. doi: 10.2307/2389824

Mann, S. (1988). Molecular recognition in biomineralization. *Nature* 332, 119–124. doi: 10.1038/332119a0

Marion, G. M., Mironenko, M. V., and Roberts, M. W. (2010). Frezchem: a geochemical model for cold aqueous solutions. *Comput. Geosci.* 36, 10–15. doi: 10.1016/j.cageo.2009.06.004

Meybeck, M., and Ragu, A. (2012). *GEMS-GLORI World River Discharge Database*. Paris: Laboratoire de Géologie Appliquée; Université Pierre et Marie Curie. doi: 10.1594/PANGAEA.804574

Millot, R., érôme Gaillardet, J., Dupré, B., and Allègre, C. J. (2003). Northern latitude chemical weathering rates: clues from the mackenzie river basin, canada. *Geochim. Cosmochim. Acta* 67, 1305–1329. doi: 10.1016/S0016-7037(02)01207-3

Montserrat, F., Renforth, P., Hartmann, J., Leermakers, M., Knops, P., and Meysman, F. J. (2017). Olivine dissolution in seawater: implications for CO_2 sequestration through enhanced weathering in coastal environments. *Environ. Sci. Technol.* 51, 3960–3972. doi: 10.1021/acs.est.6b05942

Moosdorf, N., Renforth, P., and Hartmann, J. (2014). Carbon dioxide efficiency of terrestrial enhanced weathering. *Environ. Sci. Technol.* 48, 4809–4816. doi: 10.1021/es4052022

Motavalli, P., Palm, C., Parton, W., Elliott, E., and Frey, S. (1995). Soil ph and organic c dynamics in tropical forest soils: evidence from laboratory and simulation studies. *Soil Biol. Biochem.* 27, 1589–1599. doi: 10.1016/0038-0717(95)00082-P

Narbarte-Hernandez, J., Iriarte, E., Carrancho-Alonso, Á., Olazabal-Uzkudun, A., Rad, C., Arriolabengoa, M., et al. (2021). Geochemical fingerprint of agricultural liming as a regular management practice in modern-period basque farming. *Sci. Total Environ.* 787, 147525. doi: 10.1016/j.scitotenv.2021.147525

Oh, N.-H., and Raymond, P. A. (2006). Contribution of agricultural liming to riverine bicarbonate export and CO_2 sequestration in the ohio river basin. *Glob. Biogeochem. Cycles*. 20, 2265. doi: 10.1029/2005GB002565

Oshunsanya, S. (2019). *Soil pH for Nutrient Availability and Crop Performance*. London: IntechOpen. doi: 10.5772/68057

Parkhurst, D. L., and Appelo, C. (2013). Description of input and examples for phreeqc version 3 computer program for speciation, batch-reaction, one-dimensional transport, and inverse geochemical calculations. *US Geol. Survey Techn. Methods* 6, 497. doi: 10.3133/tm6A43

Plummer, L. N., Parkhurst, D. L., and Wigley, T. M. L. (1979). Critical review of the kinetics of calcite dissolution and precipitation. *Chem. Modell. Aqueous Syst.* 93, 537–573.

Pogge von Strandmann, P. A., Tooley, C., Mulders, J. J., and Renforth, P. (2022). The dissolution of olivine added to soil at 4°C: Implications for enhanced weathering in cold regions. *Front. Climate* 8, 827698. doi: 10.3389/fclim.2022.827698

Rau, G. H., and Caldeira, K. (1999). Enhanced carbonate dissolution:: a means of sequestering waste CO_2 as ocean bicarbonate. *Energy Convers. Manag.* 40, 1803–1813. doi: 10.1016/S0196-8904(99)00071-0

Rau, G. H., Knauss, K. G., Langer, W. H., and Caldeira, K. (2007). Reducing energy-related CO_2 emissions using accelerated weathering of limestone. *Energy* 32, 1471–1477. doi: 10.1016/j.energy.2006.10.011

Raymond, P. A., Hartmann, J., Lauerwald, R., Sobek, S., McDonald, C., Hoover, M., et al. (2013). Global carbon dioxide emissions from inland waters. *Nature* 503, 355–359. doi: 10.1038/nature12760

Relph, K. E., Stevenson, E. I., Turchyn, A. V., Antler, G., Bickle, M. J., Baronas, J. J., et al. (2021). Partitioning riverine sulfate sources using oxygen and sulfur isotopes: implications for carbon budgets of large rivers. *Earth Planet Sci. Lett.* 567, 116957. doi: 10.1016/j.epsl.2021.116957

Renforth, P. (2019). The negative emission potential of alkaline materials. *Nat. Commun.* 10, 1401. doi: 10.1038/s41467-019-09475-5

Renforth, P., von Strandmann, P. P., and Henderson, G. (2015). The dissolution of olivine added to soil: implications for enhanced weathering. *Appl. Geochem.* 61, 109–118. doi: 10.1016/j.apgeochem.2015.05.016

Ridgwell, A., and Hargreaves, J. (2007). Regulation of atmospheric CO_2 by deep-sea sediments in an earth system model. *Glob. Biogeochem. Cycles* 21, 2764. doi: 10.1029/2006GB00 2764

Rigopoulos, I., Harrison, A. L., Delimitis, A., Ioannou, I., Efstathiou, A. M., Kyratsi, T., et al. (2018). Carbon sequestration via enhanced weathering of peridotites and basalts in seawater. *Appl. Geochem.* 91, 197–207. doi: 10.1016/j.apgeochem.2017.11.001

Rogerson, M., Pedley, H., Kelham, A., and Wadhawan, J. (2014). Linking mineralisation process and sedimentary product in terrestrial carbonates using a solution thermodynamic approach. *Earth Surface Dyn.* 2, 197–216. doi: 10.5194/esurf-2-197-2014

Romero-Mujalli, G., Hartmann, J., and Börker, J. (2019a). Temperature and CO_2 dependency of global carbonate weathering fluxes-implications for future carbonate weathering research. *Chem. Geol.* 527, 118874. doi: 10.1016/j.chemgeo.2018.08.010

Romero-Mujalli, G., Hartmann, J., Börker, J., Gaillardet, J., and Calmels, D. (2019b). Ecosystem controlled soil-rock CO_2 and carbonate weathering-constraints by temperature and soil water content. *Chem. Geol.* 527, 118634. doi: 10.1016/j.chemgeo.2018.01.030

Roy, S., Gaillardet, J., and Allegre, C. (1999). Geochemistry of dissolved and suspended loads of the seine river, france: anthropogenic impact, carbonate and silicate weathering. *Geochim. Cosmochim. Acta* 63, 1277–1292. doi: 10.1016/S0016-7037(99)00099-X

Schuiling, R., and Krijgsman, P. (2006). Enhanced weathering: an effective and cheap tool to sequester CO_2. *Clim. Change* 74, 349–354. doi: 10.1007/s10584-005-3485-y

Schuiling, R., and Tickell, O. (2010). Enhanced weathering of olivine to capture CO_2. *J. Appl. Geochem.* 12, 510–519.

Seifritz, W. (1990). CO_2 disposal by means of silicates. *Nature* 345, 486–486. doi: 10.1038/345486b0

Shi, Z., Allison, S. D., He, Y., Levine, P. A., Hoyt, A. M., Beem-Miller, J., et al. (2020). The age distribution of global soil carbon inferred from radiocarbon measurements. *Nat. Geosci.* 13, 555–559. doi: 10.1038/s41561-020-0596-z

Taylor, L. L., Quirk, J., Thorley, R., Kharecha, P. A., Hansen, J., Ridgwell, A., et al. (2016). Enhanced weathering strategies for stabilizing climate and averting ocean acidification. *Nat. Clim. Chang* 6, 402–406. doi: 10.1038/nclimate2882

Thomazo, C., Buoncristiani, J.-F., Vennin, E., Pellenard, P., Cocquerez, T., Mugnier, J. L., et al. (2017). Geochemical processes leading to the precipitation of subglacial carbonate crusts at bossons glacier, mont blanc massif (french alps). *Front. Earth Sci.* 5, 70. doi: 10.3389/feart.2017.00070

Tipper, E. T., Bickle, M. J., Galy, A., West, A. J., Pomiès, C., and Chapman, H. J. (2006). The short term climatic sensitivity of carbonate and silicate weathering fluxes: insight from seasonal variations in river chemistry. *Geochim. Cosmochim. Acta* 70, 2737–2754. doi: 10.1016/j.gca.2006.03.005

Tipper, E. T., Gaillardet, J., Galy, A., Louvat, P., Bickle, M., and Capmas, F. (2010). Calcium isotope ratios in the world's largest rivers: a constraint on the maximum imbalance of oceanic calcium fluxes. *Glob. Biogeochem. Cycles* 24, 3574. doi: 10.1029/2009GB003574

Torres, M. A., West, A. J., Clark, K. E., Paris, G., Bouchez, J., Ponton, C., et al. (2016). The acid and alkalinity budgets of weathering in the andes-amazon system: Insights into the erosional control of global biogeochemical cycles. *Earth Planet Sci. Lett.* 450, 381–391. doi: 10.1016/j.epsl.2016.06.012

Trumbore, S. E., Chadwick, O. A., and Amundson, R. (1996). Rapid exchange between soil carbon and atmospheric carbon dioxide driven by temperature change. *Science* 272, 393–396. doi: 10.1126/science.272.5260.393

Tunney, H., Sikora, F., Kissel, D., Wolf, A., Sonon, L., and Goulding, K. (2010). A comparison of lime requirements by five methods on grassland mineral soils in ireland. *Soil Use Manag.* 26, 126–132. doi: 10.1111/j.1475-2743.2010.00263.x

West, A. J., Galy, A., and Bickle, M. (2005). Tectonic and climatic controls on silicate weathering. *Earth Planet Sci. Lett.* 235, 211–228. doi: 10.1016/j.epsl.2005.03.020

West, T. O., and McBride, A. C. (2005). The contribution of agricultural lime to carbon dioxide emissions in the united states: dissolution, transport, and net emissions. *Agric. Ecosyst. Environ.* 108, 145–154. doi: 10.1016/j.agee.2005.01.002

White, A. F., and Brantley, S. L. (2018). *Chemical Weathering Rates of Silicate Minerals*. Berlin; Boston, MA: De Gruyter. doi: 10.1515/9781501509650

Yan, H., Liu, Z., and Sun, H. (2020). Large degrees of carbon isotope disequilibrium during precipitation-associated degassing of CO_2 in a mountain stream. *Geochim. Cosmochim.Acta* 273, 244–256. doi: 10.1016/j.gca.2020.01.012

Zamanian, K., Pustovoytov, K., and Kuzyakov, Y. (2016). Pedogenic carbonates: Forms and formation processes. *Earth Sci. Rev.* 157, 1–17. doi: 10.1016/j.earscirev.2016.03.003

Zbieranowski, A. L., and Aherne, J. (2013). Ambient concentrations of atmospheric ammonia, nitrogen dioxide and nitric acid in an intensive agricultural region. *Atmos Environ.* 70, 289–299. doi: 10.1016/j.atmosenv.2013.01.023

Zeng, S., Kaufmann, G., and Liu, Z. (2022a). Natural and anthropogenic driving forces of carbonate weathering and the related carbon sink flux: a model comparison study at global scale. *Glob. Biogeochem. Cycles* 36, e2021GB007096. doi: 10.1029/2021GB007096

Zeng, S., Liu, Z., and Groves, C. (2022b). Large-scale CO_2 removal by enhanced carbonate weathering from changes in land-use practices. *Earth Sci. Rev.* 225, 103915. doi: 10.1016/j.earscirev.2021.103915

frontiers | Frontiers in Climate

TYPE Original Research
PUBLISHED 30 August 2022
DOI 10.3389/fclim.2022.959229

OPEN ACCESS

EDITED BY
Etsushi Kato,
Institute of Applied Energy, Japan

REVIEWED BY
Thorben Amann,
University of Hamburg, Germany
Fatima Haque,
National Taiwan University, Taiwan

*CORRESPONDENCE
Christina S. Larkin
c.s.larkin@soton.ac.uk

SPECIALTY SECTION
This article was submitted to Negative Emission Technologies, a section of the journal Frontiers in Climate

RECEIVED 01 June 2022
ACCEPTED 11 August 2022
PUBLISHED 30 August 2022

CITATION
Larkin CS, Andrews MG, Pearce CR, Yeong KL, Beerling DJ, Bellamy J, Benedick S, Freckleton RP, Goring-Harford H, Sadekar S and James RH (2022) Quantification of CO_2 removal in a large-scale enhanced weathering field trial on an oil palm plantation in Sabah, Malaysia. *Front. Clim.* 4:959229. doi: 10.3389/fclim.2022.959229

Quantification of CO_2 removal in a large-scale enhanced weathering field trial on an oil palm plantation in Sabah, Malaysia

Christina S. Larkin[1]*, M. Grace Andrews[1], Christopher R. Pearce[2], Kok L. Yeong[3], David J. Beerling[3], Joshua Bellamy[1], Suzan Benedick[4], Robert P. Freckleton[3], Heather Goring-Harford[1], Satyam Sadekar[1] and Rachael H. James[1]

[1]School of Ocean and Earth Sciences, University of Southampton, Southampton, United Kingdom, [2]National Oceanography Centre, Southampton, United Kingdom, [3]Leverhulme Centre for Climate Change Mitigation, School of Biosciences, University of Sheffield, Sheffield, United Kingdom, [4]Faculty of Sustainable Agriculture, Universiti Malaysia Sabah, Kota Kinabalu, Malaysia

Modeling studies show that large-scale deployment of enhanced rock weathering on croplands has the potential to reduce levels of atmospheric carbon dioxide by the end of the century. There is, however, a pressing need to verify model predictions through long-term field trials. Here we report results from the first 3 years of an ongoing enhanced weathering field trial, carried out on an oil palm plantation in Sabah, Malaysia. Crushed silicate rock was applied to three hydrologically isolated catchments, and three adjacent (paired) reference catchments were left untreated. The drawdown of atmospheric CO_2 was quantified via the export of alkalinity in stream waters and changes in soil carbonate content. The amended and reference catchments were found to have a similar extent of CO_2 drawdown via alkalinity export [respectively, 3.8 ± 0.8 (1 SD) and 3.7 ± 0.6 (1 SD) tCO_2 ha^{-1}] when all catchments were averaged over the study period (October 2018 to July 2021). However, differences were observed between the different catchment pairs (plots): two of the plots displayed a similar extent of CO_2 removal for both the amended and reference catchments, but the third amended catchment had a higher extent of CO_2 removal of ~1 tCO_2 ha^{-1} relative to its adjacent reference catchment. The difference in CO_2 removal rates determined for this plot can likely be attributed to increased weathering of silicate minerals in the amended catchment. Soil carbonate concentrations were on average < 0.2 wt% $CaCO_3$, but we report a small increase of ~0.03 wt% $CaCO_3$ in the top 30 cm of soil in the amended soils relative to the reference catchments. The magnitude of CO_2 drawdown via alkalinity export determined for these agricultural catchments is around an order of magnitude higher than in natural forested catchments

in Sabah and similar to that of basaltic catchments. We show that these high weathering rates are primarily driven by weathering of carbonate fertilizers. The data presented from this field trial provide vital contextual information on the real-world efficacy and practicalities associated with the implementation of enhanced weathering for atmospheric CO_2 removal that will help to inform further trials as well as wider-scale deployment.

KEYWORDS

climate change mitigation, enhanced weathering, tropical croplands, carbon dioxide removal, oil palm

Introduction

To keep current global warming below dangerous levels (<2°C above pre-industrial), it is widely accepted that in addition to significant emissions reductions, carbon dioxide (CO_2) will need to be actively removed from the atmosphere (UN Environment Programme, 2017; Royal Society, 2018). This is because between about 4 and 8% of global CO_2 emissions are "hard to avoid," either because some industries are difficult to decarbonize (such as agriculture), or because of the need to uphold principles of justice including the protection of human rights (UN Environment Programme, 2017; Royal Society, 2018; IPCC, 2022).

Carbon dioxide can be removed from the atmosphere in several ways. These include nature-based methods such as afforestation and restoration of coastal habitats including mangroves and sea grass beds, as well as technological methods such as direct air capture (e.g., IPCC, 2022). Enhancing rates of rock weathering, which naturally removes about 1 Gt of CO_2 from the atmosphere every year and plays a key role in the long-term ($>10^5$ yrs) regulation of Earth's climate (e.g., Walker et al., 1981), is another proposed CO_2 removal strategy (e.g., Hartmann et al., 2013). Modeling studies have shown that the application of crushed calcium (Ca)- and magnesium (Mg)-rich silicate rocks to agricultural soils has the potential to increase weathering rates and draw down 0.5–2 Gt of CO_2 per year, equivalent to ~2.5% to 10% of Paris Agreement targets (Beerling et al., 2020). The quantity of additional CO_2 removed depends on factors such as application rate, climatic conditions, mineralogy and grain size (Schuiling and Krijgsman, 2006; Renforth, 2012; Hartmann et al., 2013; Taylor et al., 2016; Andrews and Taylor, 2019).

Weathering is a natural geological process whereby atmospheric CO_2 dissolved in rainwater or respired by plants reacts with rocks and soils, partly dissolving them (Equation 1 and Equation 2). During the weathering process, CO_2 is converted to alkalinity (principally hydrogen carbonate ions) that is transported via soil waters, groundwaters and rivers to the ocean, where it may be securely stored on timescales of $\sim 10^5$ years (e.g., Drever, 1997).

$$\overbrace{2CO_{2(aq)} + 3H_2O}^{rainwater} + \overbrace{CaAl_2Si_2O_8}^{\substack{silicate\ mineral\\(anorthite)}} \rightarrow \overbrace{2HCO_3^- + Ca^{2+}}^{soil\ water} + \overbrace{Al_2Si_2O_5(OH)_{4(s)}}^{\substack{clay\ (kaolinite)\\retained\ in\ soils}} \quad (1)$$

$$\overbrace{CO_{2(aq)} + H_2O}^{rainwater} + \overbrace{CaCO_3}^{\substack{carbonate\\mineral}} \rightarrow \overbrace{2HCO_3^- + Ca^{2+}}^{soil\ water} \quad (2)$$

Equation 1 shows that weathering of one mole of a silicate mineral (anorthite) removes two moles of atmospheric CO_2 whereas weathering of one mole of carbonate minerals removes only one mole of atmospheric CO_2 (Equation 2). However, although silicate weathering is twice as effective at removing CO_2 from the atmosphere compared to carbonate weathering, dissolution rates of carbonates are three orders of magnitude faster than those of fastest weathering silicate minerals (e.g., Lasaga, 1984; Hartmann et al., 2013). In arid to semi-arid regions were soils are alkaline carbonate minerals may precipitate from soil waters (Equation 3) forming pedogenic carbonate that is stable on timescales of $\sim 10^4$ years (e.g., Zamanian et al., 2016 and references therein). Note that precipitation of carbonates re-releases half of the CO_2 captured by silicate minerals back into the atmosphere, and dissolution and re-precipitation of carbonate minerals has no net impact on levels of atmospheric CO_2 (i.e., Equation 3 is the reverse of Equation 2).

$$\overbrace{2HCO_3^- + Ca^{2+}}^{soil\ water} \rightarrow \overbrace{CO_2 + H_2O}^{soil\ water} + \overbrace{CaCO_{3(s)}}^{soils} \quad (3)$$

Rates of rock weathering are limited by the reactivity of the minerals that make up the rock. For example, olivine and basaltic glass have fast dissolution rates (e.g., Oelkers and Gislason, 2001; Oelkers et al., 2018), whereas quartz is unreactive and has no

CO_2 removal potential (e.g., Kump et al., 2000). Weathering rates also vary as a function of particle size, with mineral crushing or high erosion rates potentially leading to greater chemical dissolution rates (Riebe et al., 2004). In addition to the availability of weatherable minerals, weathering rates are also controlled by environmental factors (kinetics), such as temperature and water availability, and the saturation state of the soil waters (West et al., 2005; Gabet and Mudd, 2009; Maher and Chamberlain, 2014). Lowland tropical regions are considered to have the fastest potential weathering rates on Earth due to high temperatures and high rainfall, but weathering can be limited by supply of fresh minerals (Stallard and Edmond, 1983) as thick heavily weathered soils develop quickly (e.g., laterites). For this reason, tropical regions are considered prime candidates for the deployment of enhanced weathering (Taylor et al., 2016; Edwards et al., 2017; Manning et al., 2017; Beerling et al., 2018, 2020).

To date, the potential of enhanced weathering for removing atmospheric CO_2 has principally been estimated using modeling studies (e.g., Renforth, 2012; Taylor et al., 2016; Beerling et al., 2020; Bullock et al., 2021), or based on results from small-scale mesocosm or laboratory experiments (e.g., Renforth et al., 2015; Amann et al., 2020; Kelland et al., 2020; Pogge von Strandmann et al., 2021). Most mesocosm and laboratory studies to date have focused on amending soils with relatively fast weathering silicate minerals, notably olivine, or fast weathering silicate rocks, such as dunite that contains a high proportion of olivine. While experiments on organic-rich acidic soils incubated with olivine revealed that gross removal of CO_2 assessed from the increase in Mg^{2+} concentrations on soil exchangeable sites was between ∼12 to 16 $tCO_2\ ha^{-1}yr^{-1}$ (depending on the olivine application rate), no net increase in CO_2 removal was observed due to increased rates of soil respiration (Dietzen et al., 2018). Similarly, application of olivine to ryegrass in a pot experiment was observed to increase gross CO_2 uptake by ∼0.5–4.4 $tCO_2\ ha^{-1}yr^{-1}$ (Berge et al., 2012), although amendment of agricultural soils (with and without crops) with olivine-bearing dunite showed significantly lower rates of CO_2 removal (0.02–0.05 $tCO_2\ ha^{-1}\ yr^{-1}$; Amann et al., 2020). Finally, pot experiments focusing on soil amendment with wollastonite (a fast-weathering silicate mineral) reported substantial increases (of up to ∼0.6 wt%) in the total inorganic carbon content of wollastonite-amended soil relative to untreated soil over a period of 8 weeks (Haque et al., 2019). Assuming a till depth of 30 cm and sustained inorganic carbon accumulation rates, this could correspond to a removal rate of up to ∼500 $tCO_2\ ha^{-1}\ yr^{-1}$.

At larger scales, only a handful of field trial studies have been carried out on the CO_2 removal potential of enhanced rock weathering (Haque et al., 2020; Taylor et al., 2021). In October 1999, in an effort to restore soil calcium that had been depleted by leaching by acid rain, 3.44 t ha^{-1} of wollastonite was applied to the Hubbard Brook Experimental Forest watershed in New Hampshire, USA. A recent re-analysis of stream water chemistry has revealed that cumulative carbon capture by carbonic acid weathering increased by 0.025–0.13 $tCO_2\ ha^{-1}$ over 15 years compared to a reference catchment (Taylor et al., 2021). A study of wollastonite-amended croplands in Ontario, Canada, has reported increased levels of CO_2 removal as soil inorganic carbon by up to 0.4 $tCO_2\ ha^{-1}$ over 5 months in a field planted with soybean; much higher rates of CO_2 removal as soil inorganic carbon were observed in fields planted with leafy vegetables (up to ∼1.9 $tCO_2\ ha^{-1}$ in 1 year) although this may partly be due to addition of carbonate fertilizers (Haque et al., 2020). Notwithstanding the differences in the results between these field studies, models and laboratory experiments are unlikely to adequately represent the natural system and laboratory experiments in particular have been shown to overestimate field weathering rates (e.g., White and Brantley, 2003). Therefore, it is imperative to conduct large-scale, multi-year field trials to determine the real-world efficacy and safety of enhanced rock weathering, as well as the practicalities associated with its deployment.

This study presents the first quantification of the rate of CO_2 drawdown via alkalinity generation as well as soil carbonate formation from an ongoing enhanced rock weathering field trial being conducted on an oil palm plantation in Sabah, Malaysia. As far as we are aware, this is the first field trial of its kind in a tropical region. We set out a methodology for accurately quantifying CO_2 removal via alkalinity generation that attributes (i) the weathering source (silicate vs. carbonate minerals) and (ii) the weathering agent (carbonic acid vs. strong acids that do not contribute to carbon dioxide removal) and discuss the challenges with quantifying carbon dioxide removal via soil carbonate formation in low pH tropical soils. The results from this ongoing field trial provide vital contextual information for the application of enhanced weathering in tropical environments.

Study site and experiment overview

Here we provide a general overview of the experiment and study site, with further analytical details given under Materials and Methods and in Supplementary Text 1. Our study site is located on an oil palm plantation in Sabah, Malaysia (Figure 1) and is characterized by a tropical climate with an annual rainfall of ∼2,000 mm and a mean annual temperature of ∼28°C (monitored by the onsite weather station, Supplementary Text 1, Figure 2). The plantation sits on heavily weathered tropical soils that are underlain by Oligocene to mid Miocene volcaniclastic deposits and Quaternary river alluvium (Lim, 1985). The oil palms are planted in terraces as the site has significant topography (Figure 1, ∼100 to 400 m elevation range).

Three plots were selected within the plantation. Each of the three plots consists of a pair of hydrologically

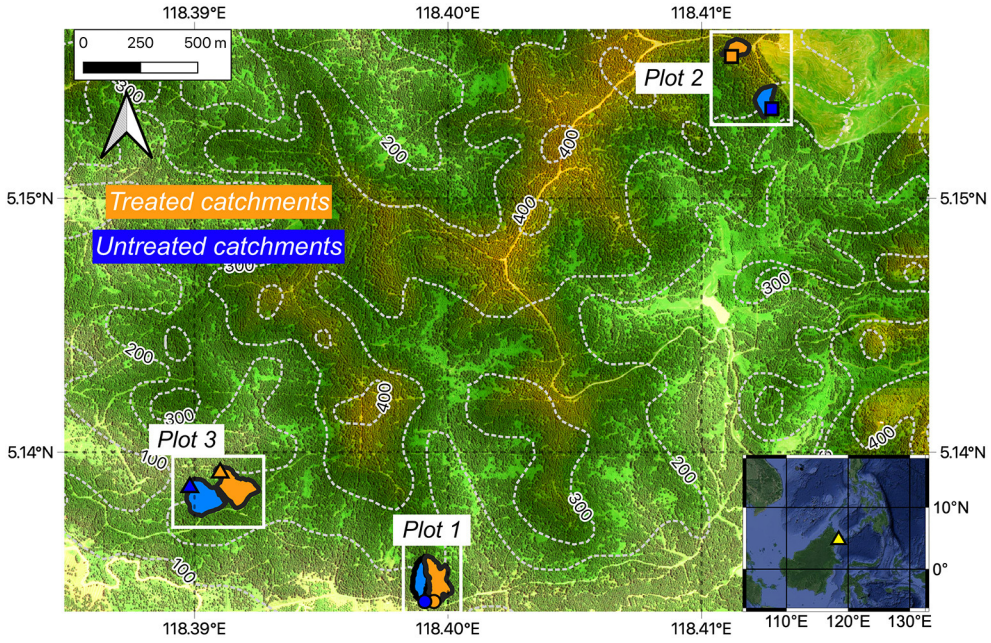

FIGURE 1
Map of the study site in Sabah, Malaysia. The three experimental plots are indicated by the white rectangles, with each plot consisting of (1) an untreated (reference) catchment and (2) a catchment amended with crushed silicate rock (treated). The two catchments within each plot are hydrologically isolated from each other. Stream sampling locations at the base of each catchment are indicated by the symbols (circles: plot 1, squares: plot 2, triangles: plot 3). Elevation is superimposed on a Google Map Satellite basemap, with dashed white contours and numbers indicating elevation (in meters). Yellow triangle in map insert (Google Satellite basemap) indicates the location of study area within Sabah Malaysia.

isolated catchments that drain into a small stream and range in size from 0.6 to 1.8 ha (Figure 1). Prior to the start of the experiment, the existing mature (20–25 year old) oil palms were felled and the plots were re-planted with young (~2–3 years old) oil palms in 2017. A cover crop was also planted to stabilize and minimize soil loss. One catchment from each plot was applied with 50 tons per hectare (t ha^{-1}) of crushed silicate rock after planting, and the other catchment was left untreated to act as a reference catchment (Figure 1). Application of crushed rock to the treated catchments was repeated every year throughout the course of the experiment, usually between August and December (Supplementary Text 1.1). The crushed rock was applied in the same way as fertilizers, that is, by hand to the base of the oil palms as well as in between the palms. Hereafter, the silicate rock-amended catchments are referred to as "treated" catchments and the reference catchments are referred to as "untreated" catchments. Note, however, that as there were pre-existing differences in stream water chemistry prior to rock application (see results, Figure 3), and the sizes of treated and untreated catchments were different (Figure 1, Supplementary Table 4), the untreated catchment stream water data cannot strictly be considered as a "control," so all stream water data were processed separately for each individual catchment.

To assess the effects of rock treatment on stream water chemistry, samples of stream water were taken from each site prior to the first application of the rock in April/May 2018, with continuous monitoring and sampling starting in October 2018. However, due to COVID-19 pandemic prevention measures, sampling was suspended between March and June 2020. Soil cores were taken to assess changes in soil chemistry between April and May 2018 prior to the first application of the crushed rock, and thereafter twice a year (Supplementary Text 1.5). The experiment is ongoing, but here we report data from the first 3 years of the experiment, up until July 2021.

Materials and methods

In this section, we firstly summarize our approach to the quantification of CO_2 removal and then secondly, we provide specific details relating to our analytical protocols. We calculate CO_2 removal as alkalinity (Equations 1 and 2) directly, via (i) measurement of elements and compounds dissolved in the stream waters and (ii) measurement of the water flux (discharge) from each catchment. This approach ensures that we capture net CO_2 removal from waters that exit the weathering zone to drainage, although we do not consider any modification to the alkalinity flux during riverine transport to the ocean. While

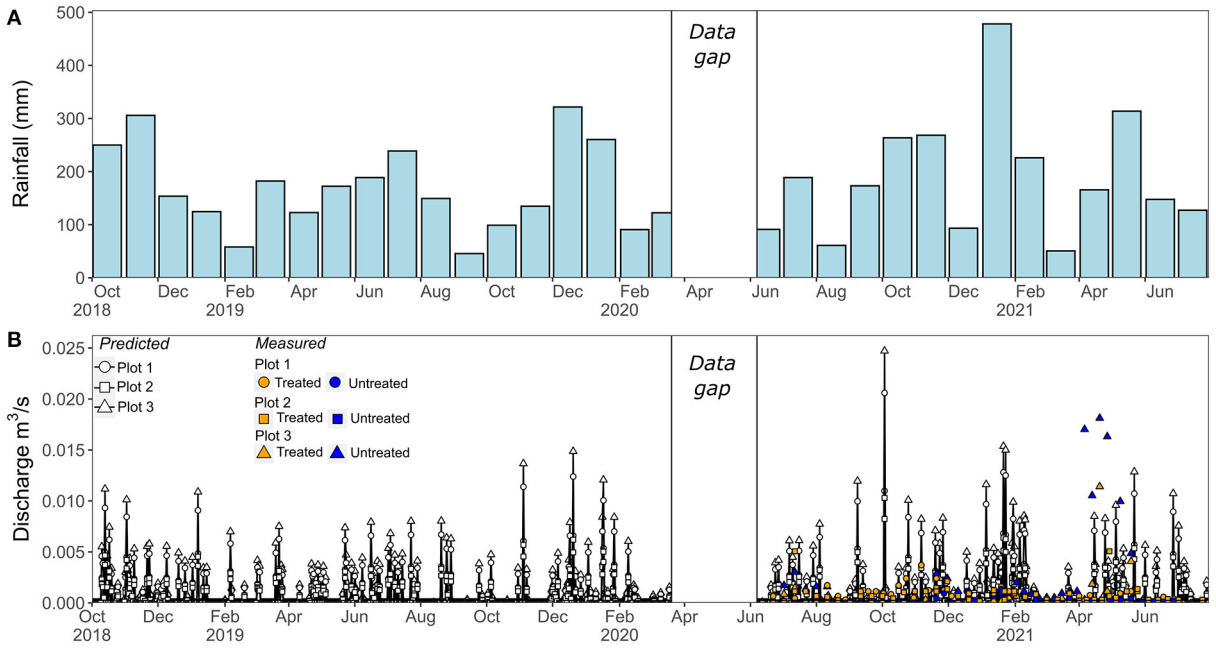

FIGURE 2
Rainfall and measured vs predicted discharge in stream catchments throughout the monitoring period (October 2018 to July 2021). **(A)** Total monthly rainfall in mm. **(B)** Predicted instantaneous daily discharge in m^3/s (black lines, and white symbols). Measured discharge (from June 2020 onwards) is also show for comparison (colored symbols). The white box indicates a data gap during the COVID-19 lockdown of 2020.

it is possible to determine weathering rates from the loss of soluble cations from the soils (e.g., Riebe et al., 2004), this is usually applied in studies aiming to characterize long-term weathering rates because soils have very high concentrations of e.g., Ca and Mg (wt% levels) relative to soil waters, making cation loss difficult to detect. Furthermore, the fate of weathering products cannot be assessed with this method. If, for example, the products of weathering are taken up by biomass or adsorbed on soil cation exchange sites, then CO_2 will be regenerated on short timescales.

In addition to characterizing water chemistry and discharge, it is also essential to determine the proportion of alkalinity derived from silicate vs. carbonate minerals, because whereas all alkalinity (HCO_3^-) generated by weathering of silicate minerals comes from CO_2 (Equation 1), only half of the alkalinity derived from weathering of carbonate minerals comes from CO_2 (the other half coming from carbonate; Equation 2). Characterization of the chemical composition of all soil mineral phases enables the relative proportion of silicate vs. carbonate weathering to be determined via measurement of cation concentrations and the radiogenic strontium isotopic composition ($^{87}Sr/^{86}Sr$) of stream waters, corrected for inputs from rainwater and water-soluble fertilizers (Section Quantification of CO_2 drawdown via pedogenic carbonate formation). The alkalinity derived from weathering reactions can be calculated from cation concentrations, as the HCO_3^- produced is charge balanced by base cations (Equations 1 and 2).

Calculation of CO_2 removal via pedogenic carbonate (inorganic carbon, predominately calcium carbonate) formation can be determined from the difference in the carbonate concentration of soils prior to the start of the experiment and those collected after application of crushed rock, although any contribution from weathering and re-precipitation of carbonate-based fertilizers (or carbonate in the applied crushed rock) needs to be subtracted because CO_2 removed during the weathering process will be re-released when the carbonate re-precipitates (Equations 2 and 3).

Measurement of stream water discharge

Stream water discharge can either be measured directly or derived from measurements of rainfall and estimated rates of evapotranspiration. Rainfall and other climate parameters (humidity, temperature, windspeed and solar radiation) were monitored at the plantation (Figure 2, Supplementary Text 1.2), allowing the predicted discharge from each catchment to be calculated daily from the difference between rainfall and potential evapotranspiration (see Supplementary Text 1.2 for full details). This approach was validated by comparing

10.3389/fclim.2022.959229

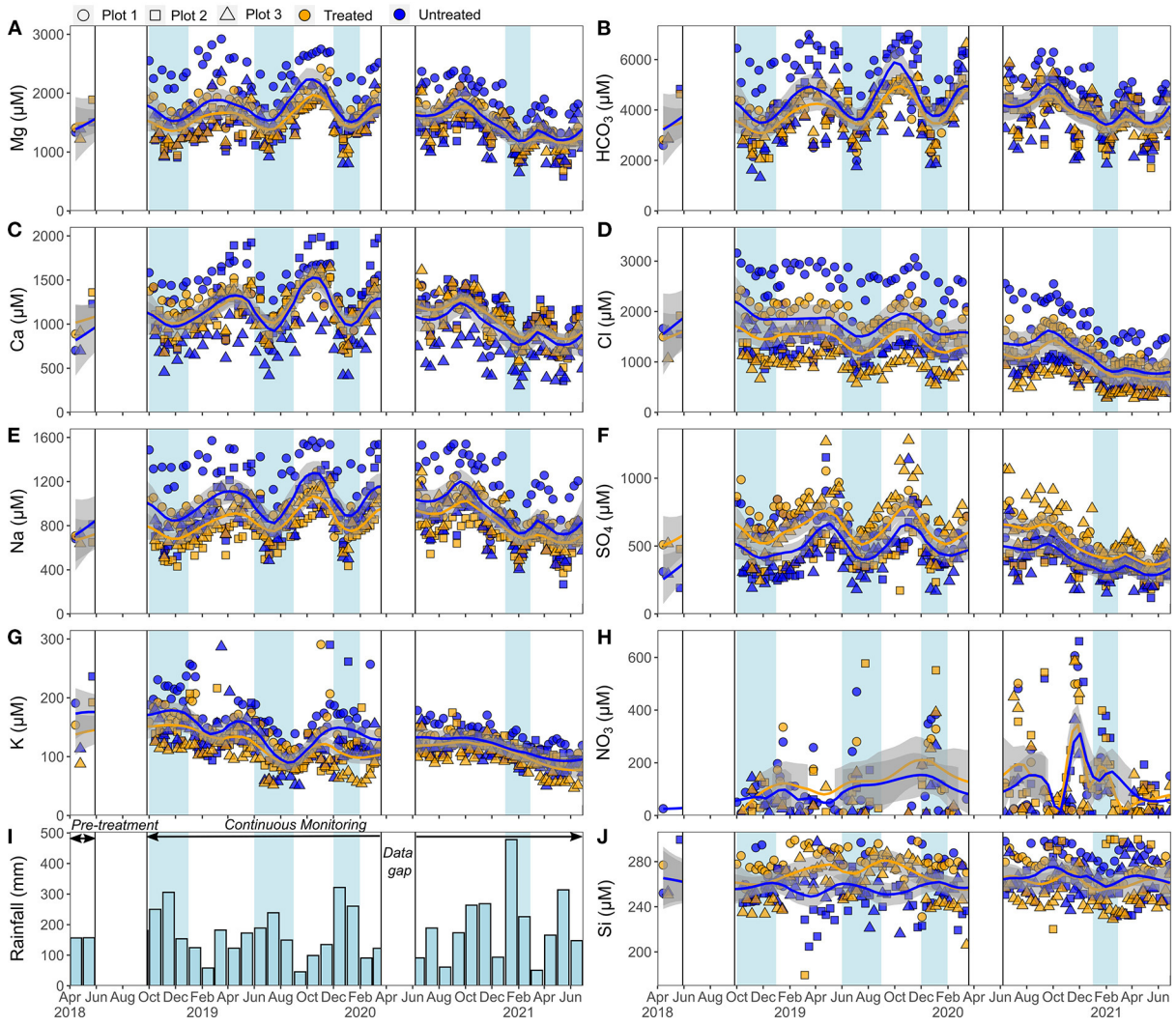

FIGURE 3
Stream water chemistry. Major cation concentrations are shown on the left-hand side **(A,C,E,G)** and major anion and silicon concentrations on the right-hand side **(B,D,F,H,J)**. Smoothed fit (lines and gray bands) through data is a Loess regression, which averages the treated and untreated datasets for all three catchments. The gray band is the 95% confidence interval on this fit. Rainfall **(I)** is the monthly sum, in mm. Light blue shading indicate times of higher rainfall that correlate with a decrease in some major elemental concentrations. White boxes indicate data gaps prior to rock application and during the COVID-19 lockdown.

predicted discharge with discharge measured bi-weekly in the streams from June 2020 onwards. Direct instantaneous measurements were obtained from readings of water depth within a Cutthroat Flume (OpenChannelFlow, 36 × 16-inch) that was installed at the water sampling points (symbols in Figure 1) at the lowest topographic point of each catchment. Measured discharge was in reasonable agreement with predicted daily discharge (Figure 2): differences can be expected as the instantaneous manual readings were only made every 2 weeks and may have missed individual rain events; in addition, readings could only be made when the streams were flowing, thus also missing periods of low or no flow (Figure 2).

Collection and analysis of stream waters and rainwater

Stream waters were collected from each catchment under free-flowing conditions at an approximately biweekly frequency, with water temperature and pH measured *in situ* at the time of sampling. Rainwater samples were periodically collected at the plantation. All waters were filtered at 0.45 μm immediately after sampling. A sub-sample of the filtered water was acidified to pH 2 with concentrated HNO_3 in acid-cleaned HDPE bottles for analysis of cations. Sub-samples for anion analysis were collected in MilliQ rinsed LPDE bottles and

were not acidified. Sub-samples for analysis of dissolved organic carbon (DOC) and total dissolved nitrogen (TDN) were collected in amber borosilicate glass vials and acidified with HCl.

Alkalinity analysis

Total alkalinity was determined for stream waters immediately after sampling using a Gran titration technique (Stumm and Morgan, 1996). Precision and accuracy were monitored using a sodium carbonate standard and were always better than ±5%. Bicarbonate (HCO_3^-) concentrations were calculated from total alkalinity, temperature and pH using CO2SYS v2.1 (Pierrot et al., 2006) using the stoichiometric equilibrium constants derived for freshwater by Millero (1979). For this calculation only [HCO_3^-], [CO_3^{2-}], [OH^-], and [H^+] were included in the definition of total alkalinity (Pierrot et al., 2006). Borate was not included in the definition of total alkalinity as measured B concentrations (see section Analysis of cation and anion concentrations and results) indicated that borate could only account for <0.1% of the total alkalinity so is considered negligible. The pH and alkalinity data indicate that >99% of stream water alkalinity consists of HCO_3^-. Moreover, as DOC concentrations are low (ranging from 75 to 540 μM C), it can be assumed that alkalinity ≈ [HCO_3^-].

Analysis of cation and anion concentrations

All concentration analyses were carried out in laboratories in the National Oceanography Centre, Southampton.

Concentrations of major and some trace elements (B, Ba, Ca, K, Mg, Na, Si, Sr) were measured on a Thermo Scientific iCAP 6000 Inductively Coupled Plasma Optical Emission Spectrometry (ICP-OES). Accuracy and precision were monitored using repeated measurements of a multi-elemental ICP standard (VWR) and an in-house drift standard, with known values reproduced always within ±10%. Aluminum concentrations in stream waters were low or below the typical detection limit (<∼0.05 ppm) in the stream waters, and so were monitored to check for potential contamination from particulate material but are not reported. The DOC and TDN concentrations in the stream waters were determined on a Total Organic Carbon Analyzer (Shimadzu TOC-VCPH). Accuracy was monitored using consensus reference material from the University of Miami (UM Hansell CRM); our values were within ±10% of the consensus values. Precision was determined via repeat measurements of the same sample ($n > 3$) and was better than ±2%.

Anion (SO_4^{2-}, NO_3^-, Cl^-) concentrations were measured by ion chromatography (IC, Thermo Scientific Dionex Aquion) with a 9 mM sodium carbonate eluent. A multi-elemental standard (Dionex Seven Anion Standard II) was repeatedly measured to monitor accuracy and precision, with values reproduced to within ±6% of known concentrations. The normalized inorganic charge balance (NCIB = $(\Sigma^+ - \Sigma^-)/(\Sigma^+ + \Sigma^-)$ in %, where Σ^+ is the sum of cations and Σ^- is the sum of anions, in equivalents) was on average 1.8% for all stream water measurements ($n = 562$) and was always better than ±10% (Supplementary Table 8).

Analysis of radiogenic Sr isotope ratios ($^{87}Sr/^{86}Sr$)

The radiogenic strontium isotopic composition ($^{87}Sr/^{86}Sr$) of the stream waters was determined by Thermal Ionization Mass Spectrometry (TIMS) at the University of Southampton. Briefly, 200 to 500 ng of Sr was separated from the rest of the sample matrix with Sr-Spec resin, using established chromatographic procedures (following Pearce et al., 2015 and Kelland et al., 2020 and references therein). The Sr fraction was loaded on a single Re filament and measured on the TIMS (Thermo Scientific). The $^{86}Sr/^{88}Sr$ ratio was normalized to 0.1194 using an exponential law. External and analytical reproducibility was monitored using standards: NBS 987 and an IAPSO seawater standard regularly passed through column chemistry (Supplementary Text 1.4). Repeated measurements of NBS 987 yielded 0.710252 ± 6 ppm (2SD, $n = 73$). The uncertainty associated with a sample measurement is taken as the uncertainty on these repeated measurements of NBS 987 (i.e., ±6 ppm).

Collection and analysis of soil samples

After collection, soil cores were split into two fractions, 0–10 cm and 10–30 cm, and dried in an oven at 80°C. Soil pH was measured at the oil palm plantation by mixing dry soil with distilled water in a 1:5 ratio.

Dried soils were first sieved to <2 mm, and then subjected to a chemical leaching procedure to separate the exchangeable (plant available), carbonate, and silicate fractions of the soils. The exchangeable fraction was isolated by leaching the soils in 1M ammonium chloride (NH_4Cl) for 24 h and the carbonate fraction was isolated by leaching the residue remaining after the NH_4Cl leach in 4M acetic acid (AcOH) for 24 h. After both leaches were completed, the residual soil was rinsed 3 times in MilliQ water, dried, and completely digested on at hotplate at 130°C in a mix of HF, HNO_3 and $HClO_4$. The residual soil is assumed to principally consist of relatively insoluble silicate minerals. The chemical compositions of each of the soil leachates, and the digested soil residue, was determined by ICP-OES as described in Sections Analysis of cation and anion concentrations; selected soil leachates were also analyzed for $^{87}Sr/^{86}Sr$ as described in Section Analysis of radiogenic Sr isotope ratios ($^{87}Sr/^{86}Sr$).

The inorganic carbon (carbonate) content of the dried and sieved soil samples was assessed using a UIC CM5015 CO_2 Coulometer in the SEAPORT Stable Isotope Lab, University of Southampton. However, the carbonate content of all the soils analyzed was below the detection limit of the instrument (<0.2 wt% $CaCO_3$). For this reason, we assessed changes in soil carbonate by chemical leaching (reaction with 4M AcOH for 24 h after the exchangeable fraction was removed, as above) on a selection of soil samples (Supplementary Table 5) from 2018 (pre-treatment), 2019 and 2020. To calculate wt% $CaCO_3$ we assumed that the Ca in the leachate measured by ICP-OES was from dissolution of $CaCO_3$. Calculated $CaCO_3$ values (see Section Composition of the soils, applied rock, and fertilizers) were consistent with the results from coulometry (i.e., <0.2 wt%). We applied inferential statistics to assess the significance of differences in carbonate content in soils between treated and untreated plots and different years. The data were normalized to homogenize the variance between data sets by transforming to a log scale with the time point (year) treated as a continuous variable. The variance was analyzed using a 3-way ANOVA (time, treatment, and plot) on the transformed model. To assess differences between years, the model was refitted with the time point (year) included as a discrete factor and contrasts and Tukey-adjusted *p*-values were then calculated.

Composition of applied crushed rock and fertilizers

The crushed rock that was applied to the treated catchments was donated by Onika Quarry (owned by Leeka Holdings) in Tawau, Sabah, and its composition is described in detail in Lewis et al. (2021). Briefly, the rock is andesitic in composition and is derived from Pleistocene magmatic-arc volcanic deposits (Lewis et al., 2021). The mineralogy is dominated by plagioclase (45 wt%), sanidine feldspar (13 wt%) and diopside (clinopyroxene, 12 wt%) minerals and has a relatively high quartz content (19 wt%). The rock also contains trace carbonate minerals (~0.8 wt%, Lewis et al., 2021). The applied rock has a grainsize of $p80 = 1{,}767\ \mu m$ and its whole rock specific surface area [determined by (BET)-N_2 adsorption] was $2.73 \pm 0.06\ m^2/g$ (Lewis et al., 2021).

The chemical composition of carbonate minerals in the applied rock was determined by leaching the ground rock in 4M acetic acid in the same way as for the soils. The material remaining after removal of the carbonate fraction, which can be assumed to represent the silicate fraction, was subsequently digested on a hotplate at 130°C in a mix of HF and HNO_3. The leachates and digestates were dried down and redissolved in 3% HNO_3 and cation concentrations and $^{87}Sr/^{86}Sr$ ratios were measured as described in Sections Analysis of cation and anion concentrations and Analysis of radiogenic Sr isotope ratios ($^{87}Sr/^{86}Sr$).

Throughout the experiment, fertilizers were applied to the oil palms in accordance with usual agricultural practice at the plantation. Fertilizers consisted of ground Mg-limestone, potash, magnesium sulfate and sodium borate, as well as various other compound (e.g., NPK) fertilizers. The full fertilizer application schedule is given in Supplementary Table 3. Most notably, ground Mg-limestone was added to all catchments between April and August 2018, and again in January 2019. Approximately 2 kg of Mg-limestone was applied to the base of each oil palm on both occasions. As carbonate minerals have high dissolution rates relative to silicate minerals, this fertilizer can be expected to undergo rapid chemical weathering and will contribute to CO_2 drawdown (Equation 2).

The chemical composition of water-soluble fertilizers (NK, NPK, Na-borate, urea, muriate of potash and $MgSO_4$) was determined by dissolving the fertilizer in MilliQ water and then acidifying to pH 2 with concentrated distilled HNO_3. Non-water-soluble fertilizers (rock phosphate and ground Mg-limestone) were digested on a hotplate at 130°C in a mix of HF, HNO_3 and $HClO_4$. The dissolved/digested fertilizers were then dried down and redissolved in 3% HNO_3 and cation concentrations were measured as described in Section Analysis of cation and anion concentrations.

Results

All data obtained in this study are available in the Supplementary Tables 1–8 and summarized here. Our data characterize the chemical composition of the stream waters, soils and different soil phases and include radiogenic strontium isotope data that can be used to trace cation sources.

Chemical composition of stream waters

Concentrations of key solutes in stream waters are shown together with rainfall data in Figure 3. The variation in concentrations followed a similar pattern across all catchments, with lower concentrations of major dissolved ions (Ca^{2+}, Mg^{2+}, Na^+, HCO_3^-) coinciding with higher rainfall (>600 mm). This likely reflects a greater influence of surface runoff during periods of high rainfall with proportionally higher base flow during drier conditions.

The DOC concentration of all the stream waters was lower than the global average river concentration (Liu and Wang, 2022, Supplementary Table 8), ranging from 75 to 540 μM C. Bicarbonate (HCO_3^-) accounted for >99% of total alkalinity (Supplementary Table 8) which is expected due to the low DOC and because the inorganic charge balance was close to zero and stream water pH was neutral [proton activity mean = 6.76 ± 0.40 (1SD, $n = 582$)]. Stream waters have HCO_3^- concentrations that are relatively high (in some cases >99% of

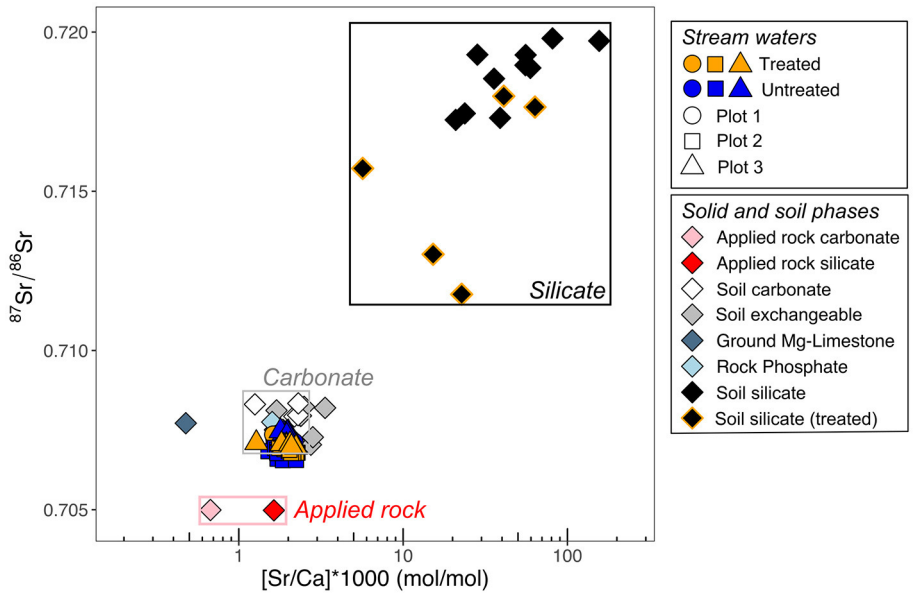

FIGURE 4
$^{87}Sr/^{86}Sr$ isotope geochemistry of stream waters, soil phases (exchangeable, carbonate and silicate, the applied rock (silicate and carbonate phases) and fertilizers. Boxes enclose the range of soil silicates, soil carbonates and the applied rock. Treated silicate refers to the silicate fraction of soils post rock application in treated catchments. Analytical error is smaller than the symbol size.

world rivers, which fall between 47 to 5,950 μeq/L; Meybeck, 2003), varying from 1,323 to 7,097 μeq/L across all catchments (n = 579). Stream water cations are dominated by Mg^{2+}, Ca^{2+}, and Na^{+}, with concentrations ranging from 584 to 2,921, 301 to 2,050, and 268 to 1,690 μM, respectively (n = 579). Sulfate and chloride concentrations are nearly always higher than the global river average (ranging from 118 to 1,280 and 281 to 3,159 μM, respectively, whereas world river average concentrations are 175 and 167 μM, respectively; Meybeck, 2003). Nitrate concentrations in stream waters were on average 122 μM and often below the typical analytical detection limit (<8 μM, Supplementary Table 8). Stream water concentrations of elemental B ranged from 9 to 66 μM, which is higher than the range of most natural waters (average value of the world's largest rivers = 0.94 μM; Gaillardet et al., 2014).

Radiogenic strontium isotopes

Radiogenic Sr isotope ($^{87}Sr/^{86}Sr$) compositions can be used to trace the weathering source in waters and soils. Since ^{87}Rb decays into ^{87}Sr (half-life = 49 Gyr), the $^{87}Sr/^{86}Sr$ ratios of waters and soils are set by source rock composition which differs according to rock type and age. Strontium is a mobile element and has a similar atomic radius to Ca, so it readily substitutes for Ca in minerals. Therefore, $^{87}Sr/^{86}Sr$ compositions of waters, sediments and soils also trace the weathering of carbonate minerals, which usually have higher $^{87}Sr/^{86}Sr$ ratios than silicate minerals (e.g., Gaillardet et al., 1999). For this reason, the Sr isotopic compositions of the stream waters, the soils and the applied rock were also measured to help determine the proportion of weathering of carbonate vs. silicate minerals (Figure 4). Stream water $^{87}Sr/^{86}Sr$ values ranged from 0.706556 to 0.707471, overlapping with soil carbonate phases (that ranged from 0.707167 to 0.708338). Silicate phases had a wide range of $^{87}Sr/^{86}Sr$ values, with the lowest values measured in post-treatment soils (Figure 4).

Composition of the soils, applied rock, and fertilizers

The soils in all catchments were acidic with soil pH = 5.10 ± 0.55 (proton activity mean, ± 1 SD, n = 402). The chemical compositions of the different soil fractions (exchangeable, carbonate and silicate), fertilizers and the applied rock, which are all potential sources of solutes in the stream waters, are summarized in Supplementary Table 5.

We estimate the soil inorganic carbon content to be on average <0.2 wt% using the Ca concentrations mobilized in the acetic acid leachates (Figure 5). Chemical extractions are imperfect and additional phases, such as phosphate minerals and potentially silicate or clay minerals, may be mobilized (Tessier et al., 1979), so estimates of carbonate concentrations derived by chemical leaching represent maximum values. Differences in the mean values of calculated calcium carbonate concentrations

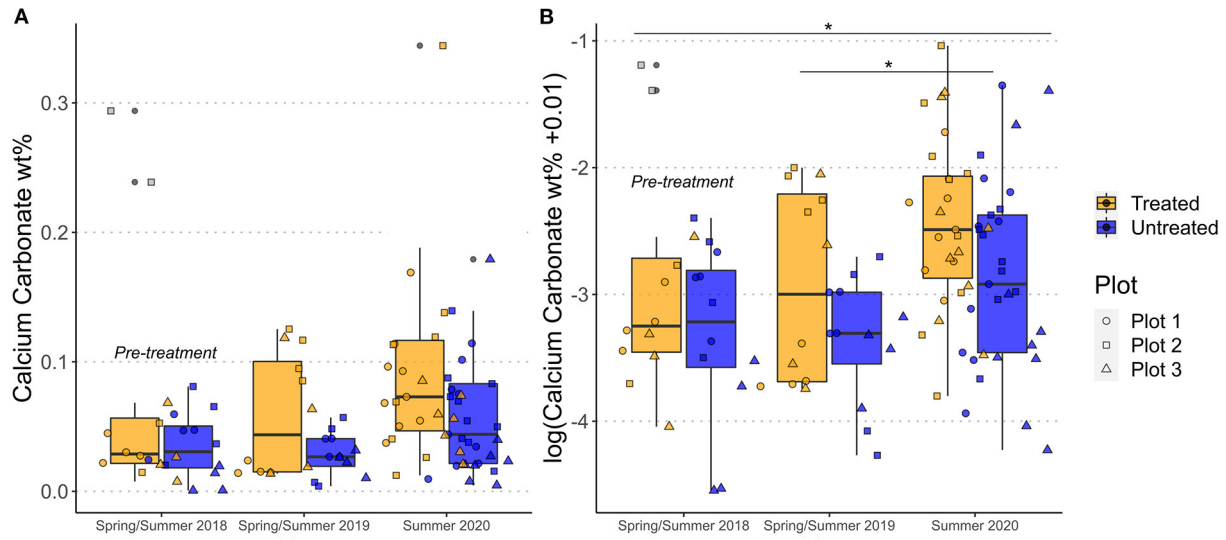

FIGURE 5
Change in soil carbonate concentration (derived from analysis of soil leachates) over the course of this study as wt% calcium carbonate **(A)** and transformed to a log scale **(B)**. Box plots are for data from all three plots, with the thick black line indicating the median value. Individual data points are the colored symbols. Gray colored squares indicate extreme outliers excluded from the data analysis. *Indicates the calculated *p*-value was between 0.01 and 0.05.

($CaCO_3$ wt%) were observed between treated and untreated plots for all 3 time points analyzed: 2018 (pre-treatment), treated = 0.032 ± 0.019 (SD) and untreated = 0.035 ± 0.026 (SD); 2019, treated = 0.059 ± 0.049 (SD) and untreated = 0.028 ± 0.016 (SD) and 2020, treated = 0.099 ± 0.079 (SD) and untreated = 0.068 ± 0.064 (SD) (Figure 5A). The calculated $CaCO_3$ concentration was ~0.03 wt% higher in the treated plot when compared to untreated plot at the final time point analyzed (2020). All three effects (year, plot, treatment) significantly contributed to the variance (plot $p = 0.010052^*$, treatment $p = 0.004561^{**}$ and year $p = 0.001734^{**}$, Figure 5B). There were also significant differences between the means of 2019 and 2020 ($p = 0.0102^*$) and of 2018 and 2020 ($p = 0.0146^*$), but no significant difference between 2018 and 2019 (Figure 5B).

The chemical composition of carbonate phases (ground Mg-limestone fertilizer and the acetic acid extractable portion of the soil and the applied rock) and the silicate phases (residual fractions of the soil and applied rock, after leaching of non-silicate phases) was also determined to partition sources of cations derived from weathering of silicate vs. carbonate phases for each individual catchment. Cross plots of Na/Σ^+, Ca/Σ^+ and Mg/Σ^+ (where Σ^+ is the sum of the base cations in equivalents), demonstrate that this approach is valid as the silicate phases are characterized by relatively high Na/Σ^+ and the carbonate phases are characterized by high Ca/Σ^+. In addition, carbonate phases all plot on a mixing line between Mg- and Ca-carbonate or rock phosphate endmembers, whereas the silicate phases lie off the mixing line (Figure 6B). Figure 5A also shows that mobilization of Na relative to other major cations was minimal in the acetic acid leach, confirming that the acetic acid leach targeted mostly carbonate phases. The chemical composition of the soil exchangeable fraction overlaps with that of carbonate (dolomite and limestone and Mg-limestone fertilizer; Figure 6); note that the soil exchangeable fraction may also include any water-soluble fertilizers present in the soil.

The chemical composition of fertilizers considered as potential cation sources applied to the oil palms over the course of this study is provided in Supplementary Table 3. The fertilizers are (i) water-soluble salts (e.g., $MgSO_4$, Na-borate, potash and NPK fertilizers) that add cations to stream waters but do not draw down any atmospheric CO_2, and (ii) rock-based fertilizers (e.g., ground Mg-limestone and rock phosphate) that will undergo chemical weathering and contribute to the CO_2 budget. Rock-based fertilizer compositions are also plotted in Figure 6.

Discussion

Here, we quantify and discuss the evidence for CO_2 removal via alkalinity generation and soil carbonate formation over the course of this field trial. Firstly, we assess CO_2 drawdown via pedogenic carbonate formation in the soils. Secondly, we set out a model framework for quantifying CO_2 removal via alkalinity generation in waters which considers inputs from fertilizers and strong acid weathering, as well as carbonic acid weathering of silicate and carbonate minerals. This model framework is similar to those applied in natural riverine and weathering studies (e.g.,

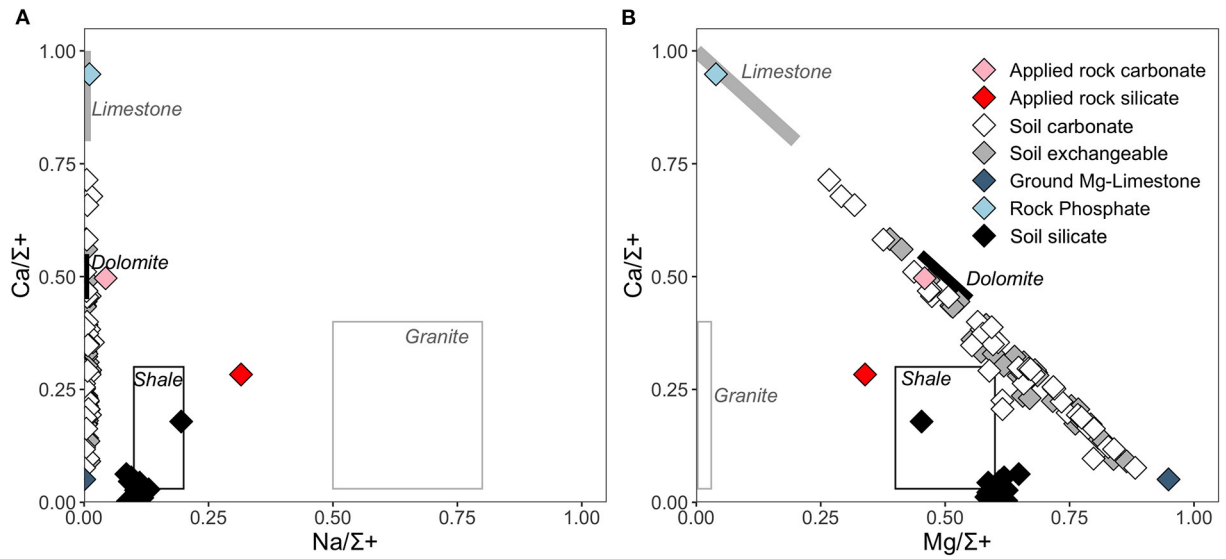

FIGURE 6
Geochemical composition of the applied rock (carbonate and silicate phases), soil phases (exchangeable, carbonate, and silicate) and rock-based fertilizers compared to generalized lithological endmember compositions spanning a wide range (silicates represented by shale and granite, carbonates represented by dolomite and limestone). **(A)** Na/Σ^+ and Ca/Σ where Σ^+ is the sum of major cations (Ca, Mg, Na, K) in equivalents and **(B)** Mg/Σ^+ and Ca/Σ^+. Composition of generalized global lithological endmembers (boxes) are from Torres et al. (2016).

Gaillardet et al., 1999; Galy and France-Lanord, 1999; Torres et al., 2016; Bufe et al., 2021; Kemeny and Torres, 2021). Finally, we place our quantifications in a global context, comparing estimations of CO_2 removal via alkalinity generation to selected comparator catchments.

Quantification of CO_2 drawdown via pedogenic carbonate formation

As shown by Equation 3, CO_2 removal associated with enhanced weathering deployed in croplands or with plants can also occur via pedogenic carbonate formation (e.g., Manning and Renforth, 2013). Soil carbonate concentrations (inferred from the chemistry of the acetic acid leaches) indicate that <0.2 wt% $CaCO_3$ was, on average, present in the soils. Over the course of the experiment, the calculated soil carbonate concentration increased significantly in all plots and in both treated and untreated catchments (Figure 5). To date (i.e., by 2020), the increase in the soil carbonate concentration is ~0.03 wt% higher in the treated catchments relative to the untreated catchments (Figure 5A). Trace carbonate minerals from the applied rock in treated catchments may contribute to this difference, as three rock applications at 50 tons per ha with 0.8 wt% calcite would result in ~0.03 wt% increase in carbonate minerals in the soil, but only if this calcite was retained in the upper 30 cm of the soil (i.e., and not weathered, or migrated deeper in the soil profile). If this increase resulted solely from silicate mineral weathering and subsequent pedogenic carbonate formation (Eqn 1 and Eqn 3) over the top 30 cm of the soil, this would be approximately equivalent to a removal of 0.51 $tCO_2\ ha^{-1}$ (assuming a bulk soil density of 1.3 g/cm^3) or 0.26 $tCO_2\ ha^{-1}\ yr^{-1}$. This idealized calculation highlights that small and difficult to detect changes in soil inorganic carbon content may equate to the removal of significant quantities of CO_2. However, we are unable to verify if this increase in soil carbonate concentration between treated and untreated plots resulted from enhanced silicate mineral weathering, as additional isotopic measurements (e.g., $\delta^{13}C_{CaCO3}$) would be needed to verify the proportion of soil inorganic carbon derived from CO_2. The low inorganic carbon content of the soils meant that $\delta^{13}C_{\ CaCO3}$ could not be measured directly on the soils from this field trial.

Overall, we emphasize that most carbonate minerals present in both the treated and untreated soils are likely to be predominately derived from fertilizer application, explaining the significant increase in calculated soil inorganic carbon content with time in both treated and untreated plots (Figure 5). This interpretation is supported by $^{87}Sr/^{86}Sr$ isotope and cation molar ratios, which indicate that the carbonate phases have high Mg and lie on a mixing line between a phosphate or limestone endmember, and a high-Mg limestone endmember (Figure 6). The radiogenic Sr isotope compositions of the soil carbonates (Figure 4) also overlap with the fertilizer endmember compositions.

Low concentrations of soil carbonate are consistent with the relatively low pH of the soils, as well as local climate conditions. Mean annual precipitation (MAP) is ~2,000 mm at our field sites (Figure 2) and soil inorganic carbon mainly forms under

dry arid conditions, so is not likely to accumulate in areas where MAP exceeds 1,000 mm (e.g., Zamanian et al., 2016). Continued monitoring of soil inorganic carbon concentration at this field site will be necessary to ascertain whether carbonate accumulates at this site long-term, thereby becoming a demonstrably permanent store of CO_2. Although the climatic conditions specific to our field site mean that pedogenic carbonate formation is not likely to be a substantial CO_2 removal pathway, carbonate formation could be an important pathway for CO_2 sequestration under different climatic and geologic regimes.

Quantification of CO_2 drawdown via alkalinity generation

Here we set out a model framework for rigorously quantifying CO_2 removal via alkalinity generation. Before the proportion of dissolved solutes derived from weathering of silicate vs. carbonate minerals can be quantified, contributions of dissolved solutes not derived from weathering need to be eliminated. These non-weathering sources are primarily atmospheric (cyclic) salts principally delivered by rainfall, and water-soluble fertilizer salts (e.g., compound fertilizers and potash).

Correction for inputs from fertilizer and atmospheric salts

The influence of fertilizers on stream chemistry is evidenced by the high sulfate and chloride concentrations sourced from $MgSO_4$ and KCl (muriate of potash) fertilizers, respectively (Figure 3). Furthermore, Mg concentrations are similar to or higher than Ca in stream waters (Figure 3), which is the opposite of most freshwater systems where typically Ca is more concentrated (Meybeck, 2003). This is consistent with the dissolution of high-Mg fertilizers ($MgSO_4$ and ground Mg-limestone). High B concentrations are indicative of input from dissolution of Na-borate fertilizer, and low DOC concentrations consistent with the lack of significant organic fertilizer input.

Atmospheric inputs to the stream waters were accounted for using average cation/chloride ratios measured in rainwater samples (see Supplementary Text 2). Following this, a series of corrections were made to subtract the contributions of water-soluble fertilizer salts (summarized in Supplementary Text 2). These corrections allow us to isolate the cation contribution to stream waters derived only from chemical weathering of silicate and carbonate minerals (referred to herein as "rock-derived" cations).

None of the water-soluble salt fertilizers were a significant source of Ca (or Sr) to the sampled stream waters. However, inputs from water-soluble salt fertilizers were significant for K^+ and Na^+, and as our fertilizer correction is non-exhaustive this likely induces unquantified error into the calculated rock-derived stream concentrations. However, the validity of our approach for extracting the rock-derived weathering signature is verified by cross plots of $[HCO_3^-]$ and $[Ca^{2+} + Mg^{2+}]_{rock}$ (Figure 7), which shows that the gradient of our rain-corrected and fertilizer-corrected $[HCO_3^-]$ and $[Ca^{2+} + Mg^{2+}]_{rock}$ data is ~2, consistent with the carbonic acid weathering of carbonate or silicate minerals (Equations 1 and 2).

Our radiogenic Sr isotope data (Figure 4) also indicate that a large proportion of stream water $[K^+]$ and $[Na^+]$ must be derived from fertilizer inputs rather than weathering of silicate minerals, because the $^{87}Sr/^{86}Sr$ ratios of the stream waters is consistent with weathering of carbonate phases.

Proportion of silicate vs. carbonate weathering

Following correction of stream water chemistry for atmospheric and fertilizer salt inputs, the proportions of cations derived from the weathering of silicate vs. carbonate minerals were assessed using an idealized two-endmember mixing model (Supplementary Text 3). In this case, the endmembers are silicate minerals and carbonate minerals, which are defined as the chemical compositions of, respectively, the soil residue (silicate phases remaining after removal of exchangeable ions and carbonate phases) and the soil carbonate phase (phases leachable in acetic acid after removal of exchangeable ions). The soils contain silicate and carbonate minerals derived from the applied rock (treated catchments), the background soil and rock-based fertilizers, and they therefore integrate all of the potential carbonate and silicate mineral endmembers. This simplified approach does not account for weathering of the rock phosphate fertilizer; however, phosphate weathering had a minor influence on stream chemistry as phosphate concentrations in stream waters were ~0.1–4 μM (Supplementary Text 4).

The model calculates the instantaneous fraction of cations derived from carbonate and silicate weathering (f_{carb} and f_{sil}, where $f_{carb} + f_{sil} = 1$) for each stream water sample, using the measured elemental molar ratios (Na/Σ^+, Ca/Σ^+ and Mg/Σ^+, corrected for atmospheric and fertilizer salt inputs) and, where available, radiogenic Sr isotopes combined with Sr/Σ^+. Radiogenic Sr isotope data were not corrected for atmospheric inputs, as rainwaters had negligible Sr concentrations (Supplementary Table 7). We solve 4 equations for f_{sil} and f_{carb} simultaneously using a Bayesian endmember mixing package in R (simmr; Parnell et al., 2010), which calculates 10,000 possible solutions, and takes account of the error in the endmember compositions (Supplementary Text 3). The f_{sil} and f_{carb} values reported are the mean and standard deviation of these possible solutions (Figure 8A).

Model results indicate that >90% of stream cations were derived from carbonate mineral weathering over the first ~1–2 years of the study for all catchments, and for the whole

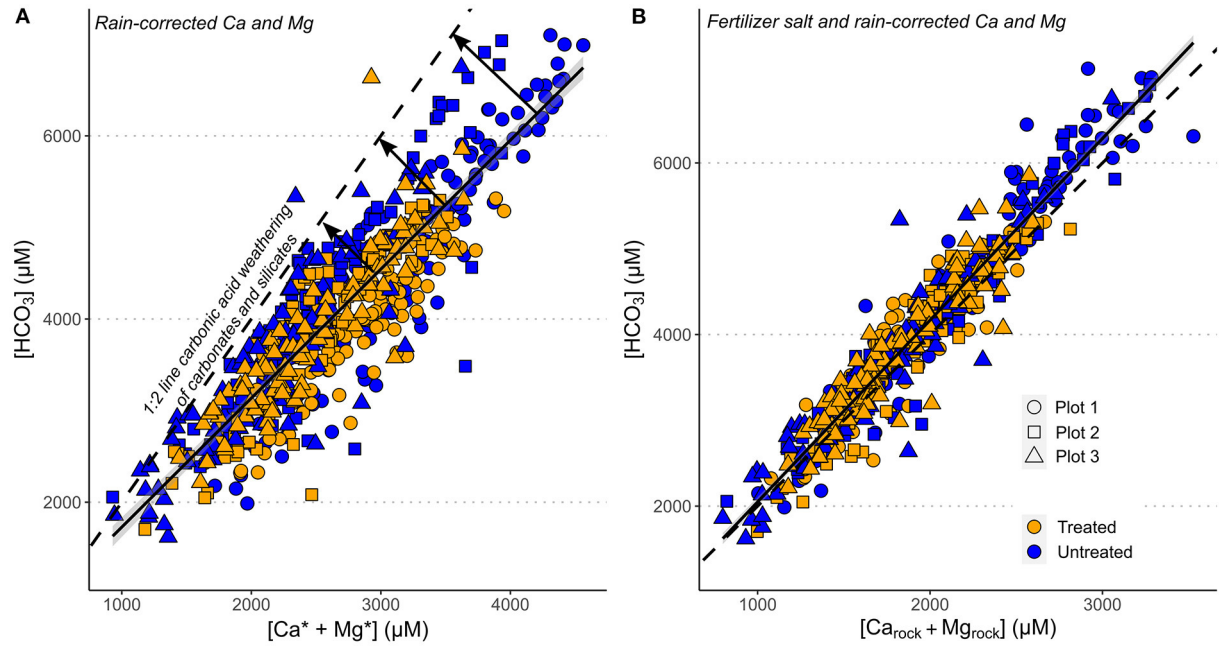

FIGURE 7
Cross plots of dissolved stream water chemistry g. **(A)** HCO_3^- vs. $Ca^{2+} + Mg^{2+}$ (corrected for atmospheric inputs). **(B)** HCO_3^- vs. fertilizer salt and rain corrected Ca and Mg concentrations ($[Ca^{2+}+Mg^{2+}]_{rock}$). Dashed black line shows the stoichiometry of carbonic acid weathering of silicate and carbonate minerals, and the solid black lines are the linear regressions through the data.

duration of the study for plots 1 and 2 (Figure 8A). The high Mg concentrations in both soil carbonate leachates and stream waters (e.g., Figures 3, 6) are indicative of significant input of cations from weathering of high-Mg carbonate, likely sourced from the ground Mg-limestone fertilizer.

Stream waters from both treated and untreated catchments in plots 1 and 2 had similar f_{sil} values [plot 1 average: untreated $f_{sil} = 0.040 \pm 0.002$ (1 SD), treated $f_{sil} = 0.08 \pm 0.07$ (1 SD) and plot 2 average: untreated $f_{sil} = 0.05 \pm 0.06$ (1 SD), treated $f_{sil} = 0.035 \pm 0.002$ (1 SD)]. Since the middle of 2019, a greater proportion of stream cations have been derived from silicate weathering in plot 3, with the treated catchment values exceeding the untreated catchment values (Figure 7A, from 25th June 2019, average f_{sil} (untreated) $= 0.19 \pm 0.17$ (1 SD) and average f_{sil} (treated) $= 0.38 \pm 0.21$(1 SD), Figure 7A).

The instantaneous amount of CO_2 transferred to the stream waters ($[CO_2]_{eq}$; Figure 7A) and converted to alkalinity per unit volume of weathering fluid is given by:

$$[CO_2]_{eq} = [NO_3^-]^* - 0.5[\text{Cations}]_{carbonate} - [\text{Cations}]_{silicate} \quad (4)$$

where concentrations of cations and anions are in equivalents. Note that Equation 4 represents the drawdown of atmospheric CO_2 as negative values, whereas the release of CO_2 from the stream waters back into the atmosphere is represented by positive values.

In addition to weathering by carbonic acid, Equation 4 also accounts for the effects of weathering by nitric acid. The weathering of carbonates by strong acids [sulfuric (H_2SO_4) and nitric (HNO_3)] can result in the release of CO_2 (Spence and Telmer, 2005; Oh and Raymond, 2006; Calmels et al., 2007; Hamilton et al., 2007; Perrin et al., 2008; Torres et al., 2014; Raymond and Hamilton, 2018; Bufe et al., 2021; Relph et al., 2021), for example:

$$\overbrace{2HNO_3}^{\textit{from nitrification}} + \overbrace{CaCO_3}^{\substack{\textit{carbonate}\\ \textit{mineral}}} \rightarrow \overbrace{CO_2 + 2NO_3^- + Ca^{2+} + H_2O}^{\textit{soil water}} \quad (5)$$

Although the absence of sulfide minerals within the soils mean that sulfuric acid weathering is unlikely to occur at our study site, the addition of N-fertilizer to the plots may result in the production of nitric acid. The extent of instantaneous CO_2 release or consumption with both carbonic and nitric acid weathering can be estimated from the measured stream water NO_3^- concentrations [similar to the approach used by Bufe et al. (2021) for sulfuric acid weathering] by removing cations charge balanced by NO_3^- to calculate a net CO_2 value (Equation 4). This CO_2 calculation does not depend on whether the nitric acid reacts with carbonates or silicates (Bufe et al.,

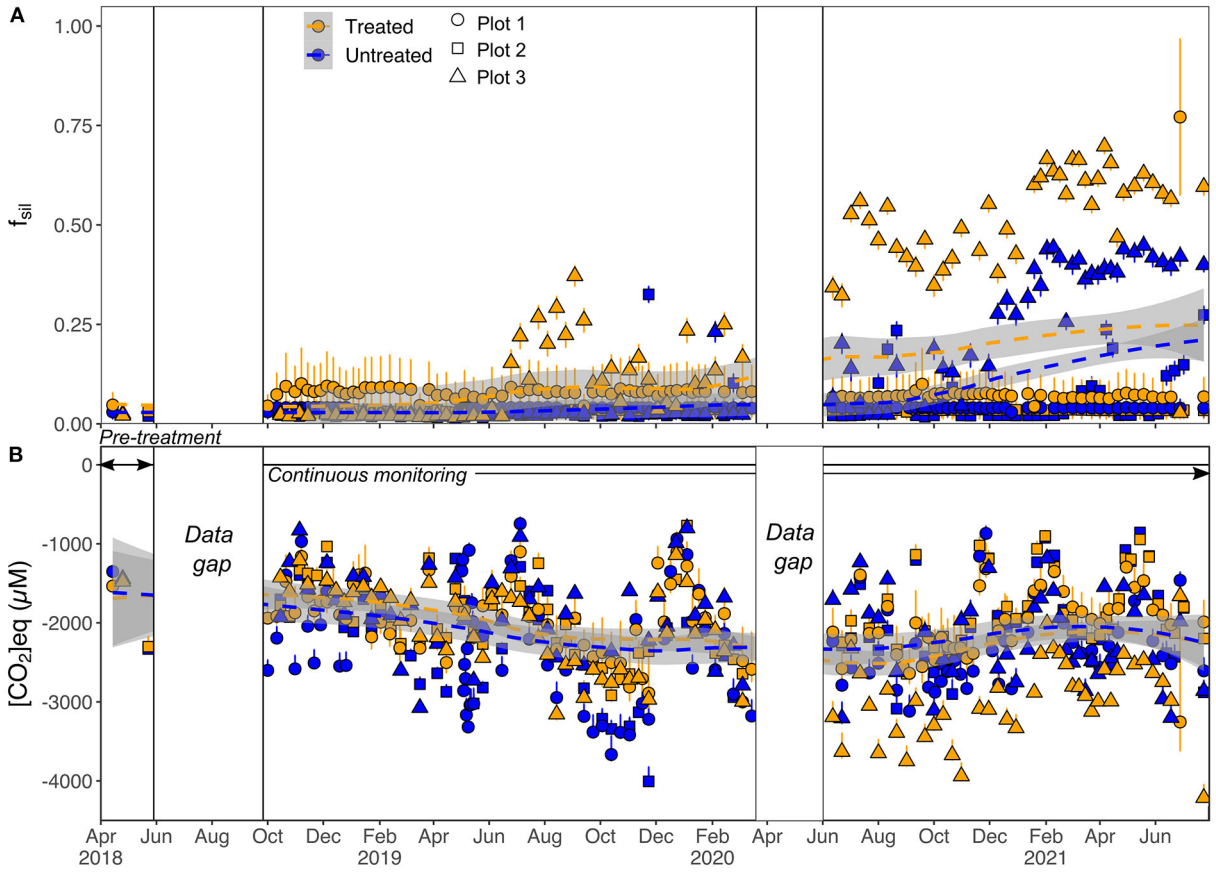

FIGURE 8
(A) Fraction of cations derived from silicate weathering (f_{sil}) in stream waters calculated using the endmember mixing model. Symbols show mean values from the Bayesian endmember mixing model, and error bars are equal to 1SD. **(B)** Calculated moles of CO_2 produced (positive) or drawn down (negative) per L of stream water as a result of rock weathering. Error bars are propagated 1SD errors from f_{sil} and f_{carb}. Smoothed fit (dashed lines and gray bands) through all catchment data is a Loess regression. White boxes indicate data gaps prior to the start of continuous monitoring, and during the COVID-19 lockdown.

2021). We note that NO_3^- concentrations were generally low (Figure 3H), and the gradient of the cross plots of $[HCO_3^-]$ and $[Ca^{2+}+Mg^{2+}]_{rock}$ is close to 2 (Figure 6B), which both suggest that carbonic acid weathering was the principal weathering agent (nitric acid weathering can be expected to shift the gradient closer to 1 or even lower; Perrin et al., 2008).

Figure 9B shows that there was net removal of CO_2 from the atmosphere via weathering in all of our study catchments over the entire sampling period. The annual variations in calculated $[CO_2]_{eq}$ and total alkalinity for each plot are compared in Figure 9. Generally, higher alkalinity values correspond to higher CO_2 removal (more negative $[CO_2]_{eq}$, Figure 9), as might be expected from Equations 1 and 2. In 2021, CO_2 removal was higher in the treated catchment in plot 3 relative to the untreated catchment, due to increased silicate weathering (Figures 8A, 9B), even though there was little difference in alkalinity between the two catchments (Figure 9A). This highlights the need to partition sources of solutes in enhanced weathering experiments to determine the relative proportions of carbonate to silicate weathering. Accurate partitioning of cation sources is particularly important when the rocks used to amend soils contain trace carbonate minerals (Lewis et al., 2021), as the fast dissolution kinetics of carbonate minerals mean they would be expected to weather first (White et al., 1999; Jacobson and Blum, 2000).

Assessment of CO_2 drawdown via alkalinity generation

The cumulative quantity of CO_2 removed from the atmosphere (in $tCO_2\ ha^{-1}$) as alkalinity since the start of continuous monitoring in our field trial can be calculated by multiplying $-[CO_2]_{eq}$ by the daily stream discharge and dividing by plot area (see Supplementary Text 5 for full details, Figure 10). Values of $[CO_2]_{eq}$ were derived by linear interpolation between the sampling points, including over the

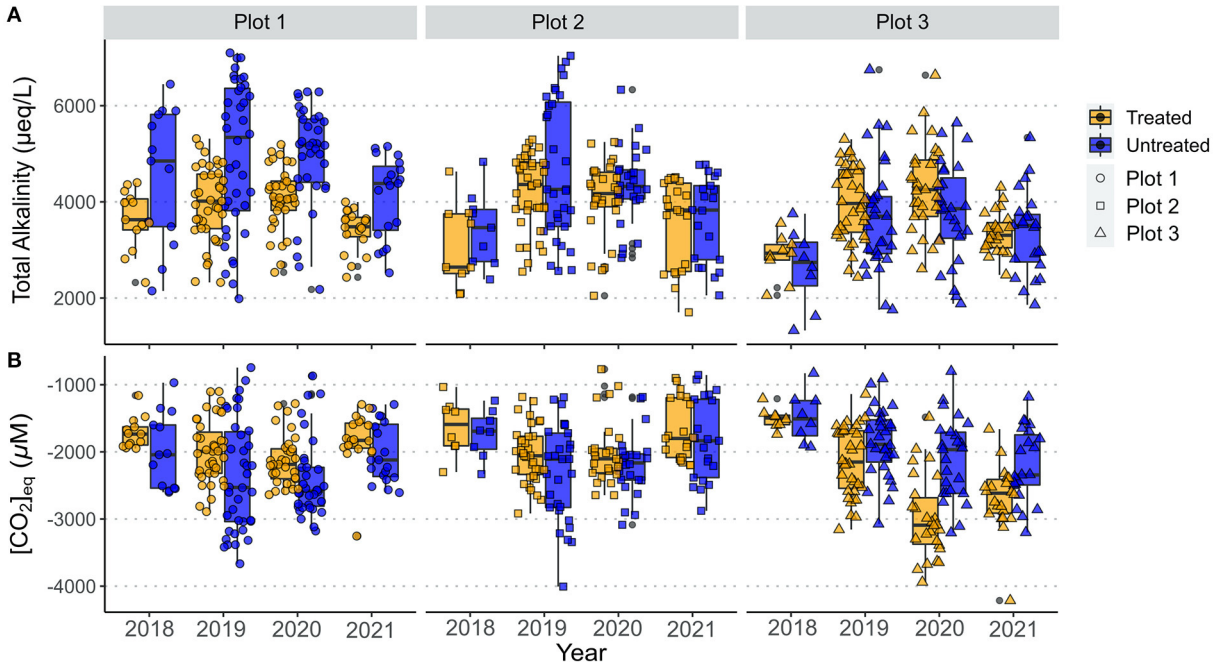

FIGURE 9
Annual variation in **(A)**. Total Alkalinity of stream waters, and **(B)**. amount of CO_2 produced (positive) or drawn down (negative) as a result of rock weathering for treated and untreated catchments in all 3 study plots. Symbols show individual data points.

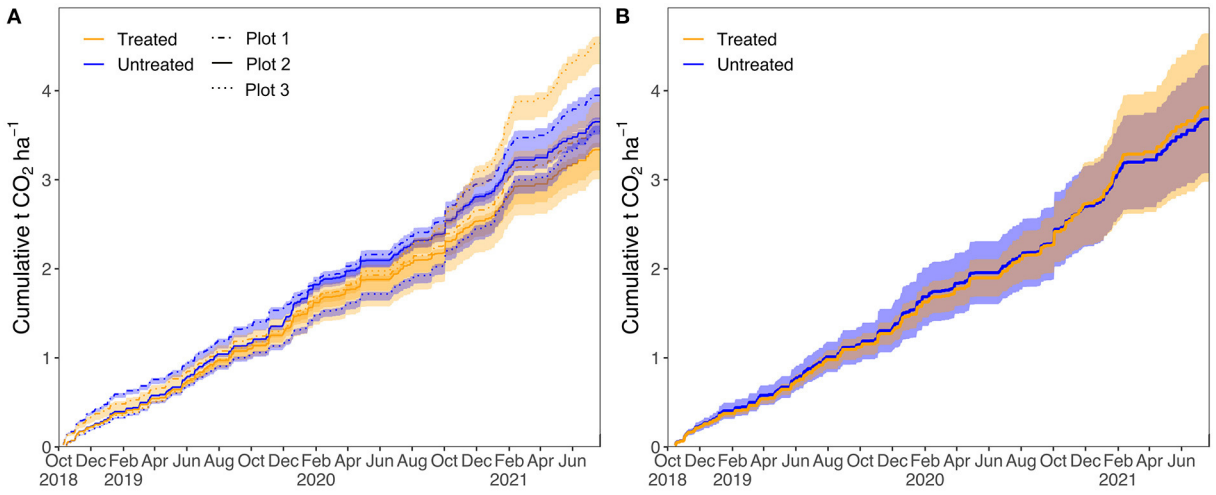

FIGURE 10
Cumulative CO_2 drawdown in tons CO_2 per hectare (tCO_2 ha^{-1}) via alkalinity generation. **(A)** Individual plots, error envelope is the propagated error [68% confidence interval (CI)]. **(B)** Mean of all three plots. Error envelope is 1 SD.

COVID-19 lockdown. Considering all three plots together, the average (±1SD) amount of CO_2 removal was 3.8 ± 0.8 tCO_2 ha^{-1} for the treated catchments and 3.7 ± 0.6 tCO_2 ha^{-1} for the untreated catchments over the continuous monitoring period (Figure 10). Thus, application of silicate rock did not result in a change in CO_2 removal via alkalinity generation outside of the error range. The quantity of CO_2 removed over the continuous monitoring period was similar for both the treated and untreated catchments in plots 1 and 2 (plot 1: treated = $3.7^{+0.2}_{-0.6}$, untreated = $3.9^{+0.1}_{-0.3}$ tCO_2 ha^{-1}, plot 2: treated = $3.3^{+0.1}_{-0.2}$, untreated =

$3.7^{+0.1}_{-0.1}$ tCO_2 ha^{-1}). However, the amount of CO_2 drawdown in plot 3 was higher in the treated catchment ($4.5^{+0.1}_{-0.2}$ tCO_2 ha^{-1}) than in the untreated catchment ($3.5^{+0.1}_{-0.2}$ tCO_2 ha^{-1}). This increase in CO_2 drawdown within the treated catchment of plot 3 corresponds to an increase in the proportion of weathering of silicate minerals (Figure 8).

There are several potential reasons for the apparent lack of an increase in silicate weathering in treated catchments in plots 1 and 2. Rock weathering releases nutrients (e.g., K) to soil waters, making them plant available. If nutrients released by chemical weathering of the applied silicate rock are not in excess of plant uptake, then they will not contribute to stream water cation or anion fluxes (e.g., Manning et al., 2017). Similarly, if cations released by enhanced weathering are retained on the cation exchange sites in soils this leads to delayed or muted signals in stream waters (e.g., Pogge von Strandmann et al., 2021). Nevertheless, our analyses of the soil exchangeable fraction did not reveal an obvious signature of enhanced weathering as, for example, the $^{87}Sr/^{86}Sr$ isotope ratio of the exchangeable fraction was similar to that of the stream waters (Figure 6). It should also be noted that the baseline rates of chemical weathering recorded in all the streams on the plantation were extremely high. For example, average alkalinity concentrations were 4,035 μM ($n = 579$) in this study, whereas the average alkalinity concentration observed in natural forested catchments in Sabah is an order of magnitude lower (407 μM, $n = 90$; Yamashita et al., 2014). The high rates of fertilizer application on oil palm plantations leads to very high levels of weathering in all catchments, making the addition of less soluble silicate rock difficult to detect. High loadings of easily-solubilised fertilizers may also inhibit dissolution of applied silicate materials as soil waters may become saturated and therefore may limit weathering rates (e.g., Maher and Chamberlain, 2014).

Although plot 1 and 2 do not show any difference in CO_2 drawdown via alkalinity generation between treated and untreated catchments, in plot 3 the difference was ∼1.1 tCO_2 ha^{-1}. A difference of ∼1.1 tCO_2 ha^{-1} is consistent with what would be expected based on reactive transport modeling of weathering of the crushed silicate rock used in this study (Lewis et al., 2021). Model results predict that one application of 50 t ha^{-1} of Tawau andesite could be expected to remove 2.9 tCO_2 ha^{-1} over a period of 15 years (Lewis et al., 2021). This is equivalent to ∼1.1 tCO_2 ha^{-1} for 3 annual applications of rock at 50 tons per hectare as was the case for the period of this study (just under 2 years). A predicted (maximum) difference of ∼1.1 tCO_2 ha^{-1} is relatively small relative to our study baseline (on the order of 3 tCO_2 ha^{-1}). As discussed above, weathering is currently dominated by weathering of fertilizers and as such the effects of enhanced weathering of the applied rock may be difficult to detect in all catchments. It is highly likely that the cumulative effect of rock application may take more time (i.e. >3 years) to become detectable. In settings with lower baseline stream water concentrations (e.g., forested regions with no fertilizer input) it may be that the signature of enhanced weathering is easier to detect.

CO_2 drawdown via alkalinity generation in a global context

Rates of CO_2 removal as alkalinity determined in this study are high relative to rates determined for natural forests in Sabah, catchments draining the world's largest rivers and carbonate rock weathering (Figure 11). Carbonate CO_2 removal rates are derived from Suchet et al., 2003 with CO_2 release from nitric acid weathering calculated after (Perrin et al., 2008). We note, however, that few of these comparator catchments have been adequately characterized with a complete CO_2 budget (e.g., taking into account CO_2 release due to strong acid weathering); most published CO_2 removal rates represent maximum values (e.g., Hilton and West, 2020). The high rates of CO_2 consumption on the palm oil plantation are not, however, unexpected, as it has long been established that agriculture and agricultural liming can enhance weathering rates and increase alkalinity fluxes relative to non-agricultural settings (Pacheco and Van der Weijden, 2002; Hamilton et al., 2007; Raymond et al., 2008).

Our study demonstrates that the high rates of weathering and CO_2 drawdown in both the treated and untreated catchments on the palm oil plantation are driven primarily by weathering of a carbonate fertilizer. The rates of weathering are on the same order of magnitude as basaltic catchments which are thought to constitute 30–35% of global continental weathering fluxes (Dessert et al., 2003), on the order of ∼1 tCO_2 ha^{-1} yr^{-1}. These values are also around an order of magnitude higher than that calculated for natural forested catchments in Sabah which experience similar climatic conditions (ranging from 0.02 to 0.08 tCO_2 ha^{-1} yr^{-1} for two catchments; Grip et al., 1994; West et al., 2005). This indicates that the tropics should be considered as a key location for further enhanced weathering trials, as their large capacity to drawdown atmospheric CO_2 via alteration of soils (in this instance with carbonate fertilizers) and enhanced chemical weathering is clear. If enhanced rock weathering was deployed without agricultural liming, and if fast weathering silicate minerals were to replace carbonates, the potential longer-term CO_2 drawdown could be higher.

Conclusion

The study provides the first quantification of the extent of atmospheric CO_2 removal via alkalinity generation in a field trial of enhanced weathering in a tropical environment. We

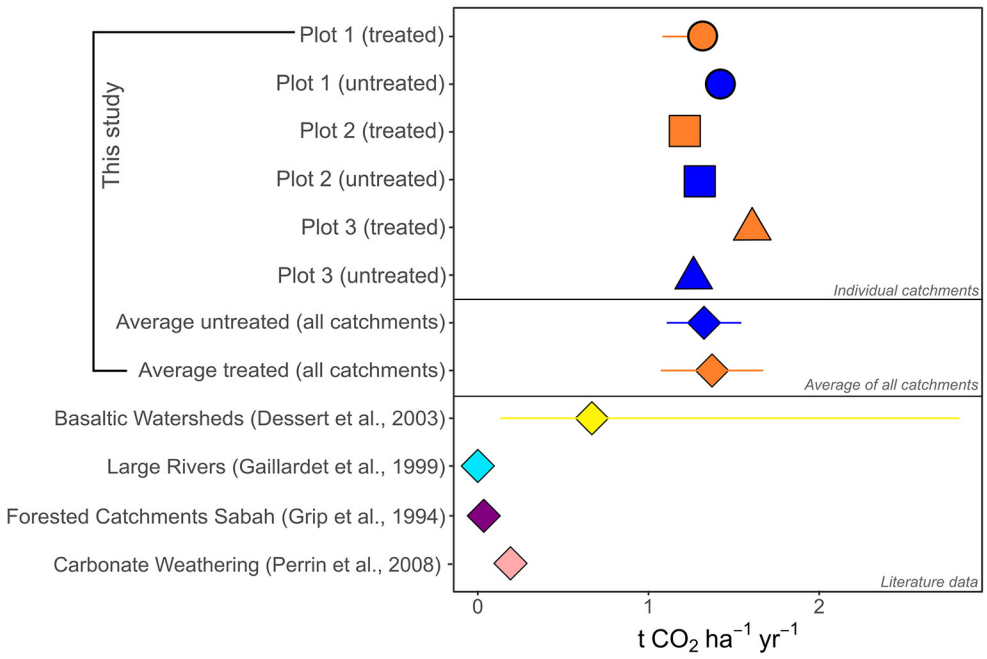

FIGURE 11
Rates of CO_2 removal via alkalinity generation calculated in this study compared to rates of CO_2 removal from: (i) carbonate weathering, (ii) natural forested catchments in Sabah, (iii) the world's largest rivers and (iii) small basaltic watersheds. For this study the individual catchments with the 1 SD propagated errors are shown (where greater than the symbol size), and the average and 1 SD error of all catchments is also shown (diamonds). For literature data (Grip et al., 1994; Gaillardet et al., 1999; Dessert et al., 2003; Perrin et al., 2008), the average is shown (symbol), and the error bar is the range. For the world's largest rivers, carbonate watersheds and forested catchments in Sabah, the range is smaller than the symbol size. CO_2 consumption data for rivers draining lowland forest in Sabah are calculated using data from Grip et al. (1994), with partitioning of carbonate and silicate weathering after West et al. (2005). This calculation does not account for any CO_2 release due to strong acid weathering, and so should be considered a maximum value. Carbonate CO_2 removal data are calculated after Perrin et al. (2008), using data from Suchet et al. (2003).

present a method for quantifying CO_2 removal via alkalinity generation that accounts for the influence of fertilizers and the potential for CO_2 release associated with the weathering of carbonate minerals by strong acids. Using this method, we show that the acidification of soils due to nitrogen fertilizer application resulted in no net CO_2 release in these catchments and that the rates of chemical weathering are high throughout the study site. Although the extent of CO_2 removal via alkalinity generation associated with soils amended with silicate rock was similar to the untreated plots when all replicated catchments were considered, the results from one plot suggest an increased removal of ~0.4 tCO_2 $ha^{-1}yr^{-1}$. This result is in agreement with the CO_2 removal predicted from modeling (Lewis et al., 2021). If the carbon dioxide removal estimates from this plot are transferable to global tropical croplands (accounting for an area of 676×10^6 ha; Edwards et al., 2017), this equates to a removal of ~0.3 Gt CO_2 yr^{-1}, which is within range of the mitigation potential of other proposed carbon dioxide removal methods (IPCC, 2022). This evidently idealized calculation does not account for any emissions resulting from implementation (i.e., crushing and transportation of the applied rock), but if valid would represent ~3% of the ~10 Gt CO_2 yr^{-1} of carbon dioxide removal by 2050 that is likely required to reach the Paris agreement target of limiting global average temperatures to 1.5°C (e.g., UN Environment Programme, 2017; IPCC, 2022).

We emphasize that this field trial is ongoing and unequivocal evidence for changes in pedogenic carbonate content, as well as the cumulative effect of rock application on weathering rates of treated vs. untreated catchments that currently show no detectable differences, may only be revealed in the coming years. Silicate mineral dissolution can be a slow process under most natural conditions, and modeling studies indicate that years to several decades may be required for the full CO_2 removal potential to be reached (e.g., Taylor et al., 2016; Lewis et al., 2021). Longer-term monitoring is also important for assessing any potential impacts to soil, plant, and stream water quality to verify the safety of enhanced rock weathering. Notwithstanding, our results demonstrate that tropical croplands have a large capacity to help draw down atmospheric CO_2, even when, as in this instance, CO_2 drawdown is driven largely by application of carbonate fertilizers.

Data availability statement

The original contributions presented in the study are included in the article/Supplementary material, further inquiries can be directed to the corresponding author/s.

Author contributions

MA, DJB, CP, RJ, RF, and KY contributed to conception and design of the study. KY and MA carried out field sampling and analysis. CL, MA, HG-H, JB, and KY conducted geochemical analysis. CL interpreted the data, carried out data analysis and calculations, and wrote the manuscript with input from all authors. All authors contributed to the article and approved the submitted version.

Funding

This research was funded through a Leverhulme Research Centre Award (RC-2015-029) from the Leverhulme Trust.

Acknowledgments

We thank Cynthia Dumousseaud, Gabriella Jardine, and Matt Cooper for technical assistance at the University of Southampton. We thank Onika Quarry for donating the rock used in this experiment as well as Glen Reynolds (Director of SEARRP) who helped to make sure the project ran smoothly. We thank the Sabah Biodiversity Centre that provided approval for both accessing the experimental site and exporting samples.

Conflict of interest

The authors declare that the research was conducted in the absence of any commercial or financial relationships that could be construed as a potential conflict of interest.

Publisher's note

Supplementary material

The Supplementary Material for this article can be found online at: https://www.frontiersin.org/articles/10.3389/fclim.2022.959229/full#supplementary-material

References

Amann, T., Hartmann, J., Struyf, E., de Oliveira Garcia, W., Fischer, E. K., Janssens, I., et al. (2020). Enhanced Weathering and related element fluxes – a cropland mesocosm approach. *Biogeosciences* 17, 103–119. doi: 10.5194/bg-17-103-2020

Andrews, M. G., and Taylor, L. L. (2019). Combating climate change through enhanced weathering of agricultural soils. *Elements* 15, 253–258. doi: 10.2138/gselements.15.4.253

Beerling, D. J., Kantzas, E. P., Lomas, M. R., Wade, P., Eufrasio, R. M., Renforth, P., et al. (2020). Potential for large-scale CO 2 removal via enhanced rock weathering with croplands. *Nature* 583, 242–248. doi: 10.1038/s41586-020-2448-9

Beerling, D. J., Leake, J. R., Long, S. P., Scholes, J. D., Ton, J., Nelson, P. N., et al. (2018). Farming with crops and rocks to address global climate, food and soil security. *Nat. Plants* 4, 138–147. doi: 10.1038/s41477-018-0108-y

Berge, H. F. M. ten, van der Meer, H. G., Steenhuizen, J. W., Goedhart, P. W., Knops, P., and Verhagen, J. (2012). Olivine weathering in soil, and its effects on growth and nutrient uptake in ryegrass (lolium perenne l.): A pot experiment. *PLoS ONE*. 7, e42098. doi: 10.1371/journal.pone.0042098

Bufe, A., Hovius, N., Emberson, R., Rugenstein, J. K. C., Galy, A., Hassenruck-Gudipati, H. J., et al. (2021). Co-variation of silicate, carbonate and sulfide weathering drives CO 2 release with erosion. *Nat. Geosci.* 14, 211–216. doi: 10.1038/s41561-021-00714-3

Bullock, L. A., James, R. H., Matter, J., Renforth, P., and Teagle, D. A. H. (2021). Global carbon dioxide removal potential of waste materials from metal and diamond mining. *Front. Clim.* 3:77. doi: 10.3389/fclim.2021.694175

Calmels, D., Gaillardet, J., Brenot, A., and France-Lanord, C. (2007). Sustained sulfide oxidation by physical erosion processes in the Mackenzie River basin: climatic perspectives. *Geology* 35, 1003–1006. doi: 10.1130/G24132A.1

Dessert, C., Dupr,é, B., Gaillardet, J., François, L. M., and Allègre, C. J. (2003). Basalt weathering laws and the impact of basalt weathering on the global carbon cycle. *Chem. Geol.* 202, 257–273. doi: 10.1016/j.chemgeo.2002.10.001

Dietzen, C., Harrison, R., and Michelsen-Correa, S. (2018). Effectiveness of enhanced mineral weathering as a carbon sequestration tool and alternative to agricultural lime: an incubation experiment. *Int. J. Greenhouse Gas Control* 74, 251–258. doi: 10.1016/j.ijggc.2018.05.007

Drever, J. I. (1997). *The Geochemistry of Natural Waters: Surface and Groundwater Environments*. Upper Saddle River, N.J.: Prentice Hall.

Edwards, D. P., Lim, F., James, R. H., Pearce, C. R., Scholes, J., Freckleton, R. P., et al. (2017). Climate change mitigation: potential benefits and pitfalls of enhanced rock weathering in tropical agriculture. *Biol. Lett.* 13:20160715. doi: 10.1098/rsbl.2016.0715

Gabet, E. J., and Mudd, S. M. (2009). A theoretical model coupling chemical weathering rates with denudation rates. *Geology* 37, 151–154. doi: 10.1130/G25270A.1

Gaillardet, J., Dupré, B., Louvat, P., and Allègre, C. J. (1999). Global silicate weathering and CO_2 consumption rates deduced from the chemistry of large rivers. *Chem. Geol.* 159, 3–30. doi: 10.1016/S0009-2541(99)00031-5

Gaillardet, J., Viers, J., and Dupré, B. (2014). "7.7 - Trace elements in river waters," in *Treatise on Geochemistry*, 2nd Edn, Eds H. D. Holland and K. K. Turekian (Oxford: Elsevier), 195–235.

Galy, A., and France-Lanord, C. (1999). Weathering processes in the Ganges–Brahmaputra basin and the riverine alkalinity budget. *Chem. Geol.* 159, 31–60. doi: 10.1016/S0009-2541(99)00033-9

Grip, H., Malmer, A., and Wong, F. K. (1994). Converting tropical rain forest to forest plantation in sabah, malaysia. Part I. Dynamics and net losses of nutrients in control catchment streams. *Hydrol. Processes* 8, 179–194. doi: 10.1002/hyp.3360080302

Hamilton, S. K., Kurzman, A. L., Arango, C., Jin, L., and Robertson, G. P. (2007). Evidence for carbon sequestration by agricultural liming. *Glob. Biochem. Cycle.* 21, GB2021. doi: 10.1029/2006GB002738

Haque, F., Santos, R. M., and Chiang, Y. W. (2020). CO2 sequestration by wollastonite-amended agricultural soils – an Ontario field study. *Int. J. Greenhouse Gas Control* 97:103017. doi: 10.1016/j.ijggc.2020.103017

Haque, F., Santos, R. M., Dutta, A., Thimmanagari, M., and Chiang, Y. W. (2019). Co-benefits of wollastonite weathering in agriculture: Co_2 sequestration and promoted plant growth. *ACS Omega* 4, 1425–1433. doi: 10.1021/acsomega.8b02477

Hartmann, J., West, A. J., Renforth, P., Köhler, P., Rocha, C. L. D. L., Wolf-Gladrow, D. A., et al. (2013). Enhanced chemical weathering as a geoengineering strategy to reduce atmospheric carbon dioxide, supply nutrients, and mitigate ocean acidification. *Rev. Geophys.* 51, 113–149. doi: 10.1002/rog.20004

Hilton, R. G., and West, A. J. (2020). Mountains, erosion and the carbon cycle. *Nat. Rev. Earth Environ.* 1, 284–299. doi: 10.1038/s43017-020-0058-6

IPCC (2022). "Climate change 2022: mitigation of climate change," in *Contribution of Working Group III to the Sixth Assessment Report of the Intergovernmental Panel on Climate Change*, Eds P.R. Shukla, J. Skea, R. Slade, A. Al Khourdajie, R. van Diemen, D. McCollum, et al. (Cambridge; New York, NY: Cambridge University Press).

Jacobson, A. D., and Blum, J. D. (2000). Ca/Sr and 87Sr/86Sr geochemistry of disseminated calcite in Himalayan silicate rocks from Nanga Parbat: Influence on river-water chemistry. *Geology* 28, 463–466. doi: 10.1130/0091-7613(2000)28andlt;463:SASGODandgt;2.0.CO;2

Kelland, M. E., Wade, P. W., Lewis, A. L., Taylor, L. L., Sarkar, B., Andrews, M. G., et al. (2020). Increased yield and CO2 sequestration potential with the C4 cereal Sorghum bicolor cultivated in basaltic rock dust-amended agricultural soil. *Glob. Chang. Biol.* 26, 3658–3676. doi: 10.1111/gcb.15089

Kemeny, P. C., and Torres, M. A. (2021). Presentation and applications of mixing elements and dissolved isotopes in rivers (MEANDIR), a customizable MATLAB model for Monte Carlo inversion of dissolved river chemistry. *Am. J. Sci.* 321, 579–642. doi: 10.2475/05.2021.03

Kump, L. R., Brantley, S. L., and Arthur, M. A. (2000). Chemical weathering, atmospheric CO2, and climate. *Annu. Rev. Earth Planet. Sci.* 28, 611–667. doi: 10.1146/annurev.earth.28.1.611

Lasaga, A. C. (1984). Chemical kinetics of water-rock interactions. *J. Geophys. Res. Solid Earth* 89, 4009–4025. doi: 10.1029/JB089iB06p04009

Lewis, A. L., Sarkar, B., Wade, P., Kemp, S. J., Hodson, M. E., Taylor, L. L., et al. (2021). Effects of mineralogy, chemistry and physical properties of basalts on carbon capture potential and plant-nutrient element release via enhanced weathering. *Appl. Geochem.* 132:105023. doi: 10.1016/j.apgeochem.2021.105023

Lim, P. S., Malaysia, and Jabatan Penyiasatan Kajibumi (1985). *Peta geologi negeri Sabah = Geological Map of Sabah*. Ipoh, Perak, Peninsular Malaysia: Director of Geological Survey of Malaysia.

Liu, F., and Wang, D. (2022). Dissolved organic carbon concentration and biodegradability across the global rivers: a meta-analysis. *Sci. Tot. Environ.* 818:151828. doi: 10.1016/j.scitotenv.2021.151828

Maher, K., and Chamberlain, C. P. (2014). Hydrologic regulation of chemical weathering and the geologic carbon cycle. *Science* 343, 1502–1504. doi: 10.1126/science.1250770

Manning, D. A. C., Baptista, J., Sanchez Limon, M., and Brandt, K. (2017). Testing the ability of plants to access potassium from framework silicate minerals. *Sci. Tot. Environ.* 574, 476–481. doi: 10.1016/j.scitotenv.2016.09.086

Manning, D. A. C., and Renforth, P. (2013). Passive sequestration of atmospheric CO_2 through coupled plant-mineral reactions in urban soils. *Environ. Sci. Technol.* 47, 135–141. doi: 10.1021/es301250j

Meybeck, M. (2003). "5.08 - global occurrence of major elements in rivers," in *Treatise on Geochemistry*, eds H. D. Holland and K. K. Turekian (Oxford: Pergamon), 207–223. doi: 10.1016/B0-08-043751-6/05164-1

Millero, F. J. (1979). The thermodynamics of the carbonate system in seawater. *Geochim. Cosmochim. Acta* 43, 1651–1661. doi: 10.1016/0016-7037(79)90184-4

Oelkers, E. H., Declercq, J., Saldi, G. D., Gislason, S. R., and Schott, J. (2018). Olivine dissolution rates: a critical review. *Chem. Geol.* 500, 1–19. doi: 10.1016/j.chemgeo.2018.10.008

Oelkers, E. H., and Gislason, S. R. (2001). The mechanism, rates and consequences of basaltic glass dissolution: I. An experimental study of the dissolution rates of basaltic glass as a function of aqueous Al, Si and oxalic acid concentration at 25°C and pH = 3 and 11. *Geochim. Cosmochim. Acta* 65, 3671–3681. doi: 10.1016/S0016-7037(01)00664-0

Oh, N.-H., and Raymond, P. A. (2006). Contribution of agricultural liming to riverine bicarbonate export and CO2 sequestration in the Ohio River basin. *Glob. Biochem. Cycle.* 20, GB3012. doi: 10.1029/2005GB002565

Pacheco, F. A. L., and Van der Weijden, C. H. (2002). Mineral weathering rates calculated from spring water data: a case study in an area with intensive agriculture, the Morais Massif, northeast Portugal. *Appl. Geochem.* 17, 583–603. doi: 10.1016/S0883-2927(01)00121-4

Parnell, A. C., Inger, R., Bearhop, S., and Jackson, A. L. (2010). Source partitioning using stable isotopes: coping with too much variation. *PLoS ONE* 5:e9672. doi: 10.1371/journal.pone.0009672

Pearce, C. R., Parkinson, I. J., Gaillardet, J., Charlier, B. L. A., Mokadem, F., and Burton, K. W. (2015). Reassessing the stable (δ88/86Sr) and radiogenic (87Sr/86Sr) strontium isotopic composition of marine inputs. *Geochim. Cosmochim. Acta* 157, 125–146. doi: 10.1016/j.gca.2015.02.029

Perrin, A.-S., Probst, A., and Probst, J.-L. (2008). Impact of nitrogenous fertilizers on carbonate dissolution in small agricultural catchments: implications for weathering CO2 uptake at regional and global scales. *Geochim. Cosmochim. Acta* 72, 3105–3123. doi: 10.1016/j.gca.2008.04.011

Pierrot, D. E., Lewis, E., Wallace, D. W. R., and Wallace, D. W. R. (2006). *MS Excel Program Developed for CO2 System Calculations*. doi: 10.3334/CDIAC/otg.CO2SYS_XLS_CDIAC105a

Pogge von Strandmann, P. A. E., Renforth, P., West, A. J., Murphy, M. J., Luu, T.-H., and Henderson, G. M. (2021). The lithium and magnesium isotope signature of olivine dissolution in soil experiments. *Chem. Geol.* 560:120008. doi: 10.1016/j.chemgeo.2020.120008

Raymond, P. A., and Hamilton, S. K. (2018). Anthropogenic influences on riverine fluxes of dissolved inorganic carbon to the oceans. *Limnol. Oceanogr. Lett.* 3, 143–155. doi: 10.1002/lol2.10069

Raymond, P. A., Oh, N.-H., Turner, R. E., and Broussard, W. (2008). Anthropogenically enhanced fluxes of water and carbon from the Mississippi River. *Nature* 451, 449–452. doi: 10.1038/nature06505

Relph, K. E., Stevenson, E. I., Turchyn, A. V., Antler, G., Bickle, M. J., Baronas, J. J., et al. (2021). Partitioning riverine sulfate sources using oxygen and sulfur isotopes: implications for carbon budgets of large rivers. *Earth Planet. Sci. Lett.* 567:116957. doi: 10.1016/j.epsl.2021.116957

Renforth, P. (2012). The potential of enhanced weathering in the UK. *Int. J. Greenhouse Gas Control* 10, 229–243. doi: 10.1016/j.ijggc.2012.06.011

Renforth, P., Pogge von Strandmann, P. A. E., and Henderson, G. M. (2015). The dissolution of olivine added to soil: implications for enhanced weathering. *Appl. Geochem.* 61, 109–118. doi: 10.1016/j.apgeochem.2015.05.016

Riebe, C. S., Kirchner, J. W., and Finkel, R. C. (2004). Erosional and climatic effects on long-term chemical weathering rates in granitic landscapes spanning diverse climate regimes. *Earth Planet. Sci. Lett.* 224, 547–562. doi: 10.1016/j.epsl.2004.05.019

Royal Society (2018). *Greenhouse Gas Removal*. Royal Society and Royal Academy of Engineering.

Schuiling, R. D., and Krijgsman, P. (2006). Enhanced weathering: an effective and cheap tool to sequester CO_2. *Clim. Change* 74, 349–354. doi: 10.1007/s10584-005-3485-y

Spence, J., and Telmer, K. (2005). The role of sulfur in chemical weathering and atmospheric CO2 fluxes: evidence from major ions, δ13CDIC, and δ34SSO4 in rivers of the Canadian Cordillera. *Geochim. Cosmochim. Acta* 69, 5441–5458. doi: 10.1016/j.gca.2005.07.011

Stallard, R. F., and Edmond, J. M. (1983). Geochemistry of the Amazon: 2. The influence of geology and weathering environment on the dissolved load. *J. Geophys. Res. Oceans* 88, 9671–9688. doi: 10.1029/JC088iC14p09671

Stumm, W., and Morgan, J. J. (1996). *Aquatic Chemistry: Chemical Equilibria and Rates in Natural Waters*. John Wiley and Sons.

Suchet, P. A., Probst, J. -L., and Ludwig, W. (2003). Worldwide distribution of continental rock lithology: Implications for the atmospheric/soil CO2 uptake by continental weathering and alkalinity river transport to the oceans. *Glob. Biochem. Cycle.* 17, 1038. doi: 10.1029/2002GB001891

Taylor, L. L., Driscoll, C. T., Groffman, P. M., Rau, G. H., Blum, J. D., and Beerling, D. J. (2021). Increased carbon capture by a silicate-treated forested watershed affected by acid deposition. *Biogeosciences* 18, 169–188. doi: 10.5194/bg-18-169-2021

Taylor, L. L., Quirk, J., Thorley, R. M. S., Kharecha, P. A., Hansen, J., Ridgwell, A., et al. (2016). Enhanced weathering strategies for stabilizing climate and averting ocean acidification. *Nat. Clim. Chang.* 6, 402–406. doi: 10.1038/nclimate2882

Tessier, A., Campbell, P. G. C., and Bisson, M. (1979). Sequential extraction procedure for the speciation of particulate trace metals. *Anal. Chem.* 51, 844–851. doi: 10.1021/ac50043a017

Torres, M. A., West, A. J., Clark, K. E., Paris, G., Bouchez, J., Ponton, C., et al. (2016). The acid and alkalinity budgets of weathering in the Andes–Amazon system: insights into the erosional control of global biogeochemical cycles. *Earth Planet. Sci. Lett.* 450, 381–391. doi: 10.1016/j.epsl.2016.06.012

Torres, M. A., West, A. J., and Li, G. (2014). Sulphide oxidation and carbonate dissolution as a source of CO_2 over geological timescales. *Nature* 507, 346–349. doi: 10.1038/nature13030

UN Environment Programme (2017). *Emissions Gap Report 2017*. UNEP - UN Environment Programme. Available online at: http://www.unep.org/resources/emissions-gap-report-2017 (accessed March 2, 2022).

Walker, J. C. G., Hays, P. B., and Kasting, J. F. (1981). A negative feedback mechanism for the long-term stabilization of Earth's surface temperature. *J. Geophys. Res. Oceans* 86, 9776–9782. doi: 10.1029/JC086iC10p09776

West, A. J., Galy, A., and Bickle, M. (2005). Tectonic and climatic controls on silicate weathering. *Earth Planet. Sci. Lett.* 235, 211–228. doi: 10.1016/j.epsl.2005.03.020

White, A. F., and Brantley, S. L. (2003). The effect of time on the weathering of silicate minerals: why do weathering rates differ in the laboratory and field? *Chem. Geol.* 202, 479–506. doi: 10.1016/j.chemgeo.2003.03.001

White, A. F., Bullen, T. D., Vivit, D. V., Schulz, M. S., and Clow, D. W. (1999). The role of disseminated calcite in the chemical weathering of granitoid rocks. *Geochim. Cosmochim. Acta* 63, 1939–1953. doi: 10.1016/S0016-7037(99)00082-4

Yamashita, N., Sase, H., Kobayashi, R., Leong, K.-P., Hanapi, J. M., Uchiyama, S., et al. (2014). Atmospheric deposition versus rock weathering in the control of streamwater chemistry in a tropical rain-forest catchment in Malaysian Borneo. *J. Trop. Ecol.* 30, 481–492. doi: 10.1017/S0266467414000303

Zamanian, K., Pustovoytov, K., and Kuzyakov, Y. (2016). Pedogenic carbonates: forms and formation processes. *Earth Sci. Rev.* 157, 1–17. doi: 10.1016/j.earscirev.2016.03.003

frontiers | Frontiers in Climate

TYPE Perspective
PUBLISHED 07 September 2022
DOI 10.3389/fclim.2022.928403

OPEN ACCESS

EDITED BY
Simona Liguori,
Clarkson University, United States

REVIEWED BY
Lyla Taylor,
The University of Sheffield,
United Kingdom
Kyle S. Hemes,
Amazon, United States

*CORRESPONDENCE
Ivan A. Janssens
ivan.janssens@uantwerpen.be

SPECIALTY SECTION
This article was submitted to Negative Emission Technologies, a section of the journal Frontiers in Climate

RECEIVED 25 April 2022
ACCEPTED 18 August 2022
PUBLISHED 07 September 2022

CITATION
Janssens IA, Roobroeck D, Sardans J, Obersteiner M, Peñuelas J, Richter A, Smith P, Verbruggen E and Vicca S (2022) Negative erosion and negative emissions: Combining multiple land-based carbon dioxide removal techniques to rebuild fertile topsoils and enhance food production. *Front. Clim.* 4:928403. doi: 10.3389/fclim.2022.928403

Negative erosion and negative emissions: Combining multiple land-based carbon dioxide removal techniques to rebuild fertile topsoils and enhance food production

Ivan A. Janssens[1]*, Dries Roobroeck[2], Jordi Sardans[3,4], Michael Obersteiner[5,6], Josep Peñuelas[3,4], Andreas Richter[6,7], Pete Smith[8], Erik Verbruggen[1] and Sara Vicca[1]

[1]Biology Department, Research Group Plants and Ecosystems, University of Antwerp, Wilrijk, Belgium, [2]Natural Resource Management Unit, International Institute of Tropical Agriculture (CGIAR), Nairobi, Kenya, [3]Global Ecology Unit, Center for Ecological Research and Forestry Applications, Spanish National Research Council, Autonomous University of Barcelona, Barcelona, Spain, [4]Center for Ecological Research and Forestry Applications (CREAF), Cerdanyola del Valles, Spain, [5]School of Geography and the Environment, Environmental Change Institute, University of Oxford, Oxford, United Kingdom, [6]Ecosystem Services and Management Program, International Institute for Applied Systems Analysis, Laxenburg, Austria, [7]Department of Microbiology and Ecosystem Science, Centre for Microbiology and Environmental Systems Science, University of Vienna, Vienna, Austria, [8]Institute of Biological and Environmental Sciences, University of Aberdeen, Aberdeen, United Kingdom

Carbon dioxide removal (CDR) that increases the area of forest cover or bio-energy crops inherently competes for land with crop and livestock systems, compromising food security, or will encroach natural lands, compromising biodiversity. Mass deployment of these terrestrial CDR technologies to reverse climate change therefore cannot be achieved without a substantial intensification of agricultural output, i.e., producing more food on less land. This poses a major challenge, particularly in regions where arable land is little available or severely degraded and where agriculture is crucial to sustain people's livelihoods, such as the Global South. Enhanced silicate weathering, biochar amendment, and soil carbon sequestration are CDR techniques that avoid this competition for land and may even bring about multiple co-benefits for food production. This paper elaborates on the idea to take these latter CDR technologies a step further and use them not only to drawdown CO_2 from the atmosphere, but also to rebuild fertile soils (*negative erosion*) in areas that suffer from pervasive land degradation and have enough water available for agriculture. This way of engineering topsoil could contribute to the fight against malnutrition in areas where crop and livestock production currently is hampered by surface erosion and nutrient depletion, and thereby alleviate pressure on intact ecosystems. The thrust of this perspective is that synergistically applying multiple soil-related CDR strategies could restore previously degraded soil, allowing it to come back into food production (or become more productive), potentially alleviating pressure

on intact ecosystems. In addition to removing CO_2 from the atmosphere, this practice could thus contribute to reducing poverty and hunger and to protection of biodiversity.

KEYWORDS

enhanced weathering, biochar, soil carbon storage, food security, undoing soil degradation, engineering soils

The conflict between using land to help solve the climate crisis or to produce more food for a growing human population

Across all Shared Socioeconomic Pathways (Riahi et al., 2017), a global increase in food demand of 35–56% is projected by 2050 relative to 2010 (van Dijk et al., 2021), implying an equally large food gap between food required in 2050 and food availability under a business-as-usual scenario (Ranganathan et al., 2018). Without drastic transformations of the agriculture and food sectors (Schmidt-Traub et al., 2019), producing 60% more food would require nearly 6 Mkm^2 nature or forest land to be converted into cropland or pasture, i.e., a growth of the current agricultural area (50 Mkm^2; Smith, 2016) by 12%. Evidently, such a dramatic land use change would have colossal adverse effects on biodiversity, environment, and climate (Ranganathan et al., 2018).

The yield per area and total production of major staple foods are globally on a decline owing to increased temperatures (Zhao et al., 2017). Especially strong impacts of climate change are experienced across the tropical belt where extreme heatwaves occur more frequently (Mbow et al., 2019) and severe droughts are already causing water stress (Porkka et al., 2016; Spinonii et al., 2021). In addition to the risk that climate change reduces productivity per unit land area, there is also a risk that the total land area available for agriculture will decline. Almost all IPCC scenarios compliant with a maximum of 1.5°C warming, which would dampen the increase in frequency and intensity of climate extremes (Hoegh-Guldberg et al., 2018), depend on large-scale deployment of carbon dioxide removal (CDR) technologies. Applying two of the most studied land-based CDR technologies, Bio-Energy with Carbon Capture and Storage (BECCS), which supports the energy transition, and afforestation/reforestation (AR), which is beneficial for biodiversity and Earth function, however, would require an estimated 4–7 Mkm^2 of land (Smith et al., 2016; Mbow et al., 2019). Reducing the current 50 Mkm^2 of agricultural land by 4–7 Mkm^2 (-8 to−14%) to enable large-scale BECCS and AR deployment is unacceptable given that 820 million people are still undernourished (Mbow et al., 2019); likewise expanding the current agricultural area with an extra 6 Mkm^2 to close the food gap would come at too large a cost for biodiversity and environment.

Food and nutritional security are furthermore threatened by decreases of soil organic matter stocks, compromising soil nutrient retention and water holding capacity (Tan et al., 2005; Ghimire et al., 2022), that moreover causes CO_2 emissions that exacerbate the climate crisis. Food security is further threatened by soil contamination (Persson et al., 2022) and soil sealing, i.e., the creation of an impermeable layer (Gardi et al., 2015). Importantly, each year erosion strips 24 billion tons of topsoil from arable land worldwide (UNCCD, 2014; FAO and ITPS, 2015), diminishing the amount of food that can be produced for many generations to come. One third of global agricultural land is already subject to human-induced land degradation (FAO, 2021), and the pace at which this takes place is rising sharply due to population growth. Soil erosion and fertility loss affect a disproportionally large area of land where climate extremes decrease yields the most, aridity increases the fastest, and majority of people's livelihoods depend on agriculture (FAO, 2021). Halting soil degradation is thus a key priority to realize the zero-hunger development goal.

Avoiding competition for land

Multiple solutions have been proposed to overcome the trade-off between using land for CDR or for agriculture, and probably all will be needed if worse climate change impacts and food shortages are to be avoided. These proposed solutions are diverse and often not mutually exclusive. One group of solutions focuses on producing more food on less land. High-yield farming of croplands, with targeted protection of biodiversity (by setting aside 20% of agricultural land as the major pathway to improving biodiversity) and spatial optimization of crop selection and fertilizer inputs to current-day climate and soil conditions, was estimated to produce similar volumes of food on 40% less land (Folberth et al., 2020). Moreover, it would reduce global irrigation needs by 20% and maintained global fertilizer applications at current-day levels (Folberth et al., 2020). In many areas where rain-fed agriculture is currently possible, droughts occur with increased frequency and intensity, so ensuring water availability will be required to reduce the

risk for crop failure during droughts. Hence, improved water management at landscape scale constitutes another important component of sustainable cropland intensification that could increase food production on less land (Rockström et al., 2010).

Besides maximizing yields, another group of solutions aims at optimizing the food chain, thus reducing the amount of food required to feed the world and enabling reductions in the agricultural land area. Reducing food wastage, for example, is one of the most low-hanging fruits: currently 30–50% of yields are wasted on their way from the field to the consumer (Lundqvist et al., 2008; FAO, 2011), implying that a drastic reduction in food wastage could substantially increase food availability, without requiring additional land. Another highly effective measure to reduce the land area needed to feed the world would be a global reduction in meat consumption. Roughly 75% of agricultural land is currently used to produce meat, which covers <25% of the calories and proteins required to feed the human population. Hence, also a reduction in global meat consumption would help reduce the land area needed to realize the zero-hunger objective and render land available for CDR (IPCC, 2022). Personal preferences and systemic behavioral patterns, however, pose major barriers to dietary change and more sustainable meat consumption (O'Riordan and Stoll-Kleemann, 2015). Moreover, livestock production also forms the backbone of pastoral communities in semi-arid zones where rainfall can only support grassland ecosystems, with approximately 200 million people worldwide depending on pure grazing (Kaufmann et al., 2019).

Another way to avoid competition for land between CDR and food production is to advance CDR techniques that can be implemented on agricultural land and therefore do not compete with food production, as is the case for enhanced weathering (EW) of silicate minerals (Beerling et al., 2018; Vicca et al., 2021; Ramos et al., 2022; Swoboda et al., 2022; Vienne et al., 2022), increased soil carbon storage (SCS; Smith, 2016; Smith et al., 2016; Rumpel et al., 2018; Amelung et al., 2020), or applying biochar (BC) from excess crop residues and other renewable biomass (Biederman and Harpole, 2013; Smith, 2016; Smith et al., 2016). While the estimated global CDR potentials of these three CDRs (EW about 1, SCS and BC both about 0.7 Gt C yr^{-1}) are lower than those of BECCS (3.3 Gt C yr^{-1}) and AR (up to 3.3 Gt C yr^{-1}) (Smith, 2016; Smith et al., 2016), the agricultural and environmental co-benefits of these approaches help in neutralizing diverse adverse human impacts on the planet and on food security. For example, EW helps counteracting acidification (potentially replacing lime) and restores depleted pools of base cations, silica, and -depending on the source materials- also phosphorus and micronutrients (Beerling et al., 2018). Increasing soil organic matter stocks through SCS and/or BC improves soil aggregation and porosity, which combined with minimizing soil disturbance reduces erodibility, and enhances infiltration, water holding capacity and nutrient retention (Razzaghi et al., 2020; Panagea et al., 2021). Especially in areas with highly weathered or degraded soils like the Global South, these co-benefits help increase crop yields (Jeffery et al., 2017; Beerling et al., 2018).

One option that has rarely been considered so far (but see Horton et al., 2021) is that these latter CDRs may actually be combined, not only to maximize the CDR per unit agricultural land, but even to create new, fertile topsoils in landscapes where agriculture is no longer viable due to surface erosion and nutrient depletion (Figure 1). As mentioned earlier, roughly 25% of the land suited for agriculture is in a severe state of degradation or is rapidly degrading, a trend that must be halted and if possible reversed. The idea to create new fertile land using CDRs originated from studying chronosequences of volcanic islands south of Iceland (the Vestmannaeyjar islands; Leblans et al., 2014). The silicate-rich sediments on the youngest island, now 50 years old, contained all elements needed for plant growth, except nitrogen (N), and the island has remained largely unvegetated since its birth. However, one part of the island harbored a seabird colony where guano deposition catalyzed rapid development of dense vegetation. Microbes subsequently transformed the plant necromass into soil organic matter, which increased soil water-and nutrient retention that further enhanced vegetation productivity, reaching similar productivity values as vegetation on other islands with well-developed, well-managed soils (Leblans et al., 2014, 2017).

This natural development of fertile soil that supports high plant productivity thus occurred because of the combination of weatherable silicate minerals, nutrient-rich fertilizers (guano), and soil organic matter accumulation. In principle, this could be engineered on unproductive land where rain-fed agriculture is possible by applying a sufficient layer of weatherable silicate minerals (EW), mixing in substantial amounts of organic matter and kick-starting productivity by fertilizing with the nutrients that are limiting plant growth the most. Co-deployment of these CDR techniques could thus enable the formation of new fertile cropland and pasture where soils are degraded and not enough food is produced to sustain livelihoods. Because this method tackles the challenges of ending hunger and mitigating emissions at the same time it can foster a high level of support and investment which will promote widespread uptake.

Realizing high-yield, carbon-negative agriculture on degraded soil

Lessons learnt about the onset of plant productivity on volcanic islands suggest that all the following features are required to create fertile soils across degraded landscapes.

Weatherable silicate minerals provide the basis of soil formation and restoring agricultural land. Usually in applications of EW the silicates are dosed at 20–50 ton ha^{-1}, i.e., a layer of a few mm, but this does not suffice for extremely

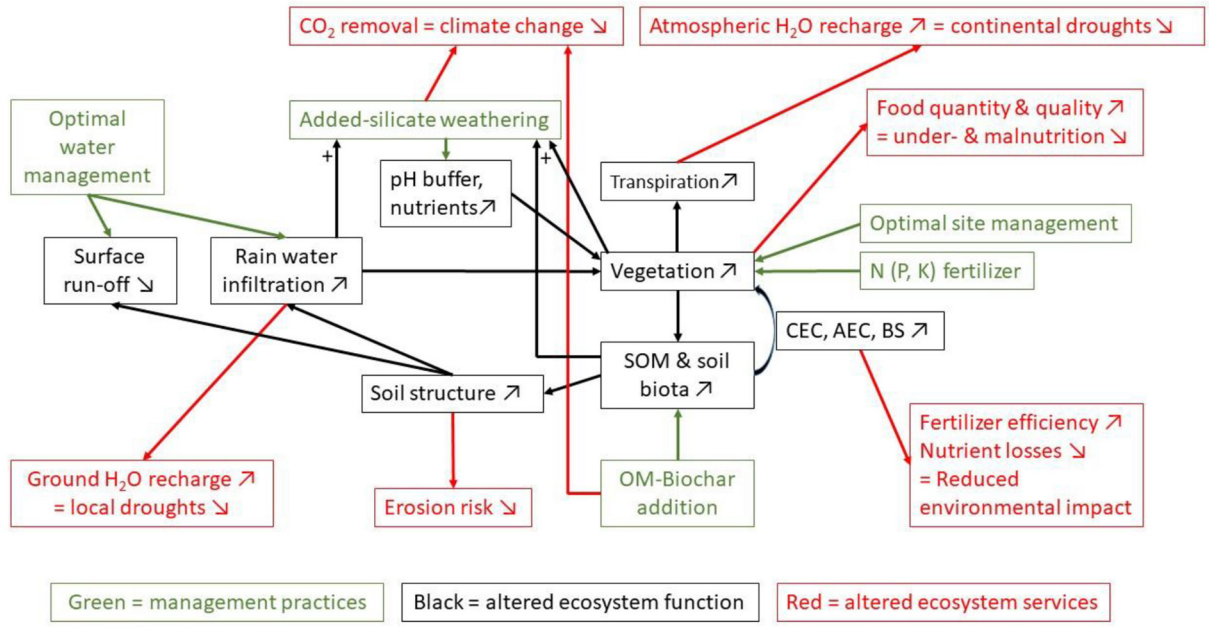

FIGURE 1
Overview of how combining CDR techniques to form new fertile soils would support functions and services in agricultural soils. CDRs and site management practices are given in green, effects on ecosystem services in red, and effects on ecosystem processes in black. Weathering of the added silicates releases a suite of nutrients and buffers soil pH, both benefiting vegetation growth. Plant growth must be supported by well-balanced addition of (in)organic fertilizers and site-specific management such as crop selection and engineered surfaces. Nutrient and water losses are best avoided through high inputs of organic matter (OM) or biochar from renewable biomass caches. These will increase cation- and anion exchange capacity (CEC and AEC) and base saturation (BS) of soils, as well as reinforce its biotic community leading to aggregate formation and improved soil structure. The latter not only protects against surface erosion, it also increases water infiltration, avoiding losses by overland flow and maximizing water retention, which stimulates plant growth. Optimal management of water through reservoirs, wells and irrigation systems further reduces water losses and increases plant-available water which helps to secure yields during extreme drought.

degraded cases where topsoils have been lost. Because of the lack of empirical studies, we can only speculate about how deep the engineered topsoil should be to enable sufficient yields. Deeper soils provide more water and nutrient storage and better anchoring for the roots. However, assuming a density of 1.5 kg dm^{-3}, every cm of engineered soil implies the transport of about 150 ton ha^{-1} of silicate minerals, that all needs to be ground and transported and requires a large financial investment and comes at an energy cost and (until the energy transition has been completed) also a CO_2 cost. Based solely on expert judgment, we speculate that a soil depth of about 10 cm would be needed to sustain viable yields. Developing a new fertile, 10-cm surface layer, would thus imply the transport of roughly 1,500 ton ha^{-1}, about 75 truckloads, and thus presents logistical and financial challenges, and comes with a large CO_2 penalty, for real-world application. Organic matter and biochar from secondary biomass residues are the finishing coat and active ingredient of new fertile soil. How much of these resources would exactly be needed to build a 10-cm surface layer is not certain and will inherently vary. Some studies have suggested application rates of OM at an equivalent rate of 1 ton C per hectare, and of biochar at 30–60 ton dry matter per hectare (e.g., Smith et al., 2016).

The climate benefit of engineering soil on degraded land through a combination of EW, SCS and BC can be preliminary evaluated with a "back-of-the-envelope" CO_2 balance. Emissions from grinding and transporting silicates reportedly amount to about 30% of the CO_2 removed during the weathering for common rates of silicate amendment, i.e., 50 ton per hectare (Smith et al., 2019). Assuming mafic basalt is applied, such a quantity could sequester a total of 15 ton CO_2/ha based on theoretical potential (i.e., 0.3 ton CO_2 per ton rock; Strefler et al., 2018), and the supply-side emission would be 4.5 ton/ha. To create new fertile soil, we suggest applying 30 times more silicates, which will proportionally increase CO_2 emission to 135 ton. However, this is compensated by different factors. If we consider that SCS and BC would realize an immediate CDR of 20 ton C or 73.5 ton CO_2 per hectare, then the remaining emission is 61.5 ton CO_2 per hectare. To achieve this offset with BC and cereal stover at a 3:1 ratio, landowners would have to apply about 25 ton/ha of BC with a low level of 50% fixed carbon (Morales et al., 2015) and about 52 ton/ha of dry cereal stover when 8% of C in the material is permanently retained in the soil (Xu et al., 2019). Further savings in CO_2 emission can be achieved on the supply-side of EW by only using the fine fractions of available waste streams and reducing the distance between mines

and soil restoration site. In this way, it is expected that the CO_2 penalty of engineering soil with EW, SCS and BC could be reduced to 30 ton per hectare. Knowing that experiments with 30–50 ton silicates per hectare found a CO_2 removal in the order of 1 ton C or 3.7 ton CO_2 per hectare per year, it would take about 8 years to become CO_2-neutral. Since much larger and longer lasting CO_2 uptake is expected at rates of 1,500 ton EW per hectare, the engineered soils can become carbon neutral within fewer years, and likely carbon-negative during following decades. While these estimates are fraught with very large uncertainties, it is clear that engineering soils makes sense in terms of CO_2 balance.

Depending on the type of applied silicate minerals, nutrients such as K, Ca, Mg, P, S may need to be supplied. Silicate minerals rich in non-acidic cations and P, and containing essential micronutrients are therefore to be preferred. However, the element that is lacking from these minerals is N. On the youngest of the Vestmannaeyjar islands, vegetation growth only took place when and where the non-geogenic nutrient, N, was deposited by the bird droppings. To estimate how much N would be needed to enable agriculture in engineered soils of 10 cm-depth, we assumed a target soil N concentration of 0.25% (average N concentration in arable soils; Nendel et al., 2019) and found that roughly 4 ton of N per hectare would be required to kick-start productivity for the 1,500 ton of silicate mineral added. We next estimated how much N would be removed with each harvest and thus needing to be resupplied to sustain high productivity in the long term. Taking maize as an example and assuming the mean global annual grain yield of 4.3 ton DM per hectare (FAO, 2009) and a N concentration of 1.2 % (Hirzel et al., 2020), an annual N supply of about 50 kg would be needed to sustain yields. Given the leakiness of the N cycle, this 50 kg is likely a low-end estimate. Replenishing stocks of N and the other nutrients missing from the applied silicate minerals is best achieved using organic fertilizers, such as manure, compost and other homologs, because also soil organic matter is needed (see below).

Supplying vegetation with ample nutrients only stimulates productivity when water is not limiting plant growth. In absence of infrastructures for water management, this restricts the engineering of new fertile soils to areas where rain-fed agriculture is possible. Advanced water conservation and application techniques, such as run-off collectors and irrigation, are therefore recommended, especially in view of extreme droughts becoming more frequent and more long-lived. Also, the greater the water infiltration rate and the higher the soil water retention capacity, the more water the soil can retain after rain events and the less vulnerable yields will be to drought. High water retention capacity could be realized by applying silt-sized silicate minerals. However, this would likely come at a great energy cost. Alternatively, infiltration rates and soil water retention capacity could also be enhanced by ensuring high soil organic matter contents. Maximizing the soil's organic matter content is crucial, not only because it contributes to CDR, but also because soil organic matter is key to almost every soil function, including nutrient retention and exchange (Figure 1). High soil organic matter inputs and stocks support active soil biota which stimulate the formation (and turnover) of soil aggregates, rich in micro- as well as macropores, that help avoid erosion. A proper balance between both pore size classes ensures high water infiltration, avoiding water losses by surface run-off, and maximizes water retention following rain events. Active soil biota also immobilize and slowly release nutrients, thereby helping to avoid nutrient losses from the system. In strongly degraded systems, microbial inoculants with beneficial microorganisms to enhance soil fertility and plant growth, i.e., bio-fertilizers, may be needed to jumpstart biological activity (D'Hondt et al., 2021).

Barriers and opportunities for real-world implementation

Where a degraded or shallow soil is present and sufficient rainfall occurs, we speculate that creating a 10-cm new topsoil layer with EW, SCS and BC may suffice to create a productive system because leaching and bioturbation tend to rapidly ameliorate subsoil conditions (e.g., buffer pH and increase organic matter content) without the need for additional deeper interventions. This 10-cm depth is a speculative prognosis based on expert opinion and has not been tested in modeling or empirical studies. A shallower depth (e.g., 5 cm) would come at lower financial and energy costs, and would thus be preferred, but may not suffice to retain sufficient rainwater and provide a healthy environment for roots and symbionts. Much deeper layers of newly created soil might be unrealistic in terms of the financial and energy requirements. Field experiments with representative rates of nutrient provision, including life cycle and economic analysis, are needed to draw sound conclusions on the optimal depth in true-life situations.

Covering earth surfaces with 10 cm of silicate minerals roughly requires 1,500 tons of rock material per hectare. Transporting such amounts is very costly and carbon-intensive if silicate minerals must be supplied from long distances by freight truck. Synthetic fertilizer inputs and water management infrastructures required to create high-yield carbon-negative agricultural land incur further production and transport costs, that all need to be assessed in life cycle assessment and—costing. While the upfront investments are large for applying EW, fertilization, SCS and BC at such high rates, a considerable part will be recovered from permanent increases of soil fertility and economic yields. Precisely for that reason farmers around the world use these practices to begin with. Furthermore, when the value of mitigated emissions and payments for ecosystem services (e.g., avoided deforestation and biodiversity loss) are considered, creating new fertile soil at large scale may become

financially viable. To enhance the viability the following options should be considered.

Using nearby waste streams

In order to minimize the cost and required energy inputs, and maximize the CDR efficiency in economic and ecological terms, silicate minerals from waste streams are the preferred sources (Beerling et al., 2020). To minimize the financial investment and especially CO_2 penalty, engineered soils must be created in the vicinity (the closer the better) of a free or cheap EW material, using whenever possible the finest fraction (<1 mm) of the silicate materials that does not require grinding (obtained e.g., by sieving). The billion tons of alkaline silicates that accumulate next to mines globally, and which are often pulverized, offer an obvious pool of substrates (Renforth et al., 2011; Renforth, 2019). Also industrial by-products such as steel slags and cement and concrete fines from demolition may provide suitable silicate substrates (Beerling et al., 2020). Yet, in as much as the economic cost of using these waste streams is relatively low, and weathering rates are typically high, their environmental and social impacts require careful investigation before they can be spread on earth surfaces. The composition of industrial by-products such as steel slags and concrete fines is notoriously heterogeneous and may require removal of pollutants to be suitable for EW applications in agriculture (e.g., Wang et al., 2018). Requirements on land accessibility by road could further restrict the area where rejuvenated soils can be constructed. This is the case in small-scale farming landscapes that are highly fragmented and have rugged topography, unless suitable logistical solutions and collective efforts are put in place.

Apply fertilizers

Research at the volcanic Vestmannaeyjar islands has indicated that on top of acquiring silicate minerals there is need for substantial N input to realize high plant productivity and, depending on the chemical composition and weathering rate of EW material that is used, other nutrients may have to be supplied. Once established, nutrient management must be tailored to the specific land use objective, i.e., food production or rangeland. The use of N_2-fixing food crops, pasture grasses, fodder crops, or tree species can help minimize the need for inorganic N fertilizer input over the long term (Rosenstock et al., 2014). Nutrient supply requirements are a function of the balance between export *via* harvest and inputs *via* manure, compost or added biomass. Thus, industrial synthetic fertilizers may not be needed if sufficient manure or organic fertilizers are added to the soils. In any case, fertilizers add to the financial and environmental costs and must be included in the life cycle analysis and—costing.

Increasing and maintaining soil organic matter stocks

Next to EW, SCS and BC are two CDR techniques that are highly beneficial for soil function. The incorporation of crop residues alone generally does not suffice to maintain high soil nutrient availabilities, nor to increase soil organic matter stocks. Cultivating green manures, legume rotations, cover crops, perennials, or deep-rooting crops, and recycling manures, composts, and other organic amendments, are indispensable to maintain or increase soil organic matter stocks and build fertile soils (Smith, 2012; Smith et al., 2020). On the volcanic Vestmannaeyjar islands, the accumulation rate of soil organic matter was strongly coupled to the availability of N, the most limiting element for plant production in those soils (Leblans et al., 2017). Microorganisms that convert plant litter into soil organic matter are usually carbon-limited, even under conditions that are nutrient-limited for autotrophic communities (Soong et al., 2021). This will be specifically true for degraded and intensively cultivated agricultural soils, that are depleted in organic matter. Combining sufficient soil nutrient availability with high organic matter inputs will likely result in high microbial carbon use efficiency, converting a larger fraction of the plant litter into microbial biomass and ultimately in stabile soil organic matter (Cotrufo et al., 2013).

In parallel to these classic techniques for building up soil organic matter, adding biochar will also help maintaining or increasing soil organic matter stocks (Smith et al., 2016). The incorporation of carbonized plant biomass into agricultural land is a CDR with high permanence and potentially large co-benefits on soil nutrient and water retention, as well as on biotic communities (Jeffery et al., 2017). A study Kenya showed that biochar-producing gasifier cookstoves incentivized farmers to collect excess residues from crops which they otherwise burn in the field, thereby displacing firewood and decreasing CO_2 emissions (Sundberg et al., 2020). Farm surveys in Uganda of available residues from common staple crops demonstrated that turning these into biochar could annually sequester 0.20 to 1.15 ton C ha^{-1}, whereas the ambitious target of the "4 per mille" initiative is 0.6 ton C ha^{-1} (Rumpel et al., 2018; Roobroeck et al., 2019). Amendment of biochar to tropical soils was proven to increase crop yields for more than a decade, under favorable and unfavorable rainfall, as a result of improved soil pH and water holding capacity (Kätterer et al., 2019). Farmer households and agribusinesses thus profit from having low-cost energy and recurrent yield gains. Plans are being developed to scale this up, with farmers bringing their residues to nearby gasification plants for captive use of heat in drying processes and/or electricity generation for lowering costs of production or selling to provide income. In this closed-loop model, biochar will be added to inorganic fertilizers and then incorporated in the soils to increase crop productivity and nutrient use efficiency and reduce N_2O emissions.

TABLE 1 Potential caveats for real-world deployment and climate impacts of the techniques in the proposed approach.

	Method	Resource supply	Costs/Benefits	CDR capacity	GHG penalties
Uncertainty (information gaps)	EW	Amount and type of silicates to build a fertile soil under various conditions	Pricing of rock products and transport at local standards; Yield and efficiency gains *(1)*	*In-situ* dissolution rate of silicates; Interactions with OM and GHG fluxes	Energy intensity and share of renewable power for processing and transport *(2)*
	SCS	Frequency and rate of OM replenishment to substitute inorganic fertilizer	Changes of OM prices and supply within high demand market; *Idem (1)*	Degree of physical and biological OM stabilization in engineered soils	*Idem (2)*; Emission factor of manure and compost production
	BC	Minimum effective dose for improving nutrient and water utilization	Fully loaded costs of feedstock aggregation and processing; *Idem (1)*	Mass balance of pyrolytic conversion; Wood and fossil fuel displacement	*Idem (2)*; Emission factor of residues from crop and agroforestry systems
Barriers (limitations for scaling)	EW	Insufficient or unsuitable local rock waste streams and deposits	Uneconomic quantity and grain size for meeting soil fertility requirements	Slow weathering of silicates due to rainfall deficit or lack of irrigation	Limited access to renewable power for processing and transport *(3)*
	SCS	Scarcity of high-quality OM like manure, compost, or legume residue	Sharp rise in OM prices due to high demand; Lag phase of productivity gain	Fast OM decomposition under intensive agriculture and global warming	*Idem (3)*; Overgrazing by livestock and high emission from manure and compost
	BC	Production constrained by feedstock supply and throughput capacity	Large capital investment and operating cost; Decline in plant growth	Sustainability standards of biomass sourcing are not observed and enforced	*Idem (3)*; No displacement of fossil and wood fuel with pyrolysis systems
Risks (unwanted effects)	EW	Heavy metal contaminants enter food chains and natural ecosystems	Unfavorable (renewable) energy tariffs; High taxes on mining and agro-inputs	Inaccurate CDR estimates due to unknown variation of process dynamics and rates	Increased fossil fuel demand and land use for mining of silicate minerals
	SCS	Leaching of N and P into environment at high application rates	Rollback on policies for compensation of additional costs by landowners	Complexity and sensitivity of OM stabilization and decay modeling	Clearing forests and natural ecosystems for resource supply *(4)*; *Idem (5)*
	BC	Adverse change in soil pH; Pollution by hazardous aromatic compounds	Disruption and shift of feedstock supply overturns financial viability	False reporting on pyrolytic conversion rates and fixed carbon ratios	*Idem (4)*; Biomass transfers cause land degradation at point of origin *(5)*

Caveats applicable to multiple CDR methods are numbered.

Water management

Even though the here-proposed practice of soil rejuvenation is best limited to areas where rain-fed agriculture is possible, water management is still preferred. Infrastructures, such as reservoirs that collect run-off water or irrigation systems, would in most cases further increase yields and reduce the risk for crop failure during anomalous droughts. Providing access to affordable renewable energy (solar or wind) would allow to pump irrigation water at little CO_2 cost. In addition, in coastal areas or in areas with saline ground water, the water present is not suitable for irrigation purposes without treatment. Affordable renewable energy could enable desalinization of this water, thereby unlocking currently unavailable water resources that may increase or secure yields. These infrastructures would come at a high cost but have the benefit of climate-proofing the investment in engineered soils, as well as their yields.

Engineering new soils that are fertile and carbon sinks on degraded land through EW, SCS and BC has strong theoretic backing yet its real-world implementation with benefits on climate and economies is not straightforward. The CDR techniques in the proposed approach have a number of potential caveats including uncertainties due to knowledge gaps, barriers that limit implementation at scale, and risks of unwanted economic and ecological effects (Table 1). All these caveats must be addressed and countered before widespread deployment is financially viable and safe provides an expert assessment of the most important gaps, challenges, and threats that have large distortional effects on the proposed approach to rebuild degraded soils. Further details about potential caveats of EW, SCS and BC are provided by Fuss et al. (2018), Nemet et al. (2018), Lefebvre et al. (2019), Smith et al. (2019), Cao et al. (2020), Haque et al. (2020), Campbell et al. (2022), Swoboda et al. (2022), and Vienne et al. (2022), among others. While there is increasing attention to the individual CDR techniques, a key uncertainty that needs to be dealt with is how EW, SCS and BC interact. Will these techniques reinforce each other, or will

antagonistic effects reduce their joint CDR and climate change mitigation potential?

In conclusion, this perspective proposes to rebuild new soils in areas where climate allows food production, but where mismanagement in previous decades has severely degraded soils, rendering them unsuited for food production. This "negative erosion" can be realized by combining multiple CDR technologies that do not compete for land. Thus, these engineered soils would contribute to multiple sustainable development goals simultaneously.

Data availability statement

The original contributions presented in the study are included in the article/supplementary material, further inquiries can be directed to the corresponding author.

Author contributions

IJ proposed the original idea. All authors helped with elaborating the idea and with writing the text, contributed to the article, and approved the submitted version.

Funding

This research was supported by the Research Foundation—Flanders (FWO) and by the European Commissions (H2020 FET-open project Super Bio-Accelerated Mineral weathering: A new climate risk hedging reactor technology—"BAM"). JS was supported by Spanish Government Project PID2020115770RB-I.

Conflict of interest

The authors declare that the research was conducted in the absence of any commercial or financial relationships that could be construed as a potential conflict of interest.

Publisher's note

All claims expressed in this article are solely those of the authors and do not necessarily represent those of their affiliated organizations, or those of the publisher, the editors and the reviewers. Any product that may be evaluated in this article, or claim that may be made by its manufacturer, is not guaranteed or endorsed by the publisher.

References

Amelung, W., Bossion, D., de Vries, W., Kögel-Knabner, I., Lehmann, J., Amundson, R., et al. (2020). Towards a global-scale soil climate mitigation strategy. *Nat. Commun.* 11, 5427. doi: 10.1038/s41467-020-18887-7

Beerling, D. J., Kantzas, E. P., Lomas, M. R., Wade, P., Eufrasio, R. M., Renforth, P., et al. (2020). Potential for large-scale CO_2 removal via enhanced rock weathering with croplands. *Nature* 583, 242–248. doi: 10.1038/s41586-020-2448-9

Beerling, D. J., Leake, J. R., Long, S. P., Scholes, J. D., Ton, J., Nelson, P. N., et al. (2018). Farming with crops and rocks to address global climate, food and soil security. *Nat. Plants* 4, 138–147. doi: 10.1038/s41477-018-0108-y

Biederman, L. A., and Harpole, W. S. (2013). Biochar and its effects on plant productivity and nutrient cycling: a meta-analysis. *GCB Bioenergy* 5, 202–214. doi: 10.1111/gcbb.12037

Campbell, J. S., Foteinis, S., Furey, V., Hawrot, O., Pike, D., Aeschlimann, S., et al. (2022). Geochemical negative emissions technologies: part I review. *Front. Clim.* 4:879133. doi: 10.3389/fclim.2022.879133

Cao,Y., Zhao, F., Zhang, Z., Zhu, T., and Xiao, H. (2020). Biotic and abiotic nitrogen immobilization in soil incorporated with crop residue. *Soil Tillage Res.* 202, 104664. doi: 10.1016/j.still.2020.104664

Cotrufo, M. F., Wallenstein, M. D., Boot, C. M., Denef, K., and Paul, E. (2013). The Microbial Efficiency-Matrix Stabilization (MEMS) framework integrates plant litter decomposition with soil organic matter stabilization: do labile plant inputs form stable soil organic matter? *Glob. Change Biol.* 19, 988–995. doi: 10.1111/gcb.12113

D'Hondt, K., Kostic, T., McDowell, R., Eudes, F., Singh, B. K., Sarkar, S., et al. (2021). Microbiome innovations for a sustainable future. *Nat. Microbiol.* 6, 138–142. doi: 10.1038/s41564-020-00857-w

FAO (2009). *"Global cereal supply and demand brief" in Crop prospect and food situation, ed.* FAO (Rome: FAO).

FAO (2011). *Global Food Losses and Food Waste – Extent, Causes and Prevention*. Rome: FAO

FAO (2021). *The State of the world's land and water resources for food and agriculture – Systems at breaking point*. Rome: FAO.

FAO and ITPS (2015). *Status of the world's soil resources (SWSR) – Main Report*. Rome: FAO.

Folberth, C., Khabarov, N., Balkovi,č, J., Skalsk,ý, R., Visconti, P., Ciais, P., et al. (2020). The global cropland-sparing potential of high-yield farming. *Nat. Sustain.* 3, 281–289. doi: 10.1038/s41893-020-0505-x

Fuss, S., Lamb, W. F., Callaghan, M. W., Hilaire, J., Creutzig, F., Amann, T., et al. (2018). Negative emissions—Part 2: costs, potentials and side effects. *Environ. Res. Lett.* 13, 063002. doi: 10.1088/1748-9326/aabf9f

Gardi, C., Panagos, P., Van Liedekerke, M., Bosco, C., and de Brogniez, D. (2015). Land take and food security: assessment of land take on the agricultural production in Europe. *J. Environ. Plan. Manag.* 58, 898–912. doi: 10.1080/09640568.2014.899490

Ghimire, R., Bista, P., and Machado, S. (2022). "Crop yield limitation by soil organic matter decline: A Case Study from the US Pacific Northwest" in *Advances in Understanding Soil Degradation. Innovations in Landscape Research,* eds. E. Saljnikov, L. Mueller, A. Lavrishchev, and F. Eulenstein (Springer, Cham.), 609–621. doi: 10.1007/978-3-030-85682-3_27

Haque, F., Chiang, Y. W., and Santos, R. M. (2020). Risk assessment of Ni, Cr, and Si release from alkaline minerals during enhanced weathering. *Open Agric.* 5:166. doi: 10.1515/opag-2020-0016

Hirzel, J., Undurraga, P., León, L., Panichini, M., Carrasco, J., González, J., et al. (2020). Maize grain production, plant nutrient concentration and soil chemical properties in response to different residue levels from two previous crops. *Acta Agric. Scand. B* 70, 285–293. doi: 10.1080/09064710.2020.1725619

Hoegh-Guldberg, O., Jacob, D., Taylor, M., Bindi, M., Brown, S., Camilloni, I., et al. (2018). "Impacts of 1.5°C Global Warming on Natural and Human Systems" in *Global Warming of 1.5°C. An IPCC Special Report on the impacts of global warming of 1.5°C above pre-industrial levels and related global greenhouse gas emission pathways, in the context of strengthening the global response to the threat*

of climate change, sustainable development, and efforts to eradicate poverty, eds. V. Masson-Delmotte, P. Zhai, H.-O. Pörtner, D. Roberts, J. Skea, P.R. Shukla, et al. (Cambridge and New York, NY: Cambridge University Press), 175–312.

Horton, P., Long, S. P., Smith, P., Banwart, S. A., and Beerling, D. J. (2021). Technologies to deliver food and climate security through agriculture. *Nat. Plants* 7, 250–255. doi: 10.1038/s41477-021-00877-2

IPCC. (2022). "Climate change 2022: Mitigation of climate change," in *Contribution of Working Group III to the Sixth Assessment Report of the Intergovernmental Panel on Climate Change*, eds P. R. Shukla, J. Skea, R. Slade, A. Al Khourdajie, R. van Diemen, D. McCollum, M. Pathak, S. Some, P. Vyas, R. Fradera, M. Belkacemi, A. Hasija, G. Lisboa, S. Luz, and J. Malley, (Cambridge; New York, NY: Cambridge University Press). doi: 10.1017/9781009157926

Jeffery, S., Abalos, D., Prodana, M., Bastos, A. C., van Groenigen, J. W., Hungate, B. A., et al. (2017). Biochar boosts tropical but not temperate crop yields. *Environ. Res. Lett.* 12, 053001. doi: 10.1088/1748-9326/aa67bd

Kätterer, T., Roobroeck, D., Andrén, O., Kimutai, G., Karltun, E., Kirchmann, H., et al. (2019). Biochar addition persistently increased soil fertility and yields in maize-soybean rotations over 10 years in sub-humid regions of Kenya. *Field Crops Res.* 235, 18–26. doi: 10.1016/j.fcr.2019.02.015

Kaufmann, B. A., Hülsebusch, C. G., and Krätli, S. (2019). "Pastoral Livestock Systems" in *Encyclopedia of Food Security and Sustainability, Vol. 3: Sustainable Food Systems and Agriculture,* eds. P. Ferranti, E. M Berry, and J. R. Anderson (Elsevier), 354–360. doi: 10.1016/B978-0-08-100596-5.22179-3

Leblans, N. I. W., Sigurdsson, B. D., Aerts, R., Vicca, S., Magnússon, B., and Janssens, I. A. (2017). Icelandic grasslands as long-term C sinks under elevated organic N inputs. *Biogeosci Discuss.* 134, 1–21. doi: 10.1007/s10533-017-0362-5

Leblans, N. I. W., Sigurdsson, B. D., Roefs, P., Thuys, R., Magnússon, B., and Janssens, I. A. (2014). Effects of seabird nitrogen input on biomass and carbon accumulation after 50 years of primary succession on a young volcanic island, Surtsey. *Biogeosciences* 11, 6237–6250. doi: 10.5194/bg-11-6237-2014

Lefebvre, D., Goglio, P., Williams, A., Manning, D. A. C., de Azevedo, A. C., Bergmann, M., et al. (2019). Assessing the potential of soil carbonation and enhanced weathering through life cycle assessment: a case study for São Paulo State, Brazil. *J. Clean. Prod.* 233, 468–481. doi: 10.1016/j.jclepro.2019.06.099

Lundqvist, J., de Fraiture, C., and Molden, D. (2008). Saving *Water: From Field to Fork – Curbing Losses and Wastage in the Food Chain.* SIWI Policy Brief. SIWI.

Mbow, C., Rosenzweig, C., Barioni, L. G., Benton, T. G., Herrero, M., Krishnapillai, M., et al. (2019). "Food Security" in *Climate Change and Land: an IPCC special report on climate change, desertification, land degradation, sustainable land management, food security, and greenhouse gas fluxes in terrestrial ecosystems*, eds. P.R. Shukla, J. Skea, E. Calvo Buendia, V. Masson-Delmotte, H.-O. Pörtner, D.C. Roberts, et al. (Cambridge and New York, NY: Cambridge University Press), 437–550.

Morales, V. L., Pérez-Reche, F. J., Hapca, S. M., Hanley, K. L., Lehmann, J., and Zhang, W. (2015). Reverse engineering of biochar. *Bioresour. Technol.* 183, 163–174, doi: 10.1016/j.biortech.2015.02.043

Nemet, G. F., Callaghan, M. W., Creutzig, F., Fuss, S., Hartmann, J., Hilaire, J., et al. (2018). Negative emissions—Part 3: innovation and upscaling. *Environ. Res. Lett.* 13, 063003. doi: 10.1088/1748-9326/aabff4

Nendel, C., Melzer, D., and Thorburn, P. J. (2019). The nitrogen nutrition potential of arable soils. *Sci. Rep.* 9, 5851. doi: 10.1038/s41598-019-42274-y

O'Riordan, T., and Stoll-Kleemann, S. (2015). The challenges of changing dietary behavior toward more sustainable consumption. *Environ. Sci. Policy Sustain. Develop.* 57, 4–13. doi: 10.1080/00139157.2015.1069093

Panagea, I. S., Berti, A., Cermak, P., Diels, J., and Elsen, A., Kusá, H., et al. (2021). Soil water retention as affected by management induced changes of soil organic carbon: analysis of long-term experiments in Europe. *Land* 10, 1362. doi: 10.3390/land10121362

Persson, L., Almroth, B. M. C., Collins, C. D., Cornell, S., de Wit, C. A., Diamond, M. L., et al. (2022). Outside the safe operating space of the planetary boundary for novel entities. *Environ. Sci. Technol.* 56, 1510–1521. doi: 10.1021/acs.est.1c04158

Porkka, M., Gerten, D., Schaphoff, S., Siebert, S., and Kummu, M. (2016). Causes and trends of water scarcity in food production. *Environ. Res. Lett.* 11, 015001. doi: 10.1088/1748-9326/11/1/015001

Ramos, C. G., Hower, J. C., Blanco, E., Silva Oliveira, M. L., and Theodoro, S. H. (2022). Possibilities of using silicate rock powder: an overview. *Geosci. Front.* 13, 101185. doi: 10.1016/j.gsf.2021.101185

Ranganathan, J., Vennard, D., Waite, R., Lipinski, B., Searchinger, T., and Dumas, P. (2018). *Shifting Diets for a Sustainable Food Future. Working Paper, Installment 11 of Creating a Sustainable Food Future.* Washington, DC: World Resources Institute.

Razzaghi, F., Obour, P. B., and Arthur, E. (2020). Does biochar improve soil water retention? a systematic review and meta-analysis. *Geoderma* 361, 114055. doi: 10.1016/j.geoderma.2019.114055

Renforth, P. (2019). The negative emission potential of alkaline materials. *Nat. Commun.* 10, 1401. doi: 10.1038/s41467-019-09475-5

Renforth, P., Washbourne, C. -L., Taylder, J., and Manning, D. A. C. (2011). Silicate production and availability for mineral carbonation. *Environ. Sci. Technol.* 45, 2035–2041. doi: 10.1021/es103241w

Riahi, K., Van Vuuren, D. P., Kriegler, E., Edmonds, J., O'neill, B. C., Fujimori, S., et al. (2017). The shared socioeconomic pathways and their energy, land use, and greenhouse gas emissions implications: an overview. *Glob. Environ. Chang.* 42, 153–168. doi: 10.1016/j.gloenvcha.2016.05.009

Rockström, J., Karlberg, L., Wani, S. P., Barron, J., Hatibu, N., Oweis, T., et al. (2010). Managing water in rainfed agriculture—The need for a paradigm shift. *Agric. Water Manag.* 97, 543–550. doi: 10.1016/j.agwat.2009.09.009

Roobroeck, D., Hood-Nowotny, R., Nakubulwa, D., Tumuhairwe, J. B., Mwanjalolo, M., Ndawula, I., et al. (2019). Biophysical potential of crop residues for biochar carbon sequestration, and co-benefits, in Uganda. *Ecol. Appl.* 29:e01984. doi: 10.1002/eap.1984

Rosenstock, T. S., Tully, K. L., Arias-Navarro, C., Neufeldt, H., Butterbach-Bahl, K., and and, Verchot, L. V. (2014). Agroforestry with N_2-fixing trees: sustainable development's friend or foe? *Curr. Opin. Environ. Sustain.* 6, 15–21. doi: 10.1016/j.cosust.2013.09.001

Rumpel, C., Amiraslani, F., Koutika, L. S., Smith, P., Whitehead, D., and Wollenberg, E. (2018). Put more carbon in soils to meet Paris climate pledges. *Nature* 564, 32–34. doi: 10.1038/d41586-018-07587-4

Schmidt-Traub, G., Obersteiner, M., and Mosnier, A. (2019). Fix the broken food system in three steps. *Nature* 569, 181–183. doi: 10.1038/d41586-019-01420-2

Smith, P. (2012). Soils and climate change. *Curr. Opin. Environ. Sustain.* 4, 539–544 doi: 10.1016/j.cosust.2012.06.005

Smith, P. (2016). Soil carbon sequestration and biochar as negative emission technologies. *Glob. Change Biol.* 22, 1315–1324. doi: 10.1111/gcb.13178

Smith, P., Adams, J., Beerling, D. J., Beringer, T., Calvin, K. V., Fuss, S., et al. (2019). Land-management options for greenhouse gas removal and their impacts on ecosystem services and the sustainable development goals. *Annu. Rev. Environ. Resour.* 44, 255–286. doi: 10.1146/annurev-environ-101718-033129

Smith, P., Calvin, K., Nkem, J., Campbell, D., Cherubini, F., and Grassi, G. (2020). Which practices co-deliver food security, climate change mitigation and adaptation, and combat land-degradation and desertification? *Glob. Change Biol.* 26, 1532–1575. doi: 10.1111/gcb.14878

Smith, P., Davis, S. J., Creutzig, F., Fuss, S., Minx, J., Gabrielle, B., et al. (2016). Biophysical and economic limits to negative CO_2 emissions. *Nat. Clim. Change* 6, 42–50. doi: 10.1038/nclimate2870

Soong, J. L., Fuchslueger, L., Marañon-Jimenez, S., Torn, M. S., Janssens, I. A., Penuelas, J., et al. (2021). Microbial carbon limitation: the need for integrating microorganisms into our understanding of ecosystem carbon cycling. *Glob. Change Biol.* 26, 1953–1961. doi: 10.1111/gcb.14962

Spinonii, J., Barbosa, P., Cherlet, M., Forzieri, G., McCormick, N., Naumann, G., et al. (2021). How will the progressive global increase of arid areas affect population and land-use in the 21st century? *Glob. Planet. Change* 205, 103597. doi: 10.1016/j.gloplacha.2021.103597

Strefler, J., Amann, T., Bauer, N., Kriegler, E., and Hartmann, J. (2018). Potential and costs of carbon dioxide removal by enhanced weathering of rocks. *Environ. Res. Lett.* 13, 034010. doi: 10.1088/1748-9326/aaa9c4

Sundberg, C., Karltun, E., Gitau, J. K., Kätterer, T., Kimutai, G. M., Mahmoud, Y., et al. (2020). Biochar from cookstoves reduces greenhouse gas emissions from smallholder farms in Africa. *Mitig. Adapt. Strateg. Glob. Change* 25, 953–967. doi: 10.1007/s11027-020-09920-7

Swoboda, P., Döring, T. F., and Hamer, M. (2022). Remineralizing soils? the agricultural usage of silicate rock powders: a review. *Sci. Total Environ.* 807, 150976. doi: 10.1016/j.scitotenv.2021.150976

Tan, Z. X., Lal, R., and Wiebe, K. D. (2005). Global soil nutrient depletion and yield reduction. *J. Sustain. Agric.* 26, 123–146. doi: 10.1300/J064v26n01_10

UNCCD (2014). *Land Degradation Neutrality: Resilience at Local, National and Regional Levels*. Bonn: UNCCD.

van Dijk, M., Morley, T., Rau, M. L., and Saghai, Y. (2021). A meta-analysis of projected global food demand and population at risk of hunger for the period 2010–2050. *Nat. Food* 2, 494–501. doi: 10.1038/s43016-021-00322-9

Vicca, S., Goll, D. S., Hagens, M., Hartmann, J., Janssens, I. A., Neubeck, A., et al. (2021). Is the climate change mitigation effect of enhanced silicate

weathering governed by biological processes? *Glob. Change Biol.* 28, 711–726. doi: 10.1111/gcb.15993

Vienne, A., Poblador, S., Portillo-Estrada, M., Hartmann, J., Ijiehon, S., Wade, P., et al. (2022). Enhanced weathering using basalt rock powder: Carbon sequestration, co-benefits and risks in a mesocosm study with Solanum tuberosum. *Front. Clim.* 4, 869456. doi: 10.3389/fclim.2022.869456

Wang, W., Zeng, C., Sardans, J., Zeng, D., Wang, C., Bartrons, M., et al. (2018). Industrial and agricultural wastes decreased greenhouse-gas emissions and increased rice grain yield in a subtropical paddy field. *Exp. Agric.* 54, 623–640. doi: 10.1017/S001447971700031X

Xu, H., Sieverding, H., Kwon, H., Clay, D., Stewart, C., Johnson, J. M. F., et al. (2019). A global meta-analysis of soil organic carbon response to corn stover removal. *GCB Bioenergy* 11, 1215–1233. doi: 10.1111/gcbb.12631

Zhao, C., Liu, B., Piao, S., Wang, X., Lobell, D. B., Huang, Y., et al. (2017). Temperature increase reduces global yields of major crops in four independent estimates. *Proc. Natl. Acad. Sci. U.S.A.* 114, 9326–9331. doi: 10.1073/pnas.1701762114

frontiers | Frontiers in Climate

TYPE Review
PUBLISHED 16 December 2022
DOI 10.3389/fclim.2022.970429

OPEN ACCESS

EDITED BY
Sara Vicca,
University of Antwerp, Belgium

REVIEWED BY
Patrick Frings,
GFZ German Research Centre for Geosciences, Germany
Jonathan Sanderman,
Woodwell Climate Research Center, United States

*CORRESPONDENCE
Maya Almaraz
almaraz@ucdavis.edu

SPECIALTY SECTION
This article was submitted to Negative Emission Technologies, a section of the journal Frontiers in Climate

RECEIVED 15 June 2022
ACCEPTED 22 November 2022
PUBLISHED 16 December 2022

CITATION
Almaraz M, Bingham NL, Holzer IO, Geoghegan EK, Goertzen H, Sohng J and Houlton BZ (2022) Methods for determining the CO_2 removal capacity of enhanced weathering in agronomic settings. *Front. Clim.* 4:970429. doi: 10.3389/fclim.2022.970429

Methods for determining the CO_2 removal capacity of enhanced weathering in agronomic settings

Maya Almaraz[1]*, Nina L. Bingham[1], Iris O. Holzer[2], Emily K. Geoghegan[2], Heath Goertzen[1], Jaeeun Sohng[2] and Benjamin Z. Houlton[3]

[1]Institute of the Environment, University of California, Davis, Davis, CA, United States, [2]Department of Land, Air and Water Resources, University of California, Davis, Davis, CA, United States, [3]Department of Global Development and Department of Ecology and Evolutionary Biology, College of Agriculture and Life Sciences, Cornell University, Ithaca, NY, United States

Recent analysis by the IPCC suggests that, across an array of scenarios, both GHG emissions reductions and various degrees of carbon removal will be required to achieve climate stabilization at a level that avoids the most dangerous climate changes in the future. Among a large number of options in the realm of natural climate solutions, atmospheric carbon dioxide removal (CDR) *via* enhanced silicate weathering (EW) in global working lands could, in theory, achieve billions of tons of CO_2 removal each year. Despite such potential, however, scientific verification and field testing of this technology are still in need of significant advancement. Increasing the number of EW field trials can be aided by formal presentation of effective study designs and methodological approaches to quantifying CO_2 removal. In particular, EW studies in working lands require interdisciplinary "convergence" research that links low temperature geochemistry and agronomy. Here, drawing on geologic and agronomic literature, as well as demonstration-scale research on quantifying EW, we provide an overview of (1) existing literature on EW experimentation as a CO_2 removal technique, (2) agronomic and geologic approaches to studying EW in field settings, (3) the scientific bases and tradeoffs behind various techniques for quantifying CO_2 removal and other relevant methodologies, and (4) the attributes of effective stakeholder engagement for translating scientific research in action. In doing so, we provide a guide for establishing interdisciplinary EW field trials, thereby advancing the verification of atmospheric CO_2 in working lands through the convergence of geochemistry and agronomy.

KEYWORDS

enhanced weathering, field study, methods, soil carbon sequestration, agriculture, working lands

Introduction

Natural climate solutions (NCS) center on improved land management techniques to remove carbon (C) from the atmosphere in the near-term and, depending on the approach, can retain C for decades to millennia. Enhanced weathering (EW; the application of pulverized silicate rock to soils) is an NCS that has been proposed to capture 1–2 billion metric tons of CO_2 from the atmosphere per year by 2100, storing it as either as calcium carbonate in soil or bicarbonate in soil pore water, which can eventually leach to the ocean through groundwater and rivers (Beerling et al., 2018). Enhanced weathering has been suggested across a wide variety of land systems, including forests, coasts, and working lands (i.e., croplands and rangelands; Schuiling and Krijgsman, 2006; Meysman and Montserrat, 2017; Beerling et al., 2018). Working lands are particularly appealing for EW applications because they are already highly managed, widely distributed across the globe, and may experience co-benefits for crop production from EW (Beerling et al., 2018). Applying novel technologies like EW to agricultural systems requires a blending of scientific knowledge from geology and agronomy, two disciplines which do not interact strongly in many field studies. While EW in working lands has garnered much attention in the literature, few field studies of EW efficacy exist; rather, most of our existing knowledge on EW and carbon dioxide removal (CDR) is sourced from examinations of natural silicate weathering coupled with small scale laboratory or mesocosm studies, which are then scaled into global models. Verification of CDR rates and other co-benefits of EW across climates, crop types, soil types, and management practices will require a dramatic increase in field studies to understand and optimize this NCS (e.g., Haque et al., 2020).

Enhanced weathering accelerates the natural geologic processes by which water and carbonic acid chemically weather silicate rocks. As part of these reactions, atmospheric CO_2 dissolves into water as carbonic acid, reacts with silicate minerals, and forms bicarbonate, calcium carbonate or other secondary minerals. While silicate weathering helps to stabilize atmospheric CO_2 levels over million-year time scales, it is too slow to reduce the pace of modern climate change. By contrast, the purposeful crushing and shattering of silicate rocks to create high surface areas can be applied to soils to greatly accelerate the natural weathering reaction kinetics and the concomitant CO_2 removal process. The mechanisms by which geologic materials sequester C have been widely studied in laboratory settings and in natural ecosystem field studies (Gaillardet et al., 1999; Dupré et al., 2003; Ibarra et al., 2016); however, the efficacy that smaller rock sizes generated for use in EW have on weathering kinetics and CO_2 removal rates are largely untested at large (acre to multi-acre) scales or in agronomic settings (Beerling et al., 2020). Instead, global models, estimates of EW, weathering kinetics, and reaction products have relied on mesocosm studies, often in greenhouses or growth chambers (Ten Berge et al., 2012; Amann et al., 2020). This is a major barrier to understanding the realized potential for EW as an NCS and deployment of the technology with confidence.

Working lands have the potential to remove CO_2 through the application of rock dust. Given that cropland and pastures span 38% of the global land surface, small management changes may have large impacts on the climate when scaled up (Beerling et al., 2018; Food Agriculture Organization of the United Nations, 2020). Because working lands, particularly croplands, are already highly managed, EW does not pose the same risks to biodiversity as in natural ecosystems. Most industrialized farms already have or use spreading equipment required for silicate rock applications and are familiar with spreading practices, which are similar to applying lime, fertilizer, or other soil amendments. Furthermore, silicate rocks are abundant and globally common–roughly 90% of Earth's crust is made up of silicate minerals–and, while not all are available to mining, such inputs have the potential to be widely available. At present, stockpiles of natural and artificial silicate by-products from mining and other industrial processes exist, however, future demands for EW may require access to unmined material for EW to be effective globally (Beerling et al., 2020). Many working land soils are highly degraded due to years of intensified agriculture that mines soils of C and nutrients, combined with erosion that has resulted in soil loss (Janssens et al., 2022). Since the dawn of agriculture, the top two meters of cultivated soils have lost 133 Gt C globally with dramatic acceleration in the past 200 years (Sanderman et al., 2017). This has resulted in a soil C pool with high potential to be rebuilt through management practices, including the restoration of both organic and inorganic pools. EW has the potential to provide crop and soil health benefits including increases in yield, soil and plant nutrients, and water holding capacity that can provide agronomic and economic benefits to farmers and ranchers (Beerling et al., 2018). Many of the soil, crop, and C benefits of EW are most likely to be observed in highly weathered, low pH, low nutrient systems, but it remains unknown whether such effects will persist across diverse soil conditions. An understanding of factors that influence EW's effectiveness will require field tests across an array of crop, climate, and soil types. Furthermore, potential negative impacts of EW (e.g., heavy metal accumulation, dust inhalation, etc.) remain largely untested under large scale or long-term field conditions. As EW in working lands is under discussion as a globally relevant approach for CO_2 removal, it is incumbent upon researchers to develop, test, verify, and scale this technology for maximum impact.

A principal barrier to EW deployment lies in scientific verification of CO_2 removal under field conditions, which, through testing and refinement of approaches, can help to advance the technological readiness of EW in agronomic settings. Here we provide an overview of geologic and

agronomic methods that can be used to assess mechanisms by which EW effectively sequesters C at field scales. This guide is intended for geologists, agronomists, hydrologists, and natural systems soil scientists, among others, who are interested in conducting EW field research in working lands for the first time. In this paper, we examine gaps in the literature related to EW field trials and describe methods to measure CO_2 removal that bridge the fields of geology and agronomy, such that EW can be deployed with less uncertainty and greater assurance in terms of C benefits. In particular, we discuss relevant geologic concepts and methodological options related to measuring geologic, agronomic, and climate relevant processes, namely CDR, factors that influence weathering kinetics, tools to trace weathering products, and soil and crop health outcomes. Finally, we conclude the paper by touching upon applied science considerations such as outreach and engagement.

Literature survey of enhanced weathering study methodology and context

To better quantify the need for EW field research development, we censused the literature on EW publications to identify the number of existing field studies relative to other methodologies and to identify the contexts in which EW research is being conducted. We used Web of Science to search *"enhanced weathering" AND "carbon" AND "soil"* which resulted in 58 publications. We then further limited our search criteria to only include studies that examined ground silicate rock applications to soils as a method for CDR. After reviewing the papers, we eliminated 17 papers that did not meet this additional criterion, many of which were either paleontological, limnological, or ecological studies that examined rock weathering across natural gradients. We also eliminated 5 papers published in 2022 since data for this year were incomplete at the time of publication. The remaining 36 papers were categorized according to (1) the methodology used (i.e., field, mesocosm, model, or review), and (2) the context in which the study took place (i.e., agriculture, grassland, mining, or non-specific). Mesocosm studies included laboratory and greenhouse pot experiments, microcosms, microplots, soil column, or soil core incubations. Modeling studies included mathematical models and life cycle analyses. Review papers included systematic reviews, meta-analyses, perspective, and opinion pieces. Non-specific contexts included global, regional, or national studies, studies that included multiple locations or settings, or those that did not specify a location/setting, which was most typical of modeling studies. One grassland study also included a forest comparison, which we categorized as a grassland study.

We found that the number of publications on EW applications to soils as a method for CDR has grown in recent years. In the last 4 years, we found 29 publications on EW, whereas a total of only 7 publications had been generated prior to 2018 then (Figure 1). Of the 36 publications our search generated, the majority of papers employed either models (13 publications) to explore the potential of EW as a CDR strategy or synthesized the literature/provided literature-based perspectives in the form of review papers (12 publications; Table 1). Only 5 publications used field-based methods and 4 of those 5 were generated by the same research group, seemingly from a single field study in Ontario, Canada (see Supplementary Data). These data suggest that there have only been data published from two field trials of EW (with a third being published since the time of our literature survey; Larkin et al., 2022). We also found that, while most of the publications included in our dataset were not specific in their context (16 publications), being modeling studies that were broad in scope, the second most common context was agriculture (15 publications; Table 2).

From our findings, it appears that EW is being most rigorously explored in agricultural settings but that such exploration is being predominantly studied using modeling and synthesis approaches and are rarely examined using field trials. In some ways this puts the cart before the horse in that EW is being proposed as a widely scalable CDR technology without adequate field trials to substantiate its effectiveness as such. Such a low frequency of field trials limits our ability to understand the capacity for EW to remove CO_2 from the atmosphere or infer other impacts that such practices may have on ecosystems. Furthermore, published field methods serve a resource for scientists seeking to embark on new field research. Without a wealth of methods to draw on, scientist may struggle to deploy field trials at a rate needed to develop this CDR technology in a timeframe relevant to climate change mitigation.

Recommendations from geology and agronomy for experimental evaluation of enhanced weathering in working lands

The settings under which weathering studies occur shape the approaches that are used to build basic scientific knowledge. A classical distinction involves whether an experimental design is derived from the landscape setting, as is often the case in the geosciences, or if the experimental design is implemented onto the landscape, common to agronomic research. Field research in geology and soil science (particularly sub-fields such as low-temperature geochemistry, geomorphology, hydropedology, and pedology) study how rocks interact with life through an ecosystem process or biogeochemical lens (Dietrich and Lohse, 2014). To address questions within this realm in the field, geological scientists use landscape settings which contain gradients in the factors they hope to study (Pickett,

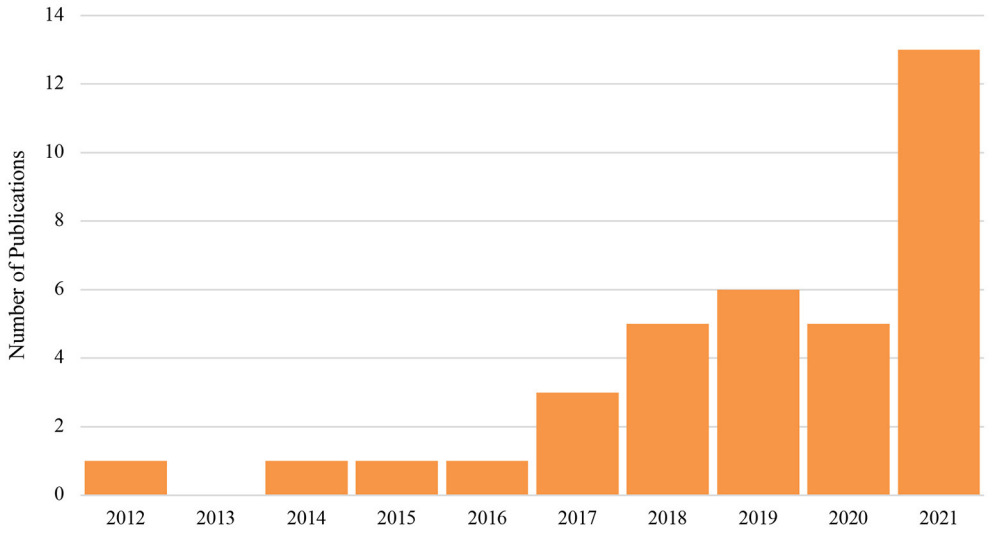

FIGURE 1
Number of publications on enhanced weathering (the application of silicate rock to soils) as a method for carbon dioxide removal in terrestrial ecosystems. Publications were generated using the search *"enhanced weathering" AND "carbon" AND "soil"* and then further refined to meet search criteria (see methods in section Literature survey of enhanced weathering study methodology and context).

TABLE 1 Literature survey results for publications that examined enhanced weathering as a method for carbon dioxide removal, categorized by methodology used in the publication (see methods in section Literature survey of enhanced weathering study methodology and context).

Methods	# of publications
Model	13
Review	12
Mesocosm	6
Field	5
Total	36

TABLE 2 Literature survey results for publications that examined enhanced weathering as a method for carbon dioxide removal, categorized by the context in which this practice was examined (see methods in section Literature survey of enhanced weathering study methodology and context).

Context	# of publications
Non-specific	16
Agriculture	15
Grasslands	3
Mining	2
Total	36

1989; Vitousek, 2004). Conversely, agronomists are principally concerned with identifying and improving issues related to crop production, and thus implement management schemes onto landscapes to test hypotheses. From these two approaches stem various decisions related to site selection, data measurement types, and sampling frequency and timing. To best assess how to study EW, we compare and contrast (Table 3) how two different fields, geoscience and agronomy, typically utilize the landscape to test hypotheses.

Applying geologic approaches to agronomic field studies designs could greatly improve our understanding of EW as a C sequestration technology at shorter time scales. Fortunately, it is likely that many geologic techniques will be more easily deployed in agricultural settings than in natural field settings, where terrain and remoteness pose challenges. At the same time, there may be difficulties (e.g., replication, frequency, etc.) associated with scaling geologic methods to agronomic settings and working around the dynamics of active farms and ranches.

There are tradeoffs associated with translating geologic methods to agronomic contexts. Geologic studies often require considerable care in choosing a study site that controls for the underlying geology, land-use history, paleoclimate influence, aspect, landscape position, and vegetation, among other factors. In contrast, agricultural systems often control for many of these factors, as most farmers select for flat fertile soils and may control for climate through irrigation. At the same time, agronomic studies call for higher replication and sampling frequency than many geologic studies. For instance, geologic measurements of water or sediment may be collected at watershed outlets which provide watershed-averaged measurements. Therefore, the number of samples is limited by the total number of watershed replicates available.

TABLE 3 Summary of the differences between geology and agronomy studies, and recommendations for geologic experimental designs in working lands.

Consideration for study type	Geologic study	Agronomic study	EW study recommendations in working lands
Timeframe under consideration	1–10^6 years or longer; shorter studies may focus on current or short-term perturbations to an ecosystem Longer studies focus on landscape and ecosystem evolution	Growing season (water-year), single or multiple (1–5+ years)	Growing season (water-year) Multiple years Long-term preferred (~10 years)
Replication	Limited by availability of appropriate sampling locations within the natural setting	Measurements are typically replicated annually, preferably over multiple years	Replication is dependent on plot size A minimum of 3 replicate plots is acceptable, but 5–9 are highly recommended in larger plots
Sampling Frequency	Studies for short-term effects often involve more frequent sampling (e.g., daily stream water sampling over 1 year) Landscape and ecosystem evolution studies may only sample one time (using space-for-time substitutions)	Multiple times over the growing season (often 3–6 times) More frequently during periods of interest (e.g., fertilization, rain/irrigation events, etc.)	Soils should be sampled annually Other measurements can be taken more frequently (e.g., soil alkalinity multiple times, lysimeters weekly, GHGs continuously, etc.)
Sampling Depth	Sampling depths for soil often extend well below surface soils into deep soil and bedrock	0–10 cm is customary Deeper sampling may occur depending on the research Sampling should consider tillage and crop root depth	0–10 cm minimum Carbon changes have been shown to occur at depth (2 m), so sampling 1–2 m deep every few years is suggested

We limit our scope to that of soil, soil water, plant material, and soil gas emission measurements.

In agronomic settings, sample size of soil and crop materials depends on heterogeneity across the land. Samples could represent land units (such as experimental plots), be divided into similar areas/sections to account for heterogeneity (for instance, drainage or sand content may vary across a site due to the presence of a creek) or represent soil layers that are affected by agronomic practices (e.g., tillage depth, plant root depth, soil horizon depth, etc.). Soil sampling depth is also a major difference between geologic and agronomic studies. For geobiologists, sampling depth is extended to capture the complete picture of how rock interacts with life (Richter and Mobley, 2009), which means sampling depths for soil often extend well below surface soils (0–10 cm) into deep soil and bedrock. In agricultural soils, though C sequestration has been detected as deep as 2 m (Tautges et al., 2019), most sampling efforts remain limited to the surface soil (~10–30 cm deep).

Sampling frequency is another consideration when translating geologic methods to agronomic settings. For geologists, the spatial and temporal scale of the geological study determines where and what type of samples are taken and how often sampling is conducted. For instance, a geomorphologist focused on landscape and ecosystem evolution may try to measure change over 10^3-10^6 years. Such long timescale-based questions can use space-for-time substitutions which target sites that span a gradient in landscape age to sample (Pickett, 1989) where samples are commonly taken one time (e.g., Long Substrate Age Gradient (LSAG), a long chronosequence sampling design in Hawai'i; Crews et al., 1995). Agronomic field studies typically take place over a growing season (or water-year) and measurements are timed according to management and plant growth (Saville, 1980). Over the course of a growing season, planting, fertilization, irrigation, and harvest are all important events to be considered with agronomic measurements, thus measurements are often taken at multiple time points and may be more intensive at certain times (e.g., rain events, fertilization events, etc.), depending on the measurement. To acquire robust data, is it important that agronomic studies include multiple years of repeated measurements to account for interannual variability (Martin et al., 2004; Smith et al., 2004).

The most critical way in which geology must conform to agriculture is in experimental study design. While geologic studies may consider the landscape as their experimental design, agronomy implements the experiment onto the field. Agronomic field studies commonly use randomized block designs (inclusive of an untreated control) that capture spatial variation within a cropped field (see Chaney, 2017 for some experimental design options). However, within this design, plot size, shape, and arrangement must consider not

only the scientific question, but also practicalities related to field equipment used for planting, harvest, irrigation, and amendment spreading. Additionally, experimental designs need to consider factors such as crop lifespan (e.g., annual vs. perennial, short vs. long lived), crop traits (e.g., row crop vs. grass crop, nitrogen fixing or not), irrigation method (e.g., flood vs. drip vs. overhead) as well as other management practices (e.g., tillage, fertilization, liming, etc.) as these may influence weathering rates. Such factors influence the length of study, the method and frequency of rock application, the spatial distribution of sampling, and scientific equipment installation, among other factors. Climatic and soil characteristics should be controlled for in a robust experimental design unless these are being systematically varied to explore their influence on EW. Since agricultural amendment studies are intended for practical application, it is common for researchers to accommodate typical farming practices into experimental designs. If farmers apply manure, use flood irrigation, practice organic farming, and so on, including such practices benefits from land manager knowledge and allows for results that are relevant to real world farming. Lastly, when working on active farms, one must adapt to necessary management changes and be prepared to terminate treatments if they cause issues to crops or aspects of the farm that are vital to production.

Methodological considerations for determining enhanced weathering efficacy

Diverse methods are available for determining the kinetics and products of EW. Many geology methods have been used in natural contexts to approach questions at geologic timescales, so translating those approaches to shorter timescales and agricultural management contexts can pose challenges. While this research is highly necessary, there are few examples of quantifying a geologic process in an agronomic setting. Approaches to quantifying EW products, CDR rates, drivers of CDR, and mechanisms by which C is stabilized are varied, as this is a nascent field. At present, techniques from geochemistry, agronomy, and soil science are being agglomerated depending on specific project objectives, researcher expertise, study system and scale, and financial constraints. In this section, we examine a range of methodological options, both proposed and implemented, for approaching experimental design, measurements of mineral weathering products, and crop and soil health. We conclude this section with a brief list of recommended measurements, acknowledging that a greater quantity of field studies will be necessary to develop best practices for EW monitoring in working lands.

Carbon dioxide removal

Assessing CDR and the mechanisms responsible as a function of EW practices in agricultural settings requires multifaceted approaches to measure different states of C. Different C pools can be targeted to determine the impact of EW technologies in croplands following the application of EW materials, such as measuring total C content of bulk soil, dissolved organic carbon (DOC) and dissolved inorganic carbon (DIC) in pore water, plant biomass C, and soil greenhouse gas (GHG) emissions, among others (Figure 2). The goal of quantifying multiple fluxes and pools of C in a system is to generate a total net C budget, which will elucidate if a crop system is a net source or a net sink of C. In this section we discuss a variety of measurement options for characterizing CO_2 removal in response to EW field trials and summarize the strengths and weaknesses of each C measurement in Table 4.

An important first step in budgeting C is to directly quantify the amount of C present in the soils, for which diverse approaches have been studied and reviewed intensively (Smith et al., 2020). To quantify soil C stocks, soil samples should be collected before the initial application of silicate rock materials (to quantify baseline stocks) as well as periodically throughout the experiment. Given that soil C sequestration can take years to observe, annual sampling should be more than adequate for monitoring changes in the soil C pool, however, being a rarely tested mechanism, further field trials will be needed to verify this frequency. Sampled soil can be processed for subsequent analyses; for example, once collected, samples may be air dried, sieved, and ground. After preparation, several approaches can be used to quantify the C present in the soil.

Measuring total (or bulk) soil C is the primary way to quantify CDR in soils. However, there are more advanced approaches measuring different C pools that can help refine C budget estimates or answer specific research questions. Conventionally, total bulk soil C, which consists of both the organic and inorganic fractions (Figure 2), can be determined using Dumas high-temperature combustion (Nelson and Sommers, 1983). Combustion methods can also be used to measure the amount of C in plant biomass such as crop harvest or crop residues. Soil C stocks can be measured using bulk density and depth measurements or by the equivalent soil mass method. Determining soil C *via* equivalent soil mass circumvents potential changes to bulk density that can arise from management practices such as tillage or additions of organic amendments (Von Haden et al., 2020). Robust measurements of soil C are required to quantify CDR rates on a per area basis. However, C stock measurements alone do not indicate the mechanisms controlling changes in C storage.

As EW methods continue to develop, it is also crucial to consider the broader scope of soil C cycling and potential methodological approaches. EW of rock amendments can interact with biogeochemical conditions of the soil matrix by

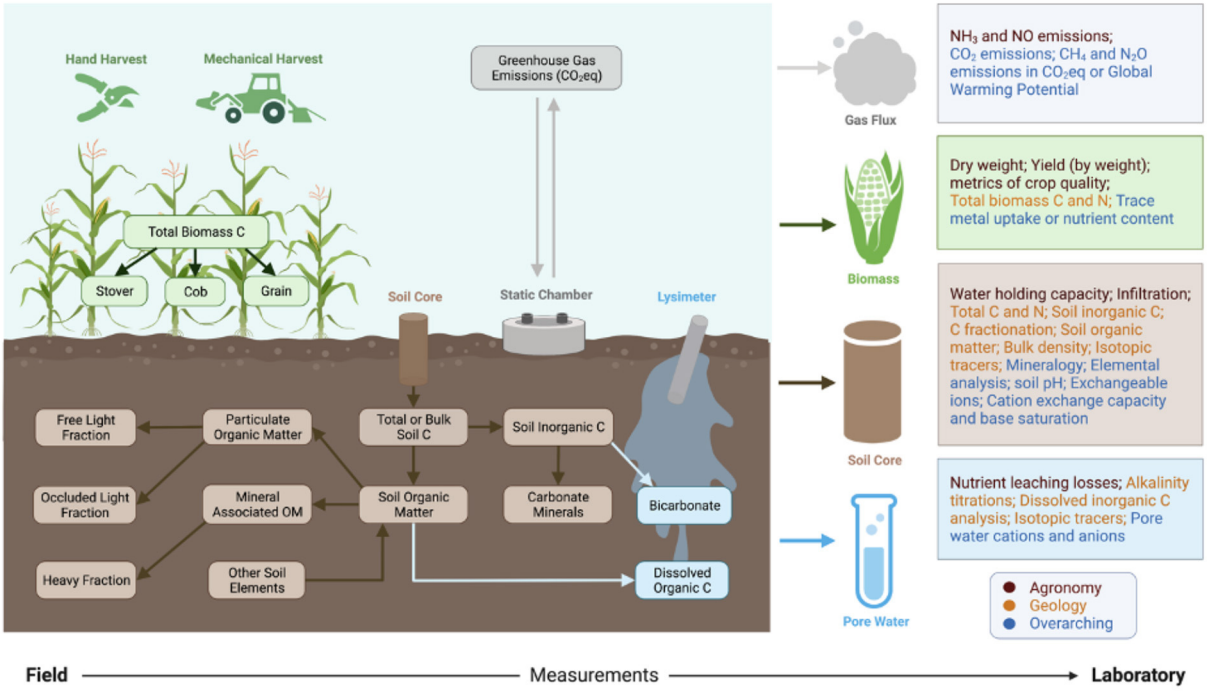

FIGURE 2
Flow chart for field measurements, sample collection, and laboratory analyses from enhanced weathering studies in working land environments.

altering soil pH, base cation pools, and mineral mass in a different range of scales. Such micro or macro environmental changes in the soil matrix can in turn influence microbial vitality, which is a major player in processing SOM into different C pools in soil. SOM is susceptible to decomposition or microbial oxidation and loss back into the atmosphere through microbial respiration.

On one hand, microbial activity can indirectly change SOM pool sizes by decomposing DOC, particulate organic matter (POM) and mineral associated organic matter (MAOM), which are key C pools of SOM (Figure 2; Cotrufo et al., 2019; Kleber et al., 2021). On the other hand, these oxidized C forms, such as organic acids derived from plant root or microbes and respired CO_2 dissolved in soil pore water, are a source of protons that have the potential to drive reactions with minerals, which will directly generate inorganic C products (HCO_3^- and $CaCO_3$; Zaharescu et al., 2020). Moreover, there has been a growing consensus that microbially-derived OM is a key ingredient in formulating stabilized soil C in a form of MAOM (Lavallee et al., 2020). Regarding direct quantification of EW impact on soil C, advanced analytical tools can be utilized to trace biological and microbial processes (stable isotope probing using labeled substrates such as ^{13}C or ^{18}O-H_2O) and to visualize and characterize OM at the sub-micrometer scale (Nano Secondary Ion Mass Spectrometry and Scanning Transmission X-ray Microscopy coupled to Near Edge X-ray Absorption Fine Structure Spectroscopy; Asano et al., 2018; Wang et al., 2019; Wilhelm et al., 2022). While these tools are helpful to identify EW impact on SOC formation and CO_2 removal mechanisms, this approach can be unrealistic for monitoring large scale EW impact in agricultural soils.

Soil inorganic carbon (SIC) pools have traditionally been examined in arid and semi-arid regions where low moisture availability and high average pH lead to carbonate precipitation in the soil (Filippi et al., 2020). In arid soil, inorganic forms of soil C are typically carbonates [CO_3(2-)] existing as solid form in carbonate minerals, which are commonly more thermodynamically stable than organic C. Because agricultural soils have highly variable water contents depending on irrigation protocols and seasonal and regional water regimes, EW impact on SIC formation in agriculture could be site specific depending on targeting pools or mechanisms of SIC formation. The major forms of soil inorganic C (SIC) to consider in EW study are not only carbonates, but also bicarbonate ions (HCO_3^-), which is a dominating DIC form in groundwater. Soil pH controls the fraction of EW-derived carbonates that are available as aqueous bicarbonate or precipitated as pedogenic carbonates (Haque et al., 2020; Vienne et al., 2022). The SIC pool can be substantial and thus measurements should be incorporated into EW field studies.

There are several options for quantifying organic and inorganic soil C pools. Combustion methods such as elemental

TABLE 4 Common carbon measurements for determining the CO_2 removal capacity of enhanced weathering in agronomic settings, inclusive of measurement definition, sample type, common methodology, strengths and weakness of each approach, and supplemental measurements best paired with each carbon measurement.

CO_2 removal measurements	Definition	Samples	Laboratory method	Strengths	Weaknesses	Paired measurements
Total carbon (TC)	Total carbon contents (organic and inorganic) of soil	Soils and rock amendments	Combustion (elemental analyzer)	Most common carbon measurement; relatively easy and affordable	Labor intensive collection and processing; does not separate organic and inorganic forms of carbon without additional treatment; difficult to detect changes against background carbon	Bulk density; equivalent soil mass (sample from three depths); dry weight; sample depth
Soil organic carbon (SOC)	Carbon associated with organic compounds	Soils and rock amendments	Loss on ignition; acid digest assay; Walkley-Black (calculated from SOM); LECO elemental analysis	SOC is the dominant carbon pool in most soils	May not differ significantly from TC; methodological inconsistencies exist	Bulk density; equivalent soil mass (sample from three depths); dry weight; sample depth
Total inorganic soil carbon (SIC)	Inorganic (carbonate minerals) forms of carbon in the soil	Soils and rock amendments	Total carbon minus organic carbon; Thermogravimetric analysis (TGA); acidification with pressure calcimeter or infrared analyzer	An important potential fate of EW	SIC pool may be small in many soils; SIC may precipitate at depths >50 cm making sampling more difficult	Bulk density; equivalent soil mass (sample from three depths); dry weight; sample depth
Soil extractable alkalinity	Carbonate alkalinity (buffering capacity) of soil saturated paste extracts, which contribute to bicarbonate and carbonate formation	Soils and rock amendments	Acidimetric titrations of soil saturated paste extract	Direct measurement of initial carbon product of weathering reaction	Scaling from extractable soil samples may miss transient fluxes of high weathering events	pH
Soil carbon pools based on size and density	Labile to recalcitrant soil carbon pools which differ in function and age (particulate organic matter 53-2000 μm in size and mineral-associated organic matter <53 μm in size; or free, occluded, and heavy light fractions)	Soils and rock amendments	Separation using a 53 μm sieve; separation via density fractionation using sodium polytungstate	Can inform about the stability of accumulated carbon	Labor and time intensive; requires specialized equipment to measure density fractionation	Dry weight; carbon contents; 14^C optional to assess age
Soil microbial biomass carbon (SMBC)	Carbon contents of microbial biomass is soils	Soils and rock amendments	Chloroform fumigation; substrate induced respiration	Can indicate the rate of potential microbial carbon transformation processes in the response to amendments	May miss the impact of rock amendments in shifting the microbial functional traits or community composition	Carbon contents

(Continued)

10.3389/fclim.2022.970429

TABLE 4 (Continued).

CO_2 removal measurements	Definition	Samples	Laboratory method	Strengths	Weaknesses	Paired measurements
Dissolved inorganic carbon (DIC) of soil pore water, leachate, or discharge	The total amount of CO_2, carbonic acid (H_2CO_3), bicarbonate (HCO_3-), and carbonate (CO_3-) in water	Soil pore water, leachate, or discharge	Coulometric and infrared detection methods; acidimetric titrations to measure carbonate alkalinity (carbonate and bicarbonate anions in a solution)	An important potential fate of EW; could be a large pool; develops relatively quickly	Quick development requires a need for frequent sampling; can be difficult to sample at high frequency, especially in drier soils	Water balance, pH
Dissolved organic carbon (DOC) of soil pore water, leachate, or discharge	Organic carbon dissolved in a water that does not include the suspended solids component	Soil pore water or leachate; water or salt extracts	Filtration (operationally defined as the fraction of organic carbon that can pass through a filter with a pore size 0.45 μm)	Reflects the imminent change of labile carbon pool size in soil	Transient pool; typically small pool in terrestrial ecosystems; should be measured with other pools	Water balance, carbon contents
Total biomass carbon	Total carbon contents of biomass	Plants	Combustion (elemental analyzer)	Can inform about carbon losses/the fate of carbon	Biomass weight can also be used as a proxy, assuming 50% of biomass is carbon	Dry weight; carbon contents by plant anatomy (grain vs. stover) optional to get agronomic implications
CO_2 and CH_4 emissions	Gaseous carbon dioxide and methane exchange between soil and the atmosphere	Atmosphere	Laboratory incubations; automatic or manually-operated static flux chambers, measured with syringe sampling and gas chromatography or in situ with a portable gas analyzer; Eddy covariance flux tower; remote sensing	Can inform about carbon losses or CH_4 consumption potential; can improve carbon budgets	Costly and time intensive	Air temperature; soil temperature; soil moisture; bulk density; chamber volume; CH_4 and N2O can be converted to CO_2 equivalents to get GWP
^{13}C	Natural abundance stable isotope	Any	Mass spectrometer elemental analyzer	Can inform about mechanisms of carbon accumulation; often included with TC measurements	Snapshot of the process of natural isotope fractionation; data interpretation can be challenging	Standard and ^{12}C values to get isotope ratios
^{14}C	Trace the fate or age of carbon	Any	Mass spectrometer elemental analyzer	Can use a labeled substrate to trace the fate of accumulated carbon; can estimate the age of carbon stored	Costly; requires specialized expertise; requires a laboratory that is ok with ^{14}C contamination	None necessary

10.3389/fclim.2022.970429

analyzer loss on ignition (LOI) or LECO elemental analysis can be used to measure SIC or calculate the portion of inorganic C (i.e., total C minus organic C). LOI measurements should be used with caution as they are very sensitive to soil texture and moisture and may produce inconsistent results (*Personal communication with Whendee Silver*). Thermogravimetric analysis (TGA) can also be used to measure carbonaceous components in the mineral (clay and oxides) components of soils (after the removal of OM) and rock samples (Pallasser et al., 2013; Kemp et al., 2022). Additionally, soil can be acidified to measure the evolved CO_2 by using a pressure calcimeter (gives bulk equivalent $CaCO_3$ content; Sherrod et al., 2002), or an infrared gas analyzer (Lin et al., 2016). Inorganic C in soil samples can also be measured using acid dissolutions followed by the manometric, titrimetric, or gravimetric determination of CO_2 (Presley, 1975; Wang et al., 2012). Similarly, carbonates can be measured using rapid titrations (soil treated with hydrochloric acid and titrated with sodium hydroxide) to get $CaCO_3$ equivalents (Rayment and Lyons, 2011). By measuring organic and inorganic soil C stocks at the field scale over time, treatment effects and CDR rates following silicate rock applications can be determined.

In addition to measuring soil organic and inorganic C, directly measuring DIC in the soil pore water is critical to quantifying the flux of C that is removed through EW. An important form of soil DIC is aqueous bicarbonate ions (HCO_3^-) present in the soil pore water. HCO_3^- concentrations may also be estimated using total alkalinity, depending on the pH of the system (Olin Neal, 2001). To obtain soil water samples for monitoring solute fluxes in natural soils, *in situ* soil water extraction methods may be used. These include vacuum lysimeters (also referred to as porous cups/tubes or suction cups), suction plate or tension plate lysimeters, pan or zero-tension lysimeters, wick samplers, and resin boxes (Weihermüller et al., 2007). Lysimeters of varied types provide a method for frequent measurement of soil pore water and may be placed at multiple depths to monitor solute movement; however, selection of a suitable sampler material depending on the solutes of interest is imperative (Weihermüller et al., 2007; Vandenbruwane et al., 2008). In agricultural systems, it is likely that lysimeters will have to be removed and reinstalled to accommodate certain machinery. HCO_3^- formed from EW processes may leach deeper into soil profiles and precipitate as carbonate minerals or eventually leach into groundwater; therefore, SIC measurements at deeper soil depth or DIC monitoring in downstream of ground watershed may be appropriate depending on the hydrologic conditions of the system (Sigfusson et al., 2006; Amann and Hartmann, 2022). Once pore water is collected, samples can be measured for pH, total alkalinity using acidimetric titration, DIC, cations and metals by inductively coupled plasma emissions spectrometry (ICP), or other measurements, enhancing understanding of EW processes. Given the central roles of water volume and flow path length in regulating chemical weathering, determining a water balance estimate is critical to scale concentration values into weathering or C fluxes (Maher and Chamberlain, 2014). In the field, this may require monitoring irrigation inputs with a flow meter, obtaining weather station precipitation data, or establishing and monitoring a site-specific weather station, as well as measuring evapotranspiration, soil moisture, infiltration, and hydraulic conductivity.

C isotopic signatures of both SOC and SIC can be useful to infer the mechanisms responsible for CDR within a system (Del Galdo et al., 2003). C isotopic fractionation of SOC and SIC can be measured by quantifying ratios of stable C isotopes (^{12}C and ^{13}C), or by conducting pulse labeling experiments using radioisotope (^{14}C) as a tracer (Smith et al., 2010). The $\delta^{13}C$ composition of SOC is largely determined by the fraction of plant litter originating from C3 or C4 species and by fractionation occurring during microbial decomposition of the resulting organic matter. For SIC, the $\delta^{13}C$ isotopic composition is controlled by the composition of soil CO_2, which is derived largely from root and microbial respiration (Cerling, 1984). The ^{14}C abundance in pedogenic carbonates, a form of SIC, is similarly determined by the relative proportion of CO_2 respired by the rhizosphere and microbially-induced SOM decomposition (Zamanian et al., 2016). The contribution of SOM decomposition determines ^{14}C abundance in pedogenic carbonates, however, is more important in deeper horizons. This is because the age of SOM increases with soil depth (i.e., the older the SOM, the more depleted the ^{14}C abundance; Amundson et al., 1994). Stable isotope data can often accompany total soil C data, however ^{14}C can be more complicated to obtain (i.e., tracers can be expensive and require special labs), and both require specialized expertise to interpret.

GHG measurements determine the net flux (gain or loss) of CO_2 and can help inform estimates of CDR rate (Whitehead et al., 2012). GHG emissions are most commonly measured using: (1) static flux chambers where measurements are taken weekly or bi-weekly (with more frequent sampling during rain or fertilization events that can produce pulse emissions), (2) automated flux chambers where measurements are taken multiple times an hour, (3) Eddy covariance flux towers that estimate net CO_2 exchange across the landscape, or (4) remote sensing (Smith et al., 2010). Of these GHG methods discussed here, static flux chambers are on the low tech/cost end of the spectrum and have the advantage of being movable, while automated chambers are most costly but are much better at capturing heterogenous fluxes. Ecosystem-scale GHG measurements (often taken using eddy covariance) account for the initial uptake of C through photosynthesis (gross primary production), and its subsequent partial losses through ecosystem respiration to give net ecosystem exchange. Eddy covariance methods can effectively determine CDR given that there are no lateral or hydrologic soil C fluxes (Arias-Ortiz et al., 2021), but instrumentation are costly, require specialized

expertise, and are limited in the number of treatments they can monitor (two). Arias-Ortiz et al. (2021) showed that sediment cores and Eddy covariance CDR estimates agreed in flooded peatlands, however this relationship broke down at the tidal wetland site where lateral C fluxes were large. Gough et al. (2008) found similar results but note that a single year of Eddy covariance data may not be consistent with long-term sediment data, thus multi-year datasets are recommended. Remote sensing is best suited for larger scale observations and also requires specialized training and skills. Eddy flux towers integrate over all C sources and sinks providing real time estimates of net ecosystem exchange (Novick et al., 2022), while static chamber measurements are more typically used to reveal differences in emissions of CO_2, nitrous oxide (N_2O) and methane (CH_4) between experimental treatments. N_2O and CH_4, which have a higher GWP potential than CO_2, can be measured and converted into CO_2 equivalents to assess the total effect of GHG emissions from agronomic systems on global warming. Currently proposed mechanisms for EW mitigation of N_2O emissions include increasing NUE through enhanced P availability or decreasing N_2O:N_2 ratios of denitrification through pH stimulated activity of N_2O reductase (Blanc-Betes et al., 2021). While CH_4 emissions can also be quantified, it is less known how EW may mechanistically influence these emissions. In combination with biomass measurements and other soil C measurements (gains from C inputs and CDR, losses from bicarbonate leaching, respiration, or biomass harvesting), GHG measurements make up one component that can contribute to the development of more accurate calculations of total C budgets in agronomic systems (Smith et al., 2010).

In addition to studying C capture potential from EW at individual field sites, scaling up CDR to regional scales is necessary for understanding the potential for EW technologies to be deployed at a larger scale. Currently, the only available assessments of the large-scale effects of EW on soil C capture are estimates derived from models. These stoichiometric models are parameterized using mass balance equations and interactions between factors such as rock-dissolution reaction rates, climate data, C dynamics, nutrient availability, plant responses, hydrology, and soil physical properties (mineralogy, grain size, soil moisture, bulk density, etc.) (Taylor et al., 2017; Cipolla et al., 2021; Goll et al., 2021). *In situ* field studies and on-the-ground measurements are necessary for both confirming and improving these model estimates across broader scales. Finally, the development of comprehensive life cycle analyses (LCA's) will be necessary to verify the net C benefit of EW, particularly given the energy demands associated with crushing and transporting rock. Existing LCA's report conflicting results regarding EW's net C benefits (Beerling et al., 2020; Taylor et al., 2021; Schlesinger, 2022), results that likely differ as a result of modeled dissolution rate assumptions, C pools incorporated, and transport methodology. In practice, the net C benefit of EW will likely vary regionally based on access to mined materials and soil conditions that support fast CDR rates, thus LCA's will be better informed when coupled with robust field data that elucidates the actualized and regionally specific CDR capacity of this emerging technology.

Influences on weathering kinetics

Terrestrial silicate weathering plays a central role in regulating Earth's atmospheric CO_2 levels. As silicate minerals weather, they react with CO_2 dissolved as carbonic acid (Equations 1 and 2), moving C from the atmosphere into the hydrosphere as bicarbonate (Equation 3), and releasing cations and silicic acid (Mitchell et al., 2010). Subsequently, bicarbonate may react further, yielding carbonate minerals such as calcite or magnesite and resulting in the release of one mole of CO_2 (Equation 4). The CDR benefit of EW may vary based on emissions associated with rock transport (i.e., life cycle emissions; Beerling et al., 2020), chemical composition of the rock, soil characteristics (like pH or texture), management practices (like irrigation or crop type), influences on carbonate formation (i.e., dust inputs of IC, parent material, upward groundwater movement; Zamanian et al., 2016), the form in which CO_2 is sequestered (with bicarbonate sequestering 2 mols and calcium carbonate sequestering 1 mol of CO_2), and whether CO_2 is released back into the atmosphere along surface water flow paths. More field data are needed to better quantify this variation.

Weathering rates and resulting solute concentrations are dictated by tectonic forces and erosion, which control availability of fresh mineral surfaces, and by runoff and water flow path lengths (Maher and Chamberlain, 2014). Additional factors that influence weathering rates include pH and temperature, as well as rock characteristics such as mineralogy and porosity (Isson et al., 2020). For this reason, areas with high rates of erosion, hotter and wetter climates, more acidic soils, or heavily irrigated management practices might expect to see faster rates of CDR in response to EW applications. Dissolution kinetics are key to understanding weathering rates of various lithologies and reaction with atmospheric CO_2 (Yadav and Chakrapani, 2006).

$$CO_2\,(g) \leftrightarrow CO_2(aq) \tag{1}$$

$$CO_2\,(aq) + H_2O \leftrightarrow H_2CO_3\,(aq) \tag{2}$$

$$CaSiO_3\,(s) + 2H_2CO_3\,(aq) + H_2O \leftrightarrow 2HCO_3^-\,(aq) + H_4SiO_4(aq) + Ca^{2+}(aq) \tag{3}$$

$$2HCO_3^-\,(aq) + H_4SiO_4\,(aq) + Ca^{2+}\,(aq) \leftrightarrow 3H_2O + CO_2\,(g) + CaCO_3\,(s) + SiO_2\,(s) \tag{4}$$

A variety of silicate rocks may be used for EW. The chemical dissolution and subsequent CDR rates vary with silicate rock type, particle size, soil characteristics, climate, and other factors. While particle size is a key determinant in weathering rate

(with small higher surface area particles weathering faster than coarse particles), from an applied perspective, extremely fine materials can be difficult to apply and may present a dust inhalation hazard. Furthermore, finely grinding rock materials requires significant energy expenditures (Strefler et al., 2018) that may exceed CDR benefits (Lewis et al., 2021). Most studies suggest that particle sizes of 10–20 microns provide the greatest CDR benefit (Rinder and von Hagke, 2021), but larger particle sizes (∼100 microns) have been used in EW research and may be more widely available (Kelland et al., 2020). More recently, researchers have suggested that larger particles may be comparable to finely ground particles in their CDR potential (Kantzas et al., 2022), highlighting the need for critical assessments that compare the efficacy of different grain sizes. Figuring out the largest grain size that is reasonably effective at CDR is critical to minimizing the energy demand of EW as well as health and safety risks associated with handling rock dust.

Mineralogy further impacts weathering rates, with minerals forming at higher temperatures and pressures, such as olivine, weathering more readily at Earth's surface (Goldich, 1938). However, ultramafic minerals that weather faster also pose a higher risk of inducing heavy metal toxicity (Beerling et al., 2018). Monitoring the content of heavy metals such as cadmium, lead, chromium, and zinc in rock and soil before and after application may help mitigate heavy metal toxicity. Moreover, global availability and proximity to mines greatly impacts the scalability of EW (Köhler et al., 2010). Basalt, though less rapidly weathering than olivine-dominated rocks, such as dunite, exists broadly and has lower risk of heavy metal accumulation when applied to soils. Site location will largely determine mine proximity and rock compositions that are accessible (Krevor et al., 2009).

Designing field experiments that not only quantify CDR, but also test the influence of various factors on CDR rates will be vital to deploying highly effective EW strategies. Randomized block designs that test the effect of particle size on CDR rate, multi-site experiments that span gradients of soil pH, or comparisons between tropical and temperate field sites are all examples of ways that field studies can examine the factors that influence weathering kinetics.

Tracing weathering products

A variety of analytical techniques common to pedology, geochemistry, agronomy, and mineralogy may be employed to elucidate the products of EW and track their movement in soil, water, and plant biomass. These products, when quantified alongside ion transport and secondary mineralization, can be used to approximate weathering and dissolution rates, trace nutrient release and movement, and monitor levels of potentially toxic metals released from applied minerals. Markers of weathering (e.g., Mg^{2+} release from olivine dissolution) may also be used to estimate CDR.

Physical and chemical characterization of silicate rock amendments, including grain size, specific surface area, mineralogy, and elemental composition, is a necessary first step in identifying expected weathering products and estimating potential CDR. Both grain size and specific surface area are relevant for estimating dissolution rates and understanding available surfaces for weathering reactions. Numerous approaches are available for characterizing grain size distributions, but a particle size analyzer (PSA) using laser diffraction is common. Additionally, the Brunauer, Emmett, and Teller (BET) method, using gas adsorption to mineral surfaces, is used to measure specific surface area. Mineralogy may be determined using X-ray diffraction (XRD; Silva et al., 2021) or quantitative evaluation of materials by Scanning Electron Microscopy (QEMSCAN), while rock elemental composition is regularly measured using lithium borate fusion coupled with X-ray fluorescence (XRF) or inductively coupled plasma atomic emission spectroscopy or mass spectroscopy (ICP-AES or ICP-MS).

To understand EW dynamics in soil, imaging approaches including scanning electron microscopy with energy dispersive spectroscopy (SEM-EDS; Haque et al., 2020), transmission electron microscopy (TEM; Bonneville et al., 2009), and nanoscale secondary ion mass spectrometry (NanoSIMS) may be relevant. Synchrotron-based x-ray absorption spectroscopy may also help reveal weathering processes and specific mineral phases (Nieva et al., 2019). As noted by Dudhaiya et al. (2019), some of these approaches for tracing weathering products, including thermogravimetric analysis (TGA; discussed in section Carbon dioxide removal), EDS, and XRD may be limited in their application in highly heterogeneous amended soils due to the small sample sizes. However, in-depth examinations of organo-mineral interactions and mineral weathering using SEM, TEM, and other approaches common in natural systems research (e.g., Jongmans et al., 1997; Bonneville et al., 2009) will likely become more common in EW studies as this field of research grows more mechanistic and detailed. Many of the aforementioned non-destructive approaches, as well as infrared spectroscopy and additional forms of x-ray spectroscopy and microanalysis, have been reviewed in detail (Haque et al., 2019a). Approaches used to characterize rock amendment mineralogy and elemental analysis are also relevant to understanding amended soils.

Beyond direct visualization and quantification of weathering products, isotopic tracers are widely used in soils and geology for dating, tracking landscape processes, and interpreting biological influences, among other applications. For example, because strontium (Sr) exhibits limited fractionation (i.e., mass-dependent fractionation is corrected for during data reduction), Sr isotopic ratios ($^{87}Sr/^{86}Sr$) may be used in soil systems as a tracer, provided all input pools (dust, parent material, rain, groundwater) are well-characterized (Capo et al., 1998). Because

of this utility, Sr has been proposed as a tracer of EW products, though this would require sufficient distinction between the rock amendment and soil parent material. Refer to the section Carbon dioxide removal for specifics concerning C isotopes in the context of EW.

Because silicate weathering occurs *via* proton-consuming reactions, increasing soil pH is a commonly observed phenomenon (e.g., Haque et al., 2019b; Amann et al., 2020). While not suitable as a direct proxy for dissolution rates, pH is important for nutrient and trace metal mobility, runoff or discharge chemistry, suitability for continued weathering and crop growth, and other ecosystem or soil effects. Tracking pH in soil and water of field experiments can help improve understanding of these dynamics. The desirability of pH shifts largely depends on the system's baseline pH (e.g., increased pH in an acidic system may alleviate some need for liming) (Ten Berge et al., 2012). While increased pH may be highly beneficial in mitigating metal toxicity and low cation exchange capacity (a measure of the soil's ability to hold positively charged ions) in tropical systems, downstream effects of pH changes on aquatic ecosystems may be negative, emphasizing the need for pH monitoring (Edwards et al., 2017).

In addition to pH controls, explicitly measuring exchange complex ions, changes in cation exchange capacity, and macro- and micronutrient pools can help identify ancillary EW effects beyond CDR, allowing for monitoring of both beneficial nutrients and potentially toxic trace metals (Ramos et al., 2022). In agricultural systems, the added step of quantifying trace metal or nutrient content of plant biomass may be relevant for assessing bioavailability of rock-derived ions, whether beneficial or detrimental, and may be quantified using acid digestion of dried plant biomass coupled with ICP-AES, ICP-MS, or AAS for elemental quantification (Ten Berge et al., 2012).

Many of the approaches applied to soil are relevant to the aquatic component of these systems, including the soil pore water, leachate or runoff, and downstream chemistry. Water pH, pore water cations and anions (quantified *via* ICP-AES, ICP-MS or atomic absorption spectroscopy (AAS), among other methods), and C species or other solutes are key metrics for tracing ion movement and export (Ten Berge et al., 2012; Amann et al., 2020; Taylor et al., 2021). A number of these measurements are highly time-sensitive (e.g., pH) and may require particular attention during sample collection (e.g., acidification for metal analysis); however, their wide application in water quality monitoring means standard collection protocols are widely available. As in soils, isotopic tracers may also be used to monitor weathering products in the aquatic component of agronomic systems.

More broadly, the roles of microbial communities, plants, and SOM in mediating mineral weathering are significant (Drever, 1994; Balogh-Brunstad et al., 2008; Bonneville et al., 2009; Taylor et al., 2012); examining these interactions in the context of EW requires a broad suite of additional tools beyond the scope of this paper, though understanding these linkages is essential to completing assessments of EW potential (Cipolla et al., 2021; Verbruggen et al., 2021; Vicca et al., 2022).

Soil health and crop outcomes

While CDR is often the main goal of EW studies, it is important to evaluate the effects of EW on properties that are important to land managers, such as soil and plant health. Soil health can be defined as the capacity of soil to function optimally within an ecosystem to sustain plants, animals, and humans. Components of soil health that are of interest to land managers due to their influence on plant health include cation exchange capacity, nutrient availability, and soil stability and infiltration. Soil available micro- and macronutrients can contribute positively to crop production and soil health. Cation exchange capacity and base saturation (the percentage of cation exchange capacity occupied) can determine nutrient stock potentials in soils. Silicate rocks typically have tradeoffs related to weathering rate and risk of heavy metal accumulation, with more readily weathered rocks having higher risks. Because heavy metals may be hazardous, potential heavy metal accumulation in soils and crops from EW practices should be assessed. Soil water measurements of interest to land managers include soil water holding capacity, infiltration rates, compaction, evapotranspiration, and salinity, among others (Corwin and Lesch, 2005; Garg et al., 2016; Li et al., 2016). The ability of soils to hold more water can reduce irrigation needs, while poor infiltration rates can lead to flooding, compaction, and increased overland flow. Similarly, increased nutrient contents or increased rates of leaching and runoff can result in contamination of water resources (Daryanto et al., 2017).

Crop yield (biomass) and quality (e.g., nutrient content, forage quality, etc.) are also important factors that should be measured during EW studies in croplands. Yield are most typically measured in the agronomic sciences using industrial methods such as mechanical harvesting instruments, but hand harvest methods that allow for observation of specific changes in biomass can also be useful (Shapiro et al., 1989; Trout and DeJonge, 2017). For instance, if corn biomass increases, but that increase is in stover, that may not be as valuable to farmers as an increase in grain. With certain crops, hand harvest may be necessary if mechanical methods (for instance, hay baling) are not accurate enough or not common (e.g., forage biomass estimates). Remote sensing methods can be employed to estimate yield (e.g., relative crop height using normalized difference vegetation index; NDVI) and crop nutrients (e.g., using near infrared spectroscopy; NIRS). Crop nutrient concentrations can also be determined by subjecting dried, finely-ground plant samples to elemental analysis [using methods such as inductively coupled plasma

emissions spectrometry (ICP)]. Crop yield and crop quality analysis may cover total plant biomass or may be divided into relevant sections of the target crop. For example, corn harvests may be divided into grain and stover yields for analysis.

In addition to measurements of GHG emissions to the atmosphere, there are other atmospheric measurements that are relevant to environmental health. For instance, ammonia (NH_3) and nitric oxide (NO) emissions are widely produced from agriculture, which have repercussions for air quality, N deposition, soil acidification, eutrophication of waterways, and adverse effects on human health (Almaraz et al., 2018; Domingo et al., 2021). Dust production from EW practices may create a health hazard for farmworkers and/or nearby residents. Furthermore, dust can have fertilization effects both near and far (Prospero et al., 2020). The degree to which dust from EW practices becomes a hazard will likely depend on grain size and application methods (e.g., tillage, wet vs. dry applications, storage, etc.). The current scarcity of EW field trials means that our understanding of dust and other hazards remains poor and requires more targeted inquiries.

Priority measurements for enhanced weathering field studies in working lands

While further field testing of EW is required to adequately develop best practices for monitoring CDR and other pertinent processes, we provide a brief list of priority measurement recommendations for those seeking to deploy EW field trials in working lands.

The primary set of measurements to include EW field trials will be those to monitor and scale CDR. Measurements of total soil C using combustion methods are the most basic assay for observing soil C sequestration, though it does not capture all pools. Since C sequestration is typically a slow process, soil sampling can occur annually and should include at least three depths (e.g., 0–10, 10–30, and 30–50 cm) so that equivalent soil mass can be used to scale these measurements, as this has been shown to be superior to traditional scaling methods based on bulk density (Von Haden et al., 2020). Deeper depths may be sampled to capture where carbonates precipitate, however, if the soil is predominately organic C, the inorganic C pool may be negligible, precluding the need to sample deeper. EW can produce both carbonates in soil and bicarbonate in soil pore water, thus measurements of soil pore water alkalinity will be critical to observing the CDR removal effect of an experiment. Soil pore water can be monitored using lysimeters sampled daily to weekly and analyzed using acidimetric titration. Lysimeter measurements should be coupled with water balance estimates to scale findings.

Secondary measurements to prioritize would be GHG emissions and yields. GHGs can be measured in a variety of ways but automated chambers are recommended as they can be moved between treatment plots to capture spatially variability, while simultaneously capturing the temporal variability that is critical to understanding the flux of these heterogenous emissions. The effects of EW on yield will be a crucial piece of data for land managers considering this practice. Mechanical yield is preferred from an agronomic perspective; however, hand harvest methods coupled with elemental analysis may better inform C cycling dynamics (i.e., C removed during harvest).

We outline an extensive list of possible measurements to explore rates and mechanisms of CDR and other soil processes that are relevant to EW's influence on the soil environment, however, the above represents a minimal set of analyses that should provide insight with regards to EW's effect on CDR. The best techniques to quantify CDR from EW trials are not yet known because we have few results from field studies across limited soil, rock, and crop types. For instance, lysimetry might pose issues in dry climates or rainfed agriculture where soil pore water is less abundant, and the importance of SIC may vary geographically based on the ratio of SOC:SIC, altering methodological needs. Further field tests will help to build a more robust set of field measurement best practices for EW trials in agronomic settings.

Applied science considerations

As researchers continue to develop robust science generated by EW field studies, the reach of this applied science work can be made more effective by incorporating a variety of stakeholders into the research process. There are numerous constituents who will be vital to developing practices that scale in a responsible and just manner. First, computational modelers can generate emission scenarios regionally or globally using field data, life cycle analyses, and process-based models. Second, sociologists and economists can help to increase an understanding of the barriers to adopting EW practices, assess costs associated with such practices as they scale, and identify potential environmental justice issues. Third, private industry can not only help facilitate EW material sourcing and shipping but have a vested interest in and experiential knowledge of market dynamics as they related to EW. Furthermore, technological industries can help to develop smartphone tools that increase uptake, knowledge, and access to EW practices. Fourth, farmers and ranchers will be vital collaborators in EW research and development, providing land on which to deploy trials, knowledge regarding field maintenance, and feedback/support related to practitioner adoption. Fifth, environmental work has a history of widening environmental injustices, thus is important to consider and incorporate local agricultural and indigenous communities into research projects from their onset; working with non-profit organizations can be a fruitful entry point into community engagement. Lastly, policy is critical for

incentivizing climate solutions; thus, partnering with policy advocates and government agencies can help translate science into action. Environmental issues, such as climate change, are highly complex in nature and thus require interdisciplinary approaches to responsible and scalable solution development.

Conclusion

Geoscientists (e.g., geologists, biogeochemists, soil scientists, etc.) are interested in the prospect of EW as a climate mitigation opportunity. While many geoscientists have the unique skill set to explore questions related to EW, few have experience working in contexts where EW is most likely to be applied (e.g., agronomy, rangeland science, forest ecology, coastal ecology, etc.). Geology and agronomy differ in their scientific approach in many ways; thus, we provide a path for incorporating robust geologic measurement techniques into agronomic field trials. While collaborations with interdisciplinary researchers and stakeholders can aid in research project facilitation, we seek to provide a framework by which researchers who are interested in the topic of EW in working lands can gain insight prior to the onset of a new project. As a new and emerging field that urgently requires more field testing across a variety of systems before becoming a viable climate mitigation strategy, we aim to shed light on the experimental design and methodological considerations for geologists and agronomists when establishing new EW field trials.

Author contributions

MA and NB formulated the concept and produced a first draft of the manuscript. EG, HG, IH, and JS contributed sections of text to the manuscript. MA, NB, IH, and EG created tables and figures. BH was the primary investigator, MA was the program manager, and NB was the postdoctoral scholar who led all co-authors in the field research project that informed this manuscript. BH helped formulate concepts on silicate rock weathering methodology and provided general guidance and feedback. MA led the writing and revision of the manuscript with input from all co-authors. All authors contributed to the article and approved the submitted version.

Acknowledgments

California's Strategic Growth Council provided funding to support the research. The Working Lands Innovation Center, housed at UC Davis' Institute of the Environment, organized the research team. The Campbell Tract Agricultural Research Station, Russell Ranch Sustainable Agriculture Facility, Bowles Farming Inc., Due Farm, the Pauma Tribe, and the Imperial Valley Desert and Sierra Foothills Research and Extension Centers provided field assistance, equipment, and facilities. Mallika Nocco, Kate Scow, Whendee Silver, Sat Darshan Khalsa, Patty Oikawa, and Nicole Tautges provided valuable input on methods development. Figures were created using BioRender.com.

Conflict of interest

The authors declare that the research was conducted in the absence of any commercial or financial relationships that could be construed as a potential conflict of interest.

Publisher's note

All claims expressed in this article are solely those of the authors and do not necessarily represent those of their affiliated organizations, or those of the publisher, the editors and the reviewers. Any product that may be evaluated in this article, or claim that may be made by its manufacturer, is not guaranteed or endorsed by the publisher.

Supplementary material

The Supplementary Material for this article can be found online at: https://www.frontiersin.org/articles/10.3389/fclim.2022.970429/full#supplementary-material

References

Almaraz, M., Bai, E., Wang, C., Trousdell, J., Conley, S., Faloona, I., et al. (2018). Agriculture is a major source of NOx pollution in California. *Sci. Adv.* 4:eaao3477. doi: 10.1126/sciadv.aao3477

Amann, T., and Hartmann, J. (2022). Carbon accounting for enhanced weathering. *Front. Climate* 54:e849948. doi: 10.3389/fclim.2022.849948

Amann, T., Hartmann, J., Struyf, E., de Oliveira Garcia, W., Fischer, E. K., Janssens, I., et al. (2020). Enhanced Weathering and related element fluxes–a cropland mesocosm approach. *Biogeosciences* 17, 103–119. doi: 10.5194/bg-17-103-2020

Amundson, R., Wang, Y., Chadwick, O., Trumbore, S., McFadden, L., McDonald, E., et al. (1994). Factors and processes governing the 14C content of carbonate in desert soils. *Earth Planet. Sci. Lett.* 125, 385–405. doi: 10.1016/0012-821X(94)90228-3

Arias-Ortiz, A., Oikawa, Y., Carlin, J., Masqu, é, Shahan, J., Kanneg, S., Paytan, A., et al. (2021). Tidal and nontidal marsh restoration: A trade-off between carbon sequestration, methane emissions, and soil accretion.

J. Geophys. Res. Biogeosci. 126:e2021JG006573. doi: 10.1029/2021JG006573

Asano, M., Wagai, R., Yamaguchi, N., Takeichi, Y., Maeda, M., Suga, H., et al. (2018). In search of a binding agent: Nano-scale evidence of preferential carbon associations with poorly-crystalline mineral phases in physically-stable, clay-sized aggregates. *Soil Syst.* 2:32. doi: 10.3390/soilsystems2020032

Balogh-Brunstad, Z., Keller, C. K., Dickinson, J. T., Stevens, F., Li, C. Y., and Bormann, B. T. (2008). Biotite weathering and nutrient uptake by ectomycorrhizal fungus, Suillus tomentosus, in liquid-culture experiments. *Geochim. Cosmochim. Acta* 72, 2601–2618. doi: 10.1016/j.gca.2008.04.003

Beerling, D. J., Kantzas, E., Lomas, M. R., Wade, Eufrasio, R. M., Renforth, Sarkar, B., Andrews, M. G., et al. (2020). Potential for large-scale CO2 removal via enhanced rock weathering with croplands. *Nature* 583, 242–248. doi: 10.1038/s41586-020-2448-9

Beerling, D. J., Leake, J. R., Long, S., Scholes, J. D., Ton, J., Nelson, N., et al. (2018). Farming with crops and rocks to address global climate, food and soil security. *Nat. Plants* 4, 138–147. doi: 10.1038/s41477-018-0108-y

Blanc-Betes, E., Kantola, I. B., Gomez-Casanovas, N., Hartman, M. D., Parton, W. J., Lewis, A. L., et al. (2021). *In silico* assessment of the potential of basalt amendments to reduce N2O emissions from bioenergy crops. *GCB Bioenergy* 13, 224–241. doi: 10.1111/gcbb.12757

Bonneville, S., Smits, M. M., Brown, A., Harrington, J., Leake, J. R., Brydson, R., et al. (2009). Plant-driven fungal weathering: Early stages of mineral alteration at the nanometer scale. *Geology* 37, 615–618. doi: 10.1130/G25699A.1

Capo, R. C., Stewart, B. W., and Chadwick, O. A. (1998). Strontium isotopes as tracers of ecosystem processes: theory and methods. *Geoderma* 82, 197–225. doi: 10.1016/S0016-7061(97)00102-X

Cerling, T. E. (1984). The stable isotopic composition of modern soil carbonate and its relationship to climate. *Earth Planet. Sci. Lett.* 71, 229–240. doi: 10.1016/0012-821X(84)90089-X

Chaney, D. (2017). *Common Research Designs for Farmers. Sustainable Agriculture Research and Education*. Available online at: https://www.sare.org/publications/how-to-conduct-research-on-your-farm-or-ranch/basics-of-experimental-design/common-research-designs-for-farmers/ (accessed October 28, 2022).

Cipolla, G., Calabrese, S., Noto, L. V., and Porporato, A. (2021). The role of hydrology on enhanced weathering for carbon sequestration II. From hydroclimatic scenarios to carbon-sequestration efficiencies. *Adv. Water Resour.* 154:103949. doi: 10.1016/j.advwatres.2021.103949

Corwin, D. L., and Lesch, S. M. (2005). Apparent soil electrical conductivity measurements in agriculture. *Comp. Electr. Agricult.* 46, 11–43. doi: 10.1016/j.compag.2004.10.005

Cotrufo, M. F., Ranalli, M. G., Haddix, M. L., Six, J., and Lugato, E. (2019). Soil carbon storage informed by particulate and mineral-associated organic matter. *Nat. Geosci.* 12, 989–994. doi: 10.1038/s41561-019-0484-6

Crews, T. E., Kitayama, K., Fownes, J. H., Riley, R. H., Herbert, D. A., Mueller-Dombois, D., et al. (1995). Changes in soil phosphorus fractions and ecosystem dynamics across a long chronosequence in Hawaii. *Ecology* 76, 1407–1424. doi: 10.2307/1938144

Daryanto, S., Wang, L., and Jacinthe, A. (2017). Impacts of no-tillage management on nitrate loss from corn, soybean and wheat cultivation: A meta-analysis. *Sci. Rep.* 7, 1–9. doi: 10.1038/s41598-017-12383-7

Del Galdo, I., Six, J., Peressotti, A., and Francesca Cotrufo, M. (2003). Assessing the impact of land-use change on soil C sequestration in agricultural soils by means of organic matter fractionation and stable C isotopes. *Glob. Chang. Biol.* 9, 1204–1213. doi: 10.1046/j.1365-2486.2003.00657.x

Dietrich, W. E., and Lohse, K. (2014). *Common Questions of the US NSF–Supported Critical Zone Observatories*. Available online at: https://czo-archive.criticalzone.org/national/publications/pub/dietrich-lohse-2014-common-questions-of-the-us-nsfsupported-critical-zone-o/ (accessed October 28, 2022).

Domingo, N. G., Balasubramanian, S., Thakrar, S. K., Clark, M. A., Adams, J., Marshall, J. D., et al. (2021). Air quality–related health damages of food. *Proc. Nat. Acad. Sci. U.S.A.* 118:e37118. doi: 10.1073/pnas.2013637118

Drever, J. I. (1994). The effect of land plants on weathering rates of silicate minerals. *Geochim. Cosmochim. Acta* 58, 2325–2332. doi: 10.1016/0016-7037(94)90013-2

Dudhaiya, A., Haque, F., Fantucci, H., and Santos, R. M. (2019). Characterization of physically fractionated wollastonite-amended agricultural soils. *Minerals* 9:635. doi: 10.3390/min9100635

Dupré, B., Dessert, C., Goddéris, Y., Viers, J., François, L., Millot, R., et al. (2003). Rivers, chemical weathering and Earth's climate. *Comptes Rendus Geoscience* 335, 1141–1160. doi: 10.1016/j.crte.2003.09.015

Edwards, D., Lim, F., James, R. H., Pearce, C. R., Scholes, J., Freckleton, R., et al. (2017). Climate change mitigation: potential benefits and pitfalls of enhanced rock weathering in tropical agriculture. *Biol. Lett.* 13:20160715. doi: 10.1098/rsbl.2016.0715

Filippi, Cattle, S. R., Pringle, M. J., and Bishop, T. F. (2020). A two-step modelling approach to map the occurrence and quantity of soil inorganic carbon. *Geoderma* 371:114382. doi: 10.1016/j.geoderma.2020.114382

Food and Agriculture Organization of the United Nations (2020). *Land Use in Agriculture by the Numbers*. Sustainable Food and Agriculture. Available online at: https://www.fao.org/sustainability/news/detail/en/c/1274219/ (accessed October 28, 2022).

Gaillardet, J., Dupré, B., Louvat, and Allegre, C. J. (1999). Global silicate weathering and CO2 consumption rates deduced from the chemistry of large rivers. *Chem. Geol.* 159, 3–30. doi: 10.1016/S0009-2541(99)00031-5

Garg, A., Munoth, and Goyal, R. (2016). "Application of soil moisture sensor in agriculture," in: *Proceedings of Internation Conference on Hydraulic* Pune.

Goldich, S. S. (1938). A study in rock-weathering. *J. Geol.* 46, 17–58. doi: 10.1086/624619

Goll, D. S., Amann, T., Buermann, W., Chang, J., Eker, S., Hartmann, J., et al. (2021). Potential CO2 removal from enhanced weathering by ecosystem responses to powdered rock. *Nat. Geosci.* 14, 545–549. doi: 10.1038/s41561-021-00798-x

Gough, C. M., Vogel, C. S., Schmid, H., Su, H. B., and Curtis, S. (2008). Multi-year convergence of biometric and meteorological estimates of forest carbon storage. *Agri. Forest Meteorol.* 148, 158–170. doi: 10.1016/j.agrformet.2007.08.004

Haque, F., Santos, R. M., and Chiang, Y. W. (2019a). Using nondestructive techniques in mineral carbonation for understanding reaction fundamentals. *Powder Technol.* 357, 134–148. doi: 10.1016/j.powtec.2019.08.089

Haque, F., Santos, R. M., and Chiang, Y. W. (2020). CO2 sequestration by wollastonite-amended agricultural soils–An Ontario field study. *Int. J. Greenhouse Gas Control* 97:103017. doi: 10.1016/j.ijggc.2020.103017

Haque, F., Santos, R. M., Dutta, A., Thimmanagari, M., and Chiang, Y. W. (2019b). Co-benefits of wollastonite weathering in agriculture: CO_2 sequestration and promoted plant growth. *ACS Omega* 4, 1425–1433. doi: 10.1021/acsomega.8b02477

Ibarra, D. E., Caves, J. K., Moon, S., Thomas, D. L., Hartmann, J., Chamberlain, C., et al. (2016). Differential weathering of basaltic and granitic catchments from concentration–discharge relationships. *Geochim. Cosmochim. Acta* 190, 265–293. doi: 10.1016/j.gca.2016.07.006

Isson, T. T., Planavsky, N. J., Coogan, L. A., Stewart, E. M., Ague, J. J., Bolton, E. W., et al. (2020). Evolution of the global carbon cycle and climate regulation on earth. *Global Biogeochem. Cycles* 34:e2018GB006061. doi: 10.1029/2018GB006061

Janssens, I. A., Roobroeck, D., Sardans, J., Obersteiner, M., Penuelas, J., Richter, A., et al. (2022). Negative erosion and negative emissions: land-based carbon dioxide removal and enhanced food production by rebuilding fertile topsoils. *Front. Climate* 169:e928403. doi: 10.3389/fclim.2022.928403

Jongmans, A. G., Van Breemen, N., Lundstrom, U. S., van Hees, A. W., Finlay, R. D., et al. (1997). Rock-eating fungi. *Nature* 289, 682–683. doi: 10.1038/39493

Kantzas, E., Val Martin, M., Lomas, M. R., Eufrasio, R. M., Renforth, Lewis, A. L., Taylor, L. L., et al. (2022). Substantial carbon drawdown potential from enhanced rock weathering in the United Kingdom. *Nat. Geosci.* 15, 382–389. doi: 10.1038/s41561-022-00925-2

Kelland, M. E., Wade, W., Lewis, A. L., Taylor, L. L., Sarkar, B., Andrews, M. G., et al. (2020). Increased yield and CO_2 sequestration potential with the C4 cereal Sorghum bicolor cultivated in basaltic rock dust-amended agricultural soil. *Glob. Chang. Biol.* 26, 3658–3676. doi: 10.1111/gcb.15089

Kemp, S. J., Lewis, A. L., and Rushton, J. C. (2022). Detection and quantification of low levels of carbonate mineral species using thermogravimetric-mass spectrometry to validate CO_2 drawdown via enhanced rock weathering. *Appl. Geochem.* 146:105465. doi: 10.1016/j.apgeochem.2022.105465

Kleber, M., Bourg, I. C., Coward, E. K., Hansel, C. M., Myneni, S. C., and Nunan, N. (2021). Dynamic interactions at the mineral–organic matter interface. *Nat. Rev. Earth Environ.* 2, 402–421. doi: 10.1038/s43017-021-00162-y

Köhler, P., Hartmann, J., and Wolf-Gladrow, D. A. (2010). Geoengineering potential of artificially enhanced silicate weathering of olivine. *Proc. Nat. Acad. Sci.* 107, 20228–20233. doi: 10.1073/pnas.1005451O

Krevor, S. C., Graves, C. R., Van Gosen, B. S., and McCafferty, A. (2009). Mapping the mineral resource base for mineral carbon-dioxide sequestration in the conterminous United States. *US Geolog. Surv.* 2009:14. doi: 10.3133/ds414

Larkin, C. S., Andrews, G., Pearce, C. R., Yeong, K. L., Beerling, D., Bellamy, J., et al. (2022). Quantification of CO_2 removal in a large-scale enhanced weathering

field trial on an oil palm plantation in Sabah, Malaysia. *Front. Climate* 161:e959229. doi: 10.3389/fclim.2022.959229

Lavallee, J. M., Soong, J. L., and Cotrufo, M. F. (2020). Conceptualizing soil organic matter into particulate and mineral-associated forms to address global change in the 21st century. *Glob. Chang. Biol.* 26, 261–273. doi: 10.1111/gcb.14859

Lewis, A. L., Sarkar, B., Kemp, S. J., Hodson, M. E., Taylor, L. L., Yeong, K. L., et al. (2021). Effects of mineralogy, chemistry and physical properties of basalts on carbon capture potential and plant-nutrient element release via enhanced weathering. *Appl. Geochem.* 2021:105023. doi: 10.1016/j.apgeochem.2021.105023

Li, S., Wang, X., Wang, S., Zhang, Y., Wang, S., and Shangguan, Z. (2016). Effects of application patterns and amount of biochar on water infiltration and evaporation. *Transact. Chin. Soc. Agri. Eng.* 32, 135–144.

Lin, Y., Prentice, I. I. I., Tran, T., Bingham, N. L., and King, J. Y. (2016). Modeling deep soil properties on California grassland hillslopes using LiDAR digital elevation models. *Geoderma Region.* 7, 67–75. doi: 10.1016/j.geodrs.2016.01.005

Maher, K., and Chamberlain, C. (2014). Hydrologic regulation of chemical weathering and the geologic carbon cycle. *Science* 343, 1502–1504. doi: 10.1126/science.1250770

Martin, C., Aquilina, L., Gascuel-Odoux, C., Molénat, J., Faucheux, M., and Ruiz, L. (2004). Seasonal and interannual variations of nitrate and chloride in stream waters related to spatial and temporal patterns of groundwater concentrations in agricultural catchments. *Hydrol. Process.* 18, 1237–1254. doi: 10.1002/hy1395

Meysman, F. J., and Montserrat, F. (2017). Negative CO2 emissions via enhanced silicate weathering in coastal environments. *Biol. Lett.* 13:20160905. doi: 10.1098/rsbl.2016.0905

Mitchell, M. J., Jensen, O. E., Cliffe, K. A., and Maroto-Valer, M. M. (2010). A model of carbon dioxide dissolution and mineral carbonation kinetics. *Proc. R. Soc. A: Mathematical Phys. Eng. Sci.* 466, 1265–1290. doi: 10.1098/rspa.2009.0349

Nelson, D. A., and Sommers, L. (1983). Total carbon, organic carbon, and organic matter. *Methods Soil Analy.* 9, 539–579. doi: 10.2134/agronmonogr9.2.2ed.c29

Nieva, N. E., Bia, G., Garcia, M. G., and Borgnino, L. (2019). Synchrotron XAS study on the As transformations during the weathering of sulfide-rich mine wastes. *Sci. Total Environ.* 669, 798–811. doi: 10.1016/j.scitotenv.2019.03.160

Novick, K. A., Metzger, S., Anderegg, W. R., Barnes, M., Cala, D. S., Guan, K., et al. (2022). Informing nature-based climate solutions for the United States with the best-available science. *Glob. Chang. Biol.* 28, 3778–3794. doi: 10.1111/gcb.16156

Olin Neal, C. (2001). Alkalinity measurements within natural waters: towards a standardized approach. *Sci. Total Environ.* 265, 99–113. doi: 10.1016/S0048-9697(00)00652-5

Pallasser, R., Minasny, B., and McBratney, A. B. (2013). Soil carbon determination by thermogravimetrics. *PeerJ* 1:e6. doi: 10.7717/peerj.6

Pickett, S. T. (1989). "Space-for-time substitution as an alternative to long-term studies," in: *Long-Term Studies in Ecology* (New York, NY: Springer).

Presley, B. J. (1975). A simple method for determining calcium carbonate in sediment samples. *J. Sedimentary Res.* 45:3.

Prospero, J. M., Barkley, A. E., Gaston, C. J., Gatineau, A., Campos y Sansano, A., and Panechou, K. (2020). Characterizing and quantifying African dust transport and deposition to South America: Implications for the phosphorus budget in the Amazon Basin. *Global Biogeochem. Cycles* 34:e2020GB006536. doi: 10.1029/2020GB006536

Ramos, C. G., Hower, J. C., Blanco, E., Oliveira, M. L. S., and Theodoro, S. H. (2022). Possibilities of using silicate rock powder: An overview. *Geosci. Front.* 13:101185. doi: 10.1016/j.gsf.2021.101185

Rayment, G. E., and Lyons, D. J. (2011). *Soil Chemical Methods: Australasia.* CSIRO publishing.

Richter, D. D., and Mobley, M. L. (2009). Monitoring Earth's critical zone. *Science* 326, 1067–1068. doi: 10.1126/science.1179117

Rinder, T., and von Hagke, C. (2021). The influence of particle size on the potential of enhanced basalt weathering for carbon dioxide removal-Insights from a regional assessment. *J. Clean. Prod.* 315, 128178. doi: 10.1016/j.jclepro.2021.128178

Sanderman, J., Hengl, T., and Fiske, G. J. (2017). Soil carbon debt of 12,000 years of human land use. *Proc. Nat. Acad. Sci. U.S.A.* 114, 9575–9580. doi: 10.1073/pnas.1706103114

Saville, D. J. (1980). Replication of field trials in space and time. *Proc. Agronomy Soc. NZ* 10, 97–99.

Schlesinger, W. H. (2022). Biogeochemical constraints on climate change mitigation through regenerative farming. *Biogeochemistry* 2022, 1—9. doi: 10.1007/s10533-022-00942-8

Schuiling, R. D., and Krijgsman (2006). Enhanced weathering: an effective and cheap tool to sequester CO2. *Clim. Change* 74, 349–354. doi: 10.1007/s10584-005-3485-y

Shapiro, C. A., Kranz, W. L., and Parkhurst, A. M. (1989). Comparison of harvest techniques for corn field demonstrations. *Am. J. Alternat. Agri.* 4, 59–64.

Sherrod, L. A., Dunn, G., Peterson, G. A., and Kolberg, R. L. (2002). Inorganic carbon analysis by modified pressure-calcimeter method. *Soil Sci. Am. J.* 66, 299–305. doi: 10.2136/sssaj2002.2990

Sigfusson, B., Paton, G. I., and Gislason, S. R. (2006). The impact of sampling techniques on soil pore water carbon measurements of an Icelandic Histic Andosol. *Sci. Total Environ.* 369, 203–219. doi: 10.1016/j.scitotenv.2006.01.012

Silva, F. M., Silva, S. H. G., Acuña-Guzman, S. F., Silva, E. A., Ribeiro, B. T., Fruett, T., et al. (2021). Chemical and mineralogical changes in the textural fractions of quartzite-derived tropical soils, along weathering, assessed by portable X-ray fluorescence spectrometry and X-ray diffraction. *J. South Am. Earth Sci.* 112, 103634. doi: 10.1016/j.jsames.2021.103634

Smith, P., Lanigan, G., Kutsch, W. L., Buchmann, N., Eugster, W., Aubinet, M., et al. (2010). Measurements necessary for assessing the net ecosystem carbon budget of croplands. *Agric. Ecosyst. Environ.* 139, 302–315. doi: 10.1016/j.agee.2010.04.004

Smith, P., Soussana, J. F., Angers, D., Schipper, L., Chenu, C., Rasse, D., et al. (2020). How to measure, report and verify soil carbon change to realize the potential of soil carbon sequestration for atmospheric greenhouse gas removal. *Glob. Chang. Biol.* 26, 219–241. doi: 10.1111/gcb.14815

Smith, W. N., Grant, B., Desjardins, R. L., Lemke, R., and Li, C. (2004). Estimates of the interannual variations of N2O emissions from agricultural soils in Canada. *Nutr. Cycl. Agroecosyst.* 68, 37–45. doi: 10.1023/B:FRES.0000012230.40684.c2

Strefler, J., Amann, T., Bauer, N., Kriegler, E., and Hartmann, J. (2018). Potential and costs of carbon dioxide removal by enhanced weathering of rocks. *Environ. Res. Lett.* 13:034010. doi: 10.1088/1748-9326/aaa9c4

Tautges, N. E., Chiartas, J. L., Gaudin, A. C., O'Geen, A. T., Herrera, I., and Scow, K. M. (2019). Deep soil inventories reveal that impacts of cover crops and compost on soil carbon sequestration differ in surface and subsurface soils. *Glob. Chang. Biol.* 25, 3753–3766. doi: 10.1111/gcb.14762

Taylor, L. L., Banwart, S. A., Valdes, J., Leake, J. R., and Beerling, D. J. (2012). Evaluating the effects of terrestrial ecosystems, climate and carbon dioxide on weathering over geological time: a global-scale process-based approach. *Philosoph. Transact. R. Soc. B: Biol. Sci.* 367, 565–582. doi: 10.1098/rstb.2011.0251

Taylor, L. L., Beerling, D. J., Quegan, S., and Banwart, S. A. (2017). Simulating carbon capture by enhanced weathering with croplands: an overview of key processes highlighting areas of future model development. *Biol. Lett.* 13:20160868. doi: 10.1098/rsbl.2016.0868

Taylor, L. L., Driscoll, C. T., Groffman, M., Rau, G. H., Blum, J. D., and Beerling, D. J. (2021). Increased carbon capture by a silicate-treated forested watershed affected by acid deposition. *Biogeosciences* 18, 169–188. doi: 10.5194/bg-18-169-2021

Ten Berge, H. F., Van der Meer, H. G., Steenhuizen, J. W., Goedhart, W., Knops, and Verhagen, J. (2012). *Olivine Weathering in Soil, and Its Effects on Growth and Nutrient Uptake in Ryegrass (Lolium perenne* L.): *A Pot Experiment.* doi: 10.1371/journal.pone.0042098

Trout, T. J., and DeJonge, K. C. (2017). Water productivity of maize in the US high plains. *Irrigat. Sci.* 35, 251–266. doi: 10.1007/s00271-017-0540-1

Vandenbruwane, J., De Neve, S., De Schrijver, A., Geudens, G., Verheyen, K., and Hofman, G. (2008). Comparison of ceramic and polytetrafluoroethene/quartz suction cups for sampling inorganic ions in soil solution. *Commun. Soil Sci. Plant Anal.* 39, 1105–1121. doi: 10.1080/00103620801925661

Verbruggen, E., Struyf, E., and Vicca, S. (2021). Can arbuscular mycorrhizal fungi speed up carbon sequestration by enhanced weathering? *Plants People Planet* 3, 445–453. doi: 10.1002/ppp3.10179

Vicca, S., Goll, D. S., Hagens, M., Hartmann, J., Janssens, I. A., Neubeck, A., et al. (2022). Is the climate change mitigation effect of enhanced silicate weathering governed by biological processes? *Glob. Chang. Biol.* 28, 711–726. doi: 10.1111/gcb.15993

Vienne, A., Poblador, S., Portillo-Estrada, M., Hartmann, J., Ijiehon, S., Wade, and Vicca, S. (2022). Enhanced weathering using basalt rock powder: carbon sequestration, co-benefits and risks in a mesocosm study with solanum tuberosum. *Front. Climate* 72. doi: 10.3389/fclim.2022.869456

Vitousek (2004). *Nutrient Cycling and Limitation: Hawai'i as a Model System*. Princeton: Princeton University Press.

Von Haden, A. C., Yang, W. H., and DeLucia, E. H. (2020). Soils' dirty little secret: Depth-based comparisons can be inadequate for quantifying changes in soil organic carbon and other mineral soil properties. *Glob. Chang. Biol.* 26, 3759–3770. doi: 10.1111/gcb.15124

Wang, X., Jelinski, N. A., Toner, B., and Yoo, K. (2019). Long-term agricultural management and erosion change soil organic matter chemistry and association with minerals. *Sci. Total Environ.* 648, 1500–1510. doi: 10.1016/j.scitotenv.2018.08.110

Wang, X., Wang, J., and Zhang, J. (2012). Comparisons of three methods for organic and inorganic carbon in calcareous soils of Northwestern China. *PLoS ONE* 7, e44334. doi: 10.1371/journal.pone.004 4334

Weihermüller, L., Siemens, J., Deurer, M., Knoblauch, S., Rupp, H., Göttlein, A., et al. (2007). In situ soil water extraction: A review. *J. Environ. Qual.* 36, 1735–1748. doi: 10.2134/jeq2007.0218

Whitehead, D., Baisden, T., Beare, M., Campbell, D., Curtin, D., Davis, M., et al. (2012). *Review of Soil Carbon Measurement Methodologies and Technologies, Including Nature and Intensity of Sampling, Their Uncertainties and Costs. Ministry for Primary Industries, Technical Paper by Landcare Research No*. 2012/36.

Wilhelm, R. C., Lynch, L., Webster, T. M., Schweizer, S., Inagaki, T. M., Tfaily, M. M., et al. (2022). Susceptibility of new soil organic carbon to mineralization during dry-wet cycling in soils from contrasting ends of a precipitation gradient. *Soil Biol. Biochem.* 169:108681. doi: 10.1016/j.soilbio.2022.108681

Yadav, S. K., and Chakrapani, G. J. (2006). Dissolution kinetics of rock–water interactions and its implications. *Curr. Sci.* 932–937.

Zaharescu, D. G., Burghelea, C. I., Dontsova, K., Reinhard, C. T., Chorover, J., and Lybrand, R. (2020). Biological weathering in the terrestrial system: an evolutionary perspective. *Biogeochem. Cycles* 2020, 1–32. doi: 10.1002/9781119413332.ch1

Zamanian, K., Pustovoytov, K., and Kuzyakov, Y. (2016). Pedogenic carbonates: Forms and formation processes. *Earth-Sci. Rev.* 157, 1–17. doi: 10.1016/j.earscirev.2016.03.003

frontiers | Frontiers in Climate

TYPE Original Research
PUBLISHED 10 January 2023
DOI 10.3389/fclim.2022.954064

OPEN ACCESS

EDITED BY
Vikram Vishal,
Indian Institute of Technology Bombay, India

REVIEWED BY
Rafael Mattos Dos Santos,
University of Guelph, Canada
Tamara Jane Zelikova,
Colorado State University, United States

*CORRESPONDENCE
Emily E. E. M. te Pas
✉ emily.tepas@wur.nl

SPECIALTY SECTION
This article was submitted to Negative Emission Technologies, a section of the journal Frontiers in Climate

RECEIVED 26 May 2022
ACCEPTED 02 December 2022
PUBLISHED 10 January 2023

CITATION
te Pas EEEM, Hagens M and Comans RNJ (2023) Assessment of the enhanced weathering potential of different silicate minerals to improve soil quality and sequester CO_2. *Front. Clim.* 4:954064. doi: 10.3389/fclim.2022.954064

Assessment of the enhanced weathering potential of different silicate minerals to improve soil quality and sequester CO_2

Emily E. E. M. te Pas*, Mathilde Hagens and Rob N. J. Comans

Soil Chemistry and Chemical Soil Quality, Wageningen University and Research, Wageningen, Netherlands

Enhanced weathering is a negative emission technology that involves the spread of crushed silicate minerals and rocks on land and water. When applied to agricultural soils, the resulting increase in soil pH and release of nutrients may co-benefit plant productivity. Silicate minerals and rocks differ in their *enhanced weathering potential*, i.e., their potential for both carbon dioxide (CO_2) sequestration and soil quality improvements. However, studies comparing silicate minerals and rocks for this dual potential are lacking. Therefore, we compared the *enhanced weathering potential* of olivine (Mg_2SiO_4), basalt, wollastonite ($CaSiO_3$), and two minerals that are novel in this context, anorthite ($CaAl_2Si_2O_8$) and albite ($NaAlSi_3O_8$). A down-flow soil column experiment was designed allowing for measurements on soils and leachate, and calculations of organic and inorganic carbon budgets. Our results showed comparatively high CO_2 capture by enhanced wollastonite and olivine weathering. Furthermore, CO_2 capture per m^2 specific surface area indicated potential for enhanced anorthite and albite weathering. Calculated carbon budgets showed that most treatments produced net CO_2 emissions from soils, likely related to the short duration of this experiment. All silicates generally improved soil quality, with soil nickel contents remaining below contamination limits. However, nickel concentrations in leachates from olivine-amended soils exceeded the groundwater threshold value, stressing the importance of monitoring nickel leaching. We found a relatively high *enhanced weathering potential* for wollastonite, while the potential for olivine may be constrained by nickel leaching. The promising results for anorthite and albite indicate the need to further quantify their *enhanced weathering potential*.

KEYWORDS

enhanced weathering potential, silicate minerals and rocks, net CO_2 sequestration, agricultural soil quality, nickel, soil column experiment

1. Introduction

Rising atmospheric carbon dioxide (CO_2) concentrations resulting from fossil fuel combustion and land use change are causing climate change (IPCC, 2014). To limit global temperature rise well below 2°C, as agreed in the Paris Agreement, large scale application of Negative Emission Technologies (NETs) is needed (IPCC, 2018). Enhanced Weathering (EW) is a NET based on the natural silicate weathering cycle that stabilizes atmospheric CO_2 concentrations and climate on geological time scales (Kump et al., 2000). When CO_2 dissolves in water, carbonic acid is formed, which weathers silicate minerals. The resulting bicarbonate (HCO_3^-) and carbonate (CO_3^{2-}) ions may leach from soils and in addition contribute to counteracting ocean acidification (Hartmann et al., 2013; Bach et al., 2019). Weathering products may also precipitate as calcium and/or magnesium carbonates ($CaCO_3$, $MgCO_3$). Although carbonates form an important soil carbon (C) sink, carbonate precipitation releases part of the consumed CO_2 back to the atmosphere, thereby limiting the overall efficiency of CO_2 sequestration (Hartmann et al., 2013; Haque et al., 2019a). EW involves the artificial acceleration of the natural silicate weathering cycle through spreading crushed silicate minerals on land and water, aimed at CO_2 sequestration at a rate significant on human time scales (Schuiling and Krijgsman, 2006; Moosdorf et al., 2014; Andrews and Taylor, 2019).

The application of crushed silicate minerals and rocks on agricultural soils may, besides capturing CO_2, improve soil quality and consequently stimulate plant productivity (Ten Berge et al., 2012; Beerling et al., 2018; Haque et al., 2019b; Kelland et al., 2020). Silicate weathering releases nutrients, such as calcium (Ca^{2+}), magnesium (Mg^{2+}), and potassium (K^+), depending on the type of silicate mineral or rock used (Harley and Gilkes, 2000; Lehmann and Possinger, 2020). Furthermore, the released silica can improve plant resistance to biotic and abiotic stresses (Beerling et al., 2018). In agriculture, carbonate minerals are often applied as liming agents, while the weathering of silicate minerals also increases soil pH (West and McBride, 2005; Dietzen et al., 2018). The increase in soil pH and formation of secondary (clay) minerals by incongruent silicate weathering may both generate negatively charged binding sites, resulting in a higher soil Cation Exchange Capacity (CEC) (Gillman, 1980). Therefore, EW can improve both the retention and availability of nutrients in soils (Gillman et al., 2002; Anda et al., 2015).

EW can be considered a long-term storage option for CO_2 in the form of Soil Inorganic Carbon (SIC), since carbonate minerals and HCO_3^- have a mean residence time in soils of 80.000–100.000 years (Andrews and Taylor, 2019). On generally shorter time scales, EW can affect Soil Organic Carbon (SOC) (Beerling et al., 2018; Andrews and Taylor, 2019; Lehmann and Possinger, 2020). The release of multivalent cations and formation of secondary minerals by EW may stabilize SOC both chemically through organo-mineral associations, and physically through aggregate formation (Paradelo et al., 2015; Beerling et al., 2018; Gao et al., 2020). Improved crop productivity due to EW may further enhance atmospheric CO_2 uptake and belowground C inputs (Vicca et al., 2022). However, increasing soil pH can enhance microbial activity, and SOC bioavailability through deprotonation of functional groups (McBride, 1994; Leifeld et al., 2013). Similar to liming, EW may stimulate SOC decomposition, potentially reducing SOC (Paradelo et al., 2015). At the same time, chemical weathering rates, and consequently CO_2 capture by EW, are generally reduced at higher pH values (Hartmann et al., 2013). Since abovementioned processes can exert opposite effects on soil C content, and considering that mining, crushing and spreading of silicates also produces CO_2 emissions (Moosdorf et al., 2014), the net CO_2 budget of EW is yet uncertain.

The main focus of EW research has so far been on olivine minerals, especially the Mg-endmember forsterite (Mg_2SiO_4), due to their potentially high weathering rates and CO_2 consumption (Hartmann et al., 2013; Oelkers et al., 2018). However, olivine weathering also releases nickel cations (Ni^{2+}). Depending on Ni concentrations and its speciation in soils, threshold values can be reached in soils, plants, and groundwater (Weng et al., 2004; Ten Berge et al., 2012; Renforth et al., 2015; Amann et al., 2020). Therefore, the use of basalt, an abundant silicate rock with lower Ni concentrations and a higher content of nutritional elements compared to olivine-rich rocks (Beerling et al., 2018), and wollastonite ($CaSiO_3$), a fast weathering and abundant Ca-bearing silicate mineral (Haque et al., 2019b), have recently received more attention. However, other silicate minerals may also have potential for EW. For example, feldspar minerals such as anorthite ($CaAl_2Si_2O_8$) and albite ($NaAlSi_3O_8$) are widely abundant (USGS, 2020). Anorthite minerals have high weathering rates (Palandri and Kharaka, 2004), and albite weathering does not result in carbonate precipitation thereby acting as a net sink for 100% of the consumed atmospheric CO_2 (Hartmann et al., 2013). Despite their potential, these minerals have to our knowledge not yet been studied in the context of EW.

Different types of silicate minerals and rocks vary in what we define as their *enhanced weathering potential*, with respect to both improving agricultural soil quality through increasing soil pH and releasing nutrients, and supporting climate change mitigation by CO_2 sequestration. However, a comparison between silicate minerals and rocks for this dual potential is lacking in current literature. Therefore, we aim to compare this *enhanced weathering potential* of five different silicates (olivine, basalt, wollastonite, anorthite, albite) using a down-flow soil column experiment. Hereby, this study supports the development of EW strategies on croplands that both improve agricultural soil quality and mitigate climate change.

2. Materials and methods

2.1. Characterization of the experimental soil and silicates

Soil samples were collected from the topsoil of a sandy grassland in Wageningen, the Netherlands (51°59'39.3"N 5°40'05.9"E) in November 2019. This field had not been used for livestock practices for 2 years and had not been fertilized since 1972. The soil was selected for its relatively low pH and geochemically reactive concentrations of base cations and Ni (Table 1). Soil samples were dried at 40°C for about 48 h, sieved over 2 mm, and homogenized.

Five types of silicates were used in this experiment. First, crushed olivine minerals were retrieved from the Aheim Gusdal Mine located in Norway, where forsterite is mined at Steinsvik (Kremer et al., 2019). Second, crushed basalt rocks were used from a mine located in between Nieder Ofleiden and Homburg, Germany (Actimin, 2019). Third, Canadian wollastonite was used, which is a crushed waste stream from mining operations at Saint Lawrence Wollastonite Deposit, Ontario, and therefore also contained some Mg impurities in the form of diopside (Haque et al., 2019b). Fourth, anorthite was retrieved from Grass Valley, California, United States. Finally, albite was obtained from a mine in Bancroft, Ontario, Canada. Anorthite and albite minerals were ordered from Ward's Science and were crushed using a jaw crusher. The silicates were characterized for their chemical composition using X-Ray Fluorescence (XRF) (ARL^{TM} PERFORM'X wavelength-dispersive sequential XRF spectrometer, ThermoFisher Scientific), Specific Surface Area (SSA) by N_2 adsorption using the Brunauer-Emmett-Teller (BET) method (Gemini model 2390p) (Table 2), and particle size distribution using laser diffraction (Coulter^{TM} LS 230, fluid module) (Figure 1).

TABLE 1 Characteristics of the experimental soil.

Parameter	Value
pH-H_2O	5.16
Ca (mg kg^{-1})[a]	214
Mg (mg kg^{-1})[a]	34.7
K (mg kg^{-1})[a]	40.0
Na (mg kg^{-1})[a]	9.00
Ni (mg kg^{-1})[a]	0.64
Total carbon (g kg^{-1})[b]	21.3
$CaCO_3$ (g kg^{-1})[b]	0.38
Organic carbon (g kg^{-1})[b]	21.3
CEC (mmol+ kg^{-1})[c]	29.9
Base saturation (%)[c]	31.0
% Sand (>50 μm)[d]	84.4
% Silt (2–50 μm)[d]	7.5
% Clay (<2 μm)[d]	3.7

[a]Geochemically reactive elemental concentrations extracted with 0.43 M HNO_3 and measured with ICP-OES (Groenenberg et al., 2017).
[b]Total C content as measured with a LECO CN analyser. IC content as determined by the Scheibler method (Allison, 1960; ISO, 1995). OC content was calculated by difference.
[c]As determined by 0.1 M $BaCl_2$ extractions followed by ICP-OES (ISO, 2018).
[d]As determined by the sieve and pipette method (NEN, 2018).

2.2. Experimental set-up

We designed a down-flow soil column experimental set-up that enabled controlling environmental conditions to ensure comparability among the different treatments, and measurements on both soil and leachate (Figure 2). Soil columns were made from polyethylene containers (180 ml) by drilling 30 (Ø2.5 mm) holes in the bottom of the containers. Each soil column was connected *via* a plastic funnel to a closed container, in which the leachate was collected and sampled every 2 to 7 days. A cellulose filter (12–25 μm pore size, Whatman 589/1) was placed at the bottom and on top of each column to prevent particle losses. Columns were filled with 150 g soil and 100 ml de-mineralised water following a five-step packing procedure in which each step consisted of one layer of 30 g soil and 20 ml de-mineralised water to reduce the chance of preferential flow paths (Gilbert et al., 2014; ISO, 2019). Aluminum foil was wrapped around the columns to prevent impact of incoming light on the soil. The experiment started after 2 days of pre-incubation, which allowed the soil to settle within the columns and redundant water to leach from the columns before the different treatments were applied, and lasted for 9 weeks (64 days). The experiment took place in a conditioned room of 20 ± 2°C.

On the 1st day of the experiment, 18.75 g (125 g kg^{-1} soil) of one of the five silicates was applied on top of each soil. This dose is in line with, though at the higher end of, the range found in current literature (Kelland et al., 2020). Each of the five treatments was studied in duplicate, being olivine (Ol1 and Ol2), basalt (Ba1 and Ba2), wollastonite (Wo1 and Wo2), anorthite (An1 and An2), and albite (Al1 and Al2). One control soil (Control) was used without silicate application. Every 2 to 4 days, 40 ml de-mineralised water was added on top of the soil columns. De-mineralised water has a pH similar to rainwater (about 5.7), but differs from rainwater in its ionic strength. Despite de-mineralised water not fully representing the effect of rainwater, the elemental concentrations measured in the leachate and

10.3389/fclim.2022.954064

TABLE 2 Specific Surface Area (SSA) and chemical composition of the silicate minerals and basalt used in this experiment.

	Olivine[a]	Basalt[a]	Wollastonite[a]	Anorthite[a]	Albite[a]
SSA ($m^2\ g^{-1}$)	3.71	3.88	1.49	0.64	1.13
SiO_2 (%)	40.24	46.41	55.26	50.75	62.03
CaO (%)	0.44	8.80	26.28	11.44	2.25
MgO (%)	43.47	10.27	5.63	5.03	0.02
K_2O (%)	0.05	1.50	1.83	0.28	0.84
Na_2O (%)	0.00	3.18	1.53	2.68	10.68
Fe_2O_3 (%)	6.66	10.44	2.46	6.36	0.15
Al_2O_3 (%)	0.65	12.91	4.11	21.79	21.12
P_2O_5 (%)	0.00	0.60	0.15	0.01	0.01
TiO_2 (%)	0.01	2.42	0.20	0.10	0.00
MnO (%)	0.09	0.18	0.05	0.13	0.04
Ni ($mg\ kg^{-1}$)	2,052	205	20	53	2
Cr ($mg\ kg^{-1}$)	1,798	468	33	54	17

[a]Chemical composition of the silicates was corrected for LOI of 6.31, 1.61, 0.94, 0.14, and 1.33% for olivine, basalt, wollastonite, anorthite, and albite, respectively.

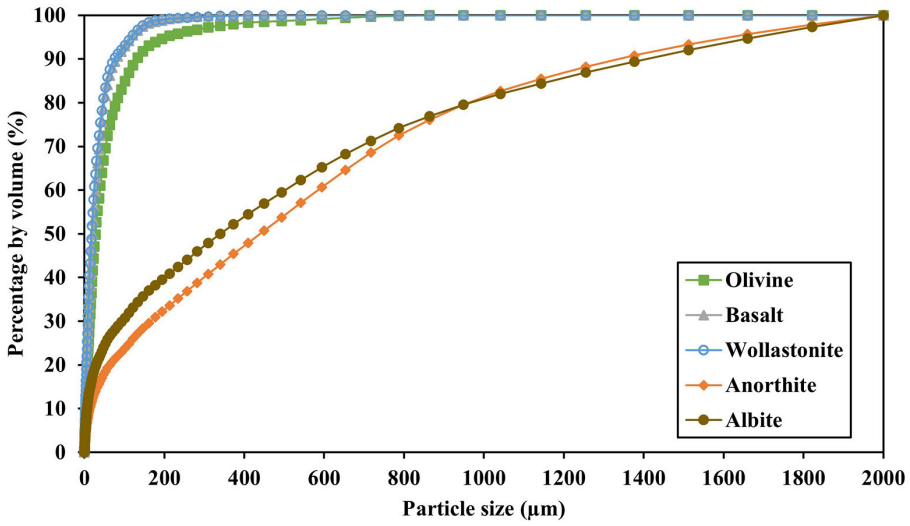

FIGURE 1
Particle size distribution of the five silicates used in this experiment, measured by laser diffraction ($n = 1$).

soil of the treatments, corrected for those measured in the leachate and soil of the control, could be solely attributed to silicate weathering, thereby allowing mass balance calculations. Although temperature and precipitation conditions during the experiment were not representative for average weather conditions in the Netherlands (average annual temperature is about 10°C lower and average annual precipitation is about three times lower compared to experimental conditions), the use of controlled conditions allowed for a comparison between the silicates, and ensured enough leachate to conduct all measurements.

2.3. Chemical analyses of leachate samples

After each water addition, leachate was collected in the containers below the columns, from which samples were taken on day 1, 3, 5, 8, 12, 17, 24, 33, and 64 of the experiment. In the leachate samples, concentrations of Ca^{2+}, Mg^{2+}, K^{+}, and sodium (Na^{+}) were measured using Inductively Coupled Plasma Optical Emission Spectrometry (ICP-OES), and Ni^{2+} concentrations were measured using High-Resolution ICP Mass Spectrometry (HR-ICP-MS). Segmented Flow Analysis

10.3389/fclim.2022.954064

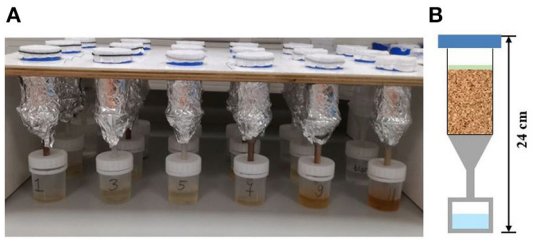

FIGURE 2
(A) Picture showing the experimental set-up. **(B)** Schematic overview of a single soil column.

(SFA) was used to measure the dissolved total C and Dissolved Inorganic Carbon (DIC) concentrations in the leachate samples, from which Dissolved Organic Carbon (DOC) concentrations were calculated. More frequent leachate samples were taken (every 2 to 7 days) to measure pH and alkalinity. First, the pH of the leachate samples was measured using a PHM 92 Lab pH electrode (Radiometer Copenhagen). Then, total alkalinity was measured by titrating 7.5 ml leachate to a pH of 4.50 (±0.05) using a 0.02 M HCl solution.

2.4. Chemical analyses of soils

After day 64, the experiment was terminated. Visually detectable silicates on top of the soils were removed using a plastic knife to minimize the occurrence of mineral particles in the soil extractions and fractionations. The soils were separately dried at 40°C for about 4 days, sieved over 2 mm, and homogenized.

Soil CEC and base cation concentrations were measured using a 0.1 M $BaCl_2$ extraction (ISO, 2018), followed by ICP-OES analysis. This data was used to calculate the base saturation, which represents the sum of Ca, Mg, K, and Na concentrations as a percentage of soil CEC. To calculate elemental mass balances and Ni release, soils were extracted with 0.43 M HNO_3 (Groenenberg et al., 2017), followed by ICP-OES analysis of Ca, Mg, K, Na, and Ni concentrations. To quantify the SIC content, the Scheibler method was used (Allison, 1960; ISO, 1995). A LECO CN analyser was used to measure total C, from which the SIC content was subtracted to calculate the SOC content.

2.5. Calculations and data analysis

Cumulative CO_2 capture was calculated using two alternative methods. The first method was based on elemental mass balances (EMB-method), using Equation 1 to calculate the weathered fraction of the applied mineral, and Equation 2 to determine CO_2 capture in this experiment. The element used to calculate the mass balance was based on the major element present in each of the silicates. Based on XRF analysis (Table 2), the Mg balance was used for olivine and basalt, the Ca balance for wollastonite and anorthite, and the Na balance for albite. Mg, Ca, and Na concentrations measured in the leachate using ICP-OES were linearly interpolated over time to calculate cumulative leaching. Soil Mg, Ca, and Na contents were measured by ICP-OES after extraction with 0.43 M HNO_3. The Mg, Ca, and Na content measured in the initial soil was used as a correction to only take into account the Mg, Ca, and Na released by silicate weathering. This method was similar to the method used by Ten Berge et al. (2012), except that we used the 0.43 M HNO_3 extraction instead of the 0.01 M $CaCl_2$ extraction to include elements adsorbed onto reactive binding sites and avoid underestimation of the weathering rate as expected by these authors. The total amounts of applied Mg, Ca, and Na were calculated based on the mineral contents as determined by XRF analysis (Table 2).

$$Fweathered = \frac{\left(\left(Mg, Ca, Na_{leachate} + Mg, Ca, Na_{soil}\right) - Mg, Ca, Na_{initial\ soil}\right)}{total\ Mg, Ca, Na\ applied} \quad (1)$$

In Equation 2, *Fweathered* was calculated with Equation 1, and the *mineral dose* was 18.75 g for all treatments. The term *stoichiometry* denoted CO_2 capture assuming ideal stoichiometric ratios during mineral dissolution, being 1.25 g CO_2 g^{-1} olivine weathered, 0.38 g CO_2 g^{-1} basalt weathered, 0.76 g CO_2 g^{-1} wollastonite weathered, 0.32 g CO_2 g^{-1} anorthite weathered, and 0.17 g CO_2 g^{-1} albite weathered (Supplementary Table S1). The results were divided by 0.15 to calculate the CO_2 capture from 150 g soil to 1 kg soil.

$$CO_2\ capture\ (g\ CO_2\ kg^{-1}\ soil) = \frac{Fweathered * mineral\ dose * stoichiometry}{0.15} \quad (2)$$

For the second method (IC-method), Equation 3 was used to calculate cumulative CO_2 capture based on alkalinity concentrations measured in the leachate and the soil carbonate content measured with the Scheibler method, representing the two pathways of IC sequestration by EW. Alkalinity concentrations were linearly interpolated to calculate cumulative alkalinity produced during this experiment, and the soil carbonate content was expressed as $CaCO_3$ (both in moles). These results were multiplied by the molar mass of CO_2 (44.0095 g mol^{-1}) and divided by 0.15 to calculate the CO_2 capture per kg soil. Finally, the carbonate content of the initial soil was subtracted to only take into account the carbonation

10.3389/fclim.2022.954064

resulting from EW.

$$CO_2\ capture\ (g\ CO_2\ kg^{-1}\ soil) = \left(\frac{Alkalinity^{*}44.0095}{0.15} + \frac{Carbonates^{*}44.0095}{0.15}\right) - initial\ soil \quad (3)$$

Furthermore, inorganic and organic CO_2 budgets were calculated and added to determine the net CO_2 budget (Equation 4), in which ΔSIC and ΔSOC were relative to the concentrations measured in the initial soil.

$$Net\ CO_2\ budget\ (g\ CO_2\ kg^{-1}\ soil) = ((\Delta SIC{+}DIC) + (\Delta SOC{+}DOC)) * \left(\frac{44.0095}{12.0107}\right) \quad (4)$$

Statistical analysis was conducted using R version 3.6.1 (R Core Team, 2020) and the package "car" (Fox and Weisberg, 2019). Data were checked for normality of residuals using the Shapiro Wilk Test, for homogeneity of variances using the Levence's Test, and for homoscedasticity of residuals by scatterplots. As the data did not meet the assumptions to allow the use of parametric tests, and as each treatment consisted of only two replicates, non-parametric Kruskal-Wallis tests were used to assess whether significant differences were found between the treatments for each variable. Since *P*-values are influenced by the number of replicates (n), we accepted a slightly lower confidence level than the most often used 95%, and considered differences between treatments significant if $P \leq 0.1$. Moreover, we focused the data analysis and interpretation mostly on the raw values, because n was limited to two. In the Results section, instead of averages, the values for both replicates of each treatment are presented, with the first value always representing the first replicate and the second value the second replicate.

3. Results

3.1. Soil quality parameters

3.1.1. pH response

pH measured in the leachate increased from 5.16 (day 0) to 7.48–7.93 for wollastonite treatments, to 7.30–7.41 for olivine treatments, to 7.42–7.10 for albite treatments, to 6.55–7.58 for basalt treatments, and to 6.87–7.24 for anorthite treatments at the end of the experiment (Figure 3). Treatments did not differ significantly in their pH response ($P = 0.387$). The pH of the control fluctuated during most of the experiment between approximately 5.5 and 6.0, and increased to 6.71 at the end of the experiment.

3.1.2. Soil nutrient content and retention

Final soil base saturation differed significantly between treatments ($P = 0.093$; Figure 4A). All treatments increased the base saturation compared to the control (41.7%), being most pronounced for the olivine (78.9–89.0%) and wollastonite (79.8–81.9%) treatments, followed by basalt (73.9–63.9%) and albite (63.7–64.3%). The anorthite treatments showed the smallest increase in base saturation (44.8–44.8%). Furthermore, significant differences between treatments were observed for soil CEC ($P = 0.089$; Figure 4B). Like with base saturation, the olivine (39.5–47.2 mmol+ kg^{-1} soil), and wollastonite (40.5–34.1 mmol+ kg^{-1} soil) treatments strongly increased soil CEC compared to the control (22.4 mmol+ kg^{-1} soil). Soil CEC of the basalt (31.9–26.5 mmol+ kg^{-1} soil) and albite (25.6–27.7 mmol+ kg^{-1} soil) treatments showed slight increases, whereas the anorthite treatments had a soil CEC (21.8–22.2 mmol+ kg^{-1} soil) that was similar to the control.

3.1.3. Nickel concentrations in soil and leachate

The treatments differed significantly in their soil Ni content as extracted by 0.43 M HNO_3 at the end of the experiment ($P = 0.093$; Figure 5). Olivine amendment resulted in the highest soil Ni concentrations (1.87–9.73 mg kg^{-1} soil), followed by basalt amendment (2.12–0.74 mg kg^{-1} soil). Wollastonite, anorthite, and albite amendment did not increase the geochemically reactive soil Ni content, as the measured concentrations were similar to those measured in the control soil (0.55 mg kg^{-1} soil). The differences in cumulative Ni leaching were also significant between treatments ($P = 0.081$), being highest for olivine (0.14–0.18 mg kg^{-1} soil), followed by wollastonite (0.11–0.10 mg kg^{-1} soil), and basalt (0.10–0.10 mg kg^{-1} soil). Ni leaching from soils amended with anorthite and albite was similar to the control (0.08 mg kg^{-1} soil). While none of the treatments produced soil Ni concentrations above the European threshold value for agricultural soils (50 mg Ni kg^{-1} soil; Tóth et al., 2016), all treatments and the control showed Ni^{2+} concentrations in individual leachate samples above the Dutch groundwater threshold value during the first 2 weeks of the experiment (Figure 6; 20 μg L^{-1}; Besluit kwaliteitseisen en monitoring water, 2009). Afterwards, all treatments and the control had Ni^{2+} concentrations below this threshold value, except for soils amended with olivine.

3.2. Soil CO_2 sequestration parameters

3.2.1. CO_2 capture by EW

Cumulative CO_2 capture was calculated using elemental mass balances (EMB-method) and IC measurements (IC-method) (Figure 7A). Using the EMB-method, CO_2 capture differed significantly between treatments ($P = 0.081$). Highest CO_2 capture was observed for soils amended with

10.3389/fclim.2022.954064

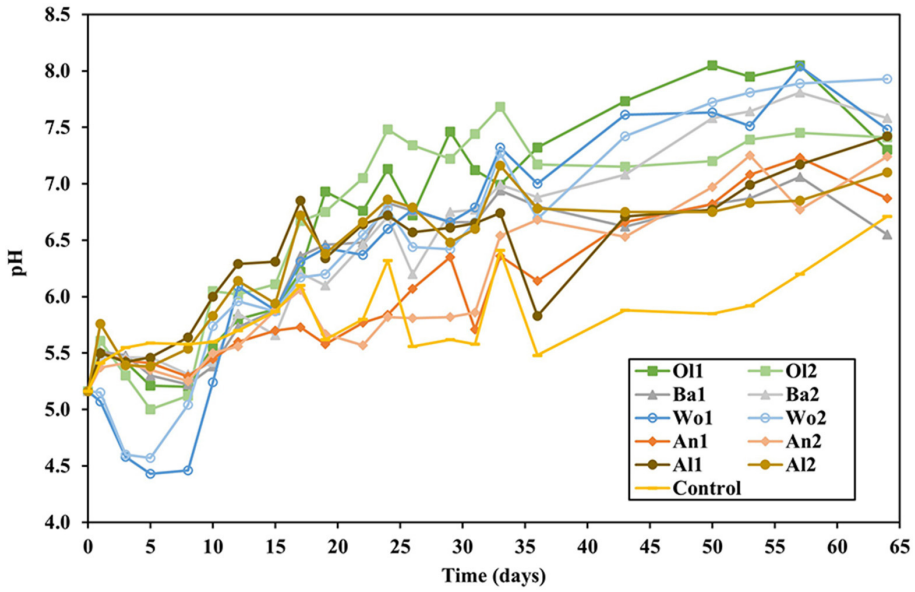

FIGURE 3
Development of pH measured in leachate samples over time.

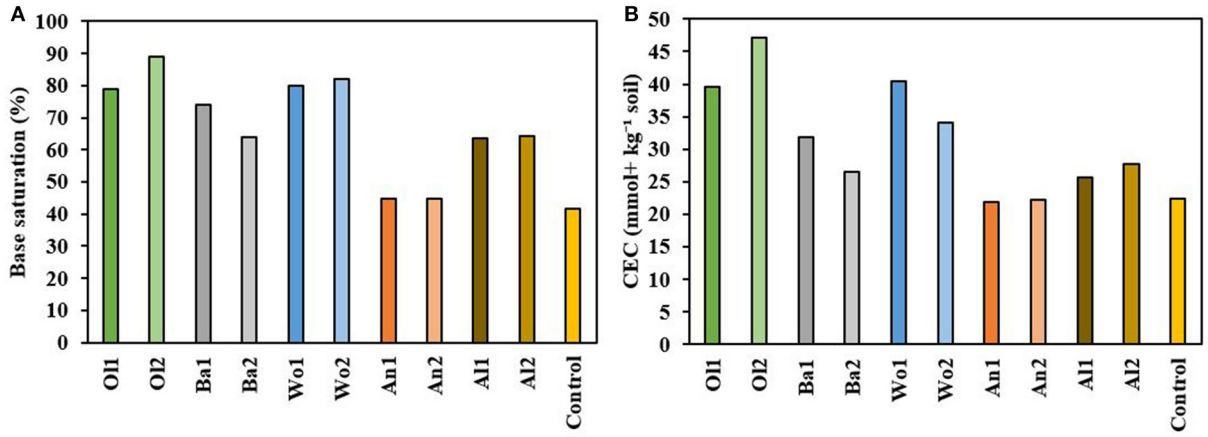

FIGURE 4
(A) Soil base saturation (%) measured at the end of the experiment. **(B)** Soil CEC (mmol+ kg^{-1} soil) measured at the end of the experiment.

olivine (1.82–4.45 g CO_2 kg^{-1} soil), and wollastonite (2.95–1.91 g CO_2 kg^{-1} soil), followed by basalt (1.61–0.41 g CO_2 kg^{-1} soil), albite (0.31–0.39 g CO_2 kg^{-1} soil), and anorthite (0.18–0.30 g CO_2 kg^{-1} soil). The IC-method resulted in a lower calculated CO_2 capture compared to the EMB-method, but similar trends were observed and treatments differed again significantly ($P = 0.078$). Using the IC-method, highest CO_2 capture was observed for wollastonite (0.61–0.63 g CO_2 kg^{-1} soil), and olivine (0.60–0.58 g CO_2 kg^{-1} soil), followed by basalt (0.38–0.47 g CO_2 kg^{-1} soil), albite (0.19–0.13 g CO_2 kg^{-1} soil), and anorthite (0.15–0.09 g CO_2 kg^{-1} soil).

Figure 1 and Table 2 show however that the silicates differed in their particle size distribution, and consequently SSA, being highest for basalt and olivine, and lowest for albite and anorthite. Corrected for these differences in SSA (Figure 7B), wollastonite weathering resulted in the highest CO_2 capture for both the EMB-method (15.8–10.3 mg CO_2 m^{-2} SSA) and IC-method (3.25–3.37 mg CO_2 m^{-2} SSA). Furthermore, Figure 7B shows a relatively higher potential for anorthite (2.22–3.70 and 1.87–1.13 mg CO_2 m^{-2} SSA) and albite (2.17–2.75 and 1.34–0.93 mg CO_2 m^{-2} SSA) using the EMB-method and IC-method, respectively, being similar to olivine weathering using

the IC-method (1.28–1.25 mg CO_2 m^{-2} SSA). For the latter, CO_2 capture based on the EMB-method (3.93–9.58 mg CO_2 m^{-2} SSA) remained substantially higher and second after wollastonite. Basalt weathering resulted on average in the lowest CO_2 capture per m^2 SSA for both the EMB-method (3.33–0.84 mg CO_2 m^{-2} SSA) and IC-method (0.77–0.97 mg CO_2 m^{-2} SSA). However, treatments did not differ significantly for SSA corrected CO_2 capture ($P = 0.120$ and $P = 0.169$, EMB-method and IC-method, respectively).

3.2.2. SOC content

SOC contents measured at the end of the experiment did not differ significantly between treatments ($P = 0.225$; Figure 8). SOC values ranged from 18.4–17.9 g SOC kg^{-1} soil for the olivine treatments to 19.9–21.6 g SOC kg^{-1} soil for the wollastonite treatments, while the other treatments had values similar to the control (19.4 g SOC kg^{-1} soil).

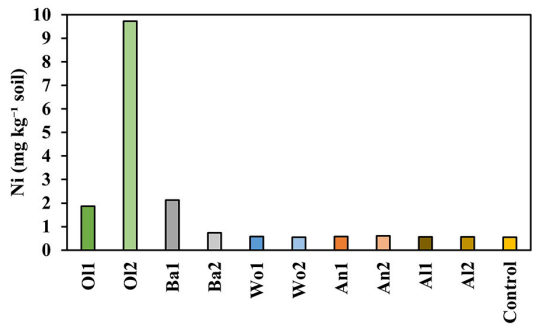

FIGURE 5
Geochemically reactive soil Ni concentrations at the end of the experiment, based on 0.43 M HNO_3 extraction.

3.2.3. Net CO_2 budgets

To assess the net effect of EW in terms of CO_2 sequestration or emissions, organic and inorganic carbon budgets were calculated, and added to determine the net CO_2 budget (Equation 4; Figure 9). IC budgets resulted in positive values for all treatments, indicating CO_2 sequestration. However, OC budgets showed generally negative values, indicating a loss of organic C as CO_2 emissions (except Wo2). Overall, the net CO_2 budget was negative for most treatments and the control, and no significant differences were observed between treatments ($P = 0.496$). These net CO_2 budgets showed that most treatments produced more CO_2 than they captured during this short-term experiment (filled bars in Figure 9), with Wo2 (3.10 g CO_2 kg^{-1} soil) as a positive exception.

4. Discussion

The aim of this study was to compare five different silicates on their *enhanced weathering potential*, including effects on both soil quality and CO_2 sequestration. Therefore, we designed a down-flow soil column experiment to allow measurements on soils and leachate. It must be noted that the water flow through some of the columns slowed down over time, resulting in a

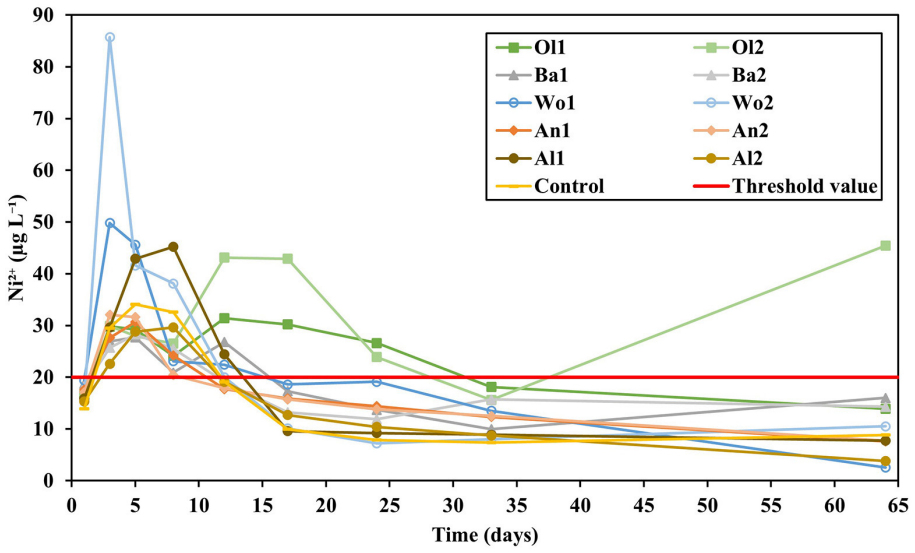

FIGURE 6
Ni^{2+} concentrations measured in the leachate over time. The red line represents the Dutch threshold value for Ni^{2+} concentrations in groundwater (Besluit kwaliteitseisen en monitoring water, 2009).

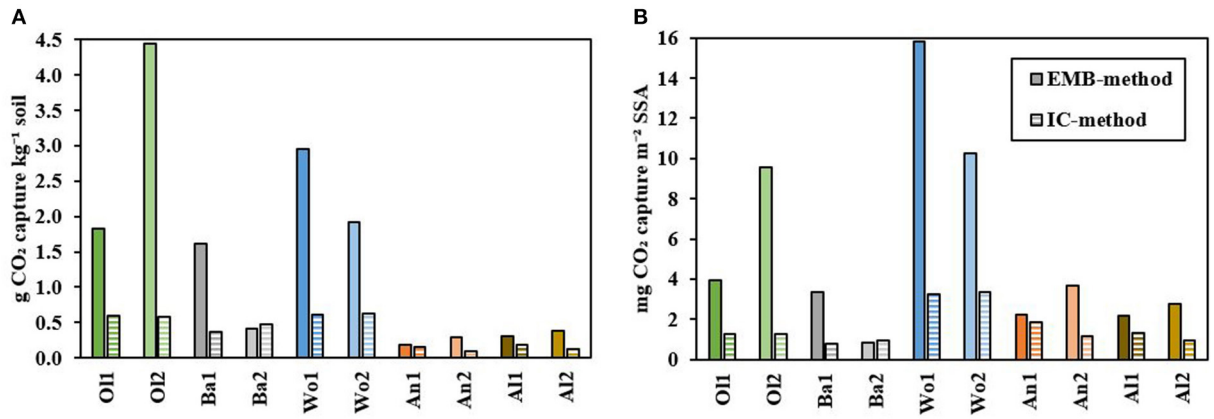

FIGURE 7
(A) Cumulative CO_2 capture calculated with the EMB-method (Equations 1 and 2; filled bars) and IC-method (Equation 3; striped bars). **(B)** CO_2 capture per m^2 specific surface area (SSA) calculated with the EMB-method (filled bars) and IC-method (striped bars).

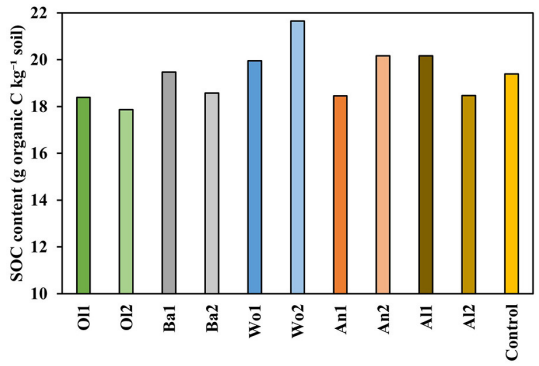

FIGURE 8
SOC content measured at the end of the experiment.

longer residence time of water in the soil. Upon dismantling the columns, dark coloring was observed suggesting reduced conditions. The release of dissolved iron (Fe^{2+}) into soil solution, and subsequent contact with oxygen supplied through the funnel, resulted in visually noticeable precipitation of Fe-oxides in the outlet of these columns, thereby reducing the through-flow of water. These features occurred especially in Ol1, Ba2, and Wo2, and to a lesser extent in An1, An2, Al1, and Control. The reduced flow of water along the mineral particles may have limited the chemical weathering rates and release of elements, likely explaining the relatively large variation between duplicates for some parameters, for example in the soil Ni content of the olivine treatments (Figure 5). Nevertheless, this study generated valuable new insights into the effects of EW on several soil quality parameters, Ni accumulation and release, and net CO_2 budgets.

4.1. Potential of EW to improve soil quality

4.1.1. Silicates as liming agents

The effects of EW on soil quality were determined through the pH response, base cation availability and retention, and Ni accumulation and release. During the first few days of the experiment, all treatments temporarily lowered pH as the cations released by EW exchanged with H^+ on negatively charged binding sites in soils (Figure 3). This observation was most pronounced for the wollastonite and olivine treatments, as their weathering mainly released multivalent cations (Ca^{2+} and Mg^{2+}), which are more strongly adsorbed onto exchange sites than K^+ and Na^+ (Supplementary Figure S1; Sparks, 2003). After about 10 days, pH started to gradually increase for all treatments as a result of proton consumption and alkalinity production by silicate weathering (Figure 3).

The optimum soil pH range for crop growth differs between species, but is generally between pH 6.0 and 8.0 (Fernández and Hoeft, 2009). Weathering of all five silicates raised pH within this optimum range without significant differences between the silicates, indicating their suitability as liming agents. Albite was the first mineral to raise pH above 6.0, within 12 days, which is likely due to its high alkalinity production (Supplementary Figure S2). Weathering of wollastonite, olivine, and basalt raised pH above 6.0 after 15 to 17 days. Anorthite weathering took 33 days to raise pH above 6.0, resulting in a longer period of soil acidity. However, the anorthite minerals used had the lowest SSA, likely explaining their lower weathering rates, and associated pH response and alkalinity production (Supplementary Figure S2). Wollastonite and olivine treatments showed the highest pH response, with individual measurements around pH 8.0 (Figure 3). These results do not necessarily indicate the occurrence of undesired

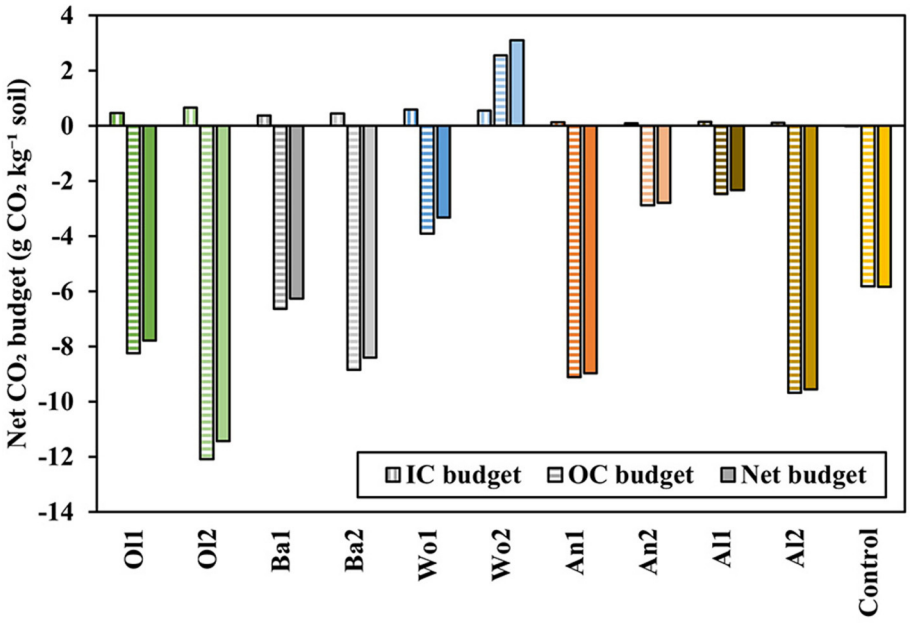

FIGURE 9
Net CO_2 budgets (Equation 4). Positive values indicate CO_2 sequestration. Negative values indicate CO_2 emissions.

pH increases in agricultural practice, as we applied a relatively high mineral dose. Furthermore, organic acids produced by plants lower pH, but these were absent in this experiment (Haque et al., 2019b; Vicca et al., 2022).

4.1.2. Silicates as fertilizers

The release of base cations by silicate weathering resulted in a significant increase in base saturation (Figure 4A). This increase was most pronounced for the wollastonite and olivine treatments, which mainly released Ca, Mg, and K into soil, three essential plant nutrients (Supplementary Figure S3; Schlesinger and Bernhardt, 2013). Relatively higher Na concentrations were measured in soils of the albite and basalt treatments, but these values are expected to have neither beneficial nor adverse effects on plant productivity (Kronzucker et al., 2013).

Olivine and wollastonite amendment almost doubled soil CEC (Figure 4B). Their strong increase in pH, and the consequent deprotonation of functional groups, likely increased soil negative charge (McBride, 1994; Anda et al., 2015), and thereby cation retention in soils. Furthermore, incongruent weathering may have resulted in the formation of secondary clay minerals that can increase soil CEC (Schlesinger and Bernhardt, 2013), but we do not have observations that confirm a significant occurrence of these processes. Basalt, anorthite, and albite treatments had only limited effect on soil CEC. For anorthite and albite these limited effects may be related to their relatively low SSA, and consequently lower weathering rates and effects on soil quality parameters measured in this study. However, previous studies applying basalt to highly weathered soils reported substantial increases in soil CEC (Anda et al., 2013, 2015) and therefore more research is suggested to understand the effects of EW application on soil CEC. If EW, in addition to releasing nutrients, also improves the retention of these and other nutrients that are not released by silicates such as nitrogen, EW could reduce the use and environmental impact of conventional fertilizers.

4.1.3. Nickel: Pollution or nutrition?

Wollastonite, anorthite, and albite amendment did not increase the Ni content of soils as extracted by 0.43 M HNO_3 (Figure 5). Basalt and especially olivine amendment increased soil Ni content, but concentrations were well below the European threshold value of 50 mg Ni kg^{-1} soil (Tóth et al., 2016). In fact, all treatments increased Ni to concentrations at which it may act as an essential micronutrient. Pot experiments fertilizing soil with 0.5–10 mg Ni kg^{-1} soil, the range in which Ni concentrations were observed in this experiment (Figure 5), showed significant increases in the yields of barley and soy beans (Kumar et al., 2018; Siqueira Freitas et al., 2018). The effect of Ni as micronutrient can be indirect through enhancing the plant uptake of other micronutrients such as iron, copper, zinc, and manganese (Kumar et al., 2018), and direct through enhancing the enzymatic activity of urease and hydrogenase supporting photosynthetic activity and nitrogen assimilation,

respectively (Kumar et al., 2018; Siqueira Freitas et al., 2018). Further research is recommended on these potential fertilization effects of Ni released by olivine and basalt weathering, as this may have implications for the application of silicates containing Ni in agricultural practice.

In contrast, Ni^{2+} concentrations measured in leachate samples of all treatments exceeded the Dutch threshold value for groundwater (20 $\mu g\ L^{-1}$; Besluit kwaliteitseisen en monitoring water, 2009) during the first 2 weeks of the experiment (Figure 6). This exceedance is not solely an effect of silicate weathering as the control also exceeded the threshold value during this period. The initial reduction in pH (Figure 3) likely underlies this observation, as Ni mobility is higher at lower pH (Dijkstra et al., 2004). The pH was most strongly reduced in the wollastonite treatments, which presumably explains the substantially higher Ni^{2+} leachate concentrations compared the control. It is therefore likely that Ni was mainly mobilized from the soil itself and less by mineral weathering considering the comparably low Ni content of wollastonite (Table 2). However, this result shows that not only silicates with a high Ni content, but also fast weathering silicates with a low Ni content can induce undesired (short-term) environmental effects through pH alterations.

After 2 weeks, the control and all treatments showed Ni^{2+} concentrations below the threshold value, except the olivine treatments. While for Ol1 Ni mobility was likely reduced under anoxic conditions (Römkens et al., 2009), Ol2 increasingly exceeded the threshold value during the second half of the experiment. It should be noted here that the measured DOC concentrations were high (Supplementary Figure S4), possibly resulting from the additions of de-mineralised water that has a lower ionic strength than rainwater. DOC may have formed complexes with Ni, thereby increasing its mobility (Dijkstra et al., 2004). As a result, in natural soil environments with rain water additions, DOC and consequently Ni^{2+} concentrations may be lower than observed in our experiment. However, in a mesocosm experiment Amann et al. (2020) also measured Ni^{2+} concentrations in the surface layers of olivine-rich dunite amended soils that exceeded drinking water threshold values. Therefore, it remains unclear whether toxic Ni^{2+} concentrations will also be reached in field conditions.

Our results show that Ni release by EW is not adversely affecting soil quality, especially since at low concentrations Ni can serve as a micronutrient, and the increase in soil pH and CEC can immobilize higher Ni concentrations (Römkens et al., 2009). However, Ni^{2+} release by olivine amendment, and mobilization of native Ni by fast weathering minerals such as wollastonite, may adversely affect groundwater quality. Therefore, we encourage others not only to monitor Ni concentrations in soils and plants, but especially also Ni^{2+} leaching. In addition, further research may establish whether an increase in soil binding capacity induced by EW can mitigate Ni^{2+} leaching.

4.2. EW as a climate change mitigation strategy

4.2.1. Comparing methods to calculate CO_2 capture by EW

Since a standardized quantification method of CO_2 capture by EW is yet to be developed, two methods based on different principles have been compared. The EMB-method was based on elemental mass balances using the concentrations of Mg for olivine and basalt, Ca for wollastonite and anorthite, and Na for albite, as measured in the leachate and extracted from soils (Equations 1 and 2; Figure 7A, filled bars). The 0.43 M HNO_3 extraction allowed to measure both bioavailable elements and those absorbed onto soil particles, to avoid an underestimation of calculated weathering rates based on a 0.01 M $CaCl_2$ extraction that only measures the bioavailable pool (Römkens et al., 2009; Ten Berge et al., 2012). However, the 0.43 M HNO_3 extraction can also partly dissolve minerals (Rodrigues et al., 2010; Groenenberg et al., 2017). Although minerals on top of the soils were visually removed, some downward transported mineral particles may have remained in the soil and partly dissolved by the extraction, thereby causing a potential overestimation of the CO_2 capture calculated with the EMB-method. To quantify the potential partial mineral dissolution, we conducted a 0.43 M HNO_3 extraction on the five silicates studied (Supplementary Table S2). For olivine, basalt, anorthite, and albite similar dissolution rates were found, being 15.0% or lower (Mg-olivine: 15.0%, Mg-basalt: 14.7%, Ca-anorthite: 2.26%, Na-albite: 12.8%). For Ca contained in wollastonite we found a substantially higher dissolution rate, namely 46.6%. However, the differences in calculated CO_2 capture between the EMB-method and IC-method are more than 15.0 and 46.6%, respectively. Mineral dissolution by the 0.43 M HNO_3 extraction can therefore only partly explain the observed discrepancy between the two methods.

For the IC-method, the alkalinity concentrations measured in the leachate and the soil carbonate content measured with the Scheibler method were used, representing the two pathways in which captured CO_2 can be stored (Equation 3; Figure 7A, striped bars). Alkalinity production and carbonate precipitation were highest for the olivine and wollastonite treatments (Supplementary Figures S2, S5), which is related to their high pH response (Figure 3) and DIC concentrations (Supplementary Figure S6). Albite weathering resulted in alkalinity concentrations similarly high as wollastonite weathering, while the soil carbonate contents of the five treatments was lowest for albite. This finding is consistent with albite releasing mainly Na^+ in the leachate while Na_2CO_3 does not precipitate (Hartmann et al., 2013), thereby making conditions for carbonate precipitation, by which part of the captured CO_2 is released, less favorable compared to the other treatments. As with the EMB-method, the

IC-method contains some uncertainties. We assumed that the measured carbonates consisted of $CaCO_3$, since $CaCO_3$ is thermodynamically more stable than $MgCO_3$ and most treatments showed relatively higher Ca^{2+} than Mg^{2+} release (Supplementary Figure S1). However, the exact carbonate mineral that was formed is unknown. Renforth et al. (2015) found in their soil column experiment using olivine that the formed carbonates consisted mainly of $CaCO_3$ with only small amounts of $MgCO_3$. Therefore, we do not expect our assumption to introduce a large error. Furthermore, alkalinity concentrations were assumed to fully consist of HCO_3^-, which seems valid as the leachate samples all had a pH between 4.50 and 8.25 in which HCO_3^- is the dominant DIC species (Verma, 2004). However, organic substances may have been present contributing to the measured alkalinity (Pearson, 1981), potentially causing an overestimation of the calculated CO_2 capture using the IC-method. Different methodologies are used in literature for quantifying CO_2 capture by EW, which are all based on different assumptions and uncertainties thereby hindering a comparison between studies. Therefore, we strongly encourage the use and comparison of multiple methodologies in future EW studies, as we have done here. Such a multiple approach can serve the development of a harmonized methodology to calculate CO_2 capture by EW, which we consider an important target to enable a robust comparison of achieved CO_2 capture in different EW studies.

To compare the silicates on CO_2 capture, we need to consider the lower SSA of anorthite, albite, and wollastonite compared to olivine and basalt (Table 2). Based on BET measurements, CO_2 capture per m^2 SSA was calculated (Figure 7B). This calculation includes the assumption that the SSA does not change during our 64-day experiment. This assumption may not be fully valid, since secondary minerals may precipitate on reactive mineral surfaces, thereby reducing the SSA available for chemical weathering, and consequently CO_2 capture over time (Huijgen et al., 2006; Amann et al., 2020). However, Scanning Electron Microscopy analysis of weathered relative to fresh mineral samples did not show visual evidence for secondary mineral precipitation on reactive surfaces (Supplementary Figure S7). Figure 7B shows that both methods indicate a high potential for CO_2 capture by wollastonite weathering, and a low potential for basalt weathering. Furthermore, when CO_2 capture is expressed per m^2 SSA, a relatively higher potential for minerals that are novel in the context of EW, anorthite and albite, was observed. Since the low SSA of the used anorthite and albite minerals likely affected the measured weathering rates in our experiment, and thereby other results presented in this study, more research on the enhanced weathering potential of these and possibly other novel minerals in the EW field is encouraged.

4.2.2. Impact of EW on SOC content

All treatments showed non-significant changes in SOC content (Figure 8). Small reductions in SOC content compared to the control soil, as observed for especially olivine treatments, were expected for a short-term experiment in which pH strongly increased and OC inputs by plants were absent. Rising soil pH enhances microbial activity and consequently SOC decomposition, especially when pH is between 6.0 and 8.0 (Maier and Pepper, 2009; Leifeld et al., 2013; Paradelo et al., 2015). In addition, the absence of plants in our study played a role. Improved productivity resulting from EW is hypothesized to increase belowground plant OC inputs, which could (partly) counterbalance SOC losses (Vicca et al., 2022). Furthermore, results might have been different if a clayey soil was used instead of a sandy soil, as clayey soils generally have a higher amount of aggregates and reactive minerals that can stabilize SOC (Hassink et al., 1997). As SOC changes generally take place on a longer time scale, we recommend to include monitoring of SOC dynamics in long-term EW experiments.

4.2.3. EW: Net CO_2 sequestration or net CO_2 emissions?

The calculated net CO_2 budgets show that for most treatments SIC sequestration by EW was counterbalanced by a loss of SOC as CO_2 emissions (Figure 9). As indicated above, we show results for a short-term experiment (64 days) in which a strong increase in pH was observed. Therefore, the strong pH effect on SOC decomposition was likely dominant over the CO_2 captured by EW. On the longer term, we hypothesize that SOC decomposition rates decrease, and CO_2 sequestration can become the dominant process, yet long-term data of EW experiments are still limited. Since we observed substantial variation between duplicates, the positive budget, i.e., net CO_2 sequestration, for Wo2 cannot be interpreted as significant. Nevertheless, these calculations demonstrate that, in addition to measuring CO_2 capture by EW, calculating net organic and inorganic carbon budgets is a valuable addition to current EW research in the context of the global transition toward net negative emissions.

CO_2 sequestration as SIC may support climate change mitigation beyond the human time scale (Andrews and Taylor, 2019; Haque et al., 2019a). However, especially when EW is applied to agricultural soils, land management strategies may control the stability of C. SIC is stable as long as land management, especially pH management, is maintained, i.e., frequent application of crushed silicates (Kantola et al., 2017; Haque et al., 2019b). Increasing soil pH favors carbonate precipitation and stability, but may have contradictory effects on SOC as outlined in the previous paragraph. Whether C storage is truly long term, i.e., beyond human time scales, is highly dependent on land management practices. Therefore, these

net CO_2 budgets are important information to land managers to maintain and enhance C storage in soils. In conclusion, we strongly encourage other authors to calculate organic and inorganic carbon budgets to allow an assessment of the net effects of EW on soil CO_2 sequestration.

5. Conclusions and outlook

The ultimate aim of this study was to compare five different silicates on their *enhanced weathering potential*, which includes impacts on both soil quality and CO_2 sequestration. A down-flow soil column experiment was used to measure effects on leachate and quantify organic and inorganic carbon budgets, both underrepresented topics in current EW literature. All silicate treatments generally improved soil quality, as indicated by their increases in pH, base saturation, and CEC. Olivine and wollastonite treatments showed the strongest increases in soil base saturation and CEC, and showed comparatively high CO_2 capture. Based on the conditions and the two methodologies to calculate CO_2 capture used in this study, application of olivine or wollastonite minerals on global cropland could capture 0.43–2.30 or 0.45–1.78 t CO_2 ha^{-1}, respectively. These values represent between 9 and 50% of global anthropogenic CO_2 emissions in 2018 as reported by Jackson et al. (2019). We should note here that chemical weathering rates measured in laboratory experiments likely differ from those measured in field conditions, and differ per soil type and climatic region (Renforth et al., 2015; Beerling et al., 2020), and that the application of a single silicate on global cropland is rather unlikely given their estimated availability and distribution. Furthermore, calculated net CO_2 budgets indicated that inorganic CO_2 sequestration was, at least on the short term, counterbalanced by a loss of organic C, highlighting the importance of quantifying net CO_2 budgets. Nevertheless, this simplified scenario shows the large potential of EW to contribute to the transition toward net negative emissions on a global scale.

We found a high *enhanced weathering potential* for wollastonite minerals, both in terms of CO_2 sequestration and soil quality improvements, while the potential of olivine minerals may be constrained by Ni^{2+} leaching. Therefore, we recommend other authors to not only measure Ni concentrations in soils and plants, but also monitor Ni^{2+} leaching. While the use of basalt was recently suggested as an alternative to olivine due to potential Ni contamination by the latter (Beerling et al., 2018; Kelland et al., 2020), we suggest that the use of feldspar minerals should also be considered, since anorthite and albite released limited Ni into soils and leachate and showed potential for high CO_2 capture. Albite treatments produced HCO_3^- concentrations similarly high as wollastonite treatments, which is not only a long-term inorganic C sink, but also contributes to mitigation of ocean acidification, an important consequence of climate change (Hartmann et al., 2013; Andrews and Taylor, 2019; Bach et al., 2019). Our anorthite and albite treatments showed promising results, however these feldspar minerals deserve further investigation as their low SSA in our experiment not fully allowed us to quantify their *enhanced weathering potential*. Finally, we also strongly encourage other authors to include silicate minerals and rocks that are novel in the EW context in their experimental design to allow a wider exploration of the full potential of EW as a NET.

Data availability statement

The original contributions presented in the study are included in the article/Supplementary material. Further inquiries can be directed to the corresponding author.

Author contributions

EP conceptualized the research and designed the experiment under the supervision of MH and RC. EP conducted the experiment and performed the chemical analyses in the laboratory, analyzed, visualized, and interpreted the data, and wrote the manuscript. MH and RC supervised the project, data analysis, writing of the manuscript, and revised and improved the manuscript. All authors approved the submitted version of the manuscript.

Funding

This work was supported through internal funding.

Acknowledgments

We thank Pol Knops for providing the olivine minerals, Huig Bergsma for providing the basalt, and Rafael Mattos Dos Santos for providing the wollastonite minerals for this experiment. Furthermore, we thank the laboratory staff, Gerlinde Vink, Miranda Vlag, Erna van den Hengel-Voskuilen, Peter Nobels, Andre van Leeuwen, Wobbe Schuurmans, Wim Pape, and Johan Uijtenbroek, for supporting the laboratory experiment and chemical analyses. We also thank Henk-Jan Koudijs for constructing the set-up of the down-flow soil column experiment. Finally, we thank the reviewers for their constructive comments that improved the quality of this manuscript.

Conflict of interest

The authors declare that the research was conducted in the absence of any commercial or financial relationships

that could be construed as a potential conflict of interest.

Publisher's note

All claims expressed in this article are solely those of the authors and do not necessarily represent those of their affiliated organizations, or those of the publisher, the editors and the reviewers. Any product that may be evaluated in this article, or claim that may be made by its manufacturer, is not guaranteed or endorsed by the publisher.

Supplementary material

The Supplementary Material for this article can be found online at: https://www.frontiersin.org/articles/10.3389/fclim.2022.954064/full#supplementary-material

References

Actimin. (2019). *Composition stonemeal Actimin-BT*. Available online at: www.actimin.nl/analyse/ (accessed October 4, 2019).

Allison, L. (1960). Wet-combustion apparatus and procedure for organic and inorganic carbon in soil. *Soil Sci. Soc. Am. J.* 24, 36–40. doi: 10.2136/sssaj1960.03615995002400010018x

Amann, T., Hartmann, J., Struyf, E., Oliveira Garcia, d. e., Fischer, W., Janssens, E. K., et al. (2020). Enhanced Weathering and related element fluxes–a cropland mesocosm approach. *Biogeosciences* 17, 103–119. doi: 10.5194/bg-17-103-2020

Anda, M., Shamshuddin, J., and Fauziah, C. (2013). Increasing negative charge and nutrient contents of a highly weathered soil using basalt and rice husk to promote cocoa growth under field conditions. *Soil Tillage Res.* 132, 1–11. doi: 10.1016/j.still.2013.04.005

Anda, M., Shamshuddin, J., and Fauziah, C. (2015). Improving chemical properties of a highly weathered soil using finely ground basalt rocks. *Catena* 124, 147–161. doi: 10.1016/j.catena.2014.09.012

Andrews, M. G., and Taylor, L. L. (2019). Combating climate change through enhanced weathering of agricultural soils. *Elem. Int. Mag. Mineral. Geochem. Petrol.* 15, 253–258. doi: 10.2138/gselements.15.4.253

Bach, L. T., Gill, S., Rickaby, R., Gore, S., and Renforth, P. (2019), CO2. removal with enhanced weathering and ocean alkalinity enhancement: Potential risks and co-benefits for marine pelagic ecosystems. *Front. Clim.* 1, 7. doi: 10.3389/fclim.2019.00007

Beerling, D. J., Kantzas, E. P., Lomas, M. R., Wade, P., Eufrasio, R. M., Renforth, P., et al. (2020). Potential for large-scale CO2 removal *via* enhanced rock weathering with croplands. *Nature* 583, 242–248. doi: 10.1038/s41586-020-2448-9

Beerling, D. J., Leake, J. R., Long, S. P., Scholes, J. D., Ton, J., Nelson, P. N., et al. (2018). Farming with crops and rocks to address global climate, food and soil security. *Nature Plants* 4, 392–392. doi: 10.1038/s41477-018-0162-5

Besluit kwaliteitseisen en monitoring water. (2009). (Decree on quality requirements and monitoring water). Available online at: https://wetten.overheid.nl/BWBR0027061/2017-01-01 (accessed September 16, 2022).

Dietzen, C., Harrison, R., and Michelsen-Correa, S. (2018). Effectiveness of enhanced mineral weathering as a carbon sequestration tool and alternative to agricultural lime: an incubation experiment. *Int. J. Greenhouse Gas Control* 74, 251–258. doi: 10.1016/j.ijggc.2018.05.007

Dijkstra, J. J., Meeussen, J. C., and Comans, R. N. (2004). Leaching of heavy metals from contaminated soils: an experimental and modeling study. *Environ. Sci. Technol.* 38, 4390–4395. doi: 10.1021/es049885v

Fernández, F. G., and Hoeft, R. G. (2009). Managing soil pH and crop nutrients. *Illinois Agron. Handbook* 24, 91–112.

Fox, J., and Weisberg, S. (2019). *An R Companion to Applied Regression (third edition)*. California: Sage.

Gao, J., Mikutta, R., Jansen, B., Guggenberger, G., Vogel, C., Kalbitz, K., et al. (2020). The multilayer model of soil mineral–organic interfaces—a review. *J. Plant Nutri. Soil Sci.* 183, 27–41. doi: 10.1002/jpln.201900530

Gilbert, O., Hernández, M., Vilanova, E., and Cornellà, O. (2014). Guidelining protocol for soil-column experiments assessing fate and transport of trace organics. *Demeau, Brussels, Belgium* 3, 54.

Gillman, G. (1980). The effect of crushed basalt scoria on the cation exchange properties of a highly weathered soil. *Soil Sci. Soc. Am. J.* 44, 465–468. doi: 10.2136/sssaj1980.03615995004400030005x

Gillman, G., Burkett, D., and Coventry, R. (2002). Amending highly weathered soils with finely ground basalt rock. *Appl. Geochem.* 17, 987–1001. doi: 10.1016/S0883-2927(02)00078-1

Groenenberg, J. E., Römkens, P. F., Zomeren, A. V., Rodrigues, S. M., and Comans, R. N. (2017). Evaluation of the single dilute (0.43 M) nitric acid extraction to determine geochemically reactive elements in soil. *Environ. Sci. Technol.* 51, 2246–2253. doi: 10.1021/acs.est.6b05151

Haque, F., Chiang, Y. W., and Santos, R. M. (2019a). Alkaline mineral soil amendment: a climate change 'stabilization wedge'? *Energies* 12, 2299. doi: 10.3390/en12122299

Haque, F., Santos, R. M., Dutta, A., Thimmanagari, M., and Chiang, Y. W. (2019b). Co-benefits of wollastonite weathering in agriculture: CO2 sequestration and promoted plant growth. *ACS Omega* 4, 1425–1433. doi: 10.1021/acsomega.8b02477

Harley, A., and Gilkes, R. (2000). Factors influencing the release of plant nutrient elements from silicate rock powders: a geochemical overview. *Nut. Cycl. Agroecosys.* 56, 11–36. doi: 10.1023/A:1009859309453

Hartmann, J., West, A. J., Renforth, P., Köhler, P., La Rocha, D. e,. C. L., Wolf-Gladrow, D. A., et al. (2013). Enhanced chemical weathering as a geoengineering strategy to reduce atmospheric carbon dioxide, supply nutrients, and mitigate ocean acidification. *Rev. Geophy.* 51, 113–149. doi: 10.1002/rog.20004

Hassink, J., Whitmore, A. P., and Kubát, J. (1997). Size and density fractionation of soil organic matter and the physical capacity of soils to protect organic matter. *Eur. J. Agron.* 7, 189–199. doi: 10.1016/S1161-0301(97)00045-2

Huijgen, W. J., Witkamp, G-. J., and Comans, R. N. (2006). Mechanisms of aqueous wollastonite carbonation as a possible CO2 sequestration process. *Chem. Eng. Sci.* 61, 4242–4251. doi: 10.1016/j.ces.2006.01.048

IPCC. (2014). *Climate Change 2014: Synthesis Report*. Fifth Assessment Report of the Intergovernmental Panel on Climate Change. In. Geneva, Switzerland.

IPCC. (2018). *Global Warming of* 1, 5.°*C*. Special Report of the Intergovernmental Panel on Climate Change. In: Incheon, South Korea.

ISO 10693. (1995). *Soil Quality - Determination of Carbonate Content - Volumetric Method*. International Organization for Standardization.

ISO 11260. (2018). *Soil Quality - Determination of Effective Cation Exchange Capacity and Base Saturation Level Using Barium Chloride Solution*. International Organization for Standardization.

ISO 21268-3. (2019). *Soil Quality - Leaching Procedures for Subsequent Chemical and Ecotoxicological Testing of Soil and Soil-Like Materials - Part 3: Up-Flow Percolation Test*. International Organization for Standardization.

Jackson, R., Friedlingstein, P., Andrew, R., Canadell, J., Le Quéré, C., Peters, G., et al. (2019). Persistent fossil fuel growth threatens the Paris agreement and planetary health. *Environ. Res. Lett.* 14, 121001. doi: 10.1088/1748-9326/ab57b3

Kantola, I. B., Masters, M. D., Beerling, D. J., Long, S. P., and DeLucia, E. H. (2017). Potential of global croplands and bioenergy crops for climate change mitigation through deployment for enhanced weathering. *Biol. Lett.* 13, 20160714. doi: 10.1098/rsbl.2016.0714

Kelland, M. E., Wade, P. W., Lewis, A. L., Taylor, L. L., Sarkar, B., Andrews, M. G., et al. (2020). Increased yield and CO2 sequestration potential with the C4 cereal Sorghum bicolor cultivated in basaltic rock dust-amended agricultural soil. *Glob. Chang. Biol.* 26, 3658–3676. doi: 10.1111/gcb.15089

Kremer, D., Etzold, S., Boldt, J., Blaum, P., Hahn, K. M., Wotruba, H., et al. (2019). Geological mapping and characterization of possible primary input materials for the mineral sequestration of carbon dioxide in Europe. *Minerals* 9, 485. doi: 10.3390/min9080485

Kronzucker, H. J., Coskun, D., Schulze, L. M., Wong, J. R., and Britto, D. T. (2013). Sodium as nutrient and toxicant. *Plant Soil* 369, 1–23. doi: 10.1007/s11104-013-1801-2

Kumar, O., Singh, S., Singh, A., Yadav, S., and Latare, A. (2018). Effect of soil application of nickel on growth, micronutrient concentration and uptake in barley (*Hordeum vulgare L.*) grown in Inceptisols of Varanasi. *J. Plant Nutr.* 41, 50–66. doi: 10.1080/01904167.2017.1381724

Kump, L. R., Brantley, S. L., and Arthur, M. A. (2000). Chemical weathering, atmospheric CO2, and climate. *Annu. Rev. Earth Planet. Sci.* 28, 611–667. doi: 10.1146/annurev.earth.28.1.611

Lehmann, J., and Possinger, A. (2020). Removal of atmospheric CO2 by rock weathering holds promise for mitigating climate change. *Nature.* 583, 204–205. doi: 10.1038/d41586-020-01965-7

Leifeld, J., Bassin, S., Conen, F., Hajdas, I., Egli, M., Fuhrer, J., et al. (2013). Control of soil pH on turnover of belowground organic matter in subalpine grassland. *Biogeochemistry* 112, 59–69. doi: 10.1007/s10533-011-9689-5

Maier, R. M., and Pepper, I. L. (2009). Earth environments. In *Environmental microbiology*: Elsevier (pp. 57-82). doi: 10.1016/B978-0-12-370519-8.00004-3

McBride, M. B. (1994). *Environmental Chemistry of Soils*. New York: Oxford University Press.

Moosdorf, N., Renforth, P., and Hartmann, J. (2014). Carbon dioxide efficiency of terrestrial enhanced weathering. *Environ. Sci. Technol.* 48, 4809–4816. doi: 10.1021/es4052022

NEN (2018). *Soil - Determination of Clay Content and Particle Size Distribution in Soil and Sediment by Sieve and Pipet.*

Oelkers, E. H., Declercq, J., Saldi, G. D., Gislason, S. R., and Schott, J. (2018). Olivine dissolution rates: a critical review. *Chem. Geol.* 500, 1–19. doi: 10.1016/j.chemgeo.2018.10.008

Palandri, J. L., and Kharaka, Y. K. (2004). *A Compilation of Rate Parameters of Water-Mineral Interaction Kinetics for Application to Geochemical Modeling*. California: U.S. Geological Survey. doi: 10.3133/ofr20041068

Paradelo, R., Virto, I., and Chenu, C. (2015). Net effect of liming on soil organic carbon stocks: a review. *Agric. Ecosyst. Environ.* 202, 98–107. doi: 10.1016/j.agee.2015.01.005

Pearson, F. (1981). Fixed endpoint alkalinity determination. *Water Pollution Control Federation* 53, 1243–1252.

R Core Team. (2020). *R: A Language and Environment for Statistical Computing*. Vienna: R Foundation for Statistical Computing. Available online at: https://www.R-project.org/

Renforth, P., von Strandmann, P. P., and Henderson, G. (2015). The dissolution of olivine added to soil: implications for enhanced weathering. *Ap. Geochem.* 61, 109–118. doi: 10.1016/j.apgeochem.2015.05.016

Rodrigues, S., Henriques, B., Silva, d. a., Pereira, E. F., and Duarte, M. A., and Römkens, P. (2010). Evaluation of an approach for the characterization of reactive and available pools of twenty potentially toxic elements in soils: Part I–The role of key soil properties in the variation of contaminants' reactivity. *Chemosphere* 81, 1549–1559. doi: 10.1016/j.chemosphere.2010.07.026

Römkens, P. F., Guo, H-. Y., Chu, C. L., Liu, T. S., Chiang, C. F., Koopmans, G. F., et al. (2009). Characterization of soil heavy metal pools in paddy fields in Taiwan: chemical extraction and solid-solution partitioning. *J. Soils Sediments* 9, 216–228. doi: 10.1007/s11368-009-0075-z

Schlesinger, W., and Bernhardt, E. (2013). *Biogeochemistry: An Analysis of Global Change (third edition)*. Oxford: Academic Press.

Schuiling, R., and Krijgsman, P. (2006). Enhanced weathering: an effective and cheap tool to sequester CO2. *Clim. Change* 74, 349–354. doi: 10.1007/s10584-005-3485-y

Siqueira Freitas, D., Wurr Rodak, B. Rodrigues dos Reis, A., de Barros Reis, F., Soares de Carvalho, T., Schulze, J., et al. (2018). Hidden nickel deficiency? Nickel fertilization via soil improves nitrogen metabolism and grain yield in soybean genotypes. *Front. Plant Sci.* 9, 614. doi: 10.3389/fpls.2018.00614

Sparks, D. L. (2003). *Environmental Soil Chemistry (Second edition ed.)*. California: Elsevier Academic Press. doi: 10.1016/B978-012656446-4/50001-3

Ten Berge, H. F., Van der Meer, H. G., Steenhuizen, J. W., Goedhart, P. W., Knops, P., Verhagen, J., et al. (2012). Olivine weathering in soil, and its effects on growth and nutrient uptake in ryegrass (*Lolium perenne L.*): a pot experiment. *PLoS ONE* 7, e42098. doi: 10.1371/journal.pone.0042098

Tóth, G., Hermann, T., Silva, D. A., and Montanarella, M. (2016). Heavy metals in agricultural soils of the European Union with implications for food safety. *Environ. Int.* 88, 299–309. doi: 10.1016/j.envint.2015.12.017

USGS. (2020). Mineral Commodity Summaries 2020. U.S. Geological Survey. Available online at: www.usgs.gov/centers/nmic/mineral-commodity-summaries (accessed June 8, 2021).

Verma, M. P. (2004). A revised analytical method for HCO3-and CO32-determinations in geothermal waters: an assessment of IAGC and IAEA interlaboratory comparisons. *Geostandards and Geoanal. Res.* 28, 391–409. doi: 10.1111/j.1751-908X.2004.tb00758.x

Vicca, S., Goll, D. S., Hagens, M., Hartmann, J., Janssens, I. A., Neubeck, A., et al. (2022). Is the climate change mitigation effect of enhanced silicate weathering governed by biological processes? *Glob. Chang. Biol.* 28, 711–726. doi: 10.1111/gcb.15993

Weng, L. P., Wolthoorn, A., Lexmond, T. M., Temminghoff, E. J., and van Riemsdijk, W. H. (2004). Understanding the effects of soil characteristics on phytotoxicity and bioavailability of nickel using speciation models. *Environ. Sci. Technol.* 38, 156–162. doi: 10.1021/es030053r

West, T. O., and McBride, A. C. (2005). The contribution of agricultural lime to carbon dioxide emissions in the United States: dissolution, transport, and net emissions. *Agric. Ecosyst. Environ.* 108, 145–154. doi: 10.1016/j.agee.2005.01.002

Frontiers in Climate

Explores solutions which can help humanity mitigate and adapt to climate change

Explores scientific advances in climate research, focusing on mitigation, adaptation, emissions and modelling. It shares research that contributes to climate policy and economic drivers, addressing societal challenges created by climate change.

Discover the latest Research Topics

See more →

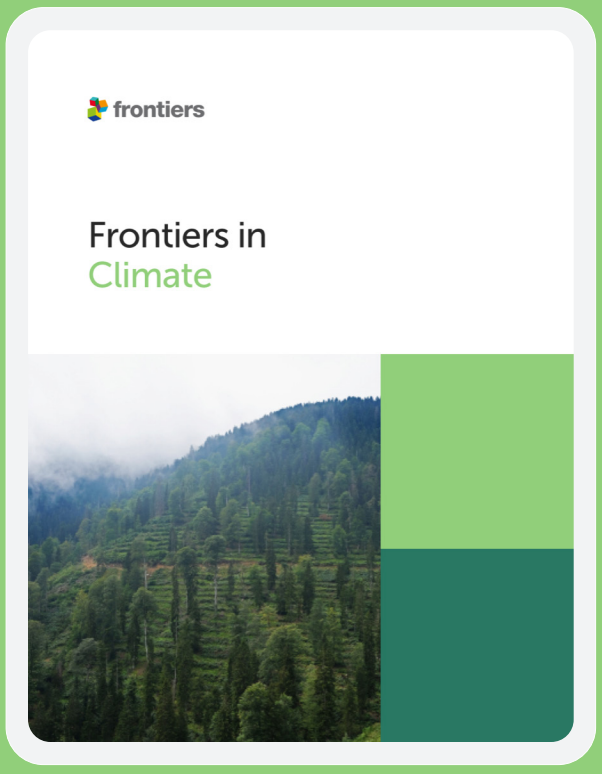

Frontiers

Avenue du Tribunal-Fédéral 34
1005 Lausanne, Switzerland
frontiersin.org

Contact us

+41 (0)21 510 17 00
frontiersin.org/about/contact